

DISSERTATION

SYNTHESIS AND CHARACTERIZATION OF IRIDIUM MODEL, AND COBALT  
AND NICKEL, INDUSTRIAL ZIEGLER–TYPE HYDROGENATION CATALYSTS  
AND THEIR PRECURSORS

Submitted by

William M. Alley

Department of Chemistry

In partial fulfillment of the requirements

For the Degree of Doctor of Philosophy

Colorado State University

Fort Collins, Colorado

Spring 2011

Doctoral Committee:

Advisor: Richard G. Finke

Eugene Y.-X. Chen

C. Michael Elliott

Nancy E. Levinger

Matthew Kipper

## ABSTRACT

### SYNTHESIS AND CHARACTERIZATION OF IRIDIUM MODEL, AND COBALT AND NICKEL, INDUSTRIAL ZIEGLER–TYPE HYDROGENATION CATALYSTS AND THEIR PRECURSORS

Following a comprehensive critical review of the pertinent literature, the research presented herein is focused on the synthesis of an Ir precursor used to model industrial Ziegler–type hydrogenation catalysts, and on catalyst characterization using both the Ir model, and genuine Co and Ni, industrial catalyst materials. The studies include: (i) the synthesis, characterization, and initial catalytic investigation of Ir (and Rh) compounds for use as models for the industrial Co and Ni Ziegler–type hydrogenation catalysts; (ii) characterization of the Ziegler–type hydrogenation catalyst made from the Ir precursor; and (iii) characterization of the authentic industrial Co and Ni Ziegler–type hydrogenation catalysts.

The synthesis and definitive characterization of Ir (and Rh) precatalysts designed to facilitate investigation into the homogeneous versus heterogeneous nature of Ziegler–type hydrogenation catalysts is described herein. Additionally, the ability of these Ir (and Rh) precatalysts to form active Ziegler–type hydrogenation catalysts upon combination with  $\text{AlEt}_3$  is demonstrated.

The homogeneous versus heterogeneous nature of the Ir Ziegler–type hydrogenation catalyst is investigated using several complementary analytical methods plus kinetic studies. Initial active catalyst solutions contain a variety of Ir species ranging from mono-Ir compounds to nanometer-scale  $\text{Ir}_n$  clusters, but on average are subnanometer,  $\text{Ir}_{\sim 4-15}$  species. However, crystalline  $\text{Ir}(0)_{\sim 40-150}$  nanoclusters are rapidly formed when the solutions are put under pressurized  $\text{H}_2$  gas, and these larger, “Ziegler nanoclusters” are shown to be the most active catalysts, an important result in comparison to all the prior, extensive literature of these important industrial catalysts.

The homogeneous versus heterogeneous nature of the authentic industrial Co- and Ni-based Ziegler–type hydrogenation catalysts are investigated using an approach parallel to that used for the Ir system, and are compared to the results from the Ir model system. The metal cluster species are essentially the same pre- and posthydrogenation; they comprise a broad distribution of  $M_n$  cluster sizes from subnanometer to nanometer in scale, with average diameters of about one nanometer, and with some amount of unreduced mono-metallic complexes also present dependent on the Al/M ratio. These findings support the primary working hypothesis present in the most recent literature, namely that Ziegler-type hydrogenation catalysis is enacted by “Ziegler nanoclusters” (as defined herein), nanoclusters of size  $M_{\geq 4}$  in the case of the industrial Co and Ni system.

## TABLE OF CONTENTS

I.	INTRODUCTION.....	1
II.	ZIEGLER–TYPE HYDROGENATION CATALYSTS MADE FROM GROUP 8–10 TRANSITION METAL PRECATALYSTS AND $\text{AlEt}_3$ : A CRITICAL REVIEW OF THE LITERATURE.....	4
	Abstract.....	6
	Introduction.....	9
	Polymer Hydrogenation.....	9
	An Important Distinction: Ziegler–type Hydrogenation Catalysts Versus Ziegler–Natta Polymerization Catalysts.....	11
	Overview of the Main Sections of This Review.....	13
	Studies of Ziegler–type Hydrogenation Catalysts.....	15
	Effect of Preparation Variables on Ziegler–type Hydrogenation Catalysts....	15
	Identities of the Precursors.....	20
	Molar Ratio of the Precursor Components (Precatalyst and Cocatalyst) and the Role of Impurities, Particularly $\text{H}_2\text{O}$ .....	23
	Solvent.....	25
	Identity of the Hydrogenation Substrate.....	25
	Other Aspects of Catalyst Synthesis.....	26
	Aging of Prepared Catalyst.....	29
	Conclusions for the Section on Catalyst Preparation Variables.....	30
	The Nature and Mechanism of Formation of Ziegler–type Hydrogenation Catalysts.....	32
	The “Ziegler–type Catalysts are Homogeneous” Hypothesis.....	34
	The “Ziegler–type Catalysts are Heterogeneous” Hypothesis.....	51
	A Closer Look at the More General Homogeneous Versus Heterogeneous Catalysis Question.....	75
	The 1994 Four-Prong Methodology.....	75
	Special Challenges with (First Row, Ni, Co, Fe) Ziegler–type Hydrogenation Catalysts.....	78
	Conclusions for the Section on the More General Homogeneous Versus Heterogeneous Catalysis Question.....	80
	Summary.....	82
	Appendix.....	88
	References.....	96
	Supporting Information.....	105
III.	MODEL ZIEGLER–TYPE HYDROGENATION CATALYST PRECURSORS, $[(1,5\text{-COD})\text{M}(\mu\text{-O}_2\text{C}_8\text{H}_{15})_2]$ (M = Ir AND Rh): SYNTHESIS, CHARACTERIZATION, AND DEMONSTRATION OF CATALYTIC ACTIVITY EN ROUTE TO IDENTIFYING THE TRUE INDUSTRIAL HYDROGENATION CATALYSTS.....	118

Abstract.....	120
Introduction.....	122
Results and Discussion.....	124
Conclusions.....	133
Experimental Section.....	135
References.....	142
Supporting Information.....	149
IV. ZIEGLER–TYPE HYDROGENATION CATALYSTS MADE FROM [(1,5-COD)Ir( $\mu$ -O <sub>2</sub> C <sub>8</sub> H <sub>15</sub> ) <sub>2</sub> ) <sub>2</sub> AND AlEt <sub>3</sub> : EVIDENCE FOR THE Ir <sub>n</sub> SPECIES PRESENT AND FOR THE TRUE CATALYST.....	183
Abstract.....	185
Introduction.....	188
Results and Discussion.....	191
Summary.....	224
Experimental Section.....	228
References.....	236
Supporting Information.....	248
V. INDUSTRIAL ZIEGLER–TYPE HYDROGENATION CATALYSTS MADE FROM Co(O <sub>2</sub> C <sub>10</sub> H <sub>19</sub> ) <sub>2</sub> OR Ni(O <sub>2</sub> C <sub>8</sub> H <sub>15</sub> ) <sub>2</sub> AND AlEt <sub>3</sub> : EVIDENCE FOR THE Co <sub>n</sub> OR Ni <sub>n</sub> SPECIES PRESENT AND FOR THE TRUE CATALYST.....	295
Abstract.....	297
Introduction.....	300
Experimental Section.....	304
Results and Discussion.....	315
Conclusions.....	340
References.....	344
Supporting Information.....	351
VI. SUMMARY.....	407
APPENDICES	
Appendix A. General Statement on “Journals-Format” Theses.....	409
Appendix B. Research Proposal.....	413

## CHAPTER I

### INTRODUCTION

The broad theme of this dissertation is the fundamental study of industrially relevant Ziegler–type hydrogenation catalysts. This dissertation is written in the “journals-format” style (see Appendix A for a discussion of this type of dissertation). It is based on three separate publications written in the format set by the American Chemical Society, plus a published literature review in the format of *Journal of Molecular Catalysis A: Chemical* (Elsevier). Continuity of this dissertation as a single document is achieved by (i) this introduction, (ii) the use of bridging paragraphs at the beginning of each chapter, and (iii) a final summary chapter. Some chapters contain important contributions from Isil K. Hamdemir. Detailed accounts of individual contributions to both the experimental and written aspects of this dissertation are given at the beginning of each chapter. A concise overview of each chapter’s contents is presented below.

Chapter II is a published literature review giving a comprehensive critical analysis of the literature of Ziegler–type hydrogenation catalysts (Alley, W. M.; Hamdemir, I. K.;

Johnson, K. A.; Finke, R. G. *J. Mol. Catal. A: Chem.* **2010**, *315*, 1–27). The literature concerning the important variables in the synthesis of Ziegler–type hydrogenation catalysts, and investigations into whether the true catalytic species are homogenous or heterogeneous in nature are discussed. The review concludes with a brief look at the general homogeneous versus heterogeneous catalysis question, which is a central question relevant to the rest of this dissertation.

Chapter III is a publication (Alley, W. M.; Girard, C. W.; Özkar, S.; Finke, R. G. *Inorg. Chem.* **2009**, *48*, 1114–1121) that describes the synthesis and characterization of Ir and Rh precursors intended for use as model industrial Ziegler–type hydrogenation catalysts. In addition, this study demonstrates that the Ir and Rh compounds synthesized do indeed form active Ziegler–type hydrogenation catalysts upon combination with  $\text{AlEt}_3$ .

Chapter IV is a publication (Alley, W. M.; Hamdemir, I. K.; Wang, Q.; Frenkel, A. I.; Li, L.; Yang, J. C.; Menard, L. D.; Nuzzo, R. G.; Özkar, S.; Johnson, K. A.; Finke, R. G. *Inorg. Chem.* **2010**, *49*, 8131–8147) reporting the use of the Ir precatalyst (whose synthesis and characterization were described in Chapter III) to investigate the homogeneous versus heterogeneous Ziegler–type hydrogenation catalysts. This work reveals that the initially active catalyst solutions contain Ir species ranging from mono-Ir compounds to  $\text{Ir}_{\sim 100}$  clusters. However, the most active catalysts obtained from this system are formed rapidly under catalytic conditions (i.e., after the introduction of  $\text{H}_2$  gas), and are crystalline  $\text{Ir}(0)_{\sim 40-150}$  “Ziegler–nanoclusters”.

Chapter V presents a paper submitted for publication in *Langmuir*. The homogeneous versus heterogeneous nature of the authentic industrial Co and Ni-based

Ziegler–type hydrogenation catalysts are investigated using an approach similar to that used with the Ir system, and with the results from the model Ir system available for comparison. The metal cluster species, both pre- and posthydrogenation, have a broad range of sizes with average diameters of about one nanometer, and unreduced mono-metallic complexes also present dependent on the Al/M ratio. Poisoning studies with the Ni system support the notion of Ziegler nanoclusters ( $M_{\geq 4}$ ) as the most active hydrogenation catalysts in this industrial system.

Chapter VI is a concise summary of the material presented in this dissertation. It also gives an indication of potentially fruitful avenues of research that could be pursued as an extension of this project.

## CHAPTER II

### ZIEGLER–TYPE HYDROGENATION CATALYSTS MADE FROM GROUP 8–10 TRANSITION METAL PRECATALYSTS AND AIR<sub>3</sub> COCATALYSTS: A CRITICAL REVIEW OF THE LITERATURE

This dissertation chapter consists of a review article published in the *Journal of Molecular Catalysis A: Chemical* **2010**, 315, 1–27. This chapter is a critical review of the existing literature on the topic of Ziegler–type hydrogenation catalysts, with a particular focus on the variables important to catalyst synthesis and what has been believed concerning the homogeneous versus heterogeneous nature of the catalysts. Despite being a review of the literature, original experimental work was performed and is reported along with the literature analysis. All original experimental work was performed by William M. Alley.

An initial, partial draft of the section concerning the homogeneous versus heterogeneous nature of Ziegler–type hydrogenation catalysts was written by Isil K. Hamdemir. Permission to reprint figures and schemes from prior publications was obtained by Isil K. Hamdemir. Preparation of the figures and schemes was performed by both William M. Alley and Isil K. Hamdemir. Literature was assembled, and tables were prepared and edited, by both Isil K. Hamdemir and William M. Alley. The writing for

the other sections of the manuscript, the subsequent drafts of the complete manuscript, including the final version and preparation of the document for publication, was accomplished by William M. Alley with light editing by Isil K. Hamdemir, Kimberly A. Johnson, and light edits (according to Prof. Finke; 16 hours) by Richard G. Finke.

The page numbers in the table of contents of this literature review article have been altered to reflect the page numbers of the contents as formatted for this dissertation. The article is otherwise unaltered. This article is reproduced with permission from Elsevier, Copyright (2010). As noted specifically in the article where applicable, certain figures and schemes are, with permission, reproduced or adapted from: K. Fischer, K. Jonas, P. Misbach, R. Stabba, G. Wilke, *Angew. Chem. Int. Ed.* 12 (1973) 943–953; M. F. Sloan, A. S. Matlack, D. S. Breslow, *J. Am. Chem. Soc.* 85 (1963) 4014–4018; J. Reguli, A. Staško, *Chem. Papers* 41 (1987) 299–310; F. K. Shmidt, L. O. Nindakova, B. A. Shainyan, V. V. Saraev, N. N. Chipanina, V. A. Umanetz, *J. Mol. Catal. A: Chem.* 235 (2005) 161–172; F. K. Shmidt, V. G. Lipovich, S. M. Krasnopol'skaya, I. V. Kalechits, *Kinetika i Kataliz* 11 (1970) 595–602; K. Angermund, M. Bühl, U. Endruschat, F. T. Mauschick, R. Mörtel, R. Mynott, B. Tesche, N. Waldöfner, H. Bönnemann, G. Köhl, H. Modrow, J. Hormes, E. Dinjus, F. Gassner, H.-G. Haubold, T. Vad, M. Kaupp, *J. Phys. Chem. B* 107 (2003) 7507–7515; and Y. Lin, R. G. Finke, *Inorg. Chem.* 33 (1994) 4891–4910.

## Review

### **Ziegler–type hydrogenation catalysts made from group 8–10 transition metal precatalysts and $\text{AlR}_3$ cocatalysts: A critical review of the literature**

William M. Alley, Isil K. Hamdemir, Kimberly A. Johnson, Richard G. Finke

#### **Abstract**

Ziegler–type hydrogenation catalysts (group 8–10 transition metal precatalysts plus  $\text{AlR}_3$  cocatalysts) are one of the most important families of industrial hydrogenation catalysts, especially for polymer hydrogenation. Despite their ~40 year history of industrial use, there is a need for improved fundamental understanding in order to make further, rationally directed improvements in these catalysts. This review examines the existing literature on Ziegler–type hydrogenation catalysts, specifically: (i) the variables important to catalyst synthesis, (ii) the catalyst formation reaction mechanism, (iii) the compositional and structural nature of the active catalyst species, and (iv) the mechanism of catalytic hydrogenation. This review also (v) discusses the current approaches to the homogeneous versus heterogeneous catalysis question, with the goal of identifying if Ziegler–type hydrogenation catalysts are homogeneous (e.g., monometallic) versus heterogeneous (e.g., nanoclusters) as the true catalyst(s). A summary of the main insights from each section of the review is also given.

## Contents

1.	Introduction.....	9
1.1.	Polymer hydrogenation.....	9
1.2.	An important distinction: Ziegler–type hydrogenation catalysts versus Ziegler–Natta polymerization catalysts.....	11
1.3.	Overview of the main sections of this review.....	13
2.	Studies of Ziegler–type hydrogenation catalysts.....	15
2.1.	Effect of preparation variables on Ziegler–type hydrogenation catalysts.....	15
2.1.1.	Identities of the precursors.....	20
2.1.2.	Molar ratio of the precursor components (precatalyst and cocatalyst) and the role of impurities, particularly H <sub>2</sub> O.....	23
2.1.3.	Solvent.....	25
2.1.4.	Identity of the hydrogenation substrate.....	25
2.1.5.	Other aspects of catalysts synthesis.....	26
2.1.6.	Aging of prepared catalyst.....	29
2.1.7.	Conclusions for the section on catalyst preparation variables.....	30
2.2.	The nature and mechanism of formation of Ziegler–type hydrogenation catalysts.....	32
2.2.1.	The “Ziegler–type catalysts are homogeneous” hypothesis.....	34
2.2.2.	The “Ziegler–type catalysts are heterogeneous” hypothesis.....	51
2.3.	A closer look at the more general homogeneous versus heterogeneous catalysis question.....	75

2.3.1.	The 1994 four-prong methodology.....	75
2.3.2.	Special challenges with (first row, Ni, Co, Fe) Ziegler–type hydrogenation catalysts.....	78
2.3.3.	Conclusions for the section on the more general homogeneous versus heterogeneous catalysis question.....	80
3.	Summary.....	82
	Acknowledgement.....	88
	Appendix A. Supplementary data.....	88
	Appendix B.....	88
	References.....	96

## 1. Introduction

In 1953, while studying the polymerization of ethylene using trialkylaluminum ( $\text{AlR}_3$ ), Ziegler and coworkers [1,2,3,4,5] discovered the “nickel effect”. When one experiment gave a majority of butene instead of the expected higher molecular weight polyethylene, a search for the cause of this unanticipated result revealed that small amounts of residual nickel salts, mostly  $\text{Ni}(\text{acac})_2$ , were present from having cleaned the metal autoclave with sulfuric acid. These nickel salts had reacted with  $\text{AlEt}_3$  to cause the observed change in catalysis, and the phenomenon was therefore termed the “nickel effect” [4]. These and other investigations into catalysts and polymerization products led to the 1963 Nobel Prize shared by Karl Ziegler and Giulio Natta [5]. The industrial and technological potential of Ziegler–Natta<sup>1</sup> catalysts was subsequently realized with remarkable speed [5]. Interest in variations on these catalysts for their potential use in *hydrogenation, particularly for polymer hydrogenation*, was considerable (Appendix A, Table A1), and began in the early 1960s [2,6].

### 1.1. Polymer hydrogenation

Diene polymers such as polyisoprene and polybutadiene, or styrenic block copolymers (SBCs, Scheme 1) that contain polyisoprene or polybutadiene blocks, have multiple commercial applications [6]. They possess the desired physical properties of

---

<sup>1</sup> Early on, Karl Ziegler [5] referred to these catalysts generally as “organometallic mixed catalysts,” and preferred the specific title “Mülheim catalysts” because of where the original work was done. Giulio Natta named them Ziegler catalysts [1,5]. They are usually now called Ziegler–Natta catalysts in the case of polymerization (as opposed to hydrogenation) catalysts.

high strength, wide range of hardness, and ease of processing. The olefins in these polymers allow them to undergo post-polymerization modification (including crosslinking, isomerization, cyclization, and hydrogenation) to create new polymers possessing desired physical and chemical properties [7]. Of the various desired types of modifications possible, hydrogenation is arguably the most important [6]. The primary purpose of polymer hydrogenation is to make the resultant polymer more resistant to the deleterious effects of thermal, oxidative, and ultraviolet radiation exposure. A main pathway for degradation of polymers containing olefinic groups occurs by autoxidation of allylic positions in the polymer to allylic –OOH groups and subsequent oxidation products [8]. Non-hydrogenated SBCs with their unsaturated olefinic midblock regions are prone to these effects.

SBCs were first produced in the early 1960s by Shell Chemical Co. with the trade name KRATON<sup>TM</sup> polymers [9]. Roughly one decade later, hydrogenated SBCs with improved thermal and oxidative stability were also being produced (see Appendix A, Table A1). Without selective hydrogenation of the olefinic blocks of SBCs, the polymers become yellow, brittle, and of little use in many applications where exposure to heat, air, and light are unavoidable. Hydrogenated SBCs would have found wider application shortly after their introduction were it not for their relatively high cost due to the extra expense of the hydrogenation step [6]. Development of more economically favorable catalytic hydrogenation processes has, and continues to, alleviate this added expense. The use of homogeneous (soluble)<sup>2</sup> [10,11,12,13,14,15,16,17,18,19] hydrogenation

---

<sup>2</sup> See the references listed [10–19] for a more in-depth discussion of the terminology of “heterogeneous vs. homogeneous” catalysts, and the problem of distinguishing between the two. Briefly, the classic use of the terms heterogeneous and homogeneous is in reference to the phase of catalyst and substrate. If the

catalysts has helped by allowing for more complete polymer hydrogenation [6]. Ziegler–type hydrogenation catalysts, the focus of this review, are one of the most important families of soluble catalyst commonly used for the purpose of polymer hydrogenation. Consequently, the timeline for the industrial development of Ziegler–type hydrogenation catalysts mirrors that of hydrogenated styrenic block copolymers (SBCs) [9].

### *1.2. An Important Distinction: Ziegler–type hydrogenation catalysts vs. Ziegler–Natta polymerization catalysts*

A broad definition of Ziegler–Natta catalysts includes any catalyst formed by reaction between a transition metal compound precatalyst and a group 1, 2, 13 or 14 alkyl or aryl halide cocatalyst [6,20,21]. It is important to make a distinction between the late-metal *Ziegler–type hydrogenation catalysts* of interest herein versus the currently popular *Ziegler–Natta polymerization catalysts*. Classic Ziegler–Natta olefin polymerization catalysts are formed by the reaction between early metals such as  $\text{TiCl}_3$  plus  $\text{Et}_2\text{AlCl}$  and are heterogeneous catalysts with active sites on  $\text{TiCl}_3$  crystallites [20,22]. Homogeneous variants of Ziegler–Natta polymerization catalysts have been developed using metallocene compounds such as  $[\text{Cp}_2\text{MX}_2]$  (Cp = cyclopentadiene, M = Ti or Zr, and X =

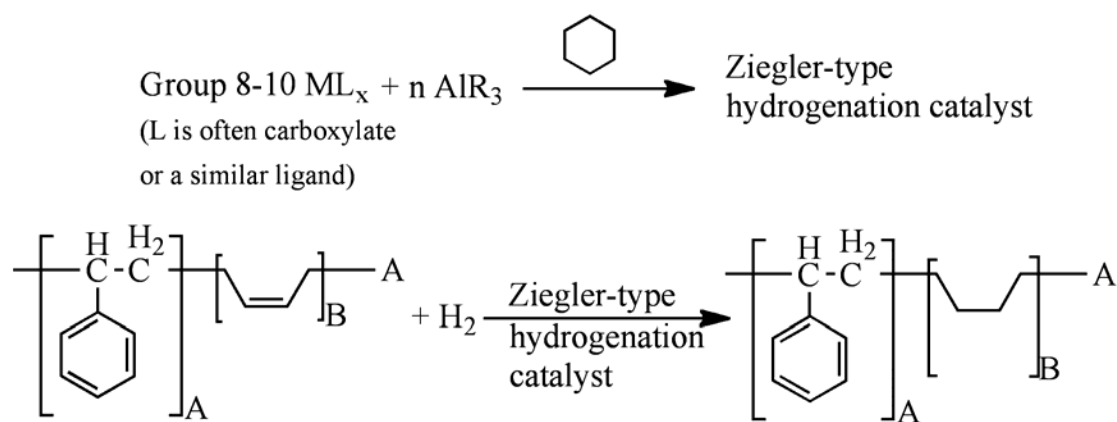
---

substrate is in solution, as is typical for hydrogenation reactions such as polymer hydrogenation, a homogeneous catalyst would be soluble whereas a heterogeneous catalyst would not. However, the true catalytically active species in catalyst systems formed of a transition metal complex under reducing conditions may be soluble metal complexes, films, powders, or nanoscale colloids formed in-situ [10]. The latter is soluble, but it shares characteristics with heterogeneous catalysts due to the heterogeneity in its active sites [11]. Such a catalyst is also sometimes called “microheterogeneous” [19]. For the sake of clarity in this review, the terms “soluble” and “insoluble” will hereafter refer to the phase of the catalyst. The terms “homogeneous” and “heterogeneous” will refer to whether the catalyst species has, respectively, only one or multiple types of active sites [16].

Cl or CH<sub>3</sub>) [21,22,23,24,25,26]. At first these precursors were tested with AlR<sub>3</sub> cocatalysts, but the discovery that small amounts of water had an activating effect led to their use with methylalumoxane (MAO), a historically enigmatic cocatalyst formed by incomplete reaction between AlMe<sub>3</sub> and water [20,21,26,27,28,29,30,31,32,33,34,35]. Metallocene compounds of early transition metals dominate the field of homogeneous Ziegler–Natta polymerization catalysis, although rare-earth metals have been used as well [21,22,36]. The bulk of research on Ziegler–Natta catalysts has been focused on *polymerization*; the term “*Ziegler–Natta catalyst*” is, therefore, practically synonymous with “*polymerization catalyst*” [5,20].

However, herein we consider a different type of Ziegler-based catalyst made from non-zero-valent group 8–10 transition metal (M) precatalysts plus AlR<sub>3</sub> cocatalysts, and used for hydrogenations. Therefore, for the purposes of this review, the term “*Ziegler–type hydrogenation catalysts*” will be reserved for catalysts prepared from group 8–10 transition metals plus AlR<sub>3</sub>. Such Ziegler–type catalysts have found wide use [37], including the hydrogenation [38] of a variety of compounds such as olefins, aromatics [2,39], and diene-based polymers as already mentioned [6,9]. The catalysts most commonly used for such industrial hydrogenation reactions are derived from first row, group 8–10 transition metal compounds [6,9]. The most frequently encountered are Co or Ni chelate compounds such as the divalent acetylacetonate (acac) or carboxylate salts, combined with AlR<sub>3</sub> cocatalysts. It is reasonable to suspect differences between this family of late transition metal Ziegler–type hydrogenation catalysts and the broader family of Ziegler–Natta catalysts based on early, high-valent transition metals [23,34], others having previously noted that the nature of these catalysts “probably is different

when nickel salts, for instance, are replaced by titanium complexes or when  $\text{AlEtCl}_2$  is substituted for  $\text{AlEt}_3$  [40]. Furthermore, we have largely excluded from discussion herein those systems which contain additives or ligands that coordinate through P or N atoms such as  $\text{PPh}_3$  or  $[(\text{CH}_3)_2\text{N}]_3\text{PO}$  [41,42,43,44,45]. Our focus herein is on what is understood, and especially on what remains unknown, about *Ziegler-type hydrogenation catalysts* based on a careful, critical examination of the existing literature.



**Scheme 1.** A Ziegler-type hydrogenation catalyst is formed by combination of a group 8–10 transition metal precatalyst and a trialkylaluminum cocatalyst in a hydrocarbon solvent. Ziegler-type hydrogenation catalysts are employed for the hydrogenation of olefins, aromatics, and polymers, for example the industrially important process of selective styrenic block copolymer (SBC) hydrogenation shown here. Ziegler–Natta or other *polymerization* catalysts are *not* a subject of this review.

### 1.3. Overview of the main sections of this review

Despite the history of the industrial application of Ziegler-type hydrogenation catalysts, opportunities remain for further improvements in hydrogenation rates, selectivity, stability, and applicability in hydrogenation of a wider range of materials [2,6,46]. Surprisingly little fundamental understanding of Ziegler-type hydrogenation catalysts exists [9,37]. Increased fundamental understanding of Ziegler-type

hydrogenation catalysts would allow for *rationally-directed* improvements [9,37,47,48]. Consequently, increased knowledge of Ziegler–type hydrogenation catalysts is highly desirable [9,37].

Published research papers seeking greater knowledge of Ziegler–type hydrogenation catalysts have generally investigated one or more of four basic issues: (i) the variables important to catalyst synthesis and their effect on catalyst properties, particularly the catalyst’s hydrogenation activity; (ii) the reaction between the transition metal precatalyst and cocatalyst components; (iii) the compositional and structural nature of the active catalyst species; and (iv) the postulated mechanism of catalytic hydrogenation. Our examination of the literature in this review is organized according to these four basic categories.

The first section of this review examines the *effects of variables* in the preparation of Ziegler–type hydrogenation catalysts, especially in terms of how they influence the resulting catalyst activity. The most important variables of catalyst preparation appear to be the: (i) identities of the transition metal precatalyst and the  $\text{AlR}_3$  cocatalyst; (ii) ratio of these two components and the role of impurities, particularly  $\text{H}_2\text{O}$ ; (iii) solvent; (iv) identity of the substrate; (v) details of component addition (such as order and rate, presence of substrate, atmosphere, and temperature); and (vi) aging of the prepared catalyst before use in hydrogenation reactions.

The second section of this review evaluates what is known about the reaction between the catalyst precursors, and whether the resulting catalysts are homogeneous (e.g., single metal organometallics) or heterogeneous (e.g., nanoclusters). Specific questions in this regard include: (i) how are the catalysts formed?; (ii) how many

transition metal atoms constitute the active catalyst species?; (iii) what are their oxidation states?; (iv) what is the form and role of the cocatalyst?; and (v) what is known about the mechanism of the catalytic hydrogenations? This second section which follows is divided into two parts; studies that support a homogeneous catalyst hypothesis are examined first, and those that support a heterogeneous catalyst hypothesis are examined second. Many authors supporting a heterogeneous catalyst hypothesis have claimed formation of nanoclusters, for which we herein coin the term “Ziegler nanoclusters” [13,49,50].<sup>3</sup>

The third section of this review is a discussion of the future outlook for additional fundamental studies of Ziegler–type hydrogenation catalysts. Possible reasons why the desired depth of understanding of Ziegler–type hydrogenation catalysts has remained elusive—despite several decades of research on the topic—are presented, along with thoughts about and what can potentially be done to improve this situation and provide the desired, additional knowledge.

## **2. Studies of Ziegler–type hydrogenation catalysts**

### *2.1. Effect of preparation variables on Ziegler–type hydrogenation catalysts*

Because of their rapid adoption by industry [5], research in Ziegler–type hydrogenation catalysts initially focused on optimization of the processes for which they were used [47,48]. This included the catalyst synthesis step, for which a wide variety of possible starting components, methods, and conditions exists. Many observations on how

---

<sup>3</sup> See the references listed for a definition of the distinction between modern nanoclusters and traditional colloids [13,49,50].

variables of catalyst synthesis affected the activity of the resulting hydrogenation catalysts were made early on. Table 1 contains a concise summary of the relevant literature, and gives an overview of the breadth of systems explored.

Catalyst preparation variables have not been exhaustively investigated despite their importance. The paucity of “systematic order” in the literature [51]<sup>4</sup> (i.e., which catalyst synthesis variables influence catalytic properties for which specific systems and why) is apparent in the many systems explored and the apparent contradictions among some of the findings (vide infra). This was noted recently by Shmidt and coworkers [19]: “contradictory published data on the interaction of catalytic system components do not allow us to interpret reliably the general concepts of the effect of the composition of the system on the properties of catalysts.” Therefore, gaining a better understanding of how variables in catalyst preparation affect the resulting catalytic properties is the first major goal of the field of Ziegler–type hydrogenation catalysts.

**Table 1. Catalyst Preparation Variables**

<b>Authors</b>	<b>Catalyst Systems</b>	<b>Results</b>	<b>Ref.</b>
Sloan, Matlack, and Breslow (1963)	Acac salts of Fe(III), Co(II and III), Ni(II), Ru(III), or Pd(II) (also Cr(III), Cu(II), Mn(II and III), Mo(VI), V(V), or Zr(IV)) + 1.2–	Most active: Co(III) > Fe(III) > Cr(III). Cu(II) salts fail to form effective hydrogenation catalysts. Use of AlClEt <sub>2</sub> , BEt <sub>3</sub> SnEt <sub>4</sub> , P(n-Bu) <sub>3</sub> , ZnEt <sub>2</sub> , or Mg(n-Bu)Br as cocatalysts results in either no reaction or an inactive ppt. at 30-50 °C and 3.7 atm H <sub>2</sub> . Ketones, aldehydes, nitriles, nitro compounds, azo compounds, and esters are <i>not</i> hydrogenated.	57

<sup>4</sup> We have found, paraphrasing what A.K. Galwey has written about a different area [51], that there is: little ability to carry out inductive prediction across ostensibly similar Ziegler–type hydrogenation catalyst systems, few established trends on which to expand, and therefore no coherent and generalized theory.

Authors	Catalyst Systems	Results	Ref.
	12.6 Al(i-Bu) <sub>3</sub> , AlH(i-Bu) <sub>2</sub> , or AlEt <sub>3</sub>		
Laporte and Schuett (1963)	Ni(2-ethylhexanoate) <sub>2</sub> + AlEt <sub>3</sub> , also Co, Fe, Cr, or Cu salts + AlEt <sub>3</sub> for arene hydrogenation	The highest catalytic activity and amount of gas evolution (> 95% ethane) is at Al/Ni = 3–4. The activity for benzene hydrogenation decreases according to Ni ≥ Co > Fe > Cr > Cu. Catalytic activity is highly dependent on the anion of the Ni(II) precursor; carboxylates, especially 2-ethylhexanoate is good, but halides are poor. Benzene hydrogenation is poisoned by PPh <sub>3</sub> .	39
Kroll (1969)	Fe(acac) <sub>3</sub> , Co(acac) <sub>2</sub> , or Ni(acac) <sub>2</sub> + Al(i-Bu) <sub>3</sub> or a <i>p</i> -dioxane adduct of Al(i-Bu) <sub>3</sub>	Relative catalytic activities are Co > Fe > Ni. The highest activities are achieved at Al/M = 6 for M(II), 8–10 for Fe(III). It is very difficult to properly adjust the Al/M ratio due to impurities such as oxygen and H <sub>2</sub> O always present, even after careful purification. The poisoning action of excess Al cocatalyst can be overcome by making a <i>p</i> -dioxane adduct of Al(i-Bu) <sub>3</sub> before catalyst synthesis. Improved kinetics are observed when the catalyst is allowed to age overnight.	75
Laporte (1969)	2-ethylhexanoate salts of Ni, Co, Fe, Cr + AlEt <sub>3</sub>	Activity order: Ni > Co > Fe > Cr. The anion of the Ni salt has a significant effect on the activity: 2-ethylhexanoate > benzoate > acac > acetate > chloride, mirroring solubility. Activities are equal for Ni(2-ethylhexanoate) <sub>2</sub> + AlEt <sub>3</sub> , Al(i-Bu) <sub>3</sub> , or Al(C <sub>6</sub> H <sub>13</sub> ) <sub>3</sub> catalysts. The highest catalytic activity is observed when Al/M=3–4 for M(II). The olefin affects the hydrogenation rate: monosubstituted > unsymmetrically disubstituted > cyclic > symmetrically disubstituted. Nitrobenzene and PPh <sub>3</sub> act as catalyst poisons.	58
Shmidt et al. (1970)	Co(C <sub>17</sub> H <sub>35</sub> CO <sub>2</sub> ) <sub>2</sub> , Fe(C <sub>5</sub> H <sub>7</sub> O <sub>2</sub> ) <sub>2</sub> , Ni(C <sub>5</sub> H <sub>7</sub> O <sub>2</sub> ) <sub>2</sub> , Ni(C <sub>6</sub> H <sub>6</sub> NO) <sub>2</sub> , Ni(C <sub>7</sub> H <sub>6</sub> NO <sub>2</sub> ) <sub>2</sub> , Ni(C <sub>9</sub> H <sub>6</sub> NO) <sub>2</sub> ,	Activity as influenced by precatalyst anion: acac > o-aminophenoxide > salicylaloximate > 8-quinolinoxide > dimethylglyoximate, the same as the decreasing order of the ligand dissociation equilibrium constant of the precatalyst. Catalytic activity is improved if the AlEt <sub>3</sub> is “added to the precatalyst in the absence of the acetylenic	42

Authors	Catalyst Systems	Results	Ref.
	Ni(C <sub>4</sub> H <sub>7</sub> N <sub>2</sub> O <sub>2</sub> ) <sub>2</sub> , or Ni(NO <sub>3</sub> ) <sub>2</sub> [P(C <sub>6</sub> H <sub>5</sub> ) <sub>3</sub> ] <sub>2</sub> (also Ti(C <sub>5</sub> H <sub>5</sub> ) <sub>2</sub> Cl <sub>2</sub> or Ti(OCH(CH <sub>3</sub> ) <sub>2</sub> ) <sub>4</sub> ) + AlEt <sub>3</sub>	hydrocarbon, and if the catalyst solution absorbs hydrogen beforehand.” Various ligands are added to the prepared catalyst solutions.	
Falk (1971)	Co(2- ethylhexanoate) <sub>2</sub> or Ni(2- ethylhexanoate) <sub>2</sub> + AlEt <sub>3</sub> or (n-Bu)Li, cyclopentyllithium, phenyllithium, ethylolithium, or (sec- Bu)Li	Catalyst prepared by slowly adding (over 90 min) the Co or Ni solution to a solution of AlEt <sub>3</sub> in a N <sub>2</sub> atmosphere. Slight impurities affect activity and change the Al or Li(alkyl)/M ratios optimal for selectivity. Li alkyls are generally inferior to AlEt <sub>3</sub> as cocatalyst. Catalyst solutions do not deteriorate after being stored for several months.	79
Esselin et al. (1986)	Ni(acac) <sub>2</sub> , Fe(acac) <sub>3</sub> , Ni(octooate) <sub>2</sub> , or Co(octooate) <sub>2</sub> + 1, 3, or, 6 AlEt <sub>3</sub> or GaEt <sub>3</sub>	Catalytic activity trends: Ni > Fe, and AlEt <sub>3</sub> > GaEt <sub>3</sub> . Optimal activity occurs at Al/M = 3 for Ni catalysts and at Al/M = 6 for Fe catalysts. Catalyst preparation is done at room temperature. Ni(acac) <sub>2</sub> •2H <sub>2</sub> O dried to ≥ 80% to give, on average, (Ni(acac) <sub>2</sub> ) <sub>3</sub> .	40
Reguli and Staško (1987)	Ni(3,5- diisopropylsalicylate) 2, Ni(acac) <sub>2</sub> , Ni(stearate) <sub>2</sub> , or Ni(benzohydroxamat e) <sub>2</sub> + 1, 2, 3, 4, 5, or 6 AlEt <sub>3</sub> , Al( <i>i</i> -Bu) <sub>3</sub> or LiBu.	Catalytic activity by precatalyst anion: diisopropylsalicylate > acac > stearate > benzohydroxamate, which correlates well with the solubility sequence of corresponding Ni salts (activity is also dependent on the solvent). The Al/M ratio strongly influences activity, the optimum is 1.5–4 depending on the catalyst precursors. Traces of O-containing compounds, especially those with acidic H, poison the catalysis, but could be partially offset by additional cocatalyst. Ni precipitates in the presence of aromatic solvents resulting in loss of catalytic activity. Order of addition: solvent, precatalyst, and then cocatalyst. Catalyst was prepared both in the presence and absence of cyclohexene substrate; the presence of cyclohexene increases the resulting catalytic activity when AlEt <sub>3</sub> or LiBu are the cocatalysts used, but the opposite effect is observed with Al( <i>i</i> -Bu) <sub>3</sub> . Temperatures from 20–45 °C during the catalyst	70

Authors	Catalyst Systems	Results	Ref.
		preparation reaction have no effect on optimal Al/M. The time of catalyst aging before use in hydrogenation, and Ar versus H <sub>2</sub> preparation atmosphere have no influence on activity.	
Alvanipour and Kispert (1988)	Co(stearate) <sub>2</sub> + 2 AlEt <sub>3</sub>	Naphthalene, quinoline, isoquinoline, 6-methylquinoline and 2-methylquinoline can be hydrogenated with the catalyst employed, but dibenzothiophene nitroquinolines and 4-chloro-2-methylquinoline cannot. Compounds containing sulfur, nitro, and chlorine groups act as poisons.	67
Barrault et al. (1994)	Co(acac) <sub>2</sub> + 0.5, 1.0, or 1.5 AlEt <sub>3</sub>	Higher Al/Co ratios give increased activity and lower selectivity. The catalyst is ~3 times more active for the hydrogenation of cinnamaldehyde than for 2-pentyl-2-nonenal. For 2-pentyl-2-nonenal, the catalyst is more active, but less selective at a given conversion when pre-treated with CO <sub>2</sub> /H <sub>2</sub> (syngas) than with just H <sub>2</sub> . "The final catalytic properties... depend on the activation process."	37
James et al. (1998)	Ni(OAc) <sub>2</sub> + 0.5 Zn(OAc) <sub>2</sub> + 4.5 AlEt <sub>3</sub>	Hydrogenation of 2-methoxy-4-propylphenol with the catalyst at 90 °C under 50 atm H <sub>2</sub> for 24 h gives a 65.2% conversion with 92.2% of the product being 2-methoxy-4-propylcyclohexanol. The catalyst is poisoned by Hg(0).	84
Šabata and Hetflejš (2002)	Ni(2-ethylhexanoate) <sub>2</sub> or Ni(acac) <sub>2</sub> + "Li-diene," <i>n</i> -BuLi, or AlEt <sub>3</sub>	Catalytic activity trends: Ni(2-ethylhexanoate) <sub>2</sub> > Ni(acac) <sub>2</sub> , and "Li-diene" > BuLi, or AlEt <sub>3</sub> . Catalytic activity depends on Li or Al/M ratio, temperature, and particular method used in catalyst formation, the optimal being: Li/Ni is 8–10, cocatalyst added rapidly to the Ni compound at 50 °C, and kept at that temperature for 10 min before allowing to cool. Batches of catalyst prepared fresh daily to avoid changes in activity due to aging.	69
Nindakova et al. (2006)	Co(acac) <sub>2</sub> • <i>n</i> H <sub>2</sub> O, <i>n</i> =0, 0.5, or 1.5; or Co(acac) <sub>3</sub> + 2, 4, 6, 8, 12, or 16 AlEt <sub>3</sub>	AlEt <sub>3</sub> added to the Co salt dropwise under an atmosphere of H <sub>2</sub> before the introduction of substrate. Using Co(acac) <sub>2</sub> • <i>n</i> H <sub>2</sub> O, the optimum Al/Co ratio depends on <i>n</i> : <i>n</i> = 0, Al/Co = 3.5–4; <i>n</i> = 0.5, Al/Co = 8–10. The <i>n</i> = 0.5 catalyst has a higher hydrogenation activity than the <i>n</i> = 0 catalyst. As [Co] decreases the optimal Al/Co ratio	19

Authors	Catalyst Systems	Results	Ref.
		increases. Higher activities are achieved in heptane solvent than in toluene.	
Belykh et al. (2006)	Pd(acac) <sub>2</sub> + 2, 4, 6, 8, 10, 15, or 16 AlEt <sub>3</sub>	AlEt <sub>3</sub> is added dropwise under flowing H <sub>2</sub> to Pd(acac) <sub>2</sub> in the absence of substrate; the optimal Al/Pd is 4. When H <sub>2</sub> O or O <sub>2</sub> traces are present, no decrease in activity at high Al/Pd is observed up to Al/Pd = 80. Use of modifiers, such as PPh <sub>3</sub> , OPPh <sub>3</sub> , ethanol, the order of component addition, the substrate used, and catalyst loading affect the catalyst activity. The effect of modifiers is dependent on Al/Pd.	81, 114
Finke and coworkers (2009)	[(1,5-COD)Ir(μ-O <sub>2</sub> C <sub>8</sub> H <sub>15</sub> ) <sub>2</sub> , Co(neodecanoate) <sub>2</sub> , or Ni(2-ethylhexanoate) <sub>2</sub> + AlEt <sub>3</sub>	At room temperature, and under an N <sub>2</sub> atmosphere, AlEt <sub>3</sub> in cyclohexane is added to a cyclohexane solution of the transition metal precatalyst with 1000 rpm stirring in the absence of olefinic substrate. However, <i>simultaneous</i> addition of Co(neodecanoate) <sub>2</sub> and AlEt <sub>3</sub> , Al/Co = 2, results in higher hydrogenation activity. Alternatively, the hydrogenation activity of the catalyst is independent of the order of addition for Al/Co = 3. The optimal Al/Ir is 1, Al/Ni is 2, and Al/Co is from 2 to 4. AlEt <sub>3</sub> was added rapidly to the Ir precatalyst and at rate of 1 drop every 5 sec for the Ni precatalyst. Rigorous drying of glassware and solvents was performed throughout these studies; however, for the Co system intentionally added H <sub>2</sub> O decreases hydrogenation activity. The following catalyst preparation variables have, at most, minor effects on hydrogenation activity of the Co system: (i) AlEt <sub>3</sub> vs. Al(t-Bu) <sub>3</sub> cocatalyst; (ii) temperature during mixing of catalyst components (e.g., 30 °C vs. 60 °C); (iii) individual vs. batch preparation; and (iv) use of neat AlEt <sub>3</sub> added at a slower rate.	52, 53, 54, 55, 56

### 2.1.1. Identities of the precursors

The first obvious variable in the synthesis of Ziegler–type hydrogenation catalysts is the identity of the specific transition metal precatalyst and AlR<sub>3</sub> cocatalyst employed.

As expected, industry favors use of the inexpensive first row metals (Fe, Co, and Ni) rather than the more expensive second and third row metals in the same groups (i.e. Ru and Os, Rh and Ir, Pd and Pt) [2,6,22]. Early studies surveyed potential catalyst precursors to ascertain which were promising as useful catalysts resulting in similar sequences for the most active metals, Ni > Co > Fe > Cr > Cu [57,58]. Also, the catalytic activities of *soluble* Ni and Co Ziegler–type hydrogenation catalysts were found to be generally superior to pre-activated, *supported* Ni or Raney Co catalysts [58]. There is a lack of agreement about whether Ni or Co systems are the most active for polymer hydrogenation, a discrepancy caused at least in part by a lack of standardization in polymer feed quality [46], differences in properties of precursor solutions such as water content or level of acidity (which, of course, readily react with the  $AlR_3$  component, thereby indirectly influencing catalytic activity) [40], or both. Whether the Ni and Co catalysts favored by industry have the absolute best activity, selectivity, and lifetime is arguable; however, the fact that they are industrially favored signifies that they likely have an advantageous balance of low cost, ease of synthesis, and desirable catalytic properties.

Another aspect of the precursor identity is the anion in the transition metal salt. The literature has included claims of the use of alkoxides [59,60,61,62,63] or halides [43,44,45,64,]. However, a catalyst poisoning effect of halides has also been reported [65,66,67]. A few patents have claimed the usefulness of sulfur-containing anions such as sulfonate, salts of sulfur-containing acids [60,68],  $M(SO_x)_n$  (and partial esters thereof), and metal salts of sulfonic acids  $M(RSO_3)_n$  [62]; however, those patents do not report the control of comparing the activity of catalysts containing S-element anions to

the activities of those made from the more common, generally favored anions acac and carboxylate. Precatalyst compounds with inexpensive 2-ethylhexanoate ligands, as well as the catalysts made from them, tend to be soluble in the hydrocarbon solvents typically used. In one study, the anion in Ni salt precatalysts had a significant effect on the resulting catalytic activity in a sequence that corresponded to the solubility of the precatalysts: 2-ethylhexanoate > benzoate > acac > acetate > chloride [58]. Similar findings correlating precursor solubility and catalytic activity have been made by others [69,70]. However, whether the increased catalytic activity is the influence of solubility, a result of the formation of different amounts of catalyst, or due to catalyst species with different activities, is not clear.

The choice of alkyls in the  $\text{AlR}_3$  cocatalyst has also been of much interest. In a 1968 patent, Kroll [64] stated that it was generally agreed, even as of 1968, that the choice of cocatalyst does affect the catalyst activity. Many studies appear to favor  $\text{AlR}_3$  with relatively short alkyl chains such as  $\text{AlMe}_3$  [71],  $\text{AlEt}_3$  [46,63,44,72,73,74], or  $\text{Al}(i\text{-Bu})_3$  [57,70,75], but use of triarylaluminum [72,76,77] has also been reported. Lapporte [58] found with  $\text{Ni}(\text{2-ethylhexanoate})_2$  that  $\text{AlEt}_3$ ,  $\text{Al}(i\text{-Bu})_3$ , and  $\text{Al}(\text{C}_6\text{H}_{13})_3$  were equivalent in the resulting catalytic activity of hydrogenation of a variety of substrates and at a variety of conditions. Some patents have described the preferred cocatalyst as  $\text{R}_{3-n}\text{AlH}_n$  where  $n = 0-2$  [59,45,65,66]. In general, the preferred cocatalyst appears to vary with the particular system; therefore, the need remains for studies elucidating the roles of the cocatalyst in both the catalyst formation and substrate hydrogenation processes.

2.1.2. *Molar ratio of the precursor components (precatalyst and cocatalyst) and the role of impurities, particularly H<sub>2</sub>O*

Several reports claim that the Al/M ratio (M = the transition metal of the precatalyst) was a key factor affecting the resulting catalyst [70,69,63]. It has been noted that when too little cocatalyst was used, it failed to adequately “activate” the catalyst, resulting in decreased activity [40]. On the other hand, it was also reported that when *too much* AlR<sub>3</sub> cocatalyst was used, it acted as a catalyst poison [75]. Most reports agree that there is an optimum Al/M. In general, the optimum Al/M seems to be highly dependent on the specific system used [57,78], and ranges from 1.5–4 are typical, at least with a Ni precatalyst [39,70].

The most important difficulty regarding optimization of Al/M appears to have been the presence of contaminants, especially those containing oxygen atoms, acidic protons, or both [75,79]. The most ubiquitous of these is almost surely H<sub>2</sub>O. Despite the occasional claim that oxygen-containing species such as water were *not* important considerations in catalyst preparation [59,77], for most systems, water and other such species are generally thought to have a significant influence. This is as expected for a system employing a water-sensitive, AlR<sub>3</sub> cocatalyst [80].

The activity of Ziegler–type hydrogenation catalyst systems are often reduced by oxygen-containing contaminants, with water being the prime example [40,63,70,72]. Reguli and Staško [70] found that this poisoning effect could be offset by the addition of more cocatalyst, the additional AlR<sub>3</sub> ostensibly acting to scavenge contaminants. Esselin and coworkers opted to use acac salts instead of M(“octoate”)<sub>2</sub> (M is Ni or Co) because solubilization of the “octoate” compounds required a variable amount of free acid in the

precatalyst solution (the term “octoate” is industry jargon for a C<sub>8</sub> carboxylate, frequently 2-ethylhexanoate) [40]. Additional potential contaminants are residual polymerization catalyst and excess alcohol from termination of the polymerization reaction [65,73]. Overall, these studies report the effects of O-containing contaminants as detrimental to the activity of the Ziegler-type hydrogenation catalyst systems used.

However, in other Ziegler-type systems the reaction of oxygen-containing species with the cocatalyst has been exploited to *improve* the catalytic system. This has been done in two ways: (i) by simply stopping the poisoning effect of excess cocatalyst [64,75,77,81], or (ii) by actually increasing the activity of the resulting catalyst [19,61,78]. In US Patent 3,937,759, Baumgartner and Balas claim that addition of one mole of AlEt<sub>3</sub> per mole of Ni to an *active* hydrogenation reaction will halt the reaction. This effect was found to be reversible by addition of a sufficient amount of alcohol to react away the AlEt<sub>3</sub> that had been added to stop the reaction [82]. In such cases where water is used, one might expect a reaction between H<sub>2</sub>O and the AlR<sub>3</sub> compound to form Al–O–Al bonded compounds known as alumoxanes [20,34,80]. Hoxmeier et al. [62], claimed that a catalyst prepared with alumoxanes was useful for hydrogenation reactions. However, the complicated effects of the interaction of the catalyst components with H<sub>2</sub>O on the resulting catalyst properties is an important, yet still incompletely understood, aspect of Ziegler-type hydrogenation catalysts, effects that depend on the AlR<sub>3</sub>/M ratio of the catalyst, as well as the amount of H<sub>2</sub>O (or ROH, etc.). The effects of H<sub>2</sub>O, ROH, and other such compounds on Ziegler-type hydrogenation catalysts is another area that begs for a more detailed and fundamental understanding, one using carefully controlled conditions beginning from a definitively characterized precatalyst.

### 2.1.3. *Solvent*

Studies of Ziegler–type hydrogenation catalysts have tended to use inert hydrocarbons, mostly alkanes such as cyclohexane [70] or heptane [57], but also aromatic solvents like benzene, toluene, or xylenes [70]. Inert hydrocarbons are commonly used because they lack lone-pair electrons that would be reactive with the Lewis acidic  $\text{AlR}_3$  cocatalyst [58,70,72]. The relative merits of such solvents have elicited only a little discussion in the literature. Catalytic activity is very dependent on solvent in the study by Reguli and Staško [70]; their  $\text{NiL}_2$  plus  $\text{AlR}_3$  or  $\text{LiBu}$  catalysts became less active in the order: cyclohexane  $\gg$  xylene  $>$  toluene  $>$  benzene  $>$  chlorobenzene. The aromatic solvents resulted in an inactive Ni precipitate being formed [70]. Shmidt and coworkers [19] reported that with their  $\text{Co}(\text{acac})_3$  plus 50  $\text{AlEt}_3$  catalyst, activity for the hydrogenation of 1-hexene was 17-fold higher in heptane instead of toluene. However, Sloan et al. [57] reported the hydrogenation of a wide variety of substrates with a wide range of catalysts in solutions of heptane or toluene, and made no mention of differences in hydrogenation rates or formation of precipitates based on which solvent was used. It is still unclear exactly how and why such prominent differences are seen with different solvents in some instances, but not others. In short, a further examination of solvents under carefully controlled conditions is another aspect of Ziegler–type hydrogenation catalysts that merits additional attention.

### 2.1.4. *Identity of the hydrogenation substrate*

Numerous substrates have been tested with Ziegler–type hydrogenation catalysts, from simple olefins to various polymers, even those with polar, acidic, or oxygen-containing functionalities [58,61,69,76]. However, not all hydrogenation attempts with a variety of substrates have been successful [57,67]. In a 1988 paper, Alvanipour and Kispert hydrogenated naphthalene and some quinolines using a  $\text{Co}(\text{stearate})_2$  plus  $\text{AlEt}_3$  catalyst [67]. However, attempts to hydrogenate 4-chloro-2-methylquinoline, nitroquinolines, or dibenzothiophene failed [67]. They believed that substrates containing chloro, nitro, and sulfur groups acted as catalyst poisons by coordinating to the catalyst [67].

In general, and as one might expect, the rate of hydrogenation was found to have some dependence on the identity of the substrate [37]. Several reports revealed a decreasing hydrogenation rate with increasing substitution about the olefinic bond while using a variety of catalysts including  $\text{Ni}(\text{2-ethylhexanoate})_2$  plus  $\text{AlEt}_3$  [58],  $\text{Ni}(\text{3,5-diisopropylsalicylate})_2$  plus  $\text{Al}(i\text{-Bu})_3$  [70], and a non-Ziegler–type, but related  $\text{Cr}(\text{acac})_3$  plus  $\text{Al}(i\text{-Bu})_3$  catalyst [57]. The known exception to this trend was reported by Sloan et al., namely that the diallyl olefin cyclohexene is among the most rapidly hydrogenated olefins [57]. Overall, the catalyst activity is dependent on the identity of the substrate as one might expect. However, the details of the effects seen require further scrutiny and explanation, for example, what rate laws are seen for the different classes of olefins?

#### *2.1.5. Other aspects of catalyst synthesis*

The catalyst component addition order, rate of component addition, and whether or not the substrate should be present during catalyst synthesis have been points of

concern in the literature. There is wide disagreement on these issues between researchers, and among different systems, as to the effects, if any, of the above-noted variables on catalysis [45,64]. Various reports have stated preferences for: (i) slow addition of the precatalyst solution to the cocatalyst solution [79]; (ii) addition in the opposite order, but still slowly [77]; or (iii) keeping Al/M molar ratios essentially constant during the reaction, either by simultaneous addition or by rapid addition of a solution of the cocatalyst to a solution of the transition metal precatalyst [63]. Likewise, different reports have expressed, oppositely, the benefits of preparing the catalyst in the presence of substrate [68], or in the absence of substrate [62]. In 1987 Reguli and Staško [70] observed that the presence of cyclohexene during the catalyst synthesis reaction increased the hydrogenation activity of the resulting catalyst when AlEt<sub>3</sub> or LiBu were used as cocatalysts, but that the presence of cyclohexene inexplicably had the *opposite* effect when Al(*i*-Bu)<sub>3</sub> was employed as the cocatalyst.

Another detail occasionally discussed is the gas present (i.e., N<sub>2</sub>, Ar, or H<sub>2</sub>) during catalyst synthesis. Shmidt and coworkers [42] obtained a higher activity if “the catalyst solution absorbs hydrogen beforehand.” However, Reguli and Staško [70] found that conducting their Ni(3,5-diisopropylsalicylate)<sub>2</sub> plus Al(*i*-Bu)<sub>3</sub> catalyst preparation in an atmosphere of either Ar or H<sub>2</sub> ultimately had no influence on the resulting catalyst activity. The question, then, is whether there is something special about using H<sub>2</sub> as opposed to the inert gasses N<sub>2</sub> or Ar (i.e., whether the key is just to provide an O<sub>2</sub> and H<sub>2</sub>O-free atmosphere, or is H<sub>2</sub> acting as a reductant during the catalyst preparation). A subtlety here may be whether one is carrying out reactions in solution under H<sub>2</sub> gas with the first row group 8–10 metals versus those with second or third row transition metals,

since only the latter are reduced to metal zero compounds under an atmosphere of hydrogen and standard conditions [83].<sup>5</sup> Overall, it appears that the primary purpose of the atmosphere employed is to ensure conditions free of O<sub>2</sub> and oxygen-containing impurities such as H<sub>2</sub>O. That said, reduction/activation of the catalyst when H<sub>2</sub> is used has not been adequately tested via careful control experiments with and without H<sub>2</sub> in Ziegler–type hydrogenation catalyst systems.

The temperature of catalyst preparation is another variable occasionally mentioned in the literature [41], with different temperatures often being employed for different systems. For example, temperatures reported for optimal catalyst preparation range from 50 °C (followed by holding the solution at that temperature for 10 min before being allowed to cool [69]), to heating the catalyst after the synthesis reaction at 90 °C under 1 atm of N<sub>2</sub> for 2 hours [84]. In general, and despite various claims of reaction temperatures that lead to an optimal catalyst, activity as a function of reaction temperature has also not been systematically studied.

The effects that temperature and other variables in catalyst preparation (order and rate of precursor addition, presence of substrate, and atmosphere) have on the activity of the resulting catalysts appear to depend on the individual system used. It is clear that they have not been adequately studied, or even reported in some cases. Additionally,

---

<sup>5</sup> Standard reduction potentials (E°, 25 °C, 1 atm) vs. SHE in volts for M<sup>n+</sup> + ne<sup>-</sup> ⇌ M, where M is: Fe<sup>3+</sup>/Fe = -0.037, Fe<sup>2+</sup>/Fe = -0.447, Co<sup>2+</sup>/Co = -0.28, Ni<sup>2+</sup>/Ni = -0.257, Ru<sup>2+</sup>/Ru = 0.455, Rh<sup>2+</sup>/Rh = 0.600, Pd<sup>2+</sup>/Pd = 0.951, Ir<sup>3+</sup>/Ir = 1.156, Pt<sup>2+</sup>/Pt = 1.18, and 2H<sup>+</sup>/H<sub>2</sub> = 0.000. The most commonly used precatalysts of first row group 8–10 transition metals Fe, Co, and Ni therefore have unfavorable potentials for reduction by H<sub>2</sub> gas under standard conditions, unlike second and third row transition metals [83]. Hence, if a second or third row transition metal precatalyst was used, pretreatment by even 1 atm of H<sub>2</sub> at standard conditions could influence the catalyst formation reaction, at least from a thermodynamic perspective.

*how* these and other variables influence catalyst activity will not be fully understood without studying how these variables are affecting first (i) the products of the catalyst synthesis reaction (i.e., the composition and structure of the resulting catalyst), and second (ii) the kinetics and mechanism of the catalysis.

#### 2.1.6. *Aging of prepared catalyst*

Another factor that has garnered mention in the literature as potentially significant for the activity of Ziegler–type catalysts is the aging of prepared catalyst solutions. The issues of whether or not prepared catalyst solutions have a significant “shelf-life” before deactivation or precipitation is related to this topic. It has been noted for some systems that in the catalyst solution, a precipitate often formed if it was stored at a high temperature for long periods of time [68]. Šabata and Hetflejš [69] took the precaution of making fresh batches of catalyst daily to avoid changes in activity due to aging. In contrast, others have allowed the prepared catalyst to age overnight [67,75], claiming that it improved reproducibility of the kinetic experiments [75]. Reguli and Staško reported that the time of catalyst aging before use in hydrogenation had no influence on activity [70]. However, the actual experimental results, including what aging times were examined, were not reported [70]. Conclusions regarding the effects of catalyst aging cannot be drawn from this assortment of results for Ziegler–type hydrogenation catalysts as a group; the outcome is dependent on the individual system, requiring independent optimization of each set of conditions. Without a more detailed understanding of the fundamental chemistry involved, the contradictory results prevent the ability to develop a consistent picture of the phenomenology of Ziegler–type hydrogenation catalyst aging.

### 2.1.7. *Conclusions for the section on catalyst preparation variables*

The above survey of variables makes apparent that there are many important details involved in preparation of Ziegler–type hydrogenation catalysts, specifically: the identities of the transition metal precatalyst and the  $\text{AlR}_3$  cocatalyst; the ratio of these two components and the role of impurities, particularly  $\text{H}_2\text{O}$ ; the solvent; the identity of the substrate; the details of component addition such as order and rate, presence of substrate, atmosphere, and temperature; and any aging of the prepared catalyst before use in hydrogenation reactions. Furthermore, the question of *how* these variables have the effects they do is an open one. The ability to explain the effects of these variables in catalyst preparation is hampered by the fact that the effects themselves are often dissimilar for ostensibly similar, but ultimately somehow different, systems. Therefore, it is desired to perform studies of the catalysts under conditions that are either optimized, industrially relevant, or both if needed. Since these catalysts are used industrially, and since faster, longer lifetime, and more selective catalysts are always of interest, there is an incentive for additional studies, along with a host of the necessary control experiments—for example, comparing the best or other’s catalysts to one’s own catalyst, all under identical conditions.

When one considers the obstacles to understanding the effects of all possible variables in Ziegler–type catalyst preparation, it becomes easier to understand why this class of industrial catalysts has not been exhaustively investigated, and why contradictory data exist. Isolation of any single variable for study is difficult because of how many variables there are (*at least* 11), the possibility that additional, still-unidentified variables

exist, and the indication [58,70] that many variables may be correlated with one another. A modern systematic and/or combinatorial study holds the potential of identifying superior industrial catalysts, for example.

Furthermore, accurate evaluation of catalyst activity, the indicator most often used for the effect on the catalyst, may be hindered by an H<sub>2</sub> gas-to-solution mass-transfer limitation (MTL) [85,86,87,88].<sup>6</sup> The presence of an H<sub>2</sub> gas-to-solution MTL in hydrogenations using Ziegler-type catalysts is especially likely because of their high catalytic activities—indeed, we have routinely run into such MTL issues in our own studies [55,56]. Additionally, when polymers are the substrate, adequate mixing is difficult to achieve in the viscous polymer solutions thereby increasing the chances that kinetics will be dominated by MTL. Despite this, *few studies discussed herein mentioned efforts to avoid MTL kinetics* [41,57,69,75]. It is possible that many of the kinetic results reported for Ziegler-type hydrogenation catalysts are questionable because their studies have fallen victim to MTL effects. Unless specifically ruled out, undetected MTL should be suspected for instances where there is disagreement about whether or not a given variable had any effect on the catalyst properties of a given system. For these reasons, all research, both the patent literature assembled in Appendix A, Table A1, and other

---

<sup>6</sup> See the references listed [85,86,87,88] for a more in-depth discussion of MTL effects and its consequences. MTL should be a concern for one attempting to measure the kinetics of any solution phase reaction where one of the reactants (H<sub>2</sub> in this case) is supplied as a gas. If the hydrogenation reaction of interest is fast relative to the mass transfer of H<sub>2</sub> gas into solution, then the overall reaction kinetics will be dominated by the slower mass-transfer step. In certain cases where there may be competing reactions, such as isomerization or olefin oligomerization [58] with Ziegler-type hydrogenation catalysts, the presence of significant MTL effects can also alter product ratios.

published studies shown in Table 1, should, in our opinion, be viewed with a critical eye and with possible MTL effects in mind.

Importantly, the effects that synthesis variables have on the catalytic properties of Ziegler-type hydrogenation catalysts (e.g., activity), are likely to be closely related to the effects of those variables on the *homogeneous or heterogeneous nature of the catalysts*. When catalyst formation of a non-Ziegler-type hydrogenation catalyst is carried out in-situ, “the lesson is that the nature of the true catalyst can change with the reaction conditions” [16]; this may be just as true for Ziegler-type hydrogenation catalysts pre-formed by the addition of  $AlR_3$ . Therefore, a way to look for answers as to *how* catalyst synthesis variables affect catalytic activity would be to study the composition and structure (i.e., the homogeneous or heterogeneous nature) of the resulting catalysts. Connecting these aspects of Ziegler-type hydrogenation catalysts—namely synthesis variables, catalytic properties, and homogeneous or heterogeneous nature—remains a, if not *the*, significant challenge for the field.

## 2.2. *The nature and mechanism of formation of Ziegler-type hydrogenation catalysts*

Because of the desire to make rationally-directed improvements to Ziegler-type hydrogenation catalysts, important topics include: the reaction between the precatalyst and the cocatalyst; the true nature of the active catalyst; and the identity of the cocatalyst species in the resulting catalyst solution. Specifically of interest are the homogeneous or heterogeneous nature of the true catalyst(s), the oxidation state of the transition metal, and the resultant form and role of the initially added, for example  $AlR_3$ , cocatalyst species. A detailed mechanism of the reaction between catalyst precursor components is

also desired, one that includes the compositions and structures of all intermediate species and the kinetics of constituent elementary steps [89]. However, this level of detail is still unrealized with Ziegler–type hydrogenation catalysts.

As noted above, a main question about Ziegler–type hydrogenation catalysts is whether they are homogeneous (e.g., single metal organometallics) or heterogeneous (e.g., nanoclusters). The patent literature (Appendix A, Table A1) has given only cursory attention to the topic; uncertainty and disagreement exist [60,77,78]. This is understandable since determining the true nature of a catalyst is a classic, non-trivial problem [16,90]. A generalized methodology for addressing this problem does exist [12,13,15,16,17,18], and has been successful at distinguishing between heterogeneous and homogeneous catalysts; it has identified catalysts of both types, even in a system where slight differences in conditions were a deciding factor [17]. One of the main ideas behind this approach is (i) to first address the question of what species are present that could be catalysts—that is, what are the main, resting forms of the (pre)catalyst, and then (ii) to *determine which species contribute to catalysis primarily via kinetic and quantitative poisoning experiments* [12,13,15,16,17,18]. In studying Ziegler–type hydrogenation catalyst systems, nearly all workers have struggled to answer the difficult question of what species are present (i.e., what are the products and the catalyst formation reaction stoichiometry?). The needed kinetic and poisoning experiments are only rarely present [57,58]; without definitive kinetic evidence, species identified in the following papers may or may not be related to the actual catalyst(s) [91].<sup>7</sup> In many cases they

---

<sup>7</sup> This point is based on two basic principles in catalysis. The first is that the majority, or even all, of the observed catalysis could be due to a minority, but highly active species [10]. The second is Bergman’s formulation, somewhat tongue-in-cheek, of “Halpern’s Rules” for catalysis, which state, “if you can isolate

might be “catalyst reservoir” species that actually are not in the catalytic cycle and therefore, may even detract from the overall rate. The classic example of this is the “catalyst reservoir” of five observable species identified in Halpern’s studies of Wilkinson’s hydrogenation (pre)catalyst; only the spectroscopically invisible, 16-electron  $\text{RhClL}_2(\text{solvent})$  and subsequent species contribute to the observed hydrogenation catalysis [10].

2.2.1. *The “Ziegler–type catalysts are homogeneous” hypothesis.*

2.2.1.1. *Systems investigated by Wilke and coworkers [4]:  $\text{Ni}(\text{acac})_2$  plus  $\text{AlMe}_3$ ,  $\text{AlEt}_3$ , or  $\text{Al}(i\text{-Bu})_3$ .* When Karl Ziegler and coworkers first discovered the “Ni effect” in 1953, it was assumed that the Ni in the complexes took the form of a metal colloid which, in attempted ethylene *polymerizations*, was responsible for chain cleavage after each insertion step [1,2,3,4,5]. Wilke and coworkers [4] have written that this assumption was based, at least in part, on the lack of knowledge at the time about metal  $\pi$ -complexes. Consequently, the work of Wilke and coworkers [4,92,93,94,95,96] was carried out with the different hypothesis that the Ni species responsible may be  $\pi$ -complexes, and *not* colloidal Ni. Wilke and coworkers [4] analyzed catalyst formation in two stages: (i) the reduction of the precatalyst by  $\text{AlR}_3$ , and (ii) the subsequent reactions between the zero-valent transition metal,  $\text{AlR}_3$ , and olefin.

The reduction of  $\text{Ni}(\text{acac})_2$  by  $\text{AlMe}_3$ , which resulted in the formation of  $\text{Ni}(0)$ ,  $\text{AlMe}_2(\text{acac})$ , and methane and ethane gases, was thought to proceed by “homolysis of

---

it, it is probably not the catalyst; if it is metastable and you can detect it, it *could* be the catalyst; and if it is highly unstable and undetectable, then it probably *is* the catalyst!” [91].



The second stage of catalyst formation consisted of the subsequent reactions of Ni(0) with  $\text{AlR}_3$  and olefin. By analogy to reactions investigated in a variety of model systems, Wilke and coworkers suggested the formation of Ni-olefin  $\pi$ -complexes similar to  $\text{Ni(0)(ethylene)}_3$  [4,97]. This and other complexes, such as allyl-Ni species, similar to the Ni-olefin  $\pi$ -complexes, have been referred to as “bare” Ni atoms [93]. The  $\pi$ -complexes were thought to interact with  $\text{AlR}_3$  via multicenter bonds comprised of Ni(0) plus Al and a bridging C atom. In Figure 1, from the work of Wilke and coworkers [4], one can see how the close proximity of the  $\text{AlR}_3$   $\beta$ -H atom to the olefinic double bond could permit an electrocyclic reorganization to give the proposed active catalyst species. A prominent feature of Wilke’s proposed catalyst is the absence of Ni-H. Ni-olefin  $\pi$ -complexes were proposed as the active catalyst species in alkyl-olefin exchange reactions between Grignard reagents ( $\text{RMgBr}$ ) and olefins by Marko and coworkers [98,99], in which H migration within the organonickel complex was suggested *without* formation of a definite Ni-H bond. However, others have studied similar Ni plus  $\text{AlR}_3$  systems and their results do implicate Ni-H species as responsible for catalysis in olefin dimerization or oligomerization reactions [41,100]. It is important to emphasize that Wilke and coworkers were *not* investigating catalysts for hydrogenation reactions [4]. Hence, their postulation of an alkyl-olefin exchange reaction without formation of Ni-H would seem to have little bearing on a mechanism of *hydrogenation* with similar systems.

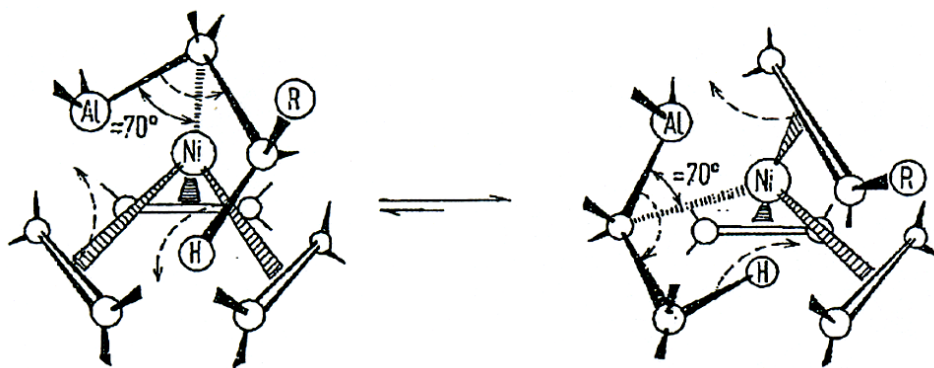


**Figure 1.** Ni(0)–olefin  $\pi$ -complexes proposed by Wilke and coworkers [4]. Interaction with  $\text{AlR}_3$  is depicted as occurring through Ni–C–Al multicenter bonds. H migration is shown in a reorganization involving the  $\text{AlR}_3$   $\beta$ -H atom, and without forming a definite Ni–H species. Reproduced with permission.

Lardicci et al. [101], studied the effect of the transition metal precatalyst on the nature of the resulting catalyst. Their observation of a difference in catalytic activity using two different precatalysts,  $\text{Ni}(\text{acac})_2$  and  $\text{Ni}(\text{N-alkylsalicylaldimino})_2$  (plus  $\text{AlR}_3$ ), lead them to the conclusion that the catalyst species formed are different in nature, thus ostensibly ruling out the “bare” Ni atoms concept [93]—that is, if the same “bare” Ni atoms were the catalyst in both systems, then the catalytic activity would have been the same, not different as observed. However, the expectation that the same catalyst would form when two different precursors are used seems flawed because the anion of the Ni precatalyst is expected to affect the catalysis as discussed previously in section 2.1.1 of this review.

Wilke and coworkers concluded that their true catalyst was likely a Ni(0) complex, although they did note that the colloidal catalyst hypothesis was impossible to disprove via their studies [4,102]. One of the important observations in the work of Wilke and coworkers [4] was that, “the extent to which a reaction follows a particular direction is dependent upon a number of external factors (purity of  $\text{Ni}(\text{acac})_2$ , hydride

content of the  $\text{Al}(\text{C}_2\text{H}_5)_3$ , solvent, temperature, presence of ligands).” For that reason, confirmation of reactions, products, and intermediates, under exact reaction conditions—and without the use of trapping agents or non-Ziegler-type model systems [103]<sup>8</sup>—although difficult, would contribute considerably to our understanding of Ziegler-type hydrogenation catalyst formation and the nature of the true catalyst.

*2.2.1.2. Systems investigated by Sloan et al. [57]:  $M(\text{acac})_n$  plus  $\text{AlEt}_3$ ,  $\text{Al}(i\text{-Bu})_3$ , or  $\text{AlH}(i\text{-Bu})_2$ ;  $M = \text{Fe(III)}$ ,  $\text{Co(II and III)}$ ,  $\text{Ni(II)}$ ,  $\text{Ru(III)}$ , or  $\text{Pd(II)}$ .* Sloan et al. [57] tested a wide variety of systems for potential catalytic hydrogenation activity, and observed similarities between the catalytic behavior of these soluble catalysts and their insoluble, heterogeneous counterparts such as Raney Ni. For example, Sloan et al. [57] reported kinetic experiments that indicated the reaction was first order in  $[\text{H}_{2,\text{gas}}]$ <sup>1</sup> and zero-order in  $[\text{olefin}]$ <sup>0</sup>, which “is the same rate behavior observed in many heterogeneous hydrogenations.” As mentioned in the previous section, they also found that, like the effects observed in heterogeneous catalysts such as Raney Ni, greater degrees of substitution on olefinic carbons generally led to slower hydrogenation. The research was conducted, in part, with the goal of being able to use soluble Ziegler-type and related hydrogenation catalysts as mechanistic models for heterogeneous hydrogenation by bulk or supported metal catalysts despite the author’s belief that the true catalysts are homogeneous [104].

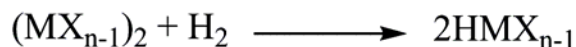
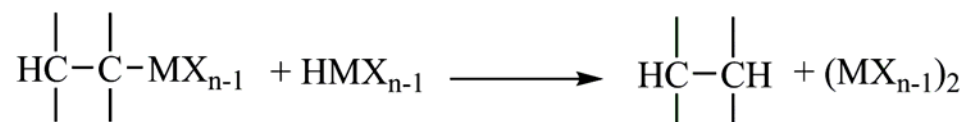
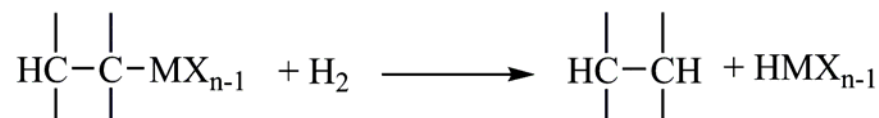
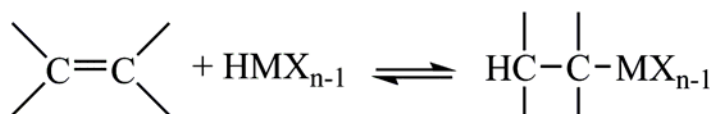
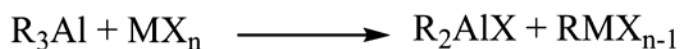
---

<sup>8</sup> In the final analysis, the use of a model system that is available for study over another system rigorously only yields information about the model (as one would logically expect). Another noteworthy general comment on models is that “all models are wrong, but some are useful,” a quote attributed to George E. P. Box [103].

In an effort to rule out either the homogeneous or heterogeneous catalyst hypothesis, the authors performed catalyst poisoning experiments—an important type of kinetics-based experiment. They observed that the addition of ethanol or acetone to the catalyst systems under investigation killed the catalytic activity. They concluded that colloidal metal must therefore be absent and the catalysts must be homogeneous. However, another interpretation of this result is plausible, namely that the observed catalyst poisoning could be due to reaction of ethanol or acetone with the  $AlR_3$ -derived components of the (heterogeneous) catalyst. Furthermore the result itself has been contradicted (albeit with other systems): Kroll [75], using a  $Co(acac)_2$  plus  $Al(i-Bu)_3$ -p-dioxane catalyst, found that the catalyst activity was decreased, but *not* killed by the addition of even a > 200 fold excess of butyl alcohol over the Al present. Schmidt and coworkers [114], studying a  $Pd(acac)_2$  plus  $AlEt_3$  system (discussed below), found that the addition of ethanol either enhanced or decreased the catalyst activity depending on the specific Al/Pd and EtOH/Al ratios used. Therefore, the Sloan et al. poisoning experiment alone cannot discern whether Ziegler-type hydrogenation catalysts are homogeneous or heterogeneous—they probably are reporting more on the  $AlR_3$ -component of the catalyst than on the  $(metal)_n$  nuclearity (n value) of the catalyst(s).

Sloan et al. proposed a generalized mechanistic scheme, shown below in Scheme 3, starting with the precursor components, showing both catalyst formation and hydrogenation of olefins. It was based on the concept that any such hydrogenation mechanism should be analogous to that of heterogeneous hydrogenation. This mechanistic scheme was noted by the authors as speculative and deliberately

oversimplified, “since the structures of the various catalysts are largely uninvestigated” [57].



**Scheme 3.** A reconstruction of a reaction scheme postulated by Sloan et al. [57]. The first step in this mechanism is alkylation of the transition metal precatalyst  $\text{MX}_n$  by the aluminum alkyl. Hydrogenolysis forming a metal hydride and olefin coordination follow. Elimination from the M-alkyl is shown as an alternative path to M-H formation (last line). Hydrogenolysis to give saturated olefin is shown as possibly involving either  $\text{H}_2$  or another molecule of metal-hydride. Redrawn with permission.

In the generalized mechanistic scheme, the transition metal precatalyst is first alkylated by the organoaluminum cocatalyst. Hydrogenolysis of the newly formed metal alkyl bond gives a metal hydride and an alkane. The authors mentioned elimination from the metal alkyl as an alternative way to generate the transition metal hydride. The reduction of transition metal and the formation of transition-metal-Al and/or transition-

metal–olefin complexes were given as other possibilities [38].<sup>9</sup> The addition of the olefin substrate was shown as a single-step insertion into the Ni–H bond leading to a new metal alkyl, but it was mentioned that it is probably preceded by complex formation with the olefin  $\pi$ -bonded to the metal.<sup>10</sup> Note that this equilibrium step (or steps) must lie to the far right in order to explain the observed zero-order olefin kinetics. The catalytic cycle is completed in this mechanism by hydrogenolysis of the M–R bond, either by molecular H<sub>2</sub> or by another molecule containing hydride followed by reduction, to give the saturated olefin and regenerate the M–H catalyst species.

The simple alternative explanation here is that the catalysts used by Sloan et al. are heterogeneous. Evidence for this alternative hypothesis are the similarities in catalytic behavior to known heterogeneous catalysts and the likely alternative interpretation of their poisoning experiment given above (i.e., that additions of ethanol or acetone react with the AlR<sub>3</sub>-derived component). In short, while an important and early effort, one that included kinetic and poisoning experiments, the homogeneous versus heterogeneous nature of the true catalysts is uncertain despite these early studies.

*2.2.1.3. Systems investigated by Lapporte [58]: M(2-ethylhexanoate)<sub>2</sub> plus m AlEt<sub>3</sub>, M= Ni or Co, m=3–4.* Similar to the work of Sloan et al. [57], Lapporte [58] had observed

---

<sup>9</sup> The timing of steps in a case like this is a standard mechanistic ambiguity; whether the addition of olefin occurs before or after H<sub>2</sub> enters and the formation of the metal hydride is possible, but often difficult, to ascertain [38].

<sup>10</sup> To test part of the proposed scheme, a solution of a Cr(acac)<sub>3</sub> plus Al(*i*-Bu)<sub>3</sub> catalyst with 2-methyl-2-butene as substrate was treated with D<sub>2</sub> gas. Analysis of the reaction products by MS showed mono-, di-, and trideuterated species, explained by reversible olefin migratory insertion to a M–D(H).

that the rate behavior of his soluble catalysts bore similarity to heterogeneous catalysts.<sup>11</sup> Lapporte pointed out that the diminished hydrogenation activity when NiCl<sub>2</sub> was used as the Ziegler-type precatalyst was analogous to the diminished rate of hydrogenation when Cl<sup>-</sup> was present using a Raney Ni catalyst. Also like Sloan et al., Lapporte was motivated by the prospect of using soluble Ziegler-type and related hydrogenation catalysts as models of heterogeneously catalyzed hydrogenation [104]. Therefore, it is no surprise that Lapporte gave a simplified mechanistic scheme (see Equations 6 and 9–11 detailed elsewhere [58]) that is quite similar to the scheme by Sloan et al.

One minor difference between the Sloan et al. and Lapporte schemes is that in the Lapporte scheme, reduction of the Ni(II) precatalyst with AlEt<sub>3</sub> to Ni(0) was shown proceeding via the formation of Ni–Et. Magnetic susceptibility measurements of the Al/Ni = 4 catalyst solutions at variable temperatures were interpreted as containing diamagnetic 3d<sup>10</sup> Ni species, although binuclear Ni(I) species could not be ruled out. Another difference is that Ni–H was shown as generated by elimination from the metal alkyl, and metal–olefin  $\pi$ -complex formation was depicted before insertion into the Ni–H bond. Like Sloan et al., Lapporte observed substrate isomerization and carried out a deuterium labeling experiment. It was noted that the observation of 1,2-dideuteroethylene and HD are consistent with Ni–ethylene  $\pi$ -complex and Ni–H intermediates, and reversible addition of the Ni–H species to the olefin double bond. Further, more direct evidence for the presence of Ni–ethylene  $\pi$ -complex and Ni–H

---

<sup>11</sup> One exception, however, was that nitrobenzene, which is easily hydrogenated using non-AlR<sub>3</sub> containing heterogeneous Ni<sub>n</sub> catalysts, showed only sparing conversion with the Ni Ziegler-type hydrogenation catalyst studied by Lapporte [58]. It is now known that nitrobenzene reduction is not a reliable indicator of heterogeneous catalysis [16].

species was obtained from low temperature  $^1\text{H}$  NMR spectra [58]. However, it was found that these signals irreversibly disappeared upon warming of the catalyst solutions to room temperature. The reasons and implications for this were not discussed, and it is not clear if the observed species are on, or off, the catalytically productive pathway. Lapporte's NMR observations are, however, a great lead for someone to pursue to see if the observed species do (or do not) show the kinetics of a catalytically competent intermediate.

Lapporte also interpreted his observations in terms of the knowledge available at the time, that is, that the true catalyst was homogeneous. Lapporte cited the "bare" Ni atoms idea of Wilke and coworkers [93] in proposing the catalysts could be mononuclear Ni(0) species solubilized by labile  $-\text{H}$ ,  $-\text{R}$ , solvent, or  $\text{Al}(\text{Et})_2(2\text{-ethylhexanoate})$  ligands that could be easily displaced by the unsaturated substrate. Additionally, Lapporte observed that gas evolution, apparently the products of reduction of the Ni(II) precatalyst by  $\text{AlEt}_3$ , was greatest at the same Al/Ni giving optimal catalytic activity, ostensibly suggesting a Ni(0) catalyst. However, like the work of Sloan et al., none of the results can be taken to rule out either homogenous or heterogeneous catalysts as the active species—indeed, we can be pretty sure now that it was pretty much impossible to solve the homogeneous versus heterogeneous catalysis question for these complex catalysts at that time [16]. The formation of a dark color upon hydrogenation of ketones to the corresponding alcohol was interpreted as "decomposition of at least some Ni to metal, albeit very finely dispersed" [58]. The black reaction mixture, though inseparable by ultracentrifugation, is consistent with  $\text{M}_n$  nanocluster formation [16], nanoparticles which

are expected to be a potent hydrogenation catalyst in the presence of moderate amounts of  $\text{AlR}_3$  and in hydrocarbon solvents under  $\text{H}_2$ .

*2.2.1.4. System investigated by Klinedinst and Boudart [105]:  $\text{Fe}(\text{acac})_3$  plus 6  $\text{AlEt}_3$ .*

Klinedinst and Boudart sought to determine the nature of Ziegler–type hydrogenation catalysts of especially Fe using IR and Mössbauer spectroscopy. An IR spectrum of the catalyst solution was similar to the superposition of spectra of  $\text{AlEt}_3$  and  $\text{AlEt}_2(\text{acac})$  obtained separately for the sake of comparison. This qualitatively indicated that the catalyst formation reaction between precursor components involved the transfer of acac from  $\text{Fe}(\text{acac})_3$  to the cocatalyst. However, exchange of ethyl from Al to Fe could not be detected by IR because the band region characteristic of the C–H stretch in “ $\text{FeEt}_2$ ” was obscured by the same C–H stretch in  $\text{AlEt}_3$ .

The authors hoped that Mössbauer spectroscopy of the catalyst solutions would confirm the presence of metallic particles too small to be detected by X-ray diffraction. Catalyst samples were prepared for Mössbauer spectroscopy in toluene at 190 K and then rapidly quenched to 77 K. The spectra obtained indicated that high spin Fe(II) were the only Fe species present. A possible explanation offered was that the reaction of  $\text{Fe}(\text{acac})_3$  with  $\text{AlEt}_3$  may be limited to a one electron reduction at these temperatures. This is depicted in Equations (1) and (2) below, reproduced from the original publication [105]. However, evidence for the gaseous products  $\text{H}_2$ , ethane and/or ethylene was not provided as part of this study and would be useful for anyone interested in reinvestigating this  $\text{Fe}(\text{acac})_2$  plus  $\text{AlEt}_3$  system.



When the catalyst sample was warmed to room temperature and then re-quenched to 77 K, it gave a Mössbauer spectrum identical to those of active catalyst samples prepared at room temperature. These Mössbauer spectra of activated catalysts showed that further reaction of the high spin Fe(II) had taken place. The most significant finding was that no metallic iron particles  $\geq 1.7$  nm were detected, which was taken to be consistent with a homogeneous catalyst hypothesis. The obvious alternative hypothesis is that the catalyst is heterogeneous, but consists entirely of particles smaller than 1.7 nm. Another possibility is that the catalysts are heterogeneous, but do not display the hyperfine pattern in Mössbauer spectra characteristic of metallic iron because they are amorphous [106,107], or are amorphous until exposed to high pressure H<sub>2</sub> [108] (these samples were not exposed to H<sub>2</sub>). However, while it provides (negative) evidence against a crystalline heterogeneous Fe<sub>n</sub>, catalyst of diameter  $\geq 1.7$  nm (which corresponds to Fe<sub>≥218</sub> if it were close-packed Fe(0), [50]),<sup>12</sup> even this clever study by Klinedinst and Boudart was unable to answer the difficult homogeneous versus heterogeneous catalysis question.

#### 2.2.1.5. System investigated by Alvanipour and Kispert [67]: Co(stearate)<sub>2</sub> plus 2 AlEt<sub>3</sub>.

Alvanipour and Kispert [67] concluded that Ziegler–type hydrogenation catalysts are

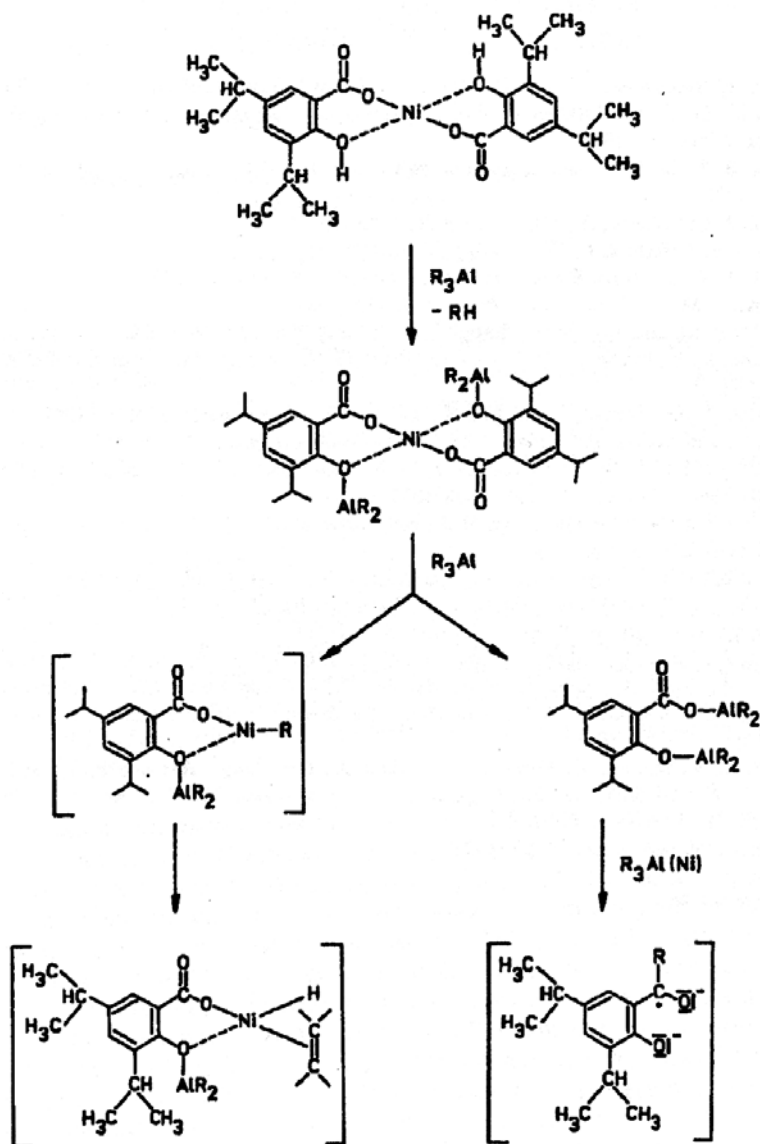
---

<sup>12</sup> The number (N) of atoms in a metal nanocluster of diameter (D) can be estimated according to the equation:  $N = (N_0\rho(4/3)\pi(D/2)^3)/M$ , where  $N_0 = 6.022 \times 10^{23} \text{ mol}^{-1}$ ,  $\rho$  = the room temperature density of the pure bulk metal, and  $M$  = atomic mass [50]. For Fe:  $\rho = 7.87 \text{ g/cm}^3$  and  $M = 55.845 \text{ g/mol}$  [83].

most likely homogeneous metal hydride or  $\pi$ -complexes. Their basis for this conclusion is their own finding that “high speed” centrifugation was unable to induce a separation in a solution of the catalyst in their  $\text{Co}(\text{stearate})_2$  plus 2  $\text{AlEt}_3$  system, and the absence of other evidence of metallic particles. In addition, they cited the results of others that suggested Ziegler–type hydrogenation catalysts are homogeneous: Wilke’s isolated  $[(\text{P}(\text{Ph})_3)_2\text{Ni}(\text{C}_2\text{H}_4)]$  complex [92], the diamagnetic  $3d^{10}$   $\text{Ni}(0)$  catalyst species proposed by Lapporte [58], and the Mössbauer spectroscopy results of Klinedinst and Boudart [105]. However, their work did not include the kinetic studies required to identify the true catalyst(s).

*2.2.1.6. Systems investigated by Reguli and Staško [70]:  $\text{NiL}_2$  plus  $\text{AlR}_3$  or  $\text{BuLi}$  ( $L = 3,5$ -diisopropylsalicylate, *acac*, *stearate*, or *benzohydroxamate*;  $R = \text{Et}$  or *i-Bu*).* The study by Reguli and Staško is noteworthy for its detailed examination of a range of variables in search of the optimum synthesis conditions for their Ziegler–type hydrogenation catalysts [70]. The authors also considered the nature of the catalyst preparation reaction and the resulting catalyst. In aliphatic solvent, EPR spectra indicated two paramagnetic species, interpreted as  $\text{Ni}(\text{I})$ , and ketylradicals ( $\text{ArCO}^{\bullet}\text{R}$ ), which were thought to form during the last stage of reaction between the precursors. The (unquantitated) concentrations of these species increased with  $\text{Al}/\text{Ni}$  to a maximum at  $\text{Al}/\text{Ni} = 8$ – $10$ , yet the catalytic activity was optimal at  $\text{Al}/\text{Ni}$  in the  $2$ – $4$  range, providing an important disconnect between the EPR signals and the (kinetic) catalysis. Based on this observation, the active catalyst species were thought to be diamagnetic species of  $\text{Ni}(\text{II})$  formed by alkylation of the precatalyst, although these results do not necessarily

mean the catalyst must be a homogeneous Ni(II) complex, only that the catalyst is not likely a Ni(I) species. A scheme depicting formation of the active catalyst species was proposed and is reproduced, Scheme 4.



**Scheme 4.** A speculative reaction scheme and structures proposed by Reguli and Staško for  $Ni(\text{diisopropylsalicylate})_2$  plus  $AlR_3$  [70]. Reproduced with permission.

2.2.1.7. *System investigated by Barrault et al. [37]: Co(acac)<sub>2</sub> plus AlEt<sub>3</sub>.* Studies by Barrault et al. investigated the catalyst formation reactions in a Co(acac)<sub>2</sub> plus AlEt<sub>3</sub> system using IR spectroscopy of the reaction solutions and GC analysis of the gas products. IR spectra at 25 min and 18 hours indicated that the timescale of reaction at room temperature was rapid, and GC showed completion of gas production after only three min of mixing. IR spectra were obtained at Al/Co = 0.5, 1.0, and 1.5. At lower Al/Co ratios they showed formation of Al(acac)<sub>3</sub>. At Al/Co = 1.5, formation of Al(Et)<sub>2</sub>(acac) and complete transfer of the acac ligands from the Co(acac)<sub>2</sub> precatalyst was observed. GC showing the production of ethane was interpreted as suggesting the disproportionation shown, Equation (3).



However, the observed ethane fraction was > 96% of the gas composition, whereas according to Equation 3 the reduction of Co(II) to Co(0) is expected to produce *equal amounts* of ethane and *ethylene*. Therefore, Barrault et al. postulated that either the disproportionation was not taking place, or that some of the ethylene was involved in  $\pi$ -binding interactions with soluble Co(0) complexes. The IR spectra obtained are at least consistent with such  $\pi$ -bonded Co(0)–ethylene complexes.

Carbonylation experiments were also carried out in which Al/Co = 1 catalyst samples were bubbled with a mixture of CO and H<sub>2</sub> gases, and monitored by IR spectroscopy. The highest  $\nu(\text{CO})$  frequency observed indicated CO binding to Co(0) centers that were more electron-donating to the  $2\pi^*$  orbital of CO than what had been

previously observed for CO surface-bound to Co(0) particles. Mononuclear Co(0) species complexed by such ligands as  $\pi$ -bound  $\text{CH}_2=\text{CH}_2$  were expected to be more electron rich than exposed Co(0) on the surface of metal particles. Therefore, this result was interpreted as evidence of such soluble mononuclear species. However, the authors were correct to conclude that, despite the fact that the carbonylation experiments showed the *presence* of complexed Co(0) species, neither these nor  $\text{Co}(0)_n$  metal particles could be ruled out as the sole active catalyst.

2.2.1.8. *Systems investigated by Shmidt and coworkers:  $\text{AlEt}_3$  plus  $\text{Co}(\text{acac})_2$  [109],  $\text{Co}(\text{acac})_3$  [110,111],  $\text{Ni}(\text{acac})_2$  [42,111],  $\text{Fe}(\text{acac})_3$ , or  $\text{Pd}(\text{acac})_2$  [111].* The reactions of  $\text{AlEt}_3$  with the above-listed metals and precursors were monitored using UV-Visible and IR spectroscopies. Transfer of acac ligands from the transition metal to Al was observed with the consequent formation of a mixture of  $\text{Al}(\text{acac})_3$  and  $\text{AlEt}_2(\text{acac})$  for  $\text{M} = \text{Fe}$ ,  $\text{Co}$  or  $\text{Ni}$ , and only  $\text{AlEt}_2(\text{acac})$  at various Al/M ratios for  $\text{M} = \text{Pd}$ . Analysis of aromatic hydrocarbon solutions of the Co catalyst with EPR spectroscopy led the authors to propose a paramagnetic Co(0) complex as the active catalyst [109], which is shown in Figure 2;  $\text{AlEt}_2(\text{acac})$  is proposed as a ligand of the Co(0) complex along with a molecule of the arene solvent, and  $\text{AlR}_3$  bound through a carbon atom. It is understood, however, that “ $\text{Et}_2\text{Al}^+$ ” cations such as that in Figure 2 are normally stabilized through coordination by a Lewis base [112].

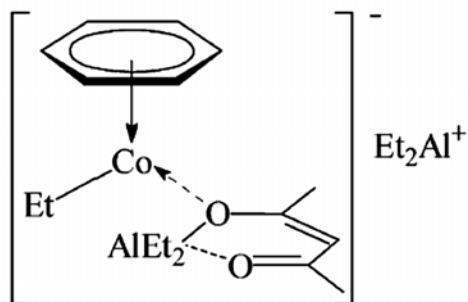


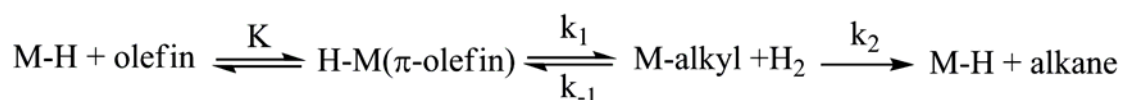
**Figure 2.** A Co(0) complex suggested as a possible active Ziegler–type hydrogenation catalyst species by Shmidt and coworkers [109,110,111]. In later work and based on additional evidence (vide infra), this species, whose presence was identified spectroscopically, was reinterpreted as the *precursor* for the  $\text{Co}(0)_n$  Ziegler nanoclusters now proposed as the active catalyst [113]. Reprinted with permission.

Magnetic measurements of the catalyst solutions appeared to confirm the reduction of transition metals to the zero-valent state. However, as clearly mentioned by the authors, the presence of low spin Co(II) or Ni(II) complexes exhibiting the same  $\mu_{\text{eff}}$  as Co(0) and Ni(0), could not be ruled out [111]. Furthermore, quantitative analysis of these magnetic susceptibility studies showed that 3–8% of the Co in the sample exists in  $\text{Co}(0)_n$  particles of up to 100 Å. Without further information, especially the necessary kinetic studies, it is entirely plausible that the observed  $\text{Co}(0)_n$  particles are responsible for some or all of the observed catalysis.

Shmidt and coworkers [42] proposed a simple mechanistic scheme for the hydrogenation of olefins using Ziegler–type catalysts. This scheme was very similar to the Sloan et al. [57] and Lapporte [58] schemes, and is shown in Scheme 5. The true catalyst was assumed to be a complex metal hydride. The idea of initial reversible olefin  $\pi$ -complex addition was supported by the observation that these catalysts cause olefin isomerization. The final step producing saturated hydrocarbon and regenerating the M–H catalyst was shown as hydrogenolysis of the metal–carbon bond as it was in the previous

schemes [57,58]. It is shown in Scheme 5 as involving a molecule of H<sub>2</sub>, which was a common depiction at the time [38], a mechanism consistent with the kinetic observations that olefin isomerization occurred at a slower rate with increasing H<sub>2</sub> pressure, and that the reaction is first order in H<sub>2</sub> pressure (by both their and other's data) [42,57,70].

However, it is now understood that such a hydrogenolysis is unlikely as an elementary mechanistic step, at least with late metal homogeneous catalysts. Moreover, such a step is probably better depicted by reductive elimination involving M–H formed by a prior oxidative addition of H<sub>2</sub> to the metal [10,89].



**Scheme 5.** A reproduction of the scheme for catalytic olefin hydrogenation using a Ziegler-type hydrogenation catalyst from Shmidt and coworkers' 1970 paper [42]. Used here with permission.

### 2.2.2. The “Ziegler-type catalysts are heterogeneous” hypothesis

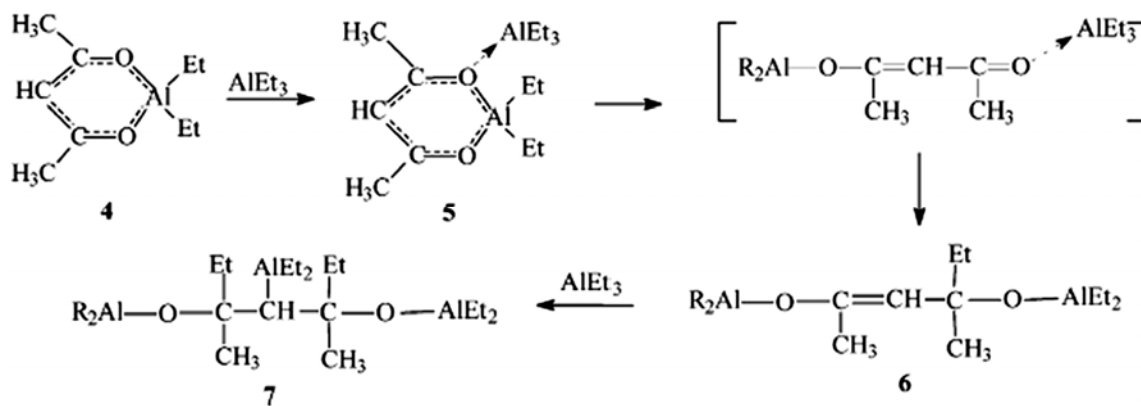
#### 2.2.2.1. Systems investigated by Shmidt and coworkers: *Co(acac)<sub>2,3</sub>* [19,113], or

*Pd(acac)<sub>2</sub>* [81,114] plus *AlEt<sub>3</sub>*. In 2005 and 2006, Shmidt and coworkers replaced their earlier conclusion of a Co(0) complex catalyst [109,110,111] with a postulate of catalysis by Co(0)<sub>n</sub> nanoclusters [19,113]. The presence of nanoclusters is consistent with the observation that dark brown solutions formed in both Co and Pd systems upon combination of the precursor components [16]. TEM images of Co samples demonstrated the presence of these clusters, and a particle size histogram displayed two maxima at 2.6 and 5.0 nm. Larger particles of 10–50 nm were thought to be agglomerates of the smaller particles. In the catalyst system prepared from Pd(acac)<sub>2</sub>,

TEM images exhibited the presence of 4.2 nm particles when Al/Pd = 4. Increasing the Al/Pd ratio to  $\geq 8$  decreased the particle size to 1–2 nm [81,114].

The Co clusters were shown to be amorphous by XRD, but formed 10 nm crystalline particles after calcination at 450 °C for 4 hours. The Co(0) complex previously proposed as the catalyst, and based on earlier UV-Visible and EPR spectroscopic results, Figure 2 [109,110,111] (*vide supra*), was reinterpreted as being the *precursor* for the Co(0)<sub>n</sub> nanoclusters, something fully consistent with Halpern's Rules (really guidelines) for catalysis [91].<sup>7</sup> The finely dispersed component observed in the earlier studies was reinterpreted as the 10–50 nm agglomerates of the smaller Co(0)<sub>n</sub> nanoparticles [19,113].

Catalyst formation and the role of AlEt<sub>3</sub> were studied using IR spectroscopy, and analysis of the gaseous and solid products. A reaction scheme based on the IR results was proposed, which showed the reaction of Et<sub>2</sub>Al(acac) with excess AlEt<sub>3</sub>, Scheme 6. The amounts of these species, the stability of the nanoclusters (as judged by the amount and time until precipitate was formed), and their catalytic activity were all found to depend on the Al/M ratio. Activity and stability varied inversely to each other, again consistent with Halpern's Rules, or guidelines, for catalysis [91],<sup>7</sup> cited earlier.



**Scheme 6.** A scheme proposed for the reaction of  $\text{Et}_2\text{Al}(\text{acac})$  with excess  $\text{AlEt}_3$  based on the results of IR spectroscopy by Shmidt and coworkers [113]. Reprinted with permission.

Based on their observations, Shmidt and coworkers proposed that the various Al-containing species and arene solvent molecules act as the nanocluster catalyst stabilizers, Figure 3. Their difference in binding strengths to the nanocluster surface could explain the ease with which they are replaced by the olefin substrate molecules, and therefore the differences in catalyst stability and activity.  $\text{AlEt}_3$  itself was thought to have the highest binding strength, which would explain the observation that increasing excesses of  $\text{AlEt}_3$  resulted in increasingly stable, yet decreasingly active catalysts.

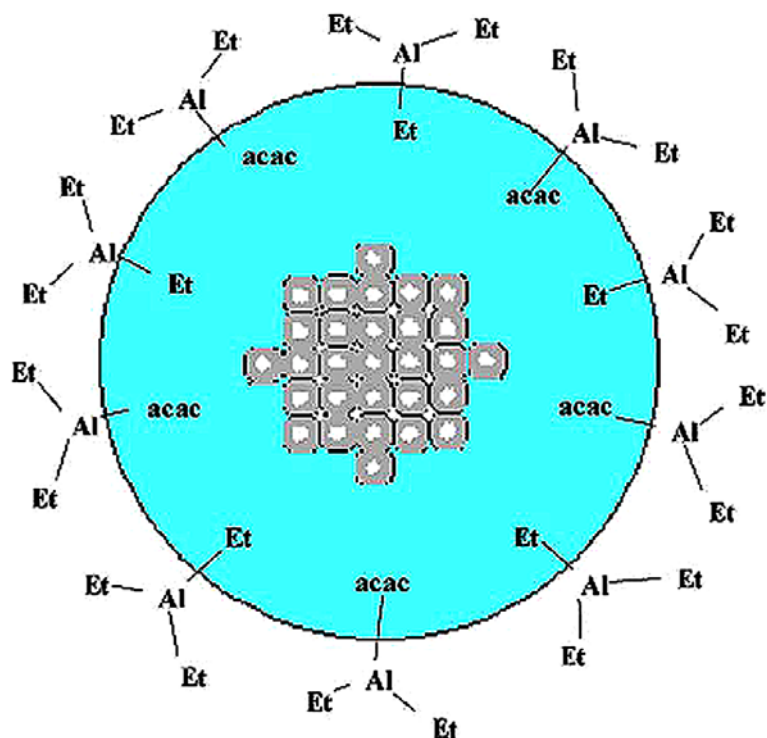


**Figure 3.** A cobalt nanoparticle and the associated organoaluminum stabilizer layer suggested by Shmidt and coworkers [113]. The gray circles in the center are Co atoms in an apparent crystalline array. Reprinted with permission.

The higher catalytic activity and immediate black precipitate formation when precatalysts with crystal  $\text{H}_2\text{O}$  were used were explained by the formation of alumoxane ( $\text{R}_2\text{AlOAlR}_2$ ) oligomers and their acac derivatives. This requires the assumption of *weaker coordination of alumoxane compounds to the nanocluster surface*, and therefore less stabilization compared to the other proposed stabilizers  $\text{AlEt}_2(\text{acac})$ ,  $\text{AlEt}_3$ , or their reaction products, a potentially important, more general conclusion. The results from IR and elemental analyses on samples of catalyst precipitates showed the remaining Al compounds were a mixture of species including oligomeric alumoxanes with characteristic Al–O–Al bonding. However, the catalyst precipitates had Al/Co ratios of 1.9–2.2 regardless of whether the initial Al/Co used in their preparation was 2, 4, or 8.

The authors suggested that this result indicated that excess AlEt<sub>3</sub> and AlEt<sub>2</sub>(acac) not bound to the catalyst surface were washed away by hexane during sample preparation. However, it is not clear why the purported stronger binding AlEt<sub>3</sub> and AlEt<sub>2</sub>(acac) would wash away instead of the supposed weaker binding alumoxane. Not all aspects of the observed nanocluster and stabilizers from this important study are fully explained [113].

Gas analysis, deuterium labeling, and radical trapping experiments were carried out, the interested reader is referred to the details of those experiments elsewhere [19,113]. The general process of catalyst formation in these studies can be summarized as follows: (i) the anions of the transition metal precatalyst are replaced by R groups from AlR<sub>3</sub>, (ii) the M-alkyl intermediate decomposes during the reduction of M, specifically for Co, the Co(0) nanocluster precursor complex forms (i.e., the complex previously thought of as the catalyst), and (iii) M(0)<sub>n</sub> nanoclusters then form from that Co(0) precursor complex, and are stabilized by Al-containing compounds, the details and identities of which depend on the initial Al/M.

This description still lacks a mechanism for formation of nanoclusters from M(0) complex intermediates. Additionally, and importantly, *in the absence of kinetic evidence, the simple observation of the presence of nanoclusters does not itself necessitate that they are the active catalysts*—although it certainly opens up that hypothesis as a dominant one to try to disprove. Schmidt and coworkers [113] observed Co concentration-dependent turnover frequencies (TOF = moles of product/(moles of catalyst × unit time) [115]), specifically *lower Co concentrations giving higher TOFs*. Since the TOF would be [Co]-independent for a mononuclear homogeneous catalyst, this indicates that either a  $\text{Co(0)}_n\text{L}_x + m\text{L} \rightleftharpoons n\text{Co(0)}\text{L}_{(x/n+m)}$  or related equilibrium is present (see p. 334 elsewhere

[16]), that the catalysts are heterogeneous, or possibly some other explanation such as a competing, bimolecular catalyst deactivation pathway. However, the explanation that catalyst solutions with lower [Co] make less-agglomerated catalysts, with higher TOF's directly contradicts the observation [19,113] that catalyst solutions with *more* agglomeration give higher catalytic rates. These studies do, however, identify kinetics as a function of metal/AlR<sub>3</sub> concentrations as key experiments for future studies. Such studies with a model Ir catalyst have recently been done [52,53,54], as will be briefly described (*vide infra*).

2.2.2.2. *System investigated by Pasykiewicz et al. [71]: Co(acac)<sub>3</sub> plus 1 AlMe<sub>3</sub> in benzene.* The 1974 paper by Pasykiewicz et al. investigated the possible reaction pathways and products of the catalyst formation reaction by IR spectroscopy of the reaction mixtures and MS analysis of the gas products. They suggested the following reaction stoichiometry, Equation (4).



The identity of Al(acac)<sub>3</sub> was confirmed by IR, NMR, and elemental analysis. The amount of each of the gaseous products was measured. The yields of the gaseous products were 60–70% based on the number of methyl groups, yet hydrolysis of the products did not result in further gas evolution, which was taken to mean that all the hydrolysable methyl groups had reacted. This leaves 30–40% of methyl groups unaccounted for by the proposed stoichiometry, so that finding the rest of the organic

products is a difficult but needed part of understanding Ziegler-type hydrogenation catalyst formation.

Analysis of the solvent after the reaction led to the detection of small amounts of toluene. When benzene-d<sub>6</sub> was used as the solvent 10% of the gas product was CH<sub>3</sub>D by MS. These observations suggested that multiple reactions are probably present (and that not all reactions are on the path to catalyst formation). A mechanistic scheme was proposed containing the following steps: (i) migration of a CH<sub>3</sub> group from Al to Co and simultaneous formation of Al(CH<sub>3</sub>)<sub>2</sub>(acac) and Co(acac)<sub>2</sub>CH<sub>3</sub>, (ii) complex formation between the Co(acac)<sub>2</sub>CH<sub>3</sub> intermediate and another molecule of AlMe<sub>3</sub>, leading to (iii) nucleophilic substitution at hydrogen, carbon, or Co atoms, and (iv) further reaction of the intermediates, ultimately resulting in metallic Co(0)<sub>n</sub> thought to be the true catalyst.

The evidence supporting the notion that metallic Co(0)<sub>n</sub> was the true catalyst consisted of: (i) the color of the reaction solution changed to black, (ii) the catalyst residue obtained from solvent evaporation reacted violently with air, methanol, or water, and (iii) reaction of this residue with HCl gave CoCl<sub>2</sub> and H<sub>2</sub>. The problem with this conclusion is that while these results suggest the presence of metallic Co(0) in the residue, they in no way definitively rule out homogeneous catalysis in solution. The kinetic studies necessary to support or refute the Co(0)<sub>n</sub> catalyst hypothesis remain to be done for this system as well.

*2.2.2.3. Systems investigated by Goulon and coworkers: M(2-ethylhexanoate)<sub>2</sub> plus AlEt<sub>3</sub> (M = Co or Ni) [40,116], or Ni(acac)<sub>2</sub> or Fe(acac)<sub>3</sub> plus AlEt<sub>3</sub> [40].* Goulon and coworkers studied Ziegler-type hydrogenation catalysts and their precursors using

EXAFS spectroscopy. In their important 1984 paper, they had greater success using the Ni precatalyst than Co because spectra of the Co catalyst solutions were overly affected by their preparation and aging [116]. EXAFS spectra of the Ni catalyst solution obtained at a series of Al/Ni ratios demonstrated Ni-Ni first-neighbors at distances equal to, or slightly larger than, those found in Ni foil. Signals were also detected for Ni-X at shorter distances, where X is C or O. The relative strength of these two signals varied with Al/M, but also with mode of preparation and aging, making truly definitive conclusions difficult. The Ni-Ni signals expected for the higher metal shells were not observed, arguing, according to one interpretation, against the presence of (extensive amounts of) Ni(0)<sub>n</sub>.

These results were interpreted by Goulon and coworkers [116] as consistent with amorphous clusters, but could also have been explained by small Ni(0)<sub>n</sub> clusters,  $n \approx 4-10$ , based on their reported Ni-Ni first shell coordination of  $3.8 \pm 1$  [117,118].<sup>13</sup> The detection of Ni-X signals by Goulon and coworkers [116] suggests the presence of ligands that may stabilize any small clusters present and is also consistent with the samples showing Ni-Ni distances slightly larger than those found in Ni foil [119,120].<sup>14</sup>

---

<sup>13</sup> See the references cited [117,118] for an explanation on how the conversion between average coordination number and number of atoms in a cluster is carried out, which is closely related to the method used for estimating number of atoms in a metal cluster of a given diameter [50].

<sup>14</sup> Goulon and coworkers tentatively discounted the data as indicative of small clusters because of the expectation that Ni-Ni distances would be shorter for metal clusters of less than about 10 atoms. However, in a recent study of Rh clusters [119], contraction of M-M distances was expected for metal nanoclusters *without ligands* according to an approximate  $n^{-1/3}$  relationship (where  $n$  = the number of atoms) [120], whereas in experimentally observed clusters *with ligands*, *larger* Rh-Rh distances were observed. This observation was explained by donation of M-M valence electrons to M-ligand bonds, thereby lengthening the M-M distance.

A shift observed in the absorption edge supported the hypothesis that Ni species were zero-valent, but incomplete reduction could not be ruled out by EXAFS. The authors pointed out that earlier magnetic susceptibility data, interpreted as ruling out the presence of metal clusters [116], may have been misleading. In light of the definitive EXAFS evidence for the existence of close M–M interactions, the earlier lack of detected ferromagnetism expected for metal clusters could be explained if “carbonaceous ‘screens’ ... prevent magnetic coupling” [116].

In their subsequent study, Goulon and coworkers [40] used other catalyst precursors in an attempt to avoid the variability problems of the initial study. They again observed EXAFS signals dominated by Ni–Ni first neighbors suggesting the presence of metal clusters. The model of molecular “[Ni,Al]” complexes or clusters was ruled out by the similarity of spectra using GaEt<sub>3</sub> as the cocatalyst, and by Ga K-edge spectra. Interestingly, EXAFS spectra of the Fe(acac)<sub>3</sub> plus 6 AlEt<sub>3</sub> catalyst system were interpreted as ruling out the presence of small Fe metal particles, but were similar to the EXAFS spectra of amorphous iron carbide. When the amorphous metal carbide model was used to fit the Ni sample spectra, the initial results were promising, but not definitive. Formation of clusters in these systems is undeniable, but whether they are small ~4–10 atom clusters, amorphous M or M–carbide clusters, or some combination is still unclear. Furthermore, the question of which species is the predominant catalyst remains open, kinetic studies being required to answer that question.

*2.2.2.4. Systems investigated by Bönnemann and coworkers: Ni(acac)<sub>2</sub> plus 3 Al(i-Bu)<sub>3</sub> [121], Pt(acac)<sub>2</sub> plus 4 AlMe<sub>3</sub> [121,122,123,124,125], or [(COD)Pt(CH<sub>3</sub>)<sub>2</sub>] plus 10*

*AlEt<sub>3</sub>*, or *Al(C<sub>8</sub>H<sub>17</sub>)<sub>3</sub>* [126]. Bönnemann and coworkers have studied the reaction between Ziegler–type precursors and have worked on characterizing the products. They observed that solutions turned brown or black upon precursor combination in the Ni(acac)<sub>2</sub> plus 3 Al(*i*-Bu)<sub>3</sub> and Pt(acac)<sub>2</sub> plus 4 AlMe<sub>3</sub> systems, which is consistent with the formation of nanoclusters [16].<sup>15</sup> In addition, TEM images of these systems revealed the presence of 3.2 ± 0.8 nm and 2.5 nm Ni and Pt nanoclusters respectively. TEM images alone, however, can be misleading as (i) the technique has been shown to be sensitive to sample preparation, especially with samples of Ziegler–type systems [9], and also (ii) can *cause* particle formation and/or crystallization under the electron beam, especially for the lighter first and second row metals [17,127]. Unlike Schmidt and coworkers who used a minimal beam current and compared images from repeated beam exposures [113], Bönnemann and coworkers [121,122,123,124,126] reported no attempt to rule out these potential TEM artifacts.

Bönnemann and coworkers focused several of their subsequent studies on the Pt(acac)<sub>2</sub> plus 4 AlMe<sub>3</sub> system. A fit of the EXAFS spectrum taken of the isolated dried colloid gave a Pt–Pt interaction with an average coordination number of 5.0 ± 0.5, and a lack of longer range Pt–Pt shells. These two observations could be explained by the predominance of clusters with ~8–13 atoms, nanoclusters with an amorphous structure, or a combination of the two. High resolution TEM images and corresponding optical diffractograms showed 1.2 nm amorphous particles. Analysis of the samples by anomalous small-angle X-ray scattering (ASAXS) spectroscopy confirmed the presence

---

<sup>15</sup> Bönnemann and coworkers use the terms “colloidal nanometals,” “transition metal nanocolloids,” and “nanosized organosols” interchangeably for what we define herein as “Ziegler nanoclusters” (and only for cases where an AlR<sub>3</sub> component is present).

of 1.2 nm amorphous nanoclusters. The different sizes of nanoclusters observed in the Pt(acac)<sub>2</sub> plus 4 AlMe<sub>3</sub> system (2.5 nm by TEM vs. 1.2 nm by HRTEM and SAXS) may be a result of the different methods used, differences in sample preparation, or a combination of the two.

Formation of nanoclusters was monitored as a function of time with in-situ SAXS, Figure 4 [124,125]. The clusters of final 1.2 nm diameter were observed within 1 hour of the start of the reaction, and stayed constant for at least 1000 hours. The constant final size of the nanoclusters, and a fit of the data by an empirical [128], exponential model, Figure 4 (bottom), were interpreted as evidence for continuous “nucleation” or “agglomeration” of reduced Pt(0) atoms into 1.2 nm diameter, Pt(0)<sub>~55</sub> nanoclusters,<sup>16</sup> without any observable contribution from nanocluster “growth” [124]. The identity of the clusters as Pt(0)<sub>~55</sub> is significant because 55 is the second of the “magic number” series of atoms for icosahedra with a full/closed outer shell, and thus more stable than non-magic number clusters [129]. To the best of our knowledge, Bönnemann and coworkers’ study is the first that has successfully monitored the in-situ formation of nanoclusters from Ziegler–type precursors, an important contribution.

Some confusion may be created by the terminology used by Bönnemann and coworkers for nanocluster formation [124], which is different than the terminology commonly used in the nucleation and growth literature [49,130,131,132]. In a range of

---

<sup>16</sup> Bönnemann and coworkers discuss the clusters as being comprised of 53 Pt atoms based on an ideal icosahedral structural model and their experimentally determined 1.2 nm diameter. This is actually an approximation since the techniques used show the clusters are amorphous (i.e., not ideally icosahedral) and that a distribution of cluster sizes exists. The clusters have been written here as Pt(0)<sub>~55</sub> to emphasize these facts according to a convention established in the literature for representing the approximate number of atoms in such (non-monodisperse) nanoclusters [50].

systems, and according to a well-precedented nanocluster formation mechanistic model (nucleation  $A \rightarrow B$  (rate constant  $k_1$ ), and autocatalytic growth  $A + B \rightarrow 2B$  (rate constant  $k_2$ ) [130], the term “nucleation” refers only to the  $k_1$  step, which is typically followed by (autocatalytic surface) “growth”, the step with rate constant  $k_2$ . Subsequent increases in size could then proceed by either continued “growth” or by, mechanistically now precedented, particle “agglomeration” (the combination of nanoparticles to form larger agglomerates) [131]. However, in the work by Bönemann and coworkers [124], “nucleation” is used to describe the formation of the final-sized 1.2 nm nanoparticles, “agglomeration” is used to describe a part of the “nucleation” process (the joining of single zero-valent Pt atoms, the other part of the “nucleation” process being the initial precursor decomposition), and “growth” is used to describe an increase in size of the 1.2 nm nanoparticles after “nucleation” has taken place (presumably occurring via continued “agglomeration”). In short, the mechanistic nomenclature used elsewhere [124] is inconsistent with the existing literature [49,130,131,132], and therefore confusing. However, despite the above nomenclature issues, the relatively slow nanoparticle development observed for this system makes it promising—if catalytically competent for hydrogenation, as is expected—for further studies aimed at determining the true nature of the catalyst and the catalyst formation mechanism. In addition, Bönemann and coworkers’ studies, along with Goulon’s and co-workers’ efforts nearly 20 years earlier [40], promise to be important classic studies in identifying what we term “Ziegler nanoclusters”.

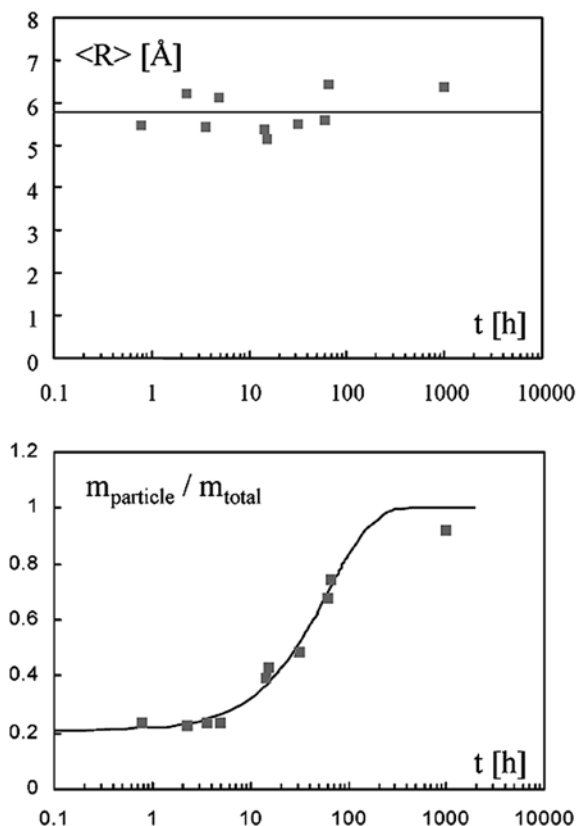


**Figure 4.** The results of in-situ ASAXS to monitor the formation of Pt(0) nanoparticles by Bönemann and coworkers [124]. The mean particle radius (top) remained essentially constant from the time particles were first detected, and up to 1000 hours attesting to particle stability (mean particle diameter = 1.2 nm). The mass fraction ( $m_{\text{particle}}/m_{\text{total}}$ ) of Pt atoms in nanoparticles as a function of time (bottom) fit with an empirical exponential model. Reprinted with permission.

A similar system, Pt(acac)<sub>2</sub> plus 4 AlEt<sub>3</sub> ([Pt] = 1.2 mM, solvent = toluene, temperature = 22.0 °C, initially 40.0 psig H<sub>2</sub>, stirring = 1000 rpm.), has been tested for its ability to catalytically hydrogenate cyclohexene. The results of following the formation of a Ziegler–type hydrogenation catalyst from this system by the cyclohexene hydrogenation reporter reaction method [50,130,133] are shown here for the first time,

Figure 5 (for complete experimental details see the Supporting Information).<sup>17</sup> The hydrogenation curves show the production of active Ziegler–type hydrogenation catalysts after an induction period, but the curves end abruptly upon total consumption of cyclohexene, and do not have a truly sigmoidal shape. The same, now well preceded nanocluster formation mechanistic model discussed above (nucleation  $A \rightarrow B$  (rate constant  $k_1$ ), and autocatalytic growth  $A + B \rightarrow 2B$  (rate constant  $k_2$ ) [130]) was employed, but failed to produce good fits in the latter portions of the curves. A representative hydrogenation curve is shown, and the fitting results are given, Figure 5. The different systems and conditions used prohibit direct comparison between these experiments and the findings of Bönemann and coworkers. However, the use of slow-forming catalysts, even if such model systems are not what are desired industrially, appears to be one important way in which new insights could be gained. Hence, the  $\text{Pt}(\text{acac})_2$  plus  $\text{AlR}_3$  system is one of interest for further studies.

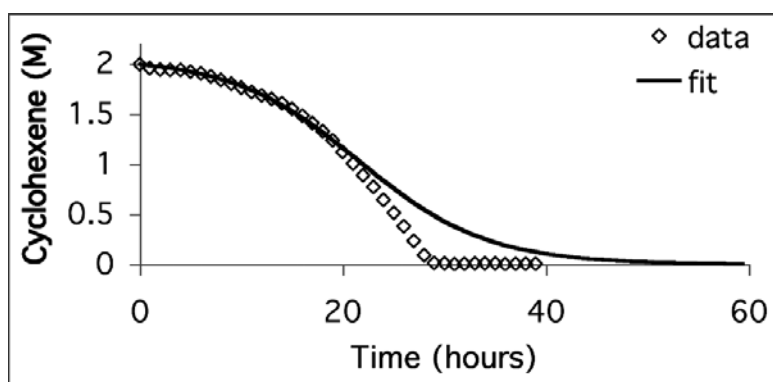


**Figure 5.** A representative reaction of  $\text{Pt}(\text{acac})_2$  plus 4  $\text{AlEt}_3$  followed by the cyclohexene hydrogenation reporter reaction method [50,130,133] ( $[\text{Pt}] = 1.2 \text{ mM}$ ,

<sup>17</sup> Other systems surveyed for use as model Ziegler–type hydrogenation catalysts are  $[(1,5\text{-COD})\text{Ir}(\text{acac})]$ ,  $[(1,5\text{-COD})\text{Rh}(\text{acac})]$ ,  $\text{Rh}(\text{acac})_3$ ,  $\text{Co}(\text{acac})_2$ . The results of these previously unpublished hydrogenation survey experiments are also given in the Supporting Information for the interested reader.

solvent = toluene, temperature = 22.0 °C, initially 40.0 psig H<sub>2</sub>, stirring = 1000 rpm), and attempted fit of the data using the now well-established A → B (rate constant k<sub>1</sub>), A + B → 2B (rate constant k<sub>2</sub>) mechanistic model for nanocluster nucleation and autocatalytic growth [130]. The resulting rate constant values taken from 5 such runs are k<sub>1</sub> = 0.004 ± 0.002, and k<sub>2</sub> = 0.09 ± 0.03. All the fits obtained were similarly poor in the last part of the curve, with a range of R<sup>2</sup> values of 0.9491–0.9954.

Bönnemann and coworkers reported the presence of a binuclear Pt complex Me<sub>4</sub>Pt(μ-AlMe)<sub>2</sub>PtMe<sub>4</sub> as an intermediate in the formation of Pt nanoparticles [122,123,124]. Its existence and structure were investigated using <sup>1</sup>H and <sup>13</sup>C NMR, MS, XPS and EXAFS studies. Decomposition of the binuclear platinum intermediate lead to “nucleation” of the 1.2 nm, Pt<sub>55</sub> nanoparticles. From the in-situ SAXS experiments, the rate of “nucleation” was found to be linearly proportional to the concentration of the binuclear intermediates. Bönnemann and coworkers concluded, therefore, that the rate-determining step in nanocluster formation is the decomposition of the binuclear intermediate. A word and picture mechanism of colloid formation from the work of Bönnemann and coworkers [124] is reproduced below, Scheme 7. In the absence of excess AlMe<sub>3</sub> or AlMe<sub>2</sub>(acac), an insoluble “Pt nanopowder” was observed made of 1.4 nm diameter clusters [123].



active Al–C bonds per Pt atom exist in the stabilizer of Pt nanoclusters. The representation of the resulting stabilized cluster is shown, Scheme 7.

Bönnemann and coworkers also analyzed the products formed upon the reaction of [(1,5-COD)Pt(CH<sub>3</sub>)<sub>2</sub>] plus 10 AlEt<sub>3</sub> or Al(C<sub>8</sub>H<sub>17</sub>)<sub>3</sub> [126]. As with other systems studied, the solution became a brown/black color upon the addition of AlR<sub>3</sub>. The presence of Pt(0)<sub>13</sub> nanoclusters was observed in TEM images showing 0.7 nm clusters. This finding was supported by comparison of experimental XANES spectrum with theoretical model spectra of 1-shell and 2-shell clusters. The zero-valent state of Pt in the Pt(0)<sub>13</sub> nanoclusters was confirmed by both XPS and XANES. Increasing the temperature during formation of the nanoclusters from room temperature to 60 °C resulted in a slight increase in size from 0.7 nm to 0.82 ± 0.19 nm, which was interpreted as a contribution from Pt<sub>55</sub> nanoclusters in addition to the major constituent, Pt<sub>13</sub> clusters. Such an interpretation could be supported by a distinct bimodal size distribution obtained from TEM images. However, this was not provided; the reported size and dispersity do not correlate well with truly monodisperse, precise 13 and 55 Pt atom particles as reported. Truly monodisperse nanoparticle samples are rare: single crystals of thiol-protected Au<sub>102</sub> nanoparticles are, for example, one case of a *truly* monodisperse nanoparticle sample [134].

The timescale of the reaction varied between 1 hour to more than one month depending on the temperature and whether Al(C<sub>8</sub>H<sub>17</sub>)<sub>3</sub> or AlEt<sub>3</sub> was used. No color change was observed using AlMe<sub>3</sub>, implying the absence of nanoclusters in the resulting solution. However, the authors did not mention the temperature or time allowed for observation, so that observation does not rule out possible nanocluster formation with

AlMe<sub>3</sub> as the cocatalyst. Bönnemann and coworkers [126] believed that β–H elimination was rate-determining in nanocluster formation, yet that explanation is not necessarily consistent with the observation of cluster formation in their own Pt(acac)<sub>2</sub> plus AlMe<sub>3</sub> system [121-125], or with catalyst formation using AlMe<sub>3</sub> in other systems [4,71]. Furthermore, if β–H elimination is rate-determining, one might have expected faster cluster formation with AlEt<sub>3</sub> than with Al(C<sub>8</sub>H<sub>17</sub>)<sub>3</sub>, since the former has 50% more β–H's (and if one assumes an equal amount of Al-alkyl is present in each case at the rate determining step). Moreover, β–H elimination is typically very facile in organometallic chemistry and rarely a rate-determining step to our knowledge [10]. Clearly, there are many aspects of the mechanism of formation of Ziegler nanoclusters that require further explanation.

Bönnemann and coworkers have several other, valuable publications dealing with interesting topics that are related to Ziegler–type hydrogenation catalysts. Other research on the Pt(acac)<sub>2</sub> plus 4 AlMe<sub>3</sub> system was focused on the characterization of networks formed by the nanoclusters [135,136]. Syntheses starting with Ni(COD)<sub>2</sub> and AlEt<sub>3</sub>, and using high temperatures, resulted in the formation of NiAl<sub>x</sub> materials [137,138]. Another system gave ~10 nm Co(0)<sub>n</sub> nanoclusters by the combination of Co<sub>2</sub>(CO)<sub>8</sub> and AlR<sub>3</sub> [139]. These studies, however, are beyond the scope of this review; the interested reader is referred to those original publications [135,136,137,138,139].

It is still unclear why *cluster* formation is relatively slow in both the Pt(acac)<sub>2</sub> plus 4 AlEt<sub>3</sub> and [(COD)Pt(CH<sub>3</sub>)<sub>2</sub>] plus 10 AlEt<sub>3</sub>, or Al(C<sub>8</sub>H<sub>17</sub>)<sub>3</sub> systems investigated by Bönnemann and coworkers, when *catalyst* formation is rapid in virtually all other systems explored [37]. One possible explanation of this is that the heterogeneous

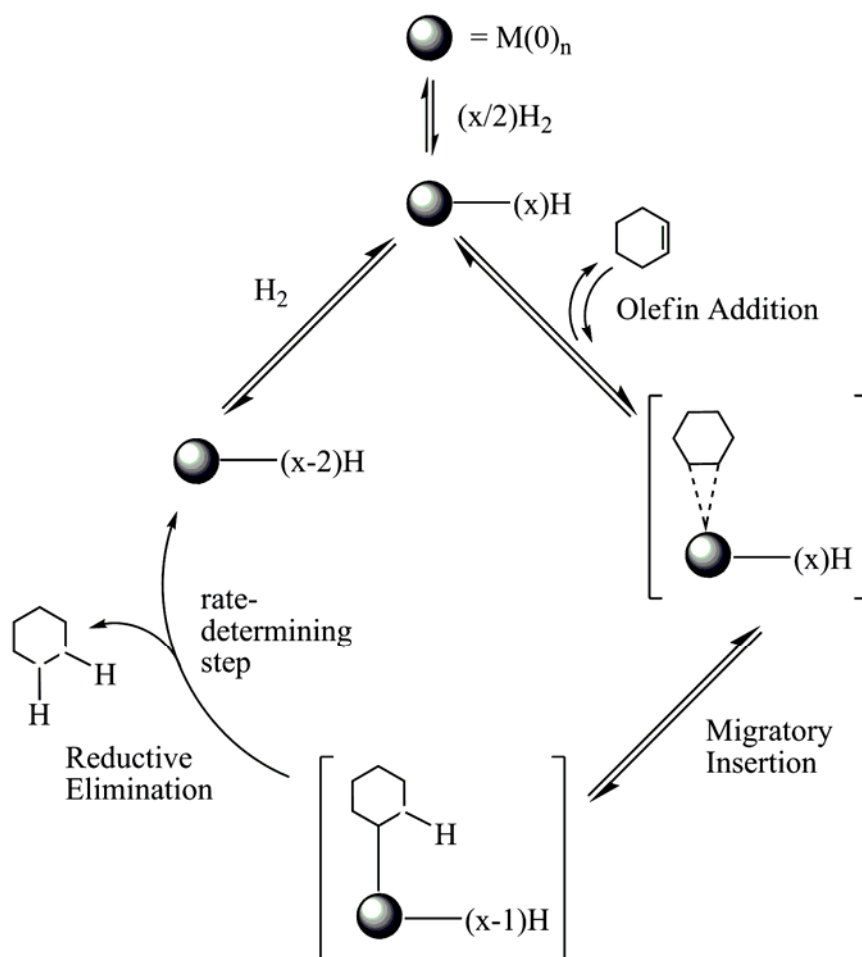
component observed in some systems is the product of catalyst deactivation, as has been observed in a Ni(diisopropylsalicylate)<sub>2</sub> plus AlR<sub>3</sub> system with aromatic solvents [70]. Another conceivable explanation, in light of the studies of Shmidt and coworkers [19,81,113,114] (who showed the presence of nanoclusters in systems of active hydrogenation catalysts) and the results in Figure 5, vide supra, showing an induction period prior to the catalytic hydrogenation of cyclohexene using a similar Pt(acac)<sub>2</sub> plus 4 AlEt<sub>3</sub> system, is that the slow cluster formation reaction is inherent to the use of these particular precursors, conditions, or both. These studies serve to again illustrate the importance of kinetic experiments in studies attempting to determine the true catalyst. Notable here is that the slow formation of these systems could be exploited in the pursuit of a more detailed investigation into the kinetics and mechanism of Ziegler–nanocluster formation, a key goal in the field of Ziegler–type hydrogenation catalysts.

*2.2.2.5. Systems investigated by Alley, Hamdemir, Wang, Frenkel, Li, Yang, Menard, Nuzzo, Özkar, Johnson, and Finke: [(1,5-COD)Ir(μ-O<sub>2</sub>C<sub>8</sub>H<sub>15</sub>)]<sub>2</sub> plus AlEt<sub>3</sub> [52,53,54], Co(neodecanoate)<sub>2</sub> plus AlEt<sub>3</sub> [55], and Ni(2-ethylhexanoate)<sub>2</sub> [56] plus AlEt<sub>3</sub>. Model and industrial Ziegler–type hydrogenation catalyst systems that have recently been under investigation by the above-noted team include AlEt<sub>3</sub> plus [(1,5-COD)Ir(μ-O<sub>2</sub>C<sub>8</sub>H<sub>15</sub>)]<sub>2</sub> [52,53,54], Co(neodecanoate)<sub>2</sub> [55], or Ni(2-ethylhexanoate)<sub>2</sub> [56]. Studies have been carried out using a variety of analytical methods including kinetic measurements, TEM, MALDI MS, EXAFS, XPS, and NMR. Interestingly, the catalytic activity of the Ir model system varies inversely with Ir concentration, similar to the [Co]-dependent TOF results reported by Shmidt and coworkers using their*

Co(acac)<sub>2,3</sub> plus AlEt<sub>3</sub> system already discussed [113]. Some of the other key results thus far appear to be that the precatalyst plus cocatalyst reactions in these Ziegler–type catalyst systems produce a mixture of sub-nanometer *and* amorphous M(0)<sub>n</sub> nanoclusters, and that this result would have gone unrealized without using a combination of analytical methods. This review is one of the necessary first steps of the studies in progress, work currently in various stages of preparation for publication [53,54,55,56].

The above group has also briefly investigated the mechanism of cyclohexene hydrogenation using a Ziegler–type hydrogenation catalyst made from Co(neodecanoate)<sub>2</sub> plus AlEt<sub>3</sub>, Al/Co = 3. A D<sub>2</sub> labeling experiment was used to determine the location of the rate-determining step with regard to the Shmidt mechanism shown back in Scheme 5. Based on those results, reported here for the first time, an updated mechanistic scheme is proposed, Scheme 8. A full description of the results and experimental details will be found by the interested reader in the Supporting Information. Briefly, the Co-based Ziegler–type hydrogenation catalyst was prepared in cyclohexane, cyclohexene substrate was added, and the vessel containing the solution was pressurized with D<sub>2</sub>. The amount of deuterium incorporation into the resulting hydrogenation product cyclohexane was analyzed by gas chromatography mass spectrometry, Figures S6 and S7, Supporting Information. The observation of a significant amount of cyclohexane containing > 2 deuterium atoms supports the precedented hypothesis, in line with the accepted mechanism for heterogeneous transition metal catalyzed hydrogenations [140], that reductive elimination, as opposed to migratory insertion [42], is the rate determining step, with prior equilibria existing in the earlier step(s). In fact,

this updated mechanism, Scheme 8, better explains the previous observation that the reaction becomes zero order in  $H_2$  at pressures above 1.5 atm [42]. A caveat on these studies is that they are not complete as of this writing, so that their full findings and resultant insights remain to be completed.



**Scheme 8.** A schematic catalytic olefin hydrogenation mechanism (shown here for cyclohexene for convenience) using Ziegler-type hydrogenation catalysts. The ball implies a transition metal nanocluster catalyst, but could also represent a monometallic catalyst. The postulated steps are oxidative addition of  $H_2$ , olefin addition, migratory insertion to form an alkyl hydride species, and irreversible, rate-determining reductive elimination yielding the saturated cyclohexane. Evidence for reductive elimination being rate limiting is our observation of multiply deuterated ( $> 2$  deuterium atoms) in the

hydrogenation product of cyclohexene (the results and experimental details are given in the Supporting Information for the interested reader). The actual timing of oxidative addition of H<sub>2</sub> versus olefin addition steps is a standard mechanistic ambiguity [38], so that the H<sub>2</sub> activation (first) pathway is shown only for the sake of illustration.

#### 2.2.2.6. *Conclusions for the section on the nature and mechanism of formation of*

*Ziegler–type hydrogenation catalysts.* The following results appear to apply across different systems: (i) the exchange of ligands between AlR<sub>3</sub> and the precatalyst has been established by IR and <sup>1</sup>H NMR spectroscopy; (ii) for M(L)<sub>2</sub> precatalysts plus AlR<sub>3</sub>, the resulting Al species present are AlR<sub>2</sub>(L), AlR(L)<sub>2</sub>, Al(L)<sub>3</sub>, or some combination of the three depending on the Al/M used, and the presence of additional impurities or additives such as H<sub>2</sub>O; (iii) the formation of alumoxanes (i.e., Al–O–Al complexes) and their contribution to the stabilizer layer of observed nanoclusters also has some precedent, but could still use additional study; and (iv) the most recent studies favor the hypothesis of M(0)<sub>n</sub> nanocluster catalysts. In these cases AlR<sub>3</sub> is generally believed to reduce the higher-valent transition metal from the precursor to the zero-valent state, and it or its reaction products are thought to ligate and stabilize the resulting M(0)<sub>n</sub> nanocluster catalyst. However, disagreement persists concerning the reaction forming Ziegler–type hydrogenation catalysts, and the nature of the catalysts themselves. Whether or not the catalysts are homogeneous or heterogeneous is still a central remaining issue, as is the composition of the active catalyst(s). In most cases, the kinetic studies required to answer the homogeneous versus heterogeneous catalysis question are lacking.

Several factors conspire to make solving the homogeneous or heterogeneous catalysis question especially difficult for Ziegler–type catalyst systems. The high sensitivity of Ziegler–type hydrogenation catalyst systems to factors such as air and

water complicates reproducible catalyst preparation, and has probably contributed to the occasional contradictory characterization results seen for otherwise ostensibly similar systems. There is also the possibility that some Ziegler–type catalyst systems are homogeneous and some are heterogeneous, especially when considering the identities of the catalyst precursor components in different systems. This sentiment was expressed by Breslow and Newburg back in 1959 [23], “It is our belief that there is not one, but a family of Ziegler–type catalysts.” Even given identical systems, the variables of the synthesis procedure affect catalyst activity and may lead to modifications in the nature of the resulting catalyst. This was recognized by Barrault et al. [37], who noted that “the nature of these complexes is largely controlled by differences in preparation.” In other words, despite the narrow definition used herein for Ziegler-type hydrogenation catalysts, the creation of fundamentally different catalysts from similar *or even identical* starting materials may occur because of differences in other variables in the catalyst preparation, or conditions employed during analysis [10,17]. This is a reflection of an insight of Halpern’s from the mechanistic study of organometallic systems [141,142], which “underlines the danger of assuming the mechanisms... or of extrapolating from one system or set of conditions to another (even closely related) one” [141]. Hence, it is certainly possible that small changes may alter the state of the transition metal from single metal complexes to multimetallic nanoclusters, which are quite different species and catalysts.

Despite the conflicting reports that exist concerning the homogeneous or heterogeneous nature of Ziegler–type polymer hydrogenation catalysts, there is good reason to believe that, in many systems and under conditions commonly employed, there

is at least a heterogeneous, nanocluster, or possibly sub-nanocluster component to the active catalysts [16]. That early researchers favored the conclusion that Ziegler-type hydrogenation catalysts are homogeneous makes perfect sense. The prior lack of examples of organic-solvent-soluble nanoclusters, and prior lack of knowledge of the kinetics and mechanism of formation of transition-metal nanoclusters, meant that it simply was not possible to routinely know when soluble nanocluster catalysts were both forming and then serving as the kinetically dominant catalyst [16].<sup>18</sup> The recent observation of Ziegler nanoclusters in some systems is a direct result of characterizations using modern methods such as TEM, XAFS, and ASAXS. The availability and improvement of other, advanced analytical methods may eventually assist in the disproof of the homogeneous or heterogeneous catalyst hypothesis for a given system and set of conditions. Another reasonable hypothesis warranting disproof is that of the simultaneous existence of both homogeneous *and* heterogeneous active catalysts in a single system. Additionally, results from studies under well-documented conditions using *well defined precursor materials* (i.e., and in comparison to the common, but somewhat ill-defined, industrially used Ni and Co precursors) promises to allow generalization of any important findings [52]. Ideally, such studies would simultaneously be able to detect the effects of catalyst preparation variables on both catalyst properties *and* catalyst composition and structure (vide infra).

---

<sup>18</sup> Ziegler-type  $M(O_2CR)_2/AlR_3$  catalysts were listed in our 2003 review [16] on the “is it homogeneous versus heterogeneous catalysis?” question as systems where heterogeneous catalysis is strongly suspected, but where studies confirming or refuting this suspicion are needed.

### 2.3. *A closer look at the more general homogeneous versus heterogeneous catalysis question*

#### 2.3.1. *The 1994 four-prong methodology*

Since it is central to the main unanswered question of industrial Ziegler–type hydrogenation catalysts, namely are they “homogeneous” or “heterogeneous” (or both), we conclude with a last section before the summary on the current methods and approaches to this historically challenging, if not perplexing, research question. In 1994, a *multi-pronged* approach with kinetic studies at its heart<sup>19</sup> was published [12]. That approach emphasizes using multiple analytical techniques and the requirement that any proposed explanation of the catalyst must satisfy *all* the data [13,16]. The approach has been shown to be successful in addressing the homogeneous versus heterogeneous catalysis question on at least four occasions [12,15,17,18]. The approach was the outgrowth of a painstaking, 5-year study that eventually identified novel, highly stabilized, as well as highly catalytically active  $\text{P}_2\text{W}_{15}\text{Nb}_3\text{O}_{62}^{9-}$  polyoxoanion-stabilized  $\text{Ir}(\text{O})_{\sim 300}$  nanoclusters as the true catalyst in hydrogenation systems beginning with [(1,5-COD)Ir•  $\text{P}_2\text{W}_{15}\text{Nb}_3\text{O}_{62}^{8-}$ ] as precatalyst under  $\text{H}_2$  and in the presence of cyclohexene, Figure 6.

---

<sup>19</sup> Support for the central importance of kinetic experiments in catalyst studies comes from, as Halpern put it, “the fact that catalysis is, by definition, purely a kinetic phenomenon” [89].

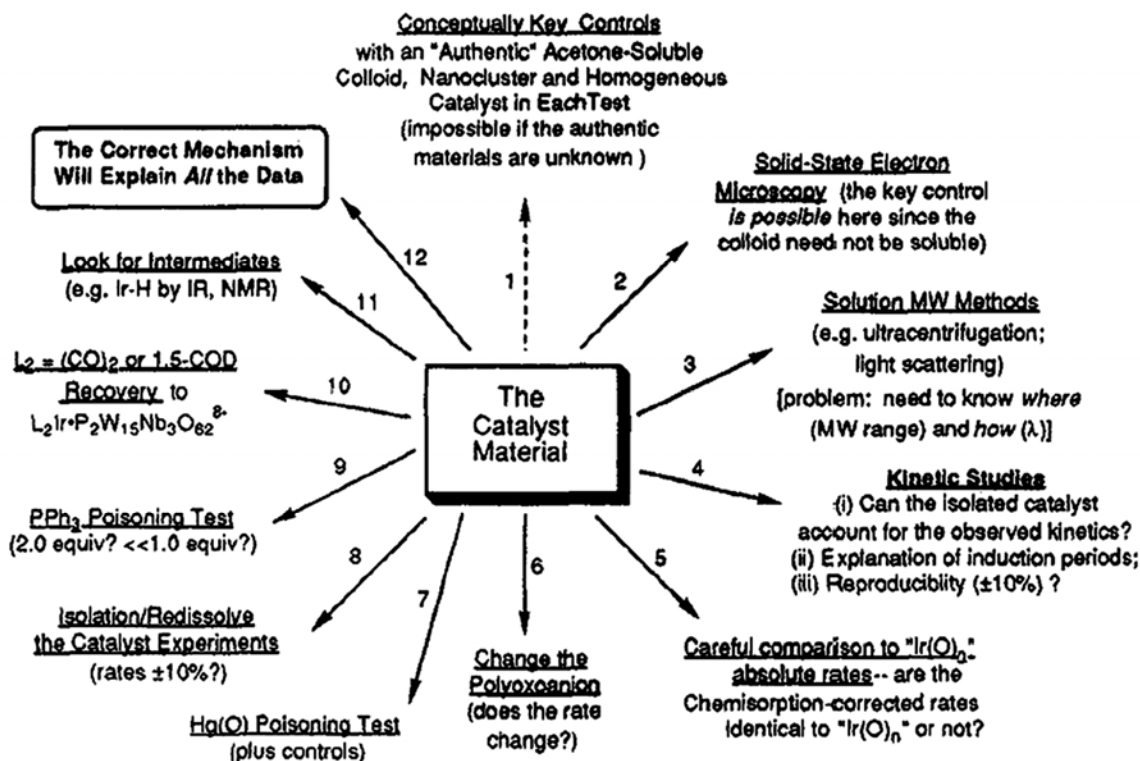


**Figure 6.** The multi-step approach developed for distinguishing homogeneous from heterogeneous catalysis in acetone-soluble Ir(0)<sub>n</sub> nanocluster systems formed from a [(1,5-COD)Ir<sup>1</sup>•P<sub>2</sub>W<sub>15</sub>Nb<sub>3</sub>O<sub>62</sub>]<sup>8-</sup> catalyst precursor under H<sub>2</sub> in acetone and in the presence of cyclohexene at room temperature [12]. Reprinted with permission.

A more general solution to the homogeneous vs. heterogeneous catalysis problem, diagrammed in a simplified form, Figure 7, resulted from that work because the polyoxoanion-stabilized nanoclusters turned out to be the most highly anionically stabilized nanocluster known at the time, and thus very "homogeneous-like" [12]. This extreme-case-developed methodology has since proven able to identify nanoparticle catalysts in at least 3 of 4 systems previously believed to be homogeneous catalysis [12,15,17,18]. The methodology even detected both homogeneous and nanocluster heterogeneous catalysis derived from a [Rh(C<sub>5</sub>Me<sub>5</sub>)Cl<sub>2</sub>]<sub>2</sub> system, in which the nature of the catalyst changed depending on the conditions used [17]. Note that the goal is not to try the impossibility of "proving" that Ziegler-type hydrogenation catalysts are

nanoclusters, but rather to have a way to rule out—that is to falsify, to disprove—all but one of the competing hypotheses for the nature of the true catalyst in a given system and for a specific set of conditions [143], leading to a set of data consistent with, and strongly supportive of, ideally one remaining hypothesis regarding the true catalyst(s). Figure 8 provides the most current, “6-prong approach” to the “is it homogeneous or heterogeneous catalysis?” question.

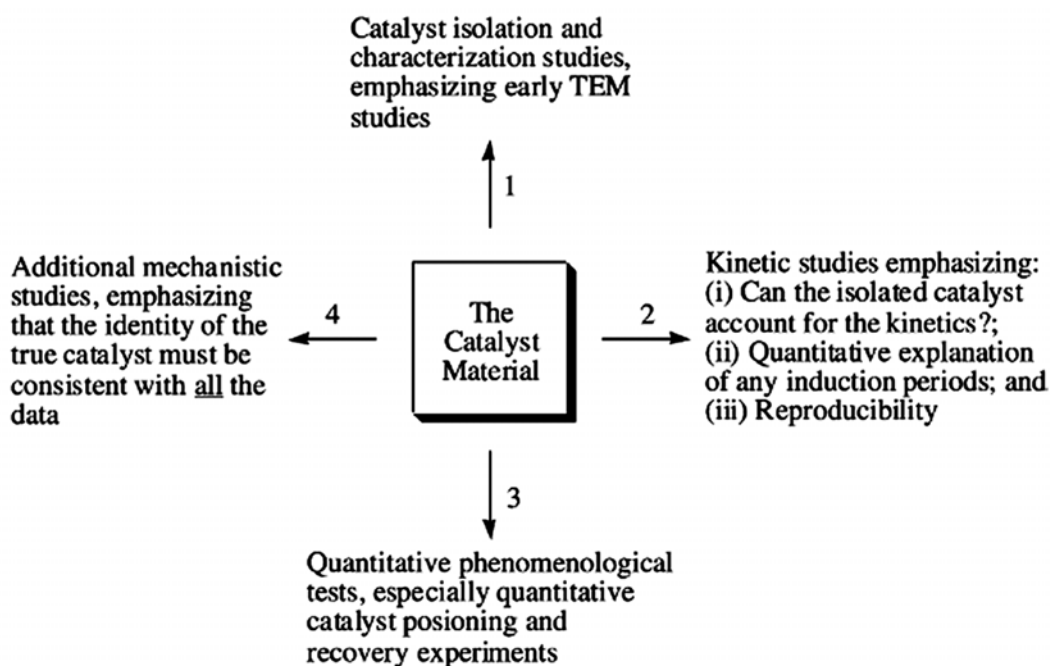


**Figure 7.** The 1994 four-prong generalized method for distinguishing homogeneous from nanocluster heterogeneous catalysts [12]. This scheme is a simplified version of the 12-step intellectual process and scheme shown in Figure 6 [12]. Reprinted with permission.

Because this methodology ideally involves the use of all relevant techniques with the realization that a proposed answer must explain all the data for a given system, any interpretation of the data is open to continued testing by use of new or improved analytical techniques. Re-interpretation would be necessary if new data is acquired that

is inconsistent with the existing explanation for the nature of the catalyst. There is an example of such an occurrence in the recent literature for researchers explicitly using the approach shown here [127,144], and a reexamination of the system using a different analytical technique, in this case XAFS [119,145]. This example serves to illustrate the importance of using all relevant, plus also kinetic studies, and understanding that any viable explanation must account for *all* the data on a given system.

### 2.3.2. *Special challenges with (first row, Ni, Co, Fe) Ziegler–type hydrogenation catalysts*

There are special challenges to answering the homogeneous versus heterogeneous catalysis question for (especially the first row, Ni, Co, Fe) Ziegler–type hydrogenation catalysts. These exist because Ziegler–type hydrogenation catalysts are: (i) notoriously sensitive to both the variables in their preparation (see section 2.1 above), and sensitive to conditions during characterization experiments; (ii) difficult to isolate for the needed kinetic studies; and (iii) prone to giving spurious results in poisoning experiments, especially since *selective* poisons for the  $\text{AlR}_3$ -derived component and, separately, for the transition-metal components are needed, but do not exist at present. Efforts to isolate Ziegler–type hydrogenation catalysts in their resting state have often met with failure (e.g.,  $\text{M}(\text{2-ethylhexanoate})_2$  plus  $m \text{ AlEt}_3$ ,  $\text{M} = \text{Ni}$  or  $\text{Co}$ ,  $m = 3\text{--}4$ , and  $\text{Co}(\text{stearate})_2$  plus  $2 \text{ AlEt}_3$  systems) [58,67]. Early successful efforts required use of non-Ziegler–type catalyst models such as  $[(\alpha,\alpha'\text{-bipyridyl})\text{NiMe}_2]$ , [4] or experiments under atypical conditions such as low temperatures [4,58,105]. The 2005 and 2006 work of Schmidt and coworkers [19,81,113], and 1999-2005 work of Bönemann and coworkers [121-

124,126], reports successful isolation of the catalyst-related material, and nanocluster materials, respectively. However, the handling procedures required for isolation of these materials, which often involves removal of the solvent under vacuum, washing the residue with hexane, and drying, may influence the nature of the material, the characterization results, or both [146]. This is especially true for the use of TEM, which despite some recent success [19,81,113,121-124,126], has also given results that were highly dependent on the method of sample preparation in some Ziegler-type catalyst systems [9]. Furthermore, and as already mentioned, without checking for artifacts when using TEM (by control experiments and complementary characterization techniques), misleading change in, or damage to, the sample from the electron beam of the TEM may occur and go undetected [17,127]. *This is especially true for TEM of Ziegler-type catalyst samples of the relatively light elements of Ni and Co*, which are more susceptible to certain types of TEM-beam-induced damage in addition to poor contrast and image quality [147].

Normally, quantitative catalyst poisoning experiments using established poisons such as CS<sub>2</sub> have the potential to give definitive results [148]. Less than 1 equivalent of poison should be needed to completely kill catalyst activity if the catalyst is a particle with only a fraction of transition metal atoms on its surface. However, if a full equivalent of poison is needed it may indicate a molecular homogeneous catalyst [16]. The use of such poisons with Ziegler-type hydrogenation catalysts is problematic because the Lewis acidic AlR<sub>3</sub> component can be expected to compete with the transition metal for the poison—again, ideally two types of selective poisons are needed. Attempts to use alcohol in catalyst poisoning led to contradictory results, as has already been discussed

[57,75,114]. Poisoning Ziegler-type hydrogenation catalysts with Hg(0)—a (non-definitive, but often useful) test of heterogeneous catalyst formation—suffers from the possibility that Hg(0) might also poison homogeneous complex catalysts or catalyst precursors [16]. Difficulties with the Hg(0) poisoning test have been discussed elsewhere [90]. Additionally, control experiments to illuminate or rule out these effects would need to take into account the fact that most Ziegler–type hydrogenation catalysts are rapidly pre-formed before use in hydrogenation.

Finally, the requirement that the correct explanation be consistent with all the data is an important, but tall order for Ziegler–type hydrogenation catalysts. A lot of conflicting data on what appears to be comparable systems exists. This requirement is, nevertheless, one that will have to be met before a systematic understanding of Ziegler–type hydrogenation catalyst systems is realized.

### *2.3.3. Conclusions for the section on the more general homogeneous versus heterogeneous catalysis question*

Despite the success of the 1994 approach in Figures 6 and 7, applying it toward determining the true nature of Ziegler–type hydrogenation catalysts is changing and upgrading that approach [53,54,55,56]. However, it must be remembered that the approach in Figures 6 and 7 is nothing more than a guideline for one’s own, creative thinking and approach for the specific, “true catalyst determination” problem and catalyst at hand. The central tenets of the methodology should still apply: (i) find what form or forms the precursor materials take in a sample of the resting state(s) of the catalyst; (ii) perform kinetic studies from resting state(s) to determine which are the kinetically

competent/dominant species; (iii) use all available/applicable techniques; and (iv) eliminate all reasonable alternative hypotheses to arrive at, ideally, a unique catalyst formulation that accounts for all the data.

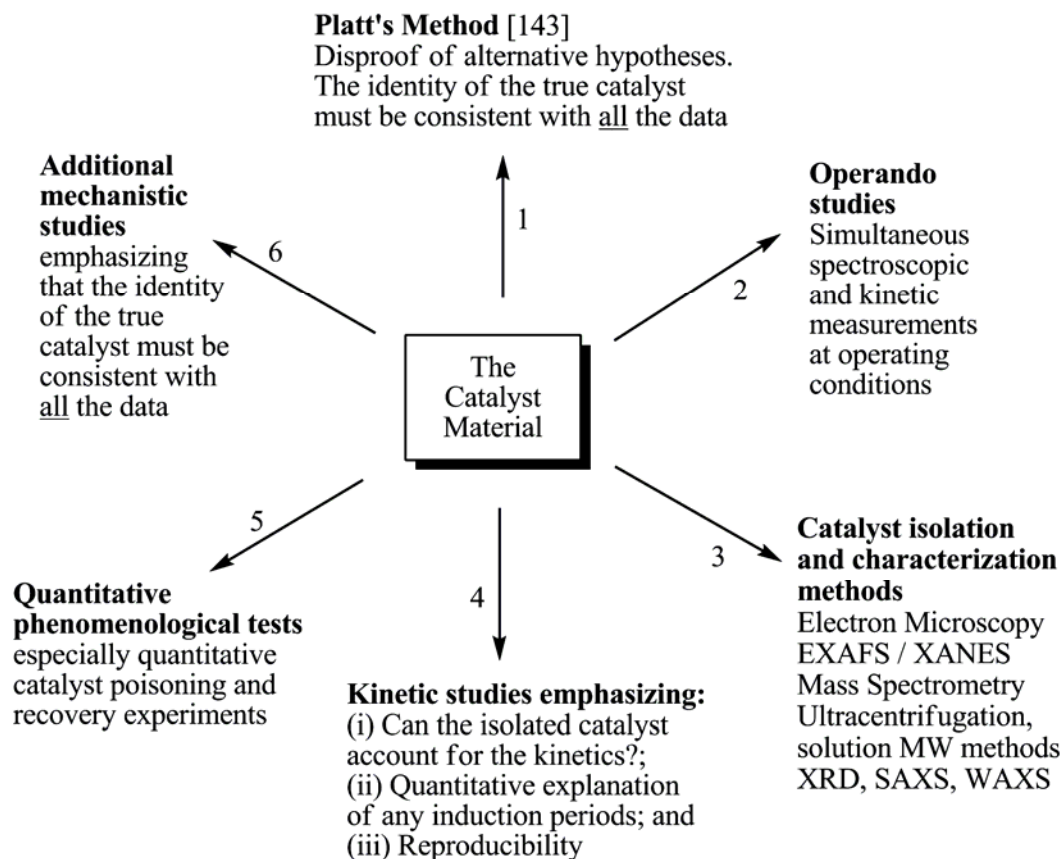


**Figure 8.** The updated “six-prong” approach for distinguishing homogeneous from heterogeneous catalysis, updated to include operando spectroscopy. The basic principles, however, remain the same: (i) find what form or forms the precursor materials take in a sample of the resting form(s) of the catalyst; (ii) perform kinetic studies from resting state(s) to determine which are the kinetically competent/dominant species; (iii) use all available/applicable techniques; and (iv) eliminate alternative hypotheses [143] to arrive at, ideally, a unique explanation that accounts for all the data.

The ideal goal in this updated approach to the “homogeneous versus heterogeneous catalysis” problem is the *simultaneous spectroscopic and kinetic analysis of a catalyst at the desired or normal operating conditions*, that is, via “operando”

spectroscopy (the term “operando” is from the Latin for “working” or “operating”) [149,150,151,152]. This combination overcomes weaknesses of using either kinetic [89,153] or spectroscopic analysis alone [152], especially if *multiple* spectroscopic techniques are simultaneously used [154]. However, the use of operando spectroscopy requires overcoming difficult challenges in experiment and reactor cell design [154]. Considerable challenges are likely to be encountered in any attempt to analyze Ziegler–type hydrogenation catalysts by operando spectroscopy. The use of an experimental setup, no matter how sophisticated, cannot supplant the importance of using Platt’s method of disproof of all reasonable alternative hypotheses [143].

### 3. Summary

The key points from the introduction section are:

- Ziegler–type hydrogenation catalysts made of group 8–10 transition metal precatalysts, particularly first row metal chelates or carboxylates, and  $\text{AlR}_3$  cocatalysts, are important for the industrial hydrogenation of a variety of unsaturated organic compounds, including diene polymers. Ziegler–type *hydrogenation* catalysts should *not* be confused with Ziegler–Natta *polymerization* catalysts, which were not a part of this review.
- Despite their relatively long history of industrial use, there is a need for an improved fundamental understanding of Ziegler–type hydrogenation catalysts. That improved understanding should, in turn, drive further *rationally-directed* synthetic, mechanistic, and industrial improvements.

- The key general areas investigated in the literature can be categorized as: (i) the variables important to catalyst synthesis and their effect on catalyst properties, particularly hydrogenation activity, (ii) the reaction between the transition metal precatalyst and cocatalyst components, (iii) the compositional and structural nature of the active catalyst species, and (iv) the mechanism of catalytic hydrogenation.

The main findings from the section on catalyst preparation variables are:

- The most important variables of catalyst preparation appear to be: (i) the identities of the transition metal precatalyst and the organometallic cocatalyst; (ii) the ratio of these two components and the role of impurities, particularly H<sub>2</sub>O; (iii) the solvent; (iv) the identity of the substrate; (v) the details of component addition (such as order and rate, presence of substrate, atmosphere, and temperature); and (vi) the aging of prepared catalyst before use in hydrogenation reactions.
- Catalysts made from Ni or Co precursors are favored by industry. They tend to have the highest activities, and have an advantageous balance of desirable properties, low cost, and relative ease of preparation.
- The anions present are another important aspect of the identity of the precatalysts. Anions such as 2-ethylhexanoate and acac are the most popular for use and study. The activity of catalysts made with these precursors appears to be positively correlated to their solubility. Some precatalyst anions, especially halogens, reduce catalyst activity, likely by acting as poisons.

- Short chain  $\text{AlR}_3$  cocatalysts, particularly  $\text{AlEt}_3$ , are most commonly used. The preferred cocatalyst varies with the particular system.
- One of the main variables appears to be the Al/M ratio. Most studies seem to agree that there is an optimum Al/M ratio for most systems. The optimum Al/M ratio has been reported to exist due to incomplete activation at too low Al/M and poisoning by excess  $\text{AlR}_3$  at high Al/M. Water and other impurities have been reported to have both beneficial and detrimental effects, depending on the particulars of the system being studied, and appear to affect the optimum Al/M ratio. The optimum Al/M ratio is one of the areas where a greater fundamental understanding of the nature of the catalyst for each given system could help to make sense of the range of results observed in the literature.
- The other variables involved in catalyst preparation (the solvent, the substrate, the order and rate of component addition, the presence or absence of substrate, the atmosphere, the temperature, and catalyst aging before use) are not universally agreed to be important. However, in most cases, they have been reported as having an effect on the activity of the resulting catalyst, but generally less so than the identity of the catalyst precursors, the Al/M ratio, and the amount of  $\text{H}_2\text{O}$  present. Many variables are likely connected to each other in complicated ways, such as the Al/M ratio and the amount of  $\text{H}_2\text{O}$ , but these relationships are incompletely understood.
- Mass transfer limitations should be suspected in many studies for these active catalysts, and unless the control experiments designed to rule out MTL were specifically done and reported in detail. This is especially true for instances

where reports claim that certain catalyst preparation variables were not important to catalytic activity, but other reports claim that they are.

- The ability to explain the effects of variables in the preparation of Ziegler–type hydrogenation catalysts is hampered by the fact that the effects themselves are often dissimilar for ostensibly similar, but in fact different systems. Answers as to *how* variables in catalyst synthesis affect catalytic activity are needed and are possible from studies of the ways in which each variable affects the mechanism of formation, composition, and resultant structure of the catalyst. Ultimately being able to connect the variables to catalyst activity, composition, structure and formation mechanism remains a significant challenge.

The main findings from the section on the nature and mechanism of formation of Ziegler–type hydrogenation catalysts are:

- The most important unknowns in Ziegler–type hydrogenation catalysis are the reaction between the catalyst precursors, whether the resulting catalysts are homogeneous or heterogeneous, and the details of the mechanism of catalytic hydrogenation? The most important of these questions is the nature of the true catalyst. Specific questions in this regard include: (i) how is the catalyst formed, (ii) how many transition metal atoms constitute the active catalyst species, (iii) what are their oxidation states, and (iv) what is the composition, structure, and role of the cocatalyst?
- Ziegler assumed early on that the catalyst of the Ni effect took the form of colloidal Ni. Early efforts by Wilke and coworkers attempted to disprove this,

and to show that the catalyst could be a homogeneous allyl-complex. That classic work laid the groundwork for subsequent researchers of Ziegler-type *hydrogenation* catalysts to propose homogeneous catalysts for those systems. More recent research, with the aid of much improved instrumentation technology and improved precedent for hydrocarbon-soluble colloids, has obtained results that suggest the true catalysts are heterogeneous, what we have termed herein as “Ziegler nanoclusters.”

- Definitive *kinetic* evidence remains to be reported for many Ziegler-type hydrogenation catalyst systems. Without that data, the homogeneous versus heterogeneous catalysis question cannot be answered.
- It may be that no single type of catalyst results for Ziegler-type hydrogenation catalyst systems. Small but important differences in outwardly similar systems may cause fundamental differences in the type(s) of catalyst(s) present. This, in turn, reveals the importance of using well-defined catalyst precursors, and carefully controlled conditions, in the needed studies attempting to identify the true catalyst(s). Additionally, some Ziegler-type hydrogenation catalyst systems may *simultaneously* contain catalytically active homogeneous *and* heterogeneous components. If so, it will take an extraordinarily careful, comprehensive, and detailed effort, all on the right/“best” system, to definitively support this particular hypothesis.

The key messages from the section taking a closer look at the more general homogeneous versus heterogeneous catalysis question are:

- A multi-pronged approach, demonstrated on multiple occasions to be successful, exists for distinguishing between homogeneous versus heterogeneous catalysis. Explicit application of that approach in addressing the homogeneous versus heterogeneous catalysis question for Ziegler–type hydrogenation catalysts, is proving useful in work underway [53,54,55,56].
- There are special challenges to answering the homogeneous versus heterogeneous catalysis question for Ziegler–type hydrogenation catalysts: (i) they are typically very sensitive to both the variables in their preparation, and conditions during characterization experiments; (ii) they have been difficult to isolate for the needed kinetic studies; and (iii) poisons selective for each of the metal and Al-based components do not currently exist.
- The multi-pronged approach to the homogeneous versus heterogeneous catalysis problem has been updated to include operando spectroscopy for catalyst characterization.

We would like to end by noting that, despite the many challenges summarized in this review, Ziegler–type hydrogenation catalysts hold considerable promise for other applications. Ziegler-type hydrogenation catalysts are, despite the homogeneous versus heterogeneous catalysis question, largely unrecognized as hydrocarbon soluble, readily self-assembled catalysts with neutral charge, high activity, and long lifetime, at least in many of the cases examined herein. Additional catalytic application, fundamental kinetic, spectroscopic, as well as other studies are strongly encouraged, regardless of whether Ziegler nanoclusters are the true catalysts in all, or even selected, cases.

## Acknowledgements

Financial support was provided by NSF Grant CHE-0611588.

## Appendix A. Supplementary data

Supplementary data associated with this article can be found, in the online version, at doi: 10.1016/j.molcata.2009.07.007.

## Appendix B

See Tables B.1–B.3.

**Table B.1.** Patent Literature

Authors (Year)	Catalyst Systems	Other Variables in Catalyst Synthesis	Ref.
Breslow and Matlack (1963)	Ti( <i>i</i> -Pr) <sub>4</sub> , V( <i>n</i> -Bu) <sub>3</sub> , Cr(acac) <sub>3</sub> , MoO <sub>2</sub> (acac) <sub>2</sub> , Mn(acac) <sub>3</sub> , Ru(acac) <sub>3</sub> , Co(acac) <sub>3</sub> , Fe(acac) <sub>3</sub> , Ni(acac) <sub>2</sub> , or Pd(acac) <sub>2</sub> + Al( <i>i</i> -Bu) <sub>3</sub>	<i>Solvent</i> : <i>n</i> -heptane, or heptanes. <i>Hydrogenation Substrate</i> : Cyclohexene, 1-octene, ethynylbenzene, polyisoprene rubber, 2-methylbutene-2, hexane-1, or tetramethylethylene. <i>Order of addition</i> : cocatalyst added to the precatalyst in both the presence and absence of substrate. <i>Synthesis atmosphere</i> : H <sub>2</sub> gas at 50 psi, 43 psi, 40 psig, 21 psig, or 35 psig. <i>Synthesis temp</i> : room temp, 40 °C, 50 °C, 30 °C.	59
Laporte, S. (1965)	Ni(acac) <sub>2</sub> , Fe(acac) <sub>2</sub> , Ni(benzoate) <sub>2</sub> , Ni(acac) <sub>2</sub> , Cr(acac) <sub>2</sub> , Co(acac) <sub>2</sub> , or Cu(acac) <sub>2</sub> + 1–5, 8 or 30 AlEt <sub>3</sub> or BEt <sub>3</sub>	<i>Solvent</i> : Benzene. <i>Hydrogenation Substrate</i> : Benzene, <i>o</i> -xylene, 1,3-butadiene, 4-vinylcyclohexane, 1,5,9-cyclododecatriene, naphthalene, methyl ethyl ketone, maleic anhydride, cinnamic acid, benzoic acid, dimethyl terephthalate, benzaldehyde, dimethylphthalate, phenol, nitrocyclohexane, isophthalonitrile, pyridine, aniline, nitrobenzene, 3-hexyne. <i>Order of addition</i> : cocatalyst added to precatalyst in the presence of substrate. <i>Synthesis atmosphere</i> : N <sub>2</sub> ; <i>Synthesis temp</i> : –50 °C to 200 °C	72
Kroll	Co(acac) <sub>2</sub> , Fe(acac) <sub>n</sub>	<i>Solvent</i> : Heptane, dimethoxyethane, triethylamine, benzene,	64

Authors (Year)	Catalyst Systems	Other Variables in Catalyst Synthesis	Ref.
(1968)	Ni(acac) <sub>n</sub> , Pt(acac) <sub>n</sub> , Cr(acac) <sub>n</sub> , V(acac) <sub>n</sub> <sup>a</sup> + 4, 6, 8, 10 or 35 Al(i-Bu) <sub>3</sub> , AlEt <sub>2</sub> (n-BuO), AlMe <sub>2</sub> (acac), AlEt <sub>3</sub> , or AlH(i-Bu) <sub>2</sub> , Al(i-Bu) <sub>3</sub> - p-dioxane, AlEt <sub>2</sub> Cl/AlEtCl <sub>2</sub>	decane, p-dioxane, p-xylene, pentane, ether, dimethoxyethane. <i>Hydrogenation Substrate:</i> Cyclohexene, cis, trans,trans-cyclododecatriene, benzonitrile, quinoline, cyclopentadiene, benzophenone, 4-vinylcyclohexene, phenylacetylene, 1-hexene, n-methylmorpholine, anisole, diphenylether, cyclododecatriene, octyne-4, dicyclopentadiene, cyclooctadiene, 3-methyl-1-butene, 2-methyl-2-butene. <i>Order of addition:</i> Precatalyst + cocatalyst (substrate is not mentioned). <i>Synthesis atmosphere:</i> N <sub>2</sub> . <i>Aging:</i> Overnight, or 5 min. Additional notes: "The stability and/or activity of Ziegler-type catalysts is markedly improved by the addition of a third component, i.e., Lewis base such as p-dioxane or SEt <sub>2</sub> , weak organic acid such as n-butanol or t-butylalcohol, oxygen, to the catalyst system."	
Yoshimoto et al. (1970)	Ni naphthenate, Co(acac) <sub>n</sub> , <sup>a</sup> Fe naphthenate, bis (salicylaldehyde)Ni, Ni cyclohexylcarboxylate, Co octanoate, or Co naphthenate + 3, 4, or 12 AlEt <sub>3</sub> , MgEt <sub>2</sub> , (n- Bu)Li, or LiAlH <sub>4</sub> , Ni benzenesulphonate or Ni p-toluene sulfonate + AlEt <sub>3</sub>	<i>Solvent:</i> Toluene, hexane, tetrahydrofuran, or n-hexane. <i>Hydrogenation Substrate:</i> Butadiene units of styrene butadiene copolymer. <i>Order of addition:</i> Precatalyst and cocatalyst are mixed in the presence of olefinically unsaturated hydrocarbon which does not act as hydrogenation substrate. <i>Synthesis atmosphere:</i> N <sub>2</sub> or H <sub>2</sub> . <i>Synthesis temp:</i> 30 °C, 29 °C, 28 °C, 80 °C, 50 °C, -78 °C. <i>Aging:</i> 5 min. Additional notes: An olefinically unsaturated hydrocarbon such as cyclohexene, 1-heptene, dicyclopentadiene, styrene or 1,7-octadiene, is added to the reaction medium to form the, so called, "three components catalyst." The use of olefinically-unsaturated hydrocarbon becomes increasingly important to the production of an effective and stable catalyst as temperatures are increased from 0–100 °C. Excess unsaturated hydrocarbon causes an, "undesirable induction period due to the auxiliary reaction in the catalyst formation."	68
Yoshimoto et al. (1970)	Ni naphthenate, Co naphthenate, bis(ethylacetoacetate) Ni, bis(acetylacetone) Ni, Fe naphthenate, Ni	<i>Solvent:</i> Toluene. <i>Hydrogenation Substrate:</i> Styrene butadiene copolymer, or polybutadiene. <i>Order of addition:</i> Substrate + H <sub>2</sub> (gas) + precatalyst and cocatalyst (order of addition of precatalyst or cocatalyst is not given). <i>Synthesis atmosphere:</i> H <sub>2</sub> . <i>Synthesis temp:</i> 30 °C. <i>Aging:</i> 5 min.	60

Authors (Year)	Catalyst Systems	Other Variables in Catalyst Synthesis	Ref.
	2-ethylhexanoate, or Co 2-ethylhexanoate + 0.6, 1.3, 2.7, 4.0, or 6.7 (n-Bu)Li, or MgEt <sub>2</sub>	Additional notes: Presence or absence of polymer to be hydrogenated is not an important factor in catalyst preparation.	
Wald and Quam (1971)	Ni acac + 2 AlEt <sub>3</sub> or Al(i-Bu) <sub>3</sub>	<i>Solvent:</i> Cyclohexane. <i>Hydrogenation Substrate:</i> Polystyrene-polyisoprene-polystyrene block copolymer. <i>Synthesis temp:</i> 40 °C. <i>Aging:</i> >15 min. Additional notes: Selectively hydrogenates the diene portions of block copolymers without hydrogenating the vinyl aromatic portions thereby reducing oxygen sensitivity, and without “appreciable degradation” (chain scission).	65
Wald and Quam (1972)	Ni octoate, or Ni acac + 2, or 3 AlEt <sub>3</sub>	<i>Solvent:</i> Cyclohexane. <i>Hydrogenation Substrate:</i> Polystyrene-poly(styrene/isoprene) copolymer. <i>Order of addition:</i> Substrate + H <sub>2</sub> (gas) + pre-prepared catalyst (order of addition of precatalyst and cocatalyst is not given), or precatalyst + cocatalyst + substrate. <i>Synthesis temp:</i> 250 °C. <i>Aging:</i> 15 min. Additional notes: Provides selectively hydrogenated block copolymers with improved processability with minimum degradation of the polymers in the form of chain scission by the hydrogenation catalyst.	66
De La Mare (1973)	Ni(octoate) <sub>2</sub> or Co(2-ethylhexanoate) <sub>2</sub> + 2.5 AlEt <sub>3</sub>	<i>Solvent:</i> Isooctane/cyclohexane. <i>Hydrogenation Substrate:</i> Butadiene-2-vinylpyridine copolymer. <i>Order of addition:</i> Substrate + solvent + pre-prepared catalyst (order of addition of precatalyst and cocatalyst is not given) + H <sub>2</sub> (gas); <i>Synthesis temp:</i> 25 °C, or 170 °C. Additional Notes: Treatment of copolymers containing blocks from polar monomers with 1–3 moles of a Lewis acid, preferably BF <sub>3</sub> , per polar group facilitates hydrogenation. Without this treatment it is not possible to use these catalysts to hydrogenate polar copolymers.	76
Loveless et al. (1976)	Ni acac, Ni naphthenate, or Fe(acac) <sub>3</sub> + 0.8, 3.0, 3.3, 6.0 or 10.0 (n-Bu)Li	<i>Solvent:</i> n-heptane, or cyclohexane. <i>Hydrogenation Substrate:</i> Polyisoprene, sulfur vulcanizable elastomers, or 1-octene. <i>Order of addition:</i> Precatalyst + substrate + H <sub>2</sub> (gas) + cocatalyst. <i>Rate of addition:</i> Cocatalyst is slowly added (i.e. 250 mmoles of (n-Bu)Li is added over 10 min). <i>Synthesis</i>	77

Authors (Year)	Catalyst Systems	Other Variables in Catalyst Synthesis	Ref.
		<i>atmosphere:</i> H <sub>2</sub> . <i>Synthesis temp:</i> room temp. <i>Aging:</i> 10 min. Additional Notes: A phenolic substance, such as p-nonyl phenol, is added to the precatalyst solution to produce soluble organometallic complex before the addition of other catalyst components. A claim is that this catalyst is superior to previous ones in, “degree and rapidity of hydrogenation which is possible.” There is no upper limit to the amount of cocatalyst that can be used, but there is no benefit to using more than the amount prescribed. “The catalyst is not sensitive to small traces of impurities such as water.”	
Baumgartner and Balas (1976)	Ni(2-ethylhexanoate) <sub>2</sub> + 2.5 or 3.0 AlEt <sub>3</sub>	<i>Solvent:</i> Cyclohexane. <i>Hydrogenation Substrate:</i> Styrene-isoprene copolymer. <i>Synthesis temp:</i> 80 °C. Additional Notes: Excess AlEt <sub>3</sub> was added after the reduction of the substrate was completed to some extent. This addition interrupted the hydrogenation. The addition of 2-ethylhexanol after the interruption caused the hydrogenation to resume.	82
Ladenberger et al. (1980)	Ni(acac) <sub>2</sub> + Al(i-Bu) <sub>3</sub>	<i>Solvent:</i> Toluene, hexane. <i>Hydrogenation Substrate:</i> Butadiene-styrene copolymer. <i>Synthesis atmosphere:</i> H <sub>2</sub> . <i>Synthesis temp:</i> 25 °C to 30 °C. Additional Notes: A more active catalyst is achieved through the addition of H <sub>2</sub> O after reaction of the precatalyst, cocatalyst and the substrate. H <sub>2</sub> uptake frequently only starts after the H <sub>2</sub> O addition. Aromatics are more readily hydrogenated if a high Al/M is used.	78
Durand et al. (1981)	Two metal chelate compounds: the first of Co or Ni, and the second of another metal Fe, Zn, Zr, Mn, Mo (all preferably acac or carboxylates), + 1.5 to 6 AlEt <sub>3</sub> , Al(i-Bu) <sub>3</sub> or LiBu	<i>Solvent:</i> Heptane, cyclohexanol, decahydronaphthalene, benzene, diisopropylether. <i>Hydrogenation Substrate:</i> Bis phenol A, phenol, cyclododecatriene, benzene, propionitrile, oleonitrile, adiponitrile. <i>Order of addition:</i> Substrate + pre-prepared catalyst (order of addition of the precatalysts and the cocatalyst is not given), or Substrate + Catalyst 1 (precatalyst 1 + cocatalyst) + Catalyst 2 (precatalyst 2 + cocatalyst). <i>Synthesis temp:</i> 90 °C. Additional Notes: if the metal salts were reacted separately with the same cocatalyst, an inferior catalyst, or even non-active solution will result. The mode of	155

Authors (Year)	Catalyst Systems	Other Variables in Catalyst Synthesis	Ref.
		catalyst preparation is not critical, but is preferably carried out in the absence of substrate in most cases.	
Willis et al. (1990)	Ni 2-ethylhexanoate + 6 or 2.3 (s-Bu)Li or AlEt <sub>3</sub>	<i>Solvent:</i> Cyclohexane, tetrahydrofuran. <i>Hydrogenation Substrate:</i> Two different styrene butadiene block copolymers. <i>Order of addition:</i> Substrate + catalyst (order of addition of precatalyst and cocatalyst is not given). <i>Synthesis temp:</i> 47 °C, room temp. Additional Notes: Water should be present when the precatalyst and the cocatalyst are combined. Catalysts so prepared are suitable for hydrogenating polymers containing acidic functionality when certain other procedures are followed. Without said procedures (the focus of the patent), acidic functional groups interfere with the hydrogenation reaction by catalyst deactivation and/or gelling of the polymer solution.	61
Abraham et al. (1991)	Fe, Co or Ni halides, acetates, or acacs Co(neodecanoate) <sub>2</sub> or Pd(PPh <sub>3</sub> ) <sub>4</sub> , Pt(PPh <sub>3</sub> ) <sub>4</sub> , or Rh(PPh <sub>3</sub> ) <sub>3</sub> + 4 AlR <sub>3</sub> where each R = alkyl has 1–4 C atoms	<i>Solvent:</i> Toluene. <i>Hydrogenation Substrate:</i> Butadiene-methacrylate copolymer. <i>Order of addition:</i> Precatalyst + cocatalyst added over substrate. <i>Synthesis atmosphere:</i> N <sub>2</sub> . <i>Synthesis temp:</i> room temp. <i>Aging:</i> 1 h. Additional Notes: The use of a complexing agent, such as phosphines (R <sub>3</sub> P) or phosphites ((RO) <sub>3</sub> P), is necessary in catalysis of hydrogenation of high MW nitrile-butadiene rubber (NBR) random copolymers. Without the complexing agent, gelation occurs due to complexation of the transition metal catalyst to the polar groups on the polymer chains.	44
Hoxmeier and Slaugh (1991)	Nickel 2-ethylhexanoate + 1, 2, 3, 4, 7, or 10 MAO (Methylalumoxane) or EAO (Ethylalumoxane), an equimolar blend of MAO/EAO, or AlEt <sub>3</sub>	<i>Solvent:</i> Cyclohexane. <i>Hydrogenation Substrate:</i> Polystyrene-polybutadiene-polystyrene triblock copolymer. <i>Order of addition:</i> Substrate + catalyst (order of addition of precatalyst and cocatalyst is not given). <i>Synthesis temp:</i> 25 °C. <i>Aging:</i> 30 min. Additional Notes: 0.5 equivalents of H <sub>2</sub> O is present in the precatalyst solution. Catalysts made in this manner with MAO offer improved control over the extent of hydrogenation in polymers containing both ethylenic and aromatic unsaturation by an initially slower hydrogenation reaction, but compared to similar catalysts made with AlR <sub>3</sub> , retain higher activities over longer time spans. However, the	62

Authors (Year)	Catalyst Systems	Other Variables in Catalyst Synthesis	Ref.
		catalyst formed with longer alkyl chain alumoxanes (C <sub>2</sub> -C <sub>8</sub> ) are more active for hydrogenation at all times than similar catalysts made with AlR <sub>3</sub> .	
Coolbaugh et al. (1991)	Ni(octoate) <sub>2</sub> or Ti(n-Bu) <sub>4</sub> + 3.6, 2.5, or 6.0 AlEt <sub>3</sub>	<i>Solvent:</i> Cyclohexane. <i>Hydrogenation Substrate:</i> Isoprene-Butadiene-isoprene triblock copolymer. <i>Order and rate of addition:</i> Precatalyst + cocatalyst, 20.80 mL of cocatalyst is added as quickly as possible (i.e. in 15 sec); or solvent + precatalyst and cocatalyst simultaneously added over 25 min. The catalyst solutions prepared as above are added over substrate. <i>Synthesis atmosphere:</i> N <sub>2</sub> . <i>Aging:</i> 10 min. Additional Notes: The molar ratio of the transition metal compound to the cocatalyst should be kept essentially constant by either simultaneous addition of solutions of the two, or by as rapid addition of the cocatalyst as possible. If added over the course of more than about 15 min a less selective catalyst results, which may also ppt. from solution. The reversal of the addition sequence is likewise detrimental. "Extreme care must be used to exclude air, moisture and other impurities capable of interfering with the delicate chemical balance involved in the synthesis of the catalyst."	63
Goodwin and Willis (1992)	Ni(2-ethylhexanoate) <sub>2</sub> + 2.6 AlEt <sub>3</sub>	<i>Solvent:</i> Cyclohexane. <i>Hydrogenation Substrate:</i> Polyisoprene, or polybutadiene. Additional Notes: Complete hydrogenation of olefinic unsaturation in low molecular weight diene polymers, particularly those having terminal hydroxyl groups, is achieved (previously not possible using these catalyst systems) by removing fine particles of ionic Li residues such as LiOR and LiOH through filtering or decanting the polymer solutions prior to hydrogenation.	73
Hergenrother et al. (1994)	Ni octoate + 3, 6, 7 Al(i-Bu) <sub>3</sub> , or AlEt <sub>3</sub>	<i>Solvent:</i> Hexane, toluene. <i>Hydrogenation Substrate:</i> Polybutadiene. <i>Order of addition:</i> Precatalyst + cocatalyst. The catalyst solution added over the substrate. <i>Synthesis atmosphere:</i> H <sub>2</sub> . <i>Synthesis temp:</i> -25 °C, or 66 °C. <i>Aging:</i> 1 h. Additional Notes: Cyclohexene is added to precatalyst solution before cocatalyst addition to stabilize the catalyst prior to hydrogenation. Hydrogenation saturation controlled	45

Authors (Year)	Catalyst Systems	Other Variables in Catalyst Synthesis	Ref.
		by treating polymers with an arylphosphine in the presence of the hydrogenation catalyst. The order of reagent addition is unimportant with either the precatalyst or the cocatalyst added incrementally throughout the hydrogenation reaction.	
Handlin et al. (1995)	Ni 2-ethylhexanoate + 2.6 AlEt <sub>3</sub>	<i>Solvent:</i> Cyclohexane. <i>Hydrogenation Substrate:</i> Polybutadiene. Additional Notes: the catalyst is used to hydrogenate butadiene polymers having terminal functional groups to give low viscosity polymers.	74
Johnson et al. (2002)	Co neodecanoate, or Ni octoate + 2.0, 2.2, or 1.3 AlEt <sub>3</sub>	<i>Solvent:</i> Cyclohexane, diethylether. <i>Hydrogenation Substrate:</i> Linear triblock copolymer of styrene and ethylene/butadiene, polystyrene-polybutadiene-polystyrene triblock copolymer, or linear polystyrene-polyisoprene-polystyrene-polyisoprene block copolymer. <i>Order and rate of addition:</i> The catalyst is prepared by slowly adding cocatalyst over the precatalyst in the absence of substrate.	46

<sup>a</sup> The “n” values of the precatalyst components are not given; they may be the same or different in different transition metal precatalyst compounds.

**Table B.2.** Nature and Mechanism of Formation of the Catalyst – the “Ziegler-type Catalysts are Homogeneous” Hypothesis

Authors (year)	Catalyst Systems	Results	Ref.
Wilke and coworkers (1973)	Ni(acac) <sub>2</sub> + AlMe <sub>3</sub> , AlEt <sub>3</sub> or Al(i-Bu) <sub>3</sub>	A homogeneous Ni(0) complex formed as a result of the reaction of Ni-olefin $\pi$ -complex with Al cocatalyst. The resulting complex is proposed to contain multicenter bonds including C, Ni(0), and Al atoms.	4
Sloan <i>et. al.</i> (1963)	Fe(acac) <sub>3</sub> , Co(acac) <sub>2</sub> , Co(acac) <sub>3</sub> , Ni(acac) <sub>2</sub> , Ru(acac) <sub>3</sub> , or Pd(acac) <sub>2</sub> + AlEt <sub>3</sub> , Al(i-Bu) <sub>3</sub> , or AlH(i-Bu) <sub>2</sub>	M-H species, given as MHX <sub>n-1</sub> , are claimed as the active catalyst. The M-H species are proposed to form by alkylation and then hydrogenolysis of the precatalyst.	57
Laporte (1969)	Ni(2-ethylhexanoate) <sub>2</sub> , or Co(2-ethylhexanoate) <sub>2</sub> + 3-4 AlEt <sub>3</sub>	Mononuclear H-M(0) -L species, L = labile -H, -R, solvent, olefin, or AlEt <sub>2</sub> (2-ethylhexanoate), is	58

Authors (year)	Catalyst Systems	Results	Ref.
		proposed as the catalyst. However, binuclear M(I) is not ruled out.	
Klinedinst and Boudart (1973)	Fe(acac) <sub>3</sub> + 6 AlEt <sub>3</sub>	Mössbauer spectroscopy shows that high spin Fe(II) are the only Fe species present at low temp. Rules out catalysis by (crystalline) metallic Fe particles ≥ 1.7 nm in diameter.	105
Alvanipour and Kispert (1988)	Co(stearate) <sub>2</sub> + 2 AlEt <sub>3</sub>	Homogeneous M(0) species are proposed to form via unstable ethyl–Ni (L <sub>3</sub> Ni–Et) and/or Ni–H (L <sub>2</sub> Ni–H–C=C) where L: solvent, CH <sub>2</sub> =CH <sub>2</sub> or RCO <sub>2</sub> AlEt <sub>2</sub> .	67
Reguli and Stasko (1987)	Ni(3,5-diisopropylsalicylate) <sub>2</sub> , Ni(acac) <sub>2</sub> , Ni(stearate) <sub>2</sub> , or Ni(benzohydraxamate) <sub>2</sub> + AlEt <sub>3</sub> , Al( <i>i</i> -Bu) <sub>3</sub> , or BuLi	Homogeneous diamagnetic Ni(II) formed by alkylation of the transition metal precatalyst is suggested as the active catalyst species. Ni colloid formation is observed in the presence of aromatic compounds.	70
Barrault et al. (1994)	Co(acac) <sub>2</sub> + AlEt <sub>3</sub>	Co(0) clusters, and Co(0) complexes are simultaneously present, neither of which can be ruled out as active catalyst species.	37
Shmidt and coworkers (1970, 1979, 1983)	Co(acac) <sub>2</sub> , Co(acac) <sub>3</sub> , Ni(acac) <sub>2</sub> , Fe(acac) <sub>3</sub> or Pd(acac) <sub>2</sub> + AlEt <sub>3</sub> , AlMe <sub>3</sub> , n-BuLi, n-PrMgBr or <i>i</i> -PrMgBr	A paramagnetic homogeneous Co(0) complex, stabilized by arene solvent, R of AlR <sub>3</sub> and acac from the Co precatalyst is thought to be the active catalyst. Presence of low spin M(II) is not ruled out. In addition, ≤ 100 Å M(0) particles are observed.	42, 109, 110, 111

**Table B.3.** Nature and Mechanism of Formation of the Catalyst – the “Ziegler-type Catalysts are Heterogeneous” Hypothesis

Authors (year)	Catalyst Systems	Results	Ref.
Shmidt and coworkers (2005, 2006)	Co(acac) <sub>2</sub> , Co(acac) <sub>3</sub> , or Pd(acac) <sub>2</sub> + AlEt <sub>3</sub>	Observe ferromagnetic β-Co(0) <sub>n</sub> or Pd(0) <sub>n</sub> nanoparticles (1–5 nm) apparently stabilized by AlEt <sub>3</sub> , and/or acetylacetonate derivatives of AlEt <sub>3</sub> including AlEt <sub>2</sub> (acac) or alumoxanes. The Co(0) complex proposed previously as the active catalyst is reinterpreted as the precursor to Co(0) <sub>n</sub> nanoclusters.	19, 113, 81, 114

Pasynkiewicz et al. (1974)	$\text{Co}(\text{acac})_3 + 1 \text{ AlMe}_3$	A mixture of Co(II), Co(I) complexes and metallic Co(0) are reported. Suggest the true catalyst is metallic Co(0). The other reaction products proposed: $[\text{Co}(\text{acac})_2\text{CH}_3]$ , $(\text{CH}_3)_2\text{Al}(\text{acac})$ , $[(\text{acac})\text{Co}=\text{CH}_2]$ , $[\text{Co}(\text{acac})]$ , $[(\text{acac})\text{Co}(\text{CH}_3)_2]$ .	71
Goulon and coworkers (1984, 1986)	$\text{Ni}(\text{acac})_2$ , $\text{Ni}(\text{2-ethylhexanoate})_2$ , $\text{Co}(\text{2-ethylhexanoate})_2$ , or $\text{Fe}(\text{acac})_3 + \text{AlEt}_3$	$\text{M}(\text{O})_n$ clusters are proposed as catalysts. However, whether they are small ~4–10 atom clusters, amorphous M or M-carbide clusters, or some combination is unclear.	40, 116
Bonnemann and coworkers (1999-2005)	$\text{Ni}(\text{acac})_2 + 3 \text{ Al}(\text{i-Bu})_3$ , $\text{Pt}(\text{acac})_2$ , $+ 4 \text{ AlMe}_3$ , $[(1,5\text{-COD})\text{Pt}(\text{CH}_3)_2]$ $+ 10 \text{ AlEt}_3$ or $\text{Al}(\text{C}_8\text{H}_{17})_3$ , and a variety of other systems	$\text{M}(\text{O})_n$ amorphous nanoclusters stabilized by an organoaluminum multilayer are observed. Catalytic activities are not tested.	121, 122, 123, 124, 125, 126

## References

- [1] K. Ziegler, E. Holzkamp, H. Breil, H. Martin, *Angew. Chem.* 67 (1955) 541–547.
- [2] G. W. Parshall, S. D. Ittel, *Homogeneous Catalysis*, second ed., John Wiley & Sons, New York, 1992.
- [3] P. W. Jolly, G. Wilke, *The Organic Chemistry of Nickel*, Vol. II, Academic Press, New York, 1975.
- [4] K. Fischer, K. Jonas, P. Misbach, R. Stabba, G. Wilke, *Angew. Chem. Int. Ed.* 12 (1973) 943–953.
- [5] K. Ziegler, *Nobel Lectures, Chemistry 1963–1970*, Elsevier Publishing Company, Amsterdam, 1972.
- [6] N. T. McManus, G. L. Rempel, *J.M.S. Rev. Macromol. Chem. Phys.* 35 (1995) 239–285.
- [7] M. P. McGrath, E. D. Sall, S. J. Tremont, *Chem. Rev.* 95 (1995) 381–398.
- [8] H. Weiner, A. Trovarelli, R. G. Finke, *J. Mol. Catal. A: Chem.* 191 (2003) 217–252.
- [9] K. A. Johnson, *Polym. Prepr.* 41 (2000) 1525–1526.
- [10] J. P. Collman, L. S. Hegedus, J. R. Norton, R. G. Finke, *Principles and Applications of Organotransition Metal Chemistry*, University Science Books, Mill Valley, 1987.
- [11] J. Schwartz, *Acc. Chem. Res.* 18 (1985) 302–308.

- 
- [12] Y. Lin, R. G. Finke, *Inorg. Chem.* 33 (1994) 4891–4910.
- [13] J. D. Aiken III, Y. Lin, R. G. Finke, *J. Mol. Catal. A: Chem.* 114 (1996) 29–51.
- [14] K. S. Weddle, J. D. Aiken III, R. G. Finke, *J. Am. Chem. Soc.* 120 (1998) 5653–5666.
- [15] J. A. Widegren, M. A. Bennett, R. G. Finke, *J. Am. Chem. Soc.* 125 (2003) 10301–10310.
- [16] J. A. Widegren, R. G. Finke, *J. Mol. Catal. A: Chem.* 198 (2003) 317–341.
- [17] C. M. Hagen, J. A. Widegren, P. M. Maitlis, R. G. Finke, *J. Am. Chem. Soc.* 127 (2005) 4423–4432.
- [18] E. E. Finney, R. G. Finke, *Inorg. Chim. Acta* 359 (2006) 2879–2887.
- [19] L. O. Nindakova, F. K. Shmidt, V. V. Saraev, B. A. Shainyan, N. N. Chipanina, V. A. Umanets, L. N. Belonogova, D.-S. D. Toryashinova, *Kinetics and Catalysis* 47 (2006) 54–63.
- [20] H. Sinn, W. Kaminsky, *Adv. Organomet. Chem.* 18 (1980) 99–149.
- [21] P. Corradini, G. Guerra, L. Cavallo, *Acc. Chem. Res.* 37 (2004) 231–241.
- [22] R. H. Crabtree *The Organometallic Chemistry of the Transition Metals*, fourth ed., John Wiley & Sons, New York, 2005.
- [23] D. S. Breslow, N. R. Newburg, *Org. Bio. Chem.* 81 (1959) 81.
- [24] G. Natta, G. Mazzanti, *Tetrahedron* 8 (1960) 86–100.
- [25] W. P. Long, D. S. Breslow, *J. Am. Chem. Soc.* 82 (1960) 1953–1957.
- [26] A. Andresen, H.-G. Cordes, J. Herwig, W. Kaminsky, A. Merck, R. Mottweiler, J. Pein, H. Sinn, H.-J. Vollmer, *Angew. Chem. Int. Ed.* 15 (1976) 630–632.
- [27] L. Resconi, S. Bossi, L. Abis, *Macromolecules* 23 (1990) 4489–4491.
- [28] M. R. Mason, J. M. Smith, S. G. Bott, A. R. Barron, *J. Am. Chem. Soc.* 115 (1993) 4971–4984.
- [29] T. Sugano, K. Matsubara, T. Fujita, T. Takahashi, *J. Mol. Catal.* 82 (1993) 93–101.
- [30] A. R. Barron, *Organometallics* 14 (1995) 3581–3583.
- [31] D. W. Imhoff, L. S. Simeral, S. A. Sangokoya, J. H. Peel, *Organometallics* 17 (1998) 1941–1945.
- [32] A. R. Barron in: J. Scheirs, W. Kaminsky (Eds.), *Metallocene-based Polyolefins*, John Wiley & Sons, New York, 2000, pp. 33–67.
- [33] A. R. Barron, *Macromol. Symp.* 97 (1995) 15–25.
- [34] E. Y.-X. Chen, T. J. Marks, *Chem. Rev.* 100 (2000) 1391–1434.

- 
- [35] A. H. Tullo, Paying Attention to Activators. *Chemical and Engineering News* (Oct 22, 2001) 38–39.
- [36] A. Fischbach, F. Perdih, E. Herdtweck, R. Anwander, *Organometallics* 25 (2006) 1626–1642.
- [37] J. Barrault, M. Blanchard, A. Derouault, M. Ksibi, M. I. Zaki, *J. Mol. Catal.* 93 (1994) 289–304.
- [38] B. R. James, *Homogeneous Hydrogenation*, John Wiley & Sons, New York, 1973.
- [39] S. J. Lapporte, W. R. Schuett, *J. Org. Chem.* 28 (1963) 1947–1948.
- [40] C. Esselin, E. Bauer-Grosse, J. Goulon, C. Williams, Y. Chauvin, D. Commereuc, E. Freund, *J. Phys. Colloques* 47 (1986) C8-243–C8-248.
- [41] W. Keim, *J. Mol. Catal.* 52 (1989) 19–25.
- [42] F. K. Shmidt, V. G. Lipovich, S. M. Krasnopol'skaya, I. V. Kalechits, *Kinetika i Kataliz* 11 (1970) 595–602.
- [43] K. Bronstert, V. Ladenberger, G. Fahrbach, *Catalytic Hydrogenation of Polymers Containing Double Bonds*. U.S. Patent 3,673,281, Jun. 27, 1972.
- [44] T. Abraham, P. H. Starmer, A. H. Jorgensen, *Composition of and a Method for Preparing High-Temperature Oil-Resistant Elastomers from Hydrogenated Butadiene-Acrylate Copolymers*. U.S. Patent 4,994,528, Feb. 19, 1991.
- [45] W. L. Hergenrother, J. M. Doshak, *Process and Catalyst for Producing Partially Hydrogenated Diene Polymers Containing Endo and Exo Chain Trisubstituted Unsaturation*. U.S. Patent 5,310,817, May 10, 1994.
- [46] K. A. Johnson, W. De Jong, D. K. Schisla, *Method for Making Selectively Hydrogenated Block Copolymers of Vinyl Aromatic Hydrocarbons and Conjugated Dienes*. U.S. Patent 7,390,856, June 24, 2008.
- [47] J. F. Haw (Ed.), *In-Situ Spectroscopy in Heterogeneous Catalysis*, Wiley VCH, Weinheim, 2002.
- [48] J. Pérez-Ramírez, E. V. Kondratenko, *Catal. Today* 121 (2007) 160–169.
- [49] R. G. Finke in: D. L. Feldheim, C. A. Foss Jr. (Eds.), *Metal Nanoparticles: Synthesis, Characterization, and Applications*, Marcel Dekker, Inc. New York, 2002, pp. 17–54.
- [50] Y. Lin, R. G. Finke, *J. Am. Chem. Soc.* 116 (1994) 8335–8353.

- 
- [51] A. K. Galwey, *Thermochim. Acta* 413 (2004) 139–183.
- [52] W. M. Alley, C. W. Girard, S. Özkar, R. G. Finke, *Inorg. Chem.* 48 (2009) 1114–1121.
- [53] W. M. Alley, I. K. Hamdemir, Q. Wang, A. Frenkel, L. Li, J. C. Yang, L. D. Menard, R. G. Nuzzo, K. A. Johnson, R. G. Finke, Ziegler-Type, Industrially Relevant Hydrogenation Catalysts Made from  $[(1,5\text{-COD})\text{Ir}(\mu\text{-O}_2\text{C}_8\text{H}_{15})_2]$  and  $\text{AlEt}_3$ : Evidence for the  $\text{Ir}(0)_n$  species present and for the true catalyst, submitted for publication.
- [54] I. K. Hamdemir, S. Özkar, K. A. Johnson, R. G. Finke, Ranking the activity and other catalytic properties of Ziegler-Type, industrially relevant hydrogenation catalysts made from  $[(1,5\text{-COD})\text{Ir}(\mu\text{-O}_2\text{C}_8\text{H}_{15})_2]$  and  $\text{AlEt}_3$ , via a modified five-criteria method, in preparation.
- [55] W. M. Alley, I. K. Hamdemir, Q. Wang, A. Frenkel, L. D. Menard, R. G. Nuzzo, S. Özkar, K. A. Johnson, R. G. Finke, Cobalt Ziegler-Type industrial hydrogenation catalysts made from  $\text{Co}(\text{neodecanoate})_2$  and  $\text{AlEt}_3$ : evidence for nanoclusters and nanocluster-based catalysis, in preparation.
- [56] W. M. Alley, I. K. Hamdemir, Q. Wang, A. Frenkel, L. Li, J. C. Yang, L. D. Menard, R. G. Nuzzo, S. Özkar, K. A. Johnson, R. G. Finke, Nickel Ziegler-Type industrial hydrogenation catalysts made from  $\text{Ni}(2\text{-ethylhexanoate})_2$  and  $\text{AlEt}_3$ : evidence for nanoclusters and nanocluster-based catalysis, in preparation.
- [57] M. F. Sloan, A. S. Matlack, D. S. Breslow, *J. Am. Chem. Soc.* 85 (1963) 4014–4018.
- [58] S. J. Lapporte, *Ann. N. Y. Acad. Sci.* 158 (1969) 510–525.
- [59] D. S. Breslow, A. S. Matlack, Hydrogenation of Unsaturated Hydrocarbons. U.S. Patent 3,113,986, Dec. 10, 1963.
- [60] T. Yoshimoto, S. Kaneko, T. Narumiya, H. Yoshii, Hydrogenation Catalysts and a Process for Hydrogenating Polymers by the Use of Them. U.S. Patent 3,541,064, Nov. 17, 1970.
- [61] C. L. Willis, L. A. Pottick, D. E. Goodwin, Method for Hydrogenating Functionalized Polymer and Products Thereof. U.S. Patent 4,970,254, Nov. 13, 1990.
- [62] R. J. Hoxmeier, L. H. Slauch, Hydrogenation Catalyst and Hydrogenation Process Wherein Said Catalyst is Used. U.S. Patent 5,057,582, Oct. 15, 1991.
- [63] T. S. Coolbaugh, F. C. Loveless, D. N. Mathews, Method of Synthesizing a Selective Olefin Hydrogenation Catalyst. Eur. Pat. Appl. 91300316.6, Jan. 16, 1991.

- 
- [64] W. R. Kroll, Hydrogenation Process Employing a Transition Metal Catalyst. U.S. Patent 3,412,174, Nov. 19, 1968.
- [65] M. M. Wald, M. G. Quam, Partially Hydrogenated Block Copolymers. U.S. Patent 3,595,942, July 27, 1971.
- [66] M. M. Wald, M. G. Quam, Selectively Hydrogenated Block Copolymers. U.S. Patent 3,700,633, Oct. 24, 1972.
- [67] A. Alvanipour, L. D. Kispert, *J. Mol. Catal.* 48 (1988) 277–283.
- [68] T. Yoshimoto, S. Kaneko, T. Narumiya, H. Yoshii, Three Component Hydrogenation Catalysts and a Process for Hydrogenating Polymers by the Use of Them. U.S. Patent 3,531,450, Sep. 29, 1970.
- [69] S. Šabata, J. Hetflejš, *J. Appl. Polym. Sci.* 85 (2002) 1185–1193.
- [70] J. Reguli, A. Staško, *Chem. Papers* 41 (1987) 299–310.
- [71] S. Pasynkiewicz, A. Pietrzykowski, K. Dowbor, *J. Organomet. Chem.* 78 (1974) 55–59.
- [72] S. J. Lapporte, Preparation of Complex Organic Metallic Hydrogenation Catalysts and Their Use. U.S. Patent 3,205,278, Sep. 7, 1965.
- [73] D. E. Goodwin, C. L. Willis, Hydrogenation of Unsaturation in Low Molecular Weight Diene Polymers. U.S. Patent 5,166,277, Nov. 24, 1992.
- [74] D. L. Handlin, D. E. Goodwin, C. L. Willis, D. J. St. Clair, J. D. Wilkey, M. J. Modic, C. A. Stevens, Butadiene Polymers Having Terminal Functional Groups. U.S. Patent 5,393,843, Feb. 28, 1995.
- [75] W. R. Kroll, *J. Catal.* 15 (1969) 281–288.
- [76] H. E. De La Mare, Process for Hydrogenation of Polar Copolymers and Complexed Copolymer Compositions. U.S. Patent 3,766,300, Oct. 16, 1973.
- [77] F. C. Loveless, D. H. Miller, Hydrogenation Catalyst. U.S. Patent 3,932,308, Jan. 13, 1976.
- [78] V. Ladenberger, K. Bronstert, G. Fahrbach, W. Groh, Catalytic Hydrogenation of Diolefin Polymers. U.S. Patent 4,207,409 Jun. 10, 1980.
- [79] J. C. Falk, *J. Polym. Sci., Part A: Polym. Chem.* 9 (1971) 2617–2623.
- [80] H. W. Roesky, M. G. Walawalkar, R. Murugavel, *Acc. Chem. Res.* 34 (2001) 201–211.
- [81] L. B. Belykh, T. V. Goremyka, N. I. Skripov, V. A. Umanets, F. K. Shmidt, *Kinetics and Catalysis* 47 (2006) 367–374.

- 
- [82] H. J. Baumgartner, J. G. Balas, Hydrogenation Process. U.S. Patent 3,937,759, Feb. 10, 1976.
- [83] D. R. Lide (Ed.), CRC Handbook of Chemistry and Physics, seventy seventh ed., CRC Press, Boca Raton, 1996.
- [84] B. R. James, Y. Wang, C. S. Alexander, T. Q. Hu, Chem. Ind. 75 (1998) 233–242.
- [85] J. Aiken III, R.G. Finke, J. Am. Chem. Soc. 120 (1998) 9545–9554.
- [86] F. Notheisz, Á. Zsigmond, M. Bartók, Z. Szegletes, G. V. Smith, Appl. Catal. A: General 120 (1994) 105–114.
- [87] B. Cornils, W. A. Herrmann (Eds.), Applied Homogeneous Catalysis with Organometallic Compounds, Vol. 2: Developments, Wiley VCH, Weinheim, 1996.
- [88] B. A. Steinhoff, S. S. Stahl, J. Am. Chem. Soc. 128 (2006) 4348–4355.
- [89] J. Halpern, Inorg. Chim. Acta 50 (1981) 11–19.
- [90] N. T. S. Phan, M. Van Der Sluys, C. W. Jones, Adv. Synth. Catal. 348 (2006) 609–679.
- [91] C. M. Hagen, L. Vieille-Petit, G. Laurenczy, G. Süß-Fink, R. G. Finke, Organometallics 24 (2005) 1819–1831.
- [92] G. Wilke, G. Herrmann, Angew. Chem. Int. Ed. 1 (1962) 549–550.
- [93] G. Wilke, B. Bogdanović, P. Hardt, P. Heimbach, W. Keim, M. Kröner, W. Oberkirch, K. Tanaka, E. Steinrücke, D. Walter, H. Zimmermann, Angew. Chem. Int. Ed. 5 (1966) 151–164.
- [94] G. Wilke, G. Herrmann, Angew. Chem. Int. Ed. 5 (1966) 581–582.
- [95] B. Bogdanović, H. Bönemann, G. Wilke, Angew. Chem. Int. Ed. 5 (1966) 582–583.
- [96] G. Wilke, H. Schott, Angew. Chem. Int. Ed. 5 (1966) 583.
- [97] N. Hebben, H.-J. Himmel, G. Eickerling, C. Herrmann, M. Reiher, V. Herz, M. Presnitz, W. Scherer, Chem.—Eur. J. 13 (2007) 10078–10087.
- [98] L. Farády, L. Bencze, L. Markó, J. Organomet. Chem. 10 (1967) 505–510.
- [99] L. Farády, L. Bencze, L. Markó, J. Organomet. Chem. 17 (1969) 107–116.
- [100] J. J. Eisch, M. W. Foxton, J. Organomet. Chem. 12 (1968) P33–P36.
- [101] L. Lardicci, G. P. Giacomelli, P. Salvadori, P. Pino, J. Am. Chem. Soc. 93 (1971) 5794–5800.
- [102] J. J. Eisch, X. Ma, M. Singh, G. Wilke, J. Organomet. Chem. 527 (1997) 301–304.

- 
- [103] H. J. Motulsky, A. Christopoulos, *Fitting Models to Biological Data using Linear and Nonlinear Regression. A practical guide to curve fitting.* GraphPad Software Inc., San Diego, CA, [www.graphpad.com](http://www.graphpad.com), 2003, p. 58.
- [104] J. Halpern, *Homogeneous and Heterogeneous Catalysis: Kinetic and Mechanistic Aspects.* In, *Relations Between Homogeneous and Heterogeneous Catalysis, Proceedings of the International Symposium on the Relations between Heterogeneous and Homogeneous Catalytic Phenomena*, Lyon, 3–6 Nov. 1977, Centre National de la Recherche Scientifique: Paris, 1978, no. 281, pp. 27–47.
- [105] K. A. Klinedinst, M. Boudart, *J. Catal.* 28 (1973) 322–328.
- [106] J. M. Greneche, F. Varret, M. Leblanc, G. Ferey, *Solid State Commun.* 61 (1987) 813–816.
- [107] G. Kataby, Yu. Koltypin, J. Rothe, J. Hormes, I. Felner, X. Cao, *A. Gedanken, Thin Solid Films* 333 (1998) 41–49.
- [108] P.-R. Cha, Yu. C. Kim, K.-B. Kim, H.-K. Seok, E. Fleury, S.-H. Han, *Scr. Mater.* 56 (2007) 609–612.
- [109] F. K. Shmidt, V. V. Sarayev, Y. S. Levkovskii, V. G. Lipovich, V. A. Gruznykh, G. V. Ratovskii, T. V. Dmitrieva, L. O. Nindakova, *React. Kinet. Catal. Lett.* 10 (1979) 195–199.
- [110] G. V. Ratovskii, T. V. Dmitrieva, L. O. Nindakova, F. K. Shmidt, *React. Kinet. Catal. Lett.* 11 (1979) 121–124.
- [111] F. K. Schmidt, G. V. Ratovskii, T. V. Dmitrieva, I. N. Ivleva, Y. G. Borodko, *J. Organomet. Chem.* 256 (1983) 309–329.
- [112] J. Klosin, G. R. Roof, E. Y.-X. Chen, K. A. Abboud, *Organometallics* 19 (2000) 4684–4686. Also see reference 22 therein.
- [113] F. K. Shmidt, L. O. Nindakova, B. A. Shainyan, V. V. Saraev, N. N. Chipanina, V. A. Umanetz, *J. Mol. Catal. A: Chem.* 235 (2005) 161–172.
- [114] L. B. Belykh, Yu. Yu. Titova, V. A. Umanets, F. K. Shmidt, *Russian Journal of Applied Chemistry* 79 (2006) 1271–1277.
- [115] B. C. Gates, *Catalytic Chemistry*, John Wiley & Sons, New York, 1992, pp. 385–386.
- [116] J. Goulon, E. Georges, C. Goulon-Ginet, Y. Chauvin, D. Commereuc, H. Dexpert, E. Freund, *Chem. Phys.* 83 (1984) 357–366.
- [117] A. I. Frenkel, C. W. Hills, R. G. Nuzzo, *J. Phys. Chem. B* 105 (2001) 12689–12703.

- 
- [118] J. M. Montejano-Carrizales, J. L. Morán-López, *Nanostruct. Mater.* 1 (1992) 397–409.
- [119] J. L. Fulton, J. C. Linehan, T. Autrey, M. Balasubramanian, Y. Chen, N. K. Szymczak, *J. Am. Chem. Soc.* 129 (2007) 11936–11949.
- [120] A. L. Ankudinov, J. J. Rehr, J. J. Low, S. R. Bare, *J. Chem. Phys.* 116 (2002) 1911–1919.
- [121] H. Bönnemann, W. Brijoux, R. Brinkmann, U. Endruschat, W. Hofstadt, K. Angermund, *Revue Roumaine de Chimie* 44 (1999) 1003–1010.
- [122] H. Bönnemann, N. Waldöfner, H.-G. Haubold, T. Vad, *Chem. Mater.* 14 (2002) 1115–1120.
- [123] K. Angermund, M. Bühl, E. Dinjus, U. Endruschat, F. Gassner, H.-G. Haubold, J. Hormes, G. Köhl, F. T. Mauschick, H. Modrow, R. Mörtel, R. Mynott, B. Tesche, T. Vad, N. Waldöfner, H. Bönnemann, *Angew. Chem. Int. Ed.* 41 (2002) 4041–4044.
- [124] K. Angermund, M. Bühl, U. Endruschat, F. T. Mauschick, R. Mörtel, R. Mynott, B. Tesche, N. Waldöfner, H. Bönnemann, G. Köhl, H. Modrow, J. Hormes, E. Dinjus, F. Gassner, H.-G. Haubold, T. Vad, M. Kaupp, *J. Phys. Chem. B* 107 (2003) 7507–7515.
- [125] H.-G. Haubold, T. Vad, N. Waldöfner, H. Bönnemann, *J. Appl. Cryst.* 36 (2003) 617–620.
- [126] F. Wen, H. Bönnemann, R. J. Mynott, B. Spliethoff, C. Weidenthaler, N. Palina, S. Zinoveva, H. Modrow, *Appl. Organomet. Chem.* 19 (2005) 827–829.
- [127] C. A. Jaska, I. Manners, *J. Am. Chem. Soc.* 126 (2004) 1334–1335.
- [128] E. E. Finney, R. G. Finke, Fitting and Interpreting Transition-Metal Nanocluster Formation and Other Sigmoidal Kinetic Data: A More Thorough Testing of Empirical, Dispersive Kinetics vs Chemical-Mechanism-Based Equations and Treatments, *Chem. Mater.* in press.
- [129] M. A. Watzky, R. G. Finke, *Chem. Mater.* 9 (1997) 3083–3095.
- [130] M. A. Watzky, R. G. Finke, *J. Am. Chem. Soc.* 119 (1997) 10382–10400.
- [131] (a) C. Besson, E. E. Finney, R. G. Finke, *J. Am. Chem. Soc.* 127 (2005) 8179–8184. (b) C. Besson, E. E. Finney, R. G. Finke, *Chem. Mater.* 17 (2005) 4925–4938.
- [132] (a) A. M. Morris, M. A. Watzky, J. N. Agar, R. G. Finke, *Biochem.* 47 (2008) 2413–2427. (b) M. A. Watzky, A. M. Morris, E. D. Ross, R. G. Finke, *Biochem.* 47 (2008) 10790–10800.
- [133] J. A. Widegren, J. D. Aiken III, S. Özkar, R. G. Finke, *Chem. Mater.* 13 (2001) 312–324.
- [134] P. D. Jadzinsky, G. Calero, C. J. Ackerson, D. A. Bushnell, R. D. Kornberg, *Science* 318 (2007) 430–433.

- 
- [135] L. Beuermann, W. Maus-Friedrichs, S. Krischok, V. Kempter, S. Bucher, H. Modrow, J. Hormes, N. Waldöfner, H. Bönemann, *Appl. Organomet. Chem.* 17 (2003) 268–276.
- [136] F. Wen, N. Waldöfner, W. Schmidt, K. Angermund, H. Bönemann, S. Modrow, S. Zinoveva, H. Modrow, J. Hormes, L. Beuermann, S. Rudenkiy, W. Maus-Friedrichs, V. Kempter, T. Vad, H.-G. Haubold, *Eur. J. Inorg. Chem.* (2005) 3625–3640.
- [137] H. Bönemann, W. Brijoux, H.-W. Hofsatdt, T. Ould-Ely, W. Schmidt, B. Waßmuth, C. Weidenthaler, *Angew. Chem. Int. Ed.* 41 (2002) 599–603.
- [138] R. Richards, G. Geibel, W. Hofstadt, H. Bönemann, *Appl. Organomet. Chem.* 16 (2002) 377–383.
- [139] H. Bönemann, W. Brijoux, R. Brinkmann, N. Matoussevitch, N. Waldöfner, N. Palina, H. Modrow, *Inorg. Chim. Acta* 350 (2003) 617–624.
- [140] R. L. Augustine, F. Yaghmaie, J. F. Van Peppen, *J. Org. Chem.* 49 (1984) 1865–1870.
- [141] J. Halpern, *Acc. Chem. Res.* 15 (1982) 332–338.
- [142] M. J. Nappa, R. Santi, J. Halpern, *Organometallics* 4 (1985) 34–41.
- [143] J. R. Platt, *Science* 146 (1964) 347.
- [144] C. A. Jaska, I. Manners, *J. Am. Chem. Soc.* 126 (2004) 9776–9785.
- [145] Y. Chen, J. L. Fulton, J. C. Linehan, T. Autrey, *J. Am. Chem. Soc.* 127 (2005) 3254–3255.
- [146] A. Duteil, G. Schmid, W. Meyer-Zaika, *Chem. Commun.* 1995 31–32.
- [147] D. B. Williams, C. B. Carter, *Transmission Electron Microscopy*, Plenum Press, New York, 1996.
- [148] B. J. Hornstein, J. D. Aiken III, R. G. Finke, *Inorg. Chem.* 41 (2002) 1625–1638.
- [149] J. M. Thomas, G. A. Somorjai, *Top. Catal.* 8 (1999) preface.
- [150] B. M. Weckhuysen, *Chem. Commun.* 2002, 97–110.
- [151] M. O. Guerrero-Pérez, M. A. Bañares, *Chem. Commun.* 2002, 1292–1293.
- [152] F. Meunier, M. Daturi, *Catal. Today* 113 (2006) 1–2.
- [153] J. Halpern, T. Okamoto, A. Zakhariyev, *J. Mol. Catal.* 2 (1976) 65–68.
- [154] S. J. Tinnemans, J. G. Mesu, K. Kervinen, T. Visser, T. A. Nijhuis, A. M. Beale, D. E. Keller, A. M.J. van der Eerden, B. M. Weckhuysen, *Catal. Today* 113 (2006) 3–15.
- [155] D. Durand, G. Hillion, C. Lassau, L. Sajus, *Process for Hydrogenating Unsaturated Compounds*. U.S. Patent 4,271,323, Jun. 2, 1981.

Supporting Information for:

**Review**

**Ziegler–type hydrogenation catalysts made from group 8–10 transition metal  
precatalysts and  $\text{AlR}_3$  cocatalysts: A critical review of the literature**

William M. Alley, Isil K. Hamdemir, Kim Johnson, Richard G. Finke

## Hydrogenations using Pt(acac)<sub>2</sub> plus AlEt<sub>3</sub>

Using ASAXS spectroscopy, Bönemann and coworkers observed the formation of 1.2 nm diameter nanoparticles from a Pt(acac)<sub>2</sub> plus AlMe<sub>3</sub> system [1]. The relatively slow nanoparticle development observed for this system makes it promising for following the kinetics of catalyst formation en route to determining the true nature of the catalyst. However, in order to do this, it is first necessary to show that the system is indeed catalytically competent for hydrogenation, as expected (i.e., to see if the system forms a Ziegler–type hydrogenation catalyst, an important experiment not reported previously). A similar system tested by us, Pt(acac)<sub>2</sub> plus AlEt<sub>3</sub>, Al/Pt = 4, exhibits the ability to catalytically hydrogenate cyclohexene. The results of following the formation of the Ziegler–type hydrogenation catalyst formed from Pt(acac)<sub>2</sub> plus AlEt<sub>3</sub>, Al/Pt = 4, by the cyclohexene hydrogenation reporter reaction method [2,3,4] are reported below, Figure S1.

In the drybox, a 9.0 mM toluene solution of Pt(acac)<sub>2</sub> precatalyst was prepared by dissolving 0.0668 g of Pt(acac)<sub>2</sub> (Strem, 98%) in 18.87 mL of toluene (Aldrich, anhydrous, 99.8%). Using a procedure similar to that employed for the Co catalyst described below, the Pt catalyst solution was prepared in the drybox by adding, in the following order, 1.7 mL of toluene to a new 22 x 175 mm Pyrex borosilicate culture tube containing a new 5/8 x 5/16 inch Teflon-coated magnetic stirbar, followed by 0.4 mL of the Pt precatalyst solution, and with 1000 rpm stirring, 0.4 mL of a 36.0 mM toluene solution of AlEt<sub>3</sub>, giving Al/Pt = 4.0. No color change of the light-yellow solutions was apparent upon the addition of AlEt<sub>3</sub>. Finally, 0.5 mM of cyclohexene was added, and the tube was sealed in a Fisher–Porter (FP) bottle. The hydrogenation procedure was also

similar to that used for the Co catalyst described below, the only differences being the use of H<sub>2</sub> (General Air, 99.5%) instead of D<sub>2</sub>, and the FP bottle was purged with 40 psig of H<sub>2</sub> once every 15 seconds for 3.5 min (15 purges total). The light-yellow solutions gradually changed color to brown during the hydrogenation runs. After pressure data acquisition, data were converted to [cyclohexene] vs. time with MS excel according to the procedure employed with the cyclohexene hydrogenation reporter reaction method [2,3,4].

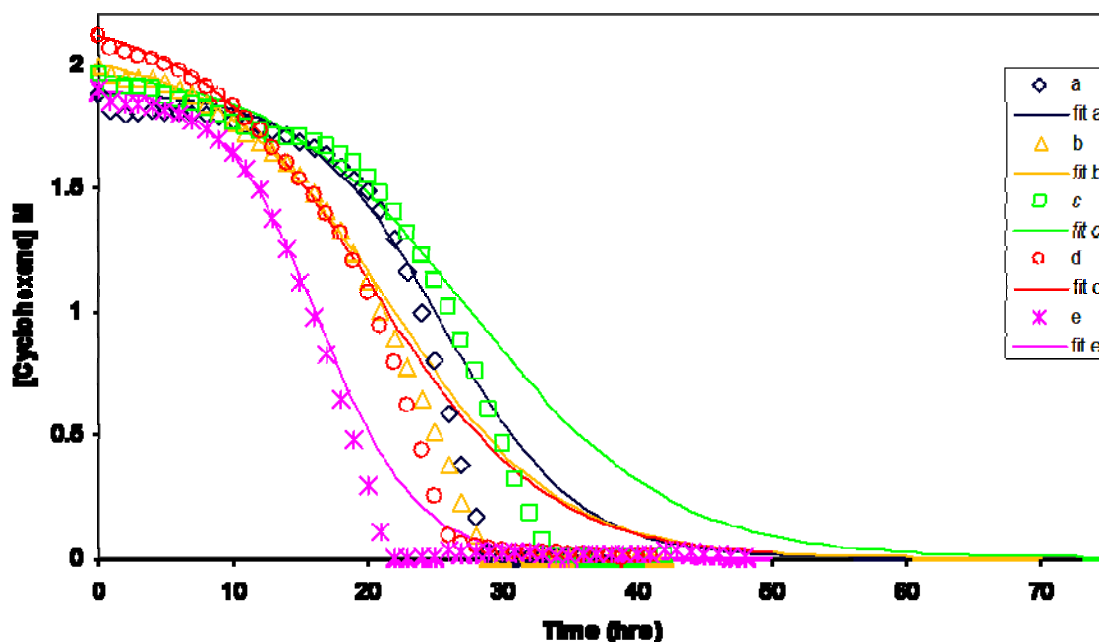


**Figure S1.** Five catalytic cyclohexene hydrogenation runs using Pt(acac)<sub>2</sub> + AlEt<sub>3</sub>, Al/Pt = 4, [Pt] = 1.2 mM, solvent = toluene, temperature = 22.0 °C, initially 40.0 psig H<sub>2</sub>, stirring = 1000 rpm. Solid lines show the attempted fits by the 2-step mechanism for nanocluster formation [3] consisting of nucleation (A → B, rate constant  $k_1$ ) followed by autocatalytic growth (A + B → 2B, rate constant  $k_2$ ), giving mean values:  $k_1 = 0.004(2) \text{ s}^{-1}$ ,  $k_2 = 0.09(3) \text{ M}^{-1}\text{s}^{-1}$ , and a range of  $R^2$  values from 0.9491 to 9954.

The near-sigmoidal-shaped curves, Figure S1, were fit using Origin by the well-precedented, 2-step mechanism of nanocluster formation consisting of nucleation (A → B, rate constant  $k_1$ ) followed by autocatalytic growth (A + B → 2B, rate constant  $k_2$ ) [3],

giving mean values of  $k_1 = 0.004(2)$  and  $k_2 = 0.09(3)$ . The kinetic model fits the initial portions of the curves well, but not the later portions, which deviate from sigmoidal by abruptly ending at the point where all the substrate has been consumed. This implies that changes involving the catalyst(s)—*specifically the evolution of a more active catalyst*—is occurring. These results show that this system, the very similar one investigated by Bönnemann and coworkers [1], or another comparable system, are of interest for studies aimed at the mechanism of formation of Ziegler–type hydrogenation catalysts.

### **Other Survey Hydrogenations En Route to Potentially Useful Ziegler–type Hydrogenation Catalyst Model Systems**

A few other precursors were combined with  $\text{AlEt}_3$  and the resulting solutions tested for their ability to catalytically hydrogenate cyclohexene, specifically the precursors  $[(1,5\text{-COD})\text{Ir}(\text{acac})]$ ,  $[(1,5\text{-COD})\text{Rh}(\text{acac})]$ ,  $\text{Rh}(\text{acac})_3$ , and  $\text{Co}(\text{acac})_2$ . The results are shown below, Figures S2–S5. Catalyst solutions were prepared similarly to as described above. In the drybox, a 3.6 mM in  $[\text{Ir}]$  solution of  $[(1,5\text{-COD})\text{Ir}(\text{acac})]$  (Strem, 99%) was prepared by weighing out 0.0237 g of  $[(1,5\text{-COD})\text{Ir}(\text{acac})]$  and dissolving in 16.48 mL of cyclohexane. The catalyst was prepared in a culture tube by adding in the following order 1.2 mL of cyclohexane, 1.0 mL of the yellow  $[(1,5\text{-COD})\text{Ir}(\text{acac})]$  solution, and with 1000 rpm stirring, 0.3 mL of a 36.0 mM  $\text{AlEt}_3$  solution in cyclohexane, making  $\text{Al}/\text{Ir} = 3$ . For  $[(1,5\text{-COD})\text{Rh}(\text{acac})]$  (Strem, 98%), 0.292 g were dissolved in 2.3 mL of cyclohexane in a culture tube. Next, 0.20 mL of a 36.0 mM cyclohexane solution of  $\text{AlEt}_3$  was then added with 1000 rpm stirring, giving  $\text{Al}/\text{Rh} = 2$ . For  $\text{Rh}(\text{acac})_3$  (Aldrich, 97%), 0.267 g was dissolved in 16.68 mL toluene. Then, 1.4 mL toluene, 0.9

mL of the Rh(acac)<sub>3</sub> solution, and afterwards, with 1000 rpm stirring, 0.2 mL of a 36.0 mM toluene solution of AlEt<sub>3</sub> were added to a culture tube, giving Al/Rh = 2. For Co(acac)<sub>2</sub>•0.34H<sub>2</sub>O (Strem; H<sub>2</sub>O determined by TGA), 0.0386 g were dissolved in 16.3 mL of toluene. Next, 0.4 mL of this solution were added to a culture tube along with 1.7 mL of toluene, and then with 1000 rpm stirring, 0.4 mL of a 36.0 mM toluene solution of AlEt<sub>3</sub> were added, making the Al/Co = 4. Lastly in each case, 0.5 mL of cyclohexene was added. The hydrogenation procedure, H<sub>2</sub> gas purge cycle, data collection, data conversion, and fitting procedure were all performed the same as described above for experiments using the Pt(acac)<sub>2</sub> precursor. (The data from the Co(acac)<sub>2</sub> system was not converted from psig H<sub>2</sub> to [cyclohexene] nor fit.) All of the precatalysts tested form active catalysts for the hydrogenation of cyclohexene. However, the most promising Ziegler-type hydrogenation catalyst system for use as a model of industrial catalysts, besides the [(1,5-COD)M(m-O<sub>2</sub>C<sub>8</sub>H<sub>15</sub>)]<sub>2</sub> (M = Rh or Ir) + AlEt<sub>3</sub> systems reported elsewhere [5], is the Pt(acac)<sub>2</sub> + AlR<sub>3</sub> system described above.

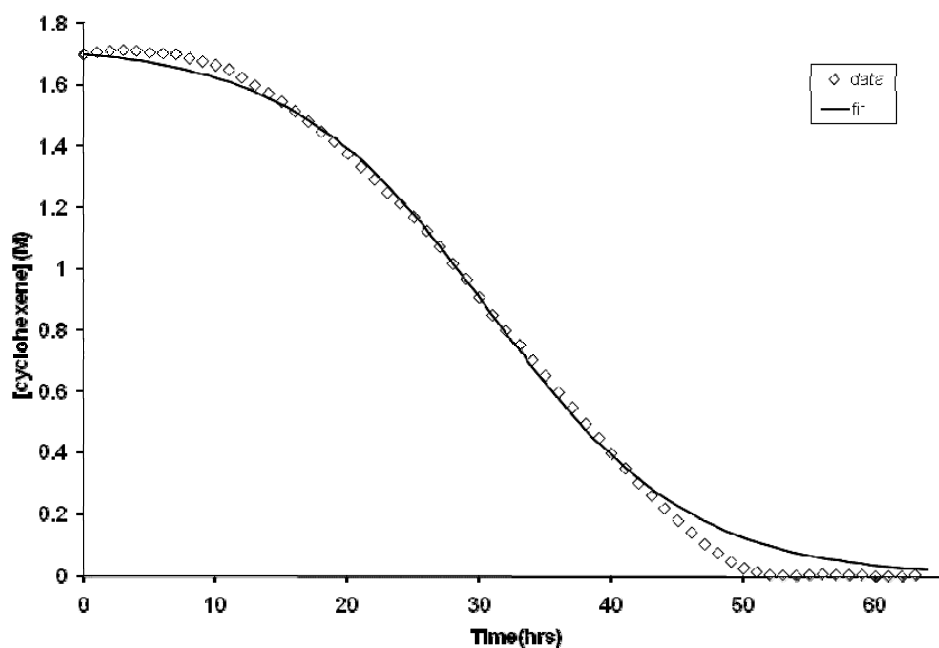


**Figure S2.** Catalytic cyclohexene hydrogenation using a Ziegler-type hydrogenation catalyst made from addition of AlEt<sub>3</sub> to [(1,5-COD)Ir(acac)], Al/Ir = 3, [Ir] = 1.2 mM, initially 40.0 psig H<sub>2</sub>, solvent = cyclohexane, temperature = 22.0 °C, stirring = 1600 rpm. The solution changed from yellow to light brown during hydrogenation. The data is reasonably well fit using the well-precedented mechanism for nanocluster formation consisting of nucleation (A → B, rate constant k<sub>1</sub>) followed by autocatalytic growth (A + B → 2B, rate constant k<sub>2</sub>) [3], giving k<sub>1</sub> = 0.0022(1) s<sup>-1</sup>, k<sub>2</sub> = 0.077(2) M<sup>-1</sup>s<sup>-1</sup>. However, small amounts of a black solid, presumably bulk Ir metal, were deposited on the stirbar and sides of the culture tube. The shape of the hydrogenation curve and apparently relatively slow catalyst formation show that this system has promise, but the formation of the insoluble black solid is an undesired feature of this system.

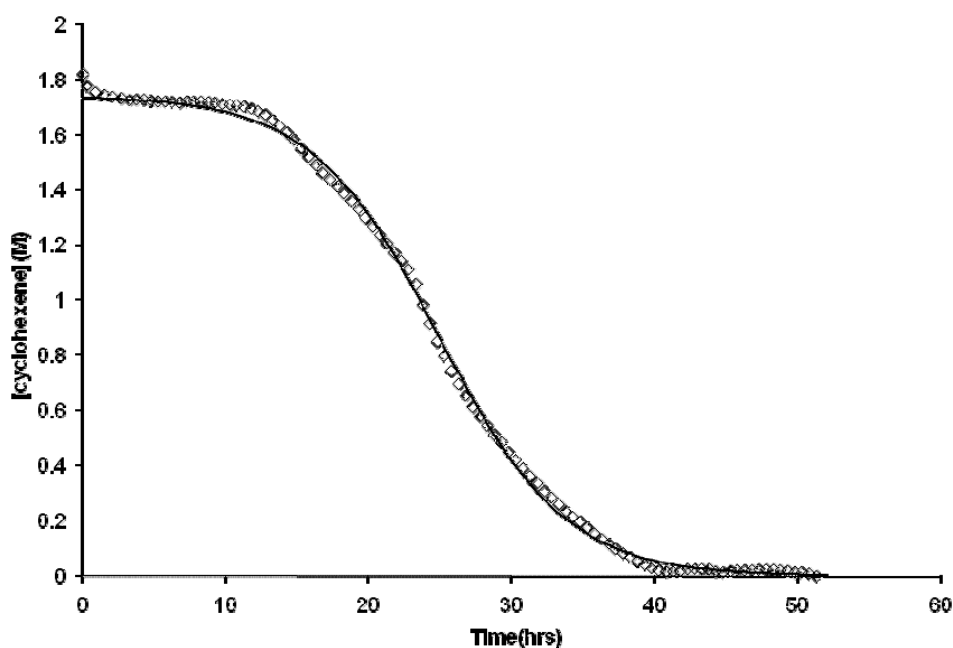


**Figure S3.** Catalytic cyclohexene hydrogenation using a Ziegler-type hydrogenation catalyst made from addition of AlEt<sub>3</sub> to [(1,5-COD)Rh(acac)], Al/Rh = 2, [Rh] = 1.2 mM, initially 40.0 psig H<sub>2</sub>, solvent = cyclohexane, temperature = 22.0 °C, stirring = 1600 rpm. The data is moderately well fit using the well-precedented mechanism for nanocluster formation consisting of nucleation (A → B, rate constant k<sub>1</sub>) followed by autocatalytic growth (A + B → 2B, rate constant k<sub>2</sub>) [3], giving k<sub>1</sub> = 0.0018(1) s<sup>-1</sup>, k<sub>2</sub> = 0.130(4) M<sup>-1</sup>s<sup>-1</sup>. However, the hydrogenation data contain several interesting and unexplained features not well accounted for by the mechanistic model used here, and as a comparison of the above data and solid fit line reveal. In addition, small amounts of a black solid, presumably bulk Rh metal, deposited on the stirbar and sides of the culture tube. The unexplained features of the hydrogenation curve make this system interesting, but the formation of the black solid is an undesired feature. Also, the precatalyst [(1,5-COD)Rh(acac)] should be stored cold.

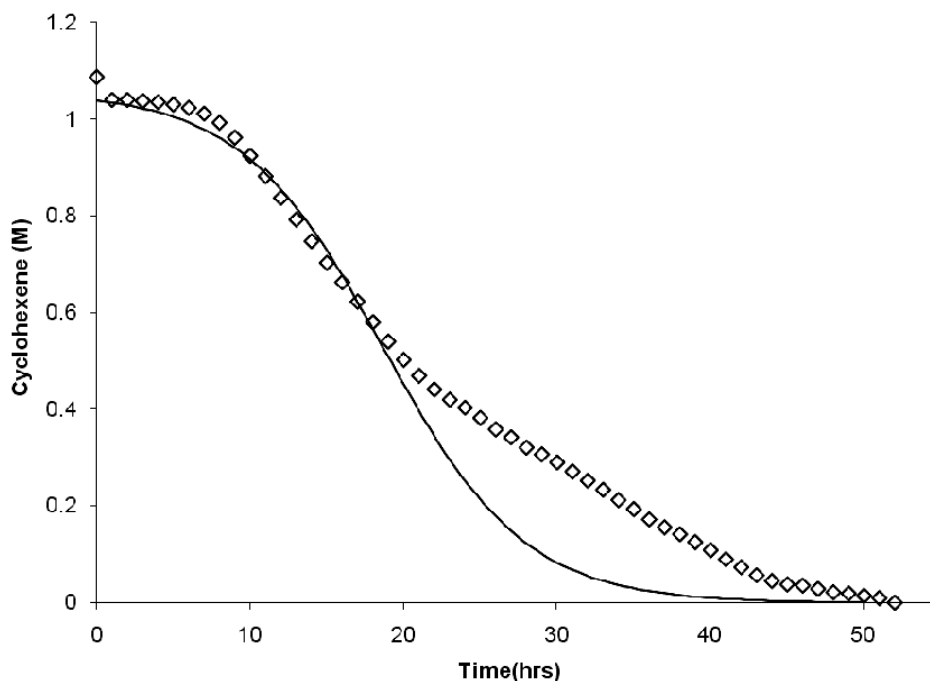


**Figure S4.** Catalytic cyclohexene hydrogenation using a Ziegler-type hydrogenation catalyst made from addition of  $\text{AlEt}_3$  to  $\text{Rh}(\text{acac})_3$ ,  $\text{Al/Rh} = 2$ ,  $[\text{Rh}] = 1.2 \text{ mM}$ , initially  $40.0 \text{ psig H}_2$ , solvent = toluene, temperature =  $22.0 \text{ }^\circ\text{C}$ , and stirring =  $1000 \text{ rpm}$ . The data are poorly fit using the 2-step mechanism of nanocluster formation consisting of nucleation ( $\text{A} \rightarrow \text{B}$ , rate constant  $k_1$ ) followed by autocatalytic growth ( $\text{A} + \text{B} \rightarrow 2\text{B}$ , rate constant  $k_2$ ) [3]; the resulting  $k_1 = 0.0038(6) \text{ s}^{-1}$  and  $k_2 = 0.20(1) \text{ M}^{-1}\text{s}^{-1}$ . This system gives an unexplained, and interestingly-shaped hydrogenation curve, but was not pursued further.

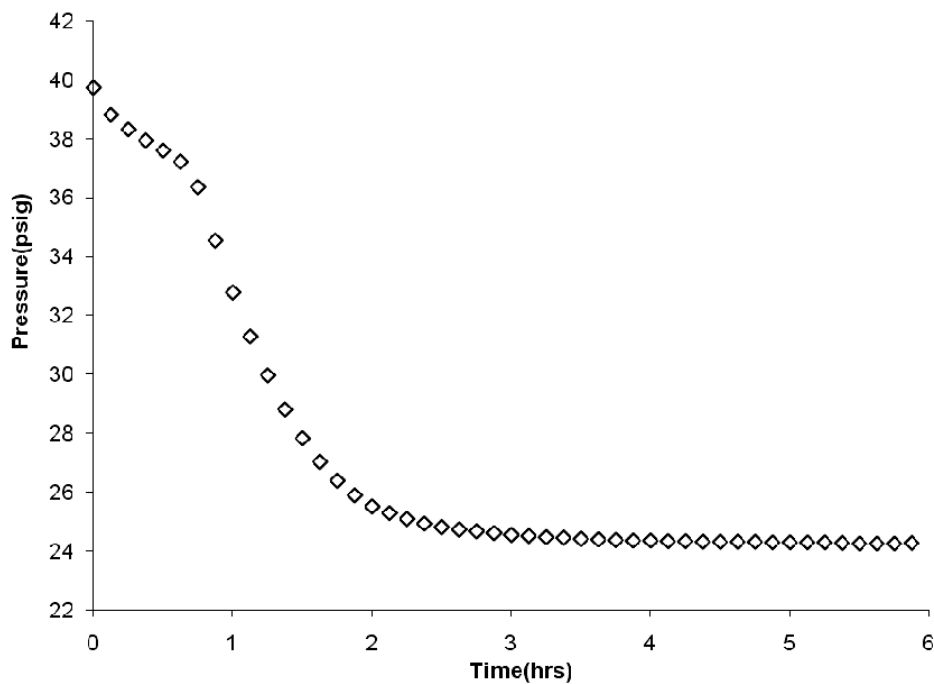
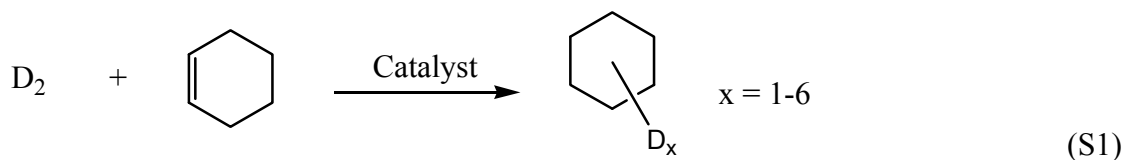


**Figure S5.** Catalytic cyclohexene hydrogenation using a Ziegler-type hydrogenation catalyst made from addition of AlEt<sub>3</sub> to Co(acac)<sub>2</sub>•0.34H<sub>2</sub>O, Al/Co = 4, [Co] = 1.2 mM, initially 40.0 psig H<sub>2</sub>, solvent = toluene, temperature = 22.0 °C, and stirring = 1000 rpm. No attempt was made to fit this irregular hydrogenation curve.

**A Deuterium Labeling Experiment [6] with a Co(neodecanoate)<sub>2</sub> plus AlEt<sub>3</sub> Catalyst leading to an Updated, Proposed Hydrogenation Mechanism for Ziegler-type Hydrogenation Catalysts**

A Ziegler-type hydrogenation catalyst made from combination of Co(neodecanoate)<sub>2</sub> and AlEt<sub>3</sub>, Al/Co = 3, was used to catalytically hydrogenate cyclohexene in a pressurized, Fisher-Porter reaction bottle. When D<sub>2</sub> gas was used, analysis of the resulting products by gas chromatography mass spectrometry (GC-MS) showed significant incorporation of multiple (i.e., > 2) deuterium atoms in the resulting cyclohexane, Equation S1. As stated in the main text, this outcome supports the

hypothesis that, at least according to a generally well-accepted mechanism for heterogeneous transition metal catalyzed hydrogenations [7], reductive elimination, as opposed to migratory insertion [8], is the rate determining step, with prior equilibria existing in the earlier step(s).



Under an N<sub>2</sub> atmosphere in a Vacuum Atmospheres drybox (O<sub>2</sub> levels were maintained at ≤ 5 ppm as monitored by a Vacuum Atmospheres O<sub>2</sub>-level monitor), an 18.0 mM in [Co] cyclohexane (Sigma-Aldrich, anhydrous, 99.5%) solution was prepared from a Co(neodecanoate)<sub>2</sub> precatalyst solution (70% Co(neodecanoate)<sub>2</sub>, 30% mineral spirits) by adding 0.58 ± 0.01 mL to a 100 mL volumetric flask and diluting to the mark. Catalyst solutions were then made individually before use by adding, in the following order, 2.0 ± 0.05 mL of cyclohexane to a new 22 x 175 mm Pyrex borosilicate culture tube containing a new 5/8 x 5/16 inch Teflon-coated magnetic stirbar, followed by 0.200 ± 0.002 mL of the Co precatalyst solution, and with stirring at 1000 rpm, 0.30 ± 0.01 mL of a 36.0 mM cyclohexane solution of AlEt<sub>3</sub> (Aldrich, 93%), giving a Al/Co = 3.0 catalyst. AlEt<sub>3</sub> was added rapidly resulting in a near instantaneous color change from the indigo Co precursor solution to dark brown. Lastly, 0.50 ± 0.01 mL of cyclohexene (Aldrich, 99%, distilled over Na under an Ar atmosphere) was added to the culture tube. The culture tube was then placed in a Fisher-Porter (FP) bottle, which was sealed and brought out of the drybox in order to attach it to the hydrogenation apparatus [3,4,9]. The F-P bottle was placed in a 22.0 °C recirculating water bath (VWR Scientific) and connected to the apparatus using TFE-sealed Swagelock quick-connects. D<sub>2</sub> gas

(Matheson, 99.5%) was purified by passing through an indicating moisture trap (Scott Specialty Gas), a disposable O<sub>2</sub> cartridge (Trigon), and an indicating O<sub>2</sub> trap (Trigon). Stirring at 1000 rpm was started, the bottle was purged with D<sub>2</sub> gas at 40 psig a total 5 times (once every 30 s), set at 40 psig, and pressure data acquisition was started by means of an Omega PX-624 pressure transducer interfaced to a PC running LabVIEW 7.0.

Pressure in the FP bottle reached a minimum value after 12 min, and after observing a constant value for > 4 min, the sealed FP bottle was detached and brought back into the drybox. Inside the drybox, samples for analysis by GC–MS were prepared by taking 40 µL of the hydrogenation reaction solution in cyclohexane and diluting with 2 mL of acetone (Burdick and Jackson). GC–MS analysis was performed on an Agilent 5973N/GC 6890 instrument equipped with a mass selective detector (70 eV) and an SPB-1, 30 m column. Temperature program: initial temperature, 10 °C (initial time 5.00 min); heating rate, 10.00 °C/min; final temperature, 100 °C. The results of analyzing the sample by GC–MS are shown below in Figure S6. The majority of the deuterated product appears at the front of the broad peak in the GC portion (top) of Figure S6. The MS portion (bottom) of Figure S6 is the segment of the GC peak at the retention time of 5.378 min.

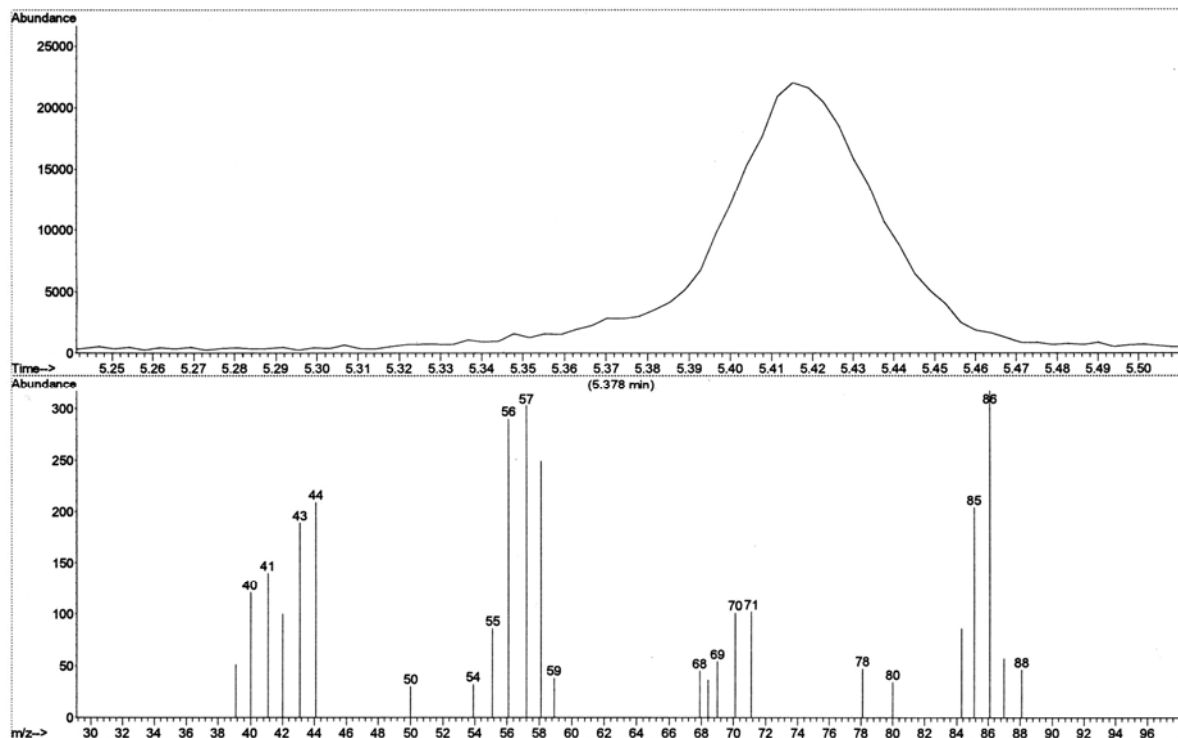


**Figure S6.** GC MS of a sample from the deuteration of cyclohexene using a  $\text{Co}(\text{neodecanoate})_2$  plus  $\text{AlEt}_3$ ,  $\text{Al/Co} = 3.0$ , Ziegler-type hydrogenation catalyst. GC (top) shows a single broad peak encompassing both undeuterated cyclohexane (the solvent) and deuterated cyclohexane, the catalytic reaction product. The deuterated cyclohexane is principally found at the leading edge of the peak, evident as the tail on the left. MS (bottom) taken at a retention time of 5.378 min contains significant amounts of multiply ( $> 2$ ) deuterated cyclohexane ( $m/z > 86$ ).

Peaks of  $m/z$  84 (cyclohexane- $\text{d}_0$ ) through  $m/z$  88 (cyclohexane- $\text{d}_4$ ) from individual mass spectra at close time intervals between 5.359min on the leading edge of the peak and the peak maximum at 5.411min were used to calculate the relative amounts of product deuteration, Figure S7. (The  $m/z$  – extent of deuterium inclusion correlations were made without regard given to the 1.1% natural abundance of  $^{13}\text{C}$ .) On the front edge of the peak there is a significant presence of triply- and quadruply-deuterated cyclohexane (about 60% of the total at 5.359 min). This result supports the hypothesis that reductive elimination is the rate determining step in the proposed cyclohexene

hydrogenation mechanism, Scheme 8 of the main text. If migratory insertion was rate-determining [8], then a maximum of two deuterium atoms per cyclohexane should have been seen.

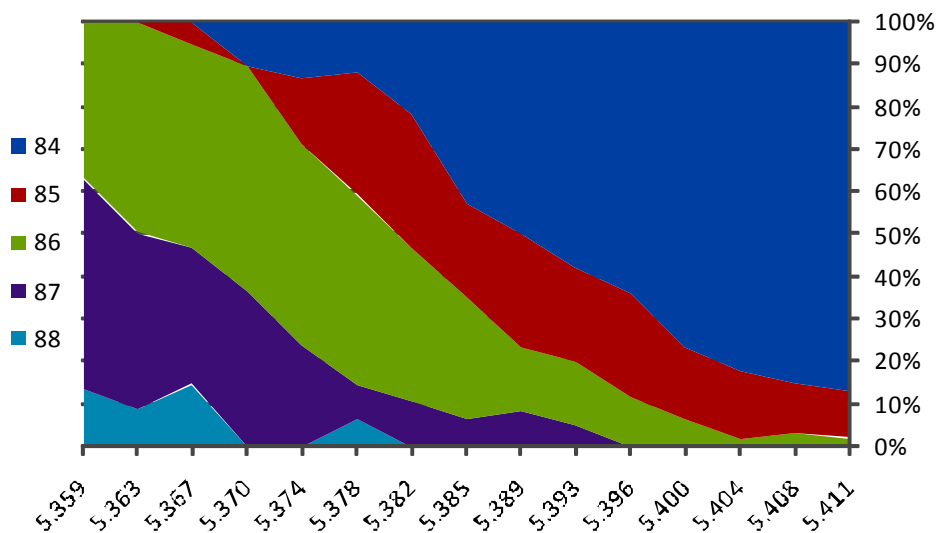


**Figure S7.** Relative abundances, as a function of retention time, of cyclohexane- $d_0$ ,  $m/z = 84$  (dark blue); cyclohexane- $d_1$ ,  $m/z = 85$  (red), cyclohexane- $d_2$ ,  $m/z = 86$  (green), cyclohexane- $d_3$ ,  $m/z = 87$  (purple), and cyclohexane- $d_4$ ,  $m/z = 88$  (light blue). The natural 1.1% abundance of  $^{13}\text{C}$  has been neglected in calculating these percentages. Triply- and quadruply-deuterated cyclohexane together make up more than 60% of the cyclohexane in the sample at the retention time of 5.359 min, supporting reductive elimination as the rate determining step in the updated cyclohexene hydrogenation mechanism, Scheme 8 of the main text.

### Other Experimental Considerations

All materials were stored and used as received in the drybox unless noted otherwise. All glassware was oven-dried at 160 °C overnight and cooled either under vacuum or an atmosphere of  $\text{N}_2$ . **Caution!** *Aluminum alkyls such as  $\text{AlEt}_3$  are toxic and pyrophoric and must therefore be handled accordingly* [10].

## References

---

- [1] K. Angermund, M. Bühl, U. Endruschat, F. Mauschick, R. Mörtel, R. Mynott, B. Tesche, N. Waldöfner, H. Bönemann, G. Köhl, H. Modrow, J. Hormes, E. Dinjus, F. Gassner, H.-G. Haubold, T. Vad, M. Kaupp, *J. Phys. Chem. B* 107 (2003) 7507–7515.
- [2] Y. Lin and R. G. Finke, *J. Am. Chem. Soc.* 116 (1994) 8335–8353.
- [3] M. A. Watzky, R. G. Finke, *J. Am. Chem. Soc.* 119 (1997) 10382–10400.
- [4] J. A. Widegren, J. D. Aiken III, S. Özkar, R. G. Finke, *Chem. Mater.* 13 (2001) 312–324.
- [5] W. M. Alley, C. W. Girard, S. Özkar, R. G. Finke *Inorg. Chem.* 48 (2009) 1114–1121.
- [6] (a) R. L. Burwell, *Acc. Chem. Res.* 2 (1969) 289. (b) K. Schrage, R. L. Burwell, *J. Am. Chem. Soc.* 88 (1966) 4555. (c) J. J. Philipson, R. L. Burwell, *J. Am. Chem. Soc.* 92 (1970) 6125.
- [7] R. L. Augustine, F. Yaghmaie, J. F. Van Peppen, *J. Org. Chem.* 49 (1984) 1865.
- [8] F. K. Schmidt, V. G. Lipovich, S. M. Krasnopol'skaya, I. V. Kalechits, *Kinetika i Kataliz*, 11 (1970) 595–602.
- [9] Y. Lin, R. G. Finke, *Inorg. Chem.* 33 (1994) 4891–4910.
- [10] D. F. Shriver, M. A. Drezdon *The Manipulation of Air-Sensitive Compounds*, second ed., John Wiley and Sons, New York, 1986.

## CHAPTER III

### MODEL ZIEGLER–TYPE HYDROGENATION CATALYST PRECURSORS, [(1,5-COD)M( $\mu$ -O<sub>2</sub>C<sub>8</sub>H<sub>15</sub>)<sub>2</sub>] (M = Ir AND Rh): SYNTHESIS, CHARACTERIZATION, AND DEMONSTRATION OF CATALYTIC ACTIVITY EN ROUTE TO IDENTIFYING THE TRUE INDUSTRIAL HYDROGENATION CATALYSTS

This dissertation chapter contains the manuscript of a paper published in *Inorganic Chemistry* **2009**, *48*, 1114–1121. It is reprinted with permission, Copyright 2009 American Chemical Society. This chapter presents the synthesis, characterization, and initial catalytic activity studies of the novel Ziegler–type hydrogenation catalyst precursors [(1,5-COD)Ir( $\mu$ -O<sub>2</sub>C<sub>8</sub>H<sub>15</sub>)<sub>2</sub>] and [(1,5-COD)Rh( $\mu$ -O<sub>2</sub>C<sub>8</sub>H<sub>15</sub>)<sub>2</sub>].

Growth of crystals of [(1,5-COD)Rh( $\mu$ -O<sub>2</sub>C<sub>8</sub>H<sub>15</sub>)<sub>2</sub>] suitable for structure determination by single crystal X-ray diffraction was performed by undergraduate research associate Chase W. Girard under the supervision of William M. Alley. Ms. Susie Miller conducted the X-ray structure determinations. All other experimental work was completed by William M. Alley with occasional suggestions from Profs. Saim Özkar and Richard G. Finke. The manuscript was written by William M. Alley, and prepared for publication by William M. Alley with a small amount of editing by Prof. Saim Özkar

and light edits (13 hours) by Prof. Richard G. Finke. Prof. Oren Anderson proofread the X-ray structure descriptions.

**Model Ziegler-Type Hydrogenation Catalyst Precursors, [(1,5-COD)M( $\mu$ -O<sub>2</sub>C<sub>8</sub>H<sub>15</sub>)<sub>2</sub>] (M = Ir and Rh): Synthesis, Characterization, and Demonstration of Catalytic Activity En Route to Identifying the True Industrial Hydrogenation Catalysts**

William M. Alley, Chase W. Girard, Saim Özkar, and Richard G. Finke

**Abstract**

The compounds [(1,5-COD)M( $\mu$ -O<sub>2</sub>C<sub>8</sub>H<sub>15</sub>)<sub>2</sub>] (COD = cyclooctadiene, M = Ir (**1**) or Rh (**2**), O<sub>2</sub>C<sub>8</sub>H<sub>15</sub> = 2-ethylhexanoate) were synthesized by addition of Bu<sub>3</sub>NH(2-ethylhexanoate) or Na(2-ethylhexanoate) to acetone suspensions of [(1,5-COD)Ir( $\mu$ -Cl)]<sub>2</sub> or [(1,5-COD)Rh( $\mu$ -Cl)]<sub>2</sub>, respectively. The synthesis of such well-defined second and third row model precursors is key to determining the true nature of commercial Ziegler-type hydrogenation catalysts (i.e., catalysts made from the combination of a non-zerovalent, group 8–10 transition metal precatalyst and a trialkylaluminum cocatalyst), an unsolved, ~40 year old problem. The characterizations of **1** and **2** were accomplished by elemental analysis, melting point, FAB-MS, FT-IR, UV–vis, NMR spectroscopy, and single crystal X-ray diffraction. The complexes, C<sub>32</sub>H<sub>54</sub>Ir<sub>2</sub>O<sub>4</sub> and C<sub>32</sub>H<sub>54</sub>O<sub>4</sub>Rh<sub>2</sub>, are isostructural: monoclinic, *P*2<sub>1</sub>/*n*, *Z* = 4. The lattice constants for **1** are *a* = 15.7748(5) Å,

$b = 9.8962(3) \text{ \AA}$ ,  $c = 20.8847(7) \text{ \AA}$ ,  $\beta = 108.408(2)^\circ$ . The lattice constants for **2** are  $a = 15.7608(4) \text{ \AA}$ ,  $b = 9.9032(3) \text{ \AA}$ ,  $c = 20.8259(5) \text{ \AA}$ ,  $\beta = 108.527(1)^\circ$ . Complexes **1** and **2** are dimeric, bridged by the 2-ethylhexanoates, and with one 1,5-COD ligand bound to each metal. The formally 16 electron metal atoms are in square ligand planes with dihedral angles between the planes of  $56.5^\circ$  for **1** and  $58.1^\circ$  for **2**. The M–M distances of  $3.2776(2)$  and  $3.3390(4) \text{ \AA}$  for **1** and **2**, respectively, fall in the range of similar structures thought to have some M–M interaction despite the lack of a formal M–M bond. Demonstration that active Ziegler-type hydrogenation catalysts are made when **1** or **2** combine with  $\text{AlEt}_3$  is provided, results that open the door to the use of **1** and **2** as well-defined third and second row congeners, respectively, of Ziegler-type hydrogenation catalysts. These compounds have proven important in addressing the previously unsolved problem of the true nature of the catalyst in industrial Ziegler-type hydrogenation catalyst systems; their high yield synthesis and unequivocal characterization reported herein are the necessary first steps of that work.

## Introduction

The selective catalytic hydrogenation of unsaturated sites in polymers, such as styrenic block copolymers, is an important industrial process used to improve the stability of the polymer toward both thermal and oxidative degradation by autoxidation processes.<sup>1,2,3</sup> According to one estimate, annual worldwide production of hydrogenated styrenic block copolymers probably exceeds  $1.7 \times 10^5$  metric tons.<sup>4</sup> An industrially important family of catalysts developed during the late 1960s and early 1970s for the purpose of polymer hydrogenation is Ziegler-type *hydrogenation* catalysts, defined as those made from a non-zerovalent, group 8–10 transition metal precatalyst and a trialkylaluminum (e.g., triethylaluminum) cocatalyst. As such, Ziegler-type *hydrogenation* catalysts are *used primarily for polymer hydrogenation*, not polymerization,<sup>1,2,5,6,7,8,9,10</sup> and should not be confused with Ziegler–Natta *polymerization* catalysts.

Surprisingly little fundamental information about Ziegler-type hydrogenation catalysts exists despite their ~40 year history of industrial application.<sup>2,11,12</sup> The single most important unanswered question is what is the true nature of Ziegler-type hydrogenation catalysts: are they single metal “homogeneous” or multiple metal “heterogeneous” catalysts?<sup>13,14,15</sup> The study of typically ill-defined industrial catalyst precursors alone has not led to a clear understanding of the true nature of these important industrial catalysts.<sup>2,8,9,16</sup>

Preparing well characterized, second and third row precursors, that yield model catalysts amenable to characterization by modern methods, is the crucial first step in attaining new insights into the true nature of Ziegler-type hydrogenation catalysts.<sup>17</sup>

Requirements for an ideal precursor are that it (i) fits the above definition of a Ziegler-type hydrogenation catalyst (i.e., that it is composed of a group 8–10 transition metal salt); (ii) has an anion such as 2-ethylhexanoate that is representative of those commonly employed industrially;<sup>2</sup> (iii) forms a catalytically active species for olefin hydrogenation upon combination with a typical alkylaluminum reagent such as AlEt<sub>3</sub>; and (iv) is readily available, preferably inexpensive and easy to prepare reproducibly in a well characterized, pure form. Additional requirements for an ideal precursor are that it (v) be soluble in solvents commonly used for olefin hydrogenation, such as cyclohexane for example; (vi) have an auxiliary ligand, such as 1,5-COD, which can be used as an analytical handle (e.g., to monitor conversion of the precatalyst to the catalyst);<sup>18</sup> (vii) employ a third row transition metal to allow transmission electron microscopy (TEM) to reliably image any polymetallic clusters that may be formed;<sup>19</sup> (viii) form the same fundamental type (i.e. homogeneous or heterogeneous) of catalyst made by industrially used precatalysts, and therefore, (ix) yield new insights into the Ziegler-type hydrogenation catalysts central to industrial polymer hydrogenation. A literature search revealed that complexes of the form [(1,5-COD)M(μ-O<sub>2</sub>C<sub>8</sub>H<sub>15</sub>)]<sub>2</sub> (COD = cyclooctadiene, M = Ir or Rh, O<sub>2</sub>C<sub>8</sub>H<sub>15</sub> = 2-ethylhexanoate) are perhaps ideal, previously unexploited, candidates for the desired precatalyst.<sup>20,21,22,23,24,25,26,27,28,29,30,31,32,33,34,35,36,37</sup> In addition, [(1,5-COD)M(μ-O<sub>2</sub>C<sub>8</sub>H<sub>15</sub>)]<sub>2</sub> (M = Ir or Rh) could prove to be of importance in a variety of other industrial applications.<sup>38</sup>

Herein we describe the synthesis, characterization, structural determination, and catalytic hydrogenation activity following the addition of AlEt<sub>3</sub> of complexes [(1,5-COD)Ir(μ-O<sub>2</sub>C<sub>8</sub>H<sub>15</sub>)]<sub>2</sub> (**1**) and [(1,5-COD)Rh(μ-O<sub>2</sub>C<sub>8</sub>H<sub>15</sub>)]<sub>2</sub> (**2**). The methods used for

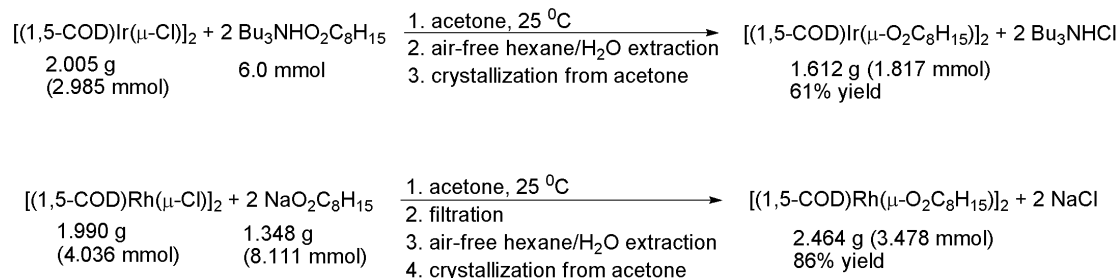
compositional and structural characterization are elemental analysis, mass spectrometry (MS), single crystal X-ray diffractometry, infrared (IR), UV–visible electronic absorption, and nuclear magnetic resonance (NMR) spectroscopy. In work to be reported separately,<sup>17</sup> we have used **1** and **2** as Ziegler-type hydrogenation catalyst precursors to investigate the problem of the true nature of industrial Ziegler-type polymer hydrogenation catalysts, a perplexing problem in the “is it homogeneous or heterogeneous catalysts?” area.<sup>14</sup> That subsequent work hinges on the high yield synthesis and unequivocal characterization of the [(1,5-COD)M( $\mu$ -O<sub>2</sub>C<sub>8</sub>H<sub>15</sub>)]<sub>2</sub> (M = Ir or Rh) precursors described herein.

## Results and Discussion

**Synthesis of [(1,5-COD)Ir( $\mu$ -O<sub>2</sub>C<sub>8</sub>H<sub>15</sub>)]<sub>2</sub> (**1**) and [(1,5-COD)Rh( $\mu$ -O<sub>2</sub>C<sub>8</sub>H<sub>15</sub>)]<sub>2</sub> (**2**).** The syntheses of **1** and **2**, Scheme 1, were modeled after earlier syntheses of similar complexes which used [(diene)M( $\mu$ -Cl)]<sub>2</sub> (diene = 1,5-COD or norbornadiene (NBD), M = Ir or Rh), and Na<sup>+</sup>, K<sup>+</sup>, or Ag<sup>+</sup> carboxylate salts as starting materials, Supporting Information, Table S1. Control experiments were performed with longer reaction times while following the formation of **1** and **2** directly with <sup>1</sup>H NMR. The reactions proceeded rapidly at room temperature (complete reaction in  $\leq 10$  min). Additionally, identical product yields were obtained if the reaction time was 10 min or 9 days. The synthesis of **1** was also accomplished using either the Na<sup>+</sup> or Ag<sup>+</sup> salt of 2-ethylhexanoate. However, use of the Na<sup>+</sup> salt requires an additional filtration step while use of the Ag<sup>+</sup> salt gave only limited amounts of **1**. Limited product formation was also observed in the attempted use of Bu<sub>3</sub>NHO<sub>2</sub>C<sub>8</sub>H<sub>15</sub> to prepare **2**. The necessity of using Na<sup>+</sup> for the synthesis of **2**

could result from different driving force requirements in the syntheses of **1** and **2**. The hexane/H<sub>2</sub>O extraction step, shown in Scheme 1, was performed outside the drybox, with the exclusion of air accomplished using Ar pressure and cannula techniques, and rigorously degassed hexane and water. Compounds **1** and **2** were easily crystallized from acetone with slow cooling, performing the extractions thoroughly to remove the residual chloride salts and/or unreacted starting materials is important, however. Compounds **1** and **2** appear to be relatively air stable in crystalline form but not in solution.<sup>39</sup> These points are discussed in greater detail in the Supporting Information for the interested reader.

**Scheme 1.** Stoichiometry and Associated Reaction Conditions for the Synthesis of **1** (Top), and **2** (Bottom)<sup>a</sup>



<sup>a</sup> Characterization for both compounds was accomplished using by elemental analysis, FAB-MS, single crystal X-ray diffraction, FT-IR, UV-Vis, and <sup>1</sup>H and <sup>13</sup>C spectroscopy, vide infra.

**X-ray Crystal Structures of 1 and 2.** The X-ray crystal structures of **1** and **2**, with atomic numbering schemes and thermal ellipsoids at a 30% probability level, are shown in Figures 1 and 2, respectively.<sup>40</sup> Compounds **1** and **2** both proved to be dimeric as expected,<sup>41</sup> and are isomorphous. Each molecule has two 2-ethylhexanoate ligands bridging the two metal centers. Each transition metal center in **1** and **2** is four-coordinate, bound to one of the oxygen atoms from each 2-ethylhexanoate, and to the two olefinic

bonds from a single  $\eta^{2:2}$ -1,5-COD. The centroids of the olefinic carbon atoms reveals square planar geometries expected for  $d^8$  Ir(I) and Rh(I). However, in both complexes the square planes are imperfect: the metal atoms are displaced from their ligand planes by 0.1522 and 0.1328 Å for Ir1 and Ir2 respectively, and likewise, by 0.1293 and 0.1180 Å for Rh1 and Rh2, respectively, bringing the metal atoms closer together than they would otherwise be. Displacement from the ligand planes has been observed in similar complexes<sup>34</sup> and has been interpreted as evidence of M–M interaction.<sup>42</sup> The dihedral angle between the planes is 56.5° for **1** and 58.1° for **2**, close to angles observed in similar complexes,<sup>42,43,44</sup> some also with bridging carboxylates.<sup>34,45</sup> The dihedral angle is influenced by the metal atom, the terminal ligands, and the type of bridging ligands for complexes of this type.<sup>46,47</sup> In addition, torsion angles about the M–M axes are 20.4° and 22.0° in **1** and **2** respectively, as determined using the [C1,C4,C5,C8] centroid–M1 and [C9,C12,C13,C16] centroid–M2 vectors. This leads to a staggering of the two 1,5-COD ligands consistent with similar established structures.<sup>33,34,43,44,46</sup>

Electron counting for complexes **1** and **2** gives formal 16 electron metal centers with no formal M–M bonds. The M–M distances of structures related to **1** and **2**, and what M–M interactions, if any, have been suggested for analogous complexes, can be found in Supporting Information, Table S2. The M–M distances in **1** and **2** of 3.2776(2) Å and 3.3390(4) Å,<sup>48</sup> respectively, agree well with precedent for those compounds in which some extent of weak M–M interaction is believed likely.<sup>28,43b,49</sup> Such axial M–M bonding interactions in dimeric, square planar,  $d^8$ – $d^8$  structures have been previously investigated,<sup>47,50</sup> with it now understood that bonding occurs as a result of donor–acceptor interactions between filled  $d_z^2$  and empty  $p_z$  orbitals.<sup>47,50</sup> Furthermore, bands in

the UV-vis absorption spectra, at  $\lambda_{\max} = 486$  nm for **1**, and  $\lambda_{\max} = 422$  nm for **2** (Supporting Information, Figure S5), correspond to bands assigned to metal-centered  $d\sigma^* - p\sigma$  transitions in the UV-vis spectra of similar compounds.<sup>44,51,52</sup>

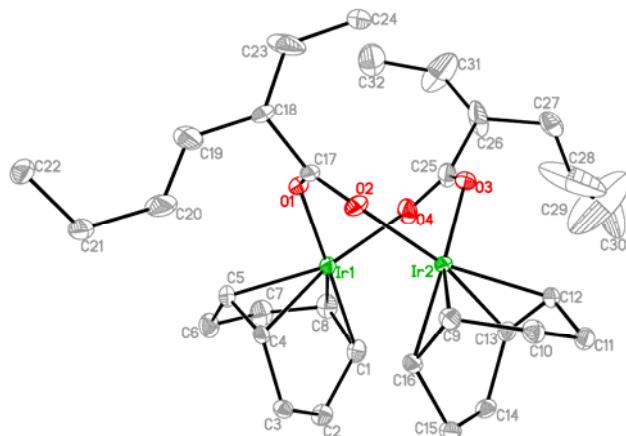


**Figure 1.** Single crystal X-ray diffraction structure and atomic numbering scheme for **1** with thermal ellipsoids at 30% probability. For the sake of clarity, hydrogen atoms are not shown. The large thermal ellipsoids for C28, C29 and C30 (here and in Figure 2) are as expected for such floppy alkyl chains.

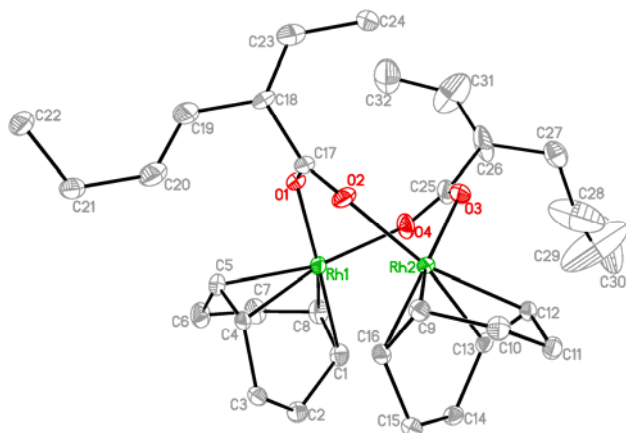


**Figure 2.** Single crystal X-ray diffraction structure and atomic numbering scheme for **2** with thermal ellipsoids at 30% probability. For the sake of clarity, hydrogen atoms are not shown.

Selected bond lengths and angles with estimated standard deviations are given in Tables 1 and 2, respectively, for both compounds. The average M–O distance for **1** is 2.092(6) Å while for **2** it is 2.090(4) Å, close to expected values.<sup>30,34,45</sup> The individual Ir–

O distances in **1** are 2.097(3) and 2.082(3) Å for one 2-ethylhexanoate ligand and 2.087(3) and 2.101(3) Å for the other, each bound to Ir1 and Ir2, respectively. Likewise, the individual Rh–O distances in **2** are 2.095(2) and 2.078(2) Å for one 2-ethylhexanoate ligand, and 2.086(2) and 2.100(2) Å for the other, for Rh1 and Rh2, respectively. These distances indicate non-symmetrical bridging of the 2-ethylhexanoate ligands. Each metal center and each 2-ethylhexanoate has one M–O bond longer than the other, with an average difference of 0.015(6) Å in **1** and 0.015(4) Å in **2**. The average M–C distance is 2.09(1) in **1** and 2.096(9) Å in **2**. The average olefinic C=C bond lengths are 1.42(1) and 1.398(9) Å in **1** and **2**, respectively. The marginally longer C=C bond in **1** could be interpreted as the result of the more electron rich Ir(I) engaging in a greater degree of  $\pi$ -back-bonding than its Rh(I) counterpart. These values and interpretations are consistent with expectations based on similar structures.<sup>33,34,43,46</sup>

**Table 1.** Selected Bond Lengths (Å) for **1** and **2**

bond	<b>1</b> , M = Ir	<b>2</b> , M = Rh
M1–C8	2.086(5)	2.093(4)
M1–C4	2.086(3)	2.088(3)
M1–O4	2.087(3)	2.086(2)
M1–C5	2.097(4)	2.104(3)
M1–O1	2.097(3)	2.095(2)
M1–C1	2.103(4)	2.105(3)
M2–O2	2.082(3)	2.078(2)
M2–C9	2.084(4)	2.087(3)
M2–C13	2.089(3)	2.092(3)
M2–C12	2.093(4)	2.098(3)

M2–C16	2.094(3)	2.101(3)
M2–O3	2.101(3)	2.100(2)
O1–C17	1.262(6)	1.251(5)
O2–C17	1.261(5)	1.266(4)
O3–C25	1.260(7)	1.262(5)
O4–C25	1.254(7)	1.254(5)

**Table 2.** Selected Bond Angles (deg) for **1** and **2**

bond	1, M = Ir	2, M = Rh
C8–M1–C4	99.17(17)	99.08(14)
C8–M1–O4	86.00(17)	86.09(13)
C4–M1–O4	166.32(14)	164.91(12)
C8–M1–C5	82.35(18)	82.55(15)
O4–M1–C5	153.88(15)	155.97(13)
C8–M1–O1	149.41(16)	150.61(13)
C4–M1–O1	91.47(13)	90.91(11)
O4–M1–O1	90.31(14)	91.36(11)
C5–M1–O1	87.98(15)	88.31(12)
C4–M1–C1	82.15(15)	82.42(13)
O4–M1–C1	94.26(16)	93.18(13)
C5–M1–C1	91.51(17)	91.18(14)
O1–M1–C1	170.54(14)	169.94(12)
O2–M2–C9	85.41(14)	85.51(12)
O2–M2–C13	166.05(15)	165.32(12)
C9–M2–C13	99.28(15)	99.02(12)
O2–M2–C12	154.13(15)	155.52(12)
C9–M2–C12	82.56(15)	82.60(13)

O2–M2–C16	93.49(13)	92.77(11)
C13–M2–C16	82.22(14)	82.44(12)
C12–M2–C16	91.69(15)	91.30(12)
O2–M2–O3	89.89(13)	90.55(10)
C9–M2–O3	151.15(15)	152.13(12)
C13–M2–O3	92.07(14)	91.72(11)
C12–M2–O3	89.72(14)	90.06(11)
C16–M2–O3	169.17(15)	168.87(12)
C17–O1–M1	130.9(3)	131.9(2)
C17–O2–M2	126.3(3)	126.5(2)
C25–O3–M2	128.7(3)	128.7(2)
C25–O4–M1	126.9(3)	127.8(3)
O2–C17–O1	125.6(4)	126.2(3)
O2–C17–C18	117.2(4)	116.5(4)
O1–C17–C18	117.2(4)	117.3(3)
O4–C25–O3	125.9(4)	125.8(3)
O4–C25–C26	118.6(6)	117.0(4)
O3–C25–C26	115.5(6)	117.2(4)

The  $\alpha$  carbon of 2-ethylhexanoate is stereogenic. Complexes **1** and **2** crystallize with (R,R) and (S,S) enantiomers in a unit cell (centrosymmetric space group  $P2_1/n$ ,  $Z = 4$ ). The possibility exists, therefore, to prepare chiral analogues of **1** and **2** (i.e., using enantiopure 2-ethylhexanoate, or analogous chiral ligands) to effect asymmetric catalysis.

**Demonstration of Catalytic Hydrogenation Activity.** It is important to demonstrate that **1** and **2** form Ziegler-type hydrogenation catalysts. This was accomplished by the addition of a cyclohexane solution of  $AlEt_3$  to a cyclohexane

solution of **1** or (separately) **2**, at an Al/M = 1 ratio; the result is an immediate change, from the orange solution of **1** to tawny yellow, or the yellow solution of **2** to clear brown. Representative cyclohexene hydrogenations are shown in Figures 3 and 4 for **1** and **2**, respectively. Active H<sub>2</sub> uptake begins immediately in both cases, suggesting that the products of the reaction between AlEt<sub>3</sub> and **1** or **2** have *preformed active Ziegler-type hydrogenation catalysts* (i.e., that the active catalysts are formed, at least in large part, from the addition of AlEt<sub>3</sub>, rather than being solely reduced or activated solely by H<sub>2</sub>). Catalyst formation from these systems is being optimized,<sup>17</sup> according to variables known to be important to Ziegler-type hydrogenation catalysts,<sup>53,54,55,56</sup> work that will be reported in due course.

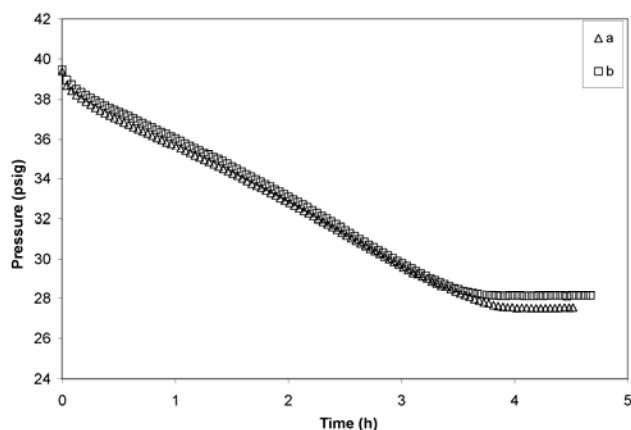


**Figure 3.** Two representative runs for the hydrogenation of cyclohexene using an Ir Ziegler-type hydrogenation catalyst formed upon combination of **1** and AlEt<sub>3</sub>, Al/Ir = 1. Experimental conditions for all hydrogenations were solvent = cyclohexane, temp. = 22.0 °C, catalyst concentration = 1.2 mM in [Metal], initial cyclohexene concentration = 1.65 M, and stirring = 1000 rpm. For clarity, only every fifth data point collected of run “a” is displayed. The absence of an induction period shows that either an active catalyst was present from the start of the hydrogenation, or conceivably formed essentially immediately once H<sub>2</sub> was added. The change of the solution during the reaction to darker brown, and the subtle changes to the slope of these curves, suggest that further catalyst evolution is taking place during the hydrogenation.<sup>17</sup>

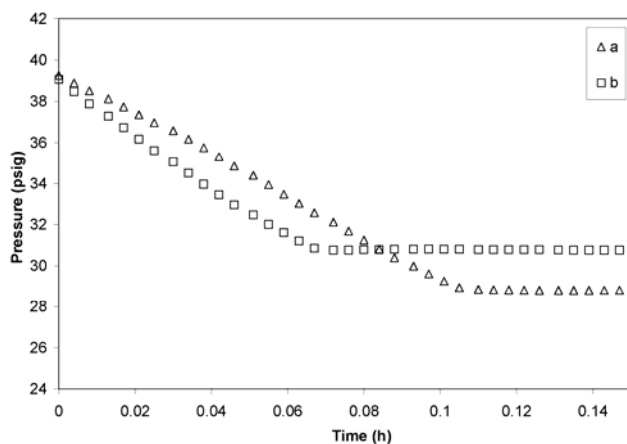


**Figure 4.** Two representative runs for the hydrogenation of cyclohexene using a Rh Ziegler-type hydrogenation catalyst formed upon combination **2** and  $\text{AlEt}_3$ ,  $\text{Al/Rh} = 1$ . Again, the absence of an induction period demonstrates that either an active catalyst is present from the start of the hydrogenation, or forms essentially immediately once  $\text{H}_2$  was added. The catalyst formed using Rh **2** is >30 fold more active than its Ir **1** counterpart. Because of this high activity, the reproducibility of the two hydrogenation curves shown here is sensitive to the reproducibility of the  $\text{H}_2$  gas purge cycle, the start of data acquisition, and the precise stirring speed, as would be characteristic of reactions influenced by  $\text{H}_2$  gas-to-solution MTL.<sup>57</sup>

The linear versus normally expected exponential shape of both the curves in Figures 3 and 4 is of interest. The Rh catalyst made from **2** is significantly more active for cyclohexene hydrogenation than the Ir catalyst made using **1** (>30 times according to linear fits to the portions of the curve during which pressure loss was occurring, Supporting Information, Figure S10 and Table S3). The rates of  $\text{H}_2$  pressure loss in Figure 4 are close to the  $\text{H}_2$  gas-to-solution MTL for the apparatus and conditions used,<sup>17</sup> which accounts for the observed linearity.<sup>57</sup> However, since the apparatus and conditions used are identical, the near-linearity of the >30-fold slower hydrogenation curves given by the catalyst made from **1**, shown in Figure 3, cannot also be explained by MTL effects. Close inspection of the hydrogenation curves for **1** reveals subtle changes in the rate of  $\text{H}_2$  uptake during the hydrogenation. An additional point is that after all the cyclohexene had been consumed, the catalyst solutions appeared unchanged in the case

of **2** (4–7 min), but had turned darker brown in the case of **1** (3.8 h). These observations imply that further catalyst development (i.e., in either consecutive or parallel reactions) is taking place as the cyclohexene hydrogenation proceeds in Figure 3. Detailed characterization studies using EXAFS, electron microscopy, and other methods are in progress,<sup>17</sup> now that **1** and **2** are available and shown to yield active Ziegler-type hydrogenation catalysts.

**Control Experiments to Determine if AlEt<sub>3</sub> is Required to Form Active Catalysts.** Since a fundamental characteristic of Ziegler-type hydrogenation catalysts is their “activation” by an organometallic cocatalyst, frequently AlR<sub>3</sub>,<sup>1,2</sup> control experiments were performed to check the necessity of AlEt<sub>3</sub> in forming active hydrogenation catalysts from **1** and **2**. Hydrogenations were performed identically to those in Figures 3 and 4, but leaving out the AlEt<sub>3</sub> while substituting an equal volume of cyclohexane for the volume introduced by the AlEt<sub>3</sub> solution. The results, Supporting Information, Figure S9, reveal that active, though poorly stabilized, nanoparticle and/or bulk metal catalysts are formed following an induction period. These control experiments confirm the need for, and value of, AlEt<sub>3</sub> in producing *long-lived* hydrogenation catalysts from **1** and **2**.

## Conclusions

The synthesis, unequivocal characterization, and utility as precursors of Ziegler-type hydrogenation catalysts of [(1,5-COD)Ir(μ-O<sub>2</sub>C<sub>8</sub>H<sub>15</sub>)<sub>2</sub>] (**1**) and [(1,5-COD)Rh(μ-O<sub>2</sub>C<sub>8</sub>H<sub>15</sub>)<sub>2</sub>] (**2**) (COD = cyclohexadiene, O<sub>2</sub>C<sub>8</sub>H<sub>15</sub> = 2-ethylhexanoate) have been

described herein. Compositional and structural characterization of these compounds was carried out by elemental analysis, FAB-MS, single crystal X-ray diffractometry, FT-IR, UV-vis, and NMR spectroscopy. X-ray crystallography showed that **1** and **2** are isostructural. The complexes are carboxylate-bridged dimers with terminal  $\eta^{2:2}$ -1,5-COD ligands. They have a bent geometry with dihedral angles of  $56.5^\circ$  and  $58.1^\circ$  for **1** and **2**, respectively, between the square ligand planes of the 4-coordinate M(I) centers. Formally non-bonding M–M distances of 3.2776(2) and 3.3390(4) Å for **1** and **2**, respectively, likely entail weak M–M bonding interactions.<sup>28,42,43b,44,47,49,50</sup>

Both **1** and **2** serve as effective precatalysts that, when combined with AlEt<sub>3</sub>, form highly active Ziegler-type hydrogenation catalysts. The Rh catalyst formed from **2** is  $\geq 30$ -fold more active than the Ir catalyst prepared from **1**. This suggests that it will prove useful to have both the Ir and Rh systems for comparison to industrial catalysts, commonly made from Ni or Co.<sup>1,2</sup> Control hydrogenations performed without AlEt<sub>3</sub> contained induction periods showing that **1** and **2** display a key feature of Ziegler-type hydrogenation catalysts by requiring “activation” by a cocatalyst, in this case AlEt<sub>3</sub>.

Publication of our work on the characterization of the catalysts formed from **1** and **2** is forthcoming.<sup>17</sup> That work teaches that the use of well-defined, model second and third row, precatalysts **1** and **2** has been instrumental in elucidating further insights into Ziegler-type hydrogenation catalysts,<sup>17</sup> a ~40 year old problem left unanswered by studies using less well-defined, first row industrial precursors.

## Experimental

**Procedures, Materials, and Instrumentation.** Unless indicated otherwise, all manipulations were performed either under N<sub>2</sub> in a Vacuum Atmospheres drybox or using air-free techniques on a Schlenk line. Oxygen levels were continuously maintained in the drybox at ≤5 ppm, monitored by a Vacuum Atmospheres O<sub>2</sub>-level monitor. All glassware was oven-dried at 160 °C overnight before use and cooled either under vacuum or under N<sub>2</sub> in the drybox. Unless noted otherwise, all solvents, compounds, and other materials below were stored in the drybox. Cyclohexane was used as received (Sigma-Aldrich 99.5%, anhydrous: water <0.001%). Both cyclohexene (Aldrich, 99%) and tributylamine (J. T. Baker Chemicals) were distilled over sodium under an argon atmosphere before being transferred to the drybox. 2-Ethylhexanoic acid (Aldrich, 99+%) was purged with argon for 30 min. Prior to storage in the drybox, acetone (Burdick and Jackson, water content <0.5%) was purged with argon for 20 min. The complexes [(1,5-COD)M(μ-Cl)]<sub>2</sub> (M = Ir, Rh), Ag(2-ethylhexanoate) (Strem, 99%), and Na(2-ethylhexanoate) (Aldrich, 97%) were used as received. KBr (Aldrich, 99+%, FT-IR grade) was oven-dried at 160 °C overnight before use. Filter paper (Whatman #4) was oven-dried at 160 °C for ≥1 h before use. Argon (General Air, 99.985%) was passed through oxygen and moisture traps consisting of activated carbon and molecular sieves prior to use. Hydrogen gas (General Air, 99.5%) was purified by passing through an indicating moisture trap (Scott Specialty Gas), a disposable O<sub>2</sub> cartridge (Trigon), and an indicating O<sub>2</sub> trap (Trigon). AlEt<sub>3</sub> was obtained (Aldrich, 93%) as the neat liquid and used as received. **Caution!** *Aluminum alkyls such as AlEt<sub>3</sub> are toxic and pyrophoric, and must be handled with extreme care using air and water-free techniques.*<sup>58</sup>

Elemental analyses were performed by Galbraith Laboratories, Knoxville, TN. Positive ion fast atom bombardment mass spectrometry (FAB-MS) data were acquired on a VG AutoSpec (Fisons Instruments). Nuclear magnetic resonance (NMR) spectra for  $^1\text{H}$  and  $^{13}\text{C}$  nuclei were obtained on a Varian Inova (JS-300) NMR spectrometer in  $\text{CD}_2\text{Cl}_2$ ,  $\text{CD}_3\text{COCD}_3$ , or  $\text{C}_6\text{D}_6$  (Cambridge Isotopes Laboratory).  $^1\text{H}$  NMR spectra were referenced to the residual impurity in the deuterated solvents and manipulated by MestRec software after initial acquisition. Samples for Fourier transform infrared (FT-IR) spectroscopy were prepared as KBr discs using a KBr die and a Carver Laboratory Press. FT-IR spectra were obtained on a Nicolet Magna-IR 760 ESP IR spectrometer. Cyclohexane solution samples for UV–visible spectroscopy were prepared in the drybox in 1 cm glass cuvettes equipped with high vacuum stopcocks. Sample concentration was 0.218 and 0.196 ( $\pm 0.001$ ) mM for **1** and **2**, respectively. UV–visible spectra were obtained using a Hewlett-Packard 8452A diode-array spectrophotometer. Melting points were acquired using a Mel-Temp II melting point measurement apparatus. Sample preparations for X-ray crystallography, FT-IR, and melting points were performed in air where brief exposure of crystalline **1** and **2** to atmospheric oxygen occurred. No degradation of crystalline **1** or **2** was apparent from this treatment.

**Synthesis of [(1,5-COD)Ir( $\mu$ -O<sub>2</sub>C<sub>8</sub>H<sub>15</sub>)<sub>2</sub>] (1) and [(1,5-COD)Rh( $\mu$ -O<sub>2</sub>C<sub>8</sub>H<sub>15</sub>)<sub>2</sub>] (2).** Detailed accounts of the synthesis procedures are given in the Supporting Information. Briefly, for the synthesis of **1**, a stoichiometric amount of  $\text{Bu}_3\text{NH}(2\text{-ethylhexanoate})$  made from combining  $\text{Bu}_3\text{N}$  and 2-ethylhexanoic acid in acetone was added to an acetone suspension of  $[(1,5\text{-COD})\text{Ir}(\mu\text{-Cl})_2]$ , causing the yellow/orange suspension to immediately turn to a deep-red solution. The product was then extracted

into cyclohexane and washed several times with portions of degassed water to remove the residual  $\text{Bu}_3\text{NH}^+\text{Cl}^-$ . It was important to ensure both air-free conditions and a thorough hexane/ $\text{H}_2\text{O}$  extraction. The hexane was then removed in vacuo, and **1** was crystallized from an acetone solution by slowly cooling to  $-78\text{ }^\circ\text{C}$ , 61% yield. Anal. Calcd for  $\text{C}_{32}\text{H}_{54}\text{Ir}_2\text{O}_4$  (mol. wt. 887.15 g/mol): C, 43.32; H, 6.14; N, 0.0; O, 7.2%. Found: C, 43.32; H, 5.94; N < 0.5; O, 7.9%. m.p.: 67–68  $^\circ\text{C}$ . FAB-MS peaks > 15% rel. intensity ( $m/z$ , rel. intensity, (estimated ion)<sup>+</sup>): 886.6, base peak,  $[(1,5\text{-COD})\text{Ir}(\text{O}_2\text{C}_8\text{H}_{15})]_2^+$ ; 741.5, 71%,  $(\text{C}_{24}\text{H}_{37}\text{Ir}_2\text{O}_2 \text{ or } \text{C}_{22}\text{H}_{29}\text{Ir}_2\text{O}_4)^+$ ; 597.0, 27%,  $(\text{C}_{11}\text{H}_{17}\text{Ir}_2\text{O}_4)^+$ ; 591.0, 76%,  $(\text{C}_{13}\text{H}_{19}\text{Ir}_2\text{O}_2)^+$ ; 443.1, 92%,  $((1,5\text{-COD})\text{Ir}(\text{O}_2\text{C}_8\text{H}_{15})\text{-1})^+$ ; 297.0, 17%,  $(\text{C}_8\text{H}_8\text{Ir})^+$ . A compelling match exists between the observed isotope distribution for the parent ion and one calculated for  $[(1,5\text{-COD})\text{Ir}(\mu\text{-O}_2\text{C}_8\text{H}_{15})]_2$  (see Supporting Information, Figure S1).  $^1\text{H}$  NMR in  $\text{C}_6\text{D}_6$ , ( $\delta$  in ppm, multiplicity, no. of H): 4.13–4.23, m, 4; 3.85–3.93, m, 4; 2.35–2.45, m, 4; 1.95–2.15, m, 6; 1.48–1.55, m, 4; 1.00–1.32, m, 20; 0.67–0.81, m, 12.  $^{13}\text{C}$  NMR in  $\text{C}_6\text{D}_6$ , ( $\delta$  in ppm): 188.4s, 64.1m, 55.8m, 50.9s, 33.4s, 32.7s, 31.9m, 30.5s, 27.0s, 23.5s, 14.6s, 12.8s. IR bands > 20% abs. ( $\text{cm}^{-1}$ ): 3030–2760m, 1560s, 1457s, 1419s, 1321s.

The procedure was very similar for the synthesis of **2**. Differences were that a solution of Na(2-ethylhexanoate) was used and the resulting crude product solution was filtered before the air-free hexane/ $\text{H}_2\text{O}$  extraction. Crystals of **2** were obtained in an 86% yield. A recrystallization of a portion of the product **2** was required to produce larger, light orange, irregularly shaped single crystals suitable for X-ray diffractometry. Anal. Calcd for  $\text{C}_{32}\text{H}_{54}\text{O}_4\text{Rh}_2$  (mol. wt. 708.57 g/mol): C, 54.24; H, 7.68; O, 9.0%; Na, 0 ppm. Found: C, 54.28; H, 7.87; O, 8.4%; Na < 46 ppm. m.p.: 57–58  $^\circ\text{C}$ . FAB-MS peaks

>15% rel. intensity ( $m/z$ , rel. intensity, (estimated ion)<sup>+</sup>): 708.4, 65%, ((1,5-COD)Rh(O<sub>2</sub>C<sub>8</sub>H<sub>15</sub>)]<sub>2</sub>)<sup>+</sup>; 565.0, 87%, ((1,5-COD)<sub>2</sub>Rh<sub>2</sub>(O<sub>2</sub>C<sub>8</sub>H<sub>15</sub>))<sup>+</sup>; 455.0, 55%, (C<sub>16</sub>H<sub>25</sub>O<sub>2</sub>Rh<sub>2</sub>)<sup>+</sup>; 415.0, 19%, ((C<sub>11</sub>H<sub>13</sub>O<sub>4</sub>Rh<sub>2</sub>)<sup>+</sup>; 353.1, base peak, ((1,5-COD)Rh(O<sub>2</sub>C<sub>8</sub>H<sub>15</sub>)-1)<sup>+</sup>; 309.9, 24%, (C<sub>13</sub>H<sub>19</sub>O<sub>2</sub>Rh)<sup>+</sup>; 211.0, 67%, ((1,5-COD)Rh)<sup>+</sup>; 147.1, 16%, (Rh(O<sub>2</sub>C))<sup>+</sup>. <sup>1</sup>H NMR in C<sub>6</sub>D<sub>6</sub>, ( $\delta$  in ppm, multiplicity, no. of H): 4.30–4.40, m, 4; 4.18–4.30, m, 4; 2.65–2.82, m, 4; 2.15–2.38, m, 6; 1.20–1.72, m, 24; 0.85–0.98, m, 12. <sup>13</sup>C NMR in C<sub>6</sub>D<sub>6</sub>, ( $\delta$  in ppm): 187.8s, 80.8d, 74.0d, 50.9s, 33.4s, 31.9s, 31.0s, 30.6s, 27.1s, 23.6s, 14.7s, 12.9s. IR bands > 20% abs. (cm<sup>-1</sup>): 3040–2760m, 1567s, 1462s, 1415s, 1324s, 952s, 817s.

**X-ray Crystallographic Structure Determination and Refinement.** X-ray diffraction data were collected on a Bruker Kappa APEXII X-ray diffractometer equipped with a beam monochromator. Corrections applied were Lorentz, polarization, and absorption (SADABS).<sup>59</sup> Data collection and cell refinement were accomplished using Bruker SMART software, and data reduction using Bruker SAINT. Both structures were solved by direct methods. Structure solution, structure refinement, and figure preparation were achieved using Bruker SHELXTL.<sup>60</sup> Refinements were accomplished by full-matrix weighted least-squares on  $F^2$  for all reflections. Anisotropic displacement parameters were used for refinement of all non-hydrogen atoms. Hydrogen atoms were included at idealized positions in structure factor calculations. Experimental details for crystal data and structural refinement of **1** and **2** are displayed in Table 3.

**Table 3.** Summary of Crystallographic Data and Refinement for Compounds **1** and **2**

compound	<b>1</b>	<b>2</b>
chemical formula	C <sub>32</sub> H <sub>54</sub> Ir <sub>2</sub> O <sub>4</sub>	C <sub>32</sub> H <sub>54</sub> O <sub>4</sub> Rh <sub>2</sub>
formula weight	887.15	708.57
<i>T</i> (K)	100(1)	100(1)
$\lambda$ (Å)	0.71073	0.71073
space group	<i>P</i> 2 <sub>1</sub> / <i>n</i>	<i>P</i> 2 <sub>1</sub> / <i>n</i>
<i>a</i> (Å)	15.7748(5)	15.7608(4)
<i>b</i> (Å)	9.8962(3)	9.9032(3)
<i>c</i> (Å)	20.8847(7)	20.8259(5)
$\beta$ (deg)	108.408(2)	108.527(1)
<i>V</i> (Å <sup>3</sup> )	3093.50(17)	3082.09(14)
$\rho_{\text{calcd}}$ (mg/m <sup>3</sup> )	1.905	1.527
<i>Z</i>	4	4
$\mu$ (mm <sup>-1</sup> )	8.629	1.105
final <i>R</i> indices <sup>a</sup>	$R_1 = 0.0443,$ $wR_2 = 0.0827$	$R_1 = 0.0504,$ $wR_2 = 0.1260$

<sup>a</sup>  $R_1$  is for  $[I > 2\sigma(I)]$ ,  $wR_2$  is for all data:  $R_1 = \sum \|F_o| - |F_c| \| / \sum |F_o|$ ,  $wR_2 = [\sum w(|F_o| - |F_c|)^2 / \sum w|F_o|^2]^{1/2}$ .

**Precatalyst and Catalyst Solution Preparation.** The Ir and Rh precatalysts **1** and **2** were used in catalyst preparation by first making a stock solution of each in cyclohexane. Specifically, a stock solution of **1**, 7.20 mM in [Ir], was prepared by weighing out  $0.0430 \pm 0.0001$  g (0.0485 mmol) of crystalline **1** and dissolving with  $13.46 \pm 0.01$  mL of cyclohexane. A stock solution of **2**, 7.20 mM in [Rh] was prepared by weighing out  $0.04337 \pm 0.0001$  g (0.0612 mmol) of crystalline **2**, and dissolving in  $17.00 \pm 0.01$  mL of cyclohexane. AlEt<sub>3</sub> was used as a 36.0 mM stock solution in cyclohexane

prepared by adding 50–70 mL of cyclohexane to a 100 mL volumetric flask, followed by  $0.53 \pm 0.01$  mL of neat AlEt<sub>3</sub> measured out by syringe, and then diluting to the mark (this included a 7% correction factor to take into account the 93% purity of the AlEt<sub>3</sub>, even though the impurities are primarily other aluminum alkyls).

Catalyst solutions were prepared individually, from the stock precatalyst and AlEt<sub>3</sub> cocatalyst solutions, in new 22 × 175 mm Pyrex borosilicate culture tubes containing new 5/8 × 5/16 in. Teflon-coated magnetic stirbars. Both culture tube and stirbar had been cleaned by rinsing three times with nanopure water prior to drying at 160 °C overnight and cooled either under vacuum or under N<sub>2</sub> in the drybox. Specifically, and using **1** as an example, a catalyst solution 1.2 mM in [Ir] was prepared individually, and in the drybox, by first adding  $0.50 \pm 0.01$  mL of 7.2 mM **1** to a culture tube, followed by  $1.90 \pm 0.02$  mL of cyclohexane (Sigma-Aldrich 99.5%, anhydrous: water < 0.001%, used as received). The level of water present is a crucial variable for these AlR<sub>3</sub>-containing catalysts.<sup>17,53</sup> Next,  $0.100 \pm 0.001$  mL of 36.0 mM AlEt<sub>3</sub> in cyclohexane was rapidly added via syringe, with stirring at  $1.0 \times 10^3$  rpm (measured with a Monarch Instruments Pocket-Tachometer 100), to make an Al/Ir = 1 solution.

**Catalytic Hydrogenation of Cyclohexene.** The procedure and apparatus for hydrogenation have been described in detail elsewhere.<sup>18a,61,62</sup> Briefly, after a catalyst solution was prepared,  $0.50 \pm 0.01$  mL of cyclohexene was added, and the culture tube was placed inside a Fisher–Porter (FP) bottle which was sealed, brought out of the drybox, placed in a temperature controlled bath set to  $22.0 \pm 0.1$  °C, and connected to the hydrogenation line<sup>18a,61,62</sup> via TFE-sealed Swagelock Quick-Connects. Stirring of 1000 rpm powered by a Fauske Super magnetic stirplate was started. The use of this stirrer

was important in ensuring continuous vortex stirring of the sample at a constant rate in an effort to diminish the influence of H<sub>2</sub> gas-to-solution mass-transfer limitations (MTL).<sup>57</sup> The FP bottle was then filled and purged with H<sub>2</sub> at 40 psig once every 15 s for three and a half-minutes for a total of 15 times. The pressure inside the FP bottle was set to 40 psig, and pressure data acquisition started at the interfaced computer,<sup>18a,61,62</sup> at a total elapsed time of 4 min after the first purge. Hydrogenation conditions: total solution volume was 3.0 mL, 1.2 mM in [M], initially 1.65 M in [cyclohexene], stirred at 1000 r.p.m., and maintained at 22.0 °C. Pressure data was collected from the FP bottle on the H<sub>2</sub> line by means of an Omega PX-621 pressure transducer interfaced to a PC running LabVIEW 7.0 and handled using Microsoft Excel.<sup>18a,61,62</sup> For control hydrogenations without added AlEt<sub>3</sub>, hydrogen pressure data was converted to cyclohexene concentration using the known 1:1 H<sub>2</sub> to cyclohexene stoichiometry.<sup>18a,61</sup> Fits to the data were obtained using Microcal Origin 7.0 according to the 2-step Finke–Watzky mechanism for nanocluster formation consisting of slow nucleation ( $A \rightarrow B$ , rate constant  $k_1$ ) followed by fast autocatalytic surface growth ( $A + B \rightarrow 2B$ , rate constant  $k_2$ ).<sup>18a</sup>

**Acknowledgement.** We thank Ms. Susie Miller for conducting the X-ray structure determinations and Prof. Oren Anderson for proofreading the X-ray structure descriptions. This work was supported by NSF Grant CHE-0611588.

**Supporting Information Available:** Tables with literature and references for previous syntheses of related Ir and Rh(1,5-COD)( $\mu$ -O<sub>2</sub>CR)-type compounds, and compounds with similar structures. Detailed synthesis procedures and observations. FAB-MS images. Spectra and discussions thereof: FT-IR; UV–vis; and <sup>1</sup>H, <sup>13</sup>C, and VT

<sup>1</sup>H NMR. Hydrogenation kinetic curves including a control experiment without added AlEt<sub>3</sub>, fits to the data, and a table of the fit results. A cif file containing the crystallographic data for both structures. This material is available free of charge via the Internet at <http://pubs.acs.org>.

## References.

---

<sup>1</sup> McManus, N. T.; Rempel, G. L. *J.M.S. Rev. Macromol. Chem. Phys.* **1995**, *35*, 239–285.

<sup>2</sup> Johnson, K. A. *Polym. Prepr.* **2000**, *41*, 1525–1526.

<sup>3</sup> Weiner, H.; Trovarelli, A.; Finke, R. G. *J. Mol. Catal. A: Chem* **2003**, *191*, 217–252.

<sup>4</sup> Johnson, K. A., Houston, TX.<sup>2</sup> Personal communication, 2008. The complete statement was: “In their March 2005 study of Syrenic Thermoplastic Elastomers (525.8600 A), SRI estimated the global 2004 SBC consumption at 1,293,000 tonnes with HSBC at 10% of that. Since then we believe demand growth rates have been of the order of 10% pa which would imply a 2007 demand in the region of 170,000 tonnes for HSBC.”

<sup>5</sup> Lapporte, S. J. Preparation of Complex Organic Metallic Hydrogenation Catalysts and Their Use. U.S. Patent 3,205,278, Sep 7, 1965.

<sup>6</sup> Cannell, L.; Magoon, E. F.; Raley, J. H. Olefin Oligomerization. U.S. Patent 3,424,815, Jan 28, 1969.

<sup>7</sup> Wald, M. M.; Quam, M. G. Selectively Hydrogenated Block Copolymers. U.S. Patent 3,700,633, Oct 24, 1972.

<sup>8</sup> Sloan, M. F.; Matlack, A. S.; Breslow, D. S. *J. Am. Chem. Soc.* **1963**, *85*, 4014–4018.

<sup>9</sup> Kroll, W. *J. Catal.* **1969**, *15*, 281–288.

<sup>10</sup> Lapporte, S. J. *Ann. N.Y. Acad. Sci.* **1969**, *158*, 510–525.

- 
- <sup>11</sup> Barrault, J.; Blanchard, M.; Derouault, A.; Ksibi, M.; Zaki, M. I. *J. Mol. Catal.* **1994**, *93*, 289–304.
- <sup>12</sup> Pasykiewicz, S.; Pietrzykowski, A.; Dowbor, K. *J. Organomet. Chem.* **1974**, *78*, 55–59.
- <sup>13</sup> Collman, J. P.; Hegedus, L. S.; Norton, J. R.; Finke, R. G. *Principles and Applications of Organotransition Metal Chemistry*; University Science Books: Mill Valley, CA, 1987.
- <sup>14</sup> Widegren, J. A.; Finke, R. G. *J. Mol. Catal. A: Chem.* **2003**, *198*, 317–341.
- <sup>15</sup> Schwartz, J. *Acc. Chem. Res.* **1985**, *18*, 302–308.
- <sup>16</sup> Falk, J. C. *J. Polym. Sci., Part A-1* **1971**, *9*, 2617–2623.
- <sup>17</sup> Alley, W. M.; Kayiran, I.; Wang, Q.; Frenkel, A.; Long, L.; Yang, J. C.; Menard, L. D.; Nuzzo, R. G.; Özkar, S.; Johnson, K. A.; Finke, R. G. Characterization of Ziegler-type Hydrogenation Catalysts Made From [(1,5-COD)Ir( $\mu$ -O<sub>2</sub>C<sub>8</sub>H<sub>15</sub>)]<sub>2</sub> and AlEt<sub>3</sub> or Al(t-Bu)<sub>3</sub>, to be submitted for publication.
- <sup>18</sup> (a) Watzky, M. A.; Finke, R. G. *J. Am. Chem. Soc.* **1997**, *119*, 10382–10400. (b) Özkar, S.; Finke, R. G. *Langmuir* **2003**, *19*, 6247–6260.
- <sup>19</sup> (a) Jaska, C. A.; Manners, I. *J. Am. Chem. Soc.* **2004**, *126*, 1334–1335. (b) Jaska, C. A.; Manners, I. *J. Am. Chem. Soc.* **2004**, *126*, 9776–9785. (c) Hagen, C. M.; Widegren, J. A.; Maitlis, P. M.; Finke, R. G. *J. Am. Chem. Soc.* **2005**, *127*, 4423–4432. (d) Hagen, C.; Vieille-Petit, L.; Laurenczy, G.; Süß-Fink, G.; Finke, R. G. *Organometallics* **2005**, *24*, 1819–1831. (e) Williams, D. B.; Carter, C. B. *Transmission Electron Microscopy*, Plenum Press: New York, 1996.
- <sup>20</sup> The similarity of [(1,5-COD)M( $\mu$ -O<sub>2</sub>C<sub>8</sub>H<sub>15</sub>)]<sub>2</sub> compounds (M = Ir or Rh, O<sub>2</sub>C<sub>8</sub>H<sub>15</sub> = 2-ethylhexanoate) to industrial catalyst precursors such as Ni(2-ethylhexanoate)<sub>2</sub> made it very likely that they would form active Ziegler-type hydrogenation catalysts upon addition of AlEt<sub>3</sub> (demonstrated herein). Additionally, complexes of the type [(1,5-

---

COD)M( $\mu$ -carboxylato)]<sub>2</sub> (COD = cyclooctadiene, M = Ir or Rh) were expected to be, and are, soluble in the same solvents as Ni(2-ethylhexanoate)<sub>2</sub> and other industrial catalyst precursors. Gas chromatographic (GC) analysis of cyclooctane (i.e., hydrogenated 1,5-COD) has proven to be an important analytical handle in past nanocluster syntheses from (1,5-COD)M<sup>+</sup> (M = Rh, Ir) precursors.<sup>18</sup> It seemed especially promising to be able to use catalysts formed from the heavier, 3<sup>rd</sup> row transition metal Ir complex, as they would more likely be amenable for use with TEM to look for the presence of metal particles than catalysts made from lighter Co and Ni counterparts. The ability to compare the Ir compound to its Rh analogue, as well as to industrial Ni and Co catalysts, is an additional advantage of the present approach and precursors.

<sup>21</sup> Although [(1,5-COD)M( $\mu$ -O<sub>2</sub>C<sub>8</sub>H<sub>15</sub>)]<sub>2</sub> (M = Ir or Rh) are not commercially available, their ready synthesis also appeared promising. Chatt and Venanzi described the original synthesis of the acetate compound [(1,5-COD)Rh( $\mu$ -O<sub>2</sub>CCH<sub>3</sub>)]<sub>2</sub> from [(1,5-COD)Rh( $\mu$ -Cl)]<sub>2</sub> and potassium acetate.<sup>26</sup> The synthesis of other [(diene)Rh( $\mu$ -O<sub>2</sub>CR)]<sub>2</sub> complexes have been reported using similar approaches, including those where the R group is CH<sub>2</sub>Cl,<sup>27</sup> CH<sub>2</sub>F,<sup>27</sup> or CF<sub>3</sub>.<sup>28,29,30</sup> Other carboxylates used include benzoate,<sup>30,31</sup>  $\square$ (+)-mandelate,<sup>24</sup> N-phenylanthranilate,<sup>32</sup> and salicylate.<sup>33</sup> Complexes with dienes other than 1,5-COD such as norbornadiene (NBD),<sup>28,28,31,34,35</sup> dicyclopentadiene,<sup>27</sup> (ethylene)<sub>2</sub>,<sup>30</sup> or (cyclooctene)<sub>2</sub>,<sup>30</sup> have been attained, usually by varying the [(diene)Rh( $\mu$ -Cl)]<sub>2</sub> starting material. Several comparable Ir compounds have been reported,<sup>27,30,36</sup> including a patent that described the synthesis of “Ir(cyclooctadiene)(2-ethylhexanoate)” by addition of triethylammonium 2-ethylhexanoate to [(1,5-COD)Ir( $\mu$ -Cl)]<sub>2</sub>.<sup>37</sup> The previous literature describing syntheses of related Rh and Ir(1,5-COD)( $\mu$ -O<sub>2</sub>CR)-type compounds is summarized in Supporting Information, Table S1.

<sup>22</sup> Mishra, S.; Daniele, S.; Hubert-Pfalzgraf, L. G. *Chem. Soc. Rev.* **2007**, *36*, 1770–1787.

<sup>23</sup> (a) Legzdins, P.; Mitchell, R. W.; Rempel, G. L.; Ruddick, J. D.; Wilkinson, G. J. *Chem. Soc. A* **1970**, 3322–3326. (b) Hui, B. C.; Rempel G. L. *Chem. Commun.* **1970**,

- 
- 1195–1196. (c) Hui, B. C. Y.; Teo, W. K.; Rempel G. L. *Inorg. Chem.* **1973**, *12*, 757–762.
- <sup>24</sup> Nagy-Magos, Z.; Vastag, S.; Heil, B.; Markó, L. *J. Organomet. Chem.* **1979**, *171*, 97–102.
- <sup>25</sup> Claver, C.; Ruiz, A.; Masdeu, A. M.; Ruiz, N. *Inorg. Chim. Acta* **1990**, *175*, 77–81.
- <sup>26</sup> Chatt, J.; Venanzi, L. M. *J. Chem. Soc.* **1957**, 4735–4741.
- <sup>27</sup> Haszeldine, R. N.; Lunt, R. J.; Parish, R. V. *J. Chem. Soc. A* **1971**, *23*, 3696–3698.
- <sup>28</sup> Azbel, B. I.; Gol’Dshleger, N. F.; Khidekel, M. L.; Sokol, V. I.; Porai-Koshits, M. A. *J. Mol. Catal.* **1987**, *40*, 57–63.
- <sup>29</sup> Lahoz, F. J.; Martin, A.; Esteruelas, M. A.; Sola, E.; Serrano, J. L.; Oro, L. A. *Organometallics* **1991**, *10*, 1794–1799.
- <sup>30</sup> Werner, H.; Poelsma, S.; Schneider, M. E.; Windmüller, B.; Barth, D. *Chem. Ber.* **1996**, *129*, 647–652.
- <sup>31</sup> Green, M.; Kuc, T. A. *J. Chem. Soc., Dalton Trans.* **1972**, 832–839.
- <sup>32</sup> Trzeciak, A. M.; Ziółkowski, J. J.; Lis, T.; Borowski, A. *Polyhedron* **1985**, *4*, 1677–1681.
- <sup>33</sup> Mieczynska, E.; Trzeciak, A. M.; Ziółkowski, J. J.; Lis, T. *Polyhedron* **1994**, *13*, 655–658.
- <sup>34</sup> Reis, A. H., Jr.; Willi, C.; Siegel, S.; Tani, B. *Inorg. Chem.* **1979**, *18*, 1859–1863.
- <sup>35</sup> Chen, M. J.; Feder, H. M. *Inorg. Chem.* **1979**, *18*, 1864–1869.
- <sup>36</sup> Burk, M. J.; Crabtree, R. H. *J. Am. Chem. Soc.* **1987**, *109*, 8025–8032.
- <sup>37</sup> Vaartstra, B. A. Metal Carboxylate Complexes for Formation of Metal-Containing Films on Semiconductor Devices. U.S. Patent 5,695,815, Dec. 9, 1997. Characterization

---

was accomplished therein by elemental analysis alone, which allowed for compositional determination but could not provide verification of the anticipated dimeric structure. Additionally, the synthesis was described therein with minimal detail, and no attempt to crystallize the compound was reported.

<sup>38</sup> The synthesis, characterization, properties, and uses of metal 2-ethylhexanoates and their derivatives have been recently reviewed by Mishra et al.<sup>22</sup> Metal 2-ethylhexanoates were described therein as “of great commercial importance” since they are used as driers in certain paints, lubricating agents, stabilizers for plastics, waterproofing agents, fuel additives, fungicides, in corrosion protection, and as desired precursors in materials science applications “to obtain nano-films, -composites, and -particles” by various deposition methods.<sup>22</sup> For this wide variety of uses, they enjoy the “advantages of being inexpensive, air-stable, non-toxic as well as commercially available for a wide number of elements.”<sup>22</sup> Metal carboxylates used in catalytic applications include Ni(2-ethylhexanoate)<sub>2</sub> + AlEt<sub>3</sub> for industrial polymer hydrogenation,<sup>1,2,22</sup> Rh<sub>2</sub>(OAc)<sub>4</sub> for olefin hydrogenation,<sup>23</sup> and [(COD)Rh(O<sub>2</sub>CR)]<sub>2</sub> + PR'<sub>3</sub> for olefin hydrogenation,<sup>24</sup> or hydroformylation.<sup>25</sup>

<sup>39</sup> It was claimed that **1** in the viscous liquid form was air stable,<sup>37</sup> but this seems unlikely to be true, especially for air exposure at long time scales. Some air sensitivity is likely common for complexes of this type; for example, the related compound [(C<sub>2</sub>H<sub>4</sub>)<sub>2</sub>Rh(μ-O<sub>2</sub>CCH<sub>3</sub>)]<sub>2</sub> was reported as “moderately air-sensitive.”<sup>30</sup>

<sup>40</sup> It has been noted that “single-crystal X-ray data on 2-ethylhexanoate... derivatives remain scarce since the long carbon chain favors disorder and, as a result, the obtained crystals are often of poor quality.”<sup>22</sup> For this reason, the relative ease with which **1** and **2** yielded X-ray diffraction-quality single crystals is notable. However, the crystal structures of **1** and **2** conform to the above statement in that disorder in the 2-ethylhexanoate alkyl chain consisting of C25-C32 is pronounced.

<sup>41</sup> Özkar, S.; Finke, R. G. *J. Organomet. Chem.* **2004**, *689*, 493–501.

- 
- <sup>42</sup> Fandos, R.; Hernández, C.; Otero, A.; Rodríguez, A.; Ruiz, M. J. *Organometallics* **1999**, *18*, 2718–2723.
- <sup>43</sup> (a) Rodman, G. S.; Mann, K. R. *Inorg. Chem.* **1985**, *24*, 3507–3508. (b) Rodman, G. S.; Mann, K. R. *Inorg. Chem.* **1988**, *27*, 3338–3346.
- <sup>44</sup> Kanematsu, N.; Ebihara, M.; Kawamura, T. *Inorg. Chim. Acta* **1999**, *292*, 244–248.
- <sup>45</sup> Schnabel, R. C.; Roddick, D. M. *Organometallics* **1996**, *15*, 3550–3555.
- <sup>46</sup> Sielisch, T.; Cowie, M. *Organometallics* **1988**, *7*, 707–714.
- <sup>47</sup> Aullón, G.; Ujaque, G.; Lledós, A.; Alvarez, S.; Alemany, P. *Inorg. Chem.* **1998**, *37*, 804–813.
- <sup>48</sup> The formally non-bonding M–M distances and estimated standard deviations cited were calculated by imposing a M–M bond, then performing an additional least-squares refinement.
- <sup>49</sup> Coleman, A. W.; Eadie, D. T.; Stobart, S. R. *J. Am. Chem. Soc.* **1982**, *104*, 922–923.
- <sup>50</sup> Aullón, G.; Alvarez, S. *Inorg. Chem.* **1996**, *35*, 3137–3144.
- <sup>51</sup> Marshall, J. L.; Stobart, S. R.; Gray, H. B. *J. Am. Chem. Soc.* **1984**, *106*, 3027–3029.
- <sup>52</sup> Rodman, G. S.; Daws, C. A.; Mann, K. R. *Inorg. Chem.* **1998**, *27*, 3347–3353.
- <sup>53</sup> Alley, W. M.; Kayiran, I.; Johnson, K.; Finke, R. G. Ziegler-type Hydrogenation Catalysts made from Group 8–10 Transition Metal Precatalysts and AlR<sub>3</sub> Cocatalysts: A Critical Review of the Literature. *J. Mol. Catal. A: Chem.*, **2009**, to be submitted for publication.
- <sup>54</sup> Šabata, S.; Hetflejš, J. *J. Appl. Polym. Sci.* **2002**, *85*, 1185–1193.
- <sup>55</sup> Reguli, J.; Staško, A. *Chem. Pap.* **1987**, *41*, 299–310.

- 
- <sup>56</sup> Coolbaugh, T. S.; Loveless, F. C.; Mathews, D. N. Method of Synthesizing a Selective Olefin Hydrogenation Catalyst. Eur. Pat. Appl. 91300316.6, Jan 16, 1991.
- <sup>57</sup> Aiken, J. D., III; Finke, R. G. *J. Am. Chem. Soc.* **1998**, *120*, 9545–9554.
- <sup>58</sup> Shriver, D. F.; Drezdson, M. A. *The Manipulation of Air-Sensitive Compounds*, 2<sup>nd</sup> ed.; John Wiley and Sons: New York, 1986.
- <sup>59</sup> Sheldrick, G. M. *SADABS, a program for Siemens Area Detection Absorption Correction*; Bruker AXS, Inc.: Madison, WI, 2000.
- <sup>60</sup> Sheldrick, G. M. *Acta Cryst. A* **2008**, *64*, 112–122.
- <sup>61</sup> Lin, Y.; Finke, R. *Inorg. Chem.* **1994**, *33*, 4891–4910.
- <sup>62</sup> Widegren, J. A.; Aiken, J. D., III; Özkar, S.; Finke, R. G. *Chem. Mater.* **2001**, *13*, 312–324.

Supporting Information for:

**Model Ziegler-Type Hydrogenation Catalyst Precursors, [(1,5-COD)M( $\mu$ -O<sub>2</sub>C<sub>8</sub>H<sub>15</sub>)<sub>2</sub> (M = Ir and Rh): Synthesis, Characterization, and Demonstration of Catalytic Activity En Route to Identifying the True Industrial Hydrogenation Catalysts**

William M. Alley, Chase W. Girard, Saim Özkar, and Richard G. Finke

**Table S1.** Syntheses and Characterizations of Related Compounds

Authors (Year)	Compounds and Syntheses	Characterization / Comments	Ref
Chatt and Venanzi (1957)	[(COD)RhOAc] <sub>2</sub> : 1 g [(COD)RhCl] <sub>2</sub> + 1 g KOAc, refluxed in acetone for 2 hrs., filtered, dried under vacuum, recrystallized from ethyl acetate	IR bands at 1530 and 1419 cm <sup>-1</sup> indicate bridging acetate ions, m.p. 197-198°, C and H analysis	<sup>1</sup>
Haszeldine et al. (1971)	[(NBD)RhOAc] <sub>2</sub> , [(NBD)RhO <sub>2</sub> CCH <sub>2</sub> Cl] <sub>2</sub> , [(NBD)RhO <sub>2</sub> CCH <sub>2</sub> F] <sub>2</sub> , [(DCPD)RhOAc] <sub>2</sub> : [(diene)RhCl] <sub>2</sub> was shaken in benzene with excess Ag(carboxylate), filtered, and recrystallized. [(COD)IrOAc] <sub>2</sub> : [(COD)IrCl] <sub>2</sub> , KOAc, and glacial HO <sub>2</sub> CCH <sub>3</sub> were mixed in acetone, filtered, dried under vacuum, and the crystals were washed with water. [(COD)IrOAc] <sub>2</sub> was unstable in solution without acetate ion, and could not be prepared from AgOAc. Other similar compounds had PPh <sub>3</sub> or ethylenediamine ligands	C and H analysis, IR showed bridging carboxylates. NMR spectra for the NBD complexes gave a quartet signal for the vinylic protons, which is explained by either coupling with Rh, or non-equivalence of the protons from bending at the carboxylate	<sup>2</sup>
Green and Kuc (1972)	[(NBD)Rh(benzoate)] <sub>2</sub> , [(NBD)RhOAc] <sub>2</sub> : in an N <sub>2</sub> atmosphere, an excess of Na(benzoate) or NaOAc was added to a CH <sub>2</sub> Cl <sub>2</sub> solution of [Rh(NBD) <sub>2</sub> ] <sup>+</sup> BF <sub>4</sub> <sup>-</sup> (i.e., 0.30 g Na(benzoate) to 0.05 g [Rh(NBD) <sub>2</sub> ] <sup>+</sup> BF <sub>4</sub> <sup>-</sup> ), stirred for 5 min, diethyl ether added, filtered, solvent removed from filtrate, and the residue recrystallized from CH <sub>2</sub> Cl <sub>2</sub> -hexane	[(NBD)Rh(benzoate)] <sub>2</sub> : 90% yield, m.p. 243-245 °C. [(NBD)RhOAc] <sub>2</sub> : 64% yield, m.p. 198-200 °C. For both: C and H analysis, MW, NMR, and IR	<sup>3</sup>
Reis et al. (1979)	[(NBD)RhOAc] <sub>2</sub> : prepared as described by Chen and Feder below	X-ray crystallography	<sup>4</sup>
Chen and Feder (1979)	[(NBD)RhOAc] <sub>2</sub> : prepared following the procedure for [(COD)RhOAc] <sub>2</sub> as described in the Chatt and Venanzi paper, but starting with [(NBD)RhCl] <sub>2</sub> instead of [(COD)RhCl] <sub>2</sub>	mp 215-218 °C compared to 198-200 °C found by Green and Kuc, <sup>13</sup> C NMR	<sup>5</sup>
Nagy-Magos et al. (1979)	[(COD)Rh(□-mandelate)] <sub>2</sub> and [(COD)RhOAc] <sub>2</sub> : 0.21 mmol [(COD)RhCl] <sub>2</sub> + 0.5 mmol Ag(□(+)-mandelate) or OAc stirred in 50 mL benzene under Ar.	IR and C, H, and Rh analysis. The time required for the reaction to complete under these conditions, as followed by IR spectroscopy, was not specified, but it was implied that it took at least several hours.	<sup>6</sup>
Trzeciak et al. (1985)	[(COD)Rh(N-phenylanthranilate)] <sub>2</sub> : 0.49 g [(COD)RhCl] <sub>2</sub> and 0.71 g Na(N-phenylanthranilate) refluxed in ethanol for 3 h, ppt. washed with H <sub>2</sub> O, then with ethanol, dried in vacuo, and recrystallized from CHCl <sub>3</sub> -ethyl ether	C, H, N, and Rh analysis and X-ray crystallography	<sup>7</sup>
Azbel et al. (1987)	[(NBD)RhO <sub>2</sub> CCF <sub>3</sub> ] <sub>2</sub> : Rh <sub>2</sub> (O <sub>2</sub> CCF <sub>3</sub> ) <sub>4</sub> was heated in either neat NBD, or a benzene solution of NBD	elemental analysis, MW (method not specified), IR, UV-Vis, and X-ray crystallography	<sup>8</sup>
Burk and Crabtree (1987)	[(COD)IrO <sub>2</sub> CCF <sub>3</sub> ] <sub>2</sub> : 0.45 mmol [(COD)IrCl] <sub>2</sub> and 0.90 mmol AgO <sub>2</sub> CCF <sub>3</sub> stirred together in 20 mL	Not characterized because it was not the	<sup>9</sup>

	of CH <sub>2</sub> Cl <sub>2</sub> in the dark for 30 min, filtered	end synthesis target	
Sheldrick and Günther (1989)	[(COD)Rh( $\mu$ -Cl)( $\mu$ -OAc)Rh(COD)]: 0.4 mmol of [(COD)RhCl] <sub>2</sub> and 0.4 mmol of either KOAc or NaOAc•10H <sub>2</sub> O refluxed in 20 mL of acetone for 3 h, solvent removed, and solid recrystallized from ethyl acetate	C and H analysis, IR, <sup>1</sup> H NMR, and X-ray crystallography, 86% yield	<sup>10</sup>
Lahoz et al. (1991)	[(COD)RhOAc] <sub>2</sub> , [(COD)RhO <sub>2</sub> CCF <sub>3</sub> ] <sub>2</sub> : a suspension of [(COD)RhOMe] <sub>2</sub> in hexane was treated with an excess of acetic or trifluoroacetic acid, stirred for 30 min, the orange crystals were filtered off, washed with hexane and dried under vacuum	C and H analysis	<sup>11</sup>
Mieczynska et al. (1994)	[(COD)Rh(salicylate)] <sub>2</sub> : 0.19 g of [(COD)RhCl] <sub>2</sub> and 0.19 g Ag(salicylate) in 25 mL heptanes, stirred for 2 h at room temp (dark yellow solution), and filtered. Solvent removed under vacuum	IR, UV-Vis, <sup>1</sup> H NMR, X-ray crystallography	<sup>12</sup>
Werner et al. (1996)	[(C <sub>2</sub> H <sub>4</sub> ) <sub>2</sub> RhOAc] <sub>2</sub> , [(C <sub>8</sub> H <sub>14</sub> ) <sub>2</sub> RhOAc] <sub>2</sub> : [(C <sub>2</sub> H <sub>4</sub> ) <sub>2</sub> RhCl] <sub>2</sub> and NaOAc in ether at -30 °C (attempts using Na or KOAc in methanol failed), slowly warmed to room temp, filtered, evaporated dry, recrystallized from pentane. [(C <sub>2</sub> H <sub>4</sub> ) <sub>2</sub> RhO <sub>2</sub> CCF <sub>3</sub> ] <sub>2</sub> , [(C <sub>2</sub> H <sub>4</sub> ) <sub>2</sub> RhO <sub>2</sub> CC <sub>6</sub> H <sub>5</sub> ] <sub>2</sub> : [(C <sub>2</sub> H <sub>4</sub> ) <sub>2</sub> RhCl] <sub>2</sub> , HO <sub>2</sub> CCF <sub>3</sub> or HO <sub>2</sub> CC <sub>6</sub> H <sub>5</sub> , and NaOH, reaction and workup same as other compounds. [(COD)IrOAc] <sub>2</sub> : [(COD)IrCl] <sub>2</sub> and AgOAc. [(C <sub>2</sub> H <sub>4</sub> ) <sub>2</sub> IrOAc] <sub>2</sub> : [(C <sub>2</sub> H <sub>4</sub> ) <sub>2</sub> IrCl] <sub>2</sub> and excess ethylene at -78 °C to give [(C <sub>2</sub> H <sub>4</sub> ) <sub>4</sub> IrCl] which was then reacted with NaOAc in ether	melting points, IR, <sup>1</sup> H NMR, C, H, and in some cases Rh analysis, MW by osmometry, X-ray crystallography for [(C <sub>2</sub> H <sub>4</sub> ) <sub>2</sub> RhOAc] <sub>2</sub> , Rh compounds were moderately air-sensitive whereas [(C <sub>2</sub> H <sub>4</sub> ) <sub>2</sub> IrOAc] <sub>2</sub> was described as extremely air-sensitive	<sup>13</sup>
Vaartstra (1997)	“Ir(I)(cyclooctadiene)(2-ethylhexanoate)”: by partially dissolving 1.2 mmol of [(COD)IrCl] <sub>2</sub> in 10 mL of acetone and adding Et <sub>3</sub> NH <sup>+</sup> O <sub>2</sub> C <sub>8</sub> H <sub>15</sub> <sup>-</sup> made by combining 2 mmol of Et <sub>3</sub> N and 10.7 mmol of 2-ethylhexanoic acid. Et <sub>3</sub> NH <sup>+</sup> Cl <sup>-</sup> was removed by adding degassed water and extracting the product into hexanes	C, H, and N analysis of the red viscous liquid, claimed to be stable in air	<sup>14</sup>

COD = 1,5-cyclooctadiene; NBD = norbornadiene; DCPD = dicyclopentadiene, OAc = CH<sub>3</sub>CO<sub>2</sub><sup>-</sup>

### *Synthesis of [(1,5-COD)Ir( $\mu$ -O<sub>2</sub>C<sub>8</sub>H<sub>15</sub>)]<sub>2</sub> (1).*

As an example of a typical synthesis performed in the drybox, 2.005 ± 0.001 g (2.985 mmol) of the orange powder starting material [(1,5-COD)IrCl]<sub>2</sub> was weighed out and transferred into a 250 mL round-bottomed flask. A stirbar and 20 ± 1 mL of acetone were added. Since [(1,5-COD)IrCl]<sub>2</sub> is only sparingly soluble in acetone, it made a clear light yellow/orange solution over the rest of the undissolved orange powder. Stirring was

started. Next,  $1.44 \pm 0.01$  mL (6.04 mmol) of tributylamine was measured into a 50 mL beaker. This was followed by  $0.96 \pm 0.01$  mL (6.0 mmol) of 2-ethylhexanoic acid. Both the tributylamine and 2-ethylhexanoic acid were added to the beaker using 1 mL disposable syringes. Acetone,  $10 \pm 1$  mL, was then added to the beaker. The clear colorless solution was swirled gently in the beaker for about one or two minutes and then poured rapidly into the light orange suspension of  $[(1,5\text{-COD})\text{IrCl}]_2$  in the 250mL round-bottomed flask with stirring. The solution turned to dark red almost immediately upon addition of the contents of the beaker. The flask was capped with a rubber septum and the dark red solution was allowed to stir for  $\geq 15$  minutes before continuing with the subsequent steps.

After  $\geq 15$  minutes of stirring, the flask, still sealed by the septum, was removed from the drybox and placed under a flow of Ar, which was first passed through oxygen and moisture traps consisting of activated carbon and molecular sieves. De-ionized water and cyclohexane were prepared ahead of time so as to be ready when the reaction flask was removed from the drybox. De-ionized water, 250 mL, was degassed by boiling for at least 20 min, followed by purging with Ar while cooling to room temperature. Cyclohexane, 150 mL, was removed from the drybox in a septum-sealed vessel and placed under Ar. Approximately 30 mL of the water was added to the dark red acetone solution in the 250 mL round-bottomed flask via cannula and under a flow of Ar. As this was done, the clear solution turned cloudy, and a black precipitate could be seen. Next, 130 mL of cyclohexane was added to the flask, again by cannula and under Ar flow, causing the disappearance of the black precipitate. The contents of the flask were stirred vigorously for 5-10 minutes. When stirring was stopped, the contents were allowed to

separate into a clear, deep-red cyclohexane phase containing the product above a cloudy yellow aqueous/acetone phase.

The aqueous/acetone phase was removed by cannula. Another 30 mL of water was added by cannula and the process was repeated. With successive extractions, the aqueous phase approached clear and colorless. A total of five such air-free extractions were performed, each using about 30 mL of water. After the final extraction, the deep-red solution in cyclohexane was removed by cannula into an awaiting flask that had been capped by a septum and purged with Ar for at least 20 minutes. Care was taken so that none of a red-brown foam, that existed primarily at the interface of the two phases, was transferred along with the solution in cyclohexane (i.e., a few mL of the cyclohexane solution was left behind). The cyclohexane was then removed by vacuum overnight leaving a dark red, almost black, viscous liquid.

The flask under vacuum was then transferred inside the drybox where the septum was removed and about 40 mL of acetone was added. The flask was swirled for a few minutes to dissolve all the viscous liquid product, **1**. The flask was then sealed with a glass stopper and removed from the drybox. It was placed in a tall reaction Dewar that contained no less than a pound of dry CO<sub>2</sub>. The flask was separated from the dry ice and the sides of the Dewar by foam packing chips to eliminate cold spots and provide a slower rate of cooling to assist in crystallization. The Dewar was then covered with Al foil and placed inside a walk-in cooler (3-5°C) to slow sublimation of the dry ice.

Dark red, rod-like crystals of **1** were observed in the flask after one or two days. The flask was then removed from the Dewar and placed in a dry ice/acetone bath with the contents under an Ar flow. The mother liquor was removed by cannula and Ar pressure.

The flask containing the crystals of **1** was then placed under vacuum overnight. Afterwards the flask was transferred to the drybox. The now dry, dark red, rod-shaped crystals were scraped from the flask with a spatula into a glass vial. Product **1** was collected in this manner, 1.612 g (1.817 mmol), a 61% yield.

The product **1** could not be isolated in pure or crystalline form if the extraction step was abridged, or otherwise not carefully performed to remove  $\text{Bu}_3\text{NH}^+\text{Cl}^-$  quantitatively. When the extraction was carefully performed, no nitrogen was detected in analysis (detection limit  $< 0.5\%$ ), and no  $\text{Bu}_3\text{NH}^+$  ion was observed in the solution NMR spectra of pure crystalline **1**. However, when  $\text{Ag}(2\text{-ethylhexanoate})$  was used instead for the attempted synthesis of pure **1**, it resulted in an opaque, dark brownish-orange reaction mixture. After 6 days, the mixture was filtered and the filtrate evacuated giving impure (by  $^1\text{H}$  NMR) dark red viscous liquid **1** in 46% yield. Subsequent attempts to crystallize **1** from this preparation were unsuccessful.

Alternatively, **1** can also be made in the same fashion as **2** (vide infra), namely by using an equimolar amount of  $\text{Na}(2\text{-ethylhexanoate})$  with respect to Ir atoms in the precursor. When this approach was used for the synthesis of **1**, an opaque, dark red reaction mixture formed almost immediately upon addition of the  $\text{Na}(2\text{-ethylhexanoate})$ . In this case, the acetone was removed in vacuo, the product was re-dissolved in cyclohexane, and then filtered using a glass fritted filter. The rest of the procedure, cyclohexane/ $\text{H}_2\text{O}$  extraction step and crystallization from an acetone solution, was carried out the same as in the synthesis using  $\text{Bu}_3\text{NH}^+\text{O}_2\text{C}_8\text{H}_{15}^-$ . This approach also gave a 61% yield of large, deep-red crystals of **1**. Also similarly, no crystals of **1** were obtained if the cyclohexane/ $\text{H}_2\text{O}$  extraction step was skipped. Whether skipping the

filtration step in the synthesis of **1** with Na(2-ethylhexanoate) would affect the yield, purity, or ability to crystallize the product was not tested. The filtration step is unnecessary in the synthesis of **1** using  $\text{Bu}_3\text{NH}^+\text{O}_2\text{C}_8\text{H}_{15}^-$ .

*Synthesis of [(1,5-COD)Rh( $\mu$ -O<sub>2</sub>C<sub>8</sub>H<sub>15</sub>)]<sub>2</sub> (**2**).*

As an example of a typical synthesis performed in the drybox,  $1.990 \pm 0.001$  g (4.036 mmol) of the yellow powder starting material [(1,5-COD)RhCl]<sub>2</sub> was weighed out and transferred into a 250 mL round-bottomed flask. A stirbar and  $20 \pm 1$  mL of acetone were added. Since [(1,5-COD)RhCl]<sub>2</sub> is only sparingly soluble in acetone it made a clear light-yellow solution over the rest of the undissolved yellow powder. Stirring was started. Next,  $1.348 \pm 0.001$  g (8.117 mmol) of Na(O<sub>2</sub>C<sub>8</sub>H<sub>15</sub>) was measured out into a small glass vial. A few mL of acetone was added to the vial and agitated with a disposable plastic pipette to dissolve the Na(O<sub>2</sub>C<sub>8</sub>H<sub>15</sub>). This solution was then added to the yellow suspension of [(1,5-COD)RhCl]<sub>2</sub> by pipette. Quantitative transfer of Na(O<sub>2</sub>C<sub>8</sub>H<sub>15</sub>) was achieved by rinsing the glass vial with several ~2 mL portions of acetone and adding these to the reaction mixture. Afterwards, enough acetone was added to the reaction flask to bring the total volume to  $50 \pm 5$  mL. The color and turbidity of the reaction mixture, an opaque yellow, did not visibly change upon addition of Na(O<sub>2</sub>C<sub>8</sub>H<sub>15</sub>). The flask was capped and the reaction mixture was allowed to stir for  $\geq 15$  minutes.

After  $\geq 15$  minutes, the flask was placed under vacuum for at least 6 hours to remove the acetone solvent. The remaining yellow or dirty mustard yellow solid was then re-dissolved in cyclohexane and a dirty white solid, presumably NaCl, was removed

by gravity filtration in the drybox. A fritted filter and vacuum filtration may expedite this step, although this was not explicitly tested. The cloudy orange cyclohexane filtrate, about  $75 \pm 5$  mL total volume, was collected in a 250 mL round-bottomed flask and a magnetic stirbar was added. The flask was then sealed with a rubber septum, removed from the drybox, and placed under a flow of Ar.

As with the synthesis of **1**, 250 mL of de-ionized water was degassed ahead of time by boiling for at least 20 min followed by purging with Ar while cooling to room temperature, so as to be ready when the flask was removed from the drybox. Approximately 50 mL of the degassed water was added by cannula between septum-sealed containers under Ar flow to the yellow cyclohexane solution in the 250 mL round-bottomed flask. The contents of the flask were then stirred vigorously for 10–15 minutes. When stirring was stopped, the contents were allowed to separate into a clear orange cyclohexane phase containing the product above a clear, very pale yellow aqueous phase with a thin foamy film in between.

The aqueous phase was removed by cannula. The process was repeated, each time using 50 mL of water, for a total of three extractions. After the final extraction, the orange solution in cyclohexane was removed by cannula into an awaiting flask that had been capped by a septum and purged with Ar for at least 20 minutes. Care was taken so that none of the foam or remaining water was transferred along with the orange solution in cyclohexane (i.e., a few mL of the cyclohexane solution was left behind). The cyclohexane was then removed by vacuum overnight leaving a viscous liquid the color of dark honey.

The flask under vacuum was then transferred inside the drybox where the septum was removed and about 40 mL of acetone was added. The flask was swirled for a few minutes to dissolve all the viscous liquid product **2** resulting in a clear orange solution. The flask was then sealed with a glass stopper and removed from the drybox. Crystallization of **2** was accomplished in the same manner as with **1**.

A yellow or yellow-orange crystalline solid **2** was observed in the flask after two or three days. The flask was then removed from the Dewar and placed in a dry ice/acetone bath and under Ar flow. A separate flask containing 20 mL of acetone was also placed in the dry ice/acetone bath and bubbled with Ar for ~10 minutes while it cooled to  $-78\text{ }^{\circ}\text{C}$ . The mother liquor was removed from the flask containing **2** by cannula and Ar pressure. The chilled 20 mL of acetone was added to the flask containing **2**, agitated briefly with the cannula tip, and then removed with Ar pressure. The flask containing **2** was then placed under vacuum overnight. Afterwards the flask was transferred to the drybox. The now dry yellow or yellow-orange crystalline solid was scraped from the flask with a spatula into a glass vial. Product **2** was collected in this manner, 2.464 g (3.478 mmol), an 86% yield.

Intriguingly, attempts to use  $\text{Bu}_3\text{NH}^+\text{O}_2\text{C}_8\text{H}_{15}^-$  for the synthesis of **2** in acetone were unsuccessful; no visibly apparent change, either in color or solubility, occurred in the yellow suspension, even after two days. Only a small amount of impure (by  $^1\text{H}$  NMR), non-crystalline product was obtained. However, when a switch to Na(2-ethylhexanoate) in acetone was made, even though the reaction mixture remained an opaque yellow-orange, **2** formed in <15 min as determined by  $^1\text{H}$  NMR (vide infra), and crystalline **2** was ultimately obtained in >80% yield.

Similar cation effects concerning the synthesis of related compounds have been reported in the literature.<sup>2,10</sup> For example, Haszeldine et al. synthesized [(1,5-COD)IrOAc]<sub>2</sub> from [(1,5-COD)IrCl]<sub>2</sub> using KOAc in glacial CH<sub>3</sub>CO<sub>2</sub>H, but found that it was unstable in solution without acetate ion, and could not be prepared by AgOAc.<sup>2,15</sup> Similarly, either KOAc or NaOAc in acetone was effective for the synthesis of [(1,5-COD)Rh(μ-Cl)(μ-OAc)Rh(1,5-COD)];<sup>10</sup> however, further reaction to give [(1,5-COD)RhOAc]<sub>2</sub> would only occur with KOAc, not NaOAc, even when the latter was used in excess. The authors stated that an obvious explanation for this difference in reactivity was lacking, but suggested the possibilities that the cation could be mechanistically involved in cleavage of the Rh–Cl bonds, solvation effects could be important, or both.<sup>10</sup> In the present work, Bu<sub>3</sub>NH<sup>+</sup>O<sub>2</sub>C<sub>8</sub>H<sub>15</sub><sup>-</sup> is successful for the synthesis of **1** yet Na(2-ethylhexanoate) is required for the synthesis of **2**. It seems possible that the extra driving force provided by use of the Na<sup>+</sup> salt as NaCl is precipitated is of different importance in the syntheses of **1** and **2**.

In the syntheses of **1** and **2** using Na(O<sub>2</sub>C<sub>8</sub>H<sub>15</sub>) the crude reaction product was re-dissolved in cyclohexane for filtration before performing the cyclohexane/H<sub>2</sub>O extraction. In the case of **2**, a semi-crystalline solid was obtained when the procedure was attempted without the cyclohexane/H<sub>2</sub>O extraction. However, analysis of this material showed it contained 485 ppm Na, attributed to residual, unreacted Na(O<sub>2</sub>C<sub>8</sub>H<sub>15</sub>), and the material could not be recrystallized to give X-ray diffraction-quality crystals. The residual Na(O<sub>2</sub>C<sub>8</sub>H<sub>15</sub>) was removed by performing the extraction with degassed water on a cyclohexane solution of **2**. The message here is that we recommend the syntheses of **1** or **2** carefully follow the procedures given for the extraction step.

*Control Experiment Directly Monitoring the Formation of 1 and 2 by <sup>1</sup>H NMR.*

To determine if the time allowed for the synthesis reactions to proceed was sufficient for maximum yield in each case, the reaction progress for the syntheses of **1** (by both Bu<sub>3</sub>NH<sup>+</sup> and Na<sup>+</sup>O<sub>2</sub>C<sub>8</sub>H<sub>15</sub><sup>-</sup>) and **2** was checked directly by <sup>1</sup>H NMR. These spectra are shown in Figure S8. Syntheses were performed as described, but scaled-down to 1/3<sup>rd</sup> in the case of **1** and 1/5<sup>th</sup> in the case of **2**, to run in 11.5 mL of acetone-d<sub>6</sub> each. NMR samples were prepared by removing a drop of the reaction mixture, depositing it in an NMR tube and diluting with additional acetone-d<sub>6</sub>. Aliquots were taken at 10 min after the reactions were started and at varying times, from a few hours, up to 34 hours after the start. Spectra of aliquots taken after 10 min of reaction and 34.5 hours are virtually identical, *vide infra*, and all appeared as expected for spectra of the products in crude reaction mixtures. This suggests that formation of product upon combination of the starting materials is rapid for both **1** and **2**. The reaction mixtures slowly changed in visual appearance, however, over the course of longer reaction times. The reaction mixture of **1** turned a somewhat darker red when stirred for 3 days, and the reaction mixture of **2** steadily turned a dirty greenish-yellow over the course of 9 days. However, individual syntheses of **2**, one for 10 min, and the other over 9 days, each yielded the same 86% of pure crystalline product. Therefore, the color change was presumably due to the formation of a minute amount of strongly colored, but unidentified side product. Therefore, one may conclude that these reactions proceed rapidly, and are complete after ≤10 min.

**Table S2.** Selected Structural Parameters of Related Compounds

Authors (Year)	Compounds	M–M (Å)	Comments	$\theta^a$ (°)	Ref
Reis et al. (1979)	[(NBD)RhOAc] <sub>2</sub>	3.1050(7)	Rh–Rh distance was thought to indicate a weak bond	50.1	<sup>4</sup>
Bonnet et al. (1979)	[Ir( $\mu$ -S <sup>t</sup> Bu)(CO)(P(OMe) <sub>3</sub> ) <sub>2</sub> ] <sub>2</sub>	3.216(2)	Reacts with H <sub>2</sub> to form a dihydridodiiridium(II) complex with a Ir–Ir single bond (Ir–Ir dist. of 2.673(1) Å)	123.2	<sup>16</sup>
Coleman et al. (1982)	[(1,5-COD)Ir( $\mu$ -pyrazolyl)] <sub>2</sub>	3.216	Distance of formally non-bonded, 16 electron Ir centers was thought suggestive of a weak ground-state interaction	Not Given	<sup>17</sup>
Beveridge et al. (1983)	[(1,5-COD)Ir( $\mu$ -pyrazolyl)] <sub>2</sub> , [(1,5-COD)Rh( $\mu$ -pyrazolyl)] <sub>2</sub> , [(1,5-COD)Ir( $\mu$ -3-CF <sub>3</sub> ,5-CF <sub>3</sub> C <sub>3</sub> N <sub>2</sub> H)] <sub>2</sub> , [(1,5-COD)Ir( $\mu$ -3-CH <sub>3</sub> ,5-CF <sub>3</sub> C <sub>3</sub> N <sub>2</sub> H)] <sub>2</sub>	3.216(1), 3.267(2), 3.073(1), 3.066(2)	Thought that relatively short M–M distances may reflect some degree of M–M interaction despite no formal bonding	78.5, 80.7, 70.1, 69.7	<sup>18</sup>
Trzeciak et al. (1985)	[(1,5-COD)Rh(N-phenylanthranilate)] <sub>2</sub>	3.424(3)	Rh–Rh distance is comparable to those similar compounds with no direct Rh–Rh bonding	Not Given	<sup>7</sup>
Azbel et al. (1987)	[(NBD)RhO <sub>2</sub> CCF <sub>3</sub> ] <sub>2</sub>	3.244	The longer Rh–Rh distance as compared to the acetate analog is consistent with a weakening of the Rh–Rh interaction by the trifluoroacetate group	Not Given	<sup>8</sup>
Rodman and Mann (1988)	[(1,5-COD)Ir( $\mu$ -mhp)] <sub>2</sub> , [(1,5-COD)Rh( $\mu$ -mhp)] <sub>2</sub> <sup>b</sup>	3.242(1), 3.367(1)	In the range of M–M distances found for weak d <sup>8</sup> –d <sup>8</sup> interaction	56, 57	<sup>19</sup>
Sielisch and Cowie (1988)	[(1,5-COD)Ir( $\mu$ -S <sub>2</sub> NC <sub>3</sub> H <sub>4</sub> )] <sub>2</sub> , [(1,5-COD)Rh( $\mu$ -S <sub>2</sub> NC <sub>3</sub> H <sub>4</sub> )] <sub>2</sub>	3.5434, 3.7154(5)	$\theta$ appears related to the bridging units	55.2, 54.3	<sup>20</sup>
Sheldrick and Günther (1989)	[(1,5-COD)Rh( $\mu$ -Cl)( $\mu$ -OAc)Rh(1,5-COD)]	3.161(1)	Similar Rh–Rh have been thought to suggest a Rh–Rh interaction	124	<sup>10</sup>
Chebi et al. (1990)	[(1,5-COD)Ir( $\mu$ -CH <sub>2</sub> -py-6Me-C,N)] <sub>2</sub> , [(1,5-COD)Rh( $\mu$ -CH <sub>2</sub> -py-6Me-C,N)] <sub>2</sub>	3.5889(3), 3.6806(3)	Long M–M distances imply little, if any, interaction	Not Given	<sup>21</sup>
Schnabel and Roddick (1993)	[(dfepe)Ir( $\mu$ -Cl)] <sub>2</sub> , [(dfepe)Rh( $\mu$ -Cl)] <sub>2</sub> <sup>c</sup>	3.236(4), 3.219(4)	See Table 1 therein for a summary of other [L <sub>2</sub> M( $\mu$ -Cl)] <sub>2</sub> complexes	128, 128	<sup>22</sup>
Mieczysława et al. (1994)	[(1,5-COD)Rh(salicylate)] <sub>2</sub>	3.325(3)	Comparable to other complexes with no direct Rh–Rh bonding	Not Given	<sup>12</sup>
Werner et al.	[(C <sub>2</sub> H <sub>4</sub> ) <sub>2</sub> RhOAc] <sub>2</sub>	3.225(1),	The 2 Rh–Rh distances	Not	<sup>13</sup>

(1996)		3.230(1)	are for the 2 independent molecules in the unit cell. These values were thought to indicate the absence of a direct Rh–Rh interaction	Given	
Schnabel and Roddick (1996)	[(dfepe)Ir( $\mu$ -O <sub>2</sub> CCF <sub>3</sub> ) <sub>2</sub> ]	4.307	Origin of the large M–M distance and $\theta$ ( $\lambda$ therein) was thought to be steric	82.7	<sup>23</sup>
Kanematsu et al. (1999)	[(1,5-COD)Ir( $\mu$ -ap)] <sub>2</sub> , <sup>d</sup> [(1,5-COD)Ir( $\mu$ -anp)] <sub>2</sub> <sup>e</sup>	3.0998(6), 3.0681(3)	No formal Ir–Ir bond, but bands observed in UV-Vis are diagnostic of d <sup>8</sup> –d <sup>8</sup> interaction	54.2, 55.1	<sup>24</sup>
Fandos et al. (1999)	[(1,5-COD)Ir(2-O-3-CN-4,6-Me <sub>2</sub> -C <sub>5</sub> HN)] <sub>2</sub>	3.092(2)	Ir atoms are out of their square planes by 0.1523(6) and 0.2271(6) Å, suggesting an Ir–Ir interaction	55.4	<sup>25</sup>
Cotton et al. (2000)	[(1,5-COD)Ir(DAniF)] <sub>2</sub> <sup>f</sup>	3.2327(6)	Ir–Ir distance was thought to indicate no bond	Not Given	<sup>26</sup>
Marciniac and coworkers (2002, 2003)	[(1,5-COD)Ir( $\mu$ -OSiMe <sub>3</sub> ) <sub>2</sub> ], [(1,5-COD)Ir( $\mu$ -OEt)] <sub>2</sub>	2.7923(6), 2.8958(11)	See references therein for analogous Rh complexes	119.7, 122.7	<sup>27</sup>
Miranda-Soto et al. (2006)	[(1,5-COD)Ir( $\mu$ - <sup>t</sup> Bu-PyS)] <sub>2</sub> , [(1,5-COD)Rh( $\mu$ - <sup>t</sup> Bu <sub>2</sub> -ImS)] <sub>2</sub>	2.9055(8), 3.4194(4)	See references therein for discussion of other related complexes	101.0 2(6), 139.0 6(5)	<sup>28</sup>
Chen et al. (2007)	[(1,5-COD) <sub>2</sub> Ir <sub>2</sub> ( $\mu$ <sub>2</sub> -S <sub>2</sub> C <sub>2</sub> B <sub>10</sub> H <sub>10</sub> )]	2.8608(11)	Interaction between the Ir atoms at this distance was seen as a certainty	107.6 27(15 )	<sup>29</sup>
Alley et al. (2008)	[(1,5-COD)Ir(O <sub>2</sub> C <sub>8</sub> H <sub>15</sub> )] <sub>2</sub> , [(1,5-COD)Rh(O <sub>2</sub> C <sub>8</sub> H <sub>15</sub> )] <sub>2</sub>	3.278(5), 3.339(5)	M–M distances agree well with precedent for those compounds in which some extent of weak M–M interaction is likely	56.5, 58.1	This Work

<sup>a</sup>  $\theta$  = dihedral angle between the square planes of the metal centers, <sup>b</sup> mhp = 6-methyl-2-hydroxyppyridinate, <sup>c</sup> dfepe = (C<sub>2</sub>F<sub>5</sub>)<sub>2</sub>PCH<sub>2</sub>CH<sub>2</sub>P(C<sub>2</sub>F<sub>5</sub>)<sub>2</sub>, <sup>d</sup> ap = 2-aminopyridinato, <sup>e</sup> anp = 2-anilinopyridinato, <sup>f</sup> DAniF = (p-anisyl)NC(H)N(p-anisyl)

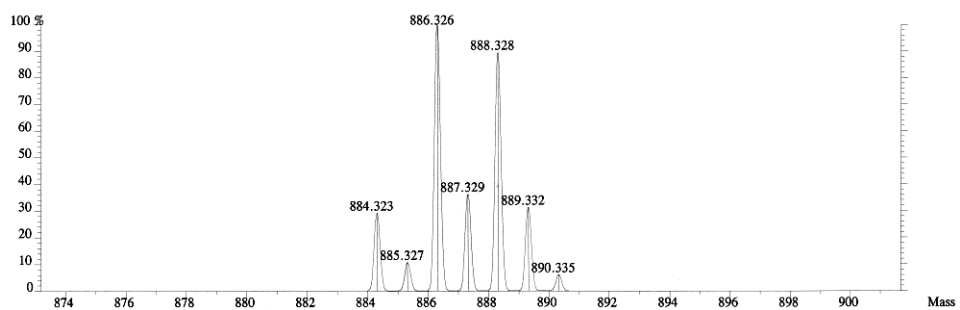
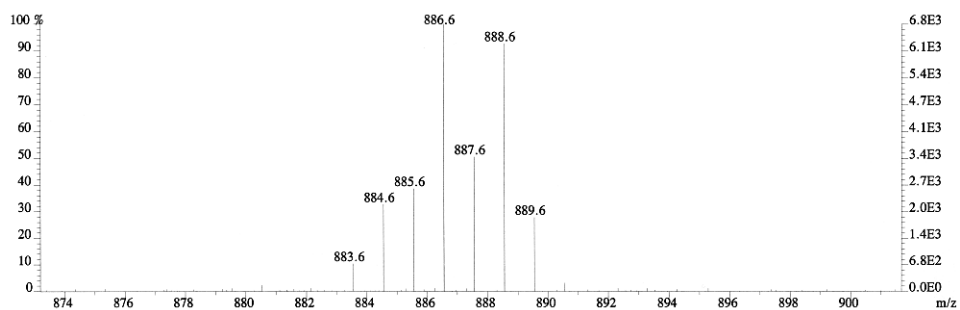
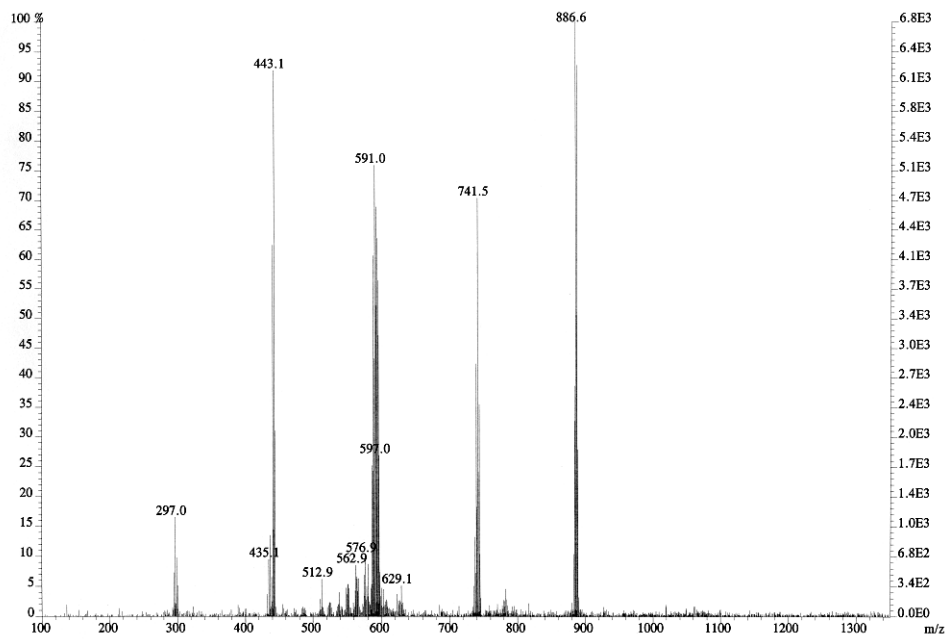


**Figure S1.** Top: FAB-MS of  $[(1,5\text{-COD})\text{Ir}(\text{O}_2\text{C}_8\text{H}_{15})]_2$  (**1**). Middle and Bottom: Observed (middle) and calculated (bottom) isotope distributions in the  $m/z = 884\text{--}890$  region diagnostic of an  $\text{Ir}_2$  formula.

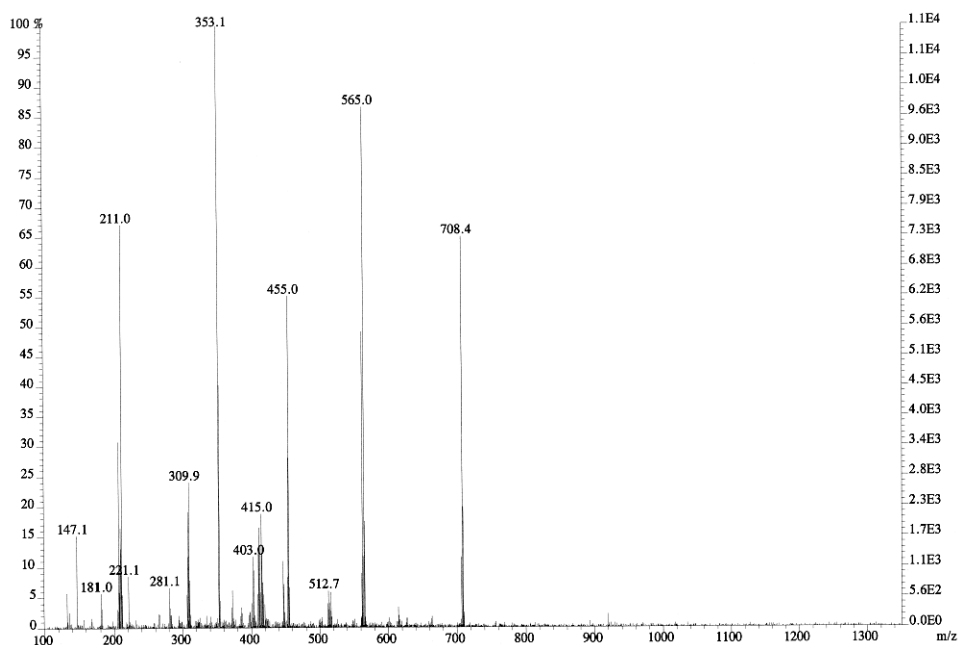


**Figure S2.** FAB-MS of [(1,5-COD)Rh(O<sub>2</sub>C<sub>8</sub>H<sub>15</sub>)<sub>2</sub>] (**2**).

### Spectroscopic Characterization

*Infrared and UV-Visible.* The FT-IR spectra of solid samples in KBr, Figures S3 and S4 for [(1,5-COD)Ir(O<sub>2</sub>C<sub>8</sub>H<sub>15</sub>)<sub>2</sub>] (**1**) and [(1,5-COD)Rh(O<sub>2</sub>C<sub>8</sub>H<sub>15</sub>)<sub>2</sub>] (**2**), respectively, are virtually identical. The single peaks at 1560 cm<sup>-1</sup> for **1** and 1567 cm<sup>-1</sup> for **2** correspond to  $\nu(\text{CO}_2^-)_{\text{asym}}$ . However, each spectrum has three peaks in the range attributable to  $\nu(\text{CO}_2^-)_{\text{sym}}$ . Therefore, the difference ( $\Delta$ ) between  $\nu(\text{CO}_2^-)_{\text{asym}}$  and  $\nu(\text{CO}_2^-)_{\text{sym}}$ , which is often used as a diagnostic for unidentate, chelating, or bridging metal-carboxylate coordination modes,<sup>1,2,13,30</sup> is ambiguous for **1** and **2**. The UV-Visible absorption spectra for **1** and **2** are shown below in Figure S5.

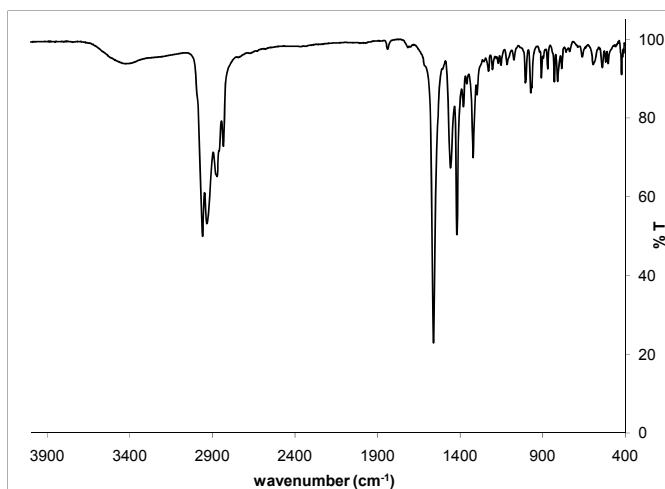


**Figure S3.** IR spectrum of **1**, KBr disc. The  $\Delta$  values between the  $\nu(\text{CO}_2^-)_{\text{asym}}$  band at  $1560\text{ cm}^{-1}$  and the 3 peaks in the range corresponding to  $\nu(\text{CO}_2^-)_{\text{sym}}$  are 103, 141, (bridging) and 239 (unidentate)  $\text{cm}^{-1}$ .

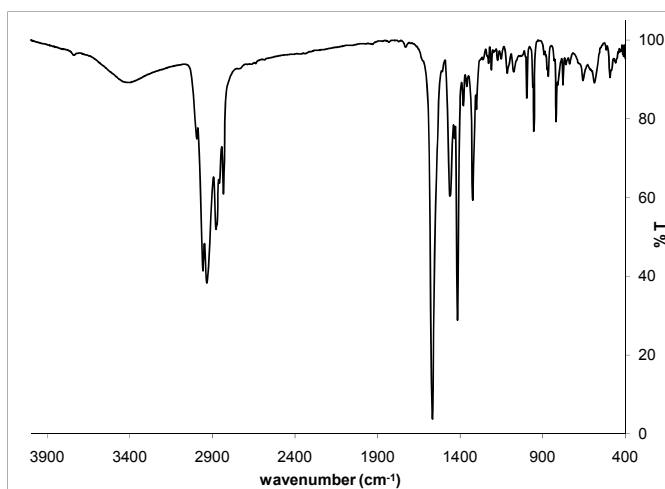


**Figure S4.** IR spectrum of  $[(\text{COD})\text{Rh}(\text{O}_2\text{C}_8\text{H}_{15})]_2$  (**2**), KBr disc. The  $\Delta$  values between the  $\nu(\text{CO}_2^-)_{\text{asym}}$  band at  $1567\text{ cm}^{-1}$  and the 3 peaks in the range corresponding to  $\nu(\text{CO}_2^-)_{\text{sym}}$  are 105, 152, (bridging) and 243 (unidentate)  $\text{cm}^{-1}$ .

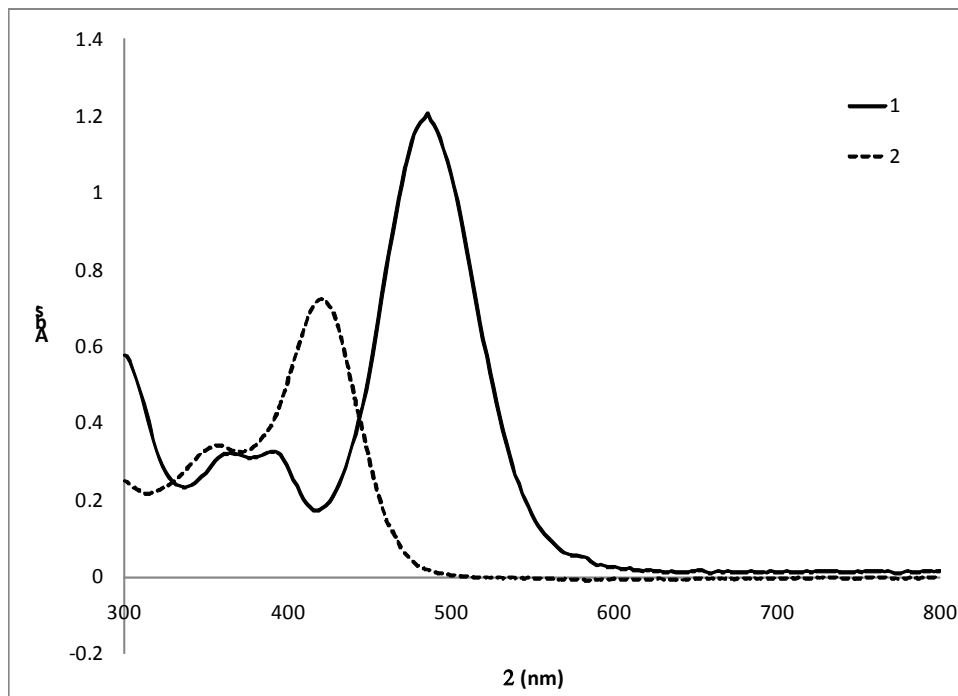
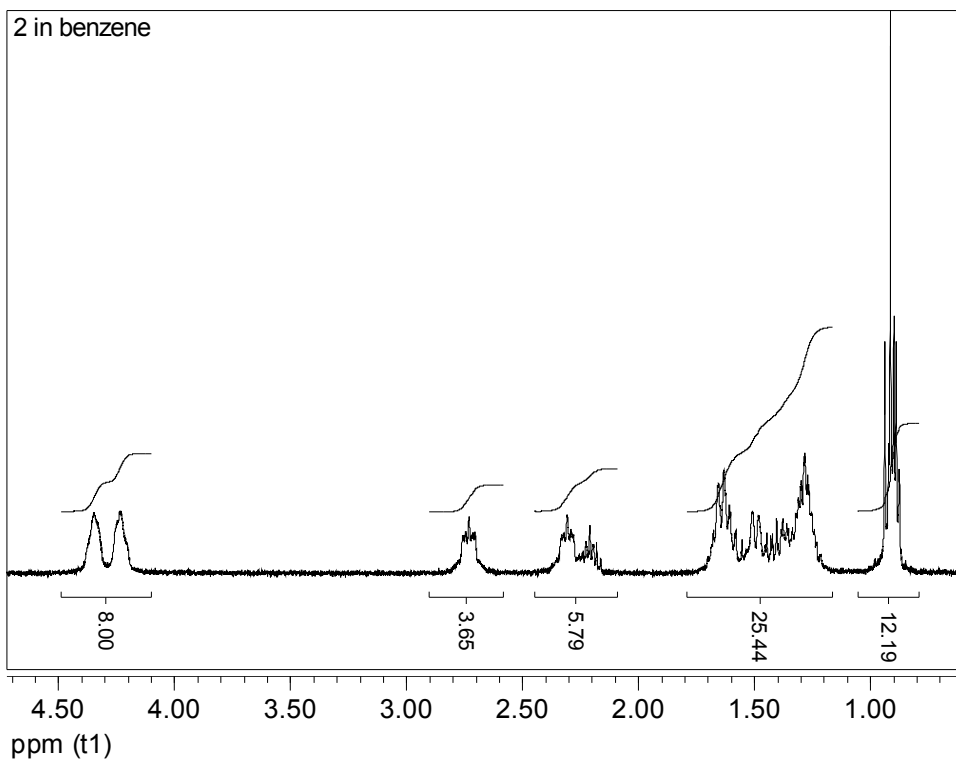
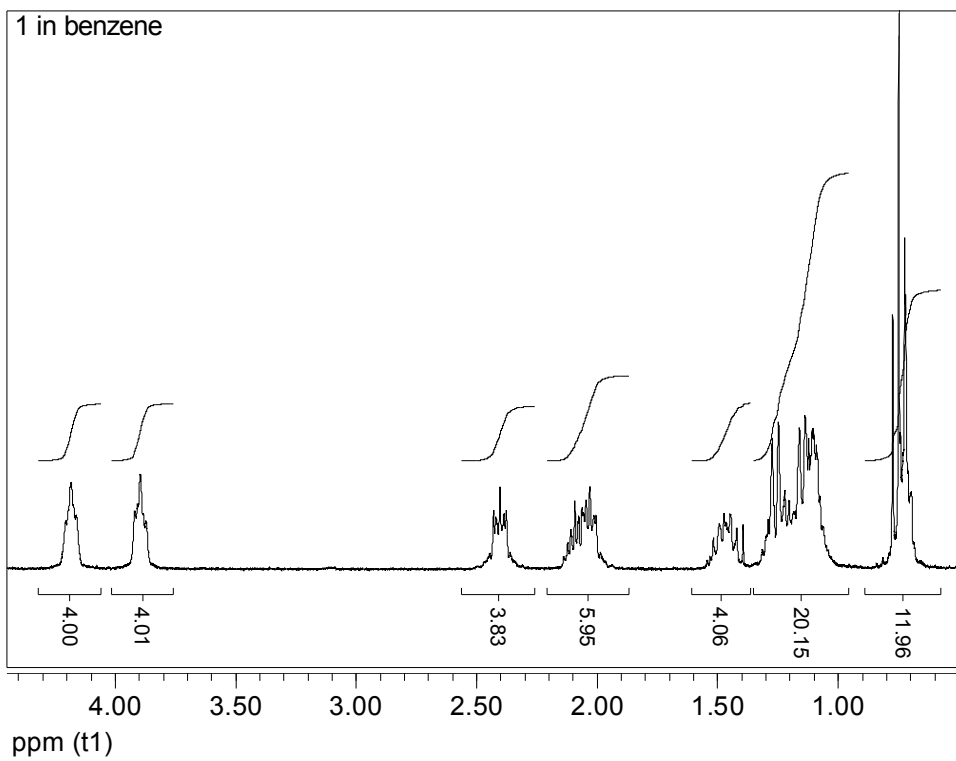


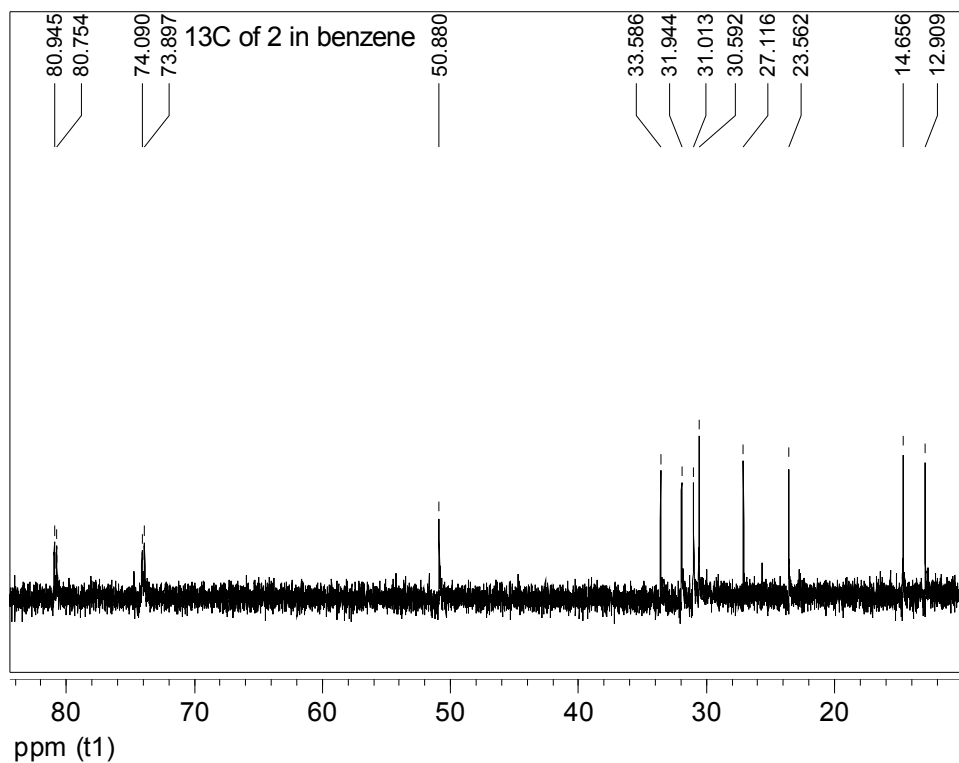
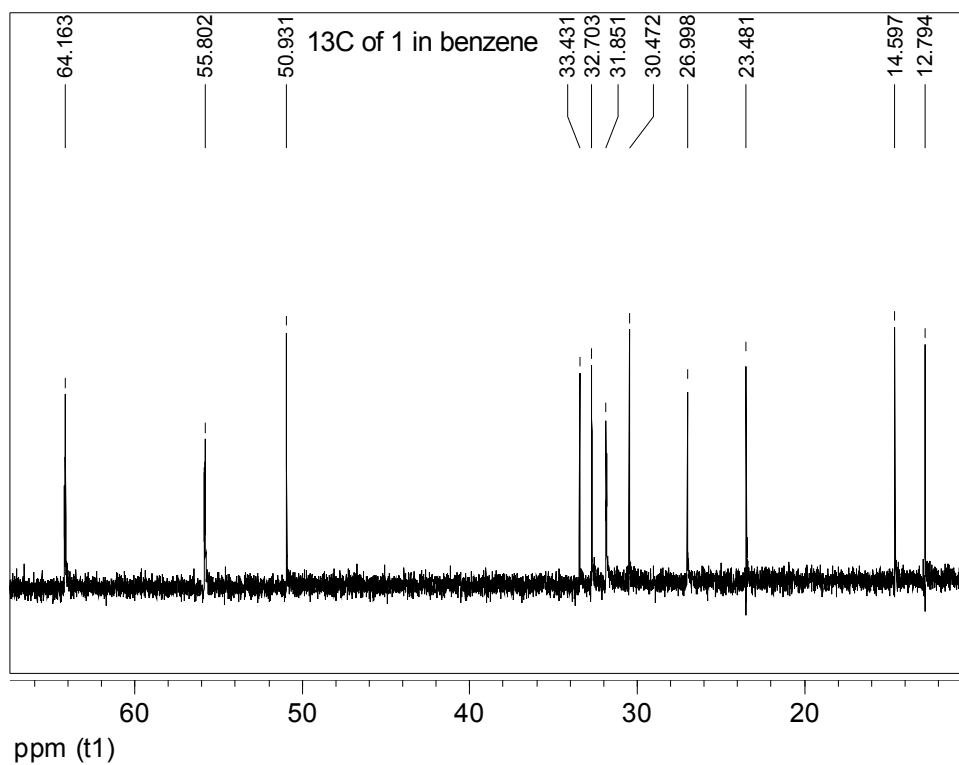
**Figure S5.** UV-Vis absorption spectra of **1** (solid line) and **2** (dashed line). The bands at  $\lambda_{\text{max}} = 486\text{ nm}$  ( $\epsilon_{\text{max}} = 5540\text{ M}^{-1}\text{ cm}^{-1}$ ) for **1**, and  $\lambda_{\text{max}} = 422\text{ nm}$  ( $\epsilon_{\text{max}} = 3700\text{ M}^{-1}\text{ cm}^{-1}$ ) for **2** correspond to metal-centered  $d\sigma^* - p\sigma$  transitions. The fact that this band is blue shifted in **2** relative to its position in the spectrum of **1** is qualitatively consistent with the longer M-M distance in **2**.<sup>31</sup>

*NMR.* The  $^1\text{H}$  and  $^{13}\text{C}$  NMR spectra for **1** and **2**, acquired at room temperature and in benzene- $d^6$  are given in Figure S6. Both compounds display two peaks assigned to olefinic protons, at 3.85–3.93 and 4.13–4.23 ppm for **1**, and at 4.18–4.30 and 4.30–4.40 ppm for **2**. Similar compounds with terminal COD ligands and bent dimeric geometries have been studied extensively by NMR spectroscopy.<sup>19,32</sup> In the  $^1\text{H}$  spectra, the non-equivalence of olefinic positions can be explained by the bent dimeric geometry, leading to resonances that correspond to “inside” or “outside” positions in reference to the distal

metal.<sup>19</sup> The <sup>13</sup>C spectrum of **2** is easily assigned: two doublet peaks, centered at 80.8 and 74.0 ppm, exist for olefinic carbons as expected based on the bent dimeric structure. The signal for the sp<sup>2</sup> carbon of the bridging carboxylates (not shown) appears at 187.8 ppm. Close inspection of the <sup>13</sup>C spectra of **1** revealed that the olefinic carbon peaks at 64.1 and 55.8 ppm, and the peak at 31.9 ppm, appear as unresolved doublets of doublets. The signal for the sp<sup>2</sup> carbon of the bridging carboxylates (not shown) appears at 188.4 ppm.

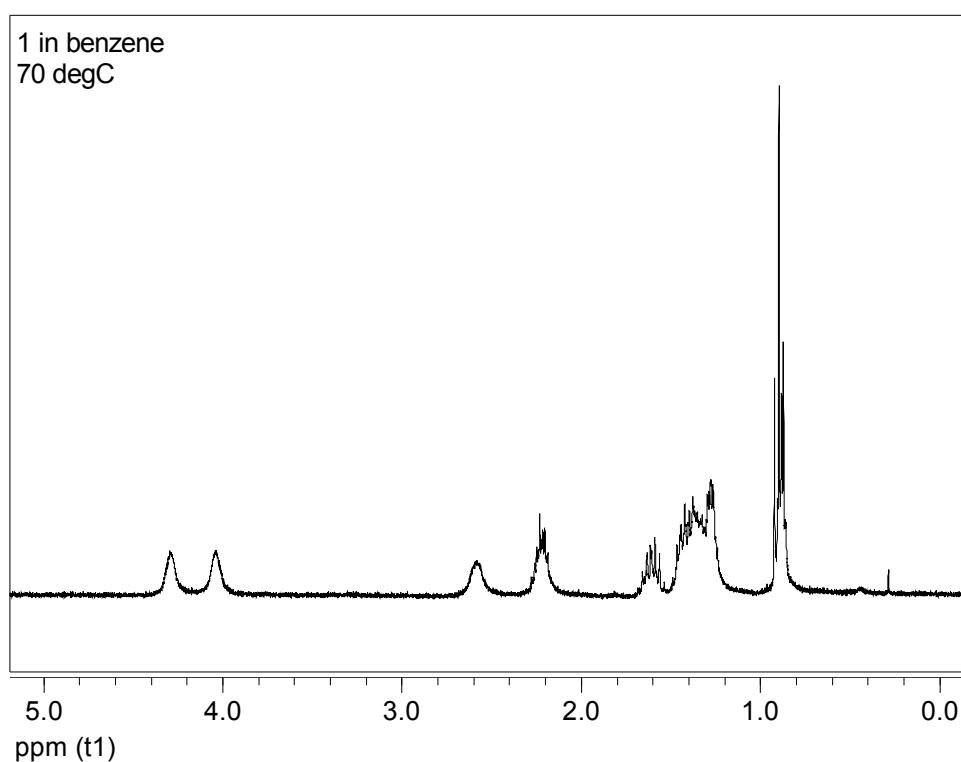
One would expect the iridium-olefin bond in **1** to be stronger than the rhodium-olefin bond in **2**, and that expectation is consistent with the larger “coordination shifts”,<sup>33</sup> observed by <sup>13</sup>C and <sup>1</sup>H NMR, of the olefinic carbon and hydrogen atoms (i.e., the coordination shift  $\equiv \delta$  in the free 1,5-COD molecule –  $\delta$  in the coordinated 1,5-COD ligand).<sup>33</sup> In benzene-d<sup>6</sup>, the coordination shifts of the olefinic resonances in **1** are 1.54 ppm for <sup>1</sup>H and 69.15 ppm for <sup>13</sup>C, whereas in **2** they are 1.29 pm for <sup>1</sup>H and 51.72 ppm for <sup>13</sup>C. The averages of the two olefinic positions of **1** and **2** were used for the calculations.

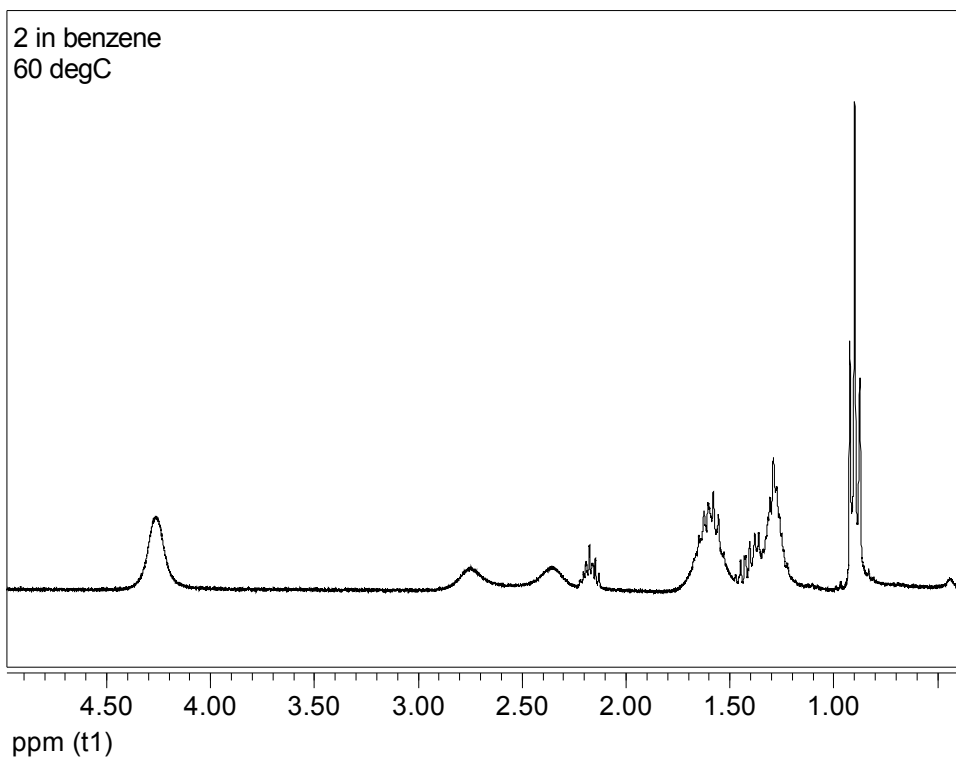
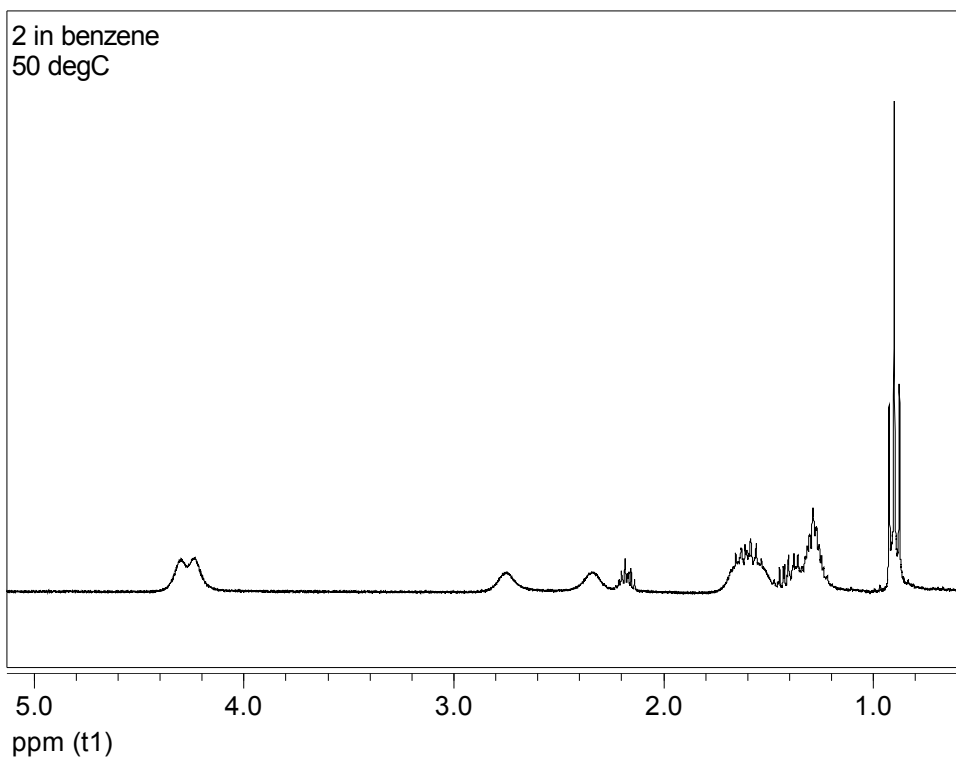


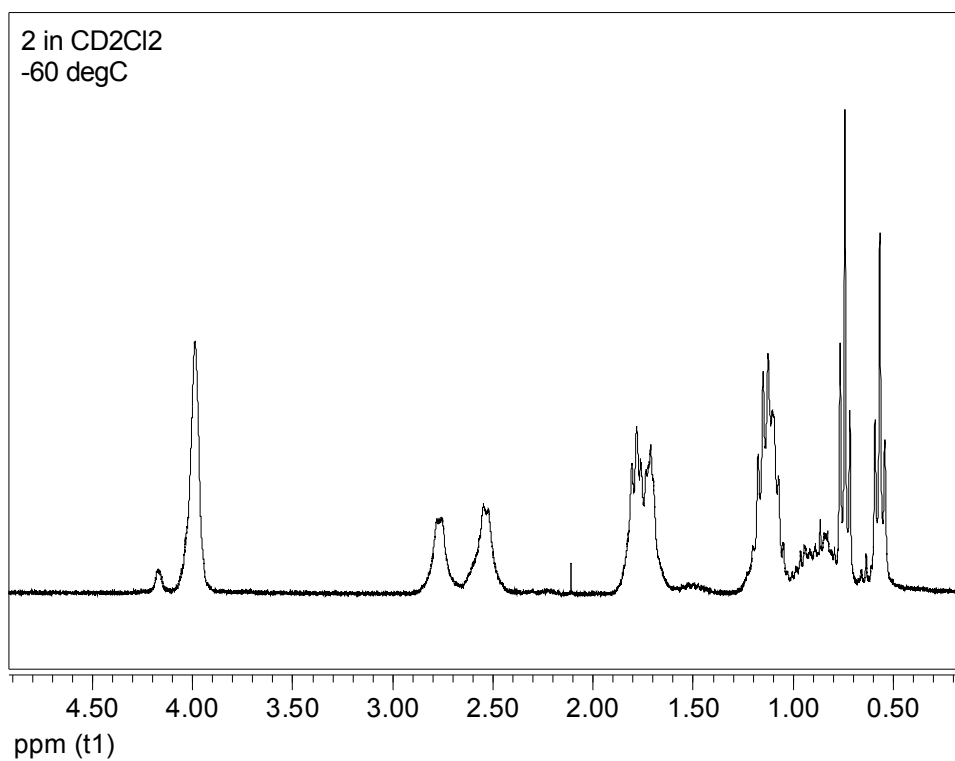
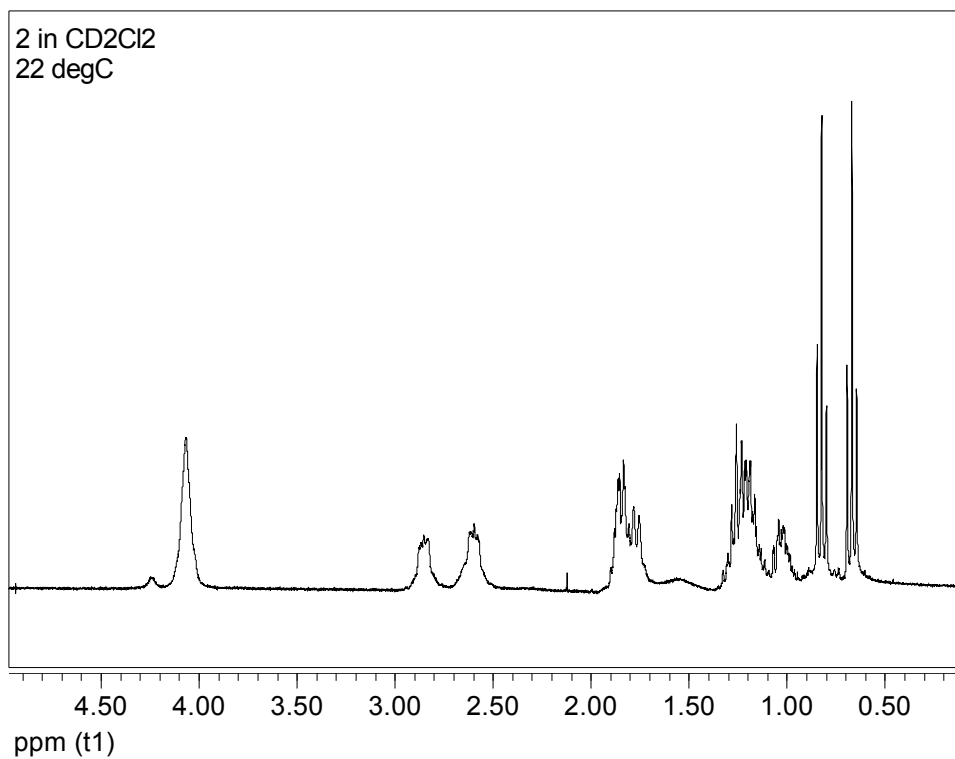


**Figure S6.** Room temperature <sup>1</sup>H and <sup>13</sup>C NMR spectra of **1** and **2**.

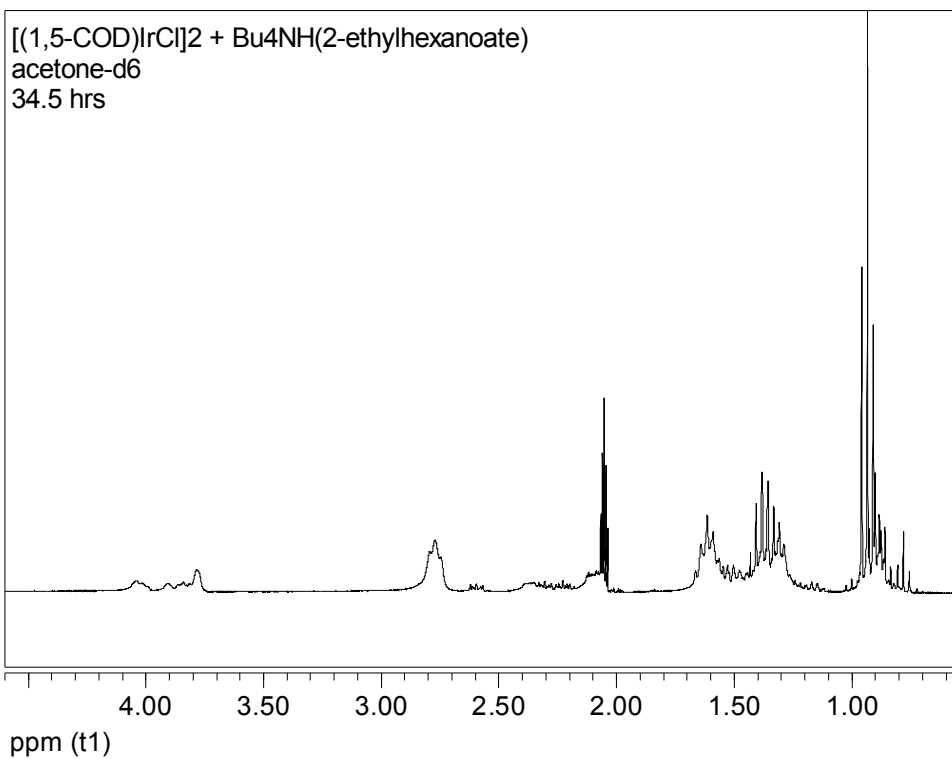
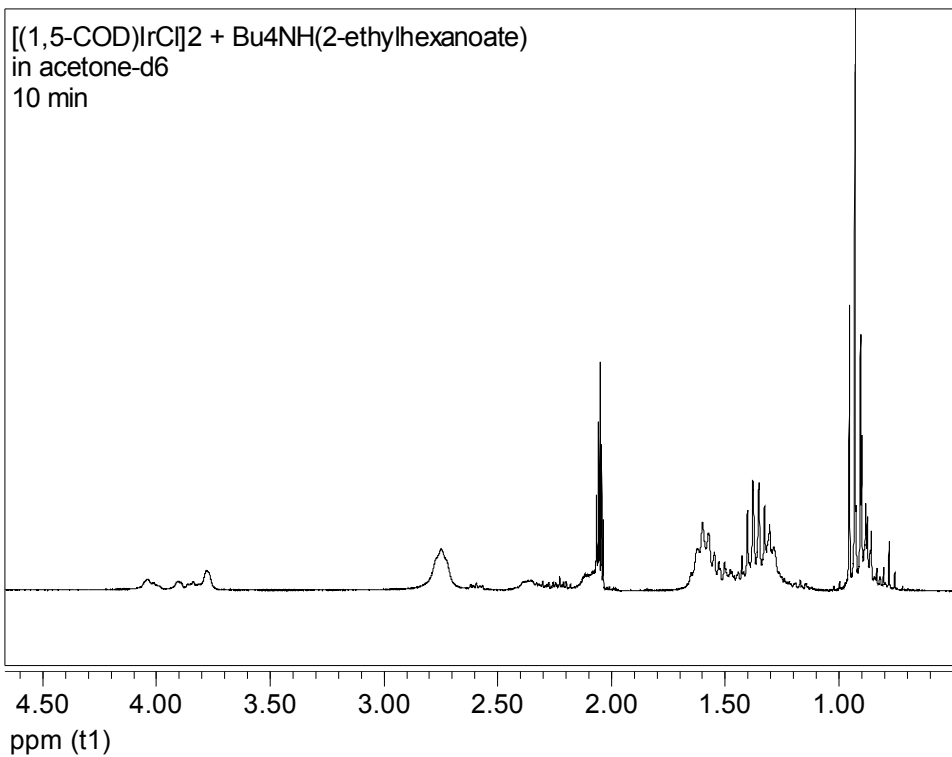
Variable temperature (VT)  $^1\text{H}$  NMR spectra were obtained for **1** and **2**, and are shown in Figure S7. In the  $^1\text{H}$  NMR spectra of **2** at high temp, or at room temp in  $\text{CD}_2\text{Cl}_2$ , the olefinic peaks converged to a single peak. Low temp spectra of **2** in  $\text{CD}_2\text{Cl}_2$  were not able to split the olefinic peak out into two peaks. Convergence of the olefinic peaks in spectra of similar structures has been attributed to either rotation of the  $(\text{diene})_2$  ligands about the  $\text{M}-(\text{diene})_2$  axis or by an inversion process.<sup>5,19,20,23,28,32</sup> The same behavior of the two olefinic peaks in the spectrum of **1** was not observed at high temp in benzene or at room temp in  $\text{CD}_2\text{Cl}_2$ . Differences in fluxionality between Ir and Rh compounds in such structures have been reported previously.<sup>20</sup>

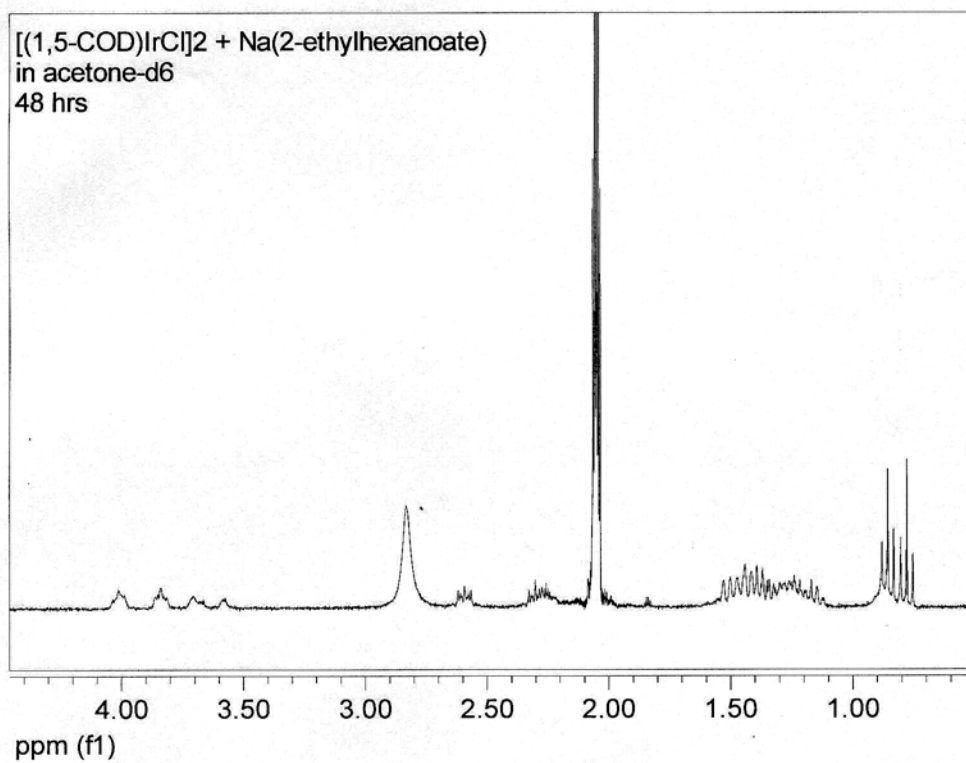
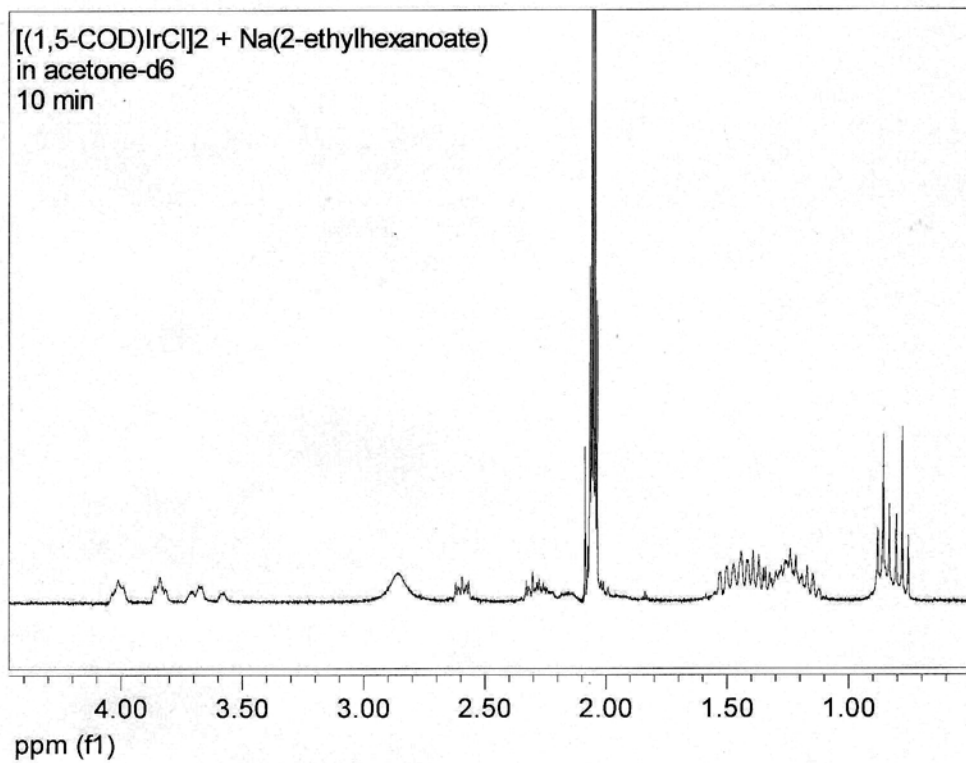






**Figure S7.** Variable temperature <sup>1</sup>H NMR spectra of **1** and **2** in either benzene-d<sup>6</sup> or CD<sub>2</sub>Cl<sub>2</sub>.





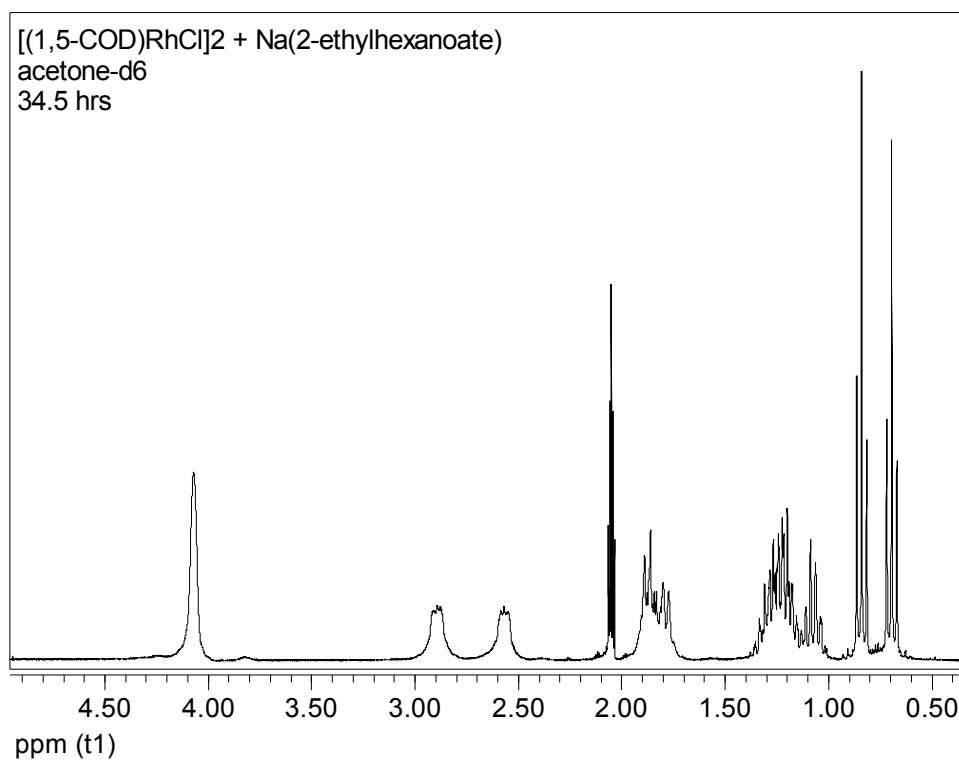
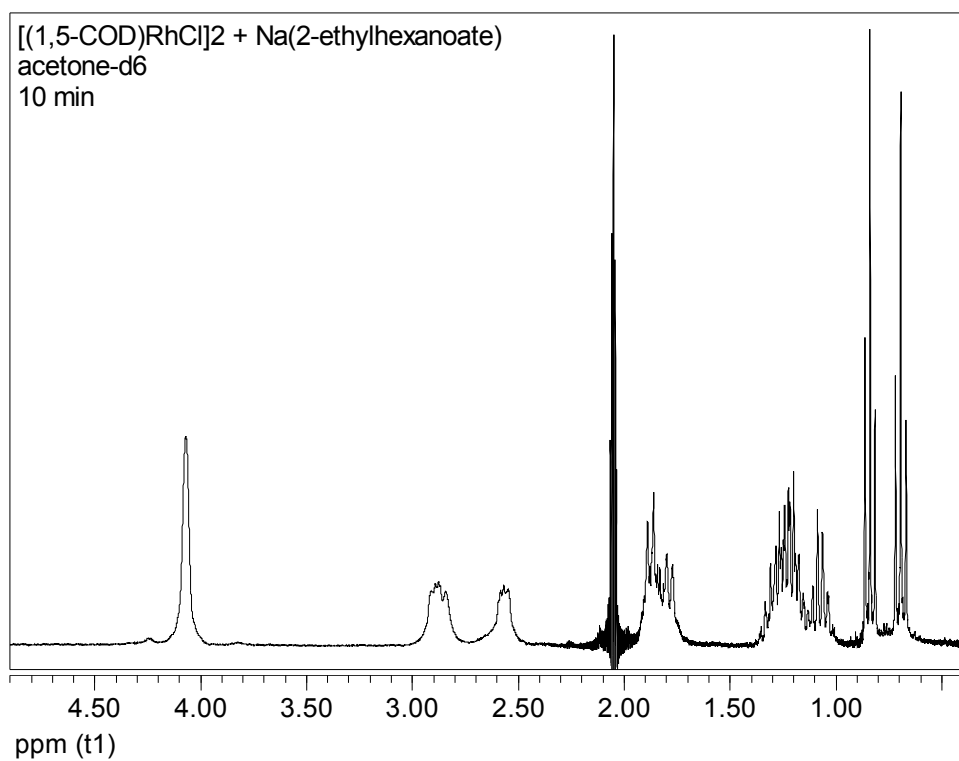


**Figure S8.** <sup>1</sup>H NMR spectra of the crude reaction mixtures of **1** and **2** in acetone-d<sup>6</sup>.

**Control Experiments to Determine if AlEt<sub>3</sub> is Required to Form Active Catalysts.**

Since a fundamental characteristic of Ziegler-type hydrogenation catalysts is their “activation” by an organometallic cocatalyst, frequently  $\text{AlR}_3$ ,<sup>34,35</sup> control experiments were performed to check the necessity of  $\text{AlEt}_3$  in forming active hydrogenation catalysts from **1** and **2**. Hydrogenations were performed identically to those in Figures 3 and 4, but leaving out the  $\text{AlEt}_3$  while substituting an equal volume of cyclohexane for the volume introduced by the  $\text{AlEt}_3$  solution. Figure S9 shows the results of these control experiments. The observation of induction periods indicates precursors **1** and **2** are not themselves active catalysts. However,  $\text{H}_2$  uptake does occur showing that catalysts do eventually form under the reductive experimental conditions (i.e., reduction by  $\text{H}_2$ ).

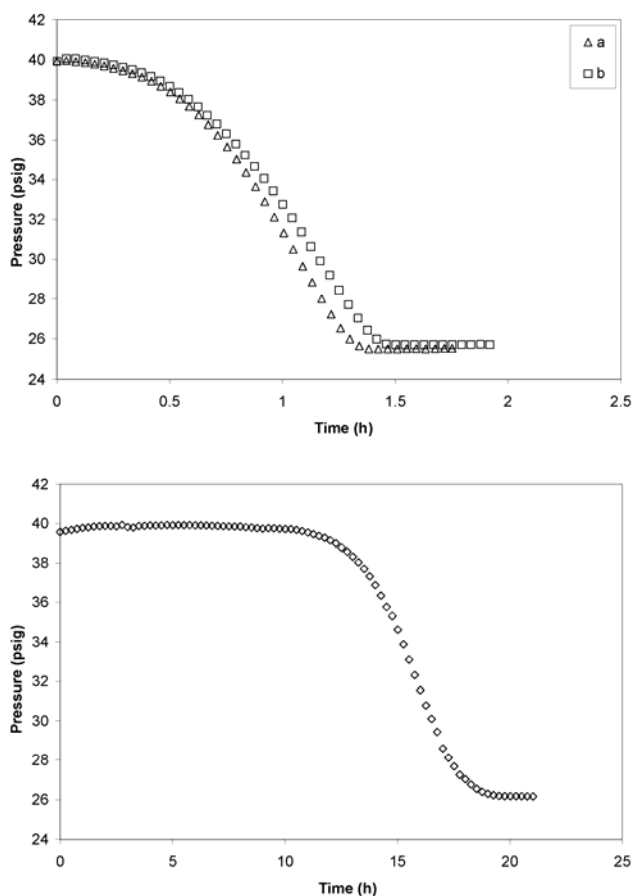


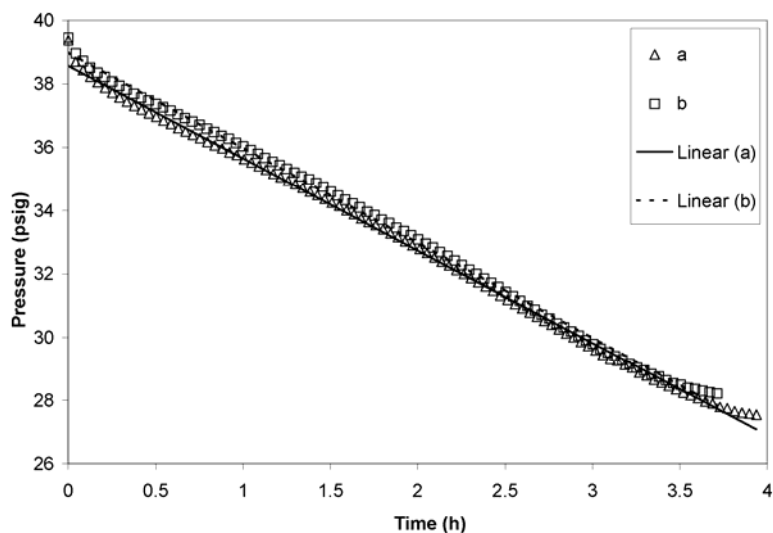
**Figure S9.** Catalytic hydrogenation of cyclohexene using the catalyst precursors  $[(1,5\text{-COD})\text{Ir}(\mu\text{-O}_2\text{C}_8\text{H}_{15})_2]_2$  (top) or  $[(1,5\text{-COD})\text{Rh}(\mu\text{-O}_2\text{C}_8\text{H}_{15})_2]_2$  (bottom) *without* added  $\text{AlEt}_3$ . For clarity, only every fifth data point collected of run “a” with **1** (top), and only

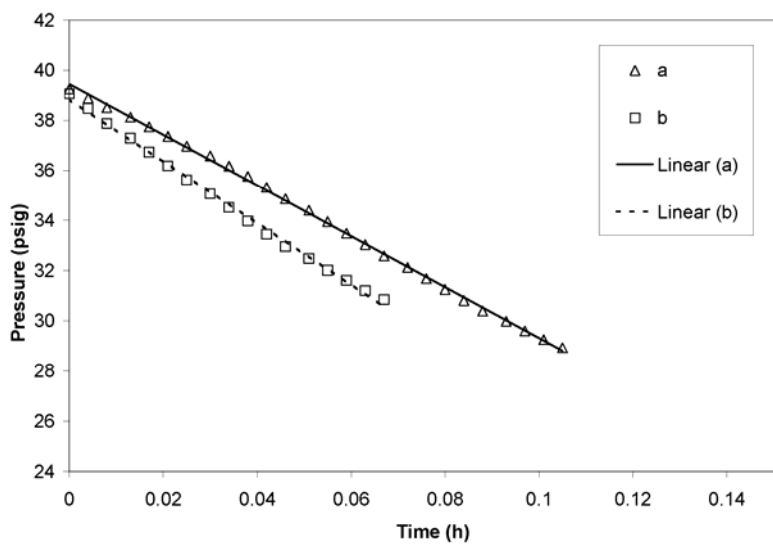
every sixth data point of the run with **2** (bottom) is displayed. The presence of an induction period indicates that **1** and **2** themselves are not active cyclohexene hydrogenation catalysts. However, hydrogenation in both cases did occur, showing that catalysts were formed under the reductive conditions of the experiment. The solutions at the end of the hydrogenation were the same orange for **1** and yellow for **2** they were at the start, but black solid had formed on the Teflon-coated magnetic stirbars suggesting catalysis by either  $M(0)_n$  nanoclusters, bulk  $M(0)$ , or conceivably both. The curves shown here for **1** are representative runs, having been reproduced at least four times. Only one other such experiment was attempted with **2**, but was aborted due to an excessively long induction period. Large variability in the induction periods of such nucleation and growth reactions that form bulk metal has been observed before in other systems.<sup>36</sup>

Such sigmoidal hydrogenation curves are characteristic of formation of nanocluster catalysts, bulk metal catalysts, or both.<sup>37,38</sup> These curves were fit using the Finke-Watzky mechanistic model for initial nanocluster formation by slow nucleation followed by fast autocatalytic surface growth, Figure S11.<sup>38,36</sup> Additionally, at the end of the hydrogenations, the solutions were the original orange and yellow colors for **1** and **2**, respectively, indicating that most of **1** and **2** were unreacted, but small amounts of a black solid had deposited on the surface of the Teflon-coated magnetic stirbars. This also suggests that small amounts of **1** and **2** have been transformed into highly active  $M(0)_n$  nanocluster catalysts, bulk  $M(0)$  catalysts, or both.<sup>37,38</sup> The average maximum rate of  $H_2$  uptake achieved using the catalyst formed by **1** under  $H_2$  without added  $AlEt_3$  is about six times greater than the  $H_2$  uptake rate attained using the catalyst formed by the Ziegler-type hydrogenation catalyst made from the combination of **1** and  $AlEt_3$ , Table S3. However, the observance of bulk metal indicates that this system is unstable towards agglomeration, and therefore is not a system of primary interest to us outside this control experiment, and certainly not of industrial interest.

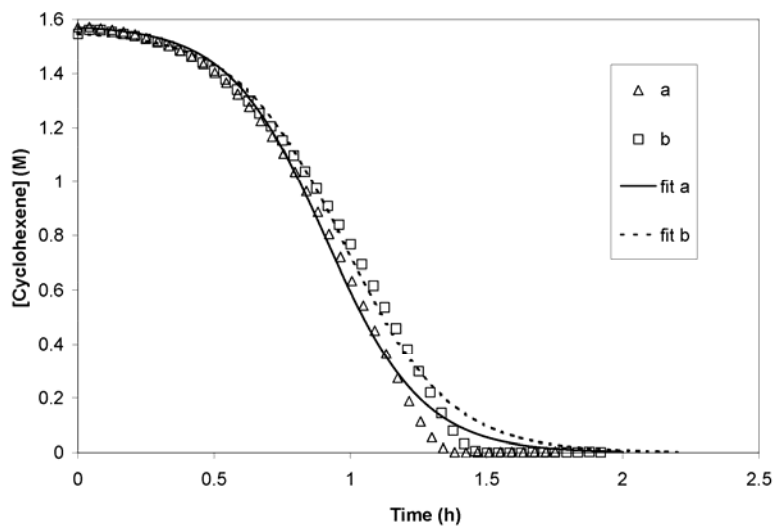
## Fitting of Cyclohexene Hydrogenation Curves

Hydrogenation curves attained using the Ziegler-type catalysts made from **1** or **2** and  $\text{AlEt}_3$  are shown in Figure S10 with linear fits to the data. For the purpose of fitting, these data series were truncated at the point at which hydrogenation uptake ceases due to complete conversion of cyclohexene. Hydrogenation curves attained using **1** or **2** *without* added  $\text{AlEt}_3$  are shown in Figure S11 along with fits to the data. The kinetic model used to fit these curves describes a mechanism of nanocluster formation in which a slow nucleation step,  $\text{A} \rightarrow \text{B}$  (rate constant  $k_1$ , A is the precursor molecule and B is a catalyst species) is followed by fast, autocatalytic surface growth  $\text{A} + \text{B} \rightarrow 2 \text{B}$  (rate constant  $k_2$ ). This model, the Finke-Watzky (F-W) mechanism, has been described in detail in the literature.<sup>36,37,38</sup> Values obtained from all fits are summarized in Table S3.





**Figure S10.** Cyclohexene hydrogenation curves using Ziegler-type catalysts made from **1** (top) and **2** (bottom) plus  $\text{AlEt}_3$ , with linear fits to the data. For the purpose of fitting, these data series are truncated at the point at which hydrogenation uptake ceases due to complete conversion of cyclohexene.



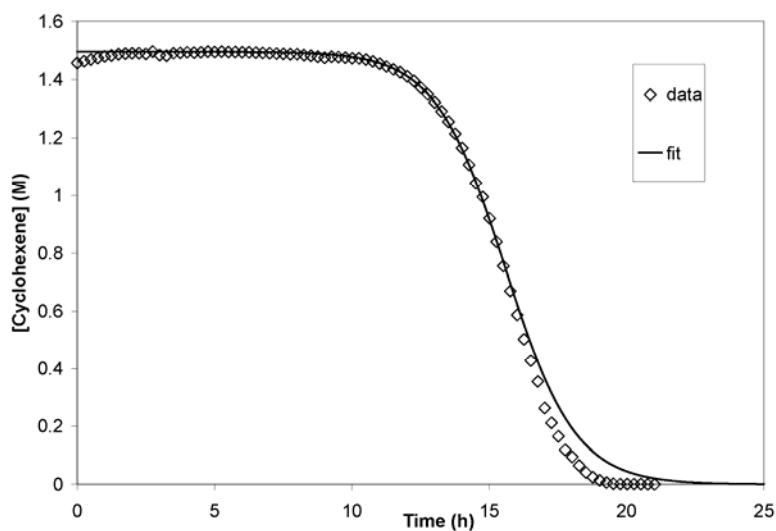


**Figure S11.** Cyclohexene hydrogenation curves using catalyst precursors **1** (top) and **2** (bottom), without added  $\text{AlEt}_3$ . Each curve is fit with the F-W 2-step model of slow nucleation followed by fast autocatalytic surface growth.

**Table S3.** Fitting Results from the Hydrogenation Curves in Figures S9 and S10.

System	Run	Fit Type	Fit Results			$R^2$
			$-\text{d}[\text{H}_2]/\text{dt}$ (pisc/hr)	$k_1$	$k_2$	
Al/Ir = 1	a	linear	2.92(1)	-	-	0.9981
Al/Ir = 1	b	linear	3.01(1)	-	-	0.9984
Al/Rh = 1	a	linear	101.4(7)	-	-	0.9989
Al/Rh = 1	b	linear	124(2)	-	-	0.997
Al/Ir = 0	a	F-W	-	$5.62(9) \times 10^{-2}$	$3.93(2) \times 10^3$	0.9998
Al/Ir = 0	b	F-W	-	$5.2(3) \times 10^{-2}$	$3.72(8) \times 10^3$	0.9974
Al/Rh = 0	-	F-W	-	$3.6(6) \times 10^{-6}$	$6.6(1) \times 10^2$	0.9966
Al/Ir = 0	a	linear	19.3(1)	-	-	0.9999
Al/Ir = 0	b	linear	17.0(1)	-	-	0.9996
Al/Rh = 0	-	linear	3.02(2)	-	-	0.9997

## References.

---

- <sup>1</sup> Chatt, J.; Venanzi, L. M. *J. Chem. Soc.* **1957**, 4735–4741.
- <sup>2</sup> Haszeldine, R. N.; Lunt, R. J.; Parish, R. V. *J. Chem. Soc. A* **1971**, 23, 3696–3698.
- <sup>3</sup> Green, M.; Kuc, T. A. *J. Chem. Soc., Dalton Trans.* **1972**, 832–839.
- <sup>4</sup> Reis, A. H., Jr.; Willi, C.; Siegel, S.; Tani, B. *Inorg. Chem.* **1979**, 18, 1859–1863.
- <sup>5</sup> Chen, M. J.; Feder, H. M. *Inorg. Chem.* **1979**, 18, 1864–1869.
- <sup>6</sup> Nagy-Magos, Z.; Vastag, S.; Heil, B.; Markó, L. *J. Organomet. Chem.* **1979**, 171, 97–102.
- <sup>7</sup> Trzeciak, A. M.; Ziółkowski, J. J.; Lis, T.; Borowski, A. *Polyhedron* **1985**, 4, 1677–1681.
- <sup>8</sup> Azbel, B. I.; Gol'dshleger, N. F.; Khidekel, M. L.; Sokol, V. I.; Porai-Koshits, M. A. *J. Mol. Catal.* **1987**, 40, 57–63.
- <sup>9</sup> Burk, M. J.; Crabtree, R. H. *J. Am. Chem. Soc.* **1987**, 109, 8025–8032.
- <sup>10</sup> Sheldrick, W. S.; Günther, B. *J. Organomet. Chem.* **1989**, 375, 233–243.
- <sup>11</sup> Lahoz, F. J.; Martin, A.; Esteruelas, M. A.; Sola, E.; Serrano, J. L.; Oro, L. A. *Organometallics* **1991**, 10, 1794–1799.
- <sup>12</sup> Mieczynska, E.; Trzeciak, A. M.; Ziółkowski, J. J.; Lis, T. *Polyhedron* **1994**, 13, 655–658.
- <sup>13</sup> Werner, H.; Poelsma, S.; Schneider, M.; Windmüller, B.; Barth, D. *Chem. Ber.* **1996**, 129, 647–652.
- <sup>14</sup> Vaartstra, Metal Carboxylate Complexes for Formation of Metal-Containing Films on Semiconductor Devices. U.S. Patent 5,695,815, Dec. 9, 1997.

- 
- <sup>15</sup> Burk and Crabtree<sup>9</sup> referenced Haszeldine et al.<sup>2</sup> in implying that [(COD)IrOAc]<sub>2</sub> could be produced by reaction between [(COD)IrCl]<sub>2</sub> and AgOAc as an intermediate in the synthesis of [IrH<sub>2</sub>(OCOCH<sub>3</sub>)(P(C<sub>6</sub>H<sub>11</sub>)<sub>3</sub>)<sub>2</sub>].
- <sup>16</sup> Bonnet, J. J.; Thorez, A.; Maisonnat, A.; Galy, J.; Poilblanc, R. *J. Am. Chem. Soc.* **1979**, *101*, 5940–5949.
- <sup>17</sup> Coleman, A. W.; Eadie, D. T.; Stobart, S. R. *J. Am. Chem. Soc.* **1982**, *104*, 922–923.
- <sup>18</sup> Beveridge, K. A.; Bushnell, G. W.; Stobart, S. R.; Atwood, J. L.; Zaworotko, M. J. *Organometallics* **1983**, *2*, 1447–1451.
- <sup>19</sup> Rodman, G. S.; Mann, K. R. *Inorg. Chem.* **1988**, *27*, 3338–3346.
- <sup>20</sup> Sielisch, T.; Cowie, M. *Organometallics* **1988**, *7*, 707–714.
- <sup>21</sup> Chebi, D. E.; Fanwick, P. E.; Rothwell, I. P. *Organometallics* **1990**, *9*, 2948–2952.
- <sup>22</sup> Schnabel, R. C.; Roddick, D. M. *Inorg. Chem.* **1993**, *32*, 1513–1518.
- <sup>23</sup> Schnabel, R. C.; Roddick, D. M. *Organometallics* **1996**, *15*, 3550–3555.
- <sup>24</sup> Kanematsu, N.; Ebihara, M.; Kawamura, T. *Inorg. Chim. Acta* **1999**, *292*, 244–248.
- <sup>25</sup> Fandos, R.; Hernández, C.; Otero, A.; Rodríguez, A.; Ruiz, M. J. *Organometallics* **1999**, *18*, 2718–2723.
- <sup>26</sup> Cotton, F. A.; Lin, C.; Murillo, C. A. *Inorg. Chem.* **2000**, *39*, 4574–4578.
- <sup>27</sup> (a) Marciniak, B.; Kownacki, I.; Kubicki, M. *Organometallics* **2002**, *21*, 3263–3270.  
(b) Kownacki, I.; Marciniak, B.; Kubicki, M. *Chem. Commun.* **2003**, 76–77.
- <sup>28</sup> Miranda-Soto, V.; Pérez-Torrente, J. J.; Oro, L. A.; Lahoz, F. J.; Martín, M. L.; Parra-Hake, M.; Grotjahn, D. B. *Organometallics* **2006**, *25*, 4374–4390.
- <sup>29</sup> Chen, Y.-Q.; Wang, J.-Q.; Jin, G.-X. *J. Organomet. Chem.* **2007**, *692*, 5190–5194.

- 
- <sup>30</sup> Nakamoto, K. *Infrared and Raman Spectra of Inorganic and Coordination Compounds*, 4<sup>th</sup> ed.; John Wiley and Sons: New York, 1986.
- <sup>31</sup> Rodman, G. S.; Daws, C. A.; Mann, K. R. *Inorg. Chem.* **1998**, *27*, 3347–3353.
- <sup>32</sup> Szajek, L. P.; Shapley, J. R. *Organometallics* **1993**, *12*, 3772–3775.
- <sup>33</sup> (a) Chisholm, M. H.; Clark, H. C.; Manzer, L. E.; Stothers, J. B. *J. Am. Chem. Soc.* **1972**, *94*, 5087–5088. (b) Mann, B. E.; Shaw, B. L.; Slade, R. L.; Stainbank, R. E. *J. Chem. Soc. A* **1971**, 2976–2980.
- <sup>34</sup> McManus, N.; Rempel, G. *J.M.S. – Rev. Macromol. Chem. Phys.* **1995**, *35*, 239–285.
- <sup>35</sup> Johnson, K. *Polym. Prepr.* **2000**, *41*, 1525–1526.
- <sup>36</sup> Widegren, J. A.; Bennett, M. A.; Finke, R. G. *J. Am. Chem. Soc.* **2003**, *125*, 10301–10310.
- <sup>37</sup> Widegren, J.; Finke, R. *J. Mol. Catal. A: Chem.* **2003**, *198*, 317–341.
- <sup>38</sup> Watzky, M. A.; Finke, R. G. *J. Am. Chem. Soc.* **1997**, *119*, 10382.

## CHAPTER IV

### IRIDIUM ZIEGLER-TYPE HYDROGENATION CATALYSTS MADE FROM [(1,5-COD)Ir( $\mu$ -O<sub>2</sub>C<sub>8</sub>H<sub>15</sub>)<sub>2</sub>] AND AlEt<sub>3</sub>: SPECTROSCOPIC AND KINETIC EVIDENCE FOR THE Ir<sub>n</sub> SPECIES PRESENT AND FOR NANOPARTICLES AS THE FASTEST CATALYST

This dissertation chapter contains a paper published in *Inorganic Chemistry* **2010**, *49*, 8131–8147. It is reprinted with permission, Copyright (2010) American Chemical Society. This chapter presents efforts to determine whether the catalyst formed using the precursors mentioned in the title is homogeneous or heterogeneous in nature. The approach taken makes use of the Ir Ziegler-type hydrogenation catalyst system made from [(1,5-COD)Ir( $\mu$ -O<sub>2</sub>C<sub>8</sub>H<sub>15</sub>)<sub>2</sub>] plus AlEt<sub>3</sub> (the synthesis and characterization of the Ir complex is described in Chapter III of this dissertation). The approach used herein also utilizes multiple analytical techniques and complementary kinetic studies.

All [(1,5-COD)Ir( $\mu$ -O<sub>2</sub>C<sub>8</sub>H<sub>15</sub>)<sub>2</sub>] used in these studies was synthesized, purified, and characterized by William M. Alley. Z-contrast STEM imaging was performed by Long Li on samples prepared by William M. Alley. XAFS data was obtained, processed, and analyzed by William M. Alley with assistance from Qi Wang, Anatoly

Frenkel, and Laurent D. Menard. MALDI MS data was collected by Isil K. Hamdemir, and interpreted by her and William M. Alley. HR- and bright field TEM, and electron diffraction imaging (Figure 8, and in the Supporting Information) were performed by JoAn Hudson of Clemson University on samples prepared by Isil K. Hamdemir. Interpretation of bright field TEM data was performed by Isil K. Hamdemir. Interpretation of the electron diffraction image was accomplished by William M. Alley. XPS was performed and analyzed by Isil K. Hamdemir. The important control experiment, Figure 11, demonstrating that a catalyst sample retains its activity after being isolated as a powder and redispersed in cyclohexene was performed by Isil K. Hamdemir. All other kinetics experiments, including Hg(0) poisoning, and all associated control experiments were performed by William M. Alley.

The manuscript was written by William M. Alley with the aid of an earlier draft of a research report written by Isil K. Hamdemir that described the experimental procedures, results, and a discussion of the work she performed. The manuscript was prepared for publication by William M. Alley with moderate editing assistance (43 hours) from Prof. Richard G. Finke. The various coauthors lightly edited and proofread the manuscript, primarily the portions that correspond to their areas of expertise.

**Iridium Ziegler-Type Hydrogenation Catalysts Made from [(1,5-COD)Ir( $\mu$ -O<sub>2</sub>C<sub>8</sub>H<sub>15</sub>)]<sub>2</sub> and AlEt<sub>3</sub>: Spectroscopic and Kinetic Evidence for the Ir<sub>n</sub> Species Present and for Nanoparticles as the Fastest Catalyst**

William M. Alley, Isil K. Hamdemir, Qi Wang, Anatoly Frenkel, Long Li, Judith C. Yang, Laurent D. Menard, Ralph G. Nuzzo, Saim Özkar, Kimberly Johnson, Richard G. Finke

**Abstract**

Ziegler-type hydrogenation catalysts, those made from a group 8–10 transition metal precatalyst and an AlR<sub>3</sub> cocatalyst, are often used for large scale industrial polymer hydrogenation; note that Ziegler-type *hydrogenation* catalysts are *not* the same as Ziegler–Natta *polymerization* catalysts. A review of prior studies of hydrogenation catalysts (Alley et al. *J. Mol. Catal. A: Chem.* **2010**, *315*, 1–27) reveals that a ~50 year old problem is identifying the metal species present before, during, and after Ziegler-type hydrogenation catalysis, and which species are the kinetically best, fastest catalysts—that is, which species are the true hydrogenation catalysts. Also of significant interest is whether what we have termed “Ziegler nanoclusters” are present and what their relative catalytic activity is. Reported herein is the characterization of an Ir

Ziegler-type hydrogenation catalyst, a valuable model (*vide infra*) for the Co-based industrial Ziegler-type hydrogenation catalyst, made from the crystallographically characterized [(1,5-COD)Ir( $\mu$ -O<sub>2</sub>C<sub>8</sub>H<sub>15</sub>)<sub>2</sub>] pre-catalyst plus AlEt<sub>3</sub>. Characterization of this Ir model system is accomplished before and after catalysis using a battery of physical methods including Z-contrast scanning transmission electron microscopy (STEM), high resolution (HR)TEM, and X-ray absorption fine structure (XAFS) spectroscopy. Kinetic studies plus Hg(0) poisoning experiments are then employed to probe which species are the fastest catalysts. The main findings herein are that (i) a combination of the catalyst precursors [(1,5-COD)Ir( $\mu$ -O<sub>2</sub>C<sub>8</sub>H<sub>15</sub>)<sub>2</sub>] and AlEt<sub>3</sub> gives catalytically active solutions containing a broad distribution of Ir<sub>n</sub> species ranging from monometallic Ir complexes to nanometer scale, noncrystalline Ir<sub>n</sub> nanoclusters (up to Ir<sub>~100</sub> by Z-contrast STEM) with the estimated mean Ir species being 0.5–0.7 nm, Ir<sub>~4–15</sub> clusters considering the similar, but not identical results from the different analytical methods; furthermore, (ii) the mean Ir<sub>n</sub> species are practically the same regardless of the Al/Ir ratio employed, suggesting that the observed changes in catalytic activity at different Al/Ir ratios are primarily the result of changes in the form or function of the Al-derived component (and not due to significant AlEt<sub>3</sub>-induced changes in initial Ir<sub>n</sub> nuclearity). However, (iii) during hydrogenation, a shift in the population of Ir species toward roughly 1.0–1.6 nm, *fcc* Ir(0)<sub>~40–150</sub>, Ziegler nanoclusters occurs with, significantly, (iv) *a concomitant increase in catalytic activity*. Importantly, and although catalysis by discrete subnanometer Ir species is not ruled out by this study, (v) the increases in activity with increased nanocluster size, plus Hg(0) poisoning studies, provide the best evidence to date that the approximately 1.0–1.6 nm, *fcc* Ir(0)<sub>~40–150</sub>,

heterogeneous Ziegler nanoclusters are the fastest catalysts in this industrially related catalytic hydrogenation system (and in the simplest, Ockham's Razor interpretation of the data). In addition, (vi) Ziegler nanoclusters are confirmed to be an unusual, hydrocarbon-soluble, highly coordinatively unsaturated, Lewis-acid containing, and highly catalytically active type of nanocluster for use in other catalytic applications and other areas.

## Introduction

Ziegler-type hydrogenation catalysts prepared, by definition, from a nonzero valent, group 8–10 transition metal precatalyst combined with an  $\text{AlR}_3$  cocatalyst, such as triethylaluminum ( $\text{AlEt}_3$ ), account for much of the worldwide industrial hydrogenation of styrenic block copolymers (SBCs).<sup>1</sup> According to one estimate, hydrogenated SBCs are produced at a rate in excess of  $1.7 \times 10^5$  metric tons annually worldwide.<sup>2</sup> The literature concerning Ziegler-type hydrogenation catalysts has recently been critically reviewed by us,<sup>3</sup> leading to the following insights: (i) Improved fundamental understanding of Ziegler-type hydrogenation catalysts is needed so that rationally directed catalyst improvements can be made. (ii) Multiple variables are important in catalyst synthesis, including the specific components used, the cocatalyst/transition metal ratio ( $\text{Al/M}$ ), the amount of  $\text{H}_2\text{O}$  present (widely observed to be connected to the amount of cocatalyst), and the order of addition of the catalyst components, and (iii) these variables influence the nature of the resulting catalysts and their catalytic properties. Other insights<sup>3</sup> are (iv) a central, unanswered question in the area of Ziegler-type industrial hydrogenation catalysts is whether the true catalyst is a homogeneous (e.g., single metal organometallic) or heterogeneous (e.g., polymetallic  $\text{M}(0)_n$  nanocluster) catalyst,<sup>4</sup> and that (v) the most recent, especially noteworthy prior work—that of Schmidt and co-workers,<sup>5</sup> and Bönemann and co-workers<sup>3,6</sup>—is starting to *suggest* that Ziegler-type hydrogenation catalysts are transition metal nanoclusters, what we have coined in our review as “Ziegler nanoclusters”.<sup>3</sup> However, (vi) compelling or even highly suggestive evidence concerning the homogeneous versus heterogeneous catalysis question for Ziegler-type hydrogenation catalysts has remained

elusive due to the use of often poorly defined precursors or the lack of application of the best current, previously successful approaches for addressing the historically perplexing “is it homogeneous or heterogeneous catalysis?” question.<sup>7</sup> *Absent in particular are definitive kinetic studies connected to knowledge of the dominant form(s) of the transition metal catalyst.* On the basis of our review of the literature, we reasoned, therefore, that (vii) the use of a well-characterized precatalyst as a model for the industrially favored, but often less well- (or clearly) characterized, Co and Ni precatalysts might allow new insights into Ziegler-type hydrogenation catalyst systems, and (viii) that our previously successful, multipronged, kinetic-containing approach for addressing the homogeneous versus heterogeneous catalysis problem<sup>3,4b,7,8</sup> should be applied to Ziegler-type, industrially relevant hydrogenation catalysts. In addition, (ix) we reasoned that the use of the third row transition metal Ir, where strong Ir–Ir bonds, and for example Ir(0)<sub>n</sub> nanoclusters that typically stable under characterization conditions,<sup>7a</sup> might prove very useful—if not necessary—in allowing identification of the dominant species present before and after catalysis without significant artifacts due to the use of ex situ or even in situ (as opposed to the ideal operando<sup>9</sup>) methods.

Herein, we report the characterization of iridium model Ziegler-type hydrogenation catalysts made from the crystallographically characterized precatalyst, [(1,5-COD)Ir(μ-O<sub>2</sub>C<sub>8</sub>H<sub>15</sub>)]<sub>2</sub>,<sup>2</sup> plus AlEt<sub>3</sub> under carefully controlled conditions. The resultant pre- and posthydrogenation catalyst materials are characterized by a variety of analytical techniques including Z-contrast scanning transmission electron microscopy (STEM), high resolution (HR)TEM, X-ray absorption fine structure (XAFS) spectroscopy, and matrix assisted laser desorption ionization mass spectrometry

(MALDI MS).<sup>10</sup> The needed kinetic and Hg(0) poisoning studies round out the work reported herein. The main findings are (i) that combining the catalyst precursors [(1,5-COD)Ir( $\mu$ -O<sub>2</sub>C<sub>8</sub>H<sub>15</sub>)<sub>2</sub>] and AlEt<sub>3</sub> gives catalytically active solutions containing Ir<sub>n</sub> clusters with a range of sizes from monometallic Ir complexes to nanometer scale, noncrystalline Ir<sub>n</sub> nanoclusters with an estimated mean 0.5–0.7 nm, Ir<sub>~4–15</sub> cluster (considering the similar, but not identical results obtained from the different analytical methods), *but* (ii) that during the hydrogenation process, the development of roughly 1.0–1.6 nm, *fcc* Ir(0)<sub>~40–150</sub> nanoclusters occurs, and (iii) that kinetic studies indicate, importantly, a concomitant *increase in catalytic activity* as the size of the Ir<sub>n</sub> nanoclusters increases. In addition, we find (iv) that this size–activity correlation, plus Hg(0) poisoning studies, suggest (as the simplest, “Ockham’s razor” interpretation of the data) that the fastest, kinetically competent catalysts are the larger, roughly 1.0–1.6 nm, Ir(0)<sub>~40–150</sub> nanoclusters rather than the monometallic complexes and 0.5–0.7 nm, Ir<sub>~4–15</sub> clusters initially present (the homogeneous catalyst component alone appears to have about 5% of the activity of the overall catalyst solution, *vide infra*).

The results are significant in comparison to even the ~50 year history of Ziegler-type hydrogenation catalysts<sup>3</sup> (a) in being the first to show that the transition metal component of the initial catalyst formation reaction is, at least for the present Ir model system, a broadly disperse mixture ranging from mono-Ir complexes to noncrystalline nanoscale clusters, with the estimated mean Ir<sub>n</sub> species being 0.5–0.7 nm, Ir<sub>~4–15</sub> clusters; (b) in being the first report of the explicit application of an established, previously successful, multiprong approach for addressing the homogeneous versus heterogeneous catalysis problem in a Ziegler-type hydrogenation catalyst system;<sup>3,4b,7,8</sup>

and (c) in providing evidence consistent with and highly supportive of the now dominant hypothesis for future research in the area, namely, that Ziegler nanoclusters appear to be the kinetically dominant catalysts—although we note that the true catalyst in the industrially fastest Co/AlR<sub>3</sub> system remains to be identified and is under investigation. As such, the findings reported herein are both believed to be important fundamentally and are expected to result in practical implications due to the large-scale industrial utilization of Ziegler-type hydrogenation catalysts.<sup>11,12,13,14</sup>

## Results and Discussion

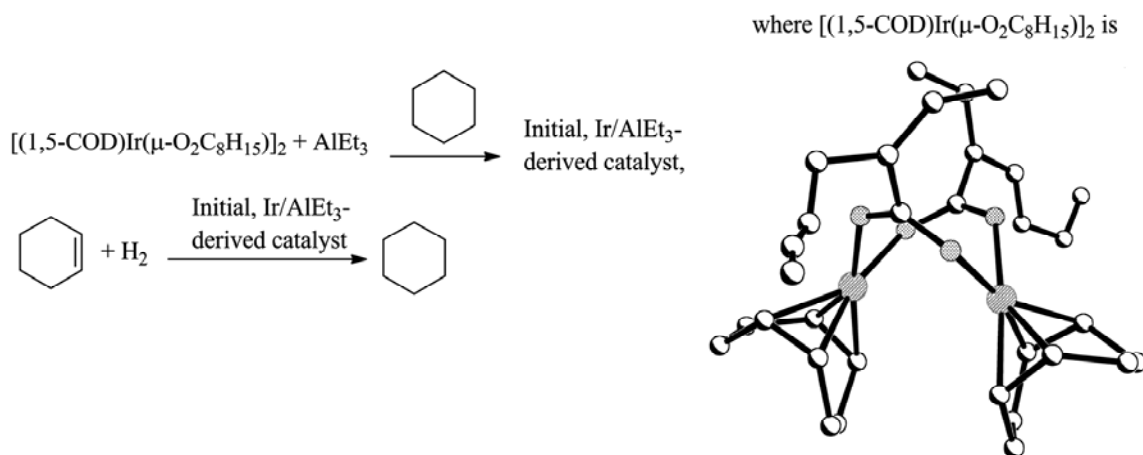
A key insight from our review of the literature of Ziegler-type hydrogenation catalysts<sup>3</sup> is that their catalytic hydrogenation activity is quite sensitive to a number of variables, including the specific conditions and details under which the catalysts are synthesized. Therefore, preliminary catalytic studies were carried out in order to determine appropriate, representative conditions for reliable and reproducible catalyst preparation and subsequent catalytic use as well as to ensure the broadest applicability of the results of the studies which follow.

**Catalyst Preparation.** Catalyst samples used in olefin hydrogenation were prepared by a combination of [(1,5-COD)Ir( $\mu$ -O<sub>2</sub>C<sub>8</sub>H<sub>15</sub>)]<sub>2</sub> and AlEt<sub>3</sub>, with Al/Ir ratios of 1.0, 2.0, 3.0, and 5.0. We previously reported the control experiment of using [(1,5-COD)Ir( $\mu$ -O<sub>2</sub>C<sub>8</sub>H<sub>15</sub>)]<sub>2</sub> for catalytic cyclohexene hydrogenation *without* AlEt<sub>3</sub>.<sup>2</sup> The resulting black, Ir(0) precipitate formed during hydrogenation indicates that the AlEt<sub>3</sub> component is crucial for the stability of the catalyst (and nanoclusters, *vide infra*). A

brief summary of those hydrogenation results without AlEt<sub>3</sub> is provided in the Supporting Information for the interested reader.

In light of what is known from the literature,<sup>3</sup> all catalyst solutions were prepared using the same materials from the same sources. Also, the procedures described below and in the Experimental Section were followed exactly for repeat kinetic runs. Specifically, an 18.0 mM cyclohexane solution of AlEt<sub>3</sub> was rapidly added to a cyclohexane solution of the precatalyst, 9.0 mM in [Ir], without the presence of the olefinic substrate, which has been reported to influence these specific catalyst formation reactions in some cases.<sup>3</sup> The addition of AlEt<sub>3</sub> to the cyclohexane solution of [(1,5-COD)Ir(μ-O<sub>2</sub>C<sub>8</sub>H<sub>15</sub>)<sub>2</sub>] resulted in an immediate change in color from orange to tawny yellow, regardless of whether an Al/Ir ratio of 1.0, 2.0, 3.0, or 5.0 was used. Catalyst solutions were then used for the catalytic hydrogenation of the model olefin, cyclohexene, as depicted in Scheme 1.

**Scheme 1.** Catalyst Preparation and Hydrogenation of Cyclohexene Plus (shown to the right) the Single-Crystal X-Ray Diffraction Determined Structure of the [(1,5-COD)Ir(μ-O<sub>2</sub>C<sub>8</sub>H<sub>15</sub>)<sub>2</sub>] Precatalyst (adapted from ref 2, copyright 2009, American Chemical Society).



### Cyclohexene Hydrogenation Curves and Catalyst Aging. Example

cyclohexene hydrogenation curves obtained by following H<sub>2</sub> pressure loss, and using the [(1,5-COD)Ir( $\mu$ -O<sub>2</sub>C<sub>8</sub>H<sub>15</sub>)<sub>2</sub>] plus AlEt<sub>3</sub> catalysts with Al/Ir ratios of 1.0, 2.0, and 3.0, are shown in Figure 1. In each case, the Ir/AlEt<sub>3</sub>-based catalysts exhibit immediate activity, but the maximum rate is attained later as the reaction proceeds, Figure 1a and b—that is, either more catalyst or a better catalyst is being formed as the reaction proceeds.

A key factor in the preparation of the catalyst is the time elapsed between mixing the [(1,5-COD)Ir( $\mu$ -O<sub>2</sub>C<sub>8</sub>H<sub>15</sub>)<sub>2</sub>] and AlEt<sub>3</sub> components prior to use of the resultant solution for the test reaction of cyclohexene hydrogenation, hereafter referred to as the *aging time*. Despite the initial reaction between the Ir precatalyst and AlEt<sub>3</sub>, hydrogenation activity approaches a maximum value if the initially prepared catalyst solutions are allowed to age by stirring under an atmosphere of N<sub>2</sub> for about 8–24 h before being placed under H<sub>2</sub> (Figure S2, Supporting Information); maximum rates of aged catalysts are ~2–7-fold greater than the maximum rates of their nonaged counterparts, depending on Al/Ir. Without aging catalyst solutions before their use, the resulting hydrogenation curves exhibit a more distinct transition from a less active—but longer-persisting—initial stage to their maximum rate stage, especially at the Al/Ir ratio of 5.0 (Figure S3, Supporting Information). However, even 33 h of aging does not completely eliminate the slower initial rate (Figure S2b of the Supporting Information). The maximum rates are ~2–10 times the initial rates in each case, depending on Al/Ir and whether or not catalyst solutions were aged. A table giving the mean initial and maximum rates from multiple runs of both aged and nonaged catalysts samples, and at various Al/Ir ratios, is given in the Supporting Information. Clearly, evolution of the

catalyst is occurring, so that it became important to determine the nature of that evolution, *vide infra*.

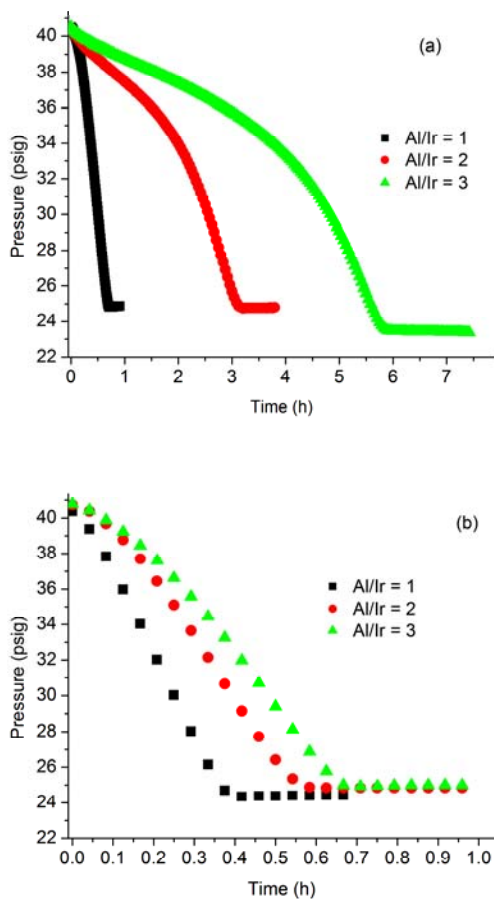


**Figure 1.** Catalytic cyclohexene hydrogenations using  $[(1,5\text{-COD})\text{Ir}(\mu\text{-O}_2\text{C}_8\text{H}_{15})_2]$  plus  $\text{AlEt}_3$  catalysts that were (a) used immediately after preparation or (b) first aged for nine h with stirring under a  $\text{N}_2$  atmosphere. Note the ca. 10-fold reduced timescale axis in part b versus that in part a—that is, the aged catalyst is about 2- to 7-fold more active, depending on the Al/Ir ratio, on the basis of the *maximum* hydrogenation rate achieved. In each case, the reaction is fastest just before the end of the catalytic run, despite the normal, rate-slowing decrease in the olefin concentration and  $\text{H}_2$  pressure (the max rate is  $\sim 2\text{--}10$  times the initial rate of a given run). Also, the effect on the initial rate of the Al/Ir ratio is significantly less when the catalyst solutions are aged before use. Reactions were performed in cyclohexane solutions, 0.6 mM in [Ir], initially 1.65 M in cyclohexene, at  $22.0\text{ }^\circ\text{C}$ , and stirred at  $1000 \pm 10$  rpm. Additional catalytic hydrogenation curves, attained using catalysts with an Al/Ir ratio of 5.0, are shown in Figure S3 of the Supporting Information.

As expected from the literature,<sup>3</sup> catalyst activity is dependent on the Al/Ir ratio. However, the magnitude of the effect of the Al/Ir ratio on the catalyst activity is diminished when the catalysts are aged. Interestingly, even 33 h of aging of the catalyst solutions does not result in further color change; yet, in all cases, the reaction solutions change color *during hydrogenation* (i.e., under H<sub>2</sub> and cyclohexene) to darker brown, results that are consistent with further catalyst development to larger Ir(0)<sub>n</sub> nanoclusters that have been identified by several physical methods, *vide infra*. Catalyst solutions sometimes give a dark brown/black precipitate within a few days of hydrogenation if the catalyst solution is transferred to a N<sub>2</sub> atmosphere shortly after complete consumption of the substrate. However, a dark brown/black precipitate (Ir(0) by XPS) plus a clear, nearly colorless solution always results if the solutions are left under pressurized H<sub>2</sub> for extended amounts of time after complete consumption of the cyclohexene substrate. The observations of brown-black catalyst solutions plus metal(0) precipitates are strongly suggestive, but by themselves not definitive, evidence for heterogeneous (e.g., nanoparticle) catalysis.<sup>4b</sup> Overall, the increased catalytic activity, color changes, and occasional bulk Ir(0) precipitate after the reaction require *at least one transformation processes of the catalyst, or possibly parallel development of different catalysts, during both the aging stage and the hydrogenation catalysis*. Nanocluster development is strongly implicated by just the color change, although verification of that by several independent methods quickly became the next objective.

The specific objectives for what follows, then, are (i) to determine the nuclearity of the Ir<sub>n</sub> species initially present and (ii) to determine the Ir<sub>n</sub> species present after the catalyst has entered the maximum rate regime. Those studies presented next comprise

the first necessary step en route (iii) to determining the nature of the active catalyst during both the initial and the maximum rate regimes. An important additional goal is to (iv) determine to what extent the rate effect of different Al/Ir ratios is due to AlEt<sub>3</sub>-induced changes in the initial Ir component of the catalyst (e.g., does Al/Ir influence initial Ir<sub>n</sub> nuclearity?) versus changes in just the AlEt<sub>3</sub>-derived component. Additional studies concerning the challenging problem of the form(s) of the AlEt<sub>3</sub>-derived species at varying Al/Ir ratios and their role in catalysis are necessarily addressed elsewhere.<sup>13</sup>

### Tabulation of the Key Pre- and Posthydrogenation Catalyst

**Characterization.** It will be easier to read what follows if we first summarize in Table 1 the key results from Z-contrast STEM, XAFS, and MALDI MS, both pre- and postcatalytic hydrogenation runs. The key findings will be that (i) a combination of the catalyst precursors [(1,5-COD)Ir(μ-O<sub>2</sub>C<sub>8</sub>H<sub>15</sub>)<sub>2</sub>] and AlEt<sub>3</sub> gives catalytically active solutions containing a broad range of Ir<sub>n</sub> species spanning from monometallic Ir complexes to noncrystalline Ir<sub>n</sub> nanoclusters, with estimated mean 0.5–0.7 nm Ir<sub>~4–15</sub> clusters. However, (ii) after a catalytic run, the population of Ir<sub>n</sub> shifts considerably toward the form of approximately 1.0–1.6 nm, *fcc* Ir(0)<sub>~40–150</sub>, Ziegler nanoclusters.

**Table 1.** Observed Ir<sub>n</sub> Cluster Diameters in the [(1,5-COD)IrO<sub>2</sub>C<sub>8</sub>H<sub>15</sub>]<sub>2</sub> Catalyst Both Pre- and Post-Catalytic Runs by Three Different Analytical Methods.

analytical method	precatalysis			postcatalysis		
	range (nm)	mean (nm)	mean Ir <sub>n</sub> nuclearity	range (nm)	mean (nm)	mean Ir <sub>n</sub> nuclearity
Z-Contrast STEM	0.2–1.4	0.5 ± 0.2	Ir <sub>~4</sub>	0.4–1.9	1.0 ± 0.3	Ir <sub>~40</sub>
XAFS	NA <sup>a</sup>	0.5	Ir <sub>~4</sub>	NA <sup>a</sup>	1.6	Ir <sub>~150</sub>
MALDI MS	0.5–1.1	0.7 ± 0.2 <sup>b</sup>	Ir <sub>~15</sub> <sup>b</sup>	0.6–1.4	0.8 ± 0.2 <sup>b</sup>	Ir <sub>~20</sub> <sup>b</sup>

<sup>a</sup> Determination of the range of Ir<sub>n</sub> clusters present is not possible by this method. <sup>b</sup> An underestimate due to the irregular shape of the peak, which includes a high *m/z* tail (vide infra). See the discussion which follows for issues with the less reliable MALDI-MS in comparison to the Z-Contrast STEM and XAFS.

### Nuclearity of the $\text{Ir}_n$ Species in Aged $\text{AlEt}_3/\text{Ir}$ Catalyst *before*

**Hydrogenation: Z-contrast Microscopy.** A selected Z-contrast STEM image of a  $[(1,5\text{-COD})\text{Ir}(\mu\text{-O}_2\text{C}_8\text{H}_{15})]_2$  plus  $\text{AlEt}_3$ ,  $\text{Al}/\text{Ir} = 2.0$ , catalyst sample, aged  $\geq 2$  days and analyzed *before* hydrogenation, shows clusters with a range of diameters, Figure 2. The size distribution histogram, also Figure 2, was constructed by measuring the full width at half-maximum (FWHM) of the intensity profile across 600 particles from images at the same levels of magnification and contrast. Most of the clusters counted in such images are subnanometer in scale. The mean cluster size is  $0.5 \pm 0.2$  nm (a cluster 0.5 nm in diameter corresponds approximately to a theoretical tetrahedral  $\text{Ir}_4$  cluster). The smallest Ir species observed appear to be mono-Ir complexes (diameter of Ir in a monometallic compound  $< 0.3$  nm),<sup>15</sup> and the histogram tails off toward larger Ir clusters present in much lower abundance, the largest observed being 1.4 nm in diameter ( $\text{Ir}_{\sim 100}$ ).<sup>16,17,18</sup>

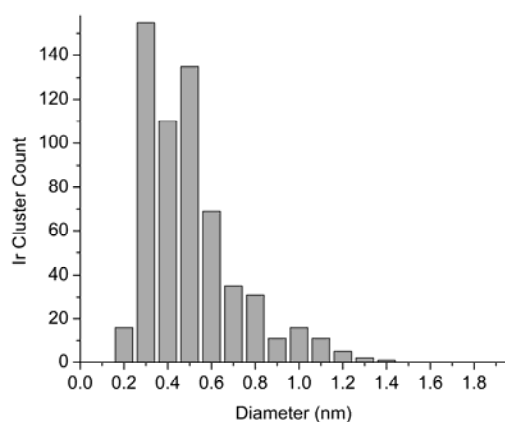
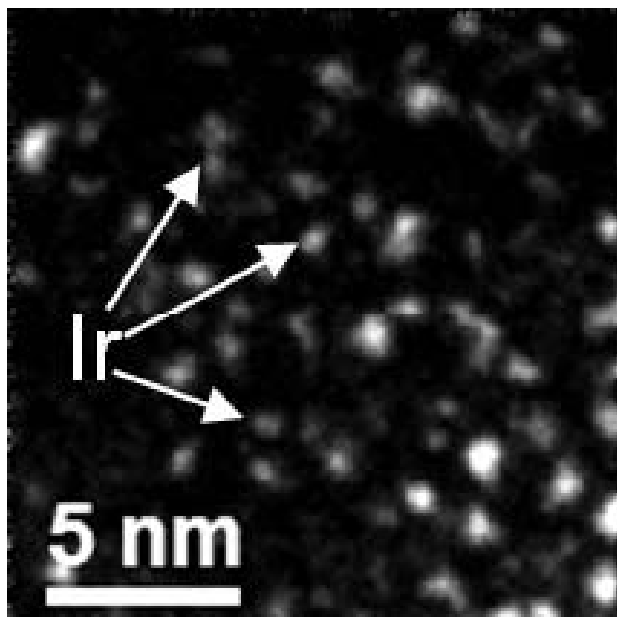


**Figure 2.** Representative Z-contrast STEM image of a  $[(1,5\text{-COD})\text{Ir}(\mu\text{-O}_2\text{C}_8\text{H}_{15})]_2$  plus  $\text{AlEt}_3$  catalyst sample with an Al/Ir ratio of 2.0. Ir appears as white spots on a dark background. A diameter measurement of 600 clusters gives an overall distribution ranging from monometallic Ir complexes to 1.4 nm,  $\text{Ir}_{\sim 100}$ , clusters and a mean cluster diameter of 0.5 nm ( $\text{Ir}_{\sim 4}$ )  $\pm$  0.2 nm.

An Ir model Ziegler-type hydrogenation catalyst was chosen for the present studies in part because prior TEM experiments and controls have shown that the (third-row metal) Ir nanoclusters and precursor compounds generally have greater stability than lighter transition metal nanoclusters or precursors in TEM electron beams.<sup>19,20,21</sup> Moreover, it has been observed previously that at least first-row metal, Ni Ziegler-type

hydrogenation catalysts are highly sensitive to sample preparation required by electron microscopy, specifically, the drying of catalyst samples on grids.<sup>1</sup> Z-contrast STEM cannot overcome the issue of sample drying but does offer the benefit of *scanning* TEM, so that potential sample damage can be minimized by using a small electron probe, low beam current, and minimum time of sample exposure to the electron beam.<sup>22</sup> In this case, the sizes and shapes of Ir spots in the images were continually monitored during image acquisition; no evidence of artifacts or modification of the sample as a result of the microscopy itself was observed, as expected for the third-row Ir system chosen in part for such superior TEM properties.<sup>7a,16</sup> In addition, *the greater resolving power of the Z-contrast method over conventional bright field TEM has permitted detection of the subnanometer clusters,*<sup>22,23,24,25</sup> which are important results. To summarize, Z-contrast microscopy indicates that aged catalyst samples before hydrogenation consist of a broad distribution of Ir<sub>n</sub> species ranging from mono-Ir complexes to 1.4 nm, Ir<sub>~100</sub> Ziegler nanoclusters. Significantly, subnanometer Ir<sub>n</sub> clusters are the most abundant species present, and the mean Ir cluster diameter of 0.5 ± 0.2 nm corresponds to Ir<sub>~4</sub> cluster compounds.

**Identification of the Ir-Containing Species in Aged AlEt<sub>3</sub>/Ir Catalyst before Hydrogenation: XAFS Spectroscopy.** XAFS data were first acquired for four reference samples: (i) an Ir black standard, (ii) HPO<sub>4</sub>-stabilized *fcc* Ir(0)<sub>n</sub> nanoclusters,<sup>26</sup> (iii) Ir<sub>4</sub>(CO)<sub>12</sub>, and (iv) the precatalyst [(1,5-COD)Ir(μ-O<sub>2</sub>C<sub>8</sub>H<sub>15</sub>)<sub>2</sub>]. XAFS data were then acquired for seven different samples of the initial, [(1,5-COD)Ir(μ-O<sub>2</sub>C<sub>8</sub>H<sub>15</sub>)<sub>2</sub> plus AlEt<sub>3</sub> catalyst solutions aged ≥ 2 days, and before their use in hydrogenation: catalysts prepared with Al/Ir ratios of 0.5, 1.0, 1.5, 2.0, 2.5, 3.0, and 5.0. Six main results from

the XAFS spectroscopy of aged catalyst samples *before hydrogenation* are that (i) all samples lack longer-range coordination shells (in r-space) that are characteristic of ordered nanoclusters. (ii) Spectra from the Al/Ir  $\leq 1.0$  samples are satisfactorily fit using a composite model created from an Ir–first-nearest-neighbor (hereafter 1NN) path from [(1,5-COD)Ir( $\mu$ -O<sub>2</sub>C<sub>8</sub>H<sub>15</sub>)<sub>2</sub>]<sub>2</sub> and the Ir–Ir first-nearest-neighbor (1NN) single scattering path (hereafter SS1) from bulk Ir, but (iii) *modeling the Al/Ir  $\geq 1.5$  samples requires incorporating the contribution of the Ir–Al path*, an important finding. In addition, (iv) small Ir–Ir 1NN coordination numbers ( $N$ ; roughly in the range of 2–3, vide infra) correspond to subnanometer Ir cluster sizes. (v) Ir–Ir 1NN distances longer than expected for bulk Ir or ordered Ir nanoclusters indicate valence-electron sharing with ligands, consistent with small, ligated molecular Ir clusters, and (vi) XANES spectra of the Ir catalyst samples differ from bulk Ir but are similar to the precursor [(1,5-COD)Ir( $\mu$ -O<sub>2</sub>C<sub>8</sub>H<sub>15</sub>)<sub>2</sub>]<sub>2</sub> and Ir<sub>4</sub>(CO)<sub>12</sub>, suggesting formally Ir(I) <sub>$n$</sub>  or Ir(0) <sub>$n$</sub>  molecular clusters of few Ir atoms ligated by relatively strongly electron-withdrawing groups. The only sources of ligands in the system other than the weakly coordinating cyclohexane solvent are AlEt<sub>3</sub>, C<sub>7</sub>H<sub>15</sub>CO<sub>2</sub><sup>−</sup>, and possibly Ir–H (given that the 1,5-COD is hydrogenated to cyclooctane in the reaction), so that the list of possible, dominant species present that could be ligands is actually rather short, primarily, AlEt<sub>3</sub>, C<sub>7</sub>H<sub>15</sub>CO<sub>2</sub>AlEt<sub>3</sub><sup>−</sup>, and possibly Ir–H–AlEt<sub>3</sub> (among a few others such as any Al–O–Al containing alumoxanes formed by trace water present, water that our experimental efforts and conditions have strived to minimize; see the Experimental Section). In short, the XAFS studies reveal that *initial catalyst* solutions lack ordered Ir(0) <sub>$n$</sub>  nanoclusters

and contain, on average, molecular Ir<sub>4</sub>, 0.5 nm clusters ligated by electron-withdrawing groups that are likely derived from the short list of ligands listed above.

Fourier transform (FT) magnitudes of the background-subtracted XAFS signals for the Al/Ir-dependent sample series are shown in Figure 3. FT magnitude data of selected reference samples and a catalyst sample with an Al/Ir ratio of 2.0 are shown together in Figure 4. For single scattering paths (SS1, SS2, etc.), the positions of isolated peaks in FT plots correspond to the distance between the absorber and its neighbors, albeit shorter than the actual distances due to the photoelectron phase shifts.<sup>27,28,29</sup> The first important observation is that in the FT magnitude sample spectra, Figure 3, there is a lack of distinct peaks in the 3–6 Å range expected for SS2–5 paths, whereas such peaks are visible in the FT magnitude plots of Ir black, Figure 4 and Figure S10, Supporting Information. The lack of these peaks indicates that before hydrogenation there is not an appreciable amount of Ir nanoclusters with ordered, periodic, atomic structures in the catalyst. Restated, the *aged catalyst samples before hydrogenation lack the XAFS longer r-range contribution expected if ordered nanoclusters were present*. Hence, the relatively few nanometer-sized clusters that are present before hydrogenation according to Z-contrast STEM (as well as bright field TEM; see the Supporting Information) appear to have significantly *disordered atomic structures* (this finding and its significance are discussed in further detail below).<sup>30,31,32,33,34,35,36,37</sup>

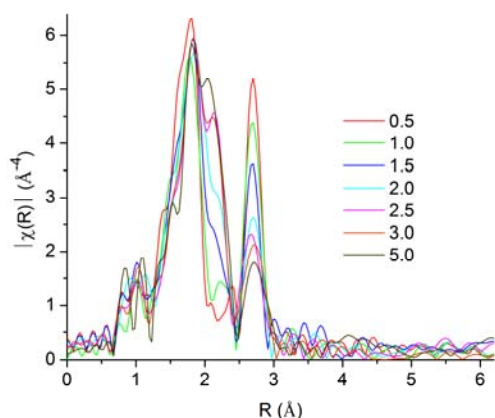


**Figure 3.** A  $k^3$ -weighted FT magnitude plot of a series of catalyst samples made from the combination of  $[(1,5\text{-COD})\text{Ir}(\mu\text{-O}_2\text{C}_8\text{H}_{15})_2]$  and  $\text{AlEt}_3$  ( $\text{Al}/\text{Ir} = 0.5, 1.0, 1.5, 2.0, 2.5, 3.0, 5.0$ ) before their use in hydrogenation. The lack of peaks in the 3–6 Å region indicates the absence of crystalline Ir particles. The large peak on the left at  $\sim 1.8$  Å represents Ir–C and/or Ir–O backscattering contributions (hereafter, “Ir–X”, since XAFS cannot distinguish between C and O backscatterers in catalyst samples, *vide infra*). The shoulder at  $\sim 2.2$  Å on the right of the larger, Ir–X peak that grows in with increasing Al/Ir ratio is well-modeled by single scattering due to Al atoms. The narrow peak at  $\sim 2.7$  Å represents single scattering from the first Ir–Ir nearest neighbor shell.  $R$  values are uncorrected for photoelectron phase shifts.

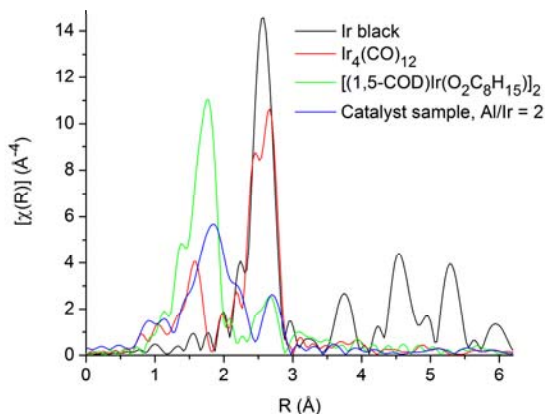


**Figure 4.** A plot of FT magnitude of the  $k^3$ -weighted XAFS data for Ir black (scaled by  $\frac{1}{4}$  for ease of comparison),  $\text{Ir}_4(\text{CO})_{12}$  (scaled by  $\frac{1}{2}$  for ease of comparison),  $[(1,5\text{-COD})\text{Ir}(\mu\text{-O}_2\text{C}_8\text{H}_{15})_2]$ , and a catalyst sample, with an Al/Ir of 2.0, for comparison. The peaks in the 3–6 Å range, seen here only in the spectrum of Ir black, are diagnostic of an ordered Ir phase.

*Fitting Results for Catalyst Samples before Hydrogenation.* XAFS spectra of Ir black, HPO<sub>4</sub>-stabilized *fcc* Ir(0) nanoclusters, Ir<sub>4</sub>(CO)<sub>12</sub>, and [(1,5-COD)Ir(μ-O<sub>2</sub>C<sub>8</sub>H<sub>15</sub>)<sub>2</sub>]<sub>2</sub> were fit using theoretical models based on the crystal structures of bulk *fcc* Ir, Ir<sub>4</sub>(CO)<sub>12</sub>,<sup>38</sup> and [(1,5-COD)Ir(μ-O<sub>2</sub>C<sub>8</sub>H<sub>15</sub>)<sub>2</sub>]<sub>2</sub>, respectively.<sup>2</sup> Fits of these standards and reference compounds are shown in Figures S10–S14, Supporting Information, and the fitting results are summarized in Tables S2–S5, Supporting Information, for the interested reader. The peaks in the spectra of Ir<sub>4</sub>(CO)<sub>12</sub>, and [(1,5-COD)Ir(μ-O<sub>2</sub>C<sub>8</sub>H<sub>15</sub>)<sub>2</sub>]<sub>2</sub> at about 1.6 Å and 1.8 Å, Figure 4, correspond to Ir–C and Ir–X first nearest neighbors (again abbreviated 1NN), respectively (X represents both C and O atoms, which were nondistinguishable by XAFS in [(1,5-COD)Ir(μ-O<sub>2</sub>C<sub>8</sub>H<sub>15</sub>)<sub>2</sub>]<sub>2</sub>, Figure S13, Supporting Information, and in the catalyst samples). The peaks in the spectra of Ir black, HPO<sub>4</sub>-stabilized Ir nanoclusters and Ir<sub>4</sub>(CO)<sub>12</sub> at about 2.5 Å correspond to Ir–Ir 1NN positions. Comparing the spectra in Figures 3 and 4, the peaks in the catalyst samples near 1.8 Å and 2.7 Å correspond, roughly, to scattering contributions from Ir–X and Ir–Ir, respectively. Therefore, scattering paths for Ir–X and Ir–Ir were used to model the catalyst sample data.

Fits of the catalyst sample data using a model created from the Ir–X path in [(1,5-COD)Ir(μ-O<sub>2</sub>C<sub>8</sub>H<sub>15</sub>)<sub>2</sub>]<sub>2</sub> and the Ir–Ir SS1 path in Ir black gave physically reasonable results only for the Al/Ir = 0.5 and 1.0 samples. For the Al/Ir ≥ 1.5 samples, the model was adapted by taking into account backscattering by Al atoms in close proximity to the absorbing Ir. This modified model better accounted for the shoulder on the right side of the leftmost (Ir–X) peak that grows in with the 1.5 and higher Al/Ir ratio samples, Figure 3. However, attempts to use the model incorporating Al to fit the Al/Ir = 0.5 and 1.0

sample data gave unreasonable results. Fits to the Al/Ir = 1.0 and 2.0 sample data using the model that neglects Al and the model that incorporates Al, respectively, are shown in Figure 5. The fitting results for all samples are summarized in Table 2. Additional spectra of the data and theoretical fits are shown in Figures S15–S21, Supporting Information.

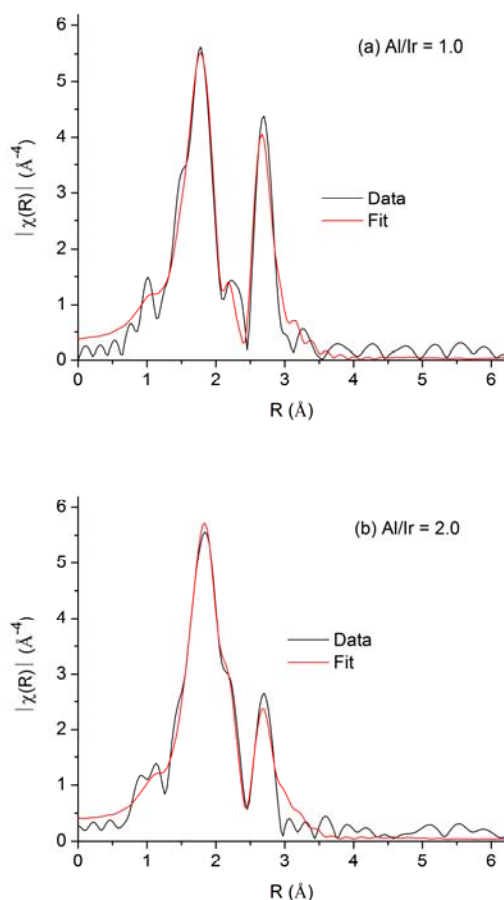


**Figure 5.** FT magnitude spectra and fits for the Al/Ir = 1.0 (a) and 2.0 (b) catalysts. The model used to fit the Al/Ir = 1.0 sample was created from the Ir–X path in [(1,5-COD)Ir( $\mu$ -O<sub>2</sub>C<sub>8</sub>H<sub>15</sub>)<sub>2</sub>]<sub>2</sub> and the Ir–Ir SS1 path in Ir black. The Al/Ir = 2.0 sample was fit by the same model but modified to account for backscattering by Al atoms in close proximity to the absorbing Ir.

**Table 2.** Fitting Results for the [(1,5-COD)Ir( $\mu$ -O<sub>2</sub>C<sub>8</sub>H<sub>15</sub>)<sub>2</sub>] Plus AlEt<sub>3</sub> Catalyst Samples before Their Use in Hydrogenation.

sample Al/Ir	Ir black	0.5	1.0	1.5	2.0	2.5	3.0	5.0
$N_{\text{Ir-Ir}}$	12 <sup>c</sup>	1.8 ± 0.4	2.8 ± 0.6	2.1 ± 0.6	3 ± 1	3 ± 1	3 ± 1	3 ± 3
$N_{\text{Ir-X}}$		6.0 ± 0.6	5.8 ± 0.6	5.4 ± 0.8	5.0 ± 0.7	4.7 ± 0.8	4.8 ± 0.8	5 ± 1
$N_{\text{Ir-Al}}$				1.0 ± 0.9	1.7 ± 0.8	2 ± 1	3 ± 1	3 ± 2
$R_{\text{Ir-Ir}} (\text{Å})^a$	2.711 ± 0.001	2.799 ± 0.005	2.797 ± 0.005	2.803 ± 0.007	2.826 ± 0.007	2.84 ± 0.01	2.849 ± 0.008	2.86 ± 0.02
$R_{\text{Ir-X}} (\text{Å})^a$		2.149 ± 0.007	2.162 ± 0.008	2.18 ± 0.01	2.19 ± 0.01	2.19 ± 0.02	2.19 ± 0.01	2.20 ± 0.03
$R_{\text{Ir-Al}} (\text{Å})^a$				2.49 ± 0.02	2.51 ± 0.01	2.51 ± 0.01	2.51 ± 0.01	2.5045 <sup>c</sup>
$\sigma^2_{\text{Ir-Ir}} (\text{Å}^2)^b$	3.5 ± 0.1	5.2 ± 0.7	7.0 ± 0.7	7 ± 1	10 ± 1	10 ± 2	10 ± 2	11 ± 4
$\sigma^2_{\text{Ir-X}} (\text{Å}^2)^b$		6.4 ± 0.9	8 ± 1	7 ± 1	7 ± 1	8 ± 2	8 ± 1	9 ± 3
$\sigma^2_{\text{Ir-Al}} (\text{Å}^2)^b$				7 ± 5	8 ± 3	8 ± 2	8 ± 3	8 ± 4

<sup>a</sup>  $R$  is the experimentally determined interatomic distance for the Ir–X, Ir–Al, and Ir–Ir single scattering paths. <sup>b</sup>  $\sigma^2$ , the Debye-Waller factor, is the mean square variation in  $R$  due to static and dynamic disorder. The values shown are  $\times 10^3$ . <sup>c</sup> For this sample only, this parameter was defined to be the value shown and not varied in the fit.

From the fit of the Al/Ir = 2.0 sample data, the 1NN Ir–Ir  $N$  of  $3 \pm 1$  indicates an Ir<sub>4</sub> cluster, which, in turn, corresponds to an Ir cluster roughly 0.5 nm in diameter.

Results for catalyst samples at all AlEt<sub>3</sub>/Ir ratios tested *are similar*, giving subnanometer, Ir<sub>4</sub>, clusters. Significantly, *XAFS and Z-contrast microscopy fortify one another in finding the same mean cluster size* within experimental error. Recall that Z-contrast STEM also reveals a broad dispersity of Ir cluster sizes in catalyst samples before hydrogenation. XAFS, on the other hand, gives ensemble-average results for local structure; it does *not* provide information regarding *distribution* of Ir cluster sizes.<sup>35</sup> In light of the larger clusters observed by electron microscopy (the tail in the histogram of Figure 2 showing some Ir <sub>$n$</sub>  clusters with nanometer scale diameters), possible explanations for the XAFS results are that the nanoscale Ir clusters could (i) have considerably disordered structures,<sup>31</sup> (ii) actually be groups of tightly associated Ir<sub>4</sub> clusters that also exist in solution,<sup>36,37</sup> or (iii) simply be artifacts brought about by

the ex situ technique itself, with the ex situ observed clusters not existing in the solutions used in cyclohexene hydrogenation and examined by XAFS spectroscopy. However, the similar Ir cluster sizes and distributions obtained by *both* Z-contrast STEM and MALDI MS (vide infra), and the XAFS-determined Ir–Ir bond lengths and bond length disorders larger than those observed in bulk Ir (see Table 2, and the text below), make the *presence* of highly disordered nanoscale Ir clusters—along with a majority of subnanometer, Ir<sub>~4</sub> clusters—a preferred explanation. The key finding by XAFS, then, is that *initial, precatalytic hydrogenation solutions are composed, on average, of Ir<sub>~4</sub>, 0.5 nm clusters.*

Significantly, the *R* values for Ir–Ir 1NNs in all samples are *larger* than the theoretical values from bulk Ir, Table 2. If transition metal nanoclusters were the dominant species present, then the M–M distances should have been *smaller* (and as we will see posthydrogenation, vide infra), distances contracted in order to minimize the surface free energy (the surface free energy of small metal clusters is elevated due to the unsatisfied bonding requirements and too-low coordination number of the surface metals).<sup>31,39</sup> However, the observed, longer Ir–Ir distances are fully consistent with subnanometer, Ir<sub>~4</sub> cluster compounds<sup>36,40,41,42</sup> coordinated to any available ligands such as those listed earlier, namely, AlEt<sub>3</sub>, C<sub>7</sub>H<sub>15</sub>CO<sub>2</sub>AlEt<sub>3</sub><sup>−</sup>, and possibly Ir–H–AlEt<sub>3</sub>. The possibility of Ir–Al bonding (or possibly Ir–X–Al, X = H or Et, bonding) is consistent with the XAFS data; fits of samples with Al/Ir ratios from 1.5–3.0 reveal Al at a distance from Ir of 2.5 Å, which is within the range found for γ-Al<sub>2</sub>O<sub>3</sub>-supported Ir<sub>4</sub> and Ir<sub>6</sub> clusters.<sup>43</sup> Additionally, the Ir to Al atom-pair distance of ca. 2.5 Å obtained by XAFS is close to crystallographically determined distances 2.456(1) Å and 2.459(1) Å in

(Cp\*(PMe<sub>3</sub>)IrAlEt)<sub>2</sub>, which possesses an Ir–Al–Ir bridging motif but is shorter than the Ir–H–Al bond distance of 2.684(2) in Cp\*(PMe<sub>3</sub>)Ir(H)<sub>2</sub>AlPh<sub>3</sub>.<sup>44</sup> These results are of considerable significance in addressing likely ligands derived from the AlEt<sub>3</sub> and C<sub>7</sub>H<sub>15</sub>CO<sub>2</sub><sup>−</sup> components of the catalyst, and under the reaction conditions.<sup>13</sup>

The three main results from fitting the XAFS spectra, then, are (i) samples with Al/Ir ratios  $\geq 1.5$  are best fit using a model incorporating backscattering from Al; (ii) low Ir–Ir first-nearest neighbor coordination numbers imply, on average, Ir<sub>~4</sub>, 0.5 nm clusters; (iii) Ir–Ir distances longer than expected for bulk Ir were found, consistent with Ir ligated by the ligands present in species such as Ir–X–Al or possible direct Ir–Al interaction. Significantly, the Z-contrast STEM and XAFS results *are consistent, giving Ir<sub>~4</sub>, 0.5 nm clusters as the mean Ir<sub>n</sub> clusters*. The identical mean cluster size results from Z-contrast STEM and XAFS argue strongly against artifacts introduced by either method, including the ex situ STEM, which in turn suggests that the *Ir<sub>~4</sub>, 0.5 nm clusters are, as the Z-contrast STEM reveals, a major part of a broad distribution of Ir<sub>n</sub> clusters*.

The X-ray absorption near-edge structure (XANES) was used to probe the oxidation state of the initial catalyst solutions. The XANES regions of Ir black, Ir<sub>4</sub>(CO)<sub>12</sub>, and [(1,5-COD)Ir(μ-O<sub>2</sub>C<sub>8</sub>H<sub>15</sub>)]<sub>2</sub> are shown in Figure 6 alongside those for the Al/Ir = 1.0 and 2.0 catalyst samples before hydrogenation. The XANES spectra of the catalyst samples are similar to the [(1,5-COD)Ir(I)(μ-O<sub>2</sub>C<sub>8</sub>H<sub>15</sub>)]<sub>2</sub> precursor and Ir(0)<sub>4</sub>(CO)<sub>12</sub> standard (formally Ir(I) and Ir(0), respectively) but unlike the Ir(0) black standard. This is the case regardless of the Al/Ir ratio of the sample and suggests that the

Ir species present are formally Ir(I) or Ir(0) ligated by the previously listed ligand possibilities.

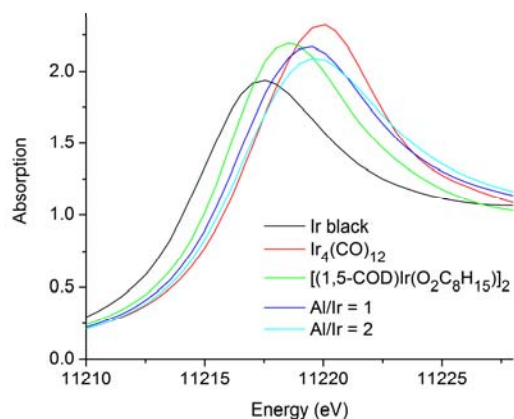


**Figure 6.** XANES portions of the normalized  $\mu(E)$  spectra for Ir black (black line),  $\text{Ir}_4(\text{CO})_{12}$  (red), the  $[(1,5\text{-COD})\text{Ir}(\mu\text{-O}_2\text{C}_8\text{H}_{15})_2]$  precatalyst (green), and the  $\text{AlEt}_3/\text{Ir} = 1.0$  and  $2.0$  samples before hydrogenation (blue and light blue). The catalyst samples before hydrogenation are comparable to the formally Ir(I) and Ir(0)  $[(1,5\text{-COD})\text{Ir}(\mu\text{-O}_2\text{C}_8\text{H}_{15})_2]$  precatalyst and  $\text{Ir}_4(\text{CO})_{12}$  standard, respectively.

A sample of the  $[(1,5\text{-COD})\text{Ir}(\mu\text{-O}_2\text{C}_8\text{H}_{15})_2]$  plus  $\text{AlEt}_3$  catalyst, Al/Ir of 2.0, was analyzed by XPS to distinguish whether the Ir species in the catalyst before hydrogenation are Ir(I) or Ir(0); experimental XPS spectra and literature reference data are given in the Supporting Information. The Ir 4f peak positions at 64.30 and 61.33 eV in the experimental XPS spectrum can be attributed to Ir(I)<sup>45</sup> but are also consistent with (i.e., indistinguishable from) Ir(0)<sub>n</sub> Ziegler nanoclusters exhibiting a final-state relaxation effect.<sup>46,47,48,49,50,51,52,53</sup> Therefore, both XANES and XPS results of catalyst samples before their use in hydrogenation are consistent with Ir(I) species as well as Ir(0)<sub>n</sub> Ziegler nanoclusters (or both), but cannot unambiguously distinguish these.

To summarize the observations from XAFS spectroscopy on the aged catalyst samples, but before hydrogenation, (i) longer range scattering peaks, expected for ordered nanoclusters, are not seen; (ii) successful fitting of the Al/Ir  $\geq 1.5$  catalyst sample spectra requires a model that includes the backscattering from Al atoms in close proximity to Ir atoms; (iii) small Ir–Ir  $N$  values are obtained that correspond to subnanometer cluster sizes; (iv) Ir–Ir bonds longer than expected for bulk or Ir(0)<sub>*n*</sub> nanoclusters, but consistent with ligated Ir<sub>~4</sub> subnanometer clusters, are seen; (v) XANES spectra are different than those of bulk Ir but are comparable to the [(1,5-COD)Ir( $\mu$ -O<sub>2</sub>C<sub>8</sub>H<sub>15</sub>)]<sub>2</sub> precursor and Ir<sub>4</sub>(CO)<sub>12</sub>. These observations suggest that the initial catalyst samples, regardless of the Al/Ir ratio, are composed on average of Ir(I) or Ir(0) subnanometer, molecular Ir<sub>~4</sub> clusters shielded from agglomeration by coordinated ligands.<sup>54,55,56,57,58,59</sup> The observations made here by XAFS on catalyst *solutions* are also fully consistent with and supported by the results from (the ex situ, solid state) Z-contrast STEM, which indicates that catalyst samples before hydrogenation are composed of a broad range of cluster sizes from mono-Ir molecules to nanometer scale noncrystalline Ir<sub>*n*</sub> clusters, the most abundant being subnanometer Ir clusters, and the mean clusters being Ir<sub>~4</sub>, 0.5 nm. The use of these complementary methods and their agreement is important; the results argue strongly against significant sample preparation and method-specific (and ex situ versus in situ) artifacts. The results confirm our design criteria of using the more-stable, third-row Ir precatalyst (i.e., with its stronger Ir–Ir bonds and resultant greater cluster and nanocluster stability) as a needed, but previously little investigated, Ziegler-type hydrogenation catalyst model system.

### Nuclearity of the $\text{Ir}_n$ Species in $\text{AlEt}_3/\text{Ir}$ Catalyst *before* Hydrogenation:

**MALDI MS.** Despite the agreement between the Z-contrast STEM and XAFS results, an additional method was used in order to further probe the  $\text{Ir}_n$  cluster size and distribution—as well as to “calibrate” that matrix assisted laser desorption ionization mass spectrometry (MALDI MS) method in this instance; is this *ex situ* method reliable? Initial catalyst samples, before their use in hydrogenation but without aging, were analyzed. The experimental methods are discussed in greater detail in the Supporting Information for the interested reader, and spectra are shown there as well. Briefly, the *ex situ* MALDI MS on dried, solid samples reveals a broad Ir-containing peak centered at about 2800  $m/z$ . The FWHM ranges from 1000–5000  $m/z$ , and the peak tails off towards the higher  $m/z$  values. With the necessary *assumptions* that the broad peak observed in the full mass spectrum is composed of only Ir atoms<sup>60,61,62</sup> and that the ionic charges are +1,<sup>60,62,63</sup> the peak maximum corresponds to  $\text{Ir}_{\sim 15}$ , 0.7-nm-diameter clusters.<sup>18</sup> Likewise, the FWHM of the peak corresponds to  $\text{Ir}_{\sim 5-26}$ , 0.5–0.9-nm-diameter clusters (used to estimate the mean  $\text{Ir}_n$  cluster size at  $0.7 \pm 0.2$  nm), and the high  $m/z$  tail gives indication of larger clusters present in relatively few numbers. The high  $m/z$  tail at one-fourth maximum intensity of the broad peak is positioned at 6000  $m/z$ , which corresponds to  $\text{Ir}_{\sim 30}$ , 0.9–1.0 nm clusters. The high  $m/z$  region of the spectrum continues to tail off indicating the presence of Ir nanoclusters, but in a much lower abundance—for example,  $\text{Ir}_{\sim 50}$ , 1.1 nm-diameter-clusters at one-eighth the maximum peak intensity (and used as the maximum range limit reported in Table 1).

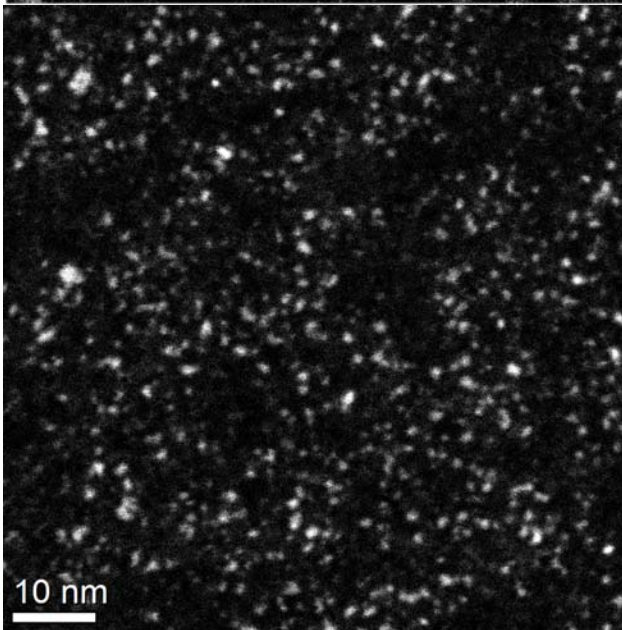
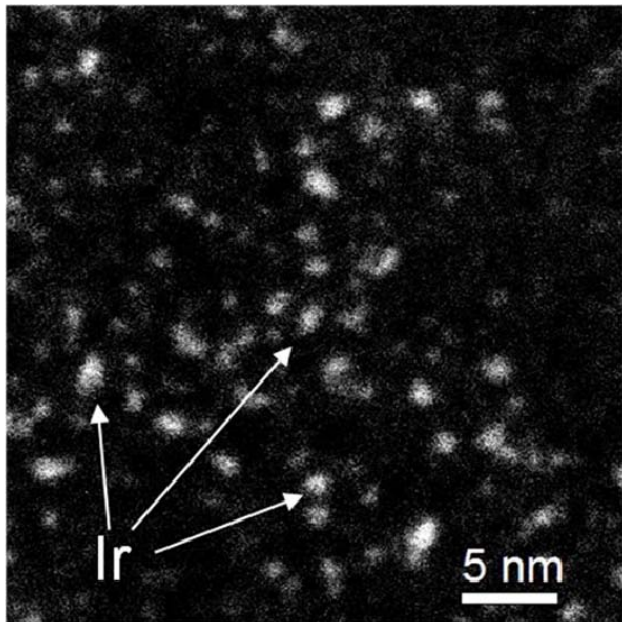
The quite different MALDI MS method proved useful in that it provides independent evidence for *similar* (albeit not identical) sizes and size distributions of  $\text{Ir}_n$

clusters. The difference between the *estimated* mean Ir<sub>~15</sub>, 0.7 nm clusters from MALDI MS and the mean Ir<sub>~4</sub>, 0.5 nm clusters indicated by both Z-contrast STEM and XAFS may be the result of (i) factors due to the differences of the methods, (ii) imperfection in the assumptions necessary for this interpretation of MALDI MS, (iii) the fact that the sample analyzed by MALDI MS was not aged whereas the Z-contrast STEM and XAFS samples were aged, or (iv) some combination thereof. Regardless, the significance here is that MALDI MS confirms, in general, the results of Z-contrast STEM by giving independent evidence that the [(1,5-COD)Ir( $\mu$ -O<sub>2</sub>C<sub>8</sub>H<sub>15</sub>)<sub>2</sub>] plus AlEt<sub>3</sub> catalyst sample, with an Al/Ir ratio of 2.0, *before* hydrogenation, is composed of a broad distribution of Ir<sub>n</sub> clusters, which are primarily subnanometer Ir<sub>n</sub> clusters, but include, to a lesser extent, Ir<sub>n</sub> nanoclusters. The generally similar results argue against *significant* artifacts caused by these three very different physical methods. The main point is that in catalyst samples before hydrogenation there is a distribution in Ir<sub>n</sub> species centered on subnanometer Ir<sub>n</sub> clusters, and that the *estimated* mean cluster sizes are 0.5–0.7 nm, Ir<sub>~4</sub>–

15.

#### **Identification of the Ir-Containing Species in the AlEt<sub>3</sub>/Ir Catalyst *after***

**Hydrogenation: Z-Contrast and HRTEM Microscopy.** The size and size distribution of Ir clusters, in a [(1,5-COD)Ir( $\mu$ -O<sub>2</sub>C<sub>8</sub>H<sub>15</sub>)<sub>2</sub>] plus AlEt<sub>3</sub> catalyst sample with an Al/Ir ratio of 2.0 and *after* its use for cyclohexene hydrogenation, were analyzed using Z-contrast microscopy. Sample Z-contrast images and a histogram are shown in Figure 7. Measurement of 635 Ir clusters resulted in a mean diameter of  $1.0 \pm 0.3$  nm, with observed Ir<sub>n</sub> cluster diameters spanning from 0.4 to 1.9 nm (two additional Ir nanoclusters, with larger diameters of 3.1 and 3.8 nm, were also observed).



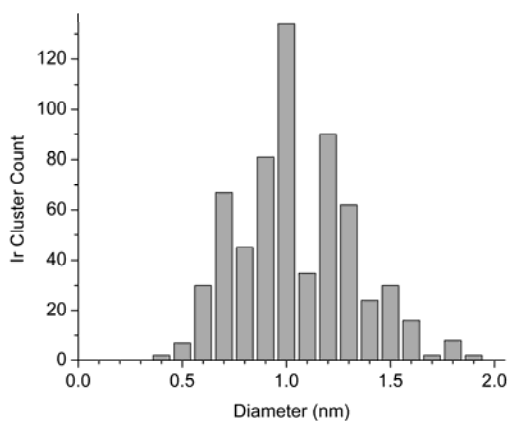


**Figure 7.** Example Z-contrast images of the [(1,5-COD)Ir( $\mu$ -O<sub>2</sub>C<sub>8</sub>H<sub>15</sub>)]<sub>2</sub> plus AlEt<sub>3</sub>, Al/Ir = 2.0, catalyst sample *after hydrogenation*. The Ir cluster histogram from the diameter measurement of 635 Ir clusters is also shown. The mean Ir cluster diameter is  $1.0 \pm 0.3$  nm, which corresponds to Ir(0)<sub>~40</sub> clusters. Two larger Ir nanoclusters with diameters of 3.1 and 3.8 nm are also observed, presumably the result of well-precedented nanocluster aggregation processes.<sup>64,65</sup>

Also obtained were HRTEM images of [(1,5-COD)Ir( $\mu$ -O<sub>2</sub>C<sub>8</sub>H<sub>15</sub>)]<sub>2</sub> plus AlEt<sub>3</sub> catalyst samples after hydrogenation, with Al/Ir ratios of 1.0, 2.0, and 5.0.<sup>66</sup> An example HRTEM image of the sample with an Al/Ir ratio of 2.0, Figure 8, shows distinct lattice fringes in the Ir particles. This result is general to all Al/Ir ratios tested; crystalline Ir Ziegler nanoclusters are observed in all HRTEM images obtained for the samples with Al/Ir ratios of 1.0, 2.0, and 5.0 (other images are shown in Figures S27–S30, Supporting Information). Electron diffraction shows that these Ziegler nanoclusters after hydrogenation are *fcc* Ir, at least under the conditions of the electron beam (Figure S31, Supporting Information). The key result, then, of the combined Z-contrast and HRTEM microscopy is that the mean Ir<sub>n</sub> clusters postcatalysis are larger, crystalline  $1.0 \pm 0.3$  nm, Ir<sub>~40</sub> nanoclusters.

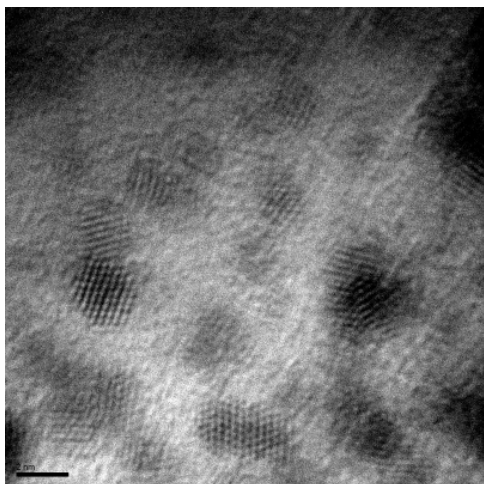


**Figure 8.** An example HRTEM image of the [(1,5-COD)Ir( $\mu$ -O<sub>2</sub>C<sub>8</sub>H<sub>15</sub>)<sub>2</sub>] plus AlEt<sub>3</sub> catalyst, Al/Ir is 2.0, after its use in cyclohexene hydrogenation (scale bar is 2 nm). The distinct lattice fringes show that the Ir particles after use in hydrogenation possess a crystalline structure under the HRTEM observation conditions. Crystalline particles are observed for all Al/Ir values tested, 1.0, 2.0, and 5.0.

#### **Identification of the Ir-Containing Species in the AlEt<sub>3</sub>/Ir Catalyst *after***

**Hydrogenation: XAFS Spectroscopy.** A sample of the [(1,5-COD)Ir( $\mu$ -O<sub>2</sub>C<sub>8</sub>H<sub>15</sub>)<sub>2</sub>] plus AlEt<sub>3</sub> catalyst, with an Al/Ir ratio of 1.0, after its use in cyclohexene hydrogenation was analyzed by XAFS spectroscopy. Peaks in the 3–6 Å range of the FT magnitude spectrum reveal that the sample is composed of Ir<sub>n</sub> particles with ordered internal atomic structures, Figure 9, consistent with the microscopy results (*vide supra*). A fit of the Fourier transform magnitude spectrum, also shown in Figure 9, gives an Ir–Ir 1NN coordination of  $9.0 \pm 0.4$ . The mean coordination number, obtained from fitting the Ir–Ir 1NN contribution, was used to estimate cluster sizes using a theoretical mean coordination number–particle diameter correlation curve<sup>16,27,67</sup> (Supporting Information). An Ir–Ir 1NN coordination of  $9.0 \pm 0.4$  according to XAFS corresponds to, on average, 1.6 nm, crystalline *fcc* Ir(0)<sub>~150</sub> clusters. Additionally, the Ir–Ir 1NN distance of  $2.688 \pm 0.001$  Å is now *shorter* than that in bulk Ir, as one would expect for

nanometer-sized, contracted surface<sup>31,39</sup> clusters. Full fitting results are given in Table S8, Supporting Information.

The XANES portion of the sample spectrum is essentially identical to the XANES spectra of Ir black, Figure 10. This shows convincingly that the oxidation state of the Ir in the sample is Ir(0). XPS confirms the predominance of Ir(0) in a catalyst sample with an Al/Ir ratio of 2.0, after hydrogenation. Additionally, the XANES result, especially with corroboration by XPS independently performed on a different sample (Supporting Information), shows definitively that the sample analyzed by XANES and XAFS was not contaminated by atmospheric oxygen. In short, the XAFS plus XANES and XPS of post hydrogenation catalyst samples shows the presence of, on average, approximately 1.6 nm, *fcc* Ir(0)<sub>~150</sub>, nanoparticles.

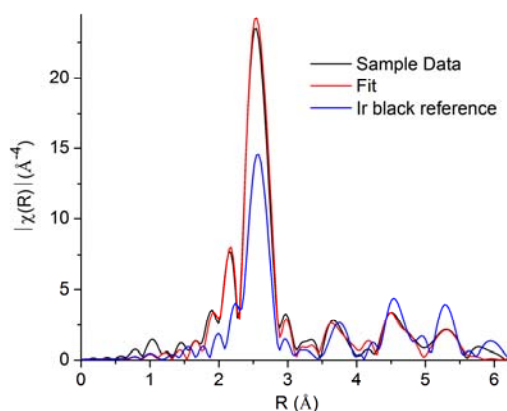


**Figure 9.** Fourier transform (FT) magnitudes of the data (black curve) and fit (red) of a powder sample of the Al/Ir = 1.0 catalyst after its use in hydrogenation. The longer range scattering peaks in the 3–6 Å range are expected for Ir nanoclusters with ordered internal structures. The Ir–Ir 1NN coordination number obtained from the fit,  $9.0 \pm 0.4$ , corresponds to, on average, approximately 1.6 nm, crystalline *fcc* Ir(0)<sub>~150</sub> clusters, according to XAFS. The FT magnitude spectrum of the Ir black reference, scaled by one-fourth, is shown for comparison (blue).

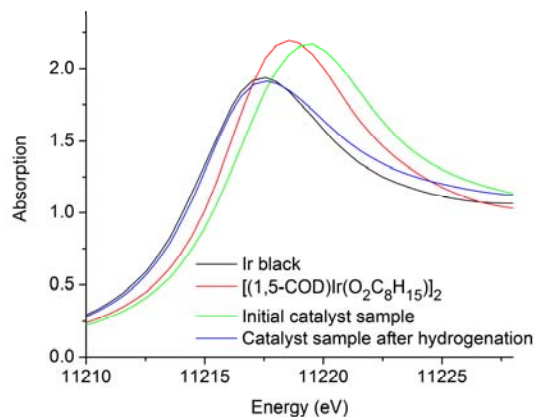


**Figure 10.** XANES spectra of Ir black (black line), the precatalyst  $[(1,5\text{-COD})\text{Ir}(\mu\text{-O}_2\text{C}_8\text{H}_{15})_2]_2$  (red), the initial  $[(1,5\text{-COD})\text{Ir}(\mu\text{-O}_2\text{C}_8\text{H}_{15})_2]_2$  plus  $\text{AlEt}_3$  catalyst (green), and the same catalyst sample after its use in the catalytic hydrogenation of cyclohexene (blue). The similarity of the Ir black and after-hydrogenation catalyst curves is compelling evidence for an Ir(0) oxidation state in the after-hydrogenation catalyst.

The difference in mean Ir cluster sizes measured by Z-contrast STEM versus those approximated by XAFS spectroscopy for the after-hydrogenation samples is possibly due to the XAFS data being collected on a powder sample. In a control experiment, precipitated catalyst material was collected after an initial cyclohexene hydrogenation run and isolated as a powder. It was then redispersed in cyclohexane, cyclohexene was added, and run in a second hydrogenation (see the Experimental Section for more details). Catalytic cyclohexene hydrogenation begins immediately using redispersed precipitate for a second run, Figure 11, and at a similar rate to the maximum rate achieved toward the end of an initial run, Figure 1. In short, this control experiment confirms that a highly active hydrogenation catalyst is retained following the procedures used to analyze the catalyst sample by XAFS and XANES. Add to this the observation, mentioned previously, that catalyst solutions sometimes precipitate after a

cyclohexene hydrogenation run under standard conditions, and the combined results argue strongly that the postcatalysis Ir cluster characterization results from XAFS are representative of the nature of the Ir species postcatalysis (although analysis of the precipitate, likely the result of well-precedented nanocluster aggregation processes,<sup>64,65</sup> probably gives a larger Ir particle size than what exists in solution before precipitation occurs). The key point is that *fcc* Ir(0)<sub>n</sub> Ziegler nanoclusters are increasing in size and abundance postcatalysis. Moreover, they likely are the fastest, best catalysts in this system (on the basis of the results of this control experiment, the increase in the rate of cyclohexene hydrogenation as catalysis proceeds, Figure 1, and also based on catalyst poisoning studies, *vide infra*).

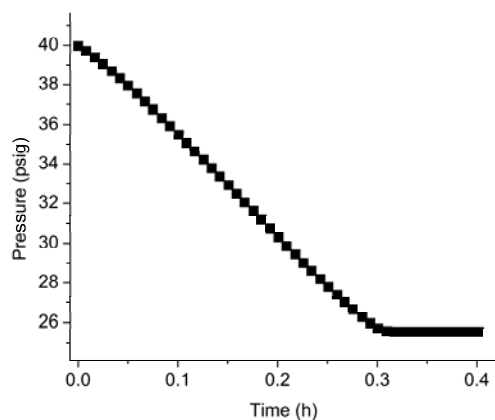


**Figure 11.** A second cyclohexene catalytic run following collection and isolation of a precipitate from a first run, and redispersion of it in cyclohexane. The initial hydrogenation rate in this experiment is 47 psig/h, and the maximum rate is 50 psig/h. Both rates are similar to the maximum hydrogenation rate observed from aged catalyst solutions during an initial run.

#### **Identification of the Ir-Containing Species in the AlEt<sub>3</sub>/Ir Catalyst *after***

**Hydrogenation: MALDI MS.** The [(1,5-COD)Ir(μ-O<sub>2</sub>C<sub>8</sub>H<sub>15</sub>)<sub>2</sub>] plus AlEt<sub>3</sub>, Al/Ir =

2.0, catalyst, after its use in cyclohexene hydrogenation, was analyzed using MALDI MS (the spectrum is shown in the Supporting Information). Similar to the MALDI MS results from the sample analyzed before hydrogenation, a broad peak representing a range of  $\text{Ir}_n$  species exists in the  $\geq 1000$   $m/z$  region, with a maximum at about 3000  $m/z$  corresponding to  $\text{Ir}_{\sim 16}$ , approximately 0.8-nm-diameter clusters. However, this posthydrogenation peak has a significant shoulder at about 5500  $m/z$ , which indicates  $\text{Ir}_{\sim 30}$ , 0.9 nm clusters, and the FWHM of the peak corresponds to  $\text{Ir}_{\sim 8-40}$ , 0.6–1.0 nm diameter clusters (the FWHM was used to estimate mean cluster diameter, Table 1, although it is an underestimation even more so than with the prehydrogenation sample because of the irregular peak shape). In addition, the curve tails off toward higher  $m/z$  values considerably less steeply than in the prehydrogenation sample spectrum—it reaches one-quarter max intensity at about 11500  $m/z$ , which corresponds to  $\text{Ir}_{\sim 60}$ , 1.2 nm clusters (nearly double the  $\sim 6000$   $m/z$  at one quarter intensity in the prehydrogenation spectrum, *vide supra*), and falls to one-eighth the maximum intensity at  $\sim 19500$   $m/z$ , which corresponds to  $\text{Ir}_{\sim 100}$ , 1.4 nm clusters (again, about double the  $m/z$  value at one-eighth maximum intensity in the prehydrogenation sample that corresponds to  $\text{Ir}_{\sim 50}$ , 1.1 nm clusters).

A broad range of  $\text{Ir}_n$  cluster sizes is again observed using MALDI MS, but compared to the prehydrogenation sample, the posthydrogenation catalyst includes even larger  $\text{Ir}_n$  nanoclusters, and a significantly greater quantity of these larger  $\text{Ir}_n$  species. Again, MALDI MS gives results that are similar, but not identical, to those from Z-contrast STEM; the possible reasons may be any combination of the factors listed previously, and an additional factor may be the difference in transit time between

completion of a catalytic run and analysis of the sample.<sup>68</sup> The key point that remains, regardless of the differences in  $\text{Ir}_n$  cluster sizes obtained using the three methods, is that Z-contrast STEM, XAFS, and MALDI MS *all show a distinct trend toward a greater population of larger, nanoscale  $\text{Ir}_n$  clusters in the posthydrogenation catalyst sample.* On the basis of the combined results of these three methods (Z-contrast giving mean  $1.0 \pm 0.3$  nm,  $\text{Ir}_{\sim 40}$  clusters; XAFS indicating mean 1.6 nm,  $\text{Ir}_{\sim 150}$ , clusters; and MALDI MS also showing a shift in the population if  $\text{Ir}_n$  species towards larger, nanometer scale clusters) we refer to these nanoscale, crystalline  $\text{Ir}(0)_n$  clusters herein as *fcc*  $\text{Ir}(0)_{40-150}$  Ziegler nanoclusters.

### **The Before-Hydrogenation-to-After-Hydrogenation Changes of Aged**

**Catalysts: A Summary.** The first step in the approach used herein to address the “is it homogeneous or heterogeneous catalyst?” question for the present catalyst system,<sup>3,4b,7,8</sup> is identification of the form(s) (e.g.,  $\text{Ir}_n$  cluster nuclearity) that the observable catalyst mass takes. A combination of analytic techniques has revealed that catalyst solutions before their use in hydrogenation contain a broadly dispersed range of  $\text{Ir}_n$  clusters extending from mono-Ir compounds to  $\text{Ir}_n$  nanoclusters with significantly disordered internal atomic structures, and with an estimated average of 0.5–0.7 nm,  $\text{Ir}(0)_{\sim 4-15}$  clusters. *The  $\text{Ir}_n$  species present are nearly the same regardless of the Al/Ir ratio employed, an important finding in its own right which, in turn, suggests that the observed changes in catalytic activity at different Al/Ir ratios are primarily the result of changes in the form and function of the Al-derived component(s) of the catalyst (i.e., the Al/Ir ratio not causing significant changes in the  $\text{Ir}_n$  nuclearity).*<sup>13</sup> During the use of these solutions in hydrogenation, a conversion toward roughly 1.0–1.6 nm, *fcc*  $\text{Ir}(0)_{\sim 40-}$

<sup>150</sup> Ziegler nanoclusters takes place,<sup>69</sup> consistent with the color change of the catalyst solutions from tawny yellow to darker brown as hydrogenation proceeds and the precipitation often seen a few days after the conclusion of a catalytic run. The conversion toward these 1.0–1.6 nm, Ir(0)<sub>~40–150</sub> Ziegler nanoclusters is independently evidenced by the results of Z-contrast STEM, XAFS spectroscopy, and MALDI MS, which show shifts in the range of Ir<sub>n</sub> clusters present toward larger Ir<sub>n</sub> clusters and increases in the mean observed clusters sizes and mean Ir<sub>n</sub> nuclearities. A key to obtaining these insights is our use of a third-row Ir system where, the evidence argues, its more stable Ir–Ir bonds mitigate against artifacts due, for example, to sample preparation and ex situ Z-contrast STEM.

#### **Additional Kinetics-Based Experiments Probing the Active Catalyst.**

Kinetics data are key to determining whether the observed catalytic activity using [(1,5-COD)Ir(μ-O<sub>2</sub>C<sub>8</sub>H<sub>15</sub>)<sub>2</sub> plus AlEt<sub>3</sub> catalysts is homogeneous (e.g., defined here as proceeding via mono-Ir compounds or subnanometer Ir<sub>~4–15</sub> cluster catalysts) or heterogeneous (e.g., defined here as proceeding via Ir(0)<sub>~40–150</sub> Ziegler nanoclusters).<sup>3,4b,7,8</sup> We have already shown that catalytic cyclohexene hydrogenation curves obtained using the [(1,5-COD)Ir(μ-O<sub>2</sub>C<sub>8</sub>H<sub>15</sub>)<sub>2</sub> plus AlEt<sub>3</sub> catalyst with an Al/Ir ratio of 2, both with and without prior aging of the catalyst solutions for 9 h, give a maximum hydrogenation rate ( $-d[H_2]/dt$ ) that is *not* the initial rate (i.e., that is faster than the initial rate). Instead, the hydrogenation rate increases concomitant with the increase in cluster size (and corresponding structural change) from Ir<sub>~4–15</sub> to *fcc* Ir(0)<sub>~40–150</sub>. This rate increase is quite pronounced when using catalyst solutions immediately after their preparation (see the switch in activity at ~2 h in Figure 12b) but is more

modest when the catalyst solutions have been aged, Figure 12a. The observed increase in the rate of hydrogenation during catalysis, plus the above studies showing (i) the *presence* of larger Ir(0)<sub>-40-150</sub> Ziegler nanoclusters post catalysis and also (ii) *high catalytic activity* when these nanoparticles are collected as a precipitate, redispersed in cyclohexane and used for a second catalytic run, strongly suggests, in the simplest (Ockham's razor) interpretation of the data, *that the fastest, best catalysts are the larger fcc Ir(0)<sub>-40-150</sub> Ziegler nanoclusters.*

To further test this hypothesis that the larger *fcc* Ir(0)<sub>-40-150</sub> Ziegler nanoclusters are the kinetically dominant catalyst, Hg(0) poisoning experiments were utilized (Hg(0) being known to poison most heterogeneous catalysts<sup>3,4b,70,71,72</sup>). Specifically, Hg(0) was added to the catalyst solutions after the cyclohexene consumption had proceeded about halfway (i.e., and once the catalytic rate had entered the maximum activity regime). The catalysis was poisoned *immediately and completely* by the Hg(0) addition, regardless of whether the initial catalyst solution was aged for 9 h prior to use (Figure 12a) or used immediately without aging (Figure 12b). This result provides additional evidence that the catalyst at the most active stage is what we defined earlier as heterogeneous—that is, due to the *fcc* Ir(0)<sub>-40-150</sub> Ziegler nanoclusters observed post hydrogenation.

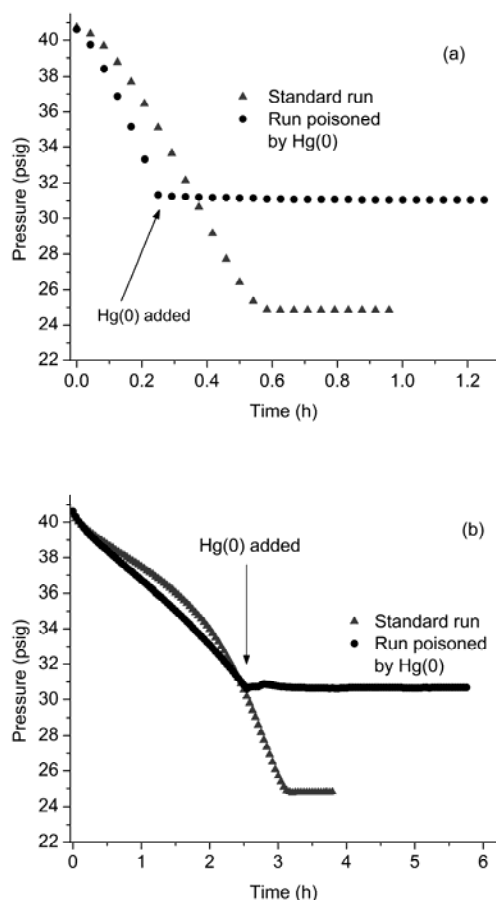


**Figure 12.** Cyclohexene hydrogenation curves for  $[(1,5\text{-COD})\text{Ir}(\mu\text{-O}_2\text{C}_8\text{H}_{15})_2]$  plus  $\text{AlEt}_3$  catalysts with Al/Ir ratios of 2.0, for (a) catalyst solutions aged 9 h, or (b) not aged, alongside hydrogenation runs poisoned by addition of  $\text{Hg}(0)$  under otherwise identical conditions. The variation in the hydrogenation runs prior to  $\text{Hg}(0)$  addition is typical for this system. For runs poisoned by  $\text{Hg}(0)$ , the catalytic hydrogenation of cyclohexene was allowed to proceed until the maximum rate regime was reached. Then, the solution was transferred to the drybox where  $\geq 300$  equivalents of  $\text{Hg}(0)$  per Ir was added and allowed to stir at 1000 rpm before putting it back on the hydrogenation line. The *subsequent* part of the hydrogenation curve shows *immediate and total* poisoning of the catalyst.

As a control experiment,  $\text{Hg}(0)$  was added to catalyst solutions, both with and without aging, *before* the start of catalytic cyclohexene hydrogenation (i.e., before being exposed to  $\text{H}_2$  gas). Near-immediate poisoning of the catalyst, Figure 13, suggests that the kinetically competent, fastest catalysts, even at the initial stage, are heterogeneous

(i.e., larger  $\text{Ir}_n$  nanoclusters, *not* the initially present mono-Ir complexes and  $\text{Ir}_{4-15}$  clusters, although one cannot rule out that  $\text{Hg}(0)$  is poisoning active  $\text{Ir}_{4-15}$  subnanoclusters). However, and interestingly, although  $\sim 95\%$  of the activity is poisoned, there is  $\sim 5\%$  activity initially, non- $\text{Hg}(0)$ -poisoned activity that implies a residual, *apparently* homogeneous catalyst, albeit one that accounts for only  $\sim 5\%$  of the catalysis.<sup>73</sup> Whether  $\text{Hg}(0)$  will or will not poison subnanometer, molecular  $\text{Ir}_n$  clusters remains an open question, one that will require the synthesis and characterization of, for example, authentic  $\text{Ir}_4$  clusters and attempts to poison their expected catalysis with  $\text{Hg}(0)$ . If, for example, the present prehydrogenation Ir clusters are actually of nominal composition  $\text{Ir}(\text{I})_4\text{H}_4$  (i.e.,  $\text{Ir}(\text{I})_4$  and not  $\text{Ir}(0)_4$ ), then that would be one *possible* explanation for their insensitivity to  $\text{Hg}(0)$ . Nevertheless, the  $\text{Hg}(0)$  poisoning experiments provide additional support for the hypothesis—now the dominant hypothesis for further studies in the area of Ziegler-type hydrogenation catalysis—that the *most active, kinetically competent catalysts* at the point of the maximum hydrogenation rate are *heterogeneous Ziegler nanoclusters analogous to the present  $\text{Ir}(0)_{40-150}$* . This is an important, previously unavailable finding. It presages an area of catalysis by hydrocarbon-soluble, Lewis-acid-containing, and thus presumably unusually coordinatively unsaturated—and certainly extremely catalytically active, industrially utilized—“Ziegler nanocluster” catalysts.

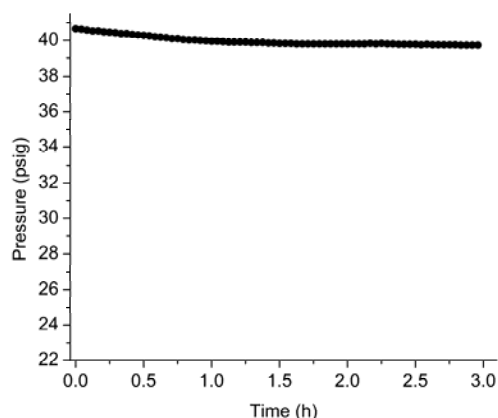


**Figure 13.** Near-immediate poisoning of the catalyst. Hg(0),  $\geq 300$  equivalents per Ir, was added to the catalyst solution after its preparation and 9 h of aging in the drybox. Sufficient mixing was ensured by stirring of the Hg(0)-containing catalyst solution for 24 h at 1000 rpm. Poisoning is 95% complete, but a small, residual, ca. 5% activity (i.e., 5% of the H<sub>2</sub>) is still consumed, mostly early in the experiment.

### Summary

The main findings of this study, then, are as follows:

- The initial [(1,5-COD)Ir( $\mu$ -O<sub>2</sub>C<sub>8</sub>H<sub>15</sub>)<sub>2</sub>] plus AlEt<sub>3</sub> Ziegler-type hydrogenation catalyst solutions, *before*-hydrogenation, are (by Z-contrast STEM, XAFS, and MALDI MS) a broad range of Ir<sub>n</sub> complexes from mono-Ir compounds to noncrystalline Ir<sub>n</sub> Ziegler nanoclusters, with the estimated mean Ir<sub>n</sub> clusters being 0.5–0.7 nm, Ir<sub>4–15</sub> subnanometer clusters. The agreement among the results, regardless of whether *ex situ* solid state Z-contrast imaging or *in situ*, solution XAFS/XANES is employed, argues against artifacts caused by these methods or the associated sample handling or preparation. Our use of MALDI MS as an additional method yielded estimated mean Ir cluster size and nuclearity results that are similar to those obtained by Z-contrast STEM and XAFS, but not identical—results that we view as a calibration of the less useful MALDI-MS method in the present case. Nevertheless, the results all yield a consistent

picture of the catalyst before hydrogenation as consisting of a broad range of  $\text{Ir}_n$  species dominated by subnanometer  $\text{Ir}_n$  clusters.

- According to XAFS, the  $\text{Ir}_n$  nuclearity results are largely unchanged regardless of the Al/Ir ratio employed. This important observation indicates that differences in catalytic activity, as a function of Al/Ir ratios, must be due just to the form or function of the Al-derived component(s),<sup>13</sup> and not to any Al/Ir- controlled or -dependent nuclearity of the initial  $\text{Ir}_n$  species present.
- At the end of their use in hydrogenation, the population of  $\text{Ir}_n$  clusters in the samples has shifted toward larger, 1.0–1.6 nm, *fcc*  $\text{Ir}(0)_{\sim 40-150}$  Ziegler nanoclusters. The average sizes of these larger nanoclusters, as determined by *Z*-contrast STEM, HRTEM, and XAFS/XANES, are similar, but not identical, depending on the technique (and associated sample preparation) used. However, the *trend* toward larger,  $\text{Ir}(0)_{\sim 40-150}$  Ziegler nanoclusters in posthydrogenation samples is verified by each method (i.e., is method-independent).
- Significantly, the development of *fcc*  $\text{Ir}(0)_{\sim 40-150}$  nanoclusters correlates with both a change in solution color (that also signals nanocluster formation) and an increase in the rate of cyclohexene hydrogenation. Furthermore, a precipitate can be collected from the catalyst solutions and, when redispersed in cyclohexene, displays immediate high activity for the hydrogenation of cyclohexene comparable to the maximum activity observed toward the end of an initial cyclohexene hydrogenation run. The evidence is consistent with and highly supportive of the now-dominant hypothesis for future research in the area, that the larger *fcc*  $\text{Ir}(0)_{\sim 40-150}$  Ziegler nanoclusters are the fastest Ziegler-type hydrogenation catalysts attained in at least the present Ir Ziegler-type

catalyst system. That said, catalysis of a ~2- to 10-fold slower rate (depending on the Al/Ir ratio and whether an aged or nonaged catalyst was used) is seen initially, when the estimated mean Ir species present are 0.5–0.7 nm, Ir<sub>4–15</sub> clusters.

- Consistent with the above “Ziegler nanocluster catalysis hypothesis”, Hg(0) added to catalyst solutions after the catalysts have entered their maximum rate regime stops the catalytic activity immediately and completely. This further supports evidence that the fastest catalysts found in this system are the *fcc* Ir(0)<sub>~40–150</sub> Ziegler nanoclusters (i.e., that “heterogeneous catalysis”<sup>3,4</sup> is present). However, it is worth noting that in solutions with Hg(0) added at the prehydrogenation stage, residual catalysis, presumably effected by unpoisoned homogeneous catalyst(s) such as monometallic Ir complexes or 0.5–0.7 nm, Ir<sub>4–15</sub> clusters, results in ~5% of the normal total H<sub>2</sub> consumption. Although significant catalysis by discrete subnanometer Ir species is not unequivocally ruled out by this study, the overall simplest interpretation of the data is that the larger, *fcc* Ir(0)<sub>~40–150</sub> nanoclusters are the more effective catalysts.

- Successfully investigating the problem of the composition and structure of a Ziegler-type hydrogenation catalyst has depended on the approach used herein: (a) the use of a third-row Ir-system with its strong Ir–Ir bonds and, therefore, more robust Ir<sub>n</sub> species that are less sensitive to various analytical methods and associated sample preparations, (b) the development<sup>2</sup> and use of the well characterized [(1,5-COD)Ir(μ-O<sub>2</sub>C<sub>8</sub>H<sub>15</sub>)<sub>2</sub>] pre-catalyst, and (c) the use of a combination of multiple, complementary analytical techniques *and* kinetic studies plus poisoning studies. That said, additional, ideally operando studies are desirable in this area,<sup>3,9</sup> and it is now possible to design them rationally and effectively.

- To our knowledge, this is the first report for a Ziegler-type hydrogenation catalyst where identification of the  $\text{Ir}_n$  species present using multiple complementary techniques has been coupled to kinetic evidence to show that the best, fastest catalysts are, in all probability,<sup>20,74,75</sup> the larger, *fcc*  $\text{Ir}(0)_{\sim 40-200}$  Ziegler nanoclusters. Nor has evidence been previously reported that a Ziegler-type hydrogenation catalyst can initially contain a homogeneous component (ca. 5% of the activity) and transition to heterogeneous catalysis during hydrogenation. That said, we wish to emphasize once again (*vide supra*; the Introduction) the important, recent contributions of, especially, Shmidt<sup>5</sup> and co-workers and Bönemann and co-workers<sup>3,6</sup> that also provide evidence for the presence of nanoclusters under Ziegler-type hydrogenation catalysis conditions.
- Further investigation of this prototype Ir Ziegler-type hydrogenation system through additional kinetic studies,<sup>12</sup> and evidence for the forms and roles of the  $\text{AlR}_3$ -derived component of the catalyst, will be reported elsewhere.<sup>13</sup> Those studies include an interesting inverse relationship between the maximum TOF and  $[\text{Ir}]$  concentration, intriguing findings which have required their own, separate study.<sup>12</sup> In addition, the results of studies analogous to those herein using the Co and Ni systems commonly employed by industry for olefin and polymer hydrogenation will be reported in due course.<sup>14</sup>

Our comprehensive review of the literature of Ziegler-type hydrogenation catalysts<sup>3</sup> shows the above insights (i.e., into the products of the precatalyst and cocatalyst reaction, how those products develop with use in a hydrogenation reaction, and the relative activities of those  $(\text{metal})_n$  products) are at the state-of-the-art for a

Ziegler-type hydrogenation catalyst—despite the industrial use of Ziegler-type hydrogenation catalysts for ~50 years to hydrogenate, currently, around  $1.7 \times 10^5$  metric tons of styrenic block copolymers annually.<sup>2</sup> One of our hopes is that the present demonstration, that at least  $\text{Ir}_n$  “Ziegler-type nanoclusters” both exist and are also the kinetically dominant, highly active catalysts, will prompt the community to begin to make use of these and other highly coordinately unsaturated, relatively “weakly ligated/labile ligand”,<sup>76</sup> hydrocarbon-soluble nanoclusters. Such Ziegler-type nanoclusters are unusual in that  $\text{RCO}_2^-$  from the starting material, *hydrocarbon* solvent, and Lewis acidic  $\text{AlEt}_3$  (plus their expected adducts, e.g.,  $\text{RCO}_2\text{AlEt}_3^-$  and any Al–O–Al-containing alumoxane from trace  $\text{H}_2\text{O}$ ) are the only possible (weakly ligating) ligands present, undoubtedly one reason for the high, industrial-level catalytic activity of Ziegler nanoclusters.

## Experimental Section

**Materials.** Unless stated otherwise, all materials were handled and stored under  $\text{N}_2$  in a Vacuum Atmospheres drybox, with  $\text{O}_2$  levels continuously maintained at  $\leq 5$  ppm according to a Vacuum Atmospheres  $\text{O}_2$ -level monitor. All solution measurements and additions done in the drybox at Colorado State University (CSU) utilized gastight syringes. Glassware was dried in an oven at  $160\text{ }^\circ\text{C}$  for  $\geq 12$  h and cooled under a vacuum or dry  $\text{N}_2$ . Cyclohexane (Sigma-Aldrich, 99.5 %,  $\text{H}_2\text{O} < 0.001$  %) was kept over activated molecular sieves for  $\geq 2$  days prior to use. Molecular sieves (Acros, 3 Å) were activated by heating at  $200\text{ }^\circ\text{C}$  for 6 hours under vacuum. The precatalyst  $[(1,5\text{-COD})\text{Ir}(\mu\text{-O}_2\text{C}_8\text{H}_{15})]_2$  was prepared as described<sup>2</sup> and used herein as a solution in

cyclohexane, typically 9.0 or 12.0 mM in [Ir]. AlEt<sub>3</sub> (Strem Chemicals, 93%) was also used as a cyclohexane solution, typically 18.0 or 36.0 mM.

***Caution!** Alkylaluminums are pyrophoric and should be handled with care using air- and moisture-free techniques.<sup>77</sup>*

Cyclohexene (Aldrich, 99%) was distilled over sodium under argon. Both Ar and H<sub>2</sub> gases were passed through moisture (Scott Specialty Gases) and oxygen traps (Trigon Technologies) prior to use. Ir black and Ir<sub>4</sub>(CO)<sub>12</sub> (Strem, 98%) were used as received. HPO<sub>4</sub>-stabilized *fcc* Ir(0)<sub>n</sub> nanos were synthesized as previously described (details are provided in the Supporting Information).<sup>26</sup>

**Catalyst Solution Preparation.** Catalyst solutions were prepared in the drybox at CSU both in batches and in smaller volumes for individual hydrogenation use (the temperature in the drybox was between 25 and 30 °C). For example, a 20 mL, [Ir] = 1.44 mM, batch of catalyst with an Al/Ir ratio of 2 was prepared by first adding 15.2 mL of cyclohexane to a 20 mL glass vial containing a 5/8 × 5/16 in. Teflon-coated magnetic stir bar. Next, 2.4 mL of a cyclohexane solution of [(1,5-COD)Ir(μ-O<sub>2</sub>C<sub>8</sub>H<sub>15</sub>)<sub>2</sub>], 12.0 mM in [Ir], was added, making an orange/light red solution. Stirring (1000 ± 200 rpm, measured with a Monarch Instruments Pocket-Tachometer 100) was started, and 1.6 mL of a 36.0 mM AlEt<sub>3</sub> solution was added rapidly.

**Catalytic Cyclohexene Hydrogenations.** All catalyst solutions for cyclohexene hydrogenation were prepared individually in 22 × 175 mm Pyrex culture tubes containing a new 5/8 × 5/16 in. Teflon-coated magnetic stir bar (both rinsed three times with ultrapure water prior to drying). For example, a 0.6 mM in [Ir], Al/Ir = 2.0, catalyst solution was prepared by adding 0.20 ± 0.01 mL of a 9.0 mM in [Ir] cyclohexane

solution of [(1,5-COD)Ir( $\mu$ -O<sub>2</sub>C<sub>8</sub>H<sub>15</sub>)<sub>2</sub>] to a culture tube followed by 0.200  $\pm$  0.002 mL of 18.0 mM AlEt<sub>3</sub> in cyclohexane, added rapidly with 1000  $\pm$  200 rpm stirring to make Al/Ir = 2.0. Cyclohexane was added to bring the total volume to 2.5 mL, and then 0.5  $\pm$  0.01 mL of cyclohexene was added, making 3.0 mL of a Al/Ir = 2 catalyst solution, 0.6 mM in [Ir] and 1.65 M in [cyclohexene].

The procedure and apparatus used for catalytic hydrogenations of cyclohexene were described in detail elsewhere.<sup>7a,78,79</sup> Briefly, once the hydrogenation reaction solution was prepared, the culture tube was placed in a Fisher–Porter (F–P) bottle, which was then sealed. The solution was then allowed to stir at 1000 rpm in the sealed F–P bottle in the drybox, typically for 9 h (see Figure S2, Supporting Information). At the end of the aging period, if any, the F–P bottle was then brought out of the drybox and placed in a bath set at 22.0  $\pm$  0.1 °C. Stirring was started at 1000  $\pm$  10 rpm employing a Fauske Super Magnetic Stirrer, and the F–P bottle was connected to a pressurized H<sub>2</sub> line using Swagelock quick-connects. The F–P bottle was purged 15 times (1 purge/15 sec). The pressure in the F–P bottle was set to 40 psig, and data collection was initiated at 4 minutes after the first purge. Hydrogen pressure vs time data were collected using a pressure transducer (Omega PX 624–100 GSV) interfaced via an Omega D1131 analog-to-digital converter connected to a PC running LabView 7.0. Data were subsequently handled using MS Excel and Origin 7. In order to quantitatively compare hydrogenation rates, and because of their shapes (i.e., more rapid H<sub>2</sub> pressure loss later in the hydrogenation, as opposed to initially), the initial and maximum rate portions of the curves were fit separately by polynomial and linear expressions, respectively (for an example, see Figure S1 of the Supporting Information).

**Catalyst Poisoning by Hg(0).** All catalyst solutions were first prepared in the drybox as described above with  $[\text{Ir}] = 0.6 \text{ mM}$ ,  $\text{Al}/\text{Ir} = 2.0$ , and an initial cyclohexene concentration of  $1.65 \text{ M}$ . Each poisoning experiment used  $\geq 300$  equivalents of  $\text{Hg}(0)$  per Ir added in the drybox. Thorough contact of the insoluble  $\text{Hg}(0)$  and the catalyst in solution was ensured by stirring at  $1000 \text{ rpm}$  in the sealed FP bottle in the drybox for  $24 \text{ h}$ . For poisoning after a partially completed hydrogenation run, the hydrogenation reaction was quenched by filling and purging with  $40 \text{ psig}$  of Ar gas five times (once every five seconds). The FP bottle was then transferred back into the drybox where  $\text{Hg}(0)$  was added. After the  $24 \text{ h}$  mixing period, the sealed FP bottle was again removed from the drybox, and hydrogenation was resumed according to the procedure already described. Time and pressure values then collected have been corrected to fit with the initial portion of the data, Figure 12. Control experiments show that  $24 \text{ h}$  of mixing the catalyst solution with  $\text{Hg}(0)$  is necessary and sufficient for catalyst poisoning (Figure S35, Supporting Information) and that the experimental procedure itself is not the cause of the loss of catalytic activity. Another control experiment showed that, for poisoning of the initial catalyst, before a hydrogenation run was started, removal of the  $\text{Hg}(0)$  from the catalyst solution made no difference in the result.

**Z-Contrast Microscopy.** Samples of the  $[(1,5\text{-COD})\text{Ir}(\mu\text{-O}_2\text{C}_8\text{H}_{15})_2]$  plus  $\text{AlEt}_3$  catalyst ( $3.00 \text{ mL}$ ,  $1.00 \text{ mM}$  in  $[\text{Ir}]$ , with an  $\text{Al}/\text{Ir}$  ratio of  $2.0$ ) were collected for Z-contrast microscopy both before and after use in cyclohexene hydrogenation, double-sealed airtight, and shipped to the Center for Microanalysis of Materials (CMM), University of Illinois at Urbana–Champaign (UIUC) for imaging. Grid preparation for Z-contrast microscopy was conducted in a glovebag filled with dry  $\text{N}_2$  at  $> 1 \text{ atm}$  and

located in the TEM room. The solution sample was diluted with cyclohexane to twice its original volume. Next, 2–3 drops were dispersed onto a TEM grid with an ultrathin carbon film on a holey carbon support (Ted Pella, Inc.) and dried at room temperature under N<sub>2</sub> for  $\geq 10$  min. Once dried, a TEM grid was transferred quickly into the TEM column to reduce oxidation of the sample. Images were acquired using a field-emission JEM 2010 (scanning) transmission electron microscope operated at 200 kV. The samples were first treated with a high-intensity electron beam (electron beam shower) for  $\sim 15$  min each time in the TEM column (with vacuum better than  $3 \times 10^{-6}$  Torr) to assist in high quality imaging. The high-angle scattering electrons were collected with a JEOL ADF detector at a camera length of 8 cm, with a 0.2 nm (nominal) diameter probe. High-angle annular dark-field (HAADF) images were collected at 2 M (million) magnification and were  $1024 \times 1024$  pixels in dimension. Cluster diameters were measured at the full width at half-maximum (FWHM) of the intensity profile across  $\geq 600$  clusters from images at the same levels of magnification and contrast (an example intensity profile is shown in the Supporting Information).

**XAFS Spectroscopy.** Sample solutions were prepared at CSU in 6.0 mL batches at 5.0, 6.0, or 7.2 mM in [Ir]. Containers were double-sealed airtight and transported to the National Synchrotron Light Source (NSLS) at Brookhaven National Laboratory (BNL), Upton, NY (two days transit time). At the NSLS, all catalyst samples were handled and stored in a N<sub>2</sub> atmosphere glovebox maintained at  $\leq 10$  ppm O<sub>2</sub>. Solution samples were loaded into a custom-designed airtight sample cell composed of a stainless steel frame made to press Kapton film windows onto a Teflon block with a  $\sim 1.5$  mL sample cavity. The samples were loaded using glass pipettes into threaded

ports in the Teflon block, which were then sealed using Teflon screws. Airtight seals in the threaded ports and windows were ensured by using Kalrez o-rings.

A portion of the Al/Ir = 1.0 catalyst sample was used for catalytic hydrogenation of cyclohexene and then collected for XAFS analysis. The brown solution had precipitated as a dark brown powder in transit to the NSLS where the XAFS experiments were performed. This is not unusual however because, as already noted, catalyst solutions kept in the drybox sometimes precipitate within a few days after completion of a catalytic run. The powder was isolated by centrifugation followed by evaporation in vacuo. The powder was then brushed onto the adhesive side of a strip of Kapton tape. The tape was then folded repeatedly and held in place with additional Kapton tape to ensure an airtight seal. Reference samples of Ir black and Ir<sub>4</sub>(CO)<sub>12</sub> powders were prepared in this manner; however, preparation of Ir black was done outside the drybox. As already mentioned, a lack of contamination by atmospheric O<sub>2</sub> during posthydrogenation XAFS analysis was confirmed from the XAFS, XANES, and independently performed XPS results, all showing that the sample consisted of Ir(0). Control experiments were performed to test whether the treatment of catalyst material necessary for analysis by XAFS and XANES *after* use in cyclohexene hydrogenation affects its activity. Samples of the catalyst after their use for cyclohexene hydrogenation were collected by bringing the F-P bottle back into the drybox after the H<sub>2</sub> consumption had ceased and removing the cyclohexane solvent under a vacuum. This provided isolated catalyst powder analogous to that analyzed by XAFS and XANES. The powder was then redissolved in 2.5 mL of cyclohexane and transferred into a new culture tube in

a F–P bottle followed by 0.5 mL of cyclohexene. A second cyclohexene hydrogenation performed following this treatment gave the activity results shown in Figure 11.

XAFS experiments were performed on a bending magnet beamline, X18b of the NSLS, which uses a Si(111) channel-cut monochromator. X-ray absorption data were collected at room temperature. Samples were mounted and positioned at 45° in the beam path with the help of a motorized sample stage. Gas ion chamber detectors were used for incident, transmitted, fluorescence, and reference channels. Absorption edge calibration was performed prior to XAFS scans using an Ir black standard, for which energy was swept from 150 eV below to 1800 eV above the Ir L3 edge (11215 eV). Energy was swept from 150 eV below to 2000 eV above the Ir L3 edge for all other samples, except in the case of data collection on the [(1,5-COD)Ir( $\mu$ -O<sub>2</sub>C<sub>8</sub>H<sub>15</sub>)<sub>2</sub>] precatalyst, when the energy was swept to 1800 eV above the L3 edge. Reference spectra were obtained simultaneously in the transmission mode for all sample scans using the Ir black standard. The number of scans performed was 2, 29, 6, and 9 for Ir black, HPO<sub>4</sub>-stabilized Ir nanoclusters, Ir<sub>4</sub>(CO)<sub>12</sub>, and [(1,5-COD)Ir( $\mu$ -O<sub>2</sub>C<sub>8</sub>H<sub>15</sub>)<sub>2</sub>], respectively. For the Al/Ir = 0.5, 1.0, 1.5, 2.0, 2.5, 3.0, and 5.0 catalyst samples before hydrogenation, 5, 5, 10, 10, 10, 3, and 6 scans were performed, respectively. Three scans were performed on an Al/Ir = 10.0 sample, but the data were excessively noisy (Figure S22, Supporting Information), precluding reliable analysis and fitting. For the Al/Ir = 1.0 sample after hydrogenation, 17 scans were performed. Fluorescence data were deemed inferior in quality to the transmission data and therefore disregarded.

Data processing was accomplished using IFEFFIT.<sup>80</sup> The reference spectra were used for scan alignment. The threshold energy ( $E_0$ ) was assigned a value that

corresponded to approximately half the normalized edge step, 11213 eV, and multiple scans of a single sample were merged (averaged). The range of data deemed to have a sufficient signal-to-noise ratio was selected using a Hanning window function for Fourier transforms (FTs), Figures S10–S21 of the Supporting Information.

A drift in the scans of the Al/Ir = 1.5, 2.0, and 2.5 catalysts before hydrogenation was observed, Figure S24, Supporting Information. A control experiment performed in an attempt to rule out possible sample damage caused by the X-ray beam suggests that no beam damage was occurring, Figure S25, Supporting Information. The reason for the observed drift is not apparent, but to lessen its effect on the analysis, the first two scans in each case were merged, and the others were discarded.

**Acknowledgment.** We thank J.-G. Wen, C.-H. Lei, and the user facilities at the CMM, UIUC. We thank JoAn Hudson of Clemson University for bright field TEM and HRTEM imaging. Mass spectra were obtained with the expert assistance of Phil Ryan (now deceased) of the Macromolecular Resources Lab at CSU. XPS was accomplished thanks to the help of Patrick McCurdy at CSU. This work was supported by NSF Grant CHE-0611588 at Colorado State University. We thank Nebojsa Marinkovic and Syed Khalid at the NSLS. AIF, JCY and RGN acknowledge support by DOE BES Grant DE-FG02-03ER15476. Use of the NSLS was supported by the U.S. Department of Energy, Office of Science, Office of Basic Energy Sciences, under Contract No. DE-AC02-98CH10886. Beamline X18B at the NSLS is supported in part by the Synchrotron Catalysis Consortium, U.S. Department of Energy Grant No DE-FG02-05ER15688.

Special thanks go to five reviewers and the editor, each of whose careful readings and constructive criticisms helped improve the final manuscript.

**Supporting Information Available:** Additional experimental information and control experiments for cyclohexene hydrogenations. Bright-field TEM images, corresponding particle size histograms, and images from TEM and HRTEM control experiments. MALDI mass spectra and results of associated control experiments. XAFS spectra with fits, tables of fitting results, and associated XAFS control experiments. Survey and high-resolution XPS spectra. HR and other TEM images of catalysts after hydrogenation. XAFS-determined coordination number-particle diameter correlation curve. Hg(0) poisoning control experiments. A full list of the authors of reference 6d. This material is available free of charge via the Internet at <http://pubs.acs.org>.

## References

- 
- <sup>1</sup> Johnson, K. A. *Polym. Prepr.* **2000**, *41*, 1525–1526.
- <sup>2</sup> Alley, W. M.; Girard, C. W.; Özkar, S.; Finke, R. G. *Inorg. Chem.* **2009**, *48*, 1114–1121.
- <sup>3</sup> Alley, W. M.; Hamdemir, I. K.; Johnson, K. A.; Finke, R. G. *J. Mol. Catal. A: Chem.* **2010**, *315*, 1–27.
- <sup>4</sup> (a) Collman, J. P.; Hegedus, L. S.; Norton, J. R.; Finke, R. G. *Principles and Applications of Organotransition Metal Chemistry*; University Science Books: Mill Valley, CA, 1987. (b) Widegren, J.; Finke, R. *J. Mol. Catal. A: Chem.* **2003**, *198*, 317–341. (c) Schwartz, J. *Acc. Chem. Res.* **1985**, *18*, 302–308.

---

<sup>5</sup> (a) Shmidt, F. K.; Nindakova, L. O.; Shainyan, B. A.; Saraev, V. V.; Chipanina, N. N.; Umanetz, V. A. *J. Mol. Catal. A: Chem.* **2005**, *235*, 161–172. (b) Belykh, L. B.; Titova, Yu. Yu.; Umanets, V. A.; Shmidt, F. K. *Russ. J. Appl. Chem.* **2006**, *79*, 1271–1277. (c) Nindakova, L. O.; Shmidt, F. K.; Saraev, V. V.; Shainyan, B. A.; Chipanina, N. N.; Umanets, V. A.; Belonogova, L. N.; Toryashinova, D.-S. D. *Kinet. Catal.* **2006**, *47*, 54–63. (d) Belykh, L. B.; Goremyka, T. V.; Skripov, N. I.; Umanets, V. A.; Shmidt, F. K. *Kinet. Catal.* **2006**, *47*, 367–374.

<sup>6</sup> (a) Bönnemann, H.; Brijoux, W.; Brinkmann, R.; Endruschat, U.; Hofstadt, W.; Angermund, K. *Rev. Roum. Chim.* **1999**, *44*, 1003–1010. (b) Bönnemann, H.; Waldöfner, N.; Haubold, H.-G.; Vad, T. *Chem. Mater.* **2002**, *14*, 1115–1120. (c) Angermund, K.; Bühl, M.; Dinjus, E.; Endruschat, U.; Gassner, F.; Haubold, H.-G.; Hormes, J.; Köhl, G.; Mauschick, F. T.; Modrow, H.; Mörtel, R.; Mynott, R.; Tesche, B.; Vad, T.; Waldöfner, N.; Bönnemann, H. *Angew. Chem., Int. Ed.* **2002**, *41*, 4041–4044. (d) Angermund, K.; et al. *J. Phys. Chem. B* **2003**, *107*, 7507–7515. (e) Haubold, H.-G.; Vad, T.; Waldöfner, N.; Bönnemann, H. *J. Appl. Crystallogr.* **2003**, *36*, 617–620. (f) Wen, F.; Bönnemann, H.; Mynott, R. J.; Spliethoff, B.; Weidenthaler, C.; Palina, N.; Zinoveva, S.; Modrow, H. *Appl. Organomet. Chem.* **2005**, *19*, 827–829.

<sup>7</sup> (a) Lin, Y.; Finke, R. G. *Inorg. Chem.* **1994**, *33*, 4891–4910. (b) Aiken, J. D., III; Lin, Y.; Finke, R. G. *J. Mol. Catal. A: Chem.* **1996**, *114*, 29–51. (c) Widegren, J. A.; Bennett, M. A.; Finke, R. G. *J. Am. Chem. Soc.* **2003**, *125*, 10301–10310. (d) Hagen, C. M.; Widegren, J. A.; Maitlis, P. M.; Finke, R. G. *J. Am. Chem. Soc.* **2005**, *127*, 4423–4432. (e) Finney, E. E.; Finke, R. G. *Inorg. Chim. Acta* **2006**, *359*, 2879–2887.

<sup>8</sup> (a) Jaska, C. A.; Manners, I. *J. Am. Chem. Soc.* **2004**, *126*, 1334–1335. (b) Jaska, C. A.; Manners, I. *J. Am. Chem. Soc.* **2004**, *126*, 9776–9785. (c) Zahmakiran, M.; Özkar, S. *Inorg. Chem.* **2009**, *48*, 8955–8964.

<sup>9</sup> For lead references to operando studies of catalysis and their importance, see: (a) Thomas, J. M.; Somorjai, G. A. *Top. Catal.* **1999**, *8* (preface). (b) Weckhuysen, B. M. *Chem. Commun.* **2002**, 97–110; (c) Guerrero-Pérez, M. O.; Bañares, M. A. *Chem. Commun.* **2002**, 1292–1293. (d) Meunier, F.; Daturi, M. *Catal. Today* **2006**, *113*, 1–2.

---

<sup>10</sup> We were made aware of XAFS as a potentially highly valuable analytical technique for the study of Ziegler-type hydrogenation catalyst systems by the following excellent early studies: (a) Goulon, J.; Georges, E.; Goulon-Ginet, C.; Chauvin, Y.; Commereuc, D.; Dexpert, H.; Freund, E. *Chem. Phys.* **1984**, *83*, 357–366. (b) Esselin, C.; Bauer-Grosse, E.; Goulon, J.; Williams, C.; Chauvin, Y.; Commereuc, D.; Freund, E. *J. Phys. Colloques* **1986**, *47*, C8–243–C8–248.

<sup>11</sup> Further analysis of this catalyst system using additional kinetic studies reveals an *increase* in catalyst turnover frequency with *decreasing* [Ir] concentration and will be reported elsewhere.<sup>12</sup> Another important remaining question, one beyond the scope of this work, is what happens to the AlEt<sub>3</sub> cocatalyst; that is, what are the forms and roles of the AlR<sub>3</sub>-derived component in the catalysis? That work is also currently underway and will be addressed in a separate paper.<sup>13</sup> Also addressed elsewhere is the question of the true active catalyst species in industrial Co and Ni Ziegler-type hydrogenation catalyst systems.<sup>14</sup>

<sup>12</sup> Alley, W. M.; Li, L.; Yang, J. C.; Özkar, S.; Finke, R. G. Manuscript in preparation.

<sup>13</sup> Hamdemir, I. K.; Özkar, S.; Johnson, K. A.; Finke, R. G. Manuscript in preparation.

<sup>14</sup> Alley, W. M.; Hamdemir, I. K.; Li, L.; Yang, J. C.; Wang, Q.; Frenkel, A.; Menard, L. D.; Nuzzo, R. G.; Özkar, S.; Johnson, K. A.; Finke, R. G. Manuscript in preparation.

<sup>15</sup> Cordero, B.; Gómez, V.; Platero-Prats, A. E.; Revés, M.; Echeverría, J.; Cremades, E.; Barragán, F.; Alvarez, S. *Dalton Trans.* **2008**, 2832–2838.

<sup>16</sup> Lin, Y.; Finke, R. G. *J. Am. Chem. Soc.* **1994**, *116*, 8335–8353.

<sup>17</sup> *CRC Handbook of Chemistry and Physics*, 77th ed.; Lide, D. R., Frederikse, H. P. R., Eds.; CRC Press: Boca Raton, FL, 1996.

<sup>18</sup> With the simplifying assumption of fcc clusters, the number ( $n$ ) of atoms in a transition metal nanocluster of diameter  $D$  can be estimated according to  $n = (N_0\rho(4/3)\pi(D/2)^3)/W$ ,<sup>16</sup> where  $N_0 = 6.022 \times 10^{23} \text{ mol}^{-1}$ ,  $\rho$  = the room temperature

---

density of the pure bulk metal, and  $W$  = atomic weight of the transition metal. For Ir,  $\rho$  = 22.5 g/cm<sup>3</sup> and  $W$  = 192.22 g/mol.<sup>17</sup> According to this estimate, the largest, 1.4-nm-diameter Ir clusters are Ir(0)<sub>~100</sub>.

<sup>19</sup> Starkey Ott, L.; Cline, M. L.; Deetlefs, M.; Seddon, K. R.; Finke, R. G. *J. Am. Chem. Soc.* **2005**, *127*, 5758–5759.

<sup>20</sup> Hagen, C. M.; Vieille-Petit, L.; Laurency, G.; Süss-Fink, Finke, R. G. *Organometallics* **2005**, *24*, 1819–1831.

<sup>21</sup> Williams, D. B.; Carter, C. B. *Transmission Electron Microscopy*; Plenum Press: New York, 1996.

<sup>22</sup> Pyrz, W. D.; Buttrey, D. J. *Langmuir* **2008**, *24*, 11350–11360.

<sup>23</sup> Menard, L. D.; Gao, S.-P.; Xu, H.; Twesten, R. D.; Harper, A. S.; Song, Y.; Wang, G.; Douglas, A. D.; Yang, J. C.; Frenkel, A. I.; Nuzzo, R. G.; Murray, R. W. *J. Phys. Chem. B* **2006**, *110*, 12874–12883.

<sup>24</sup> The results of bright field TEM used to analyze the initial [(1,5-COD)Ir( $\mu$ -O<sub>2</sub>C<sub>8</sub>H<sub>15</sub>)<sub>2</sub>] plus AlEt<sub>3</sub> catalyst samples, before their use in hydrogenation, are shown and discussed in the Supporting Information. An image obtained before hydrogenation of an Al/Ir = 2.0 catalyst sample shows 1.1  $\pm$  0.3 nm diameter Ziegler nanoclusters. This larger mean diameter is a consequence of the inability of bright-field TEM to detect the  $\leq$  ~1.0 nm Ir clusters. In addition, an image of the [(1,5-COD)Ir( $\mu$ -O<sub>2</sub>C<sub>8</sub>H<sub>15</sub>)<sub>2</sub>] precatalyst alone as a control experiment contains dark spots that are likely artifacts of the image background. Hence, the bright-field TEM results were deemphasized in this study. HRTEM was also used to image catalyst samples before hydrogenation. However, images of reasonable quality were not obtained. A sample image and an explanation of the findings are given in the Supporting Information.

<sup>25</sup> Finney, E. E.; Finke, R. G. *J. Colloid Interface Sci.* **2008**, *317*, 351–374. Also see refs 45–49 therein.

---

<sup>26</sup> (a) Özkar, S.; Finke, R. G. *J. Organomet. Chem.* **2004**, *689*, 493–501. (b) Özkar, S.; Finke, R. G. *Langmuir* **2003**, *19*, 6247–6260.

<sup>27</sup> Frenkel, A. I.; Hills, C. W.; Nuzzo, R. G. *J. Phys. Chem. B* **2001**, *105*, 12689–12703.

<sup>28</sup> In *X-ray Absorption: Principles, Applications, Techniques of EXAFS, SEXAFS, and XANES*; Koningsberger, D. C., Prins, R., Eds.; Wiley: New York, 1988.

<sup>29</sup> Stern, E. A.; Heald, S. M. In *Handbook on Synchrotron Radiation*; Koch, E. E., Ed.; North-Holland: New York, 1983; Vol. 1.

<sup>30</sup> The atomic-scale structure of transition metal nanoclusters is a topic of interest in the literature.<sup>31–34</sup> Theoretical and experimental studies have predicted and observed, respectively, the internal atomic structures of transition metal clusters from a variety of different systems,<sup>31</sup> including supported clusters.<sup>32</sup> It is found from such studies that nanoscale clusters can possess an assortment of internal structures and exhibit large degrees of structural disorder, or an amorphous-like nature, even while maintaining some signatures of periodicity.<sup>31f</sup> However, precise determination of the internal atomic structures at the nanoscale is a non-trivial problem,<sup>33</sup> especially since examples of systems that are amenable to such structural analysis are rare.<sup>34</sup>

<sup>31</sup> (a) Duff, D. G.; Curtis, A. C.; Edwards, P. P.; Jefferson, D. A.; Johnson, B. F. G.; Logan, D. E. *J. Chem. Soc., Chem. Commun.* **1987**, 1264–1266. (b) Ankudinov, A. L.; Rehr, J. J.; Low, J. J.; Bare, S. R. *J. Chem. Phys.* **2002**, *116*, 1911–1919. (c) Garzón, I. L.; Reyes-Nava, J. A.; Rodríguez-Hernández, J. I.; Sigal, I.; Beltrán M. R.; Michaelian, K. *Phys. Rev. B* **2002**, *66*, 073403–1–073403–4. (d) Petkov, V.; Ohta, T.; Hou, Y.; Ren, Y. *J. Phys. Chem. C* **2007**, *111*, 714–720. (e) Sanchez, S. I.; Small, M. W. Zuo, J.-M.; Nuzzo, R. G. *J. Am. Chem. Soc.* **2009**, *131*, 8683–8689. (f) Petkov, V.; Bedford, N.; Knecht, M. R.; Weir, M. G.; Crooks, R. M.; Tang, W.; Henkelman, G.; Frenkel, A. J. *J. Phys. Chem. C* **2008**, *112*, 8907–8911. (g) Sun, Y.; Zhuang, L.; Lu, J.; Hong, X.; Liu, P. *J. Am. Chem. Soc.* **2007**, *129*, 15465–15467. Interestingly these authors also see that larger (Pt) nanoparticles have an increased activity, and that the smaller  $\leq 1$  nm Pt nanoparticles are amorphous (perhaps due to Pt–O or other surface ligands).

- 
- <sup>32</sup> (a) Vila, F.; Rehr, J. J.; Kas, J.; Nuzzo, R. G.; Frenkel, A. I. *Phys. Rev. B* **2008**, *78*, 121404–1–121404–4. (b) Sanchez, S. I.; Menard, L. D.; Bram, A.; Kang, J. H.; Small, M. W.; Nuzzo, R. G.; Frenkel, A. I. *J. Am. Chem. Soc.* **2009**, *131*, 7040–7054.
- <sup>33</sup> (a) Gilbert, B.; Huang, F.; Zhang, H.; Waychunas, G. A.; Banfield, J. F. *Science* **2004**, *305*, 651–654. (b) Billinge, S. J. L.; Levin, I. *Science* **2007**, *316*, 561–565.
- <sup>34</sup> Jadzinsky, P. D.; Calero, G.; Ackerson, J. C.; Bushnell, D. A.; Kornberg, R. D. *Science* **2007**, *318*, 430–433.
- <sup>35</sup> (a) Sun, Y.; Frenkel, A. I.; Isseroff, R.; Shonbrun, C.; Forman, M.; Shin, K.; Koga, T.; White, H.; Zhang, L.; Zhu, Y.; Rafailovich, M. H.; Sokolov, J. C. *Langmuir* **2006**, *22*, 807–816. (b) Menard, L. D.; Xu, H.; Gao, S.-P.; Twisten, R. D.; Harper, A. S.; Song, Y.; Wang, G.; Douglas, A. D.; Yang, J. C.; Frenkel, A. I.; Murray, R. W.; Nuzzo, R. G. *J. Phys. Chem. B* **2006**, *110*, 14564–14573. (c) Soler, J. M.; Beltrán, M. R.; Michaelian, K.; Garzón, I. L.; Ordejón, P.; Sánchez-Portal, D.; Artacho, E. *Phys. Rev. B* **2000**, *61*, 5771–5780.
- <sup>36</sup> Fulton, J. L.; Linehan, J. C.; Autrey, T.; Balasubramanian, M.; Chen, Y.; Szymczak, N. K. *J. Am. Chem. Soc.* **2007**, *129*, 11936–11949.
- <sup>37</sup> Harada, M.; Asakura, K.; Toshima, N. *J. Phys. Chem.* **1994**, *98*, 2653–2662.
- <sup>38</sup> Churchill, M. R.; Hutchinson, J. P. *Inorg. Chem.* **1978**, *17*, 3528–3535.
- <sup>39</sup> Finke, R. G.; Özkar, S. *Coord. Chem. Rev.* **2004**, *248*, 135–146.
- <sup>40</sup> Shido, T.; Okazaki, T.; Ichikawa, M. *J. Mol. Catal. A: Chem.* **1997**, *120*, 33–45.
- <sup>41</sup> Cho, S. J.; Lee, J.; Lee, Y. S.; Kim, D. P. *Catal. Lett.* **2006**, *109*, 181–187.
- <sup>42</sup> Garlaschelli, L.; Greco, F.; Peli, G.; Manassero, M.; Sansoni, M.; Gobetto, R.; Salassa, L.; Pergola, R. D. *Eur. J. Inorg. Chem.* **2003**, 2108–2112.
- <sup>43</sup> Argo, A. M.; Odzak, J. F.; Gates, B. C. *J. Am. Chem. Soc.* **2003**, *125*, 7107–7115.

- 
- <sup>44</sup> Golden, J. T.; Peterson, T. H.; Holland, P. L.; Bergman, R. G.; Andersen, R. A. *J. Am. Chem. Soc.* **1998**, *120*, 223–224.
- <sup>45</sup> El-Issa, B. D.; Katrib, A.; Ghodsian, R.; Salsa, B. A.; Addassi, S. H. *Int. J. Quantum Chem.* **1988**, *33*, 195–216.
- <sup>46</sup> According to the final-state-relaxation phenomenon, electron photoemission results in a positive charge on the nanocluster surface, which has a lifetime longer than the time scale of the photoemission ( $10^{-16}$  s). This results in an electron binding energy that is shifted higher by 0.1–2.0 eV. The final state relaxation phenomenon has been previously observed for  $\text{Au}_n$ ,<sup>47,53</sup>  $\text{Pt}_n$ ,<sup>48,49,51,52</sup> and  $\text{Pd}_n$ ,<sup>52</sup> nanoclusters 1–10 nm in diameter. Therefore, the ~0.5 eV positive shift of the Ir 4f peaks in the experimental XPS spectrum (at 64.30 and 61.33 eV) with respect to literature values for bulk Ir(0) could be explained by the final state relaxation effect.
- <sup>47</sup> Wertheim, G. K.; DiCenzo, S. B.; Youngquist, S. E. *Phys. Rev. Lett.* **1983**, *51*, 2310–2313.
- <sup>48</sup> Fu, X.; Wang, Y.; Wu, N.; Gui, L.; Tang, Y. *J. Colloid Interface Sci.* **2001**, *243*, 326–330.
- <sup>49</sup> Tu, W.; Takai, K.; Fukui, K.; Miyazaki, A.; Enoki, T. *J. Phys. Chem. B* **2003**, *107*, 10134–10140.
- <sup>50</sup> De Heer, W. A. *Rev. Mod. Phys.* **1993**, *65*, 611–676.
- <sup>51</sup> Eberhardt, W.; Fayet, P.; Cox, D. M.; Fu, Z.; Kaldor, A.; Sherwood, R.; Sondricker, D. *Phys. Rev. Lett.* **1990**, *64*, 780–783.
- <sup>52</sup> Cheung, T. T. P. *Surf. Sci.* **1984**, *140*, 151–164.
- <sup>53</sup> Ohgi, T.; Fujita, D. *Phys. Rev. B* **2002**, *66*, 115410.
- <sup>54</sup> The formally Ir(I) “[ $(1,5\text{-COD})\text{IrH}$ ]<sub>4</sub>” is one reasonable hypothesis for an actual form of initial “Ir<sub>4</sub>” species in this system consistent with the XANES spectra and XPS results (both methods being unable to distinguish unambiguously whether the, mean Ir<sub>~4</sub>, 0.5

---

nm species by XAFS are Ir(I) or Ir(0)). In fact, the previously unknown [(1,5-COD)Ir( $\mu$ -H)]<sub>4</sub> has recently been prepared<sup>13</sup> by us by analogy to the synthesis for the known, formally Rh(I) compound, [(1,5-COD)RhH]<sub>4</sub>.<sup>55</sup> Other known “Ir<sub>4</sub>H<sub>x</sub>” species are [( $\eta^5$ -C<sub>5</sub>Me<sub>5</sub>Ir)<sub>4</sub>H<sub>4</sub>](BF<sub>4</sub>)<sub>2</sub><sup>56</sup> and [Ir<sub>4</sub>H<sub>8</sub>(CO)<sub>4</sub>(PPh<sub>3</sub>)<sub>4</sub>].<sup>42</sup> Additionally, M<sub>4</sub>H<sub>4</sub>-type clusters have been of interest as catalysts (or catalyst precursors) in other systems, often with the metal being Ru or Os.<sup>56,57</sup> Noteworthy here is that the formation,<sup>58</sup> and hydrogenation activity,<sup>59</sup> of oxide-supported, tetrahedral Ir<sub>4</sub> clusters have been studied extensively by Gates and co-workers.

<sup>55</sup> (a) Kulzick, M.; Price, R. T.; Muetterties, E. L.; Day, V. W. *Organometallics* **1982**, *1*, 1256–1258. (b) Duan, Z.; Hampden-Smith, M. J. *Chem. Mater.* **1992**, *4*, 1146–1148.

<sup>56</sup> Cabeza, J. A.; Nutton, A.; Mann, B. E.; Brevard, C.; Maitlis, P. M. *Inorg. Chim. Acta* **1986**, *115*, L47–L48.

<sup>57</sup> (a) Frediani, P.; Matteoli, U.; Bianchi, M.; Piacenti, F.; Menchi, G. *J. Organomet. Chem.* **1978**, *150*, 273–278. (b) Bradley, J. S. *J. Am. Chem. Soc.* **1979**, *101*, 7419–7421. (c) Doi, Y.; Koshizuka, K.; Keii, T. *Inorg. Chem.* **1982**, *21*, 2732–2736. (d) Doi, Y.; Tamura, S.; Koshizuka, K. *J. Mol. Catal.* **1983**, *19*, 213–222. (e) Sánchez-Delgado, R. A.; Andriollo, A.; Puga, J.; Martín, G. *Inorg. Chem.* **1987**, *26*, 1867–1870. (f) Bhaduri, S.; Sharma, K. *J. Chem. Soc., Chem. Commun.* **1988**, 173–174. (g) Bhaduri, S.; Sharma, K.; Mukesh, D. *J. Chem. Soc., Dalton Trans.* **1992**, 77–81. (h) Adams, R. D.; Falloon, S. B. *Organometallics* **1995**, *14*, 4594–4600.

<sup>58</sup> (a) Goellner, J. F.; Guzman, J.; Gates, B. C. *J. Phys. Chem. B* **2002**, *106*, 1229–1238. (b) Li, F.; Gates, B. C. *J. Phys. Chem. B* **2003**, *107*, 11589–11596. (c) Li, F.; Gates, B. C. *J. Phys. Chem. B* **2004**, *108*, 11259–11264. (d) Uzun, A.; Gates, B. C. *Angew. Chem., Int. Ed.* **2008**, *47*, 9245–9248.

<sup>59</sup> (a) Xu, Z.; Xiao, F.- S.; Purnell, S. K.; Alexeev, O.; Kawi, S.; Deutsch, S. E.; Gates, B. C. *Nature* **1994**, *372*, 346–348. (b) Argo, A. M.; Odzak, J. F.; Lai, F. S.; Gates, B. C. *Nature* **2002**, *415*, 623–626.

---

<sup>60</sup> Whetten, R. L.; Khoury, J. T.; Alvarez, M. M.; Murthy, S.; Vezmar, I.; Wang, Z. L.; Stephens, P. W.; Cleveland, C. L.; Luedtke, W. D.; Landman, U. *Adv. Mater.* **1996**, *8*, 428–433.

<sup>61</sup> Khitrov, G. A.; Strouse, G. F. *J. Am. Chem. Soc.* **2003**, *125*, 10465–10469.

<sup>62</sup> Kuzuya, T.; Tai, Y.; Yamamuro, S.; Sumiyama, K. *Chem. Phys. Lett.* **2005**, *407*, 460–463.

<sup>63</sup> Maya, L.; Chen, C. H.; Stevenson, K. A.; Kenik, E. A.; Allman, S. L.; Thundat, T. G. *J. Nanoparticle Res.* **2002**, *4*, 417–422.

<sup>64</sup> Hornstein, B. J.; Finke, R. G. *Chem. Mater.* **2004**, *16*, 139–150.

<sup>65</sup> (a) Besson, C.; Finney, E. E.; Finke, R. G. *J. Am. Chem. Soc.* **2005**, *127*, 8179–8184.

(b) Finney, E. E.; Finke, R. G. *Chem. Mater.* **2008**, *20*, 1956–1970.

<sup>66</sup> Images of catalyst samples *after* their use in hydrogenation were also obtained using bright field TEM. The images can be found in the Supporting Information.

<sup>67</sup> Montejano-Carrizales, J. M.; Morán López, J. L. *Nanostruct. Mater.* **1992**, *1*, 397–409.

<sup>68</sup> MALDI MS experiments were performed directly after the end of catalytic runs, whereas Z-contrast STEM (and XAFS spectroscopy) required  $\geq 2$  days between the end of the catalytic run and analysis (primarily for transit). This difference in procedures could affect the particle sizes measured, which makes some sense; catalyst samples sometimes precipitate a dark brown powder after the end of a catalytic run under standard conditions anyway. The observation of a precipitate suggests that Ir<sub>n</sub> cluster agglomeration or growth processes initiated during catalysis continue post-catalysis. Ultimately, these observations argue against the reliability of precise, *specific* Ir<sub>n</sub> cluster sizes as measured by Z-contrast STEM, MALDI MS, and XAFS spectroscopy, but strongly argue *for* the development of *fcc* Ir(0)<sub>n</sub> Ziegler nanoclusters in this system in general.

---

<sup>69</sup> The details of this structural transformation are currently unknown in this system, although for a report of a similar phenomenon in rhodium particles upon exposure to H<sub>2</sub>, see: Choukroun, R.; De Caro, D.; Chaudret, B.; Lecante, P.; Snoeck, E. *New J. Chem.* **2001**, *25*, 525–527.

<sup>70</sup> Phan, N. T. S.; Van Der Sluys, M.; Jones, C. W. *Adv. Synth. Catal.* **2006**, *348*, 609–679.

<sup>71</sup> Weddle, K. S.; Aiken, J. D.; Finke, R. G. *J. Am. Chem. Soc.* **1998**, *120*, 5653–5666.

<sup>72</sup> Catalyst poisoning by Hg(0) is, by itself, an imperfect test for homogeneity or heterogeneity, as has been pointed out previously.<sup>4b,70</sup> However, it can be useful, especially considering the challenges posed by identifying Ziegler-type hydrogenation catalysts.<sup>3</sup> One concern with the Hg(0) catalyst poisoning test is that, due to the insolubility of Hg(0), it may be difficult to thoroughly contact/react the Hg(0) with all of the catalyst in solution.<sup>4b</sup> This concern was addressed herein by using > 300 equivalents of Hg(0) per Ir each time, and by a series of control experiments showing the 24 h of mixing time allowed was necessary and sufficient for poisoning of these particular catalysts. That effective procedure was followed for each subsequent Hg(0) poisoning experiment.

<sup>73</sup> Two of the three trials using catalysts without aging gave poisoning results similar to that in Figure 13 (i.e., nearly complete poisoning after an initial small H<sub>2</sub> pressure loss). Interestingly, however, even with the  $\geq 300$  equivalents of Hg(0) per Ir used and an identical procedure used in each case, in one of the three trials, the Hg(0) only disturbed the shape of the hydrogenation curve but failed to prevent substrate hydrogenation. The implication is that an initial homogeneous Ir catalyst has at least some resistance to reaction with, or poisoning by, Hg(0) (although, Hg(0) is also believed to be able to poison homogeneous catalysts in some cases<sup>70</sup>). These other Hg(0) poisoning control experiments are shown in the Supporting Information for the interested reader.

<sup>74</sup> Liang, A. J.; Gates, B. C. *J. Phys. Chem. C* **2008**, *112*, 18039–18049.

---

<sup>75</sup> (a) One, of course, never *proves* anything in science, including the form of the catalyst. Bergman's formulation of "Halpern's Guidelines or Rules for Catalysis" apply here—that the observable species are many times not the catalyst.<sup>20</sup> That said, nonpoisoned nanoclusters are a somewhat different case, at least according to all of our knowledge of metal particle catalysis. Restated, any Ir(0)<sub>n</sub> nanocluster that is not poisoned by basic ligands is expected to be a (good hydrogenation) catalyst. This is especially true in the present case, the current Ir/AlEt<sub>3</sub> Lewis acid/cyclohexane catalyst system, where the best (~only) ligands are the cyclohexene and H<sub>2</sub> reactants (i.e., AlEt<sub>3</sub> and cyclohexane being poor "Lewis bases"). Hence, the dominant observable form(s) and sizes of the nanoclusters are expected—and assumed herein if you like—to correlate closely with the dominant catalyst for the present *structure insensitive* hydrogenation reactions. One alternative possibility is that the active catalysts are the result of fragmentation of the observed clusters under catalytic conditions. For example, Gates and co-workers have shown that the nuclearity of *oxide-supported* Rh<sub>n</sub> and Ir<sub>n</sub> species can be reversibly altered on the basis of the composition of an ethylene–H<sub>2</sub> gas mixture to which they are exposed;<sup>58d,74</sup> small M<sub>2–4</sub> cluster species oxidatively fragment to M<sub>1</sub> under ethylene (i.e., catalytic conditions with substrate present) but can reform under H<sub>2</sub>. However, the conditions of those studies (oxide-supported catalysts, gas phase substrate, no solvent) are very different than those employed herein. Another, perhaps more relevant example is the current debate concerning the true catalyst species in Pd-catalyzed coupling reactions such as Suzuki coupling and Heck arylation. There is disagreement as to whether catalysis is affected by the Pd nanoparticles themselves, or by molecular Pd species that fragment from the larger, inactive clusters.<sup>70</sup> In the final analysis, the result of the present study is to present Ir(0)<sub>~40–150</sub> Ziegler-type nanocluster hydrogenation catalysts as the leading hypothesis for future studies of the true catalyst.

<sup>76</sup> For lead references, see the following and references therein: (a) Mondloch, J. E.; Wang, Qi; Frenkel, A. I.; Finke, R. G. *J. Am. Chem. Soc.* **2010**, *132*, 9701–9714. (b) Bayram, E.; Zahmakiran, M.; Özkar, S.; Finke, R. G. *Langmuir* **2010**, *26*, 12455–12464.

<sup>77</sup> Shriver, D. F.; Drezdson, M. A. *The Manipulation of Air-Sensitive Compounds*, 2nd ed.; John Wiley and Sons: New York, 1986.

---

<sup>78</sup> Watzky, M. A.; Finke, R. G. *J. Am. Chem. Soc.* **1997**, *119*, 10382–10400.

<sup>79</sup> Widegren, J. A.; Aiken, J. D., III; Özkar, S.; Finke, R. G. *Chem. Mater.* **2001**, *13*, 312–324.

<sup>80</sup> (a) Newville, M. *J. Synchrotron Radiat.* **2001**, *8*, 322–324. (b) Ravel, B.; Newville, M. *J. Synchrotron Radiat.* **2005**, *12*, 537–541.

Supporting Information for:

**Iridium Ziegler-type Hydrogenation Catalysts Made from [(1,5-COD)Ir( $\mu$ - $O_2C_8H_{15}$ )]<sub>2</sub> and AlEt<sub>3</sub>: Spectroscopic and Kinetic Evidence for the Ir<sub>n</sub> Species Present and for Nanoparticles as the Fastest Catalyst**

William M. Alley, Isil K. Hamdemir, Qi Wang, Anatoly Frenkel, Long Li, Judith C. Yang, Laurent D. Menard, Ralph G. Nuzzo, Saim Özkar, Kimberly Johnson, Richard G. Finke

## Cyclohexene Hydrogenations

### Standard Catalyst Preparation and Cyclohexene Hydrogenation Conditions.

It is known that the hydrogenation activity and other properties of Ziegler–type hydrogenation catalysts can be very sensitive to conditions under which they are both synthesized and used.<sup>1</sup> Therefore, it was important to first establish procedures to be followed for the preparation and study of Ziegler–type hydrogenation catalysts from  $[(1,5\text{-COD})\text{Ir}(\mu\text{-O}_2\text{C}_8\text{H}_{15})]_2$  and  $\text{AlEt}_3$ . The following section contains some of the initial studies pertaining to catalyst preparation. Unless otherwise noted, hydrogenations were conducted using the following experimental conditions: solvent = cyclohexane, temp. = 22.0 °C, catalyst concentration = 0.6 mM in  $[\text{Ir}]$ ,  $\text{Al}/\text{Ir} = 2.0$ , initial cyclohexene concentration = 1.65 M, and stirring rate =  $1000 \pm 10$  rpm.

**Control Experiment Without Added  $\text{AlEt}_3$ .** In a previous control experiment already published elsewhere,<sup>2</sup>  $[(1,5\text{-COD})\text{Ir}(\mu\text{-O}_2\text{C}_8\text{H}_{15})]_2$  was used for cyclohexene hydrogenation *without added  $\text{AlR}_3$* . Hydrogenation activity developed after an induction period, but by the end of the hydrogenation, a black solid precipitate had formed suggesting catalysis by either  $\text{Ir}(0)_n$  nanoclusters, bulk  $\text{Ir}(0)$ , or both. An identical control experiment was repeated for this study with the same results as those reported previously,<sup>2</sup> specifically hydrogenation of cyclohexene occurred after a definite induction period and a black  $\text{Ir}(0)$  precipitate (*vide infra*) formed as the once brown catalyst solution became clear and colorless.

**Method of Fitting Cyclohexene Hydrogenation Kinetic Curves.** In order to compare hydrogenation rates, and because of the shapes of the curves (i.e., in almost all cases the catalysts are immediately active, but the initial rates are not the maximum

rates), initial and maximum (final) rate regimes of the cyclohexene hydrogenation kinetic curves were fit separately by polynomial and linear expressions, respectively, Figure S1. This method of fitting hydrogenation curves was employed both for catalyst solutions used immediately after preparation and those allowed to age for up to 33 hours before use.

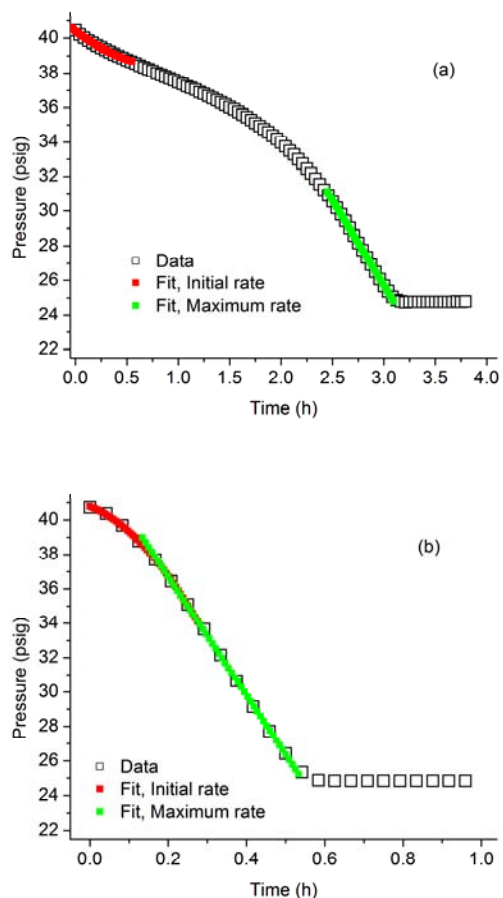


**Figure S1.** Example catalytic cyclohexene hydrogenations and fits of the curves to give initial and maximum rates using  $[(1,5\text{-COD})\text{Ir}(\mu\text{-O}_2\text{C}_8\text{H}_{15})_2]_2$  plus  $\text{AlEt}_3$  catalysts prepared and used under standard conditions (a) without catalyst aging prior to use, and (b) with nine hours aging of the catalyst solution prior to use. Second-order polynomial expressions were used to fit the initial portions (shown in red) and linear fits were used for the maximum rate portions (shown in green).

## Catalyst Aging.

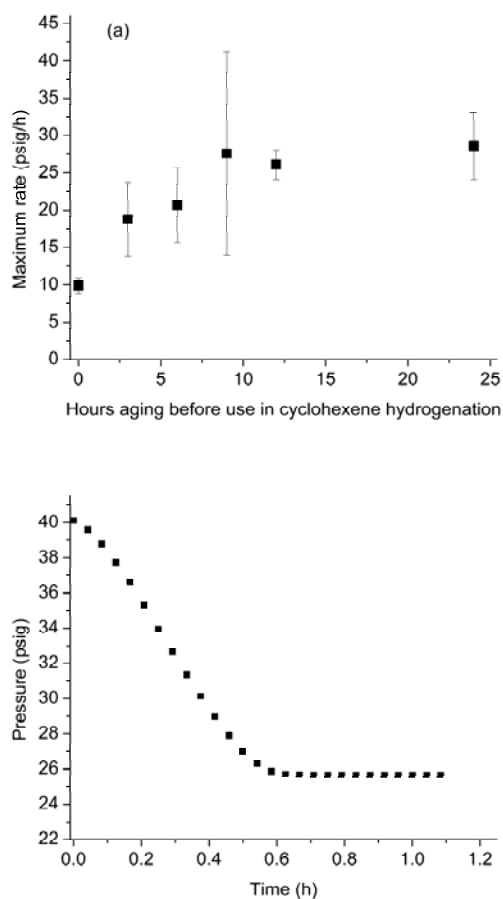


**Figure S2.** (a) Comparison of maximum hydrogenation rates using catalyst solutions with different aging times after initial preparation. Hydrogenation activity approaches a maximum value if prepared catalyst solutions are allowed to stir under  $N_2$  for about 8–24 hours. (b) Example hydrogenation curve with 33 h of aging time before use in hydrogenation. Even with the extended aging time of 33 h, the initial rate is *not* the maximum rate. Therefore, and unless stated otherwise, catalyst solutions were aged in an inert atmosphere ( $N_2$ ) drybox for nine hours before use in catalytic cyclohexene hydrogenations (nine hours being sufficient to achieve the maximum rate seen in Figure S2, part (a)).

### Catalytic Cyclohexene Hydrogenation Curves at Varying Al/Ir Ratios.

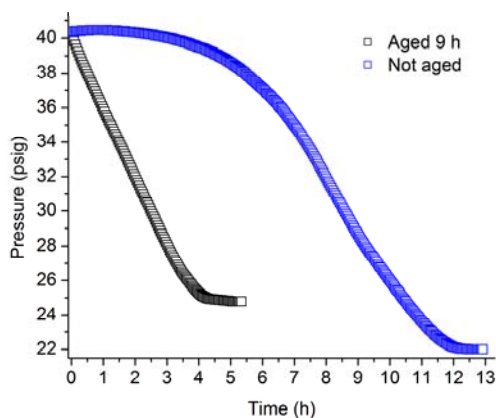


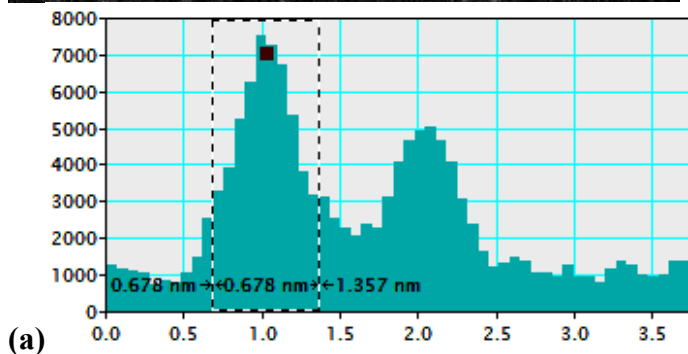
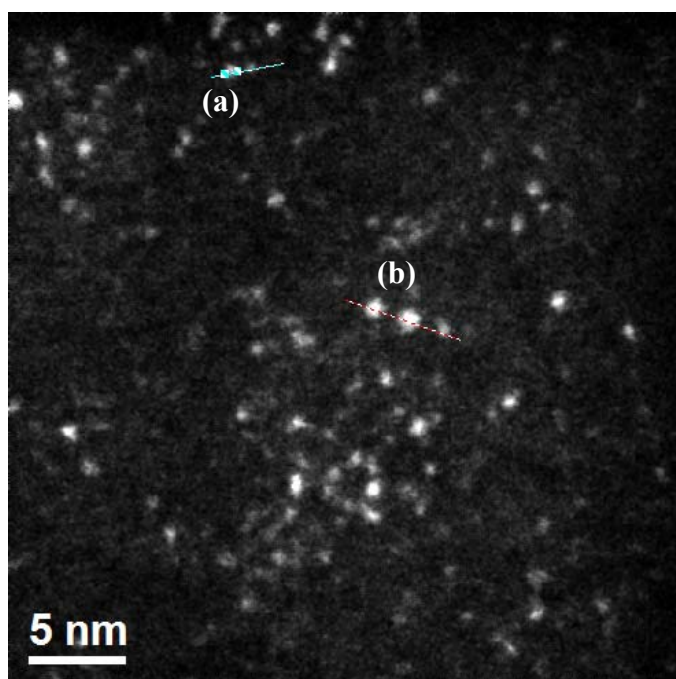
**Figure S3.** The Al/Ir = 5.0 catalyst sample hydrogenation curves, aged for nine hours (black) and non-aged prior to use (blue). When the aged Al/Ir = 5.0 catalyst is used the hydrogenation occurs much more slowly than catalysts with lower Al/Ir ratios, and the curve is essentially linear.

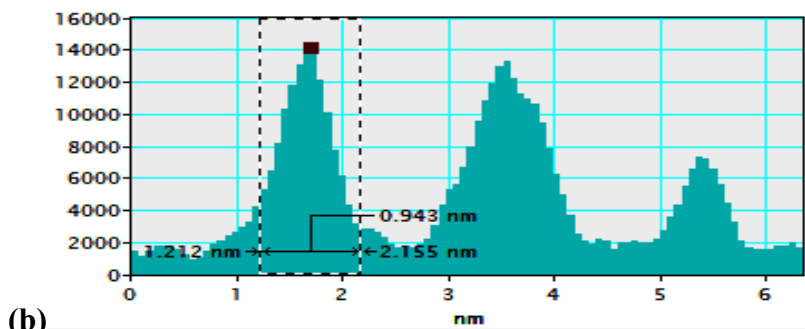
**Table S1.** Mean hydrogenation rates using  $[(1,5\text{-COD})\text{Ir}(\mu\text{-O}_2\text{C}_8\text{H}_{15})_2]$  plus  $\text{AlEt}_3$  catalysts prepared and used without catalyst aging prior to use, and with nine hours aging of the catalyst solution prior to use at a variety of Al/Ir ratios.

Al/Ir	Aging	Mean Initial Rate (psig/hr)	Mean Maximum Rate (psig/hr)
1.0	No	$2.9 \pm 0.4$	$28 \pm 2$
	9 h	$21 \pm 1$	$57 \pm 15$
2.0	No	$5.4 \pm 0.5$	$10 \pm 1$
	9 h	$12 \pm 6$	$31 \pm 14$
3.0	No	$2.2 \pm 0.5$	$6.6 \pm 0.5$
	9 h	$13 \pm 3$	$47 \pm 24$
5.0	No	0	$3.5 \pm 0.4$
	9h	$4.2 \pm 0.4$	$4.2 \pm 0.4$

**Identification of the Ir-containing species in the initial AlEt<sub>3</sub>/Ir catalyst *before* hydrogenation**

**Z-contrast STEM.** The particle size histogram of Ir particle diameters shown in Figure 2 of the main text was created by measuring the FWHM of the intensity profile across 600 Ir particles in a series of images, all at the same levels of magnification and contrast. Intensity profiles were created using Gatan Digital Micrograph; examples are shown in Figure S4.



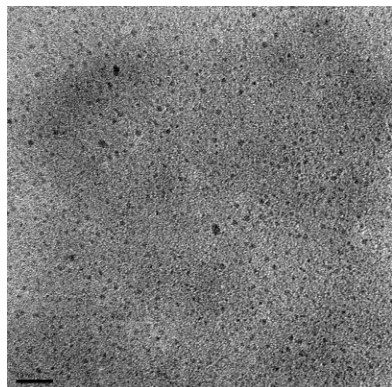


**(b)** **Figure S4.** Example intensity profiles created using Gatan Digital Micrograph, and used to measure Ir particle diameters. Both examples (a) and (b) are typical of the diameter measurement method used; the intensity profiles display clear transitions between particle edge and background despite the fuzzy or diffuse appearance of the particle boundaries in the images themselves. In a case such as this, where particle boundaries appear fuzzy in the images, but are much more clearly defined in the intensity profiles, using FWHM of the intensity profiles is an effective diameter measurement method. The histogram in Figure 2 of the main text is created from the diameters of 600 particles measured in this fashion. Of those 600 particles measured, some relatively larger Ir particles, with diameters approaching or even larger than one nm were observed. These particles were measured and included in the histogram, as shown in example (b) of this Figure, and in Figure 2 of the main text. Particles larger than those represented in the histogram in Figure 2 were not observed in any of the Z-contrast STEM images obtained; the histogram in Figure 2 is statistically representative of the sample images.

**Bright field TEM.** Sample solutions for bright-field TEM were prepared (at Colorado State University) by first diluting with cyclohexane 0.1 mL of a catalyst solution not used in cyclohexene hydrogenation,  $[\text{Ir}] = 1.44 \text{ mM}$ , to 0.6 mL in a 5 mL glass vial. Catalyst samples after hydrogenation (vide infra),  $[\text{Ir}] = 1.2 \text{ mM}$ , were prepared by the same method. TEM grids (ultrathin carbon film on a holey carbon support, Ted Pella, Inc.) were then immersed into a sample solution, and dried under an  $\text{N}_2$  atmosphere in the drybox for  $\sim 1$  min. The grids were then placed in 5-mL glass vials, sealed, and sent to Dr. JoAn Hudson at Clemson University for imaging at  $\geq 0.5\text{M}$  magnification on a Hitachi H7600T operated at 120 kV. Particle sizes were measured manually. The Al/Ir = 2.0 catalyst sample before hydrogenation was imaged on a SiO

grid (particle sizes determined by TEM on SiO or holey carbon-coated grids were found to be the same within experimental error, vide infra, Figure S30).

Images were obtained of  $[(1,5\text{-COD})\text{Ir}(\mu\text{-O}_2\text{C}_8\text{H}_{15})]_2$  plus  $\text{AlEt}_3$ ,  $\text{Al}/\text{Ir} = 2.0$ , catalyst samples before their use in hydrogenation. An example image of the  $\text{Al}/\text{Ir} = 2.0$  catalyst before hydrogenation and corresponding particle size histogram show the presence of nanoclusters with a mean diameter of  $1.1 \pm 0.3 \text{ nm}$  ( $1\sigma$ ), Figure S5, which corresponds to  $\text{Ir}(0)_{\sim 55}$  nanoclusters assuming a close-packed structure. An example TEM image of the  $[(1,5\text{-COD})\text{Ir}(\mu\text{-O}_2\text{C}_8\text{H}_{15})]_2$  precatalyst alone, collected as a control experiment, Figure S6, contains dark spots that may be clusters of Ir formed under the TEM beam or artifacts of the image background.<sup>3</sup> The larger mean size measured using bright field TEM as compared to the mean sizes measured using other methods may be explained by the inability to distinguish and measure particles with diameters of  $<1 \text{ nm}$  in TEM images, thereby demonstrating the value of the multiple-physical-methods approach used herein.



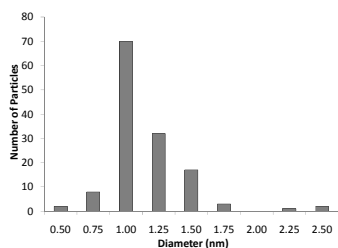


**Figure S5.** An example TEM image and particle size histogram of the  $[(1,5\text{-COD})\text{Ir}(\mu\text{-O}_2\text{C}_8\text{H}_{15})_2 + \text{AlEt}_3, \text{Al}/\text{Ir} = 2.0$ , catalyst before use in hydrogenation. The mean diameter is  $1.1 \pm 0.3$  nm from counting 135 clusters in this image (scale bar = 10 nm), corresponding, for the sake of illustration, to roughly  $\text{Ir}(0)_{\sim 55}$  assuming close-packed  $\text{Ir}(0)$ .

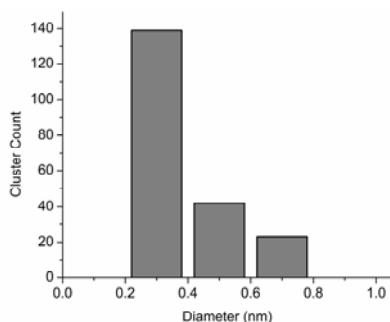
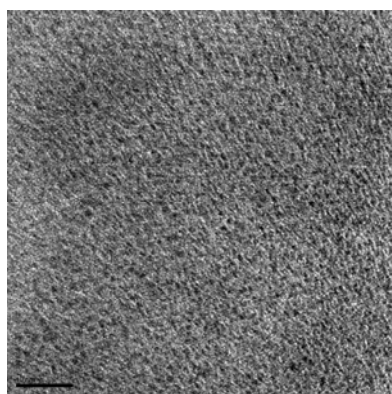


**Figure S6.** An example TEM image and apparent particle-size histogram of  $[(1,5\text{-COD})\text{Ir}(\mu\text{-O}_2\text{C}_8\text{H}_{15})_2$ , precursor solution in cyclohexane on holey carbon-coated TEM grid, scale bar = 10 nm. The dark spots may be Ir clusters formed under the TEM beam or, as seems more likely based on the histogram shown, artifacts of the background. Therefore, as was explained in the main text, bright-field TEM was deemphasized in this study. The Z-contrast results were instead used as the primary microscopic evidence in the main text.

**HRTEM.** Attempts to analyze samples of the catalyst before hydrogenation using HRTEM did not yield high quality images, an example is shown in Figure S7. The reasons for the poor HRTEM imaging of these samples can be understood in light of the findings from Z-contrast microscopy and XAFS. The large majority of Ir clusters in samples before hydrogenation are of sub-nanometer dimensions whereas the ultrathin carbon film upon which they are deposited for microscopy is ~3 nm thick. HRTEM imaging is based on phase contrast, and the resulting image contrast is influenced by the atomic periodicity of the sample.<sup>4</sup> One can picture how an overlay of sub-nm Ir clusters, nm-scale Ir clusters with significant Ir–Ir bond length disorder (and thus significant atomic aperiodicity, see the main text), and a 3-nm thick carbon film can result in an HRTEM image with poor contrast. In short, XAFS shows there are no crystalline Ir particles in samples before hydrogenation (within the detection limits), and this is consistent with the inability to obtain a useful quality HRTEM image.

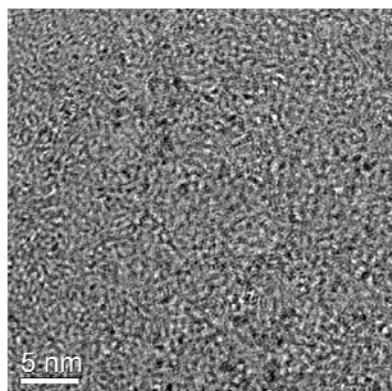


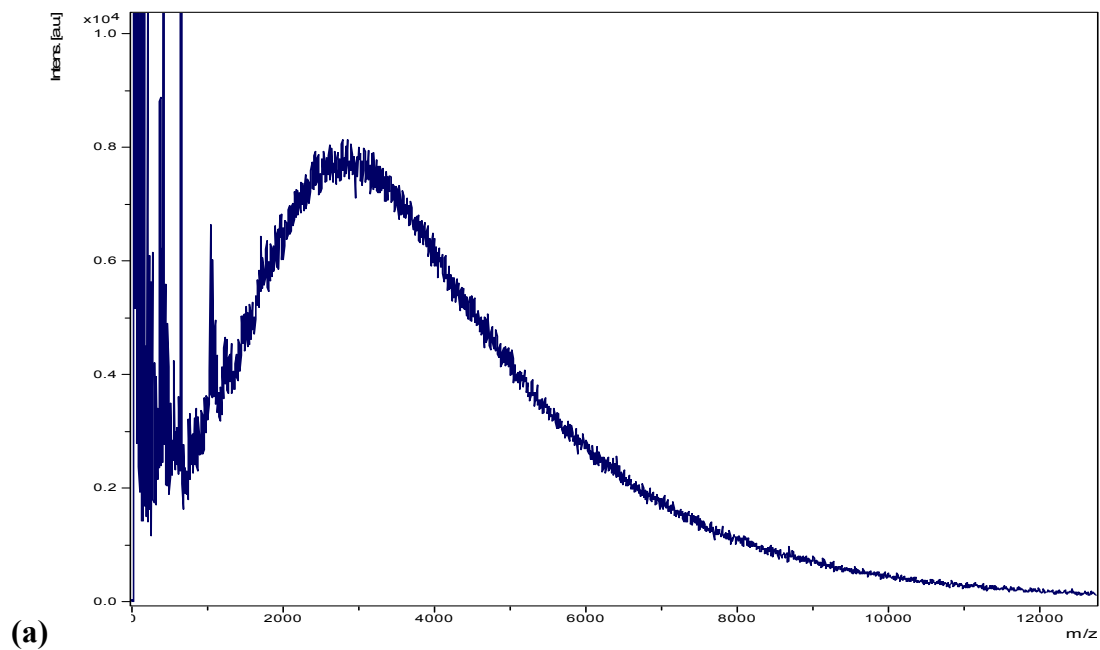
**Figure S7.** HRTEM of the [(1,5-COD)Ir( $\mu$ -O<sub>2</sub>C<sub>8</sub>H<sub>15</sub>)]<sub>2</sub> plus AlEt<sub>3</sub>, Al/Ir = 2.0, catalyst before use in hydrogenation. The poor image contrast is consistent with a lack of periodicity in nanometer scale Ir clusters in the sample.

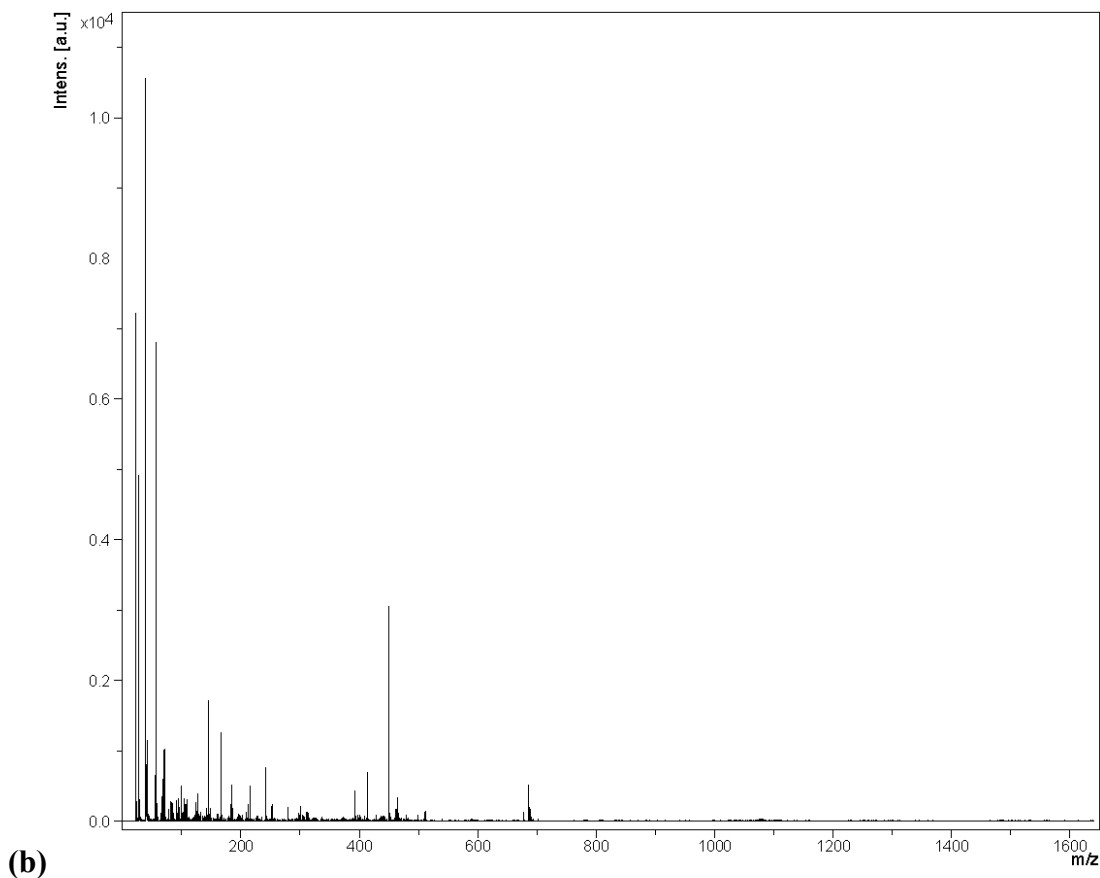
**MALDI MS of the [(1,5-COD)Ir( $\mu$ -O<sub>2</sub>C<sub>8</sub>H<sub>15</sub>)]<sub>2</sub> plus AlEt<sub>3</sub> catalyst, Al/Ir = 2.0, before its use in hydrogenation.** A 0.5  $\mu$ L, 100 mM NaI ionizing agent solution in water was prepared and hand-spotted on an MS sample plate with a pipette and air-dried.

Next, a 1  $\mu\text{L}$ , 100 mM suspension of graphite powder (Sigma-Aldrich, <20 micron) was applied as a suspension in cyclohexane over the ionizing agent spot using a pipette and air-dried (i.e., the dried-droplet method). The plate was transferred into the drybox. Sample solutions (1  $\mu\text{L}$ ,  $[\text{Ir}] = 1.44 \text{ mM}$ ) were applied onto the spot where ionizing agent and matrix had been previously deposited. The plate was then covered with its plastic capping plate and placed into a desiccator, which was sealed and brought out of the drybox. The plate was transferred in air (~30 sec. exposure) from the desiccators to the vacuum chamber of the MALDI-MS instrument, and MALDI-MS spectra were taken immediately thereafter. Mass spectra were obtained at CSU on a Bruker Ultraflex TOF-TOF instrument in reflectron mode, with acceleration voltage at 25 kV, and in positive ion mode. A nitrogen laser ( $\lambda = 337 \text{ nm}$ ) with a 3 ns pulse width was focused over a 1 mm diameter spot. Data were collected with the highest laser power possible, for a higher S/N, but which still maximized resolution and avoided sample fragmentation. Calibration was done using Bradykinin, Angiotensin\_I, Angiotensin\_II, Substance\_P, Bombesin, Renin\_Substrate, ACTH\_clip and Somatostatin (purchased as a mixture of all these peptides from Bruker-Daltonics). Experimental spectra are shown in Figure S8, and a control experiment performed using THAP (2'-4'-6'-trihydroxyacetophenone, Aldrich, 98%) as an alternative matrix, Figure S9a, gives virtually the same results as when graphite is used as the matrix. Solid THAP was stored and used outside of the drybox, and applied as an aqueous solution.

The full spectrum from MALDI MS of the  $[(1,5\text{-COD})\text{Ir}(\mu\text{-O}_2\text{C}_8\text{H}_{15})]_2$  plus  $\text{AlEt}_3$ , catalyst before its use in hydrogenation,  $\text{Al}/\text{Ir} = 2.0$ , is shown in Figure S8a. It exhibits a broad peak extending from 0-10000  $m/z$ , and that tails off towards higher  $m/z$ .

A high resolution spectrum of the low  $m/z$  region ( $m/z = 0-1600$ ) of the same sample solution applied onto the same spot was also collected, Figure S8b. The lack of characteristic Ir isotope peak distributions in the high resolution spectrum from 0-1000  $m/z$  rules out the presence of Ir atoms in these species.

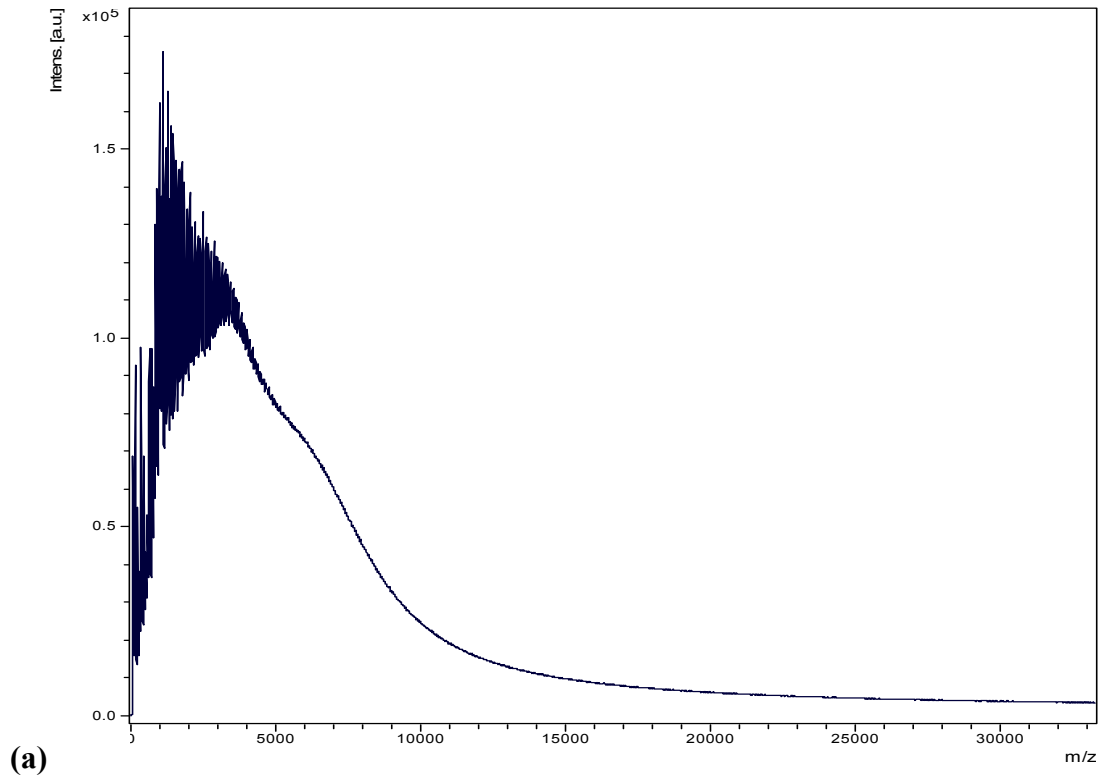


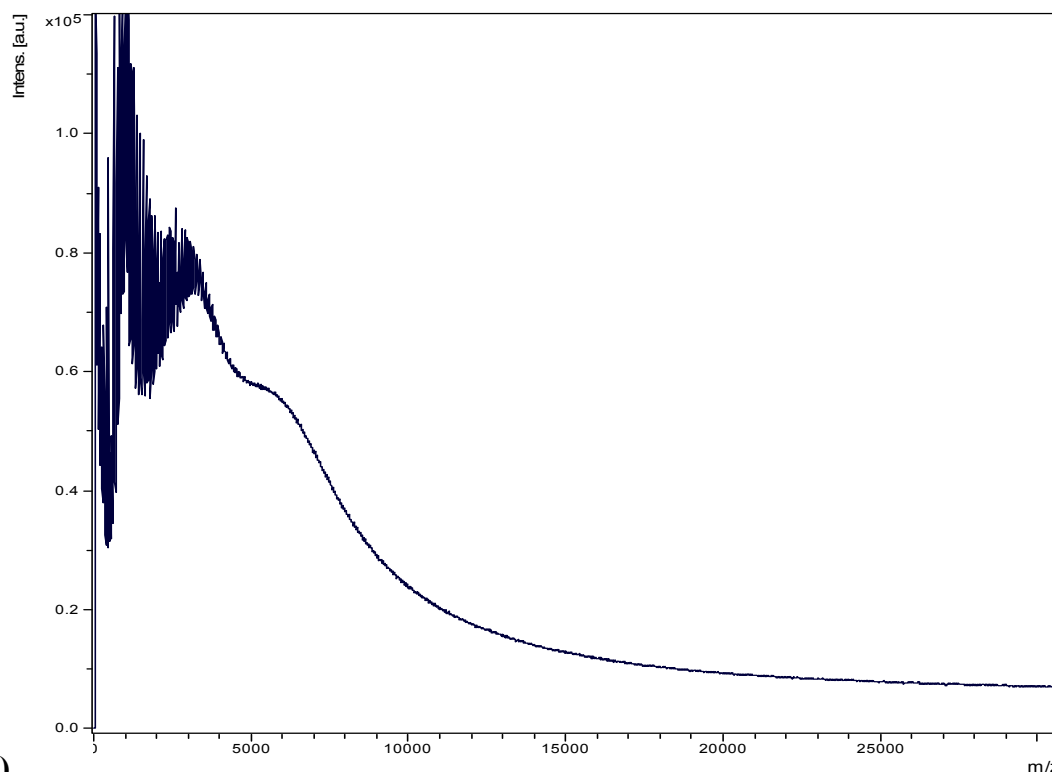


**Figure S8.** (a) The full MALDI-TOF mass spectrum of the [(1,5-COD)Ir( $\mu$ -O<sub>2</sub>C<sub>8</sub>H<sub>15</sub>)<sub>2</sub>] plus AlEt<sub>3</sub> catalyst, Al/Ir = 2.0, before hydrogenation. (b) A high resolution spectrum of the low m/z region (m/z = 0–1600) of the same sample. The lack of characteristic Ir isotope peak distributions rules out the presence of Ir atoms in this m/z = 0–1600 spectrum.

Two assumptions are required to calculate the number of Ir atoms in Ir<sub>n</sub> clusters from the MALDI mass spectra in Figure S8a. The first assumption is that (i) the ions forming the broad peaks are composed of only Ir atoms (i.e., that the Ir clusters and their stabilizers have been separated during the desorption process, a precedented assumption,<sup>5,6,7</sup> consistent with the presence of peaks lacking Ir in the 0-1000 m/z region of high resolution spectra, Figure S8b). The second assumption is that (ii) the charge of the observed ions is +1, a common assumption in the literature.<sup>5,7,8</sup> The diameter of Ir<sub>n</sub> clusters was estimated from the number of Ir atoms as described in the main text.<sup>9,10</sup>

Significantly, the results of MALDI MS are consistent with the Z-contrast STEM results in showing a sub-nanometer estimated mean  $\text{Ir}_n$  cluster diameter and broad size distribution.





**(b)** **Figure S9.** (a) The MALDI MS of the  $[(1,5\text{-COD})\text{Ir}(\mu\text{-O}_2\text{C}_8\text{H}_{15})]_2$  plus  $\text{AlEt}_3$ ,  $\text{Al}/\text{Ir} = 2$ , catalysts before use in hydrogenation using THAP (trihydroxyacetophenone) as the matrix instead of graphite. The resulting Ir nanocluster size from this spectrum is approximately the same within experimental error as the result when graphite was used as the matrix. (b) The MALDI MS of the  $[(1,5\text{-COD})\text{Ir}(\mu\text{-O}_2\text{C}_8\text{H}_{15})]_2$  plus  $\text{AlEt}_3$ ,  $\text{Al}/\text{Ir} = 2$ , catalyst *after* use in hydrogenation, also obtained using THAP as the matrix instead of graphite, reveals a shift towards larger diameter Ir clusters.

**XAFS Spectroscopy.** Additional XAFS spectra and detailed fitting results for standards and reference compounds are given below. The value for the passive electron reduction factor ( $S_0^2 = 0.84 \pm 0.04$ ) was determined from the fit to the Ir black standard, verified using the fit to the  $\text{Ir}_4(\text{CO})_{12}$  sample, and applied for fitting the other sample spectra.

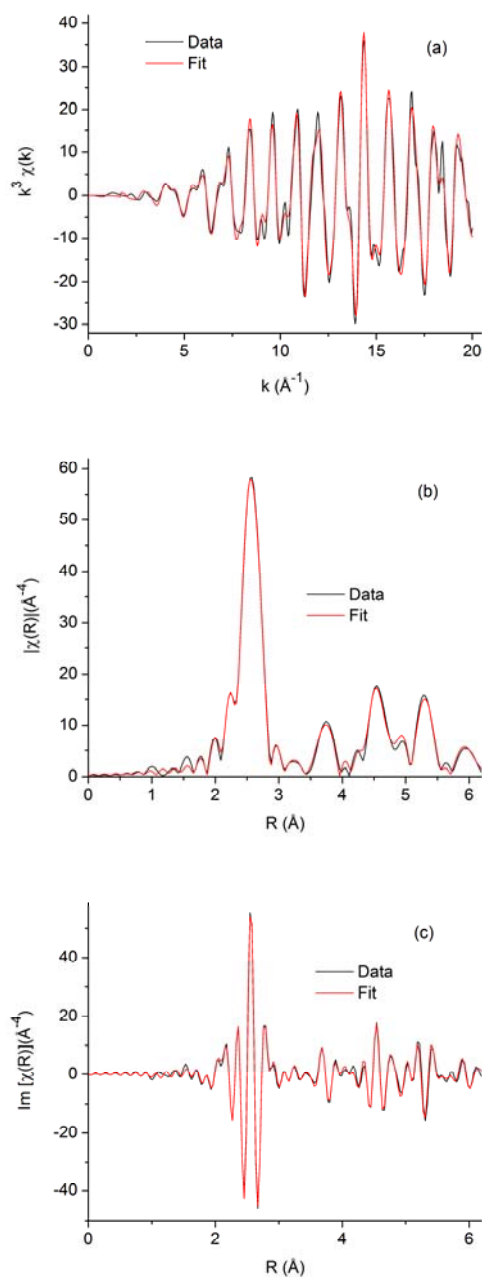


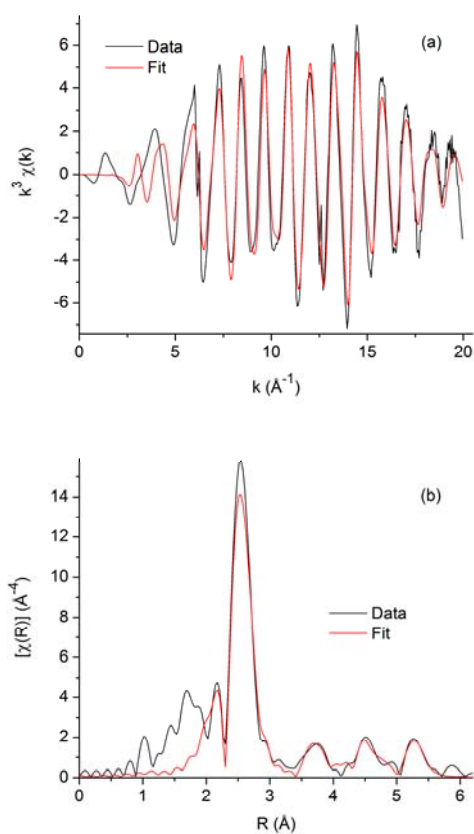
**Figure S10.** Experimental data and fit for the XAFS spectrum of the Ir black standard using the theory of *fcc* bulk Ir plotted as  $\chi(k)$  (a), and the magnitude (b) and imaginary part (c) of the Fourier Transform (FT) ( $k$ -range for FT = 2–19.49).

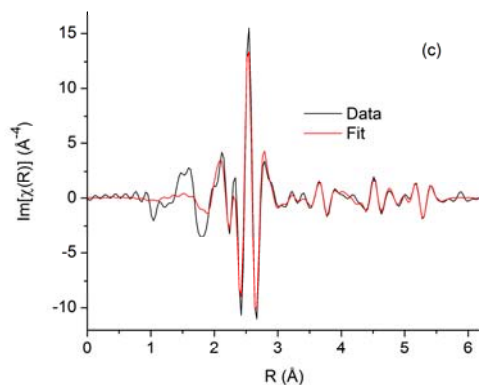
**Table S2.** Fit results for Ir black including triangular (TR) and co-linear (CL) scattering paths. Values of  $N$  were fixed so that a value for the passive electron reduction factor ( $S_0^2 = 0.84 \pm 0.04$ ) could be determined and applied for fitting sample spectra.  $\Delta E_0 = 10.5 \pm 0.5$  eV.  $k$ -weighting and  $R$ -range used for the fit are  $k^3$  and 1.0–6.2, respectively.

Path	N	R <sub>eff</sub> (Å)	R (Å)	$\sigma^2 \times 10^3$ (Å <sup>2</sup> )
SS1	12	2.7147	2.711 ± 0.001	3.5 ± 0.1
SS2	6	3.8392	3.833 ± 0.001	4.4 ± 0.3
SS3	24	4.7020	4.695 ± 0.002	4.3 ± 0.3
TR3,1	96	5.0657	5.058 ± 0.002	2.9 ± 0.7
SS4	12	5.4294	5.421 ± 0.002	4.3 ± 0.2
CL4,1	24	5.4294	5.421 ± 0.002	4.3 ± 0.2
CL1,[+],1	12	5.4294	5.421 ± 0.002	4.3 ± 0.2
CL1,4,1	12	5.4294	5.421 ± 0.002	4.3 ± 0.2
SS5	24	6.0703	6.061 ± 0.002	6.6 ± 0.6

*Synthesis and isolation of HPO<sub>4</sub>-stabilized fcc Ir(0) nanoclusters.* HPO<sub>4</sub>-stabilized fcc Ir(0)<sub>n</sub> nanoclusters were synthesized according to the literature procedure previously described.<sup>11</sup> In the drybox at Colorado State University, 0.576 mL of a 1.0 M solution of Bu<sub>4</sub>NOH in methanol (Aldrich, opened fresh before use and stored in a refrigerator) was added to 97.6 mg (0.288 mmol) of (Bu<sub>4</sub>N)H<sub>2</sub>PO<sub>4</sub> (Aldrich, 97%, used as received). The two were mixed, the solvent was removed in vacuo, and diluted to 100 mL with acetone (Burdick and Jackson, H<sub>2</sub>O ≤ 0.32%, purged with Ar for ≥ 20 minutes before transferring into the drybox) to make a 2.88 mM (Bu<sub>4</sub>N)<sub>2</sub>HPO<sub>4</sub> solution. Next, 10.0 mL of this solution was added to 13.5 mg (28.8 μmol) of [(1,5-COD)Ir(NCCH<sub>3</sub>)<sub>2</sub>]BF<sub>4</sub>, (prepared according to the literature procedure for the analogous PF<sub>6</sub><sup>-</sup> salt,<sup>12</sup> and characterized by NMR,<sup>11</sup> courtesy of Chris Graham at Colorado State University) and 9.2 mg (42.9 μmol) of Proton Sponge (1,8-

bis(dimethylamino)naphthalene, Aldrich, 99%, used as received) giving a clear yellow solution. Multiple 2.5 mL portions of this solution and another batch prepared the same way were used in the hydrogenation of cyclohexene (same general procedure as already described), resulting in dark brown solutions, which were collected and dried in vacuo to give enough dark brown powder for analysis by XAFS as an *fcc* Ir(0) nanocluster standard.<sup>11b</sup>

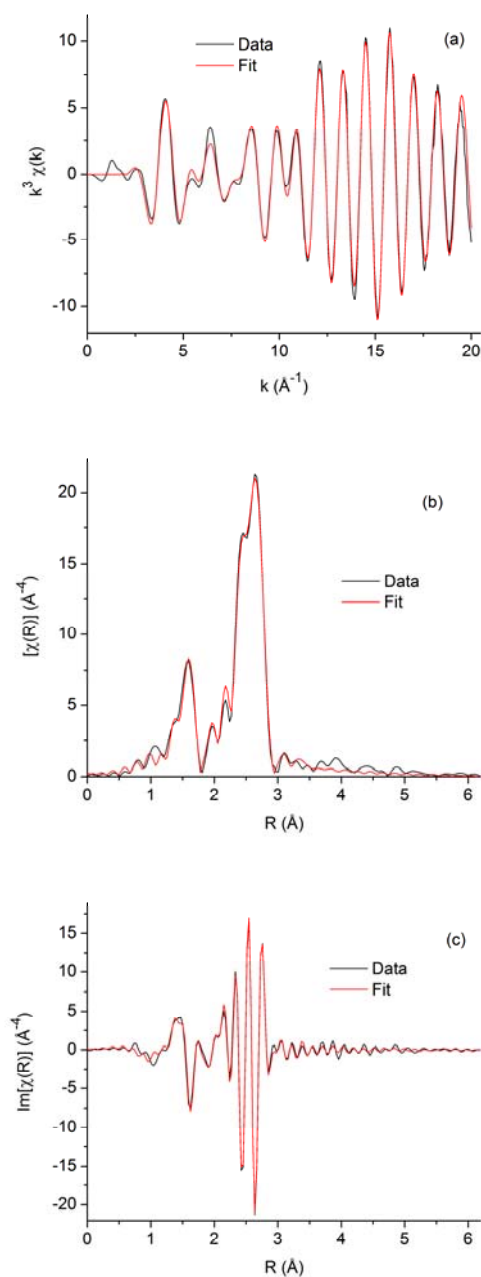




**Figure S11.** Experimental data and fit for the XAFS spectrum of the  $\text{HPO}_4$ -stabilized *fcc*  $\text{Ir}(0)_n$  nanoclusters standard<sup>11</sup> using the theory of *fcc* bulk Ir in a  $\chi(k)$  plot (a), and the magnitude (b) and imaginary part (c) of the FT ( $k$ -range for FT = 2–19.49).

**Table S3.** Fit results for *fcc*  $\text{Ir}(0)_n$  nanoclusters,  $\Delta E_0 = 10.6 \pm 0.8$ . The SS1 value of  $7 \pm 1$  suggests nanoclusters with a mean diameter of  $0.9 \pm 0.2$  nm, which is smaller than the TEM-determined literature value of  $1.8 \pm 0.4$  nm.<sup>11b</sup> This discrepancy may be explained by the inability to include  $<1.0$  nm clusters in the size calculation based on TEM alone,<sup>11b</sup> consistent with the findings herein.  $K$ -weighting and  $R$ -range used for the fit are  $k^3$  and 1.0–5.6, respectively.

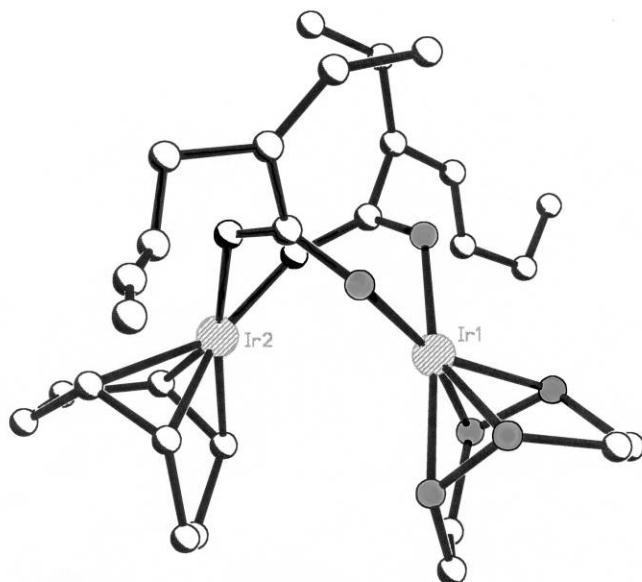
Path	N	$R_{\text{eff}}$ (Å)	R (Å)	$\sigma^2 \times 10^3$ (Å <sup>2</sup> )
SS1	$7 \pm 1$	2.7147	$2.687 \pm 0.004$	$5.7 \pm 0.4$
SS2	$2.2 \pm 0.6$	3.8392	$3.814 \pm 0.006$	$6.5 \pm 0.9$
SS3	$5 \pm 1$	4.7020	$4.682 \pm 0.006$	$7.1 \pm 0.8$
SS4; CL4,1; CL1,4,1	$1.8 \pm 0.4$	5.4294	$5.389 \pm 0.006$	$6.8 \pm 0.7$



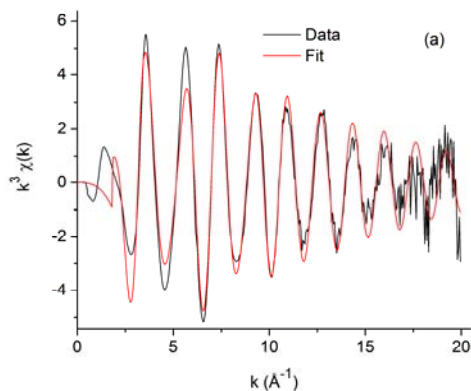
**Figure S12.** Experimental data and fit for the XAFS spectra of the  $\text{Ir}_4(\text{CO})_{12}$  standard using the crystal structure<sup>13</sup> of  $\text{Ir}_4(\text{CO})_{12}$  in a  $\chi(k)$  plot (a), and the magnitude (b) and imaginary part (c) of the FT (k-range for FT = 2–19.49).

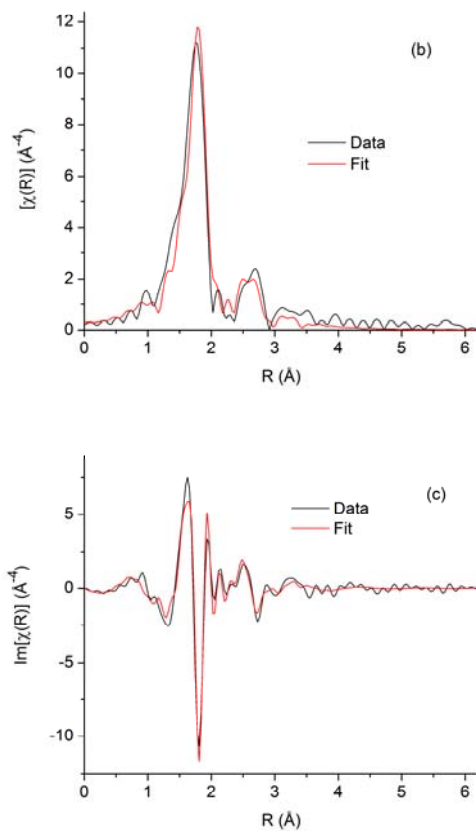
**Table S4.** Fit results for  $\text{Ir}_4(\text{CO})_{12}$ , N values were fixed so that an independent value of  $S_0^2$  could be determined ( $S_0^2 = 0.87 \pm 0.05$ , the same within experimental error as determined from the fit of Ir black). In addition,  $\Delta E_0 = 14.7 \pm 0.5$  eV. K-weighting and R-range used for the fit are  $k^2$  and 1.0–3.05, respectively.

Path	N	$R_{\text{eff}}$ (Å)	R (Å)	$\sigma^2 \times 10^3$ (Å <sup>2</sup> )
Ir-C	3	1.9539	$1.929 \pm 0.006$	$2.2 \pm 0.7$
Ir-Ir	3	2.6887	$2.689 \pm 0.002$	$2.7 \pm 0.1$
Ir-O	12	3.0932	$3.075 \pm 0.006$	$2.7 \pm 0.6$



**Figure S13.** The crystal structure of  $[(1,5\text{-COD})\text{Ir}(\mu\text{-O}_2\text{C}_8\text{H}_{15})]_2$  published previously.<sup>2</sup> The oxygen atoms from the two bridging 2-ethylhexanoate ligands are at nearly the same distance from Ir1 as the four olefinic carbon atoms. Since XAFS cannot distinguish between these relatively light scatterers, these six atoms were approximated as a single scattering shell, designated Ir–X (shaded atoms).

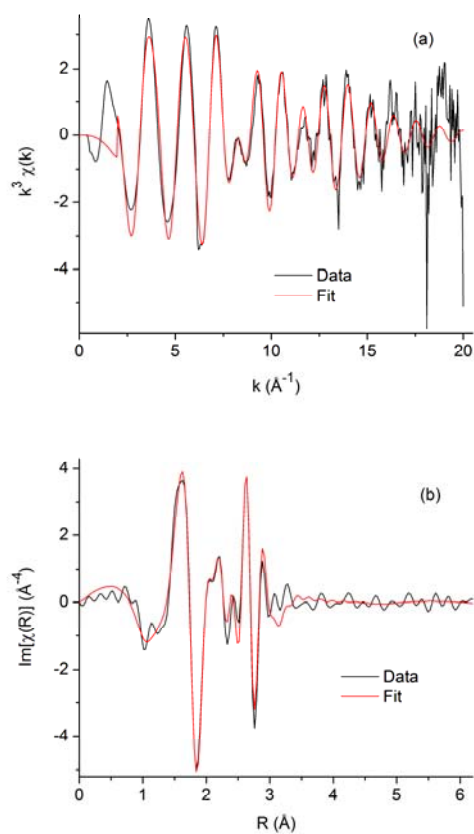




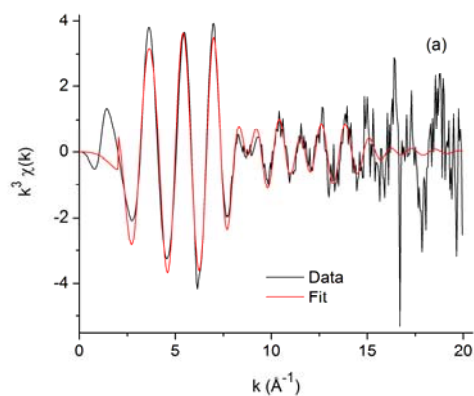
**Figure S14.** Experimental data and fit for the XAFS spectra of the [(1,5-COD)Ir( $\mu$ -O<sub>2</sub>C<sub>8</sub>H<sub>15</sub>)<sub>2</sub>] precatalyst using the published crystal structure<sup>2</sup> in a  $\chi(k)$  plot (a), and the magnitude (b) and imaginary part (c) of the FT (k-range for FT = 3–18.5).

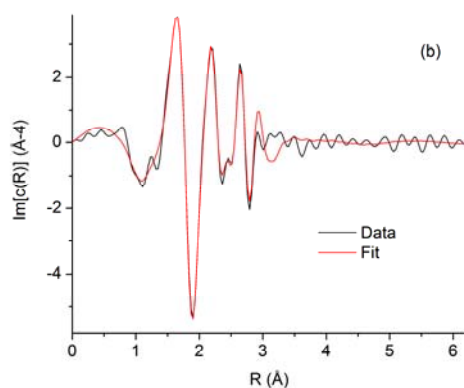
**Table S5.** Fit results for [(1,5-COD)Ir( $\mu$ -O<sub>2</sub>C<sub>8</sub>H<sub>15</sub>)<sub>2</sub>], N values were fixed,  $\Delta E_0$  (eV) =  $12.5 \pm 0.8$ . K-weighting and R-range used for the fit are  $k^2$  and 1.0–3.5, respectively.

Path	N	$R_{\text{eff}}$ (Å)	R (Å)	$\sigma^2 \times 10^3$ (Å <sup>2</sup> )
Ir-X	6	2.0848	$2.109 \pm 0.006$	$2.0 \pm 0.4$
Ir-C	6	3.0039	$3.03 \pm 0.03$	$9 \pm 4$
Ir-Ir	1	3.2769	$3.4 \pm 0.2$	$12 \pm 18$

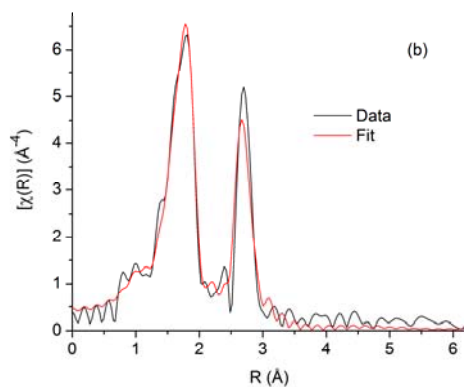
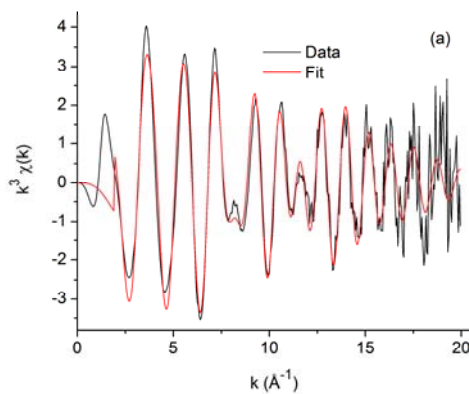


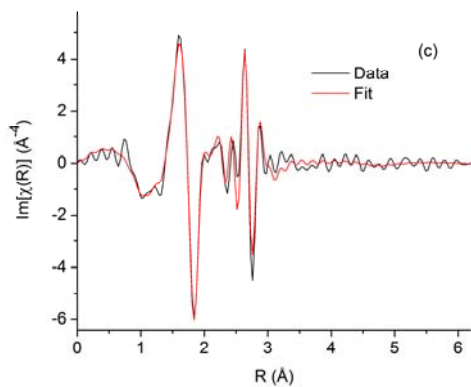
**Figure S15.** Experimental data and fit for the XAFS spectra of the of the AlEt<sub>3</sub>/Ir = 1.0 catalyst sample spectra in a  $\chi(k)$  plot (a) and the imaginary part of the FT (b). The magnitude of the FT is shown in Figure 5a of the main text ( $k$ -range for FT = 2–17).  $k$ -weighting and  $R$ -range used for the fit are  $k^3$  and 1.0–3.0, respectively.



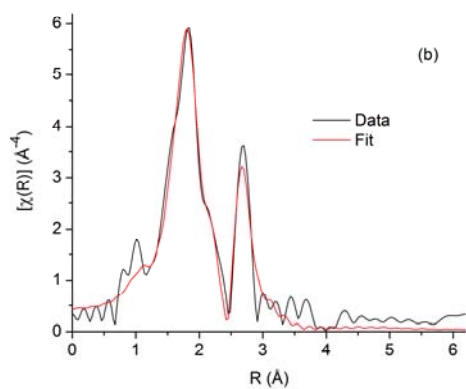
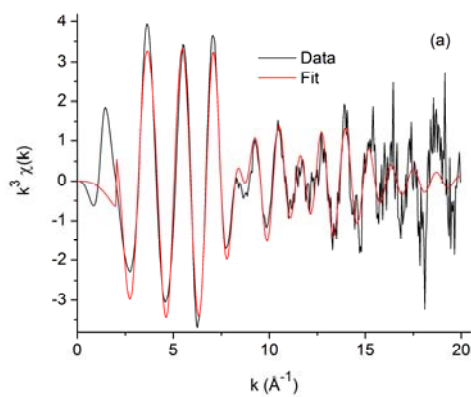


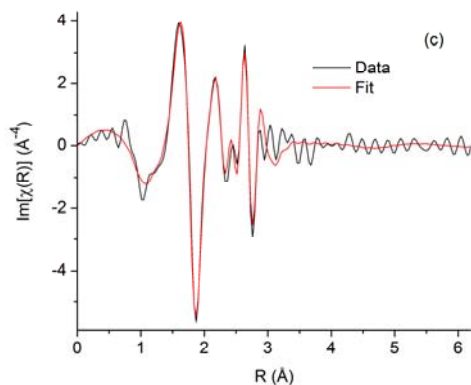
**Figure S16.** Experimental data and fit for the XAFS spectra of the of the  $\text{AlEt}_3/\text{Ir} = 2.0$  catalyst sample spectra in a  $\chi(k)$  plot (a) and the imaginary part of the FT (b). The magnitude of the FT is shown in Figure 5b of the main text ( $k$ -range for FT = 2–16).  $k$ -weighting and  $R$ -range used for the fit are  $k^3$  and 1.26–3.03, respectively.



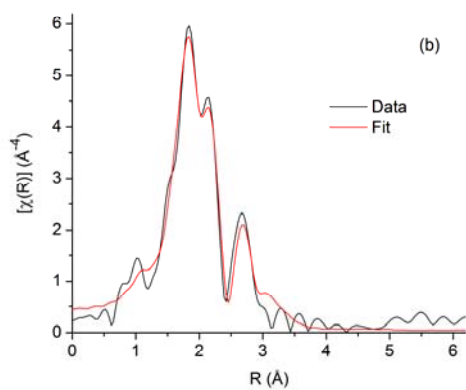
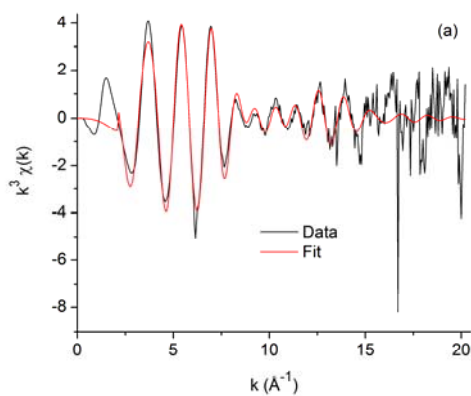


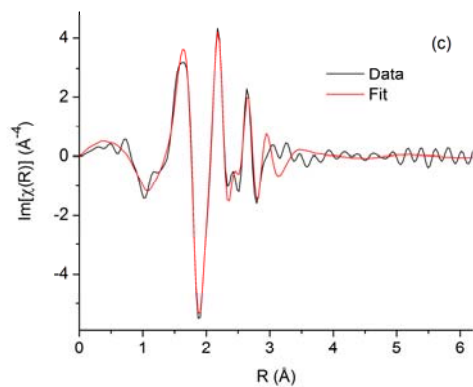
**Figure S17.** Experimental data and fit for the XAFS spectra of the AlEt<sub>3</sub>/Ir = 0.5 catalyst sample in a  $\chi(k)$  plot (a), and the magnitude (b) and imaginary part (c) of the FT (k-range for FT = 2–18.5). K-weighting and R-range used for the fit are  $k^3$  and 1.0–3.0, respectively.



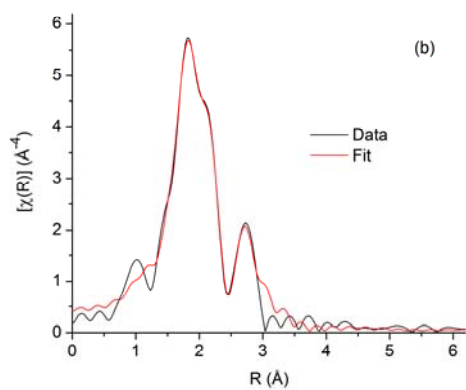
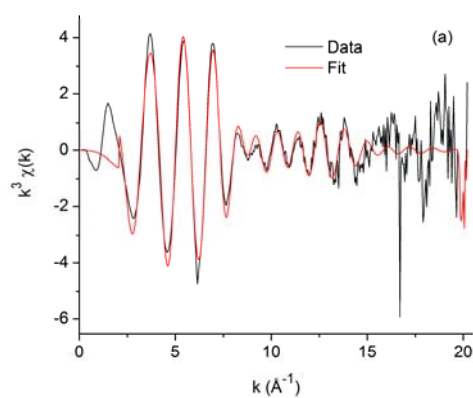


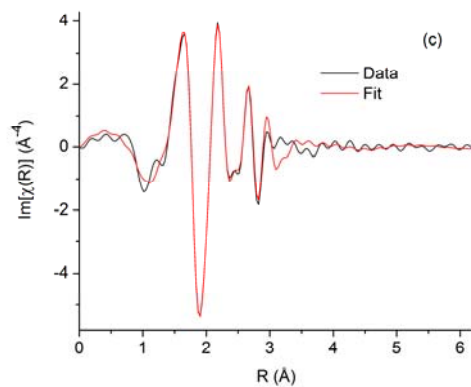
**Figure S18.** Experimental data and fit for the XAFS spectra of the AlEt<sub>3</sub>/Ir = 1.5 catalyst sample in a  $\chi(k)$  plot (a), and the magnitude (b) and imaginary part (c) of the FT (k-range for FT = 2–18). K-weighting and R-range used for the fit are  $k^3$  and 1.0–3.0, respectively.



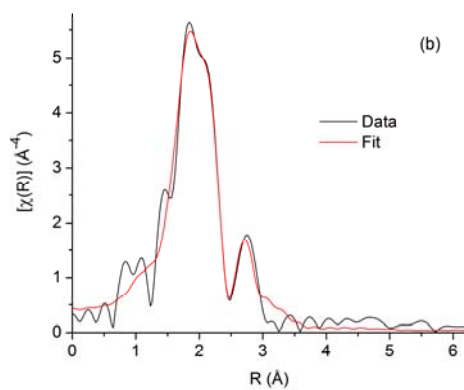
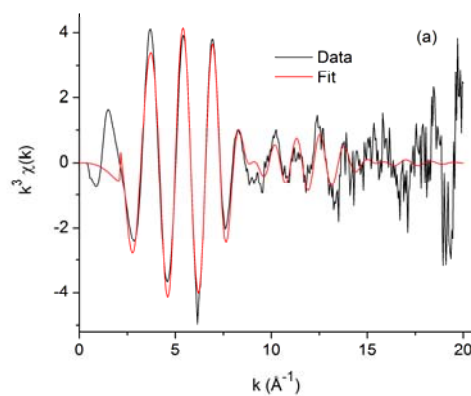


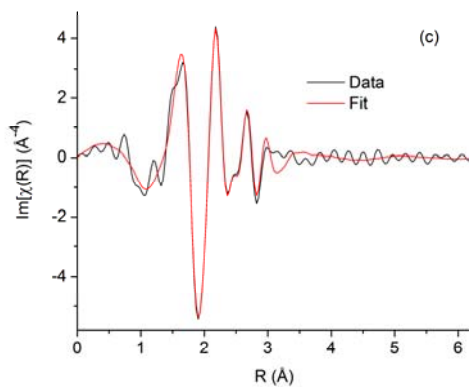
**Figure S19.** Experimental data and fit for the XAFS spectra of AlEt<sub>3</sub>/Ir = 2.5 catalyst sample in a  $\chi(k)$  plot (a), and the magnitude (b) and imaginary part (c) of the FT (k-range for FT = 2–16). K-weighting and R-range used for the fit are  $k^3$  and 1.0–3.0, respectively.



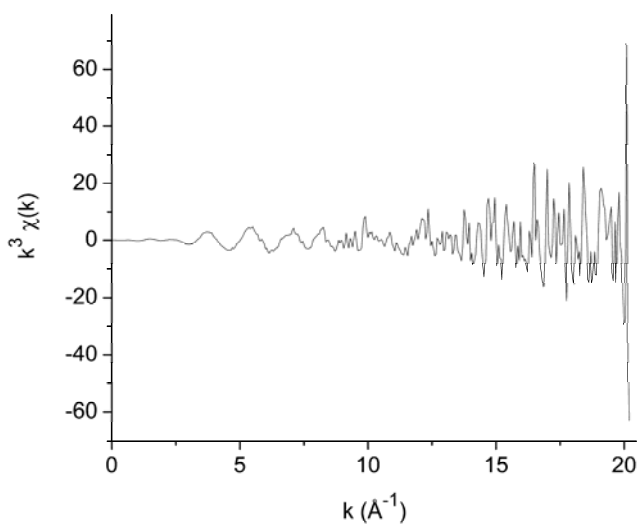


**Figure S20.** Experimental data and fit for the XAFS spectra of AlEt<sub>3</sub>/Ir = 3.0 catalyst sample in a  $\chi(k)$  plot (a), and the magnitude (b) and imaginary part (c) of the FT (k-range for FT = 2–14). K-weighting and R-range used for the fit are  $k^3$  and 1.26–3.0, respectively.

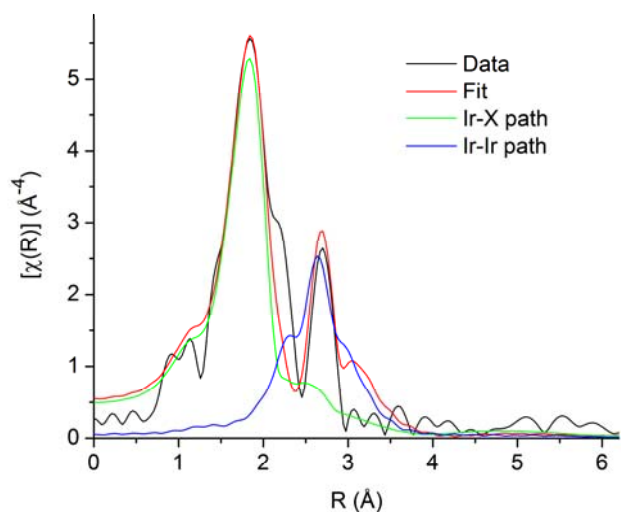




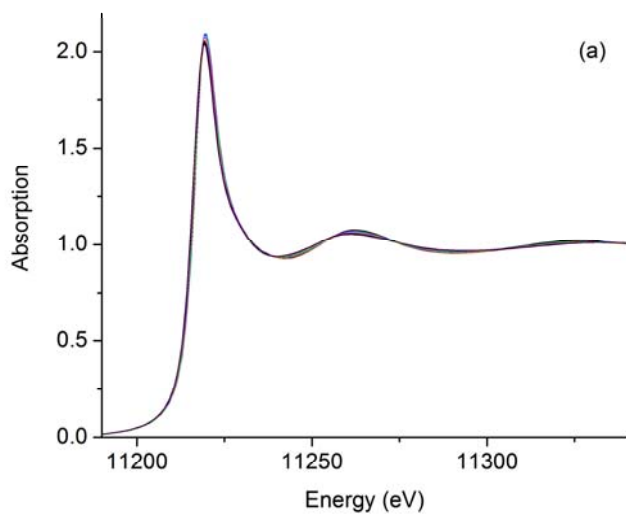
**Figure S21.** Experimental data and fit for the XAFS spectra of AlEt<sub>3</sub>/Ir = 5.0 catalyst sample in a  $\chi(k)$  plot (a), and the magnitude (b) and imaginary part (c) of the FT (k-range for FT = 2.1–14.8). K-weighting and R-range used for the fit are  $k^3$  and 1.2–3.0, respectively.



**Figure S22.** The  $\chi(k)$  spectrum for the Al/Ir = 10.0 sample. The excessive noise prevents reliable fitting and analysis.



**Figure S23.** Experimental spectrum and attempted fit of the  $\text{AlEt}_3/\text{Ir} = 2.0$  sample using the model composed of only Ir–X (green) and Ir–Ir (blue) paths. Note the shoulder at  $\sim 2.2$  on the right side of the Ir–X peak that is inadequately accounted for by the shoulder on the left side of the Ir–Ir path. Including a backscattering contribution from a theoretical Ir–Al path accounts for this feature.



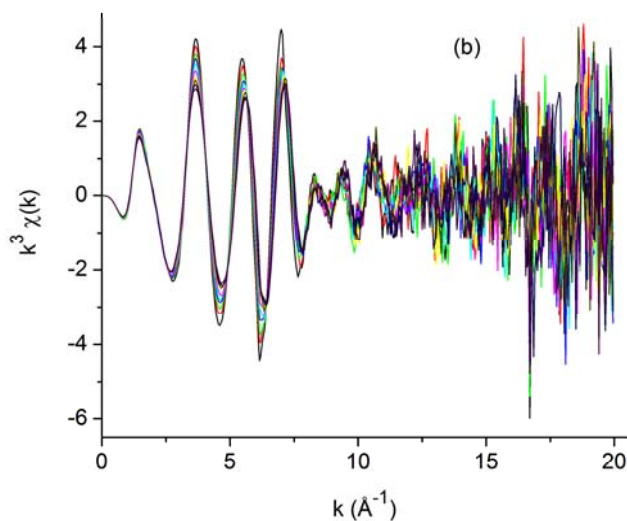


**Figure S24.** Drift in the  $[(1,5\text{-COD})\text{Ir}(\mu\text{-O}_2\text{C}_8\text{H}_{15})_2]$  plus  $\text{AlEt}_3$ ,  $\text{Al}/\text{Ir} = 2.0$ , catalyst sample data, shown in the  $\mu(E)$  (a) and  $\chi(k)$  (b) spectra. Drift in the  $\text{Al}/\text{Ir} = 1.5$  and  $2.5$  samples was very similar. An explanation is not apparent. To eliminate the effects, only the first two scans of each of these samples were merged for use in further analysis.

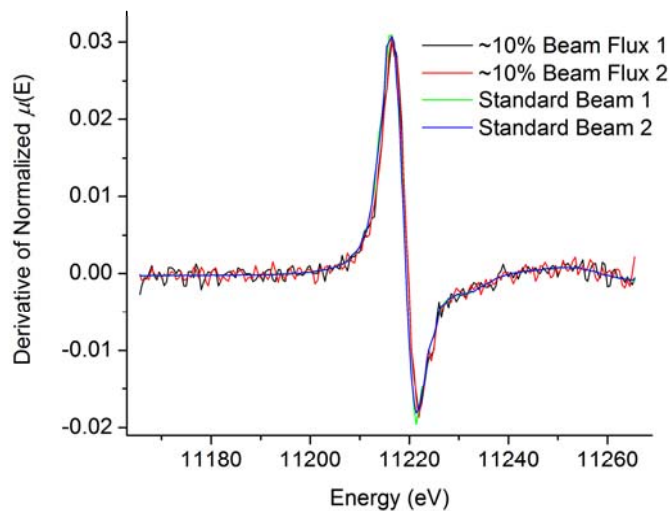
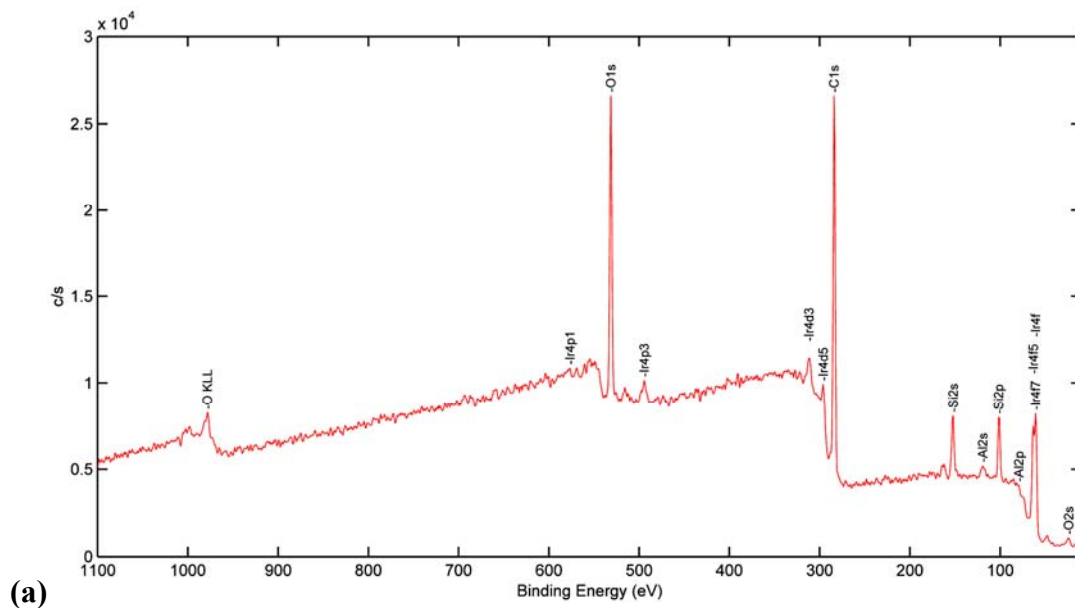


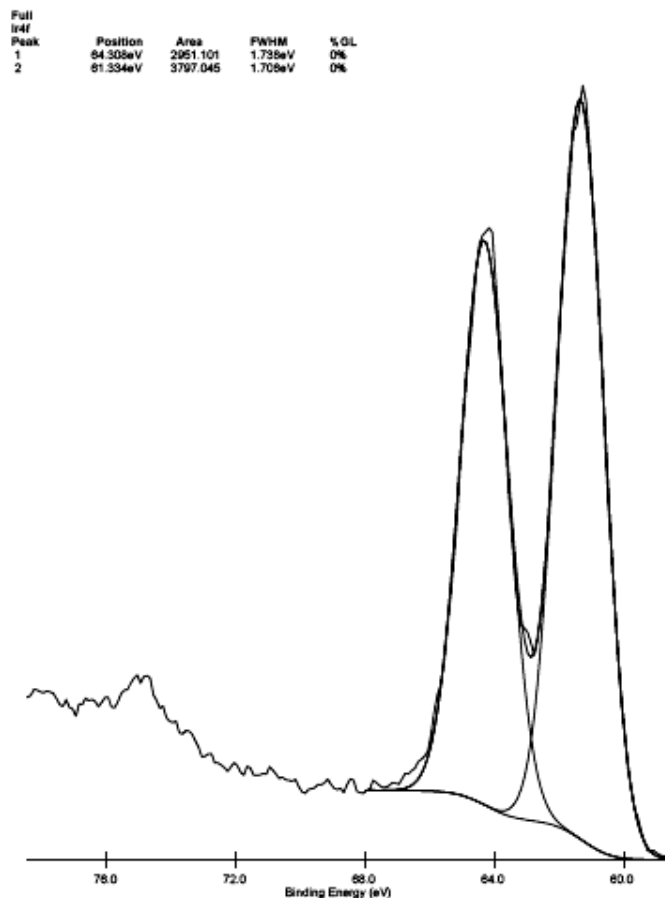
**Figure S25.** Derivative spectra of the Ir L3 edge step region of the  $\text{AlEt}_3/\text{Ir} = 0.5$  catalyst sample as a control experiment testing possible sample damage caused by the X-ray beam. Two scans were taken at  $\sim 10\%$  of the normal operating beam flux (black and red), and two more at the normal flux (green and blue). The scans are essentially identical (aside from the expected, decreased S/N ratio of the low flux scans) suggesting that either damage to the sample from the X-ray beam is the same regardless of flux (which is unlikely) or that no sample damage is occurring.

**XPS Before Hydrogenation.** In the drybox at CSU, 20 mL of a  $\text{AlEt}_3/\text{Ir} = 2.0$ ,  $[\text{Ir}] = 1.44 \text{ mM}$ , catalyst sample was prepared. A 0.2 mL aliquot of the catalyst sample was then transferred onto an XPS sample holder. The sample holder was placed in a desiccator while still in the drybox. The sealed desiccator was then taken out of the drybox and placed in a glovebag which, using sealant tape, was sealed to the sample exchange window of the XPS and purged three times with Ar. The XPS sample was transferred to the instrument under flowing Ar. Analysis was carried out on a 2000 Physical Electron 5800 ultra-high vacuum XPS-Auger spectrometer equipped with a hemispherical analyzer. A monochromatic Al X-ray source at 1486.6 eV was used with an operating power of 350.0 W. The spectra were taken at an angle of  $45.0^\circ$ , and a 23.50 eV pass energy was employed. All spectra were referenced to the hydrocarbon C 1s peak at 284.8 eV. The fitting procedure was performed using XPSPEAK 41.

Atomic composition analysis was carried out using XPS on the  $[(1,5\text{-COD})\text{Ir}(\mu\text{-O}_2\text{C}_8\text{H}_{15})_2 \text{ plus } \text{AlEt}_3, \text{Al}/\text{Ir} = 2.0$ , catalyst before its use in hydrogenation. Figure S26a shows the survey spectrum. The peak at 100.75 eV is assigned to Si 2p, which presumably originates from an impurity (e.g., molecular sieves that were added into the cyclohexane) and is therefore disregarded. Atomic composition results generally agree with the stoichiometry of the added components, as expected; the catalyst sample has an atomic composition of  $3.0 \pm 0.2 \%$  Ir,  $7.0 \pm 0.4 \%$  Al,  $26 \pm 1 \%$  O, and  $64 \pm 3 \%$  C. Figure S26b shows the high resolution spectrum of the Ir 4f peaks and Table S6 lists the Ir 4f peak positions of reference compounds. The exclusion of air was achieved by preparing the samples in a drybox and transferring them to the instrument under flowing

Ar inside a glovebag sealed to the sample exchange window. Analysis of the Ir 4f region rules out significant air-oxidation of Ir in the samples by the absence of peaks corresponding to IrO<sub>2</sub>.<sup>14</sup> The peak positions at 64.30 eV and 61.33 eV are consistent with Ir(I)<sup>15</sup> and/or Ir(0)<sub>n</sub> Ziegler nanoclusters.





(b)

**Figure S26.** (a) XPS survey spectrum of the AlEt<sub>3</sub>/Ir = 2.0, catalyst before hydrogenation. The spectrum gives % atomic composition by integration. (b) High resolution XPS spectra of the Ir 4f peaks of the AlEt<sub>3</sub>/Ir = 2.0, catalyst before hydrogenation.

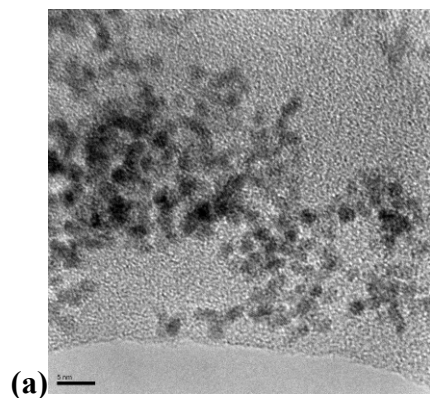
**Table S6.** Ir peak positions from the XPS spectrum of the [(1,5-COD)Ir(μ-O<sub>2</sub>C<sub>8</sub>H<sub>15</sub>)<sub>2</sub>] plus AlEt<sub>3</sub> catalyst, Al/Ir = 2.0, before its use in hydrogenation, and of reference compounds.

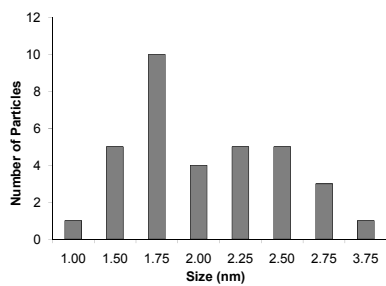
sample	peak	binding energy (eV)	ref.
Al/Ir = 2.0 catalyst	Ir 4f <sub>5/2</sub>	64.30	This Work
	Ir 4f <sub>7/2</sub>	61.33	
IrO <sub>2</sub>	Ir 4f <sub>7/2</sub>	62.3	14
	Ir 4f <sub>5/2</sub>	65.7	
bulk Ir(0)	Ir 4f <sub>5/2</sub>	63.8	16,17

	Ir 4f <sub>7/2</sub>	60.80	16,18,19,20,21
Ir <sub>n</sub> nanoclusters stabilized by Al(O)(OH)	Ir 4f <sub>5/2</sub>	64.4	14
	Ir 4f <sub>7/2</sub>	61.1	

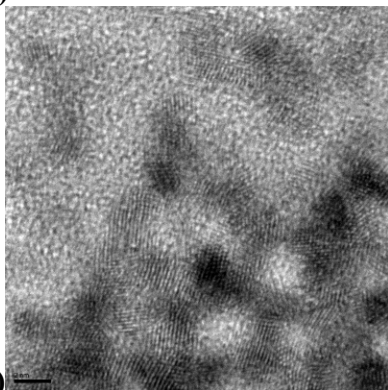
### Identification of the Ir-containing species in the AlEt<sub>3</sub>/Ir catalyst *after*-hydrogenation

**Bright field and High Resolution (HR)TEM.** Images were obtained of [(1,5-COD)Ir(μ-O<sub>2</sub>C<sub>8</sub>H<sub>15</sub>)<sub>2</sub>] plus AlEt<sub>3</sub>, Al/Ir = 1.0, 2.0, and 5.0 catalyst samples after hydrogenation using bright field TEM. Ziegler nanoclusters with a mean diameter of 1.4 ± 0.3 nm (1σ) (corresponding to Ir(0)<sub>~100</sub>) are clearly seen, for example, in the TEM image of the Al/Ir = 2.0 catalyst sample after hydrogenation, Figure S28. The TEM results are shown in Figures S27–S30, and summarized in Table S7.





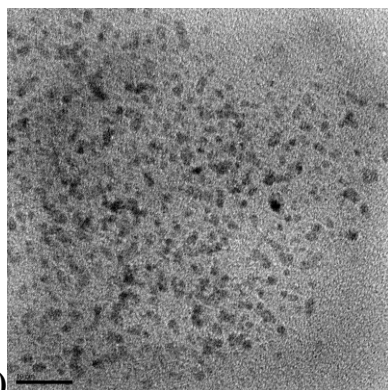
(b)

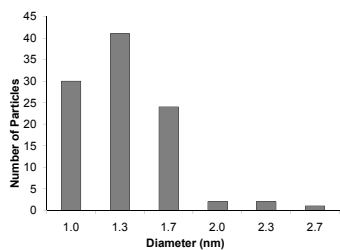


(c)

**Figure S27.** Example TEM image (a, scale bar = 5 nm), corresponding particle size histogram (b), and HRTEM image (c, scale bar = 2 nm) of the AlEt<sub>3</sub>/Ir = 1.0 catalyst after use in hydrogenation. The mean diameter from measurement of 34 particles in (a) is  $2.1 \pm 0.5$  nm.

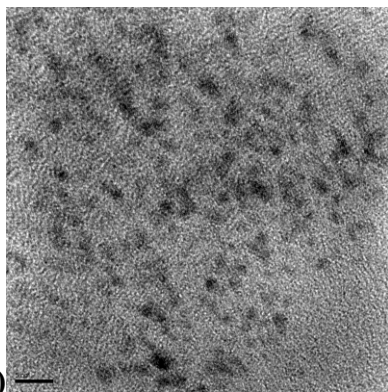
(a)



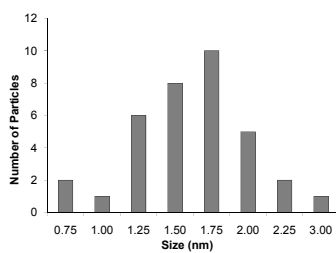


(b)

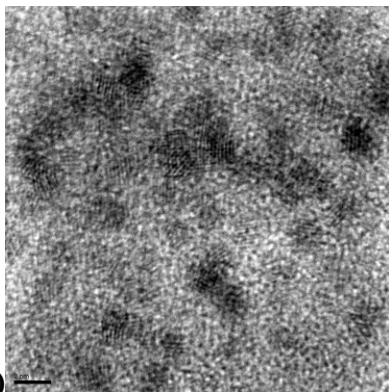
**Figure S28.** TEM image of the  $[(1,5\text{-COD})\text{Ir}(\mu\text{-O}_2\text{C}_8\text{H}_{15})_2 + \text{AlEt}_3$  catalyst, Al/Ir = 2.0, after its use in cyclohexene hydrogenation (a, scale bar = 10 nm) and corresponding particle size histogram (b). The size and size distribution is  $1.4 \pm 0.3$  nm in diameter from counting 100 clusters in image (a).



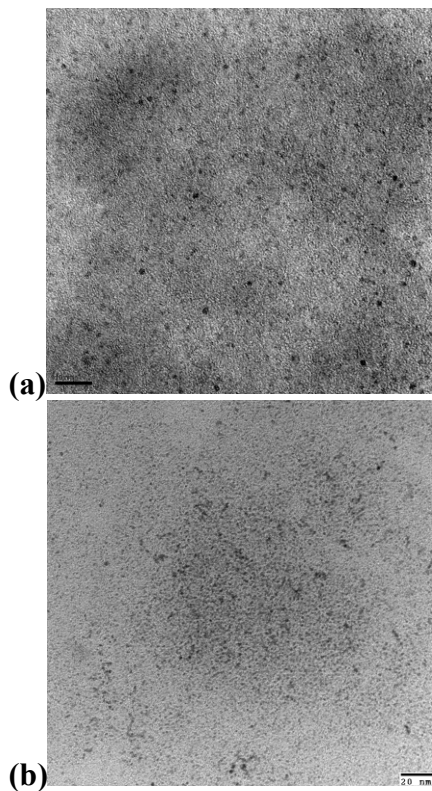
(a)



(b)



(c) **Figure S29.** Example TEM image (a, scale bar = 5 nm), corresponding particle size histogram (b), and HRTEM image (c, scale bar = 2 nm) of the  $\text{AlEt}_3/\text{Ir} = 5.0$  catalyst after use in hydrogenation. The mean diameter from measurement of 35 particles in (a) is  $1.6 \pm 0.4$  nm.



(a) (b) **Figure S30.** Example TEM image of the  $[(1,5\text{-COD})\text{Ir}(\mu\text{-O}_2\text{C}_8\text{H}_{15})]_2$  plus  $\text{AlEt}_3$  (scale bar = 10 nm),  $\text{Al}/\text{Ir} = 2.0$ , catalyst after use in hydrogenation. Images were obtained on  $\text{SiO}_2$ -coated Cu grids (Ted Pella, Type-A, 300 M). Mean particle diameter measured from these images of  $1.0 \pm 0.3$  is the same within experimental error as when holey carbon coated grids were used to image the same samples, Figure S28.

**Table S7.** Size and size distribution results from analyzing selected TEM images of the [(1,5-COD)Ir( $\mu$ -O<sub>2</sub>C<sub>8</sub>H<sub>15</sub>)<sub>2</sub>] + AlR<sub>3</sub> catalyst samples after hydrogenation.

AlR <sub>3</sub>	Al/Ir	Mean Diameter (nm)
AlEt <sub>3</sub>	1	2.1 ± 0.5 (1 $\sigma$ )
AlEt <sub>3</sub>	2	1.4 ± 0.3 (1 $\sigma$ )
AlEt <sub>3</sub>	5	1.6 ± 0.4 (1 $\sigma$ )

**Electron Diffraction.** A [(1,5-COD)Ir( $\mu$ -O<sub>2</sub>C<sub>8</sub>H<sub>15</sub>)<sub>2</sub>] plus AlEt<sub>3</sub> catalyst sample, Al/Ir = 2.0, *after* its use in hydrogenation that was analyzed using electron diffraction. An example diffraction image, Figure S31, closely matches that of genuine *fcc* Ir(0) by comparison of the relative ring distance ratios.

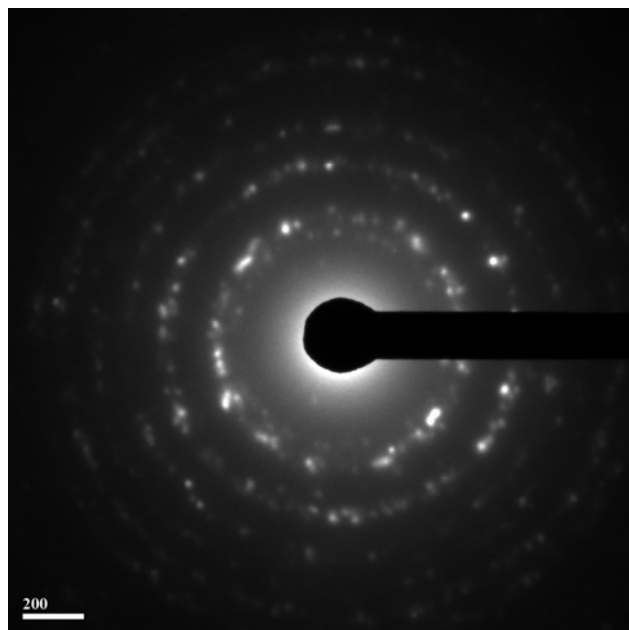


**Figure S31.** The relative ring distances in an electron diffraction image of an Al/Ir = 2.0 catalyst after hydrogenation matches *fcc* Ir(0).

**XAFS Spectroscopy.** Analysis of a sample of the  $[(1,5\text{-COD})\text{Ir}(\mu\text{-O}_2\text{C}_8\text{H}_{15})]_2$  plus  $\text{AlEt}_3$  catalyst,  $\text{Al}/\text{Ir} = 1.0$ , after its use in hydrogenation by XAFS spectroscopy shows that it consists of, on average, 1.6 nm, *fcc*  $\text{Ir}(0)_{\sim 150}$  Ziegler nanoclusters, Figure 9 of the main text. Additional spectra and the full fitting results are shown here.

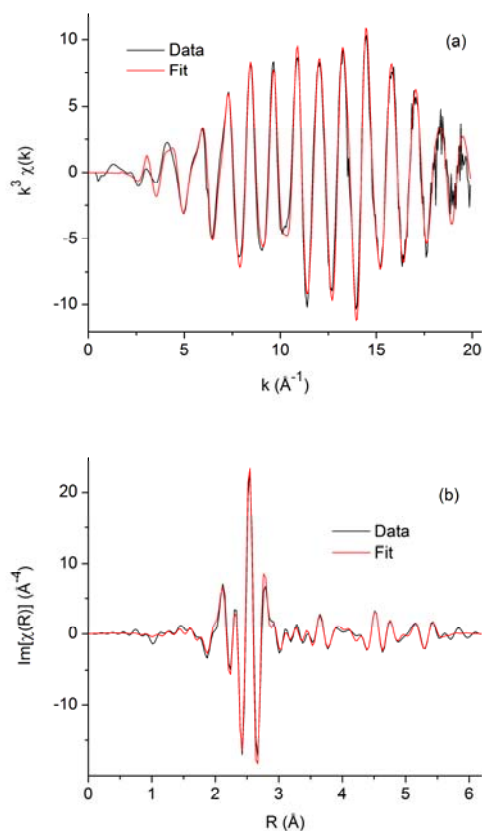


**Figure S32.** Experimental data and fit for a  $\chi(k)$  plot of the  $\text{AlEt}_3/\text{Ir} = 1.0$  catalyst sample, after hydrogenation, in a  $\chi(k)$  plot (a), and the imaginary part of the FT (b). The magnitude of the FT is shown in Figure 9 of the main text ( $k$ -range for FT = 2–18).

**Table S8.** Fit results for the  $\text{Al}/\text{Ir} = 1.0$  catalyst sample after hydrogenation.  $\Delta E_0 = 10.7 \pm 0.9$  eV.  $k$ -weighting and  $R$ -range used for the fit are  $k^3$  and 1.0–5.6, respectively.

Path	N	$R_{\text{eff}}$ ( $\text{\AA}$ )	$R$ ( $\text{\AA}$ )	$\sigma^2 \times 10^3$ ( $\text{\AA}^2$ )
SS1	$9.0 \pm 0.4$	2.7147	$2.688 \pm 0.001$	$5.1 \pm 0.1$

SS2	$2.9 \pm 0.9$	3.8392	$3.819 \pm 0.006$	$6 \pm 1$
SS3	$7 \pm 2$	4.7020	$4.682 \pm 0.005$	$6.0 \pm 0.7$
SS4; CL4,1; CL1,4,1	$3.6 \pm 0.9$	5.4294	$5.389 \pm 0.008$	$9 \pm 1$

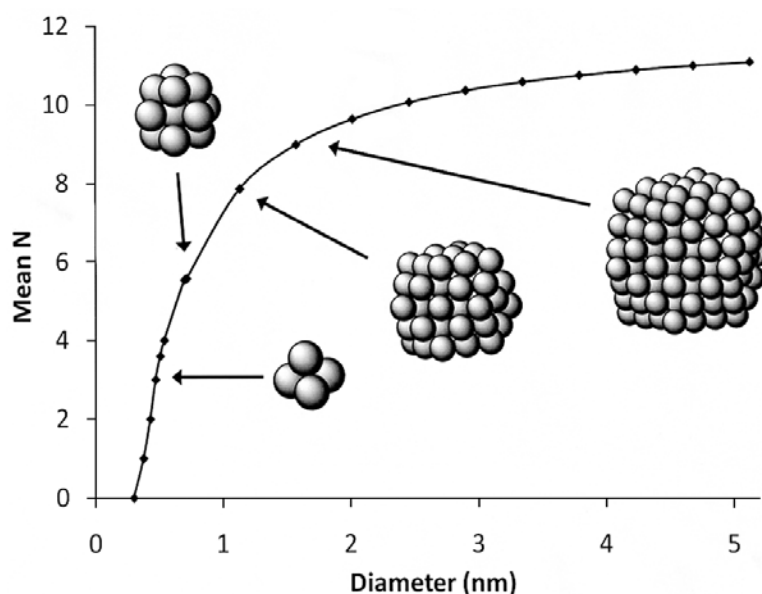


**Figure S33.** Mean 1<sup>st</sup> nearest neighbor N-particle diameter correlation curve calculated for theoretical, cuboctahedral, *fcc* Ir. The examples shown: a mean N value of 3 corresponds to an Ir<sub>4</sub> cluster 0.5 nm in diameter, a mean N of 5.5 corresponds to a 0.7 nm Ir<sub>13</sub> cluster, a mean N of 7.8 corresponds to a 1.1 nm Ir<sub>55</sub> cluster, and a mean N of 9 corresponds to a 1.6 nm Ir<sub>147</sub> cluster. The mean N value approaches the bulk Ir metal value of 12 as particles size increases.

**XPS After Hydrogenation.** A [(1,5-COD)Ir( $\mu$ -O<sub>2</sub>C<sub>8</sub>H<sub>15</sub>)<sub>2</sub>] plus AlEt<sub>3</sub> catalyst sample, Al/Ir = 2, was prepared, used in a cyclohexene hydrogenation under standard conditions, and collected for analysis by XPS. The high resolution spectrum of the Ir 4f peaks, Figure S34, is consistent with the sample being composed of Ir(0).

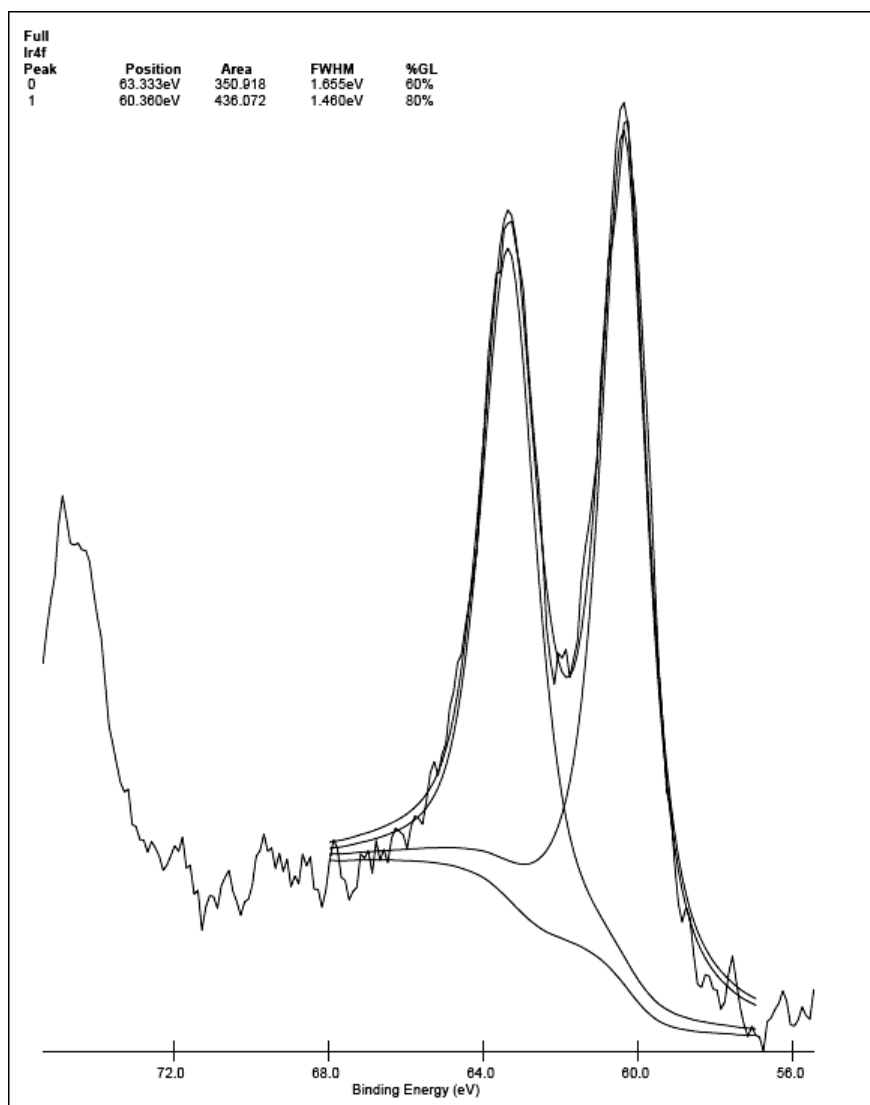


**Figure S34.** High resolution XPS spectrum of the Ir 4f peaks (and their fits) of the  $\text{AlEt}_3/\text{Ir} = 2.0$  catalyst after hydrogenation.

### **Kinetics-based experiments probing the active catalyst**

Control experiments were performed to determine the amount of mixing necessary to allow thorough contact between the insoluble  $\text{Hg}(0)$  and the catalyst in solution. The results of these experiments are shown in Figure S35. Both these control experiments and using  $\geq 300$  equivalents of  $\text{Hg}(0)$  per Ir each time were vital to establishing a procedure whereby any failure to poison the catalyst is not due to

insufficient mixing of the catalyst solution with Hg(0), a potential weakness of Hg(0) poisoning experiments.<sup>22,23</sup> Additionally, for each type of Hg(0) poisoning experiment performed using a [(1,5-COD)Ir( $\mu$ -O<sub>2</sub>C<sub>8</sub>H<sub>15</sub>)<sub>2</sub>] plus AlEt<sub>3</sub> catalyst, a control experiment was performed where the catalyst solution was subjected to the exact procedure used for Hg(0) poisoning, but without actual addition of Hg(0). These experiments were designed to show whether the result of the poisoning experiment was due to poisoning by Hg(0) or, conceivably, some problem in the procedure itself. In each case, active cyclohexene hydrogenation resumed. Therefore, these control experiments confirm that the experimental procedure itself is not the cause of the observed catalyst poisoning. Control experiments were also carried out wherein Hg(0) was added to the initial catalyst solutions, before their use in the catalytic hydrogenation of cyclohexene (i.e., before exposure to H<sub>2</sub> gas). These control experiments are discussed in the main text and one example using an aged catalyst solution is shown there; runs using a non-aged catalyst solution are shown here in Figure S36.

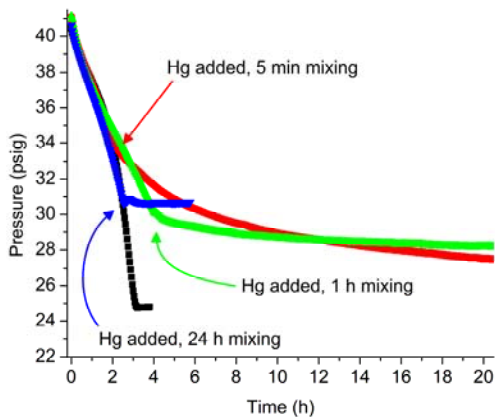


**Figure S35.** Control experiments testing the amount of mixing time required for Hg(0) poisoning using [(1,5-COD)Ir( $\mu$ -O<sub>2</sub>C<sub>8</sub>H<sub>15</sub>)<sub>2</sub>] plus AlEt<sub>3</sub> catalysts ([Ir] = 0.6 mM, Al/Ir = 2.0, initial [cyclohexene] = 1.65 M, hydrogenations performed at 22.0 °C, and with 1000 rpm stirring) and a standard hydrogenation run without Hg(0) poisoning for comparison (black). After  $\geq 300$  equivalents of Hg(0) per Ir were added, the solutions were stirred at

1000 rpm for 5 minutes (red), 1 hour (green), or 24 hours (blue) before the hydrogenation was resumed. This shows 24 hours of mixing is sufficient for total catalyst poisoning. Hence, 24 hours of mixing was used as the procedure for all the Hg(0) poisoning experiments.

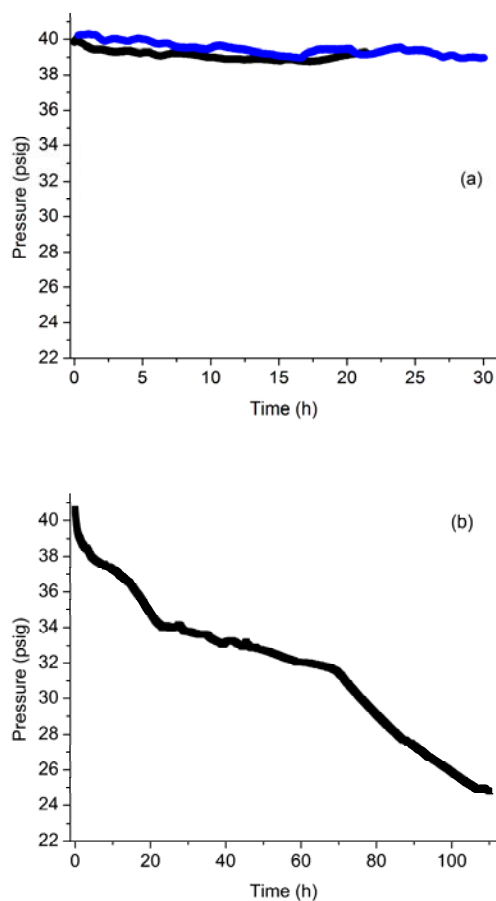


**Figure S36.** Control experiments where Hg(0) was added to the initial catalyst solutions after their preparation in the drybox, but without aging and before their use in catalytic cyclohexene hydrogenation. (b) In two control experiments prepared and performed identically, the catalyst was poisoned, albeit after a slight initial pressure loss. The results in (a) are consistent with that showed in the main text for poisoning of the initial catalyst, aged for 9 hours in that case. The poisoning implies that the primary catalyst is heterogeneous in nature (i.e., the Ir Ziegler nanoclusters observed by Z-contrast microscopy, for example). (b) In a third, ostensibly identical control experiment, the hydrogenation process was been disturbed, but still occurs roughly to completion after >100 hours Both the initial pressure loss in (a), and in the complete cyclohexene hydrogenation in (b), are consistent with some amount of a non Hg(0)-poisonable, active, and apparently homogeneous catalyst component being present initially.

The full list authors in reference 6d of the main text is:

Angermund, K.; Bühl, M.; Endruschat, U.; Mauschick, F. T.; Mörtel, R.; Mynott, R.; Tesche, B.; Waldöfner, N.; Bönnemann, H.; Köhl, G.; Modrow, H.; Hormes, J.; Dinjus, E.; Gassner, F.; Haubold, H.-G.; Vad, T.; Kaupp, M. *J. Phys. Chem. B* **2003**, *107*, 7507–7515.

### References

---

<sup>1</sup> Alley, W. M.; Hamdemir, I. K.; Johnson, K. A.; Finke, R. G. *J. Mol. Catal. A: Chem.* **2010**, *315*, 1–27.

<sup>2</sup> Alley, W. M.; Girard, C. W.; Özkar, S.; Finke, R. G. *Inorg. Chem.* **2009**, *48*, 1114–1121.

<sup>3</sup> Aiken, J. D., III; Finke, R. G. *J. Mol. Catal. A: Chem.* **1999**, *145*, 1–44.

<sup>4</sup> Williams, D. B.; Carter, C. B. *Transmission Electron Microscopy*; Plenum Press: New York, 1996.

<sup>5</sup> Whetten, R. L.; Khoury, J. T.; Alvarez, M. M.; Murthy, S.; Vezmar, I.; Wang, Z. L.; Stephens, P. W.; Cleveland, C. L.; Luedtke, W. D.; Landman, U. *Adv. Mater.* **1996**, *8*, 428–433.

<sup>6</sup> Khitrov, G. A.; Strouse, G. F. *J. Am. Chem. Soc.* **2003**, *125*, 10465–10469.

<sup>7</sup> Kuzuya, T.; Tai, Y.; Yamamuro, S.; Sumiyama, K. *Chem. Phys. Lett.* **2005**, *407*, 460–463.

<sup>8</sup> Maya, L.; Chen, C. H.; Stevenson, K. A.; Kenik, E. A.; Allman, S. L.; Thundat, T. G. *J. Nanoparticle Res.* **2002**, *4*, 417–422.

- 
- <sup>9</sup> Lin, Y.; Finke, R. G. *J. Am. Chem. Soc.* **1994**, *116*, 8335–8353.
- <sup>10</sup> *CRC Handbook of Chemistry and Physics*; 77<sup>th</sup> ed.; Lide, D. R., Frederikse, H. P. R., Eds.; CRC Press, Boca Raton, 1996.
- <sup>11</sup> (a) Özkar, S.; Finke, R. G. *J. Organomet. Chem.* **2004**, *689*, 493–501. (b) Özkar, S.; Finke, R. G. *Langmuir* **2003**, *19*, 6247–6260.
- <sup>12</sup> Day, V. W.; Klemperer, W. G.; Main, D. J. *Inorg. Chem.* **1990**, *29*, 2345–2355.
- <sup>13</sup> Churchill, M. R.; Hutchinson, J. P. *Inorg. Chem.* **1978**, *17*, 3528–3535.
- <sup>14</sup> Park, I. S. Kwon, M. S.; Kang, K. Y.; Lee, J. S.; Park, J. *Adv. Synth Catal.* **2007**, *349*, 2039–2047.
- <sup>15</sup> El-Issa, B. D.; Katrib, A.; Ghodsian, R.; Salsa, B. A.; Addassi, S. H. *Int. J. Quantum Chem.* **1988**, *33*, 195–216.
- <sup>16</sup> Marinova, T. S.; Kostov, K. L. *Surf. Sci.* **1987**, *181*, 573–585.
- <sup>17</sup> Rogers, J. D.; Sundaram, V. S.; Kleiman, G. G.; Castro, C. G. C.; Douglas, R. A.; Peterlevitz, A. C. *J. Phys. F.* **1982**, *12*, 2097–2102.
- <sup>18</sup> Wittmer, M.; Oelhafen, P.; Tu, K. N. *Phys. Rev. B* **1986**, *33*, 5391–5400.
- <sup>19</sup> Baer, Y.; Heden, P. F.; Hedman, J.; Klasson, M.; Nodling, C.; Siegbahn, K. *Phys. Scr.* **1970**, *1*, 55–56.
- <sup>20</sup> Nyholm R.; Berndtsson A.; Martensson N. *J. Phys. C: Solid St. Phys.* **1980**, *13*, L1091–1096.
- <sup>21</sup> Wagner, C. D.; Riggs, W. M.; Davis, L. E.; Moulder, J. F.; Muilenberg, G. E. *Handbook of X-Ray Photoelectron Spectroscopy*; Perkin-Elmer Corporation, Physical Electronics Division: Eden Prairie, 1979.
- <sup>22</sup> Widegren, J.; Finke, R. *J. Mol. Catal. A: Chem.* **2003**, *198*, 317–341.

---

<sup>23</sup> Phan, N. T. S.; Van Der Sluys, M.; Jones, C. W. *Adv. Synth. Catal.* **2006**, *348*, 609–679.

## CHAPTER V

### INDUSTRIAL ZIEGLER-TYPE HYDROGENATION CATALYSTS MADE FROM Co(neodecanoate)<sub>2</sub> OR Ni(2-ethylhexanoate)<sub>2</sub>, AND AlEt<sub>3</sub>: EVIDENCE FOR NANOCLUSTERS AND SUB-NANOCLUSTER OR LARGER ZIEGLER- NANOCLUSTER BASED CATALYSIS

This dissertation chapter contains a manuscript submitted for publication, as a full article, to *Langmuir*. It is reproduced with permission, unpublished work copyright 2011 American Chemical Society. This chapter presents efforts to determine whether the catalysts formed using the authentic industrial precursors mentioned in the title are homogeneous or heterogeneous in nature. The approach taken parallels the one used for the Ir model system made from [(1,5-COD)Ir( $\mu$ -O<sub>2</sub>C<sub>8</sub>H<sub>15</sub>)]<sub>2</sub> plus AlEt<sub>3</sub>, as described in Chapter IV of this dissertation, and utilizes a similar set of analytical techniques and complementary kinetic studies.

The initial control hydrogenations testing the variables of catalyst synthesis and use were carried out by both Isil. K. Hamdemir and William M. Alley. Z-contrast STEM imaging was performed by Long Li on samples prepared by William M. Alley. XAFS data was obtained, processed, and analyzed by William M. Alley with assistance from Qi Wang, Anatoly Frenkel, and Laurent D. Menard. MALDI MS data was collected by Isil

K. Hamdemir, and interpreted by her and William M. Alley. TEM control experiments including HR- and bright field TEM (given in the Supporting Information) were performed by either Long Li or JoAn Hudson of Clemson University on samples prepared by William M. Alley or Isil K. Hamdemir, respectively. Interpretation of bright field TEM data was performed by Isil K. Hamdemir. All other kinetics experiments, including Hg(0) poisoning, and associated control experiments were performed by William M. Alley.

The manuscript was written by William M. Alley with the aid of earlier paper drafts written by Isil K. Hamdemir that described the relevant literature, experimental procedures, results, and a discussion of the work she performed. The manuscript has been prepared for submission to *Langmuir* by William M. Alley with helpful comments from the coauthors plus light edits (9 hours) by Prof. Finke.

**Industrial Ziegler-type Hydrogenation Catalysts made from Co(neodecanoate)<sub>2</sub> or Ni(2-ethylhexanoate)<sub>2</sub>, and AlEt<sub>3</sub>: Evidence for Nanoclusters and Sub-Nanocluster or Larger Ziegler-Nanocluster Based Catalysis**

William M. Alley, Isil K. Hamdemir, Qi Wang, Anatoly I. Frenkel, Long Li, Judith C. Yang, Laurent D. Menard, Ralph G. Nuzzo, Saim Özkar, Kimberly Johnson, Richard G. Finke

**Abstract**

Ziegler-type hydrogenation catalysts are important for industrial processes, namely the large scale selective hydrogenation of styrenic block copolymers. Ziegler-type hydrogenation catalysts are composed of a group 8–10 transition metal precatalyst plus an alkylaluminum cocatalyst (and they are not the same as Ziegler-Natta *polymerization* catalysts). However, for ~50 years two unsettled issues central to Ziegler-type hydrogenation catalysis are the nature of the metal species present after catalyst synthesis, and whether the species primarily responsible for catalytic hydrogenation activity are homogeneous (e.g., mono-metallic complexes) or heterogeneous (e.g., Ziegler nanoclusters defined as metal nanoclusters made from combination of Ziegler-type hydrogenation catalyst precursors). A critical review of the existing literature (Alley

et al. *J. Mol. Catal. A: Chem.* **2010**, *315*, 1–27) and a recently published study using an Ir model system (Alley et al. *Inorg. Chem.* **2010**, *49*, 8131–8147) help to guide the present investigation of Ziegler-type hydrogenation catalysts made from the industrially favored precursors Co(neodecanoate)<sub>2</sub> or Ni(2-ethylhexanoate)<sub>2</sub>, plus AlEt<sub>3</sub>. The approach and methods used herein parallel those used in the study of the Ir model system. Specifically, a combination of Z-contrast scanning transmission electron microscopy (STEM), matrix assisted laser desorption ionization mass spectrometry (MALDI MS), and X-ray absorption fine structure (XAFS) spectroscopy are used to characterize the transition metal species both before and after hydrogenation. Kinetic studies including Hg(0) poisoning experiments are utilized to test which species are the most active catalysts. The main findings are that, both before and after catalytic cyclohexene hydrogenation, the species present comprise a broad distribution of metal cluster sizes from subnanometer to nanometer scale particles, with estimated mean cluster diameters of about 1 nm for both Co and Ni. The XAFS results also imply that the catalyst solutions are a mixture of the metal clusters described above, plus unreduced metal ions. The kinetics-based Hg(0) poisoning evidence suggests that the Ziegler nanoclusters (i.e.,  $\geq M_4$ ) are the most active hydrogenation catalysts in the Ni system; the Hg(0) poisoning tests in the Co system proved inconclusive. Overall, the novelty and primary conclusions of this study are: (i) this study examines Co and Ni-based catalysts made from the *actual industrial* precursor materials, which make catalysts that are notoriously problematic regarding their characterization; (ii) the Z-contrast STEM results reported herein represent, to our knowledge, the best microscopic analysis of the industrial Co and Ni Ziegler-type hydrogenation catalysts; (iii) this study is the first explicit application of an

established method, using multiple analytical methods and kinetics-based studies, for distinguishing homogeneous from heterogeneous catalysis; and (iv) this study parallels the successful study of an Ir model Ziegler catalyst system, thereby benefiting from a comparison to those previously unavailable findings, although the greater M–M bond energy, and tendency to agglomerate, of Ir versus Ni or Co are important differences to be noted. Therefore, the leading hypothesis to try to refute in future work is that Ziegler-type sub-(i.e.,  $M_4$ ) to larger nanoclusters are the dominant, industrial, Co- and Ni- plus  $AlR_3$  catalysts.

## Introduction

Ziegler-type hydrogenation catalysts are, by definition, formed from a non-zerovalent group 8–10 transition metal (M) precatalyst such as Co(neodecanoate)<sub>2</sub> or Ni(2-ethylhexanoate)<sub>2</sub> plus a trialkylaluminum cocatalyst such as triethylaluminum (AlEt<sub>3</sub>). Ziegler-type hydrogenation catalysts should not be confused, however, with Ziegler–Natta or other common polymerization catalysts, which are not a subject of this study. The relatively inexpensive Co- or Ni-based catalysts made from Co(neodecanoate)<sub>2</sub> or Ni(2-ethylhexanoate)<sub>2</sub>, respectively, are very significant industrially as they are used in the production of  $\sim 1.7 \times 10^5$  metric tons of hydrogenated styrenic block copolymers per year.<sup>1</sup> Several important fundamental questions about Ziegler-type hydrogenation catalysts persist despite the use of these catalysts for five decades.<sup>1,2,3</sup> One of the most important remaining questions is the  $\sim 50$  year old problem of whether the true nature of Ziegler-type hydrogenation catalysis is homogeneous (e.g., single metal organometallic) versus heterogeneous (e.g., nanoclusters).<sup>1,3,4,5,6</sup>

A recently published critical review of Ziegler-type hydrogenation catalysts includes an examination of the prior evidence concerning their homogeneous versus heterogeneous nature, and finds that the reasons for the longevity of this problem in this class of catalysts include their sensitivity to variables and conditions in their preparation and use, and their resistance to characterization by physical methods and isolation for kinetic studies.<sup>2,3</sup> The literature review<sup>3</sup> led to the suggestion that answering the homogeneous versus heterogeneous catalysis question for Ziegler-type hydrogenation catalysts could be facilitated through the use of a well characterized, third-row transition-metal precatalyst in combination with a multi-pronged, previously successful approach to

solving the homogeneous versus heterogeneous catalysis problem in a variety of other catalyst systems.<sup>3,6,7,8,9,10,11,12,13,14,15</sup> The central concepts of this multi-prong approach towards answering the homogeneous versus heterogeneous catalysis question are (i) identification of the potential catalyst species using multiple complementary techniques, and then (ii) kinetic studies to determine the catalytic competency of those species.

Such studies using a Ziegler-type hydrogenation catalyst made from the crystallographically characterized precatalyst, [(1,5-COD)Ir( $\mu$ -O<sub>2</sub>C<sub>8</sub>H<sub>15</sub>)<sub>2</sub>], plus AlEt<sub>3</sub> have been recently published.<sup>14</sup> Among the multiple analytical methods used were Z-contrast scanning transmission electron microscopy (STEM), matrix assisted laser desorption ionization mass spectrometry (MALDI MS), and X-ray absorption fine structure (XAFS) spectroscopy.<sup>14</sup> Since “catalysis is, by definition, a wholly kinetic phenomenon”,<sup>16</sup> kinetic studies were performed as a necessary component of addressing the homogeneous versus heterogeneous catalysis question.<sup>3,14</sup> Those studies revealed that after the initial catalyst preparation (i.e., after the addition of AlEt<sub>3</sub> to [(1,5-COD)Ir( $\mu$ -O<sub>2</sub>C<sub>8</sub>H<sub>15</sub>)<sub>2</sub>] in cyclohexane), but before use for catalytic cyclohexene hydrogenation (i.e., before exposure to pressurized H<sub>2</sub> gas), the catalyst solutions contain a wide range of Ir species from mono-Ir complexes up to structurally-disordered Ir<sub>~100</sub> Ziegler nanoclusters, with an estimated mean of 0.5–0.7 nm, Ir<sub>~4–15</sub> clusters.<sup>14</sup> However, after using catalyst solutions for cyclohexene hydrogenation, the Ir present was in the form of *fcc* Ir(0)<sub>~40–150</sub> Ziegler nanoclusters.<sup>14</sup> Moreover, poisoning and other kinetic studies suggested that the *fcc* Ir(0)<sub>~40–150</sub> Ziegler nanoclusters are the fastest catalysts.<sup>14</sup>

The goal of the present study is to repeat the analyses performed on the Ir model Ziegler-type hydrogenation catalyst system with Co- and Ni-based catalysts made from

the authentic Co(neodecanoate)<sub>2</sub> or Ni(2-ethylhexanoate)<sub>2</sub> precursor materials used for industrial polymer hydrogenation. As such, this work not only expands on our own previous study using the Ir model system,<sup>14</sup> but also on the results of others—notably the valuable studies by Schmidt and co-workers,<sup>17</sup> and Bönemann and co-workers<sup>18</sup> that suggest transition metal nanoclusters are the catalysts in the Ziegler-type systems studied by them. Our main hypotheses for the present work are (i) that the approach that proved useful with the homogeneous vs heterogeneous catalysis question in the Ir system<sup>14</sup> will be applicable to the industrial Co- and Ni-based systems, and (ii) that the results will be similar in that the fastest catalysts will be revealed to consist of Co or Ni Ziegler nanoclusters, even if as small as Co<sub>4</sub> or Ni<sub>4</sub>. Many of the same analytical techniques are employed herein, namely, Z-contrast STEM, MALDI MS, XAFS spectroscopy (through its two complementary modifications, x-ray absorption near edge structure, or XANES, and extended XAFS, or EXAFS), and Hg(0) poisoning kinetics studies. Analogous to the previous study on the Ir model system,<sup>14</sup> the specific objectives entail (i) determining the nuclearity of the M<sub>n</sub> species present initially (M is Co or Ni), (ii) establishing what M<sub>n</sub> species are present directly after use of the catalysts for cyclohexene hydrogenation, and (iii) using Hg(0) poisoning as a kinetics-based test of the homogeneous vs heterogeneous nature of the active catalyst.<sup>3</sup> The challenging, yet crucial issues of the form(s) taken, and role(s) played by the AlEt<sub>3</sub> component in Ziegler-type hydrogenation catalysts are currently being investigated, and will be reported in due course elsewhere.<sup>19</sup>

Before the use of catalyst solutions for cyclohexene hydrogenation, the Z-contrast STEM and MALDI MS results, which follow reveal that M<sub>n</sub> clusters with a wide range of sizes are obtained from combining Co(neodecanoate)<sub>2</sub> or Ni(2-ethylhexanoate)<sub>2</sub>, and

AlEt<sub>3</sub>, and the average cluster sizes are between 0.9 and 1.4 nm in diameter. The results of the Z-contrast STEM herein are, to our knowledge, the best existing microscopic analysis of *industrial* Co and Ni Ziegler-type hydrogenation catalysts. The XANES spectroscopy results suggest that a combination of nanoclusters and unreduced metal ions exists, with the ratio of the two phases depending, as one might expect, on the Al/M ratio. EXAFS spectroscopic analysis of both Co and Ni catalyst samples gives mean 1NN coordination number ( $N$ ) values for both metals in the 3–4 range. The most plausible, self-consistent interpretation of the evidence from multiple, complementary techniques is that the transition metal contents of the catalyst solutions are a combination of disordered nanoclusters and unreduced, mono-metallic species. In addition, Z-contrast STEM, MALDI MS, and XAFS all show that the transition metal species in catalyst solutions remain essentially unchanged by their use for cyclohexene hydrogenation. Furthermore, Hg(0) poisoning studies with the Ni system suggest that catalysis is heterogeneous (i.e., occurs via the observed Ni nanoclusters), but the Hg(0) poisoning experiments are inconclusive for the Co catalyst. Through the use of an established approach to distinguish homogeneous from heterogeneous catalysis,<sup>3,6–15</sup> and with the additional advantage of now being able to compare the results to those from a parallel study of an Ir model system, this study provides the best existing evidence suggesting catalysis by what appear to be Ziegler nanoclusters (i.e.,  $\geq M_4$ ) in Ziegler-type hydrogenation catalysts made from the *actual* industrial Co and Ni precatalyst materials. Noteworthy here is that since control experiments (vide infra and in the Supporting Information) show that AlEt<sub>3</sub> is required to generate an active catalyst (that XANES shows is reduced from Co(II)),

species like Co–Et that can  $\beta$ –hydrogen eliminate to ethylene plus Co–H, and thus plausible species such as  $\text{Co}_4\text{H}_4$ , all become candidates for the true catalyst.

## Experimental

**Materials and Instruments.** Material sources used to prepare catalyst solutions were kept consistent in order to obtain reproducible results (*vide infra*). All materials were stored and handled under a  $\text{N}_2$  atmosphere in a Vacuum Atmospheres drybox, unless stated otherwise. Drybox  $\text{O}_2$  levels were continuously monitored via a Vacuum Atmospheres  $\text{O}_2$ -level indicator and maintained at  $\leq 5$  ppm. Gastight syringes were used to carry out all solution measurements and additions done in the Finke group drybox at Colorado State University (CSU). Procedures used to control the amount of  $\text{H}_2\text{O}$  present were followed consistently to ensure reproducibility (*vide infra*); glassware was rinsed with nanopure water, dried overnight at  $160\text{ }^\circ\text{C}$ , and cooled under a vacuum or  $\text{N}_2$  atmosphere. Cyclohexane (Sigma-Aldrich, 99.5 %,  $\text{H}_2\text{O} < 0.001$  %) was kept over molecular sieves (Acros, 3 Å, activated by heating at  $200\text{ }^\circ\text{C}$  for 6 hours under vacuum) for  $\geq 2$  days prior to use with the Co catalyst, but used as received with the Ni catalyst (*vide infra*). Cyclohexene (Aldrich, 99%) was distilled over Na under argon. Precatalysts were obtained from OMG, as solutions in mineral spirits,  $\text{Co}(\text{neodecanoate})_2$ , 12% wt. Co, and  $\text{Ni}(\text{2-ethylhexanoate})_2$ , 8% wt. Ni (product names: 12% Co ten-cem and 8% Ni hex-cem). The industrial precatalyst sources of  $\text{Co}(\text{neodecanoate})_2$  or  $\text{Ni}(\text{2-ethylhexanoate})_2$  are neither relatively pure nor well-characterized structurally compared to the Ir model  $[(1,5\text{-COD})\text{Ir}(\text{2-ethylhexanoate})]_2$  precatalyst, which was characterized via single crystal X-ray diffractometry and used as

the pure crystalline starting material for the preparation of catalyst solutions.<sup>1,14</sup> These Co(neodecanoate)<sub>2</sub> and Ni(2-ethylhexanoate)<sub>2</sub> precatalyst solutions were used after diluting with cyclohexane to 12.0 mM in [M]. AlEt<sub>3</sub> (Strem Chemicals, 93%) was used as a solution in cyclohexane. Both Ar and H<sub>2</sub> gases were passed through moisture (Scott Specialty Gases) and oxygen traps (Trigon Technologies) prior to use. THAP (2'-4'-6'-trihydroxyacetophenone, Aldrich, 98%), used in the MALDI MS experiments as a matrix, was stored and used outside of the drybox, and applied as an aqueous solution.

#### **Catalyst Solution Preparation and Catalytic Cyclohexene Hydrogenations.**

Previous investigation into both the existing literature,<sup>3</sup> and the Ir model system<sup>14</sup> have made it clear that Ziegler-type hydrogenation catalysts are sensitive to the conditions and procedures used in their synthesis. We therefore carried out a variety of initial control experiments—testing the effects of catalyst aging, the Al/M ratio, the volume and concentration of catalyst solution prepared, the amount of H<sub>2</sub>O present, temperature, concentration of AlEt<sub>3</sub> used, and order and rate of precursor component combination—all with the goal of ensuring that the characterization results obtained herein would be both reproducible and representative of active Ziegler-type hydrogenation catalysts. The results from these control experiments are summarized here and given in greater detail in the Supporting Information for the interested reader. One of the important findings from these control experiments is the presence of gas-to-solution mass transfer limitation (MTL) effects in our current hydrogenation apparatus, which limits the *measurable* hydrogenation uptake rate to the rate of H<sub>2</sub> gas transfer into solution where the catalytic reaction takes place.<sup>20</sup> However, we have used catalyst preparation methods and conditions for this study that (i) result in catalytic cyclohexene hydrogenation rates that

are at least as rapid as we can observe due to the MTL effects present, (ii) are consistent with the most favorable methods and conditions described in the majority of the literature,<sup>3</sup> and (iii) are similar to, or the same as those used for the model Ir Ziegler-type hydrogenation catalyst made from [(1,5-COD)Ir( $\mu$ -O<sub>2</sub>C<sub>8</sub>H<sub>15</sub>)<sub>2</sub>] and AlEt<sub>3</sub>.<sup>1,14</sup> In short, the MTL kinetics present for these exceptionally active, industrial Ziegler-type hydrogenation catalysts did not preclude our determination of conditions and procedures for catalyst synthesis necessary to give results that are both reproducible and representative of active Ziegler-type hydrogenation catalysts standardized to that MTL limit.

Once established, the procedures for preparing and using catalyst solutions (referred to hereafter as the *standard conditions*) were followed consistently for repeat experiments unless specified otherwise. Control experiments demonstrate that the presence of (deliberately added) water during catalyst synthesis negatively affects the cyclohexene hydrogenation activity of the resulting catalysts. Therefore, all glassware was carefully dried as was the cyclohexane solvent for use with the Co-based catalyst (cyclohexane drying was not beneficial for the Ni catalysts, see the Supporting Information). The catalyst solutions were made under a N<sub>2</sub> atmosphere by combination of a 36.0 mM cyclohexane solution of AlEt<sub>3</sub> with a 12.0mM Co(neodecanoate)<sub>2</sub> or Ni(2-ethylhexanoate)<sub>2</sub> precatalyst stock solution. The ratios Al/Co = 3 and Al/Ni = 2 were used for the standard conditions on the basis of control experiments testing catalysts prepared with a range of Al/M values. Control experiments were performed with an Al/M ratio of zero for both Co and Ni, and it was found that no H<sub>2</sub> gas uptake occurred

without added  $\text{AlEt}_3$ , which shows the importance of the alkylaluminum cocatalyst in making active Ziegler-type hydrogenation catalysts.

Synthesis of catalyst solutions in batches up to 20 mL, as opposed to the 2.5 mL of catalyst solution prepared for use in a single hydrogenation run, had no observable effect on catalyst activity. Likewise, batch catalyst preparation at 7.2 mM in [M] had no observable effect on catalyst activity in comparison to the 1.44 mM in [M] catalyst solutions prepared for use in a single hydrogenation run (diluted after preparation to 1.2 mM in [M] with the addition of 0.5 mL of cyclohexene). Therefore, it was possible to prepare catalyst solutions either individually or batchwise as necessary, and at concentrations necessary for the subsequent type of analysis. Catalyst synthesis carried out with solutions heated to 60 °C resulted in catalyst solutions with lower cyclohexene hydrogenation activity (Supporting Information); hence, catalyst synthesis at the ambient drybox temperature of ~25 °C was established as a standard condition. For the sake of consistency, and unless noted otherwise, catalyst solutions were prepared by adding the  $\text{AlEt}_3$  solution to either the  $\text{Co}(\text{neodecanoate})_2$  or  $\text{Ni}(\text{2-ethylhexanoate})_2$  solution dropwise but rapidly (at a rate  $\geq 1$  drop every 5 sec), and with  $1000 \pm 200$  rpm stirring (measured with a Monarch Instruments Pocket-Tachometer 100). As an example of batch catalyst preparation, 20 mL of catalyst solution was prepared by first adding 16.8 mL of cyclohexane to a 20 mL glass vial containing a new  $5/8 \times 5/16$  inch Teflon-coated magnetic stir bar. Next, 1.6 mL of a 12.0 mM cyclohexane solution of  $\text{Ni}(\text{2-ethylhexanoate})_2$  was added. Stirring was started, followed by addition of 1.6 mL of a 36.0 mM  $\text{AlEt}_3$  solution. Stirring in the drybox was continued for 30 minutes, after which aliquots of the catalyst solution were taken for analysis or transferred to a new 22

× 175 mm Pyrex borosilicate culture tube containing a new 5/8 × 5/16 inch Teflon-coated magnetic stir bar for kinetic studies via use in cyclohexene hydrogenation. Since, as noted above, volume and concentration had no effect on hydrogenation, catalyst solutions were also prepared directly in the culture tubes for individual hydrogenation runs by, for example, first adding 1.9 mL of cyclohexane to a culture tube followed by 0.3 mL of a cyclohexane solution of Co(neodecanoate)<sub>2</sub>, 12.0 mM in [Co]. Stirring was started and then 0.3 mL of the 36.0 mM AlEt<sub>3</sub> solution in cyclohexane was added. Cyclohexene, 0.5 mL, was added last. In general, the procedures used in this study were very similar to, and in a number of cases the same as, those used previously for the Ir model system.<sup>14</sup>

After combination of the precursor components, cyclohexene was added to catalyst solutions used for catalytic hydrogenation runs. Control experiments show that aging prepared catalyst solutions resulted in *decreased* catalyst activity (Supporting Information), so catalysts were used for hydrogenation or otherwise analyzed as soon as possible after preparation. The procedure and apparatus used for catalytic cyclohexene hydrogenation have been described in detail elsewhere.<sup>21</sup> Briefly, the culture tube containing the catalyst solution was placed in a Fisher-Porter (F-P) bottle, sealed, and transferred out of the drybox. The F-P bottle was placed in a temperature regulating bath, stirring was begun, and the F-P bottle was connected to a pressurized H<sub>2</sub> line using Swagelock quick-connects. The F-P bottle was purged 15 times (1 purge/15 s) before setting the pressure to 40 psig. Data collection was then started at 4 min after the first purge. H<sub>2</sub> pressure data as a function of time was collected using an Omega PX 624-100 GSV pressure transducer, which was connected to a PC running LabView 7.0 by an Omega D1131 analog-to-digital converter. Data was subsequently handled using MS

Excel and Origin 7. Standard conditions for hydrogenation runs are: solvent = cyclohexane,  $[M] = 1.2 \text{ mM}$ , initial [cyclohexene] = 1.65 M, temp = 22.0 °C, initial H<sub>2</sub> pressure = 40 psig, and stirring rate = 1000 ± 10 rpm. The main point is that in both catalyst synthesis and subsequent hydrogenations, variables with the potential to influence the resulting catalytic activity have been tested and optimized (to the MTL limit), thereby allowing the development of standard conditions for the preparation and use of the highly active Ziegler-type hydrogenation catalysts used herein. This in turn ensures that the subsequent analytical results should be both reproducible and representative of active Ziegler-type hydrogenation catalysts.

**Z-Contrast STEM.** Catalyst samples were prepared according to standard conditions as described and collected for Z-contrast microscopy both before and after use in cyclohexene hydrogenation. Sample solutions were double-sealed air-tight, and shipped to the University of Pittsburgh for imaging (2–3 days between preparation and analysis). Preparation of samples on TEM grids was carried out in a glove-bag filled with dry N<sub>2</sub> at >1 atm, and located in the TEM room. Sample solutions were diluted with cyclohexane to twice their original volume, and 2–3 drops were dispersed onto a TEM grid with an ultrathin carbon film on a holey carbon support (Ted Pella, Inc.). These were dried at room temperature under N<sub>2</sub> for ≥10 minutes before being transferred into the TEM instrument. Transfer was done quickly to reduce possible oxidation of the sample. Samples were first treated with a high-intensity electron beam (electron beam shower) for ~15 minutes each time in the TEM column (with vacuum better than  $3 \times 10^{-6}$  Torr). Images were acquired using a field-emission JEM 2010 (scanning) transmission electron microscope operated at 200 kV. The high-angle scattering electrons were

collected with a JEOL ADF detector at a camera length of 8 cm, with a 0.2 nm (nominal) diameter probe. High-angle annular dark-field (HAADF) images were collected at 2M (million) magnification, and were  $1024 \times 1024$  pixels in dimension. Cluster diameters were measured manually at the full width at half maximum (FWHM) of the intensity profile across  $\geq 600$  clusters from images at the same levels of magnification and contrast using Gatan Digital Micrograph.

Control experiments were performed to determine whether the metal clusters observed were artifacts of the microscopy itself.  $\text{Co}(\text{neodecanoate})_2$ , without added  $\text{AlEt}_3$ , was deposited on a TEM grid (ultrathin carbon film supported by a lacey carbon film on a 400 Mesh copper grid, Ted Pella), and imaged following the methods noted above (i.e., including the electron beam shower). No Co clusters could be observed suggesting that neither sample preparation procedures nor Z-contrast STEM conditions are responsible for creating the observed clusters in catalyst samples. No Co clusters were observed when this same control experiment was carried out using high resolution (HR)TEM. (The fact that Co in  $\text{Co}(\text{neodecanoate})_2$  could not be observed in Z-contrast STEM images *without* Co cluster formation has a bearing on the interpretation of the EXAFS results, *vide infra*, specifically it leaves open the possibility that mono-metallic, unreduced metal ions are present.) Additionally,  $\text{Co}(\text{neodecanoate})_2$ , without added  $\text{AlEt}_3$ , was deposited on special TEM grids with 25 nm thick  $\text{SiO}_2$  windows (Dune Sciences).<sup>22</sup> However, for this sample on the special  $\text{SiO}_2$  grids, imaging using bright field TEM, Z-contrast STEM, and HRTEM all revealed the presence of nanometer-scale clusters, ostensibly the result of Co cluster formation under the TEM beam. These control experiments suggest that the clusters observed using Z-contrast STEM to image

catalyst samples deposited on ultrathin carbon grids, and measured to construct the cluster size histograms, are not artifacts resulting from the required sample handling or microscopy itself. Images from control experiments and additional microscopy are provided in the Supporting Information for the interested reader.

**MALDI MS.** Catalyst samples were prepared for analysis by MALDI MS in a manner almost identical to that described previously using the Ir model system.<sup>14</sup> A 0.5  $\mu\text{L}$ , 100 mM aqueous NaI ionizing agent solution was hand-spotted on a steel MS sample plate and air-dried, which was followed by 1  $\mu\text{L}$  of 2'-4'-6'-trihydroxyacetophenone (THAP) over the same spot and then also air-dried. The plate was then transferred into the drybox where sample solutions (1  $\mu\text{L}$ ,  $[\text{M}] = 1.44 \text{ mM}$ ) were applied onto the spot of deposited ionizing agent and matrix. The plate was then covered with its plastic capping plate and placed into a desiccator, which was sealed and removed from the drybox. The plate was transferred in air (exposure of  $\sim 30 \text{ sec}$ ) from the desiccator to the vacuum of the MALDI MS instrument, and MALDI MS spectra were taken immediately thereafter. Mass spectra were obtained at CSU on a Bruker Ultraflex TOF-TOF instrument in linear mode, with acceleration voltage at 25 kV, and in positive ion mode. A nitrogen laser ( $\lambda = 337 \text{ nm}$ ) with a 3 ns pulse width was focused over a 1 mm diameter spot. Data were collected with the highest laser power possible, for a higher S/N, but which still maximized resolution and avoided sample fragmentation. Calibration was done using Bradykinin, Angiotensin\_I, Angiotensin\_II, Substance\_P, Bombesin, Renin\_Substrate, ACTH\_clip and Somatostatin (purchased as a mixture of all these peptides from Bruker-Daltonics).

**XAFS.** Procedures for XAFS spectroscopy herein are similar to those used previously for the analysis of the Ir model system.<sup>14</sup> Solution samples of  $\text{Co}(\text{neodecanoate})_2$ ,  $\text{Ni}(\text{2-ethylhexanoate})_2$ , and catalysts made from these plus  $\text{AlEt}_3$  were prepared at Colorado State University, in 6.0 mL batches at 7.2 mM concentration in [M]. Aliquots of catalyst samples were used for cyclohexene hydrogenation in order to obtain both pre- and posthydrogenation catalyst samples. All samples were then sealed air-tight, and transported to the National Synchrotron Light Source (NSLS) at Brookhaven National Laboratory (BNL), Upton NY (2 days transit). At the NSLS, catalyst samples were handled and stored in an  $\text{N}_2$  atmosphere glovebox maintained at  $\leq 10$  ppm  $\text{O}_2$ . Catalyst samples were loaded, via glass pipette, into a custom-designed, airtight,  $\sim 1.5$  mL capacity, solution sample cell composed of a stainless steel frame made to press Kapton film windows onto a Teflon block. Threaded ports in the Teflon block allow for sample loading, which were then sealed using Teflon screws. Airtight seals in the threaded ports and windows were ensured by using Kalrez o-rings. XAFS experiments were performed at room temperature either on beamline X18b or X11a, which are sourced by bending magnets, and employ Si(111) channel-cut monochromators. Samples were loaded into an airtight sample cell, then mounted and positioned at  $45^\circ$  in the beam path. Three 30 cm long ion chambers filled with suitable gas mixtures were employed to record in transmission mode the incident, transmitted, and reference beam. A Lytle detector was used to measure fluorescence data simultaneously with transmission, but the fluorescence spectra were deemed of inferior quality to the transmission spectra and not used in the analysis. Co or Ni foils were used both for absorption edge calibration of the Co (7709 eV) and Ni (8333 eV) K edges prior to XAFS

scans. Co and Ni foils were also used to obtain reference spectra simultaneously in transmission mode for all sample scans. Six to eight scans were typically performed for each sample, and during data processing, multiple scans of a single sample were merged (averaged).

Data processing was accomplished using IFEFFIT.<sup>23</sup> For background removal, threshold energy values ( $E_0$ ) for both Co and Ni were assigned values corresponding to the inflection point in the normalized absorption edges. A Hanning window function was used to select data ranges in  $k$ -space with sufficient signal to noise ratio for Fourier Transforms (FTs), Supporting Information. The passive electron reduction factors ( $S_0^2$ ) for Co and Ni were acquired from fitting the Co and Ni foil standards, respectively (Supporting Information). Parameters including the coordination numbers ( $N$ ) bond lengths ( $R$ ) and their disorders ( $\sigma^2$ ) were varied in the fitting of catalyst sample spectra, as well as the correction to the photoelectron energy origin ( $\Delta E_0$ ). Details of fitting EXAFS spectra are given in the Supporting Information.

**Hg(0) poisoning.** Catalyst solutions for use in Hg(0) poisoning experiments were first prepared in the drybox according to the standard conditions as described with [M] concentration of 1.2 mM (M is Co or Ni), an Al/Co ratio of 3.0, or an Al/Ni ratio of 2.0, and initial cyclohexene concentrations of 1.65 M. Hg(0) was added to the catalyst solutions before cyclohexene hydrogenation catalysis was started and allowed to mix for the specified time. The bottle containing the catalyst solution and Hg(0) was then transferred to the pressurized  $H_2$  to collect pressure data using normal procedures.

In another version of the Hg(0) poisoning experiment, a standard conditions hydrogenation using the Ni catalyst was stopped after about half the cyclohexene had

been consumed by filling and purging the F–P bottle five times with Ar gas pressurized to 40 psig. The F–P bottle was then transferred back into the drybox where the Hg(0) was added. The F–P bottle was then reconnected to the hydrogenation line, refilled with H<sub>2</sub> gas using the standard procedure and data acquisition was restarted. Time and pressure values collected after Hg(0) addition were corrected to fit with the data collected before Hg(0) addition.

The results of Hg(0) poisoning control experiments are shown in the Supporting Information for the interested reader. Control experiments using various quantities of Hg(0) added to prepared catalyst solutions followed by various mixing times before their use in hydrogenation show that a procedure using  $\geq 300$  equivalents of Hg(0) per Ni and  $\geq 1.5$  hours of stirring (at 1000 rpm in a sealed FP bottle in the drybox) is adequate to thoroughly contact the Hg(0) with all of the Ni catalyst in solution; this procedure was then strictly followed.

In the case of the Co catalyst, control experiments showed that using even  $\sim 1770$  equivalents of Hg(0) per Co, plus 24 h of 1000 rpm stirring, are insufficient to completely and immediately poison all of the Co catalyst in solution. Additionally poisoning results are irreproducible (Supporting Information). This implies that the Hg(0) poisoning results with the Co catalyst cannot be interpreted in terms of catalyst homo- or heterogeneity; they are inconclusive. Other control experiments show that both the Ni and Co catalyst solutions retain catalytic activity when subjected to the handling procedures required for Hg(0) addition, but in the absence of Hg(0). Restated, those additional controls show that it is the Hg(0) itself, and not the procedures, that poison the catalysis.

## Results and Discussion

### Initial Observations, Plus an Overview of the Key Pre- and

**Posthydrogenation Characterization Results.** As noted in a review of the literature of the homogeneous versus heterogeneous catalysis problem,<sup>6</sup> initial observations of the catalyst solutions alone make industrial Ziegler-type catalysts candidates for study regarding the homogeneous vs. heterogeneous catalysis question. Specifically, dark brown or black solutions are frequently observed in literature catalyst systems now known to involve heterogeneous (e.g., nanoparticle) catalysis, making such an observation, by itself, *suggestive* of heterogeneous catalysis.<sup>6</sup> In the present study, there are several noteworthy observations from the synthesis of the industrial Co- and Ni-based catalysts, especially in comparison with the observations from the Ir model system.<sup>14</sup> For example, addition of the clear and colorless solution of AlEt<sub>3</sub> to the clear, deep-blue Co(neodecanoate)<sub>2</sub> solution results in an immediate change to a *dark brown, almost black solution*. Likewise, addition of the AlEt<sub>3</sub> solution to the clear, light-green solution of Ni(2-ethylhexanoate)<sub>2</sub> causes an immediate change to a *dark brown solution* (but one that is a lighter shade of brown than the Co/AlEt<sub>3</sub> catalyst solution). Unlike with the [(1,5-COD)IrO<sub>2</sub>C<sub>8</sub>H<sub>15</sub>]<sub>2</sub> plus AlEt<sub>3</sub> catalyst system, which is a much lighter, yellow-brown after addition of AlEt<sub>3</sub> but darkens during a cyclohexene hydrogenation run, and will occasionally precipitate a dark brown powder a few days after the completion of a hydrogenation run,<sup>14</sup> these industrial Co- or Ni-based catalysts do not exhibit observable color change or insoluble particle formation upon use for, or post, hydrogenation. Using the Ir model catalyst, it was found that H<sub>2</sub> uptake begins initially at a slower rate, then

accelerates to achieve its maximum rate after the start of hydrogenation (i.e., the initial rate is not the maximum rate).<sup>14</sup> Furthermore, this increase in cyclohexene hydrogenation rate during the hydrogenation itself observed using the model Ir catalyst is accompanied by the observation of, on average, Ir<sub>4-15</sub> clusters prehydrogenation, but *fcc* Ir(0)<sub>~40-150</sub> clusters posthydrogenation.

In contrast, with the industrial Co-, or Ni-based catalysts, H<sub>2</sub> uptake begins immediately at the apparent H<sub>2</sub> gas-to-solution MTL rate ( $\sim 80 \pm 20$  psig/h at 1000 rpm stirring, Supporting Information) or at  $\sim 30\%$  of the apparent H<sub>2</sub> gas-to-solution MTL rate respectively, Figure 1. This implies that in the industrial Co- or Ni-based catalysts, very active catalyst species are present initially (or possibly are formed essentially immediately) upon the introduction of H<sub>2</sub> gas. In short, the initial observations from catalyst preparation alone are consistent with the presence of Co and Ni Ziegler nanoclusters in catalyst solutions both initially, and throughout, the hydrogenation process.

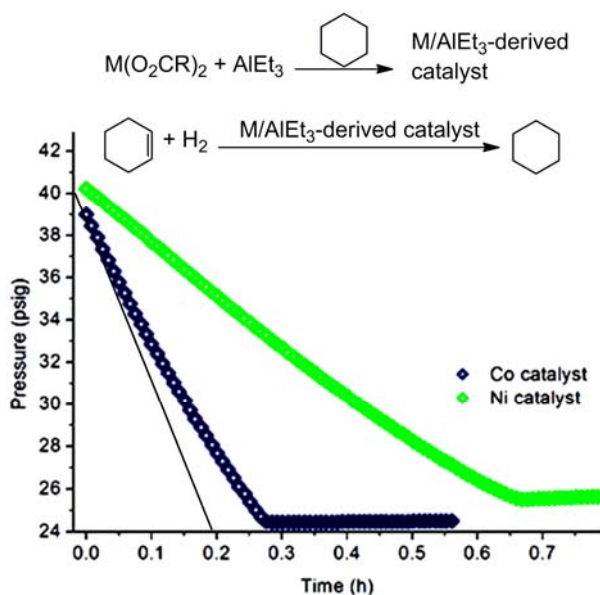


**Figure 1.** General steps for the synthesis of Co- or Ni-based Ziegler-type hydrogenation catalyst solutions. M(O<sub>2</sub>CR)<sub>2</sub> is either of the authentic industrial precatalysts,

Co(neodecanoate)<sub>2</sub> or Ni(2-ethylhexanoate)<sub>2</sub>. Catalyst solutions were made by combining a cyclohexane solution of one of the precatalysts, 12.0 mM in [M], with a 36.0 mM cyclohexane solution of AlEt<sub>3</sub>. Example catalytic cyclohexene hydrogenation curves using standard conditions of solvent = cyclohexane, [M] = 1.2 mM, initial [cyclohexene] = 1.65 M, temp = 22.0 °C, and stirring rate = 1000 ± 10 rpm are shown. The apparent MTL value, depicted here as a black line, is ~80 ± 20 psig/h in this apparatus and at these conditions (e.g., the 1000 ± 10 rpm stirring rate).

These initial observations of just the dark colors of the catalyst solutions explain why the specific objectives herein necessarily entail: (i) determining the nuclearity of the M<sub>n</sub> species present *initially*, and (ii) establishing what M<sub>n</sub> species are present *directly after* use of the catalysts for cyclohexene hydrogenation. These are the necessary first steps in probing the homogeneous versus heterogeneous nature of the most active catalyst in these industrial systems.

A summary of the results obtained from the analysis of catalyst samples pre- and posthydrogenation by Z-contrast STEM and MALDI MS is given in Table 1 alongside the results from the Ir model system for comparison. The key findings for both the Co- and Ni-based catalysts are (i) Z-contrast STEM and MALDI MS reveal nanometer-scale clusters for both Co and Ni samples, both before and after hydrogenation, and (ii) the XAFS data indicate that unreduced metal ions are present in solution, depending on the Al/M ratio, with the nanometer-scale Co<sub>n</sub> or Ni<sub>n</sub> clusters present. In addition, the XAFS shows those Co<sub>n</sub> and Ni<sub>n</sub> clusters possess disordered atomic structures. In short, disordered transition metal Ziegler nanoclusters appear to be the predominant clusters formed by the industrial Co- and Ni-based precatalysts upon addition of AlEt<sub>3</sub>, both before and after hydrogenation, yet monometallic (homogeneous) species appear to be present as well. In addition, the ability to directly compare the results obtained herein to

the results from the prior, analogous study of the model Ir system,<sup>14</sup> is a valuable, unique feature of the present study.

**Table 1.** Summary of results from investigation of metal cluster sizes using Z-contrast STEM and MALDI MS for industrial Ziegler-type hydrogenation catalysts made from Co(neodecanoate)<sub>2</sub> or Ni(2-ethylhexanoate)<sub>2</sub> plus AlEt<sub>3</sub> (Al/Co is 3.0, Al/Ni is 2.0), and for comparison an Ir Ziegler-type hydrogenation catalyst made from [(1,5-COD)Ir(μ-O<sub>2</sub>C<sub>8</sub>H<sub>15</sub>)<sub>2</sub>] plus AlEt<sub>3</sub> (Al/Ir is 2.0), both before and after use for cyclohexene hydrogenation.

analytical method	precatalysis			postcatalysis			
	range (nm)	average <sup>a</sup> (nm)	average <sup>a</sup> M <sub>n</sub> nuclearity	range (nm)	average <sup>a</sup> (nm)	average <sup>a</sup> M <sub>n</sub> nuclearity	
Co	Z-contrast STEM	0.6–3.3	1.4	Co <sub>~130</sub>	0.5–2.5	1.4	Co <sub>~130</sub>
	MALDI MS	0.8–1.8	1.2	Co <sub>~80</sub>	0.8–1.8	1.1	Co <sub>~60</sub>
Ni	Z-contrast STEM	0.4–3.5	1.3	Ni <sub>~100</sub>	0.6–4.0	1.4	Ni <sub>~130</sub>
	MALDI MS	0.8–1.7	0.9	Ni <sub>~34</sub>	0.8–1.6	0.9	Ni <sub>~34</sub>
Ir <sup>b</sup>	Z-contrast STEM	0.2–1.4	0.5	Ir <sub>~4</sub>	0.4–1.9	1.0	Ir <sub>~40</sub>
	MALDI MS	0.5–1.1	0.7	Ir <sub>~15</sub>	0.6–1.4	0.8	Ir <sub>~20</sub>

<sup>a</sup> The average values are calculated mean cluster diameters from Z-contrast STEM, and estimated mean nuclearities from MALDI MS. Explanations for how these values were determined and how the cluster diameter-nuclearity conversion is performed are given below. <sup>b</sup> Results from a previously published study,<sup>14</sup> provided here for comparison.

**Nuclearity of M<sub>n</sub> Species before Hydrogenation: Z-Contrast STEM.** Samples of the Co(neodecanoate)<sub>2</sub> plus AlEt<sub>3</sub> catalyst, with an Al/Co ratio of 3.0, *before* use for cyclohexene hydrogenation were imaged using Z-contrast STEM. Measurement of 604 clusters shows a range of Co cluster sizes from 0.6 to 3.3 nm in diameter, with a mode and median of 1.3 nm clusters, and a mean Co cluster diameter of 1.4 ± 0.4 nm. These cluster diameters correspond to cluster nuclearities with a range from Co<sub>~10</sub> to Co<sub>~1700</sub>, a mode and median of Co<sub>~100</sub>, and a mean of Co<sub>~130</sub>.<sup>24,25,26</sup> Figure 2 shows an example image and the histogram.

Samples of the Ni(2-ethylhexanoate)<sub>2</sub> plus AlEt<sub>3</sub> catalyst, with an Al/Ni ratio of 2.0, *before* use for cyclohexene hydrogenation were also imaged using Z-contrast STEM.

An example image and the histogram are shown in Figure 3. Measurement of 650 clusters in Z-contrast STEM images reveals a range of Ni cluster sizes from 0.4 nm to 3.5 nm in diameter. The mode, median, and mean Ni cluster diameters are 1.1 nm, 1.2 nm, and  $1.3 \pm 0.5$  nm, respectively. These diameters correspond to cluster nuclearities ranging from Ni<sub>3</sub> to Ni<sub>2050</sub>, the mode, median, and mean being Ni<sub>60</sub>, Ni<sub>80</sub>, and Ni<sub>100</sub>, respectively.<sup>24,25,26</sup>

For both Co and Ni samples, Z-contrast STEM shows the presence of metal clusters with a broad distribution of sizes ranging from sub-nanometer to several nanometers in diameter. Cluster diameter measurements were made using the full width at half-maximum (FWHM) of line intensity profiles across individual clusters. These Z-contrast microscopy results by themselves should not be considered absolutely definitive, however, due to the possibility that the observed clusters are artifacts of the microscopy itself, especially given that lighter (first-row) transition metal clusters and precursors are known to be less stable in TEM electron beams than their heavier (third-row) analogs—a key reason we began our studies with our now-published third-row metal, Ir-model system.<sup>14,27,28,29</sup> More specifically, Ni Ziegler-type hydrogenation catalysts have been observed to be sensitive to electron microscopy sample treatment processes, namely, drying of the Ni catalyst solution on TEM grids.<sup>2</sup> However, the possibility of artifactual results is mitigated herein by the use of *scanning* TEM,<sup>30</sup> which diminishes the potential for beam-induced sample damage via a small electron probe, low beam current, and minimal beam exposure time.<sup>31</sup> The images herein were watched during image acquisition for signs of the influence of the TEM beam on the catalyst sample, and no changes in cluster size or shape were observed. In addition, control experiments

(described in the Experimental Section, images shown in the Supporting Information) suggest that the clusters observed using Z-contrast STEM, and measured to construct the cluster size histograms, are not artifacts. To summarize, Z-contrast microscopy shows that Co and Ni catalyst samples, *before* hydrogenation, each contain a wide range of  $M_n$  clusters,  $1.4 \pm 0.4$  nm,  $\text{Co}_{\sim 130}$ , and  $1.3 \pm 0.5$  nm,  $\text{Ni}_{\sim 100}$ , being the mean cluster size and nuclearity in each case respectively. To the extent of our knowledge, the results of the Z-contrast STEM herein are the best existing microscopic analysis of *industrial* Co and Ni Ziegler-type hydrogenation catalysts.

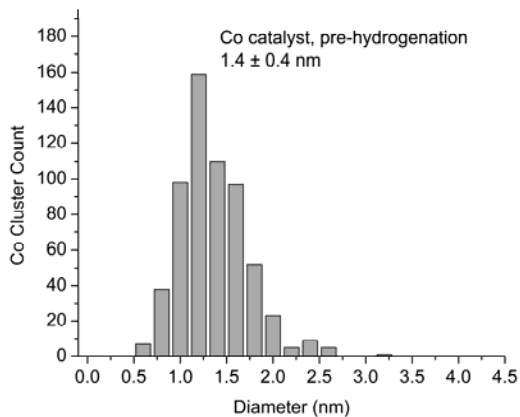
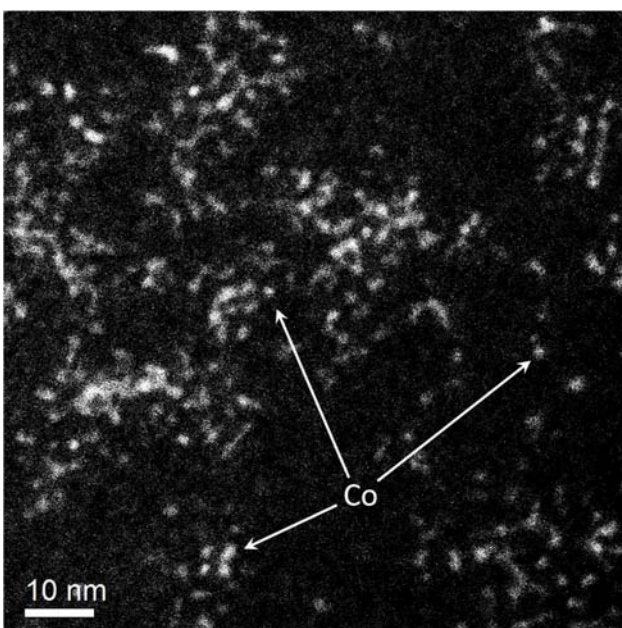


**Figure 2.** Example Z-contrast STEM image of the  $\text{Co}(\text{neodecanoate})_2$  plus  $\text{AlEt}_3$  catalyst, with an Al/Co ratio of 3.0, and before its use for cyclohexene hydrogenation. The histogram from measuring 604 Co clusters reveals an overall range of Co clusters observed from 0.6 to 3.3 nm in diameter, which correspond to  $\text{Co}_{\sim 10}$  to  $\text{Co}_{\sim 1700}$  clusters. The Co clusters measured have a mode and median of 1.3 nm, and a mean diameter of  $1.4 \pm 0.4$ , corresponding to  $\text{Co}_{\sim 100}$  and  $\text{Co}_{\sim 130}$  clusters, respectively.<sup>24,25,26</sup>

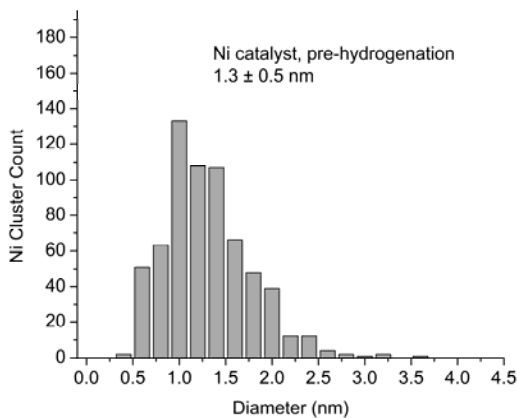
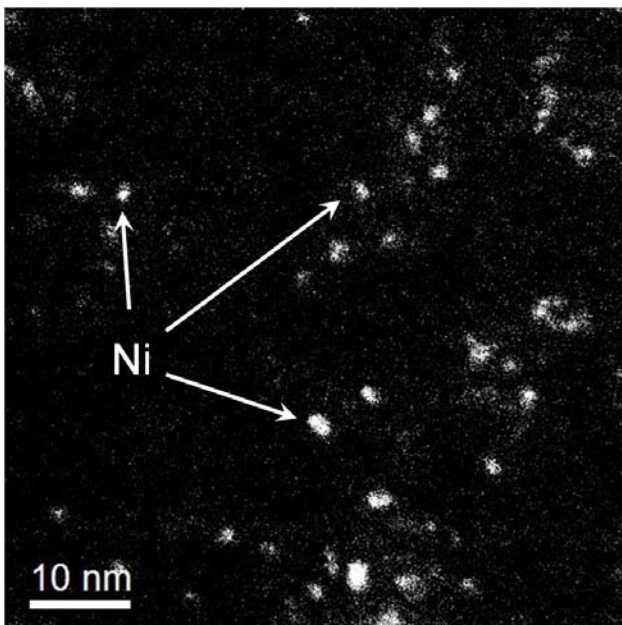


**Figure 3.** Example Z-contrast STEM image of the  $\text{Ni}(\text{2-ethylhexanoate})_2$  plus  $\text{AlEt}_3$  catalyst with an Al/Ni ratio of 2.0, and before use for cyclohexene hydrogenation. The histogram made from measurement of 650 Ni clusters shows Ni cluster sizes ranging from 0.4 to 3.5 nm in diameter, which correspond to  $\text{Ni}_{\sim 3}$  to  $\text{Ni}_{\sim 2050}$  clusters. The Ni clusters measured have a mode of 1.1 nm, a median of 1.2 nm, and a mean diameter of  $1.3 \pm 0.5$  nm, corresponding to  $\text{Ni}_{\sim 60}$ ,  $\text{Ni}_{\sim 80}$ , and  $\text{Ni}_{\sim 100}$ , respectively.<sup>24,25,26</sup>

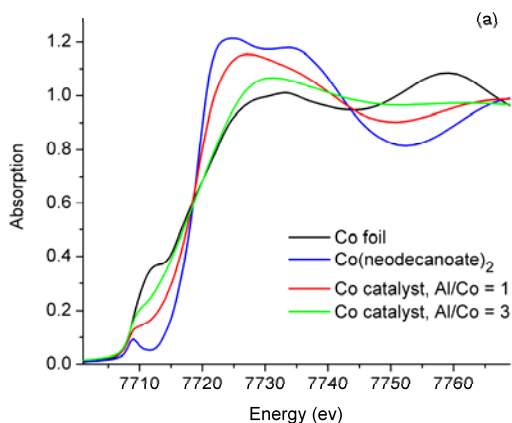
**Nuclearity of  $M_n$  Species *before* Hydrogenation: MALDI MS.** Samples of the Co(neodecanoate)<sub>2</sub> plus AlEt<sub>3</sub> catalyst, with an Al/Co ratio of 3.0, were also analyzed using MALDI MS before their use in cyclohexene hydrogenation. A broad peak is observed with a maximum intensity at ~4500 *m/z* (Figures are shown in the Supporting Information). With the assumptions that the ions forming the broad peaks are composed of only Co atoms,<sup>32,33,34</sup> and that the ionic charge is +1,<sup>14,32,34,35</sup> the maximum intensity of the MALDI MS peak at ~4500 *m/z* corresponds to Co<sub>~80</sub> clusters. This, in turn, corresponds to a diameter approaching ~1.2 nm (used as an estimate of the average Co clusters reported in Table 1). Furthermore, the broad MALDI MS peak also indicates a wide size dispersity of the Co clusters present, similar to the wide size dispersity of the Co clusters observed using Z-contrast STEM. The FWHM of the broad, asymmetrically shaped MALDI MS peak is from ~2000–9000 *m/z*, and tails off towards higher *m/z* values. The peak reaches one-fourth maximum intensity at ~12000 *m/z*, and one-eighth maximum intensity at ~16000 *m/z*; these *m/z* values correspond to approximately Co<sub>~30–150</sub>, Co<sub>~200</sub>, and Co<sub>~270</sub> clusters, respectively, which in turn correspond to approximately 0.9–1.5, 1.6, and 1.8 nm Co clusters, respectively.

Samples of the Ni(2-ethylhexanoate)<sub>2</sub> plus AlEt<sub>3</sub> catalyst, with an Al/Ni ratio of 2.0, were also analyzed using MALDI MS before their use in cyclohexene hydrogenation. A broad peak is observed with a maximum intensity at *m/z* of 2000. However, the presence of Ni atoms in species below 1500 *m/z* is ruled out by the absence of characteristic Ni isotope peak distributions in that region. In a control experiment, the MALDI MS of a blank sample containing only the matrix, trihydroxyacetophenone (THAP), and ionizing agent, NaI contains peaks in the 0–1500 *m/z* range (Supporting

Information). Therefore, the 0–1500  $m/z$  range was excluded from the mass spectrum region used to calculate number of transition metal atoms (M) in the  $M_n$  clusters, and corresponding diameters, for both Co and Ni catalyst samples; the  $m/z$  values of 1500–16000 for Co, and 1500–13500 for Ni were used to calculate the cluster diameter ranges reported in Table 1. Using the same assumptions employed for the Co system above, as well as previously in the literature,<sup>14,32,33,34,35</sup> the maximum intensity of the broad peak at  $m/z$  of  $\sim 2000$  indicates  $Ni_{\sim 34}$  clusters, corresponding to  $\sim 0.9$  nm diameter Ni nanoclusters, (used as an estimate of the average Ni clusters reported in Table 1). Much like the MALDI MS peak of the Co catalyst (and of the Ir model system<sup>14</sup>), the broad, asymmetrically shaped peak of the Ni catalyst also tails off towards higher  $m/z$  values reaching  $\sim 6000$   $m/z$  at half maximum intensity,  $\sim 9000$   $m/z$  at one-fourth maximum intensity, and  $\sim 13500$   $m/z$  at one-eighth maximum intensity, which correspond to approximately  $Ni_{\sim 100}$ ,  $Ni_{\sim 150}$ , and  $Ni_{\sim 230}$ , respectively. These nuclearities correspond, in turn, to approximately 1.3, 1.5, and 1.7 nm Ni nanoclusters, respectively.

Somewhat as an aside, but interestingly, this study, and the previous one of the Ir model system,<sup>14</sup> are unique tests of the value of MALDI MS as an analytical method for measuring the size and size distribution of transition metal nanoclusters in that the obtain MALDI MS data on systems where Z-contrast STEM (and XAFS, vide infra) data are available for comparison. Overall, the MALDI MS-determined nanocluster sizes and size distributions for both Co and Ni prehydrogenation catalysts are generally consistent with those determined using Z-contrast STEM in showing cluster sizes in the range of 0.8–1.8 nm for Co, and 0.8–1.7 nm for Ni are present.

**Nuclearity of  $M_n$  Species *before* Hydrogenation: XAFS (i.e., XANES plus EXAFS) Spectroscopy.** The XANES spectra of both Co and Ni catalysts are compared to those of the corresponding metal foils and catalyst precursors in Figure 4. In each case, the XANES spectra of the catalyst solution becomes less like the precursor solution and more like the metal foil with higher Al/M ratios. This suggests that, in terms of composite average formal oxidation state, the Co or Ni metals in catalyst solutions become progressively less like their M(II) precatalysts, and progressively more resembling of M(0), as the Al/M ratios increase from 1.0 to 3.0. These results imply that unreduced metal ions are likely present in catalyst solutions in amounts that decrease with additional  $AlEt_3$ . Given the  $M_n$  nanoclusters observed using both Z-contrast STEM and MALDI MS, these results suggest that catalyst solutions contain a combination of  $M_n$  clusters with a wide range of diameters *and* unreduced metal ions, with the proportion of M atoms in the cluster versus ion phases depending on the Al/M ratio used in catalyst preparation.



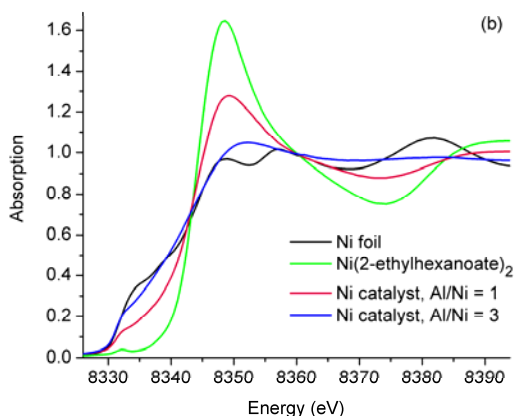


**Figure 4.** (a) XANES spectra of Co foil (black) the Co(neodecanoate)<sub>2</sub> catalyst precursor without added AlEt<sub>3</sub> (blue), and Co(neodecanoate)<sub>2</sub> plus AlEt<sub>3</sub> catalysts with Al/Co ratios of 1.0 (red) and 3.0 (green). (b) XANES spectra of Ni foil (black), the Ni(2-ethylhexanoate)<sub>2</sub> catalyst precursor without added AlEt<sub>3</sub> (green), and Ni(2-ethylhexanoate)<sub>2</sub> plus AlEt<sub>3</sub> catalysts with Al/Ni ratios of 1.0 (pink) and 3.0 (blue). In each case, with additional AlEt<sub>3</sub>, the XANES spectra of the catalyst solution becomes less like the precursor solution and more like the metal foil.

The potential of EXAFS spectroscopy for the characterization of Ziegler–type hydrogenation catalysts, especially the industrially favored Co and Ni catalysts, was made apparent to us by the valuable prior studies of Goulon and co-workers.<sup>36</sup> Specifically, those authors found Ni–Ni first nearest neighbors indicating the presence of Ni metal clusters.<sup>36</sup> However, additional study using modern EXAFS analysis methods that use *ab initio* theory for the quantitative modeling and analysis of experimental EXAFS spectra proved worthwhile,<sup>37</sup> especially when considered alongside results of complementary Z-contrast STEM and MALDI MS techniques used herein, the Hg(0) poisoning studies, and the now possible comparison to the results obtained from the Ir model system.<sup>14</sup>

First, EXAFS data were collected separately for Co and Ni foils, and cyclohexane solutions of the Co(neodecanoate)<sub>2</sub> and Ni(2-ethylhexanoate)<sub>2</sub> precatalysts, without

added AlEt<sub>3</sub>, for use as reference samples (see the Supporting Information for the full results, including fits to the data). Solution samples of the catalysts prepared by addition of AlEt<sub>3</sub>, but *before* their use in cyclohexene hydrogenation, were then analyzed by EXAFS. Spectra were collected for catalyst samples with Al/M ratios of 0.5, 1.0, 1.5, 2.0, 2.5, 3.0, and 5.0. However, the EXAFS spectra of many of these samples were of sufficiently poor quality to make fitting and interpretation unreliable. The highest quality spectra were obtained for the Al/M = 1.0 and 3.0 samples; therefore, the spectra and fitting results of the Al/M = 1.0 and 3.0 samples are shown here, but the spectra and fitting results from samples prepared at other Al/M ratios are shown in the Supporting Information.<sup>38</sup> For both Co and Ni catalysts, sample spectra show peaks that correspond to the first nearest neighbor (1NN) M–O peak in the precatalyst spectra, and to the 1NN M–M peak in the M foil spectra, Figure 5. This is analogous to the catalyst spectra of the Ir model catalyst system,<sup>14</sup> and so the fitting strategy used herein for the Co- or Ni-based catalysts is analogous to the one employed to fit the EXAFS spectra of the Ir model catalyst samples.<sup>14</sup> The Co and Ni catalyst spectra were fit using composite models created from the 1NN M–O path of the precatalyst and the 1NN M–M path of the bulk metal. Examples of fitting results are shown in Figure 6, and given in Tables 2 and 3.

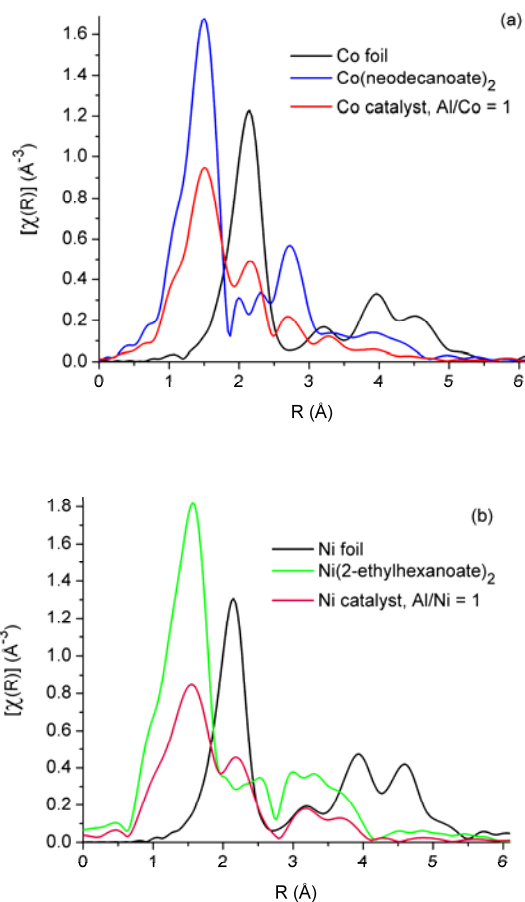


**Figure 5.** (a) Fourier transform magnitudes of the  $k^2$ -weighted EXAFS spectra of Co metal foil (black), the  $\text{Co}(\text{neodecanoate})_2$  precatalyst without added  $\text{AlEt}_3$  (blue), and a sample of the  $\text{Co}(\text{neodecanoate})_2$  plus  $\text{AlEt}_3$  catalyst with an Al/Co ratio of 1.0 before its use for hydrogenation (red). (b) Fourier transform magnitudes of the  $k^2$ -weighted EXAFS spectra of Ni foil (black), the  $\text{Ni}(\text{2-ethylhexanoate})_2$  precatalyst without added  $\text{AlEt}_3$  (green) and a sample of the  $\text{Ni}(\text{2-ethylhexanoate})_2$  plus  $\text{AlEt}_3$  catalyst with an Al/Ni ratio of 1.0 before its use for hydrogenation (pink). Upon addition of  $\text{AlEt}_3$ , the Co and Ni catalyst samples still show a peak corresponding to the 1NN, M–O peak of the  $\text{Co}(\text{neodecanoate})_2$  and  $\text{Ni}(\text{2-ethylhexanoate})_2$  precatalysts, respectively, but also display a peak corresponding to the 1NN, M–M peak from the spectrum of the bulk metal. Also, and significantly, catalyst samples lack peaks in the 3–6 Å range characteristic of ordered, metallic structure. Spectra for Co and Ni foils are shown at one-fourth intensity scale for the purpose of comparison.

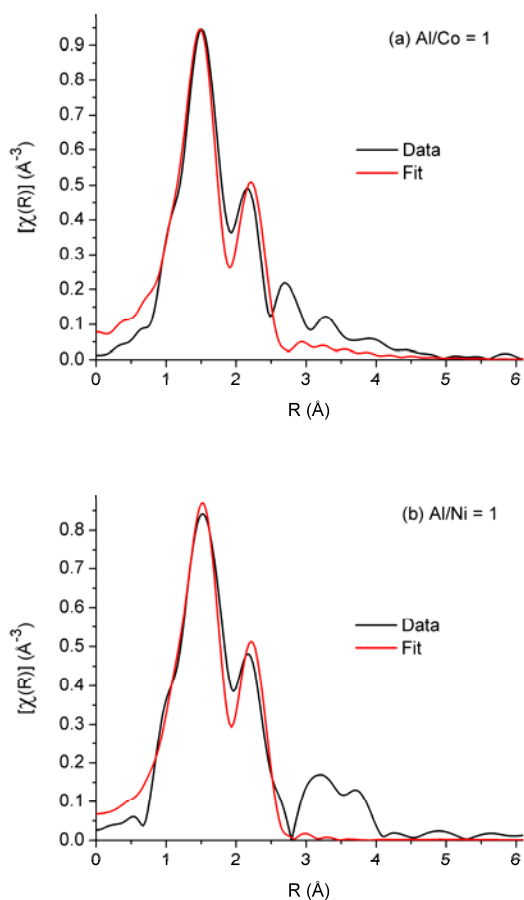


**Figure 6.** Data and fits for (a)  $\text{Co}(\text{neodecanoate})_2$  plus  $\text{AlEt}_3$  catalyst, and (b)  $\text{Ni}(\text{2-ethylhexanoate})_2$  plus  $\text{AlEt}_3$  catalyst, with an Al/M ratio of 1.0 in each case. The highest quality spectra were obtained for the Al/M = 1.0 and 3.0 samples; the experimental spectra and fits to the Al/M = 1.0 data are shown here as examples—spectra and fitting results from samples prepared at other Al/M ratios are shown in the Supporting Information.

**Table 2.** Fitting results from EXAFS spectroscopic analysis of Co reference samples and  $\text{Co}(\text{neodecanoate})_2$  plus  $\text{AlEt}_3$  catalyst samples before hydrogenation.

Sample	Co foil	$\text{Co}(\text{O}_2\text{CR})_2^{\text{a}}$	Co catalyst Al/Co	Co catalyst Al/Co
$N_{\text{Co-Co}}$	12 <sup>d</sup>		$3 \pm 2$	$3.9 \pm 0.4$
$N_{\text{Co-O}}$		$4.7 \pm 0.4$	$3.5 \pm 0.9$	$3 \pm 2$
$R_{\text{Co-Co}} (\text{\AA})^{\text{b}}$	$2.492 \pm 0.002$		$2.51 \pm 0.02$	$2.432 \pm 0.009$
$R_{\text{Co-O}} (\text{\AA})^{\text{b}}$		$1.959 \pm 0.005$	$1.95 \pm 0.02$	$1.86 \pm 0.02$
$\sigma^2_{\text{Co-Co}} (\text{\AA}^2)^{\text{c}}$	$6.7 \pm 0.3$		$15 \pm 6$	$12 \pm 1$
$\sigma^2_{\text{Co-O}} (\text{\AA}^2)^{\text{c}}$		$4.6 \pm 0.7$	$7 \pm 3$	$20 \pm 7$

<sup>a</sup>  $\text{Co}(\text{O}_2\text{CR})_2$  is the catalyst precursor  $\text{Co}(\text{neodecanoate})_2$  without added  $\text{AlEt}_3$ . The full analysis of  $\text{Co}(\text{neodecanoate})_2$  is given in the Supporting Information. <sup>b</sup> R stands for the interatomic distance corresponding to the single scattering paths. <sup>c</sup>  $\sigma^2$  represents the mean square variation in R due to both

static and dynamic disorder (also known as the EXAFS Debye-Waller factor), and values shown are  $\times 10^3$ .  
<sup>d</sup> For Co foil, this parameter was defined as the value shown (i.e., not varied in the fit).

**Table 3.** Fitting results from EXAFS spectroscopic analysis of Ni reference samples and Ni(2-ethylhexanoate)<sub>2</sub> plus AlEt<sub>3</sub> catalyst samples before hydrogenation.

Sample	Ni foil	Ni(O <sub>2</sub> CR) <sub>2</sub> <sup>a</sup>	Ni catalyst	Ni catalyst
Al/Ni			1.0	3.0
N <sub>Ni-Ni</sub>	12 <sup>d</sup>		3 ± 1	4.4 ± 0.3
N <sub>Ni-O</sub>		5.8 ± 0.3	2.8 ± 0.5	1.2 ± 0.3
R <sub>Ni-Ni</sub> (Å) <sup>b</sup>	2.490±0.003		2.51 ± 0.02	2.447±0.006
R <sub>Ni-O</sub> (Å) <sup>b</sup>		2.035±0.005	2.00 ± 0.02	1.85 ± 0.01
σ <sup>2</sup> <sub>Ni-Ni</sub> (Å <sup>2</sup> ) <sup>c</sup>	6.9 ± 0.5		13 ± 4	12.4 ± 0.8
σ <sup>2</sup> <sub>Ni-O</sub> (Å <sup>2</sup> ) <sup>c</sup>		7.4 ± 0.7	8 ± 3	14 ± 5

<sup>a</sup> Ni(O<sub>2</sub>CR)<sub>2</sub> is the catalyst precursor Ni(2-ethylhexanoate)<sub>2</sub> without added AlEt<sub>3</sub>. The full analysis of Ni(2-ethylhexanoate)<sub>2</sub> is given in the Supporting Information. <sup>b</sup> R stands for the interatomic distance corresponding to the single scattering paths. <sup>c</sup> σ<sup>2</sup> represents the mean square variation in R due to both static and dynamic disorder (also known as the EXAFS Debye-Waller factor), and values shown are  $\times 10^3$ .  
<sup>d</sup> For Ni foil, this parameter was defined as the value shown (i.e., not varied in the fit).

The main results from EXAFS are as follows: (i) peaks in the 3–6 Å range in the R-space EXAFS spectra (indicative of ordered metallic structures and evident in the Co and Ni foil reference spectra, Figure 5), are *absent* for both Co and Ni catalyst samples. This same result was also obtained from previous EXAFS analysis of the Ir model system,<sup>14</sup> and the lack of the large distance peaks observed here suggests that Co and Ni catalyst samples are either (a) composed of metal species such as sub-nanometer metal clusters too small to have contributions to that interatomic distance range (b) composed of larger metal nanoclusters with a high degree of atomic disorder, or (c) some combination of the two. (ii) Spectra are fit reasonably well using a composite model analogous to the one employed for the Ir model system.<sup>14</sup> *Significantly, and unlike in the Ir model system, the catalyst samples with an Al/M ratio of 3.0 did not require incorporating a backscattering contribution from M–Al into the model.* Furthermore, the spectra themselves, Figure 6, lack the feature observed in the spectra of the Ir model system that “grew in” with successively greater Al/M ratios. From fitting the data, (iii)

the 1NN M–M coordination numbers observed for Co and Ni samples are, like those observed in the Ir model system studied previously,<sup>14</sup> roughly in the 3–4 range, and could point towards the predominance of, on average, sub-nanometer, M<sub>4–6</sub>, metal clusters in catalyst solutions before hydrogenation.<sup>39</sup> Alternatively, low 1NN M–M coordination numbers could signify large degrees of structural disorder in relatively large metal nanoclusters.<sup>14,40</sup> The  $\sigma_{M-M}^2$  values of the catalyst samples are approximately twice the experimentally determined bulk metal values (Tables 3 and 4), which is also suggestive of disordered nanoclusters. Another possibility is that the metal species in catalyst solutions exist as some combination of disordered clusters, and unreduced metal ions.

An additional main result from EXAFS, (iv) the closest M–M distances, given by 1NN  $R_{M-M}$  values, overlap within experimental error with the corresponding bulk metals for both Co and Ni samples with Al/M ratios of 1.0, but are *shorter than* the bulk metal M–M distances for both Co and Ni Al/M = 3.0 samples. M–M distances in nanometer scale metal particles with a bulk-like atomic structure are expected to be shorter on average than the corresponding bulk M–M distances due to M–M bond contraction required to counteract (i.e., decrease) the high surface free energy of the small metal clusters.<sup>40a-d,41</sup> Therefore, the implication is that the Co or Ni catalyst materials are becoming *structurally* more like nanoscale metal particles with increasing amounts of AlEt<sub>3</sub>, but not to the point that the 1NN  $N_{M-M}$  values increase significantly or long range metallic order becomes apparent in the 3–6 Å range in the *R*-space EXAFS spectra (which is also consistent with the changes in the XANES spectra given above).

Interpretation of the EXAFS results from the Co and Ni samples must be carried out in light of the Z-contrast STEM, MALDI MS, and XANES results. For example, the

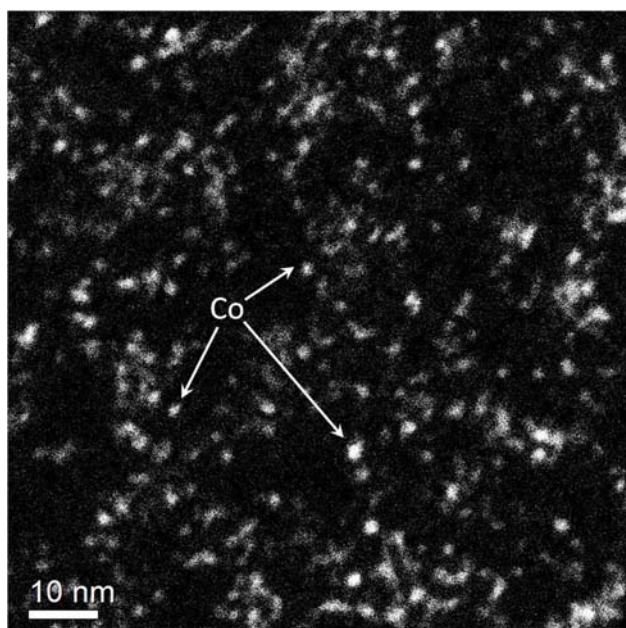
1NN  $N_{M-M}$  values from EXAFS of roughly 3–4 seem, at first take, to imply on average  $M_{4-6}$  clusters analogous to the Ir results, but Z-contrast STEM reveals mean Co or Ni cluster diameters of 1.4 or 1.3 nm, respectively, that is  $M_{-130}$  to  $M_{-100}$  clusters. Therefore, the most plausible explanation of the results from combining the Z-contrast STEM, MALDI MS, and XAFS (i.e., XANES and EXAFS) spectroscopy appears to be that a combination of nanoclusters (which are structurally disordered resulting in the absence of peaks at larger distances in the  $R$ -space EXAFS spectra, and distorted 1NN  $N_{M-M}$  values from fits of the EXAFS spectra<sup>42)</sup> and unreduced metal ions are present, with these two phases of M species both contributing to the mean  $N_{M-M}$  value.<sup>40i,43</sup> The possibility of mono-metallic, unreduced metal ions being present is supported by the control experiments for Z-contrast STEM in which no Co was observable when only  $\text{Co}(\text{neodecanoate})_2$ , without  $\text{AlEt}_3$ , was on the sample grid. In other words, the metal-containing species in Co and Ni catalyst solutions appear to consist of disordered metal clusters with a broad distribution of sizes, the mean diameters of which are given by Z-contrast STEM and MALDI MS, plus some mono-metallic complexes present as unreduced metal ionic species.

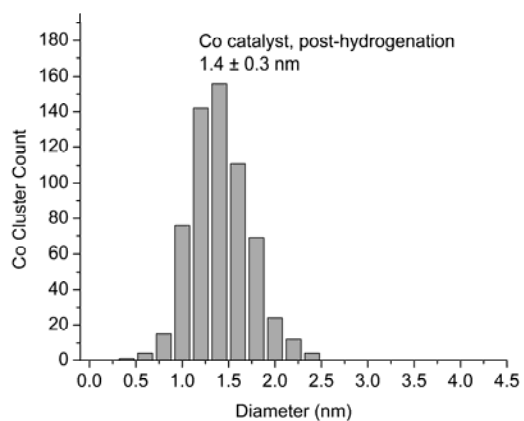
**Nuclearity of  $M_n$  species after hydrogenation: Z-contrast STEM.** The  $\text{Co}(\text{neodecanoate})_2$  plus  $\text{AlEt}_3$  catalyst, with an Al/Co ratio of 3.0, and *after* its use for cyclohexene hydrogenation was imaged using Z-contrast STEM. Measurement of 614 clusters shows a range of Co cluster sizes 0.5–2.5 nm in diameter. The mode, median, and mean Co cluster diameters are 1.3, 1.4, and  $1.4 \pm 0.3$  nm, corresponding to  $\text{Co}_{-100}$  and  $\text{Co}_{-130}$ , accordingly. Figure 7 shows an example image and the histogram.

The Ni(2-ethylhexanoate)<sub>2</sub> plus AlEt<sub>3</sub> catalyst, with an Al/Ni ratio of 2.0, *after* its use for cyclohexene hydrogenation was also imaged using Z-contrast STEM.

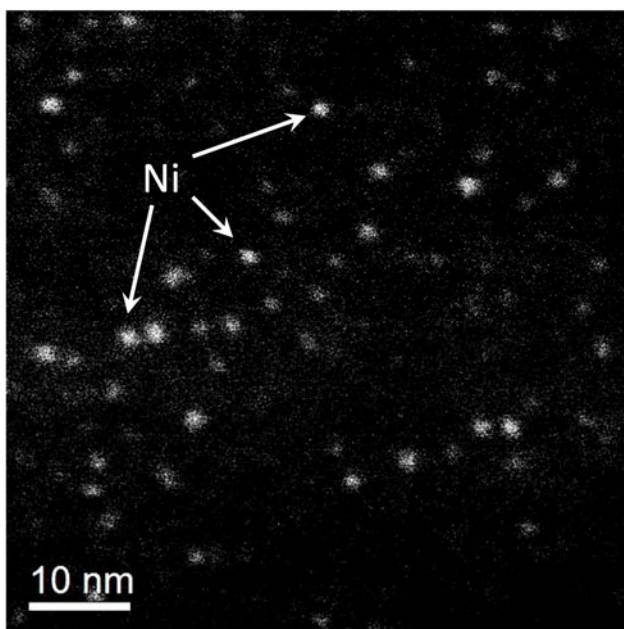
Measurement of 650 clusters in Z-contrast STEM images reveals a range of Ni cluster sizes 0.6–4.0 nm in diameter. The mode and median Ni cluster diameter is 1.4 nm and the mean is  $1.4 \pm 0.4$  nm. These diameters correspond to Ni<sub>~130</sub>. An example image and the histogram are shown in Figure 8.

Z-contrast STEM shows that using these Co and Ni Ziegler-type hydrogenation catalysts for cyclohexene hydrogenation does not induce a change in the sizes of the metal cluster species present in either Co or Ni catalyst samples, at least under the conditions used herein. Although this differs from the distinct increase in metal cluster size and change in structure exhibited by the Ir model system,<sup>14</sup> it is consistent with the lack of changes in catalyst solution color, no observation of precipitates in post-hydrogenation solutions (unlike the Ir model system<sup>14</sup>). In short, catalytic cyclohexene hydrogenation induces essentially no changes in size or size distribution of the Co or Ni clusters observed by Z-contrast STEM.





**Figure 7.** Example Z-contrast STEM image of a  $\text{Co}(\text{neodecanoate})_2$  plus  $\text{AlEt}_3$  catalyst sample after its use in hydrogenation. The histogram shows the results from measuring the diameters of 614 Co clusters in such images; measured cluster diameters range from 0.5 to 2.5 nm, which correspond to Co cluster nuclearities from  $\text{Co}_{\sim 6}$  to  $\text{Co}_{\sim 740}$ . The mode, median, and mean diameters of Co clusters are 1.3, 1.4, and  $1.4 \pm 0.3$  nm, corresponding to  $\text{Co}_{\sim 100}$  or  $\text{Co}_{\sim 130}$  accordingly.



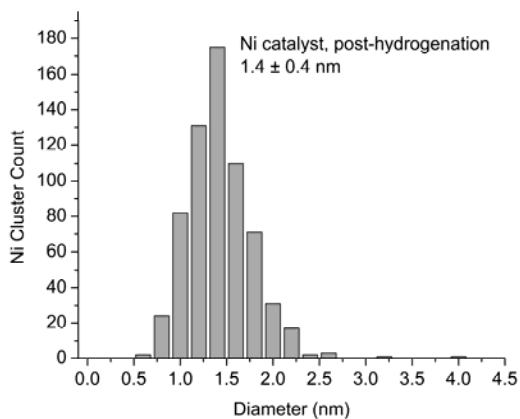


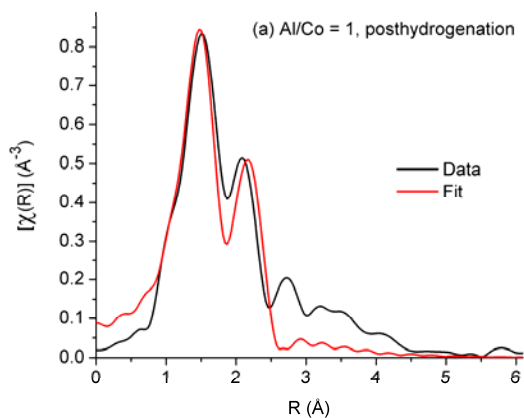
**Figure 8.** Example Z-contrast STEM image of a Ni(2-ethylhexanoate)<sub>2</sub> plus AlEt<sub>3</sub> catalyst sample after its use in hydrogenation. The corresponding histogram shows the results from measuring the diameters of 650 Ni clusters in such images, and reveals a range of Ni clusters with diameters from 0.6 to 4.0 nm, corresponding to Ni<sub>10</sub> to Ni<sub>3060</sub>. The mode and median diameters are 1.4 nm, and the mean is Ni 1.4 ± 0.4 nm, corresponding to mean Ni<sub>130</sub> clusters.

**Nuclearity of the M<sub>n</sub> species *after* hydrogenation: MALDI MS.** Samples of the Co(neodecanoate)<sub>2</sub> plus AlEt<sub>3</sub> catalyst, with an Al/Co ratio of 3.0, were analyzed using MALDI MS *after* their use in cyclohexene hydrogenation (Figures are shown in the Supporting Information). MALDI MS of the Co catalyst results in a broad peak with maximum intensity at ~3500 *m/z* (reported as the average Co cluster in Table 1), and a shoulder at ~6000 *m/z*. Using the same necessary assumptions as before, that the broad peaks are composed of only +1 charged ions,<sup>14,32,33,34,35</sup> the peak at ~3500 *m/z* indicates Co<sub>60</sub> clusters, corresponding to a diameter of ~1.1 nm. The peak of the post-hydrogenation Co catalyst tails off toward higher *m/z* values; FWHM of the peak is from ~1500–9500 *m/z*, the peak reaches one-fourth maximum intensity at ~12000 *m/z*, and one-eighth maximum intensity at ~17000 *m/z* (1500–17000 is used to report the range of Co clusters in Table 1), which correspond to 0.8–1.5 nm, Co<sub>25–160</sub>; 1.6 nm, Co<sub>200</sub>; and

1.8 nm, Co<sub>~290</sub> clusters, respectively—essentially the same as the prehydrogenation results.

The Ni(2-ethylhexanoate)<sub>2</sub> plus AlEt<sub>3</sub> catalyst, with an Al/Ni ratio of 2.0, was also analyzed using MALDI MS *after* it had been used for cyclohexene hydrogenation, giving a broad peak with a maximum intensity at ~2000 *m/z*, which again indicates Ni<sub>~34</sub> clusters, corresponding to ~0.9 nm diameter Ni nanoclusters (reported as the average cluster size in Table 1). (As in the catalyst sample before hydrogenation, the presence of Ni atoms in species below 1500 *m/z* is ruled out by the absence of characteristic Ni isotope peak distributions in that region.) The broad, asymmetrically shaped MALDI MS peak of the catalyst sample *after* hydrogenation also tails off towards higher *m/z* values, but isn't completely identical to the peak of the sample before hydrogenation; the post-hydrogenation peak displays two slight shoulders at ~3000 and ~6000 *m/z*. Nevertheless, the broad peak in the sample after hydrogenation reaches ~6500 *m/z* at half maximum intensity, ~8500 *m/z* at one-fourth maximum intensity, and ~11000 *m/z* at one-eighth maximum intensity (1500–11000 *m/z* is used to report the range of Ni clusters in Table 1), which correspond to 1.3 nm, Ni<sub>~110</sub>; 1.5 nm, Ni<sub>~145</sub>; and 1.6 nm, Ni<sub>~190</sub>, respectively. These Ni cluster size and nuclearity values are very similar to those from the prehydrogenation sample. In short, the MALDI MS-determined sizes and size distributions of both Co and Ni clusters in post-hydrogenation samples (i) agree closely with the analysis of posthydrogenation catalyst samples using Z-contrast STEM, and consistent with the Z-contrast STEM, (ii) indicate no significant change in the sizes of the metal clusters present upon their use for the catalytic hydrogenation of cyclohexene.

**Nuclearity of  $M_n$  species *after* hydrogenation: XAFS (i.e., XANES and EXAFS) Spectroscopy.** Solution samples of both  $\text{Co}(\text{neodecanoate})_2$  plus  $\text{AlEt}_3$ , and  $\text{Ni}(\text{2-ethylhexanoate})_2$  plus  $\text{AlEt}_3$  catalysts, with Al/M ratios of 1.0, were analyzed using XAFS *after* their use in hydrogenation reactions. The XANES spectra of the Co and Ni catalyst solutions posthydrogenation are nearly the same as their prehydrogenation counterparts. XANES spectra collected after hydrogenation are shown and compared to the prehydrogenation spectra in the Supporting Information for the interested reader. For both Co and Ni catalysts, the EXAFS spectra after hydrogenation also appear very similar to the sample spectra before hydrogenation. The spectra are fit using the same models employed for fitting the catalyst samples before hydrogenation. The results are shown in Figure 9 and summarized in Table 3. Complete fit information and additional spectra are in the Supporting Information.



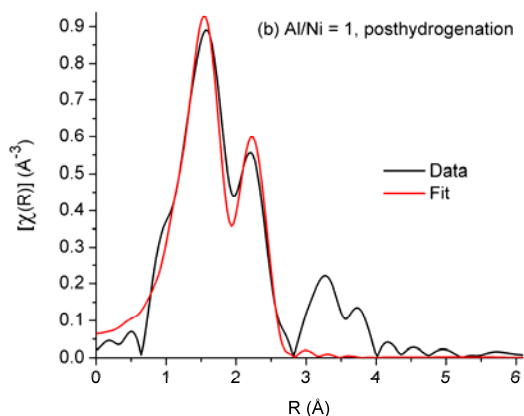


**Figure 9.** Data and fits of (a) the Co(neodecanoate)<sub>2</sub> plus AlEt<sub>3</sub> catalyst, Al/Co ratio of 1.0; and (b) the Ni(2-ethylhexanoate)<sub>2</sub> plus AlEt<sub>3</sub> catalyst, Al/Ni ratio of 1.0, both after use for the catalytic hydrogenation of cyclohexene.

**Table 3.** Summary of fit results for posthydrogenation Co and Ni catalyst spectra.

Sample	Co	Ni
$N_{M-M}$	$3 \pm 2$	$3 \pm 1$
$N_{M-O}$	$3 \pm 1$	$2.7 \pm 0.4$
$R_{M-M}$ (Å) <sup>a</sup>	$2.48 \pm 0.02$	$2.52 \pm 0.01$
$R_{M-O}$ (Å) <sup>a</sup>	$1.96 \pm 0.02$	$2.02 \pm 0.01$
$\sigma_{M-M}^2$ (Å <sup>2</sup> ) <sup>b</sup>	$15 \pm 7$	$13 \pm 3$
$\sigma_{M-O}^2$ (Å <sup>2</sup> ) <sup>b</sup>	$7 \pm 4$	$7 \pm 2$

<sup>a</sup> R stands for the interatomic distance corresponding to the single scattering paths. <sup>b</sup>  $\sigma^2$  represents the mean square variation in R due to both static and dynamic disorder (the EXAFS Debye-Waller factor), and values shown are  $\times 10^3$ .

The most plausible interpretation of the EXAFS spectra and fitting results is essentially the same for the catalyst samples after hydrogenation as for the samples before hydrogenation. The lack of peaks in the 3–6 Å range implies that no Co or Ni species with ordered metallic structures on that scale are present, and 1NN single scattering  $N_{M-M}$  values of  $\sim 3$  were obtained for both Co and Ni catalysts. Additionally, the  $R_{M-M}$  values from both Co and Ni samples posthydrogenation are the same as their prehydrogenation counterparts within experimental error, and are very close to the experimental bulk metal values (within  $\leq 0.03$  Å). Recall from the discussion of the prehydrogenation XAFS results that bulk metal-like  $R_{M-M}$  values are in contrast to the

larger  $R_{M-M}$  values expected for subnanometer  $M_n$  clusters ligated by Lewis acid species (i.e.,  $AlEt_3$  and its derivatives). Lastly, the  $\sigma^2_{M-M}$  values of the catalyst samples are again roughly twice the experimentally determined bulk metal values. Considered in light of the posthydrogenation Z-contrast and MALDI MS results, which reveal a predominance of nanometer scale clusters as part of wide size distributions, the self-consistent interpretation of all measurements (made already for the prehydrogenation samples) is that a combination of disordered nanoclusters and unreduced, mono-metallic species are present in catalyst solutions posthydrogenation. In short, both the XANES and EXAFS spectra confirm that use of catalyst solutions for cyclohexene hydrogenation has a negligible effect on the oxidation state and form of the transition metal catalyst material.

**Kinetics Studies: Hg(0) catalyst poisoning.** The observation of  $M_n$  clusters before and after catalysis does not necessitate that these species are the active hydrogenation catalysts—kinetic studies are required to determine the most active catalyst(s) from sample solutions. Catalyst poisoning by Hg(0) is a useful kinetics-based test for distinguishing homogeneous from heterogeneous Ziegler–type hydrogenation catalysis, as has been shown previously.<sup>14</sup> Hence, Hg(0) poisoning experiments were utilized to test whether the observed catalytic activity of the industrial Ziegler–type hydrogenation catalysts made from  $Ni(2\text{-ethylhexanoate})_2$  or  $Co(\text{neodecanoate})_2$  and  $AlEt_3$  is “homogeneous” (e.g., via single metal organometallic) or heterogeneous (e.g., via small  $M_4$  or larger nanoclusters), Figure 10. (Due to the outcomes of the Hg(0) poisoning experiments, the results for Ni are discussed here before those for Co.) One benefit of using Hg(0) poisoning in this case is that the results are not affected by MTL

kinetics (vide supra, and in the Supporting Information). Hg(0) addition to the Ni catalyst prior to the start of cyclohexene hydrogenation poisons catalysis *immediately and completely*, Figure 10. When Hg(0) is added to the Ni catalyst solution after about half the cyclohexene had been consumed, the Hg(0) also poisons the catalysis *immediately and completely*. These results suggest that catalysis in the Ni Ziegler-type hydrogenation system, made from authentic industrial Ni(2-ethylhexanoate)<sub>2</sub> precatalyst plus AlEt<sub>3</sub> is heterogeneous (i.e., via the observed sub (~M<sub>4</sub>) to larger nanoclusters).

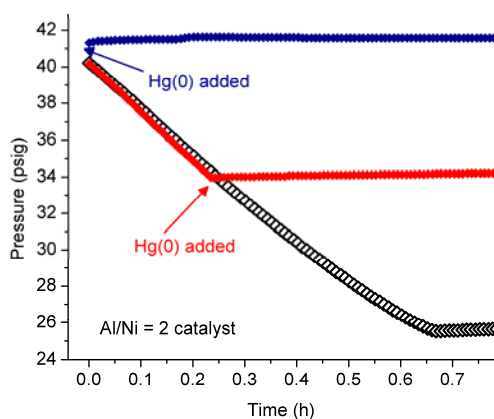


**Figure 10.** Poisoning experiments using the Ni(2-ethylhexanoate)<sub>2</sub> plus AlEt<sub>3</sub> catalyst with an Al/Ni ratio of 2.0 are shown next to standard example cyclohexene hydrogenation runs for comparison (black curve). Immediate and complete poisoning of catalysis by addition of Hg(0) after preparation of the catalyst, but before hydrogenation is begun (blue), and partway through a catalytic run (red), suggests that catalysis in the Ni catalyst system is heterogeneous (i.e., via the observed Ni nanoclusters).

It is known that one potential difficulty with Hg(0) poisoning experiments is that it may be difficult to thoroughly contact the Hg(0) with all of the catalyst in solution due to the insolubility of Hg(0).<sup>44</sup> Control experiments with the Ni system allowed the determination that a procedure using  $\geq 300$  equivalents of Hg(0) per Ni and  $\geq 1.5$  hours of 1000 rpm stirring is adequate to thoroughly contact the Hg(0) with all of the Ni catalyst in solution. However, control experiments show that the degree of poisoning

with the Co catalyst is with regard to the amount of Hg(0) used and the length of time it is mixed with the catalyst solution prior to data acquisition, is irreproducible (Experimental Section and Supporting Information). Unfortunately, then, the Hg(0) poisoning experiments with the Co catalyst proved inconclusive. Nevertheless, the Hg(0) poisoning results suggest catalysis with the Ni system is heterogeneous (i.e., proceeds via the observed Ni Ziegler sub-to-higher nanoclusters).

### **Conclusions and Needed Future Studies.**

Catalysts made from either of the industrial precursors Co(neodecanoate)<sub>2</sub> or Ni(2-ethylhexanoate)<sub>2</sub>, plus AlEt<sub>3</sub>, were analyzed by Z-contrast STEM, MALDI MS, XAFS (i.e., XANES and EXAFS), and Hg(0) poisoning studies, producing the following observations: (i) Co and Ni Ziegler-type hydrogenation catalyst solutions turn dark brown upon the initial combination of the Co(neodecanoate)<sub>2</sub> or Ni(2-ethylhexanoate)<sub>2</sub> precatalyst solutions with the AlEt<sub>3</sub> solution, and not during hydrogenation catalysis; and (ii) hydrogenation proceeds immediately with the start of data acquisition at, or very near, the maximum observable rate. (iii) Z-contrast STEM reveals, for the prehydrogenation Co sample, a 0.6–3.3 nm range of particle diameters with a mean of  $1.4 \pm 0.4$  nm, which corresponds to Co<sub>~130</sub>. For the prehydrogenation Ni sample, Z-contrast STEM reveals a 0.4–3.5 nm range of particle diameters with a mean of  $1.3 \pm 0.5$  nm, which corresponds to Ni<sub>~100</sub>. (iv) MALDI MS is used to estimate, for the prehydrogenation Co sample, a 0.8–1.8 nm range of particle diameters and an average of 1.2 nm, which corresponds to Co<sub>~80</sub>. For the prehydrogenation Ni sample, MALDI MS is used to estimate a 0.8–1.7 nm range of particle diameters and an average of 0.9 nm, which corresponds to Ni<sub>~34</sub>. (v)

XANES spectra show that the Co or Ni metals in prehydrogenation catalyst solutions become progressively less like their M(II) precatalysts, in terms of composite average formal oxidation state, and progressively more like the M(0) metal foils as the Al/M ratios increase from 1.0 to 3.0, implying that unreduced metal ions are present in catalyst solutions in amounts that decrease with additional AlEt<sub>3</sub>. (vi) EXAFS spectroscopic analysis of prehydrogenation samples reveals a lack of the R-space peaks in the 3–6 Å range indicative of ordered metallic structures. Fitting the spectra of both metals using composite models analogous to that used for the Ir model system,<sup>14</sup> gives mean 1NN M–M coordination numbers in the 3–4 range. Fitting the EXAFS spectra also gives 1NN  $R_{M-M}$  values that overlap, within experimental error, with the corresponding bulk metals for both Co and Ni samples with Al/M ratios of 1.0, but 1NN  $R_{M-M}$  values that are *shorter than* the bulk metal M–M distances for both Co and Ni Al/M = 3.0 samples. Fitting the EXAFS spectra also reveal  $\sigma^2_{M-M}$  values that are approximately twice the experimentally determined bulk metal values, indicative of disordered metal clusters. In addition, (vii) the Z-contrast STEM, MALDI MS, and XAFS results all show that cyclohexene hydrogenation does not significantly change the transition metal contents of the catalyst solutions. Finally, (viii) Hg(0) poisons the Ni catalyst immediately and completely, regardless of whether the Hg(0) is added before, or in the middle of a hydrogenation run.

The self-consistent interpretation of all results from the complementary techniques used herein is that the transition metal components of catalysts made from either of the industrial precursors Co(neodecanoate)<sub>2</sub> or Ni(2-ethylhexanoate)<sub>2</sub>, plus AlEt<sub>3</sub>, consist of a combination of M<sub>n</sub> clusters with a broad range of sizes and a large

degree of structural disorder, and unreduced, mono-metallic species, the distribution between the two phases depending on the Al/M ratio. Furthermore, the Hg(0) poisoning in particular suggests that Ziegler nanoclusters are the most active catalysts in the industrial Ni Ziegler-type hydrogenation catalyst system (i.e., that the catalysis is heterogeneous, and if one includes  $\geq \text{Ni}_4$  within the definition of heterogeneous). This work expands on the results of others—notably the important studies by Schmidt and co-workers,<sup>17</sup> and Bönemann and co-workers,<sup>18</sup> which suggest transition metal nanoclusters are the catalysts in the Co, Pd, Ni, and Pt Ziegler-type systems they studied. The combined results present the best evidence to date consistent with the “Ziegler nanocluster hypothesis” as the correct answer to the ~50 year old problem of what is the true nature of the industrial Ni-, and presumably also Co-based catalysts. Hence, the notion that industrial Ziegler-type hydrogenation catalysis proceeds via Ziegler nanoclusters is the leading hypothesis going forward to try to disprove.

Much remains to be done, however. Operando spectroscopy studies of both the formation of, and catalysis by, both the Ni and Co industrial catalyst systems remain to be accomplished.<sup>45</sup> A full kinetic study and rate law determination under non-MTL conditions also remain to be done, and promises to be challenging due to the high rates of these superior catalysts. In addition, the differences regarding the backscattering contribution from M–Al between the EXAFS spectra of the Ir model system (which show the presence of Al),<sup>14</sup> and those of the industrial Co and Ni-based catalysts studied herein (which do not show the presence of Al), are surprising and remain to be explored—could a  $\text{M}_4\text{H}_4$  type catalyst explain this discrepancy, for example? Another important difference between the Ir and Co, Ni catalysts is that catalyst aging slows the rates for the

Co, Ni catalysts, opposite to what is seen for Ir, so that future studies characterizing the aged Co and Ni catalysts is another, important future objective. Furthermore, specific determination of the form(s) taken, and role(s) played by the AlEt<sub>3</sub> component, both in the initial synthesis of the catalyst and during catalytic cyclohexene hydrogenation, remain to be fully understood.<sup>19</sup>

Despite the work remaining to be done, this investigation of the homogeneous versus heterogeneous nature of Ziegler-type hydrogenation catalysts is significant for at least four reasons: (i) this study examines Co and Ni-based catalysts made from the *actual industrial* precursor materials, which make catalysts that are notoriously problematic regarding their characterization;<sup>2,3</sup> (ii) the Z-contrast STEM results reported herein represent, to our knowledge,<sup>3</sup> the best microscopic analysis of the industrial Co and Ni Ziegler-type hydrogenation catalysts; (iii) this study is the first explicit application of an established method, using multiple analytical methods and kinetics-based studies, for distinguishing homogeneous from heterogeneous catalysis;<sup>3,6-15</sup> and (iv) this study parallels the successful study of an Ir model Ziegler catalyst system, thereby benefiting from a comparison to those previously unavailable findings,<sup>14</sup> although the greater M–M bond energy, and tendency to agglomerate, of Ir versus Ni or Co are important differences to be noted.<sup>46</sup> Overall, the leading hypothesis to try to refute in future work is that Ziegler-type sub-(i.e., M<sub>4</sub>) to larger nanoclusters are the dominant, industrial, Co- and Ni- plus AlR<sub>3</sub> catalysts.

**Acknowledgments.** Work was supported by NSF Grant CHE-0611588 at Colorado State University. MALDI MS were obtained with the expert assistance of Phil

Ryan (now deceased) of the Macromolecular Resources Lab at CSU. AIF, JCY and RGN acknowledge support by DOE BES Grant DE-FG02-03ER15476. We thank Nebojsa Marinkovic and Syed Khalid at the NSLS, the use of which was supported by the U.S. Department of Energy, Office of Science, Office of Basic Energy Sciences, under Contract No. DE-AC02-98CH10886. Beamline X18B at the NSLS is supported in part by the Synchrotron Catalysis Consortium, U. S. Department of Energy Grant No DE-FG02-05ER15688. We thank JoAn Hudson of Clemson University for the additional TEM imaging.

**Supporting Information Available.** Experimental information and results of control experiments for cyclohexene hydrogenations used to help establish standard conditions for catalyst preparation and use; additional TEM images; figures showing the MALDI MS results; EXAFS spectra with fits; Hg(0) poisoning control experiments; and a full list of the authors of reference 18d. This material is available free of charge via the Internet at <http://pubs.acs.org>.

## References

---

<sup>1</sup> Alley, W. M.; Girard, C. W.; Özkar, S.; Finke, R. G. *Inorg. Chem.* **2009**, *48*, 1114–1121.

<sup>2</sup> Johnson, K. A. *Polym. Prepr.* **2000**, *41*, 1525–1526.

<sup>3</sup> Alley, W. M.; Hamdemir, I. K.; Johnson, K. A.; Finke, R. G. *J. Mol. Catal. A: Chem.* **2010**, *315*, 1–27.

<sup>4</sup> Collman, J. P.; Hegedus, L. S.; Norton, J. R.; Finke, R. G. *Principles and Applications of Organotransition Metal Chemistry*; University Science Books: Mill Valley, CA, 1987.

- 
- <sup>5</sup> Schwartz, J. *Acc. Chem. Res.* **1985**, *18*, 302–308.
- <sup>6</sup> Widegren, J. A.; Finke, R. G. *J. Mol. Catal. A: Chem.* **2003**, *198*, 317–341.
- <sup>7</sup> Lin, Y.; Finke, R. G. *Inorg. Chem.* **1994**, *33*, 4891–4910.
- <sup>8</sup> Aiken, J. D., III; Lin, Y.; Finke, R. G. *J. Mol. Catal. A: Chem.* **1996**, *114*, 29–51.
- <sup>9</sup> Widegren, J. A.; Bennett, M. A.; Finke, R. G. *J. Am. Chem. Soc.* **2003**, *125*, 10301–10310.
- <sup>10</sup> Hagen, C. M.; Widegren, J. A.; Maitlis, P. M.; Finke, R. G. *J. Am. Chem. Soc.* **2005**, *127*, 4423–4432.
- <sup>11</sup> Finney, E. E.; Finke, R. G. *Inorg. Chim. Acta* **2006**, *359*, 2879–2887.
- <sup>12</sup> Jaska, C. A.; Manners, I. *J. Am. Chem. Soc.* **2004**, *126*, 1334–1335.
- <sup>13</sup> Jaska, C. A.; Manners, I. *J. Am. Chem. Soc.* **2004**, *126*, 9776–9785.
- <sup>14</sup> Alley, W. M.; Hamdemir, I. K.; Wang, Q.; Frenkel, A.; Li, L.; Yang, J. C.; Menard, L. D.; Nuzzo, R. G.; Özkar, S.; Johnson, K.; Finke, R. G. *Inorg. Chem.* **2010**, *49*, 8131–3147.
- <sup>15</sup> Zahmakiran, M.; Özkar, S. *Inorg. Chem.* **2009**, *48*, 8955–8964.
- <sup>16</sup> Halpern, J. *Inorg. Chim. Acta* **1981**, *50*, 11–19.
- <sup>17</sup> (a) Shmidt, F. K.; Nindakova, L. O.; Shainyan, B. A.; Saraev, V. V.; Chipanina, N. N.; Umanetz, V. A. *J. Mol. Catal. A: Chem.* **2005**, *235*, 161–172. (b) Belykh, L. B.; Titova, Yu. Yu.; Umanets, V. A.; Shmidt, F. K. *Russian Journal of Applied Chemistry* **2006**, *79*, 1271–1277. (c) Nindakova, L. O.; Shmidt, F. K.; Saraev, V. V.; Shainyan, B. A.; Chipanina, N. N.; Umanets, V. A.; Belonogova, L. N.; Toryashinova, D.-S. D. *Kinetics and Catalysis* **2006**, *47*, 54–63. (d) Belykh, L. B.; Goremyka, T. V.; Skripov, N. I.; Umanets, V. A.; Shmidt, F. K. *Kinetics and Catalysis* **2006**, *47*, 367–374.

---

<sup>18</sup> Studies by Bönemann and co-workers do not focus on hydrogenation catalysis using Ziegler-type systems, but do demonstrate the synthesis and identification of nanoclusters from Ni or Pt Ziegler-type systems. (a) Bönemann, H.; Brijoux, W.; Brinkmann, R.; Endruschat, U.; Hofstadt, W.; Angermund, K. *Revue Roumaine de Chimie* **1999**, *44*, 1003–1010. (b) Bönemann, H.; Waldöfner, N.; Haubold, H.-G.; Vad, T. *Chem. Mater.* **2002**, *14*, 1115–1120. (c) Angermund, K.; Bühl, M.; Dinjus, E.; Endruschat, U.; Gassner, F.; Haubold, H.-G.; Hormes, J.; Köhl, G.; Mauschick, F. T.; Modrow, H.; Mörtel, R.; Mynott, R.; Tesche, B.; Vad, T.; Waldöfner, N.; Bönemann, H. *Angew. Chem. Int. Ed.* **2002**, *41*, 4041–4044. (d) Angermund, K.; et al. *J. Phys. Chem. B* **2003**, *107*, 7507–7515. (e) Haubold, H.-G.; Vad, T.; Waldöfner, N.; Bönemann, H. *J. Appl. Cryst.* **2003**, *36*, 617–620. (f) Wen, F.; Bönemann, H.; Mynott, R. J.; Spliethoff, B.; Weidenthaler, C.; Palina, N.; Zinoveva, S.; Modrow, H. *Appl. Organomet. Chem.* **2005**, *19*, 827–829.

<sup>19</sup> Hamdemir, I. K.; Özkar, S.; Johnson, K. A.; Finke, R. G., manuscript in preparation.

<sup>20</sup> Aiken, J. D., III; Finke, R. G. *J. Am. Chem. Soc.* **1998**, *120*, 9545–9554.

<sup>21</sup> (a) Lin, Y.; Finke, R. G. *Inorg. Chem.* **1994**, *33*, 4891–4910; (b) Watzky, M. A.; Finke, R. G. *J. Am. Chem. Soc.* **1997**, *119*, 10382–10400; and (c) Widegren, J. A.; Aiken, J. D., III; Özkar, S.; Finke, R. G. *Chem. Mater.* **2001**, *13*, 312–324.

<sup>22</sup> Kearns, G. J.; Foster, E. W.; Hutchison, J. E. *Anal. Chem.* **2006**, *78*, 298–303.

<sup>23</sup> (a) Newville, M. *J. Synchrotron Rad.* **2001**, *8*, 322–324. (b) Ravel, B.; Newville, M. *J. Synchrotron Rad.* **2005**, *12*, 537–541.

<sup>24</sup> Lin, Y.; Finke, R. G. *J. Am. Chem. Soc.* **1994**, *116*, 8335–8353.

<sup>25</sup> *CRC Handbook of Chemistry and Physics*; 77<sup>th</sup> ed.; Lide, D. R., Frederikse, H. P. R., Eds.; CRC Press, Boca Raton, 1996.

<sup>26</sup> The number of atoms in a transition metal nanocluster (n) may be estimated making the necessary approximation that the nanoclusters have the same close-packed atomic structure as the bulk metal (either face centered cubic (fcc) or hexagonal close packed

---

(hcp)), and using the following formula:  $n = (N_0\rho(4/3)\pi(D/2)^3)/W$ .<sup>24</sup> According to this approach  $N_0$  is  $6.022 \times 10^{23} \text{ mol}^{-1}$ ,  $\rho$  is the room temperature density of the pure bulk metal,  $D$  is the measured cluster diameter, and  $W$  is the atomic weight of the transition metal. For Ni,  $\rho$  is  $8.90 \text{ g/cm}^3$ , and  $W$  is  $58.69 \text{ g/mol}$ .<sup>25</sup> For Co,  $\rho$  is  $8.86 \text{ g/cm}^3$ , and  $W$  is  $58.93 \text{ g/mol}$ .<sup>25</sup> For example, a Ni cluster diameter of 1.3 nm corresponds to Ni<sub>100</sub>.

<sup>27</sup> Starkey Ott, L.; Cline, M. L.; Deetlefs, M.; Seddon, K. R.; Finke, R. G. *J. Am. Chem. Soc.* **2005**, *127*, 5758–5759.

<sup>28</sup> Hagen, C. M.; Vieille-Petit, L.; Laurency, G.; Süss-Fink, Finke, R. G. *Organometallics* **2005**, *24*, 1819–1831.

<sup>29</sup> Williams, D. B.; Carter, C. B. *Transmission Electron Microscopy*; Plenum Press: New York, 1996.

<sup>30</sup> Catalyst samples, both before and after hydrogenation, were also analyzed using bright field and high resolution (HR)TEM as control experiments. Images and a short discussion of those results can be found in the Supporting Information.

<sup>31</sup> Pyrz, W. D.; Buttrey, D. J. *Langmuir* **2008**, *24*, 11350–11360.

<sup>32</sup> Whetten, R. L.; Khoury, J. T.; Alvarez, M. M.; Murthy, S.; Vezmar, I.; Wang, Z. L.; Stephens, P. W.; Cleveland, C. L.; Luedtke, W. D.; Landman, U. *Adv. Mater.* **1996**, *8*, 428.

<sup>33</sup> Khitrov, G. A.; Strouse, G. F. *J. Am. Chem. Soc.* **2003**, *125*, 10465.

<sup>34</sup> Kuzuya, T.; Tai, Y.; Yamamuro, S.; Sumiyama, K. *Chem. Phys. Lett.* **2005**, *407*, 460–463.

<sup>35</sup> Maya, L.; Chen, C. H.; Stevenson, K. A.; Kenik, E. A.; Allman, S. L.; Thundat, T. G.; *J. Nanoparticle Res.* **2002**, *4*, 417.

<sup>36</sup> Goulon, J.; Georges, E.; Goulon-Ginet, C.; Chauvin, Y.; Commereuc, D.; Dexpert, H.; Freund, E. *Chem. Phys.* **1984**, *83*, 357–366. (b) Esselin, C.; Bauer-Grosse, E.; Goulon,

---

J.; Williams, C.; Chauvin, Y.; Commereuc, D.; Freund, E. *J. Phys. Colloques* **1986**, *47*, C8-243–C8-248.

<sup>37</sup> Frenkel, A. I.; Hills, C. W.; Nuzzo, R. G. *J. Phys. Chem. B* **2001**, *105*, 12689–12703.

<sup>38</sup> Since much of the other data presented herein is for the Al/Ni = 2.0 catalyst, we carefully considered if it was important to have higher quality data from the Al/Ni = 2.0 sample in order to support the conclusions in the present study. We reasoned that such data are not necessary, primarily on the basis of the following four reasons. First, the XANES spectra of these samples show a smooth progression of the samples from the Al/Ni = 1.0 to Al/Ni = 3.0 ratios. Second, there is considerable similarity between the Al/Ni = 2.0 and 3.0 spectra when plotted as  $\chi(k)$ , and despite the additional noise apparent in the Al/Ni = 2.0 sample (relevant spectra comparisons are given in the Supporting Information). Third, these first two observations, together with the similarity between the fitting results from catalyst samples with Al/Ni ratios of 1.0 and 3.0, demonstrate that reliable fitting results for the Al/Ni = 2.0 sample should have values between those obtained from the Al/Ni = 1.0 and 3.0 samples. And fourth, the interpretation of the XAFS data herein, that 1NN M–M coordination numbers are not representative of cluster nuclearity, means that a direct comparison between the results from XAFS and cluster size measurements using other methods such as Z-contrast STEM is not straightforward; this is the case even if higher quality data for the Al/Ni = 2.0 sample were in hand. In short, obtaining higher quality data for the Al/Ni = 2.0 sample is not expected to improve or change any of the conclusions reached in the present study.

<sup>39</sup> One possible interpretation is that  $M_{4-6}$  clusters remain tightly associated (i.e.,  $(M_{4-6})_n$ ). (a) Fulton, J. L.; Linehan, J. C.; Autrey, T.; Balasubramanian, M.; Chen, Y.; Szymczak, N. K. *J. Am. Chem. Soc.* **2007**, *129*, 11936–11949. (b) Harada, M.; Asakura, K.; Toshima, N. *J. Phys. Chem.* **1994**, *98*, 2653–2662.

<sup>40</sup> (a) Ankudinov, A. L.; Rehr, J. J.; Low, J. J.; Bare, S. R. *J. Chem. Phys.* **2002**, *116*, 1911–1919. (b) Petkov, V.; Ohta, T.; Hou, Y.; Ren, Y. *J. Phys. Chem. C* **2007**, *111*, 714–720. (c) Petkov, V.; Bedford, N.; Knecht, M. R.; Weir, M. G.; Crooks, R. M.; Tang, W.;

---

Henkelman, G.; Frenkel, A. *J. Phys. Chem. C* **2008**, *112*, 8907–8911. (d) Sun, Y.; Zhuang, L.; Lu, J.; Hong, X.; Liu, P. *J. Am. Chem. Soc.* **2007**, *129*, 15465–15467. (e) Vila, F.; Rehr, J. J.; Kas, J.; Nuzzo, R. G.; Frenkel, A. I. *Phys. Rev. B* **2008**, *78*, 121404-1–121404-4. (f) Sanchez, S. I.; Menard, L. D.; Bram, A.; Kang, J. H.; Small, M. W.; Nuzzo, R. G.; Frenkel, A. I. *J. Am. Chem. Soc.* **2009**, *131*, 7040–7054. (g) Gilbert, B.; Huang, F.; Zhang, H.; Waychunas, G. A.; Banfield, J. F. *Science* **2004**, *305*, 651–654. (h) Billinge, S. J. L.; Levin, I. *Science* **2007**, *316*, 561–565. (i) Sun, Y.; Frenkel, A. I.; Isseroff, R.; Shonbrun, C.; Forman, M.; Shin, K.; Koga, T.; White, H.; Zhang, L.; Zhu, Y.; Rafailovich, M. H.; Sokolov, J. C. *Langmuir* **2006**, *22*, 807–816. (j) Menard, L. D.; Xu, H.; Gao, S.-P.; Twisten, R. D.; Harper, A. S.; Song, Y.; Wang, G.; Douglas, A. D.; Yang, J. C.; Frenkel, A. I.; Murray, R. W.; Nuzzo, R. G. *J. Phys. Chem. B* **2006**, *110*, 14564–14573.

<sup>41</sup> Finke, R. G.; Özkar, S. *Coord. Chem. Rev.* **2004**, *248*, 135–146.

<sup>42</sup> Yevick, A.; Frenkel, A. I. *Phys. Rev. B* **2010**, *81*, 115451.

<sup>43</sup> In addition, the explanation of the low XAFS  $N_{M-M}$  values involving disordered structure alone requires a degree of  $N_{M-M}$  distortion of considerably greater magnitude than reported in the literature.<sup>42</sup> The expected, non-distorted,  $N_{M-M}$  value for mean 1.4–1.3 nm Co and Ni clusters (determined by Z-contrast STEM) is approximately 8.6–8.9. The observed values from the XAFS results herein, Tables 2 and 3, are decreased by about 50%, as opposed to a disorder-induced decrease in  $N_{M-M}$  of 8% calculated in a previous study.<sup>42</sup>

<sup>44</sup> (a) The potential weaknesses and pitfalls of Hg(0) as a test for the homogeneous versus heterogeneous nature of a catalyst are discussed elsewhere.<sup>6</sup> (b) Also see, Phan, N. T. S.; Van Der Sluys, M.; Jones, C. W. *Adv. Synth. Catal.* **2006**, *348*, 609–679.

<sup>45</sup> (a) Thomas, J. M.; Somorjai, G. A. *Top. Catal.* **1999**, *8* (preface); (b) Weckhuysen, B. M. *Chem. Commun.* **2002**, 97–110; (c) Guerrero-Pérez, M. O.; Bañares, M. A. *Chem. Commun.* **2002**, 1292–1293. (d) Meunier, F.; Daturi, M. *Catal. Today* **2006**, *113*, 1–2.

---

<sup>46</sup> (a) The standard heats of formation of Ir, Co, and Ni gases are 159.0, 101.5, and 102.7 kcal/mol, respectively.<sup>25</sup> This means that at least naked, unligated Ir<sub>n</sub> clusters have a greater thermodynamic tendency to agglomerate to the thermodynamic minimum of a bulk Ir(0) mirror compared to Co(0) or Ni(0) clusters. The presence of hydrides or surface ligands, such as in a putative M<sub>4</sub>H<sub>4</sub>L<sub>y</sub>, mitigates this driving force some, however, since Ir–H and Ir–L bond energies should be stronger than Co or Ni ones. (b) A useful reference on this point is: Kilic, C. *Solid State Communications* **2010**, *150*, 2333–2336. (c) The difference in aging effects on the catalysts, the Ir system becoming faster, while aging the Co and Ni catalysts for 24 h has either a slight or significant slowing effect, respectively, (see the Supporting Information) is noteworthy here, and shows an important difference in the Co and Ni versus Ir samples, which in turn shows that characterization of the Co and Ni samples as a function of aging is an important future goal.

Supporting Information for:

**Industrial Ziegler-type Hydrogenation Catalysts made from Co(neodecanoate)<sub>2</sub> or Ni(2-ethylhexanoate)<sub>2</sub>, and AlEt<sub>3</sub>: Evidence for Nanoclusters and Sub-Nanocluster or Larger Ziegler-Nanocluster Based Catalysis**

William M. Alley, Isil K. Hamdemir, Qi Wang, Anatoly I. Frenkel, Long Li, Judith C. Yang, Laurent D. Menard, Ralph G. Nuzzo, Saim Özkar, Kimberly Johnson, Richard G.

Finke

### **Conditions and Procedures for Catalyst Synthesis and Use for Hydrogenations.**

Before study of Ziegler-type hydrogenation catalysts made by combination of authentic industrial precatalysts  $\text{Co}(\text{neodecanoate})_2$  or  $\text{Ni}(\text{2-ethylhexanoate})_2$  with  $\text{AlEt}_3$  could proceed in earnest, it was necessary to ensure initially that the results obtained would be both reproducible and representative of active (ideally optimized) catalysts. We began by testing a variety of conditions and procedures for both catalyst preparation and use for cyclohexene hydrogenation. What follows is an account of the findings from these preliminary kinetic studies that led to the development and use of “standard conditions” herein.

**Determination of Hydrogenation Rate from Kinetic Data.** Hydrogenation rate ( $-\text{d}[\text{H}_2]/\text{dt}$ ) is determined from kinetic data by a linear fit of individual hydrogenation curves consisting of  $\text{H}_2$  pressure (psig) versus time (h) data, Figure S1. The hydrogenation curves resulting from catalysts prepared using “standard conditions” (vide infra) are themselves nearly linear, Figures 1 and S1. However, when different preparation procedures or conditions were used, and hydrogenation curve near-linearity is not the case, the hydrogenation rate reported is from a linear fit to the steepest part of the curve, or “maximum rate”, unless stated otherwise. In order to obtain consistent results, the portion of a hydrogenation curve used for fitting was the maximum number of data points that would give a fit  $R^2$  value of at least 0.9995.

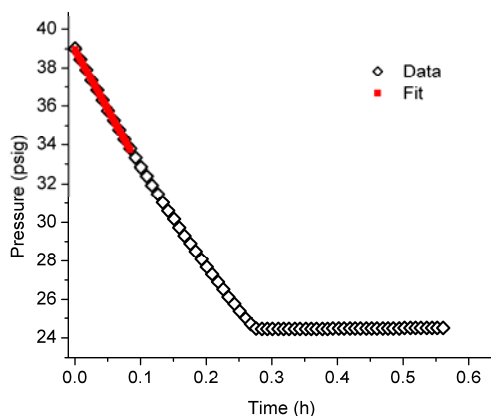


**Figure S1.** Example hydrogenation curve with linear-least-squares fit to an  $R^2$  value of 0.9995 over the steepest part of the (nearly linear) curve. The hydrogenation rate given by this fitting procedure is  $62.1 \pm 0.5$  psig  $\text{H}_2/\text{h}$  for this hydrogenation curve. This example curve was obtained using “standard conditions” (i.e., solvent = cyclohexane,  $[\text{Co}] = 1.2$  mM,  $\text{Al}/\text{Co} = 3$ , initial  $[\text{cyclohexene}] = 1.65$  M, hydrogenation temp =  $22.0$  °C, and stirring of 1000 rpm during hydrogenation).

**Mass Transfer Limitation Effects.** In our hydrogenation apparatus, the Co- and Ni-based catalysts are so highly active for the hydrogenation of cyclohexene that rate measurements from hydrogenation runs are prone to gas-to-solution mass transfer limitation (MTL) effects, Figure S2. MTL effects are frequently seen in systems in which one of the reactants is supplied as a gas, in this case the  $\text{H}_2$ , and the other reactant is in solution, in this case the cyclohexene.<sup>1</sup> In our review of the literature of Ziegler-type hydrogenation catalysts,<sup>2</sup> we commented on the fact that not all prior research in the area reported the steps taken, if any, to account for possible MTL effects in their catalyst studies. Furthermore, we proposed that one possible explanation for some of the contradictory observations concerning the importance and effect of variables in catalyst preparation conditions and procedures *is that MTL effects are an unappreciated factor in some studies.*<sup>2</sup> The significance of having observed MTL effects in this study is that it puts an upper bound on the measureable rate of catalytic activity, preventing us from

completing certain types of kinetic studies and from knowing if the catalyst systems are fully optimizing. This is one reason we have focused on Hg(0) poisoning studies as a kinetics-based probe of the nature of the catalyst, since their outcomes are unaffected by MTL kinetics. In short, due to the effects of MTL, we cannot discern the effects of different conditions and procedures for catalyst synthesis and use in cyclohexene hydrogenation when they give catalysts with activities the same as or greater than the mass-transfer limit (MTL). However, we *can* determine whether conditions and procedures for catalyst synthesis give catalysts that, for the Co catalyst, are as active as that high, mass-transfer limit. Therefore, we have used catalyst preparation methods and conditions for this study that (i) result in catalytic cyclohexene hydrogenation rates that are at least as rapid as we can observe due to the MTL present, (ii) are consistent with the most favorable methods and conditions described in the literature,<sup>2</sup> and (iii) are similar to, or the same as those used for the model Ir Ziegler-type hydrogenation catalyst made from [(1,5-COD)Ir( $\mu$ -O<sub>2</sub>C<sub>8</sub>H<sub>15</sub>)]<sub>2</sub> and AlEt<sub>3</sub>, and where MTL was not an issue.<sup>3,4</sup> Despite the limitations posed by the effects of MTL kinetics, our efforts to test the effects of different methods and conditions for catalyst synthesis and use for cyclohexene hydrogenation are valuable in order to ensure that the results obtained from our study are both reproducible and representative of the active, industrial catalysts.

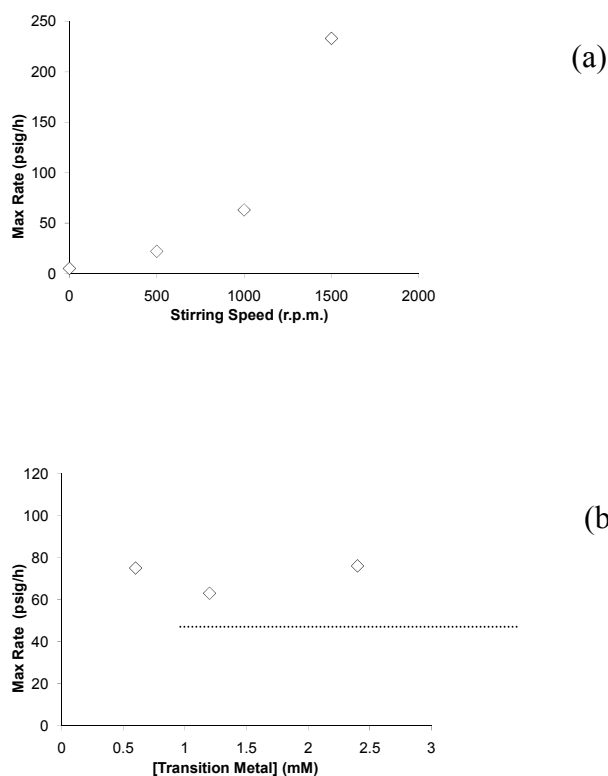


**Figure S2.** Control hydrogenations performed to test whether the cyclohexene hydrogenation kinetics measured in our hydrogenation apparatus using catalysts made from  $\text{Co}(\text{neodecanoate})_2$  or  $\text{Ni}(\text{2-ethylhexanoate})_2$ , plus  $\text{AlEt}_3$  are prone to mass transfer limitation (MTL) effects. Hydrogenation curves were collected using the  $\text{Co}(\text{neodecanoate})_2$  plus  $\text{AlEt}_3$  catalyst as a function of stirring speed (a) and as a function of  $[\text{Co}]$  concentration (b), but were otherwise, performed using “standard conditions” (i.e., solvent = cyclohexane,  $[\text{Co}] = 1.2 \text{ mM}$ ,  $\text{Al/Co} = 3$ , initial  $[\text{cyclohexene}] = 1.65 \text{ M}$ , hydrogenation temp =  $22.0 \text{ }^\circ\text{C}$ , stirring of 1000 rpm during hydrogenation). The set of hydrogenations as a function of stirring speed (a) shows that the the  $\text{H}_2$  uptake rate is strongly influenced by the stirring speed, which is a clear sign of MTL kinetics. (The stirring speed of  $1.6 \times 10^3 \text{ rpm}$  was achieved using a Fisher Jumbo magnetic stirplate that was necessary to obtain this data point, but not favored for our studies because it gives much less reproducible mixing than the Fauske Super magnetic stirplate, which has a maximum speed of 1000 rpm. The set of hydrogenations as a function of  $[\text{Co}]$  (b) give roughly the same rate values (within experimental error and the reproducibility of mixing) regardless of the  $[\text{Co}]$  used, which suggests MTL kinetics. If MTL kinetics were not present, one could reasonably expect different hydrogenation rates using different  $[\text{Co}]$  concentrations. These two sets of hydrogenations show that MTL kinetics are present for the apparatus and conditions used, which, due to the similarities regarding the  $\text{Ni}(\text{2-ethylhexanoate})_2$  plus  $\text{AlEt}_3$  catalyst, apply to that system as well. The apparent MTL value is  $\sim 80 \text{ psig/h}$  in this apparatus, and at standard conditions (dashed line).

**Catalyst Aging Prior to Use for Cyclohexene Hydrogenation.** Unlike with the previously studied model Ir system, aging the prepared Co- or Ni-based catalyst solutions before beginning a hydrogenation run does not improve the catalyst activity. In fact, aging the prepared catalyst solutions before use for cyclohexene hydrogenation has a generally negative (slowing) effect, which is very slight in the case of the Co catalyst but pronounced in the case of the Ni catalyst, Figure S3. Catalyst solutions were therefore used for hydrogenation or otherwise analyzed as soon as possible after preparation.

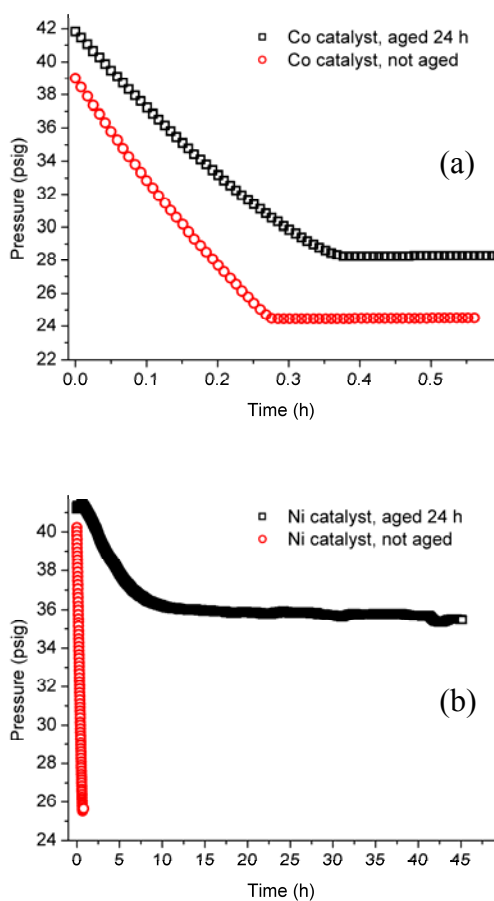


**Figure S3.** Example hydrogenation curves using catalysts aged 24 h before the start of cyclohexene hydrogenation. The slight effect of aging in the case of the Co catalyst (a) and the more significant effect of aging in the case of the Ni catalyst (b) led to lower rates for the catalytic hydrogenation of cyclohexene. Therefore, use of catalyst solutions *without* aging became the standard procedure for the studies herein. Catalyst solution aging was accomplished by sealing a catalyst solution prepared normally in a Fisher-

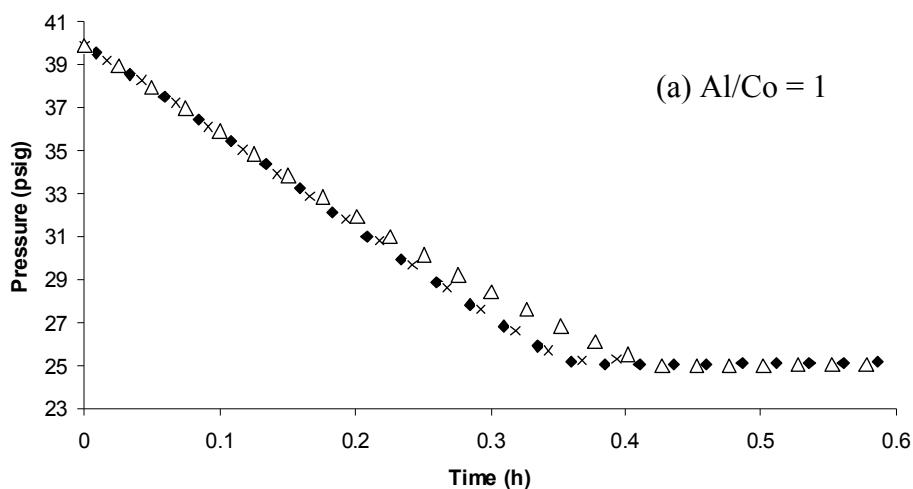
Porter bottle in the drybox, and stirring at  $1000 \pm 200$  rpm for the specified amount of time, here 24 h. Aside from the aging step, the example hydrogenation runs shown here were obtained using “standard conditions” (i.e., solvent = cyclohexane,  $[M] = 1.2$  mM, Al/Co = 3 or Al/Ni = 2, initial [cyclohexene] = 1.65 M, hydrogenation temp = 22.0 °C, and stirring of 1000 rpm during hydrogenation).

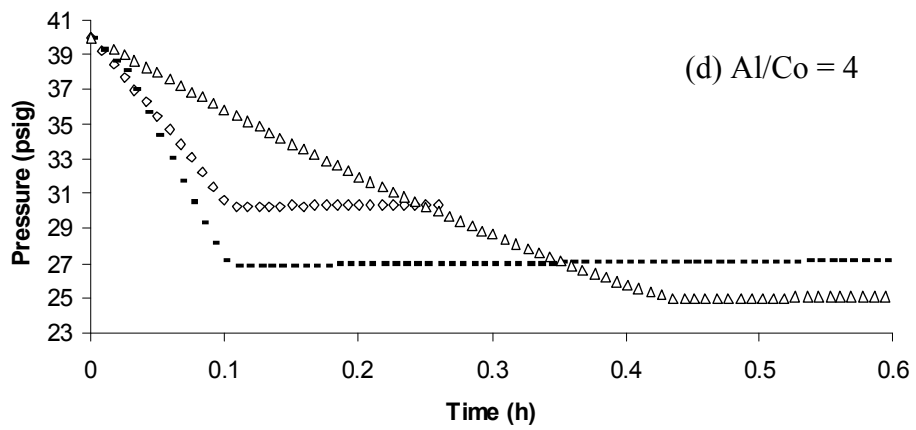
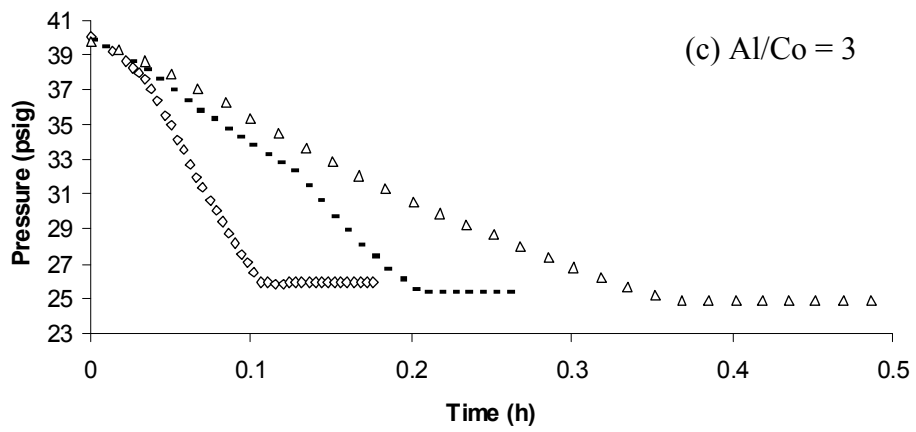
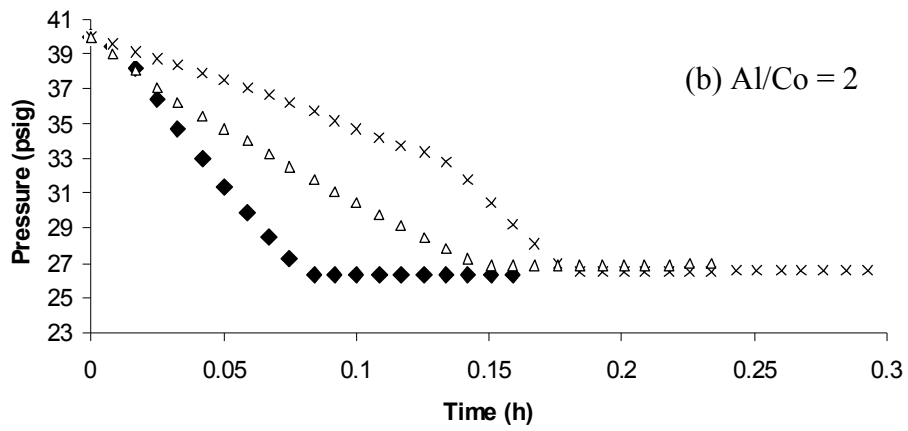
**Effects of the Al/M Ratio (M = Co or Ni), Control Hydrogenations using Catalyst Samples with Different Al/M Ratios for XAFS Spectroscopy, and Batch vs Individual Catalyst Preparation.** One of the most important variables in the synthesis of Ziegler-type hydrogenation catalysts is the Al/M ratio.<sup>2</sup> We tested various Al/M ratios with the Co(neodecanoate)<sub>2</sub> or Ni(2-ethylhexanoate)<sub>2</sub>, plus AlEt<sub>3</sub> catalysts for the effects on the rate of catalytic cyclohexene hydrogenation. Results from initial studies on the effect of the Al/Co ratio, conducted prior to identification of MTL kinetics in this system and apparatus, are given in Figure S4. For hydrogenation kinetics heavily influenced by the presence of MTL effects, the observed reproducibility of the H<sub>2</sub> uptake rate is indicative of the reproducibility of mixing. Note the lack of reproducibility in the runs shown in Figure S4, for which a Fisher Jumbo magnetic stirplate was used giving stirring of  $1000 \pm 200$  rpm. Conversely, hydrogenations performed using a Fauske Super magnetic stirplate, which allows for a more precise, continuously controlled stirring rate of  $1000 \pm 10$  rpm, display a greater degree of reproducibility in the rate of H<sub>2</sub> uptake, Figure S5. Regardless of the limitations posed by imprecise control over mixing and the presence of MTL effects, these initial hydrogenation runs demonstrate that the optimal Al/Co ratio is in the 2–4 range.

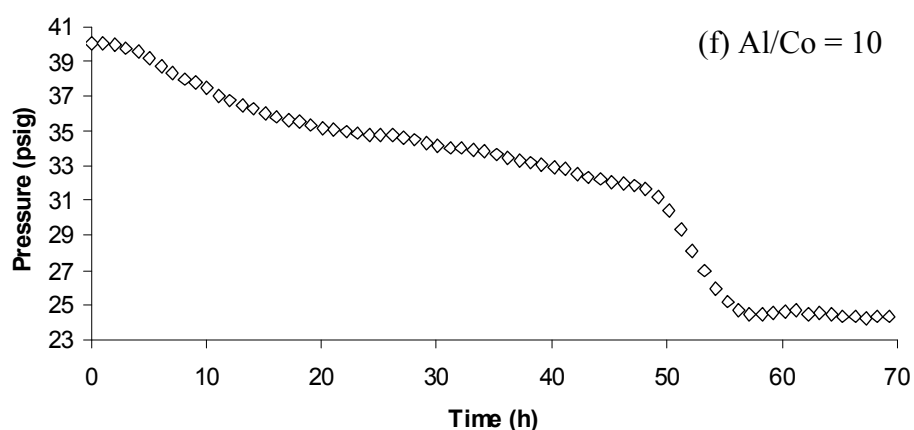
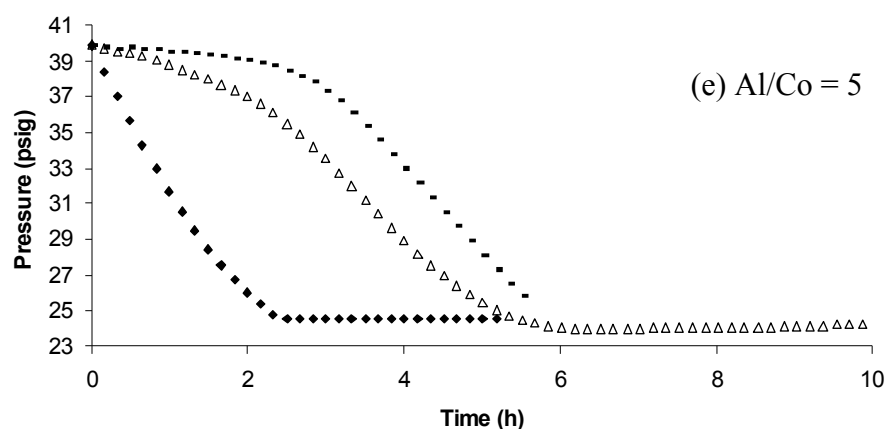
Figure S6 shows catalytic cyclohexene hydrogenation runs performed using the catalyst samples prepared at different Al/M ratios used for analysis by XAFS. For the purposes of XAFS spectroscopy, these catalyst solutions were prepared in 6.0 mL

batches, 7.2 mM in [M], M = Co or Ni. The hydrogenation curves given by these Co or Ni catalyst samples are essentially the same as those observed with catalyst samples prepared individually (i.e., prepared at the smaller, 2.5 mL, scale, and at 1.2 mM in [M]). Additional, independently performed hydrogenations (not shown) confirm that catalyst preparation in up to 20 mL batches at 1.2 mM [M] also did not give catalyst solutions with different hydrogenation activities. These control experiments show that the scale or [M] concentration of catalyst solution preparation is not a significant factor in the resulting catalyst activity, at least for the range of volumes and concentrations tested.

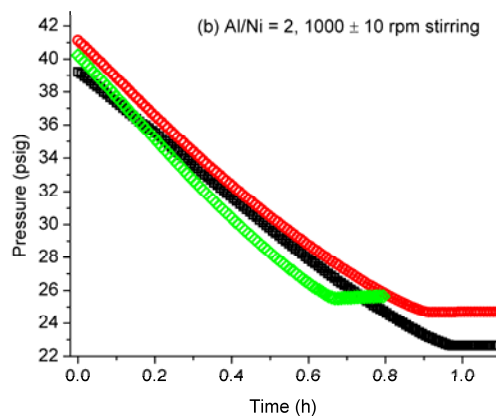
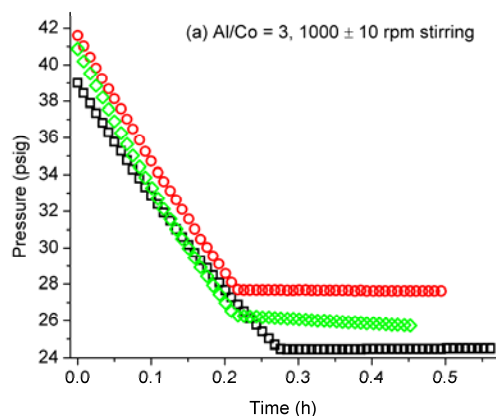
The hydrogenation activities of  $\text{Co}(\text{neodecanoate})_2$ , and separately, the  $\text{Ni}(\text{2-ethylhexanoate})_2$  *precatalyst* samples analyzed by XAFS (i.e., *without* added  $\text{AlEt}_3$ ) were also tested.  $\text{H}_2$  uptake was not observed in either case, Figure S7, demonstrating the critical role played by the  $\text{AlEt}_3$  cocatalyst in obtaining active Ziegler-type hydrogenation catalysts. On the basis of both the experimental observations made herein by us, and because of what is known from the studies of similar catalyst systems reported in the literature,<sup>2</sup> we used ratios of  $\text{Al/Co} = 3$  and  $\text{Al/Ni} = 2$  as our standard conditions.



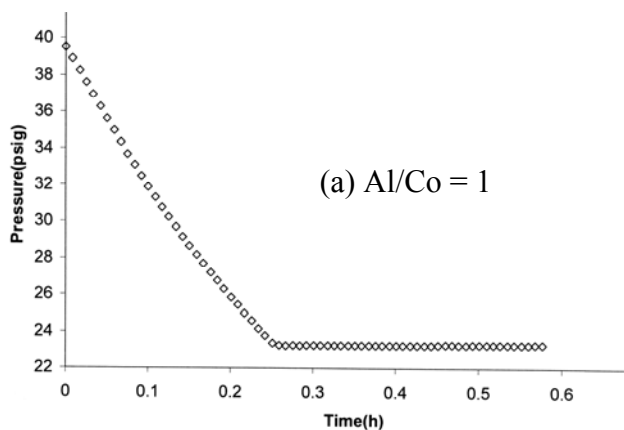




**Figure S4.** Example cyclohexene hydrogenation curves using  $\text{Co}(\text{neodecanoate})_2$  plus  $\text{AlEt}_3$  catalysts with different Al/Co ratios. (a) Al/Co = 1, the mean maximum hydrogenation rate is  $40 \pm 1$  psig/h. (b) Al/Co = 2, the mean maximum hydrogenation rate is  $140 \pm 42$  psig/h. (c) Al/Co = 3, the mean maximum hydrogenation rate is  $97 \pm 42$  psig/h. (d) Al/Co = 4, the mean maximum hydrogenation rate is  $97 \pm 58$  psig/h. (e) Al/Co = 5, the mean maximum hydrogenation rate is  $6 \pm 2$  psig/h. (f) Al/Co = 10, the maximum hydrogenation rate is about 1 psig/h. Imprecise control over the highest attainable speed of stirring ( $1000 \pm 200$  rpm; needed to raise the  $\text{H}_2$  gas-to-solution MTL rate) during hydrogenation influenced by MTL kinetics makes these experiments less informative than they otherwise could be. Nevertheless, these initial hydrogenation runs suffice for demonstrating that the optimal Al/Co ratio in the 2–4 range.



**Figure S5.** Example hydrogenations using the  $\text{Co}(\text{neodecanoate})_2$  plus  $\text{AlEt}_3$  catalyst (top),  $\text{Al/Co} = 3$ , and the  $\text{Ni}(\text{2-ethylhexanoate})_2$  plus  $\text{AlEt}_3$  catalyst (bottom),  $\text{Al/Ni} = 2$ . Standard conditions were used including  $1000 \pm 10$  rpm stirring during hydrogenation, achieved with a Fauske Super magnetic stirplate. The mean maximum hydrogenation rate for Co is  $68 \pm 7$  psig/h, and for Ni is  $22 \pm 3$  psig/h. Compare the hydrogenations with the Co catalyst here (top) with those shown in Fig S4c; the improved reproducibility is due, at least in part, to improved stirring rpm control.



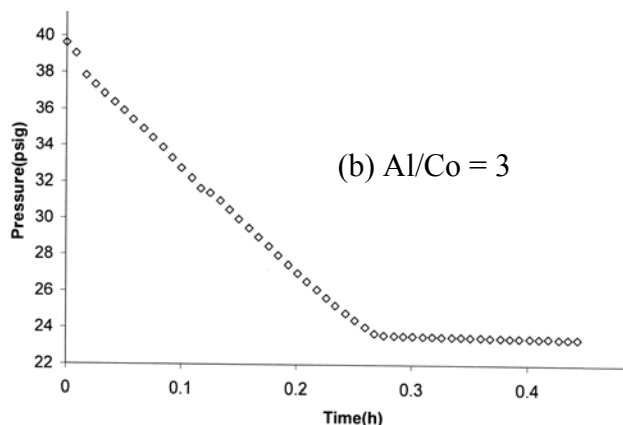


**Figure S6.** Additional cyclohexane hydrogenation curves using  $\text{Co}(\text{neodecanoate})_2$  plus  $\text{AlEt}_3$  catalysts, with Al/Co ratios of 1.0 and 3.0. Aliquots were taken from 6.0 mL batches of the catalyst solution and at 7.2 mM in [M]. The similarity of the hydrogenation curve in part (a) of this Figure to the curves in Fig S4a, and the similarity of the hydrogenation curve in part (b) of this Figure to the curves in Fig S5a argue that the volume and [M] concentration of catalyst preparation are unimportant to catalyst activity, at least within the ranges tested.

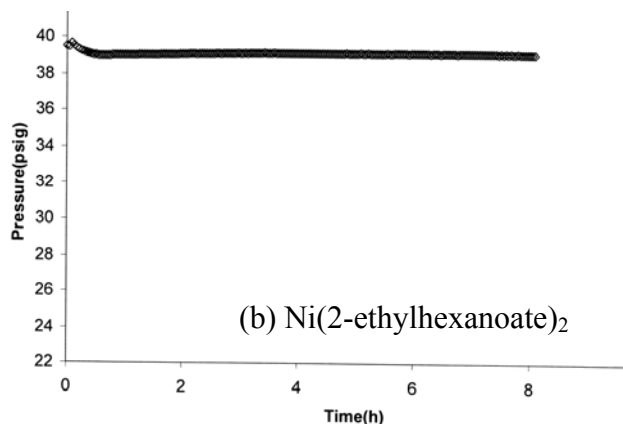
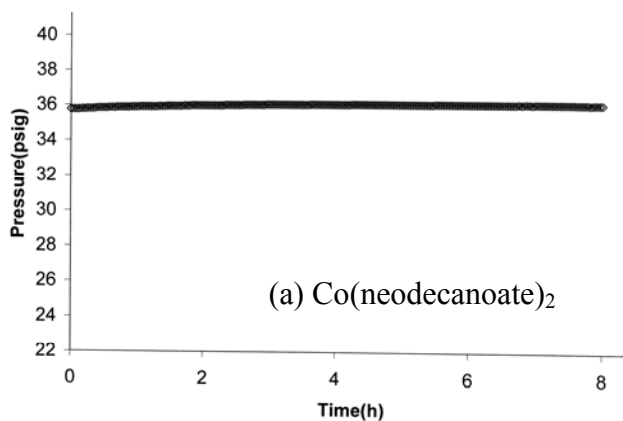
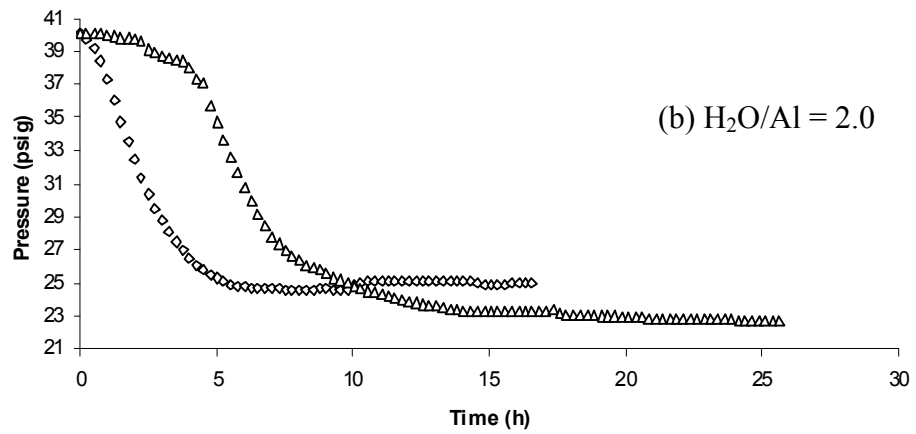
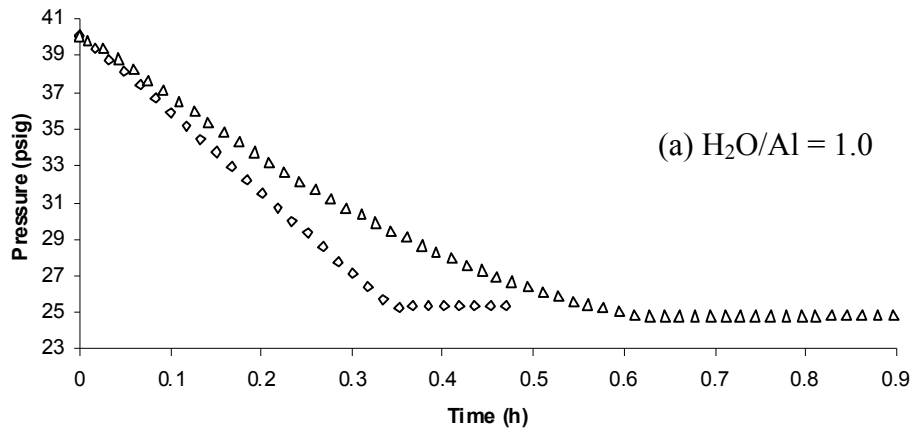


**Figure S7.** Attempted catalytic cyclohexene hydrogenation runs using  $\text{Co}(\text{neodecanoate})_2$  (a) and separately,  $\text{Ni}(\text{2-ethylhexanoate})_2$  (b) *precatalysts without*

added AlEt<sub>3</sub> (i.e., Al/M = 0). These important controls show that H<sub>2</sub> uptake is not observed in either case, demonstrating the critical role played by the AlEt<sub>3</sub> cocatalyst in obtaining active Ziegler-type hydrogenation catalysts. These runs were carried out using aliquots of the catalyst solutions prepared for analysis by XAFS.

**The Effects of H<sub>2</sub>O on Catalyst Activity.** The amount of H<sub>2</sub>O present is another important variable in the preparation and use of Ziegler-type hydrogenation catalysts, the effects of which are reported in the literature as beneficial in some cases and detrimental in others.<sup>2</sup> We tested the effects of different amounts of H<sub>2</sub>O *added intentionally* to the cyclohexene solvent in which Co(neodecanoate)<sub>2</sub> and AlEt<sub>3</sub> were simultaneously combined to give Al/Co = 3 catalyst solutions. It was found that the added water had a detrimental effect on the catalyst activity, and that catalyst activity became progressively lower with increasing amounts of added H<sub>2</sub>O; examples of the results are given in Figure S8. On the basis of these observations, we established the “standard conditions” to include rigorous drying of glassware and solvents. Specifically, and as described in the Experimental Section of the main text, all glassware was dried overnight at 160 °C and cooled either under vacuum or dry N<sub>2</sub>. Cyclohexane (Sigma-Aldrich, 99.5 %, H<sub>2</sub>O < 0.001 %) was kept over activated molecular sieves for ≥ 2 days prior to use, and cyclohexene (Aldrich, 99%) was distilled over Na under argon. Strict adherence to these drying procedures proved to be necessary in obtaining catalyst solutions with consistent cyclohexene hydrogenation activities using the Co catalyst. Cyclohexene hydrogenations performed using the Ni catalyst do not display any slowing if the cyclohexane used was not kept over molecular sieves and, in fact, slower hydrogenation runs were occasionally obtained when using cyclohexane solvent kept over molecular sieves, Figure S9 (although it is not known for sure if that was the precise cause of the slowing in those

specific experiments). On the basis of these observations, cyclohexane was used as received for the Ni catalyst, but all other water control considerations were identical to those used for the Co catalyst.



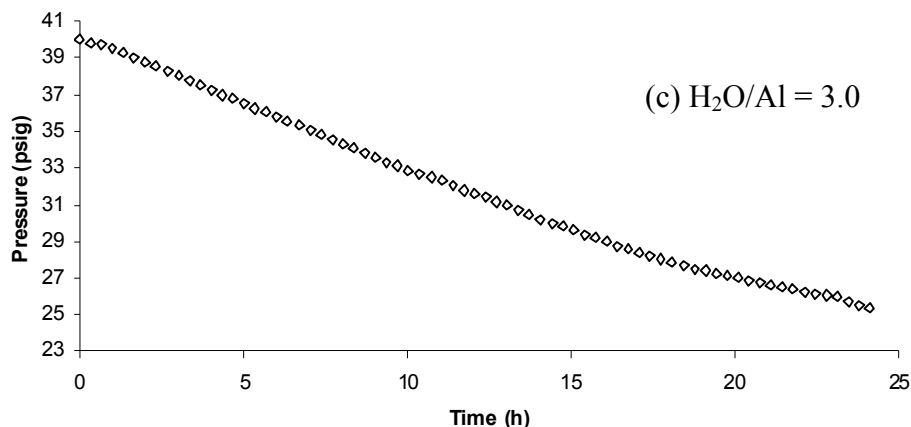


**Figure S8.** Examples of catalytic cyclohexene hydrogenation curves obtained using catalyst solutions made from  $\text{Co}(\text{neodecanoate})_2$  and  $\text{AlEt}_3$ ,  $\text{Al/Co} = 3$ , combined in cyclohexane solvent to which different amounts of  $\text{H}_2\text{O}$  had been added. (Note the different timescales in parts (a), (b), and (c) of Figure S8.) For the two example curves shown in part (a), the  $\text{H}_2\text{O/Al}$  ratio of 1.0 results in a mean maximum hydrogenation rate of  $37 \pm 4$  psig/h, as opposed to the maximum hydrogenation rate of 62 psig/h observed when the catalyst is prepared without added water, Figure S1. For the two example curves shown in part (b), the  $\text{H}_2\text{O/Al}$  ratio was 2.0 resulting in a further decrease in maximum catalyst activity. The mean maximum hydrogenation rate from experiments using an  $\text{H}_2\text{O/Al}$  ratio of 2.0 is  $5 \pm 1$  psig/h. A  $\text{H}_2\text{O/Al}$  ratio of 3.0 was used for part (c) giving a cyclohexene hydrogenation curve with a maximum hydrogenation rates of only about 1 psig/h. Clearly, the presence of  $\text{H}_2\text{O}$  in the cyclohexane solvent during the combination of the  $\text{Co}(\text{neodecanoate})_2$  and  $\text{AlEt}_3$  is detrimental to the resulting cyclohexene hydrogenation activity of the catalyst solution.

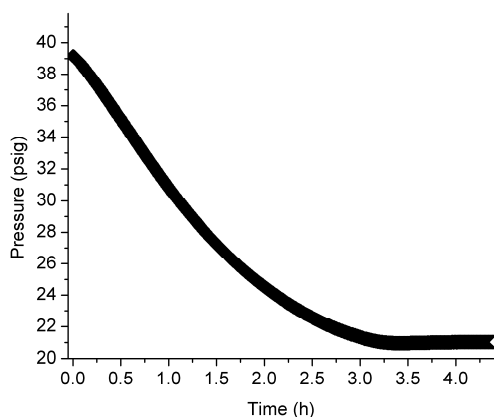


**Figure S9.** Example hydrogenation using the  $\text{Ni}(\text{2-ethylhexanoate})_2$  plus  $\text{AlEt}_3$  catalyst,  $\text{Al/Ni} = 2$ , prepared using cyclohexane kept over molecular sieves. The maximum hydrogenation rate of this run is 8.5 psig/h. Hydrogenations with lower  $\text{H}_2$  uptake rates such as this example were *occasionally* obtained when using the cyclohexane kept over molecular sieves as opposed to using the cyclohexane as received.

**Effect of Temperature During Catalyst Synthesis.** Several control hydrogenations were performed to test whether the temperature during catalyst synthesis plays an important role in catalyst activity.  $\text{Co}(\text{neodecanoate})_2$  and  $\text{AlEt}_3$  were combined to make catalyst solutions in the drybox with the solutions heated to  $60\text{ }^\circ\text{C}$  as opposed to the ambient drybox temp of  $\sim 25\text{ }^\circ\text{C}$ . Use of elevated temperature during catalyst synthesis, although reportedly important for catalyst activity optimization in some cases,<sup>2</sup> result in this case by lowering catalyst activity (see Fig S4b) to  $57 \pm 4$  psig/h, Figure S10. On the basis of this observation, standard conditions involve catalyst preparation at the ambient drybox temp of  $\sim 25\text{ }^\circ\text{C}$ .

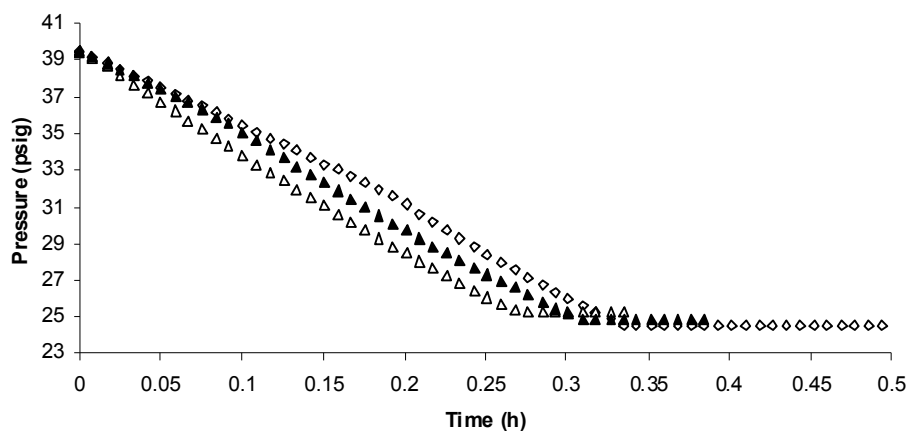


**Figure S10.** Cyclohexene hydrogenation curves using  $\text{Co}(\text{neodecanoate})_2$  plus  $\text{AlEt}_3$ , catalysts,  $\text{Al/Co} = 2$ , prepared at  $60\text{ }^\circ\text{C}$ . The mean maximum hydrogenation rate is  $57 \pm 4$  psig/h, which is lower than (otherwise identical) hydrogenations performed using catalyst solutions prepared at the ambient drybox temp of  $\sim 25\text{ }^\circ\text{C}$  (see Fig S4b). The amount of variations observed between the 3 runs shown here is typical, and is largely the result of variations in mixing combined with MTL kinetics. Other conditions not mentioned were “standard” (i.e., solvent = cyclohexane,  $[\text{Co}] = 1.2\text{ mM}$ , initial  $[\text{cyclohexene}] = 1.65\text{ M}$ , hydrogenation temp =  $22.0\text{ }^\circ\text{C}$ , and stirring of 1000 rpm during hydrogenation).

**Concentration of  $\text{AlEt}_3$  used in Catalyst Synthesis.** Control experiments were performed to test whether the use of  $\text{AlEt}_3$  in catalyst synthesis as a 36 mM solution in

cyclohexane versus neat has an effect on the cyclohexene hydrogenation activity of the resulting catalyst. The slightly lower mean maximum hydrogenation rate of  $49 \pm 7$  psig/h provides justification for instead using AlEt<sub>3</sub> as a 36.0 mM solution in cyclohexane as part of the standard conditions, Figure S11.

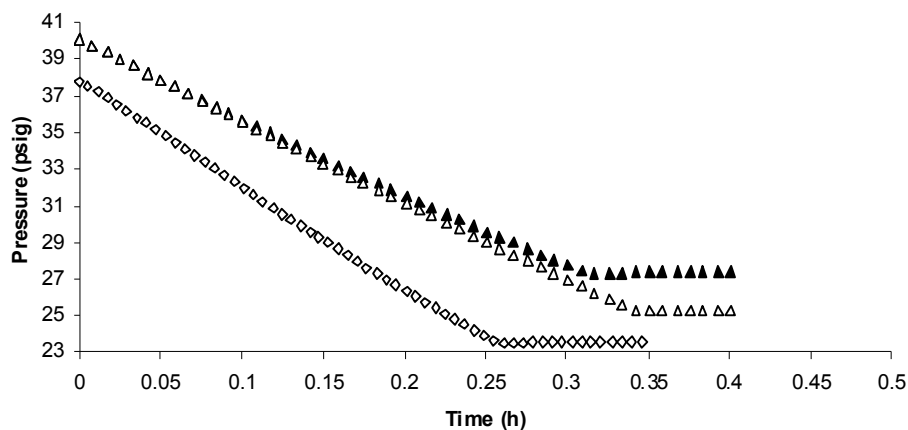


**Figure S11.** Control hydrogenations performed using Co(neodecanoate)<sub>2</sub> plus AlEt<sub>3</sub> catalyst, Al/Co = 3, made using neat AlEt<sub>3</sub> in the catalyst synthesis step. The slightly lower mean maximum hydrogenation rate of  $49 \pm 7$  psig/h provides justification for instead using AlEt<sub>3</sub> as a 36.0 mM solution in cyclohexane as part of the standard conditions.

**Order and Rate of Combination of the Precursor Components.** With Al/Co = 2, rapid (over 1 to 2 sec), *simultaneous* combination of Co(neodecanoate)<sub>2</sub> and AlEt<sub>3</sub> appears to give catalysts with higher activities than when AlEt<sub>3</sub> is added to the the Co(neodecanoate)<sub>2</sub> solution. However, this observation could be due to a combination MTL kinetics and poor reproducibility of mixing during hydrogenation. For example, with Al/Co = 3, rapid, simultaneous combination of Co(neodecanoate)<sub>2</sub> and AlEt<sub>3</sub> makes no difference in the observed H<sub>2</sub> uptake rate. In short, studies attempting to determine the optimal order and rate of precursor component combination were inconclusive. Nevertheless, considerable irreproducibility of hydrogenation rates observed using either

the Co- or Ni-based catalyst synthesized *without stirring* during combination of Co(neodecanoate)<sub>2</sub> or Ni(2-ethylhexanoate)<sub>2</sub>, and AlEt<sub>3</sub> suggests that rapid mixing at this key, incompletely understood stage of catalyst synthesis is vital (1000 ± 200 rpm stirring was used herein).

The goal of the preliminary catalytic studies was to establish standard conditions of catalyst synthesis and use in hydrogenation that necessary to ensure the subsequent studies were accomplished with catalyst samples made as reproducibly as possible and representative of active Ziegler-type hydrogenation catalysts. One of the main points is (i) that important factors in catalyst synthesis that strongly influence the activity of the resulting catalysts have been thoroughly sought out. Others are (ii) that the catalyst synthesis conditions and methods used give catalytic hydrogenation rates that are as optimized as possible, and (iii) that catalyst syntheses are repeated according to the standard conditions. These efforts ensure that the results obtained are both as reproducible as possible and are representative of active catalysts.

**Nuclearity of M<sub>n</sub> Species *before* Hydrogenation: Z-Contrast STEM and Bright Field TEM.** For each catalyst sample, cluster diameters were measured from multiple Z-contrast images at the same levels of magnification and contrast giving the histograms shown in the main text. Additional example Z-contrast images are shown here in Figure S12. Images from control experiments suggesting that neither sample preparation procedures nor Z-contrast STEM conditions are responsible for creating the clusters observed on ultrathin carbon grids are shown, Figures S13 and S14.

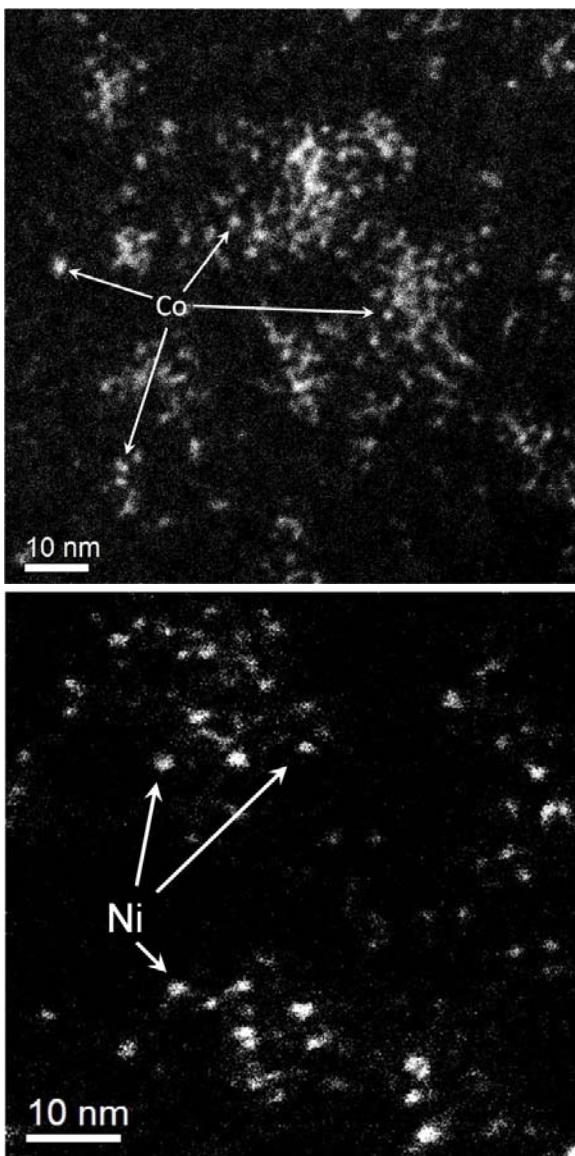


**Figure S12.** Additional example Z-contrast STEM images of catalyst samples made from  $\text{Co}(\text{neodecanoate})_2$  and  $\text{AlEt}_3$  (top), or  $\text{Ni}(\text{2-ethylhexanoate})_2$ , and  $\text{AlEt}_3$  (bottom) *before* their use for catalytic cyclohexene hydrogenation. The histograms shown in the main text include cluster diameter measurements from several images at the same levels of magnification and contrast.

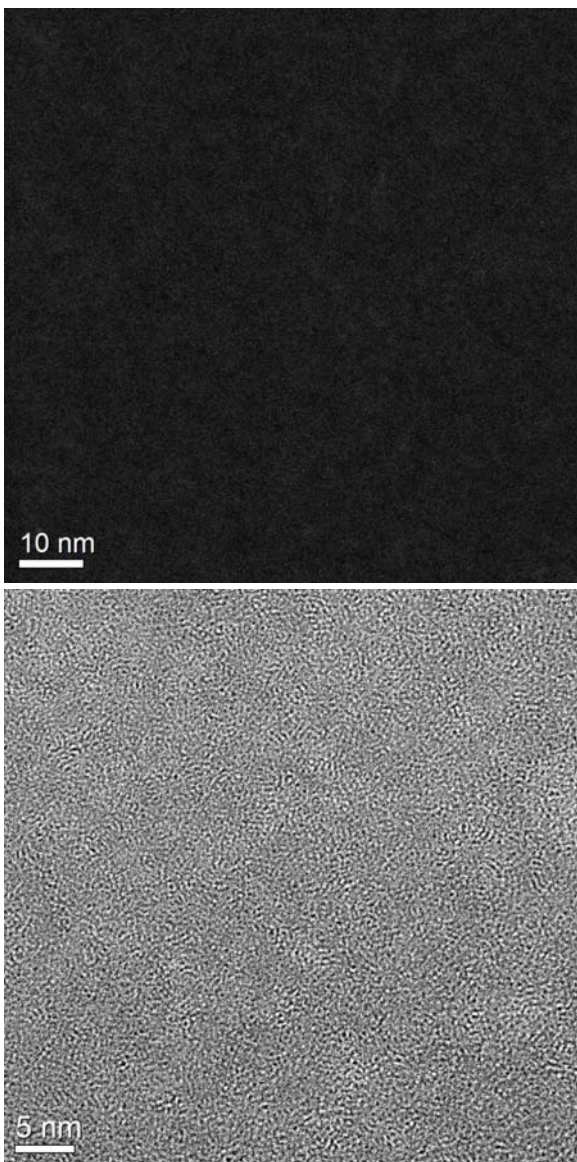


**Figure S13.** Example images from control experiments using  $\text{Co}(\text{neodecanoate})_2$  samples, without added  $\text{AlEt}_3$ , deposited on ultrathin carbon grids. Images using both Z-contrast STEM (top) and HRTEM (bottom) reveal an *absence of Co clusters*, suggesting that the Co clusters observed in the catalyst sample images shown in Fig S12 and in the main text are not artifacts of the microscopic conditions and sample preparation methods used.

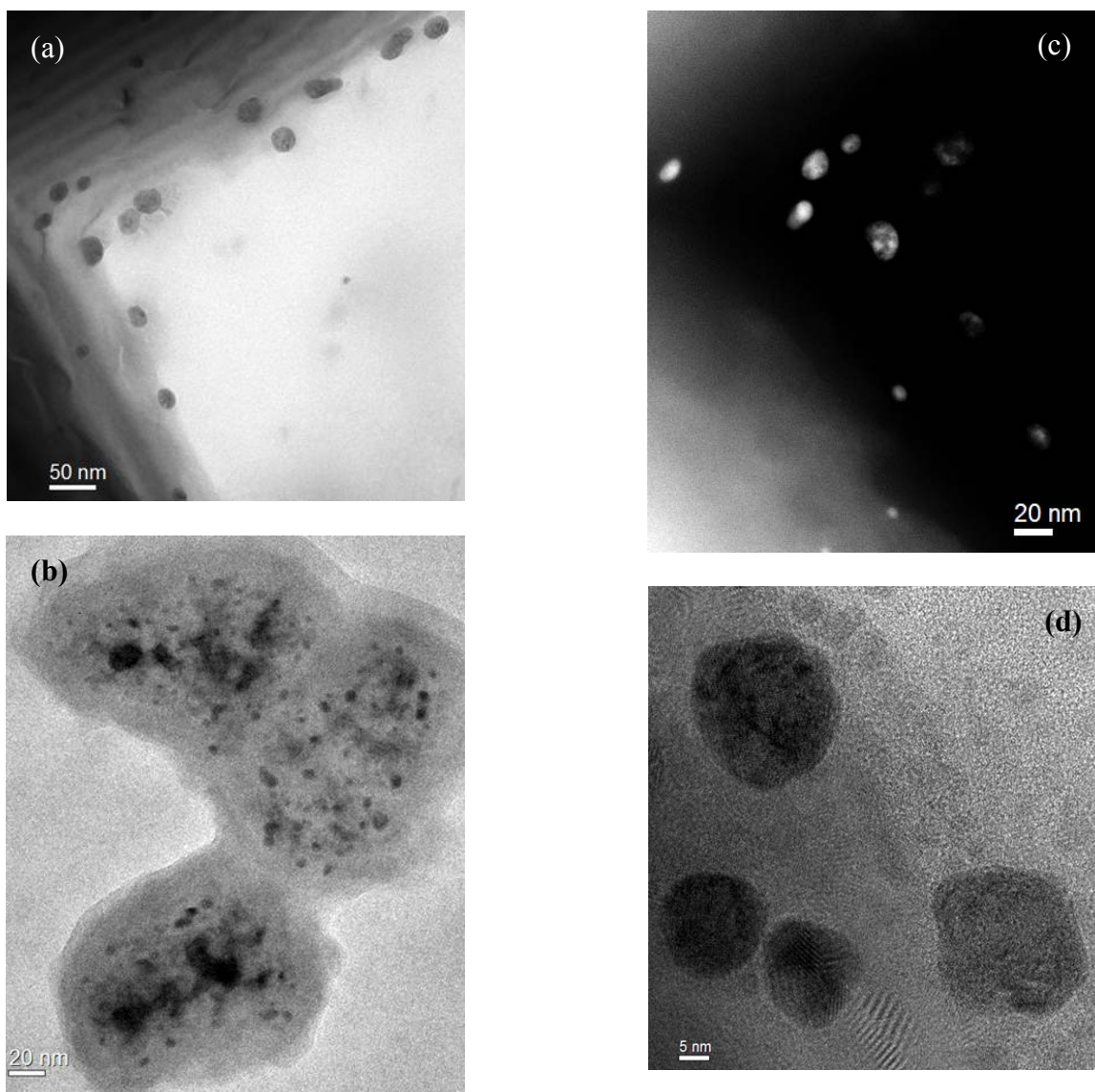
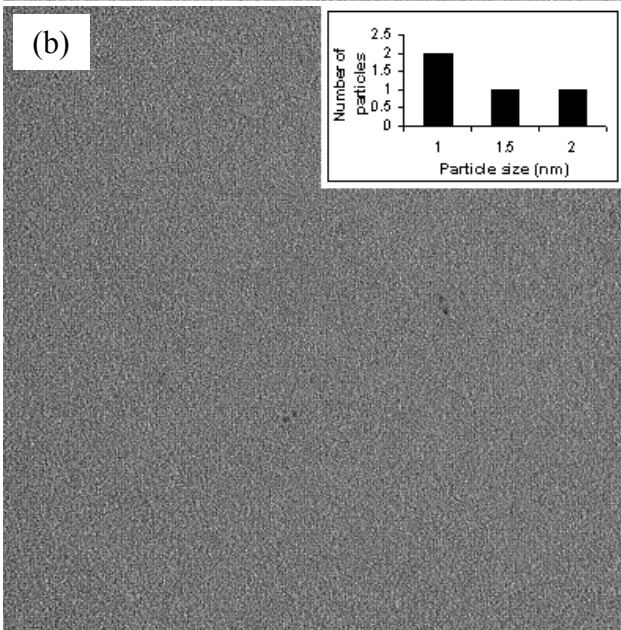
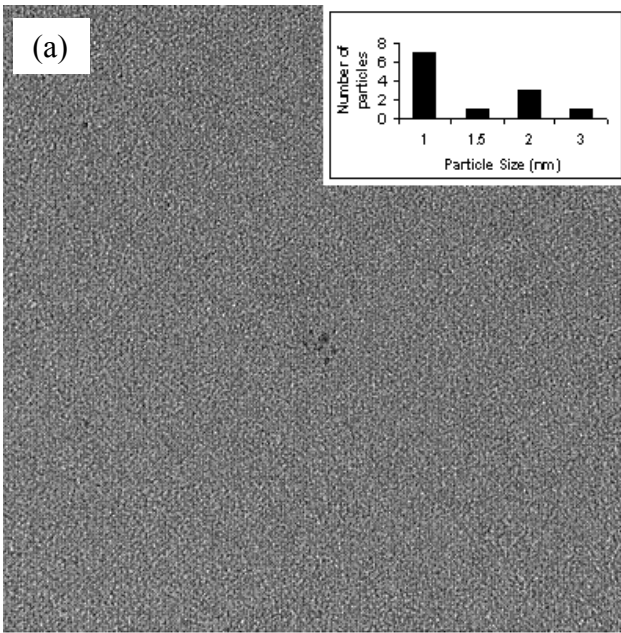


**Figure S14.** Example images from control experiments using  $\text{Co}(\text{neodecanoate})_2$  samples, without added  $\text{AlEt}_3$ , deposited on special  $\text{SiO}_2$  grids; bright field TEM (a and b), Z-contrast STEM (c), and HRTEM (d) all revealed the presence of nanometer-scale clusters. Therefore, the  $\text{SiO}_2$  grids were not used to image samples of the  $\text{Co}(\text{neodecanoate})_2$  plus  $\text{AlEt}_3$  catalyst samples. However, these findings are useful in that they reinforce the interpretation of a *lack* of observed clusters in images of the same sample deposited on ultrathin carbon grids, as an indication that the Co clusters observed in the catalyst sample images are not artifacts of the microscopic conditions and sample preparation methods used.

Images of Co and Ni catalyst samples were collected using bright field TEM, Figures S15 and S16. Measurement of the relatively limited number of particles that appear in these images reveals Co and Ni clusters with mean diameters of  $1.4 \pm 0.5$  nm, and  $1.7 \pm 0.7$ , respectively.

Similar to what was found previously using the Ir model system,<sup>4</sup> the results of bright field TEM are biased somewhat towards larger particles because the relatively poorer resolving power of conventional bright field TEM compared to Z-contrast STEM does not permit counting of any smaller particles present. The results from using bright field TEM are given here for the sake of completeness despite having been deemphasized in this study for the reasons stated.

Samples were prepared for bright field TEM by first diluting 0.1 mL of catalyst solution with cyclohexane to 0.6 mL. TEM grids (ultrathin carbon film supported by a lacey carbon film on a 400 Mesh copper grid, Ted Pella, Inc.) were then immersed into the dilute solution, and dried under an N<sub>2</sub> atmosphere in the drybox for ~1 min. The grids were then sealed air-tight in 5-mL glass vials, and sent to Dr. JoAn Hudson at Clemson University for imaging at  $\geq 0.5M$  magnification on a Hitachi H7600T operated at 120 kV. Particle sizes were measured manually. In a control experiment using the Co(neodecanoate)<sub>2</sub> precatalyst without added AlEt<sub>3</sub>, Co clusters are absent, at least within detection limit of the TEM instrument, Figure S17. This control experiment, just as the same one conducted using Z-contrast STEM before it (Fig S13), argues against TEM beam-induced formation of Co<sub>n</sub> nanoclusters, at least in the absence of AlEt<sub>3</sub>.



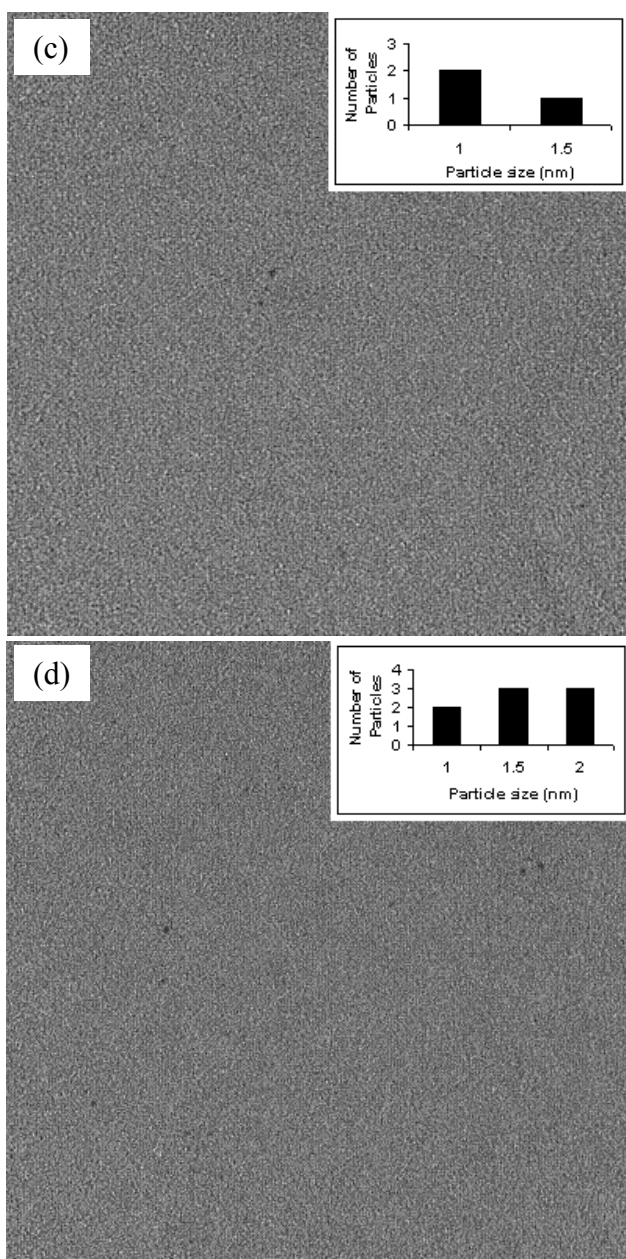


**Figure S15.** TEM images of the  $\text{Co}(\text{neodecanoate})_2$  plus  $\text{AlEt}_3$  catalyst sample, with an Al/Co ratio of 3, *before* its use in cyclohexene hydrogenation, and corresponding particle size histograms for each image. Images contain very few particles (i.e. 12, 4, 3, and 8 in images (a), (b), (c) and (d), respectively).

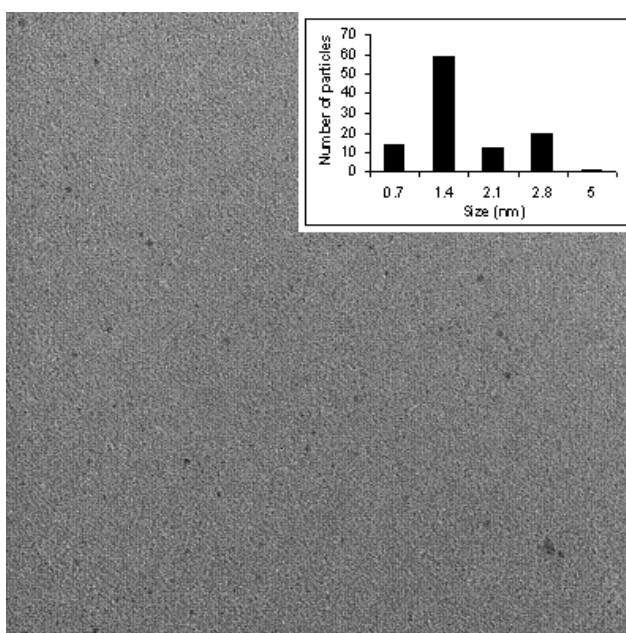


**Figure S16.** TEM and corresponding particle size histogram of the Ni(2-ethylhexanoate)<sub>2</sub> plus AlEt<sub>3</sub> catalyst, with an Al/Ni ratio of 2.0, *before* its use in cyclohexene hydrogenation. The size of the observed nanoclusters is  $1.7 \pm 0.7$  nm.

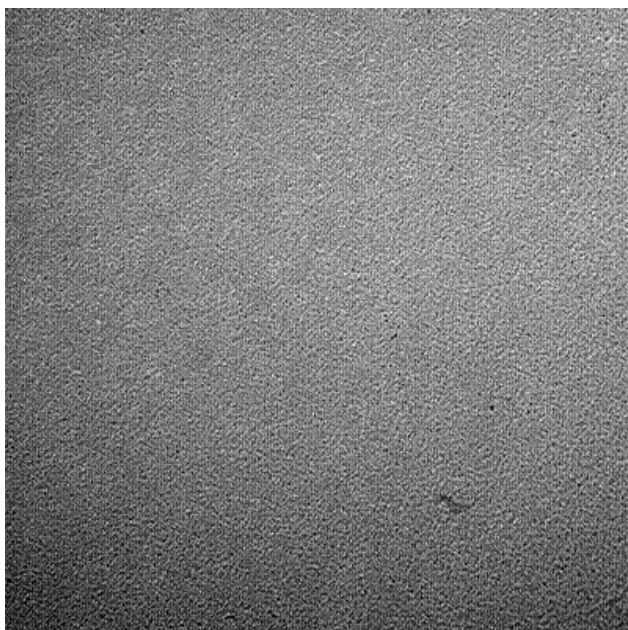
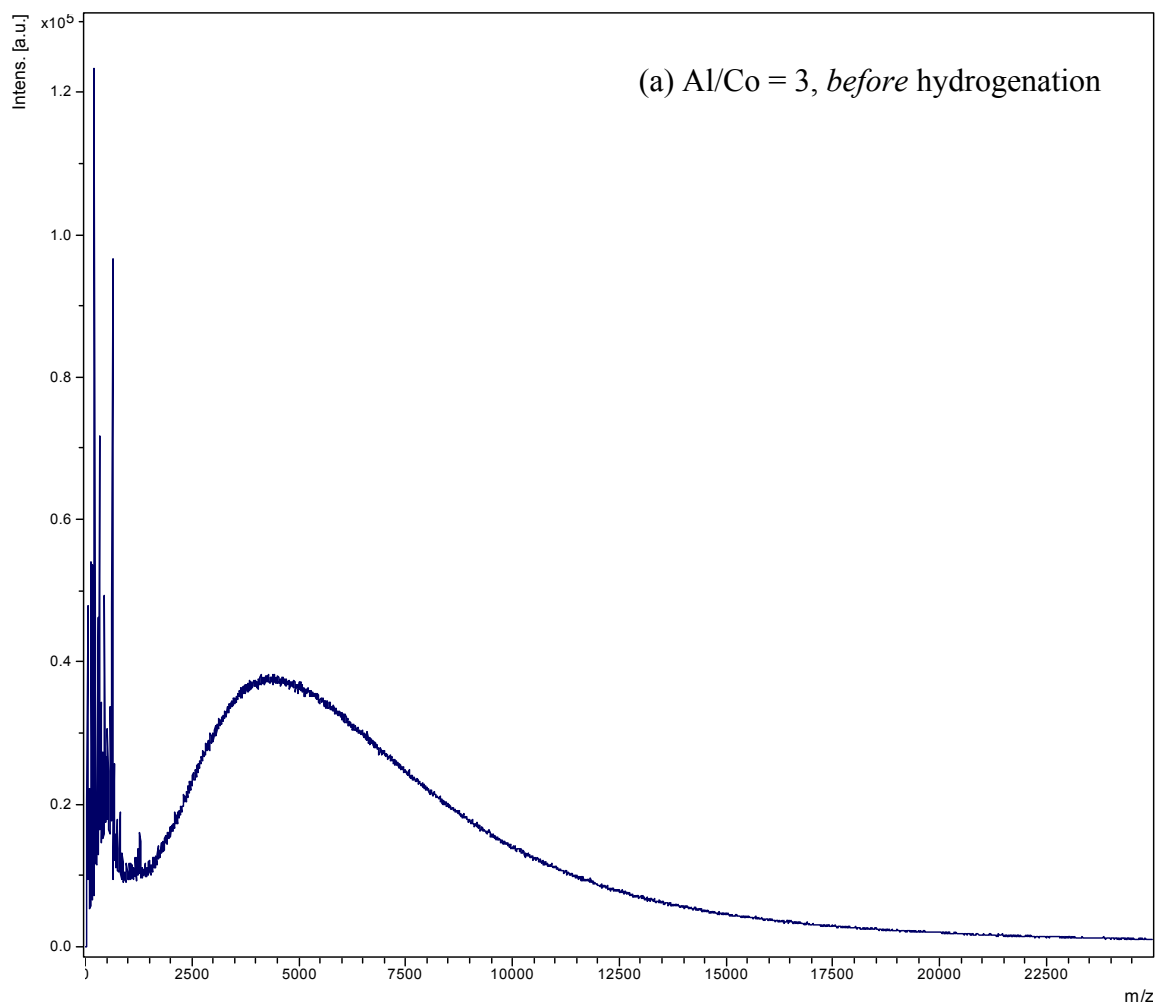


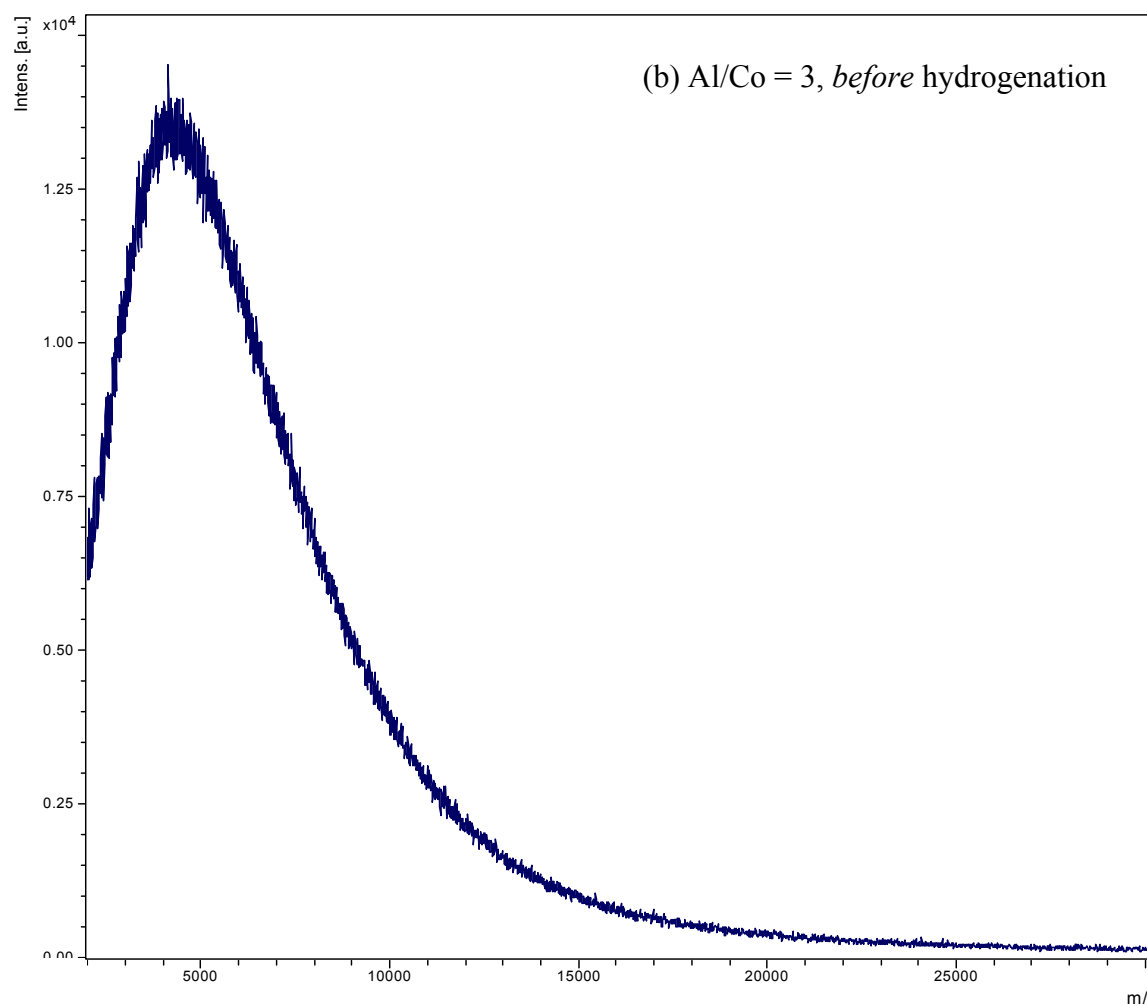
**Figure S17.** TEM image of Co(neodecanoate)<sub>2</sub> precatalyst without added AlEt<sub>3</sub>. Nanoparticles are not observed at least within detection limit of the TEM instrument, which argues against TEM beam-induced formation of Co<sub>n</sub> nanoparticles from the Co(neodecanoate)<sub>2</sub> precatalyst. Also see Fig S13 above.

**Nuclearity of M<sub>n</sub> Species *before* Hydrogenation: MALDI MS.** The MALDI MS

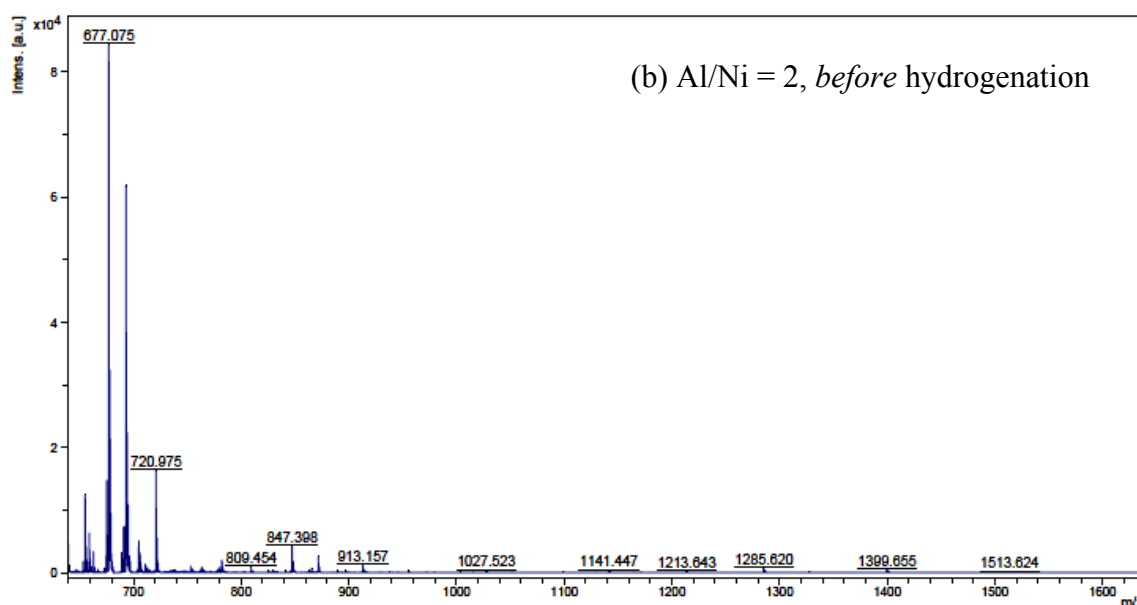
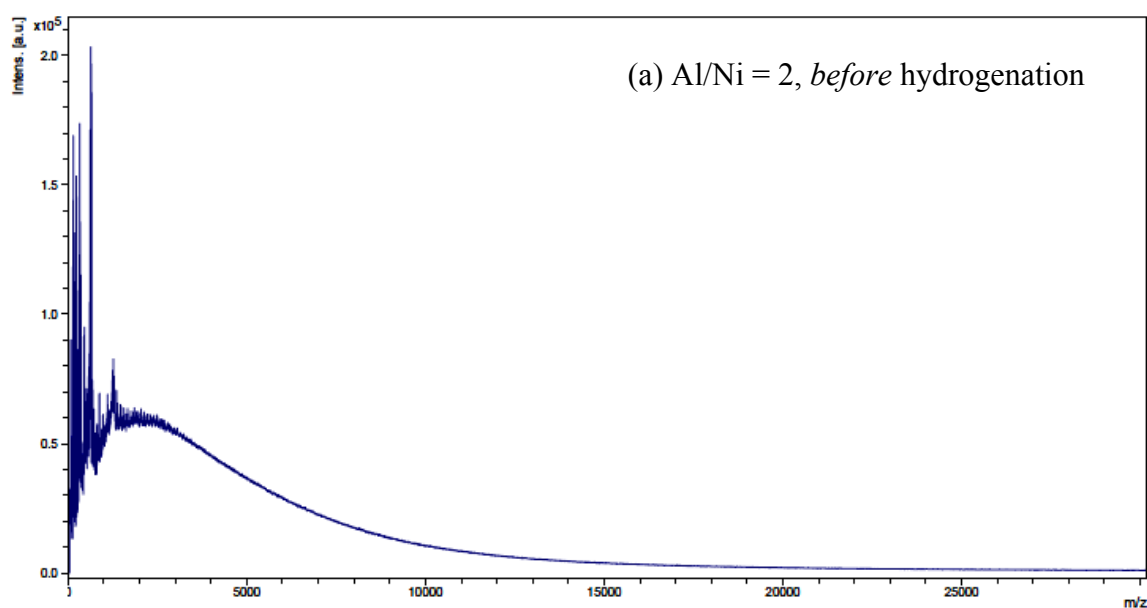
results from analyzing catalyst samples made from Co(neodecanoate)<sub>2</sub> plus AlEt<sub>3</sub>, with an Al/Co

ratio of 3, and from Ni(2-ethylhexanoate)<sub>2</sub> plus AlEt<sub>3</sub>, with an Al/Ni ratio of 2, both before hydrogenation are shown in Figures S18 and S19, respectively. Repeat experiments show that the MALDI MS peaks are reproducible for both Co and Ni catalyst samples, even when taken from separately prepared catalyst batches (this holds true for catalyst samples both *before* and *after* their use for cyclohexene hydrogenation); an example repeat MALDI MS of the Co catalyst is shown in Figure S18b. An example hi-resolution spectrum of the low  $m/z$  region is shown in Figure S19b. A blank sample containing only the matrix, trihydroxyacetophenone (THAP), and ionizing agent, NaI was analyzed, Figure S20; the matrix and ionizing agent may contribute to peaks observed in the 0–1500  $m/z$  region of catalyst sample spectra. Therefore, the 0–1500  $m/z$  region was excluded from the  $m/z$  range of the species used to calculate number of transition metal atoms (M) in the M<sub>n</sub> clusters.

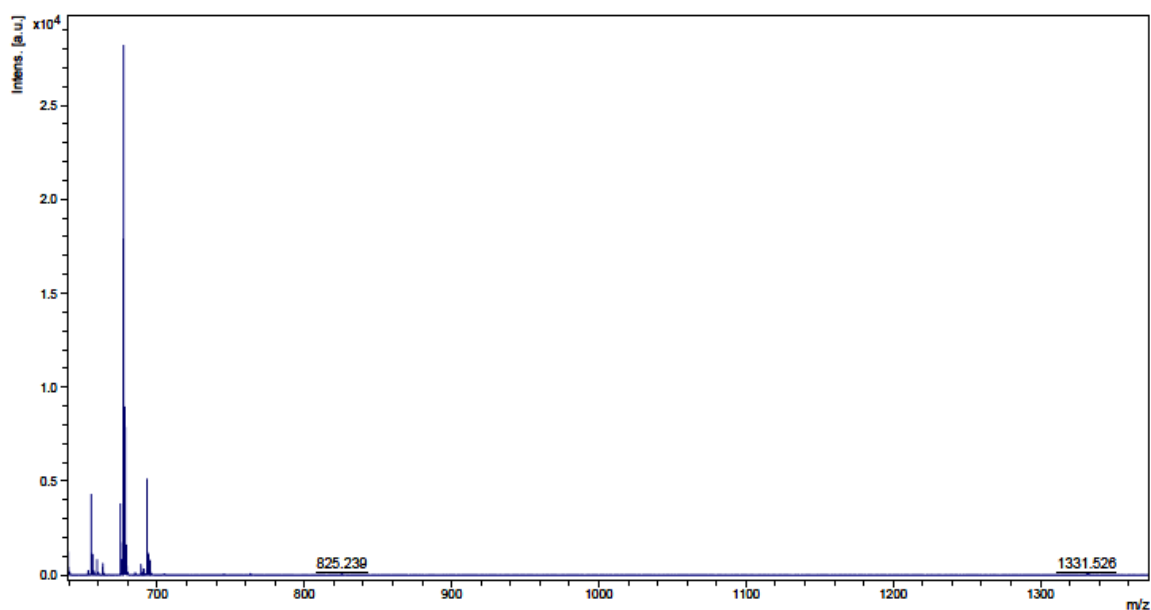




**Figure S18.** (a) MALDI MS of the  $\text{Co}(\text{neodecanoate})_2$  plus  $\text{AlEt}_3$  catalyst, with an Al/Co ratio of 3, before its use in cyclohexene hydrogenation. (b) MALDI MS of a  $\text{Co}(\text{neodecanoate})_2$  plus  $\text{AlEt}_3$  catalyst sample, with an Al/Co ratio of 3, before its use in cyclohexene hydrogenation, and prepared separately from the sample analyzed in (a). The spectrum in (b), although shown at a different scale, is consistent with the one in (a), demonstrating that the MALDI MS observations are reproducible for these catalyst samples.



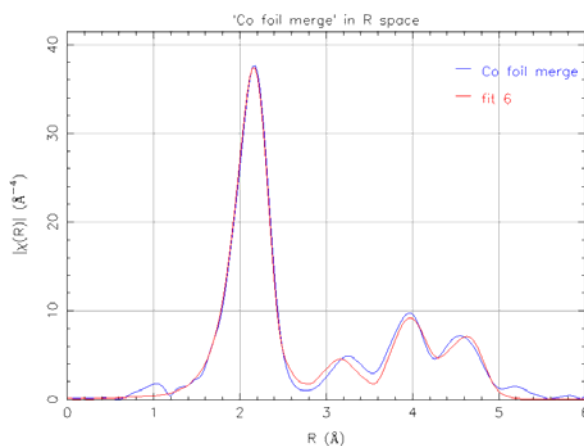
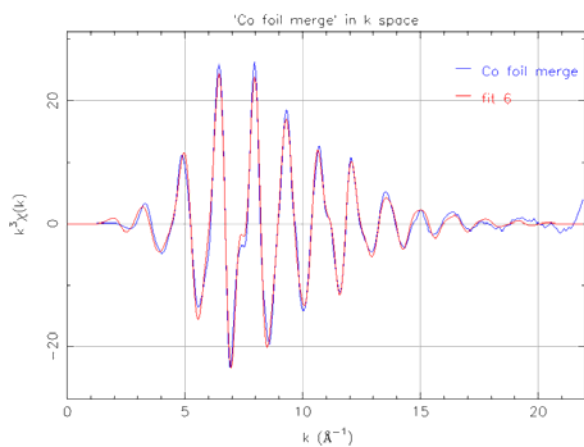
**Figure S19.** (a) MALDI MS of the Ni(2-ethylhexanoate)<sub>2</sub> plus AlEt<sub>3</sub> catalyst, with an Al/Ni ratio of 2.0, *before* its use in cyclohexene hydrogenation. (b) High resolution MALDI MS of the Ni(2-ethylhexanoate)<sub>2</sub> plus AlEt<sub>3</sub> catalyst sample, with Al/Ni ratio of 2.0, *before* it is used in cyclohexene hydrogenation. The observed peaks represent species that do not contain Ni, evidenced by the absence of characteristic Ni isotope peak distributions. Therefore, they can be assigned to either detached stabilizer species, trihydroxyacetophenone (THAP, used as the matrix), or both. Regardless, on the basis, in part, of the lack of Ni in the region up to 1500 *m/z*, the 0–1500 *m/z* region was not considered in the analysis of cluster sizes by MALDI MS.



**Figure S20.** High resolution MALDI MS of THAP plus NaI used as matrix and ionization agent, respectively. This blank sample shows that some of the peaks in the low  $m/z$  region of both Co and Ni catalyst sample spectra may be due to the THAP matrix. On the basis of this and the result shown in Fig S19b, the 0–1500  $m/z$  region was disregarded in the analysis of cluster sizes by MALDI MS.

**Nuclearity of  $M_n$  species before hydrogenation: EXAFS.** Co foil data is modeled using a theoretical bulk hcp Co signal, that includes single scattering (SS), triangular (TR), and co-linear (CL) scattering paths. Values of  $N$  were fixed so that a value for the passive electron reduction factor ( $S_0^2 = 0.84 \pm 0.03$ ) could be determined and applied for fitting sample spectra.  $\Delta E_0 = -2.1 \pm 0.5$  eV.  $k$ -weighting and  $R$ -range used for the fit were  $k^3$  and 1.0–5.1 Å, respectively, complete fitting results are given in Table S1. The XAFS spectra of the Co(neodecanoate)<sub>2</sub> precatalyst, without added AlEt<sub>3</sub> was fit using the crystal structure of [Co<sub>2</sub>(OPh)<sub>6</sub>]<sup>2-</sup> as a starting point; the fitting results are given in Table S3.<sup>5</sup> The metallic and non-metallic contributions in the XAFS spectra of Co(neodecanoate)<sub>2</sub> plus AlEt<sub>3</sub> catalysts samples were modeled using the first nearest neighbor (1NN) single scattering path, Co–Co, from the theoretical crystal structure of bulk Co, and the 1NN, Co–O path from the crystal structure of [Co<sub>2</sub>(OPh)<sub>6</sub>]<sup>2-</sup>,<sup>5</sup> respectively. Fits and the resulting data are given in the main text, and in the following Figures and Tables herein.

The Ni foil data was fit in a manner similar to Co foil, but using bulk fcc Ni as the model. The  $S_0^2$  value determined for use in fitting Ni sample spectra was  $0.92 \pm 0.06$ .  $\Delta E_0 = -3.2 \pm 0.5$  eV. K-weighting and R-range used for the fit were  $k^2$  and 1.0–4.9 Å, respectively. The complete fitting results are given in Table S2. The EXAFS spectra of the Ni(2-ethylhexanoate)<sub>2</sub> precatalyst, without added AlEt<sub>3</sub>, was fit using the crystal structure of Ni(OAc)<sub>2</sub>•4H<sub>2</sub>O,<sup>6</sup> and the results are tabulated in the main text. The metallic and non-metallic contributions in the EXAFS spectra of Ni(2-ethylhexanoate)<sub>2</sub> plus AlEt<sub>3</sub> catalysts samples were modeled using a combination of the 1NN, single scattering Ni–Ni path from the theoretical crystal structure of bulk Ni, and the 1NN single scattering Ni–O path from the crystal structure of Ni(OAc)<sub>2</sub>•4H<sub>2</sub>O,<sup>6</sup> respectively. The fits to the data and their results are given in the main text and in the following Figures and Tables herein.



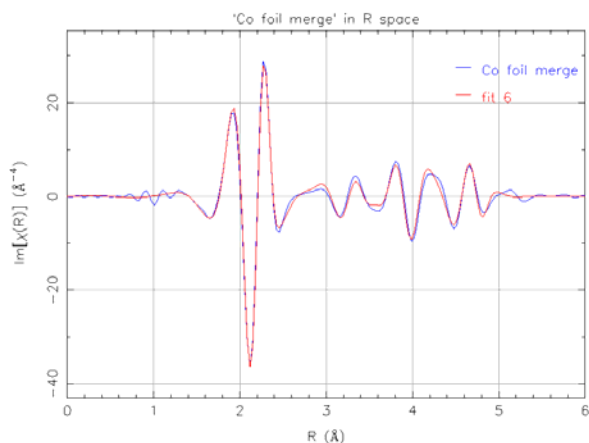


**Figure S21.** Data and fit of the EXAFS spectrum of Co foil plotted as (a)  $\chi(k)$ ; (b) the magnitude of the FT; and (c) the imaginary portion of the FT. The fit was achieved by using the FEFF6 theory of bulk hcp Co. The  $k$ -range used for FT was 2–20  $\text{\AA}^{-1}$ .

**Table S1.** Fit results for Co foil.

Path	N	$R_{\text{eff}}$ ( $\text{\AA}$ )	R ( $\text{\AA}$ )	$\sigma^2 \times 10^3$ ( $\text{\AA}^2$ )
SS1 <sup>a</sup>	6	2.4982	$2.492 \pm 0.002$	$6.7 \pm 0.3$
SS4	6	3.5413	$3.532 \pm 0.003$	$10 \pm 1$
TR3,2 <sup>b</sup>	24	3.7532	$3.744 \pm 0.003$	$5 \pm 4$
SS6	2	4.0700	$4.060 \pm 0.004$	$7 \pm 2$
SS7 <sup>c</sup>	12	4.3407	$4.330 \pm 0.004$	$10.1 \pm 0.7$
SS11	12	4.7817	$4.770 \pm 0.004$	$15 \pm 3$
SS12	6	5.0200	$5.007 \pm 0.005$	$8.0 \pm 0.6$
CL12,3	12	5.0200	$5.007 \pm 0.005$	$8.0 \pm 0.6$
CL3,12,3	6	5.0200	$5.007 \pm 0.005$	$8.0 \pm 0.6$

<sup>a</sup> In order to minimize the number of variables used, and because the difference in  $R_{\text{eff}}$  values between SS1 and SS3 is only 0.0118  $\text{\AA}$ , the contribution to the experimental Co foil spectrum from the SS3 path ( $N = 6$ ) was accounted for by multiplying  $S_0^2$  for the SS1 path by a factor of two. <sup>b</sup> The contributions from the TR2,1 ( $R_{\text{eff}} = 3.7532 \text{\AA}$ ,  $N = 12$ ) and TR3,3 ( $R_{\text{eff}} = 3.7650 \text{\AA}$ ,  $N = 12$ ) paths were accounted for by multiplying  $S_0^2$  for the TR3,2 path by a factor of two. <sup>c</sup> The contribution from the SS10 path ( $R_{\text{eff}} = 4.3474 \text{\AA}$ ,  $N = 6$ ) was accounted for by multiplying  $S_0^2$  for the SS7 path by a factor of 1.5.

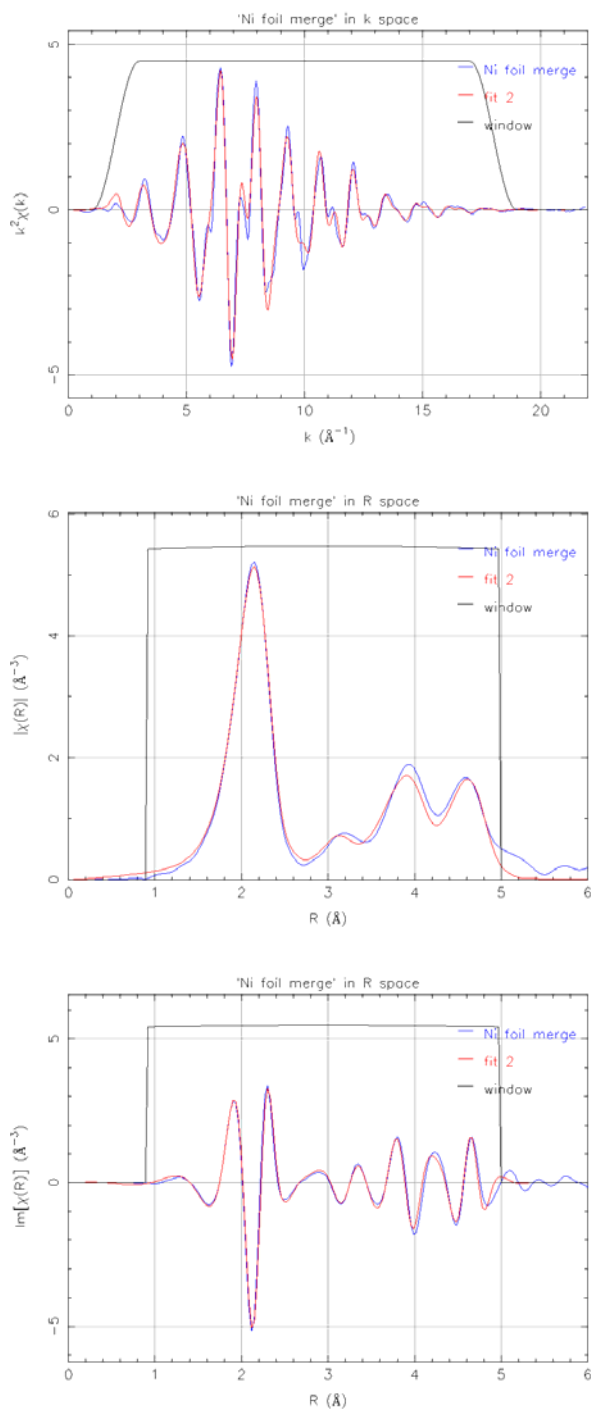
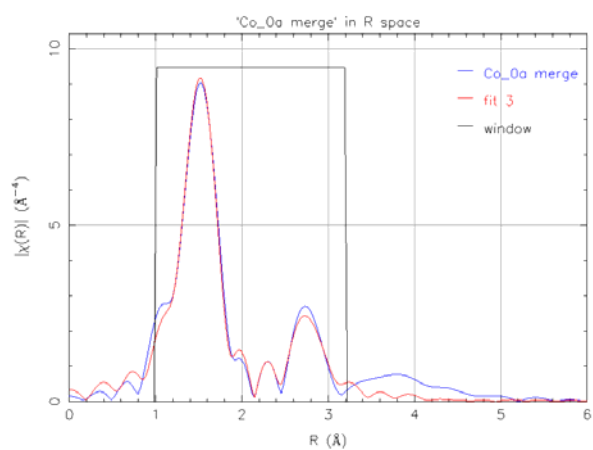
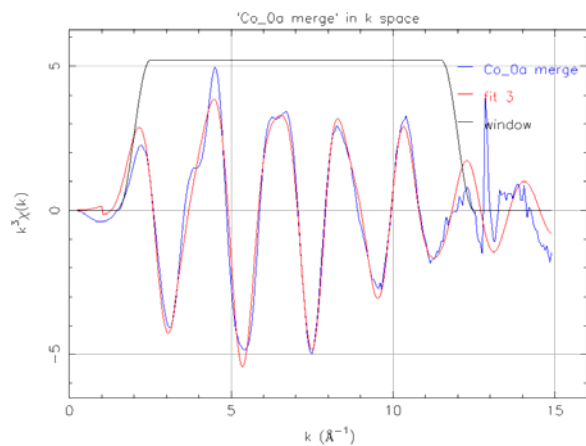


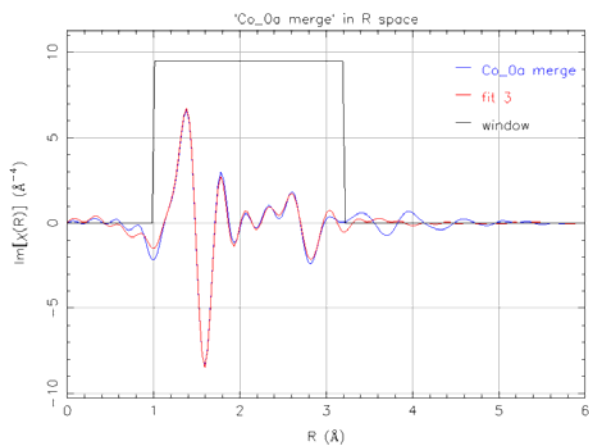
**Figure S22.** Data and fit of the EXAFS spectrum of Ni foil plotted as (a)  $\chi(k)$ ; (b) the magnitude of the FT; and (c) the imaginary portion of the FT. The fit was achieved by using the FEFF6 theory of bulk fcc Ni. The k-range used for FT was 2–18  $\text{\AA}^{-1}$ .

**Table S2.** Fit results for Ni foil.

Path	N	$R_{\text{eff}}$ ( $\text{\AA}$ )	$R$ ( $\text{\AA}$ )	$\sigma^2 \times 10^3$ ( $\text{\AA}^2$ )
SS1	12	2.4890	$2.490 \pm 0.003$	$6.9 \pm 0.5$
SS2	6	3.5200	$3.522 \pm 0.005$	$11 \pm 2$

TR1,1	48	3.7335	$3.735 \pm 0.005$	$12 \pm 10$
TR2,1	48	4.2490	$4.251 \pm 0.006$	$5 \pm 4$
SS3	24	4.3111	$4.313 \pm 0.006$	$9.7 \pm 0.9$
SS4	12	4.9780	$4.981 \pm 0.007$	$7.6 \pm 0.6$
CL4,1	24	4.9780	$4.981 \pm 0.007$	$7.6 \pm 0.6$
CL1,4,1	12	4.9780	$4.981 \pm 0.007$	$7.6 \pm 0.6$

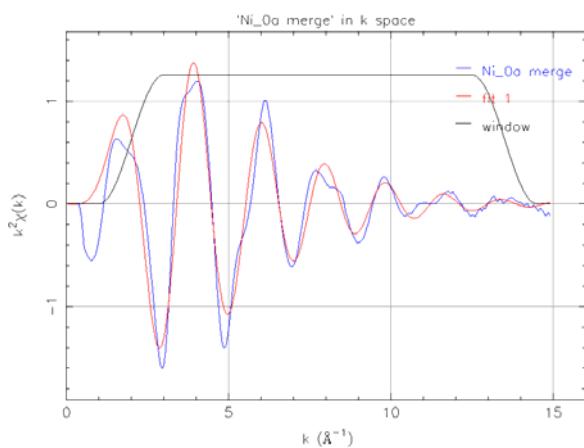


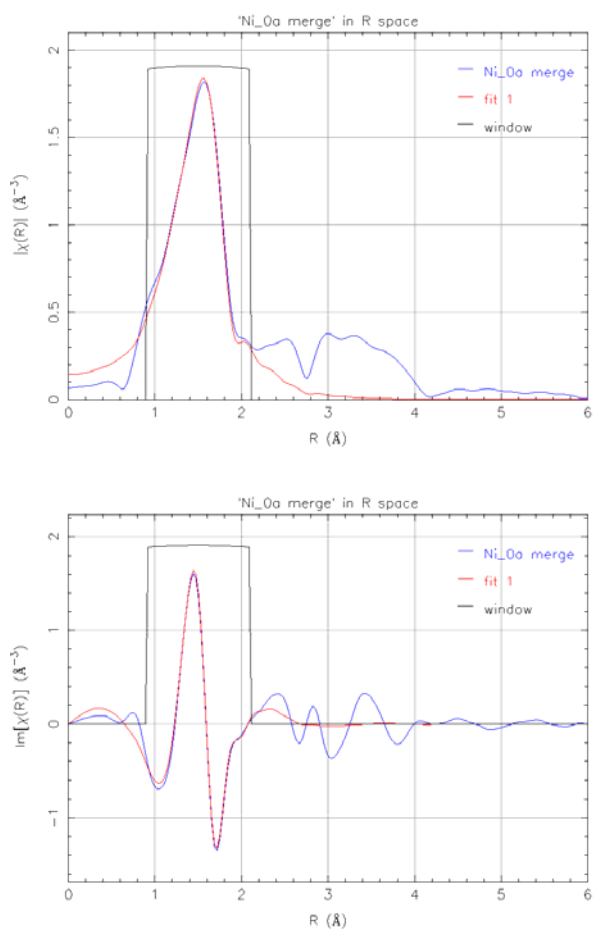


**Figure S23.** Data and fit of the EXAFS spectrum of Co(neodecanoate)<sub>2</sub> plotted as (a)  $\chi(k)$ ; (b) the magnitude of the FT; and (c) the imaginary portion of the FT. The  $k$ -range used for FT was 2–12  $\text{\AA}^{-1}$ .

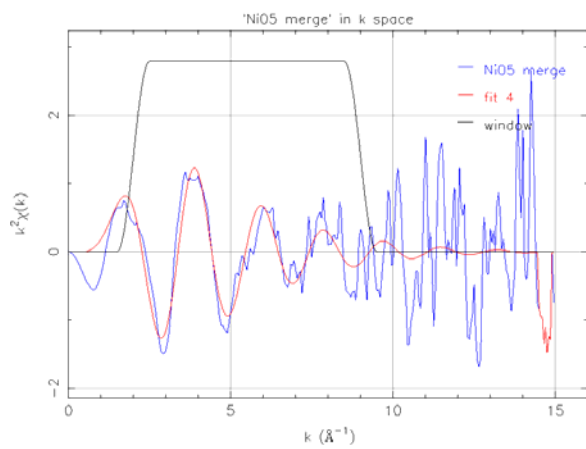
**Table S3.** Fit results for Co(neodecanoate)<sub>2</sub> without added AlEt<sub>3</sub>.  $\Delta E_0 = 4 \pm 1$  eV.

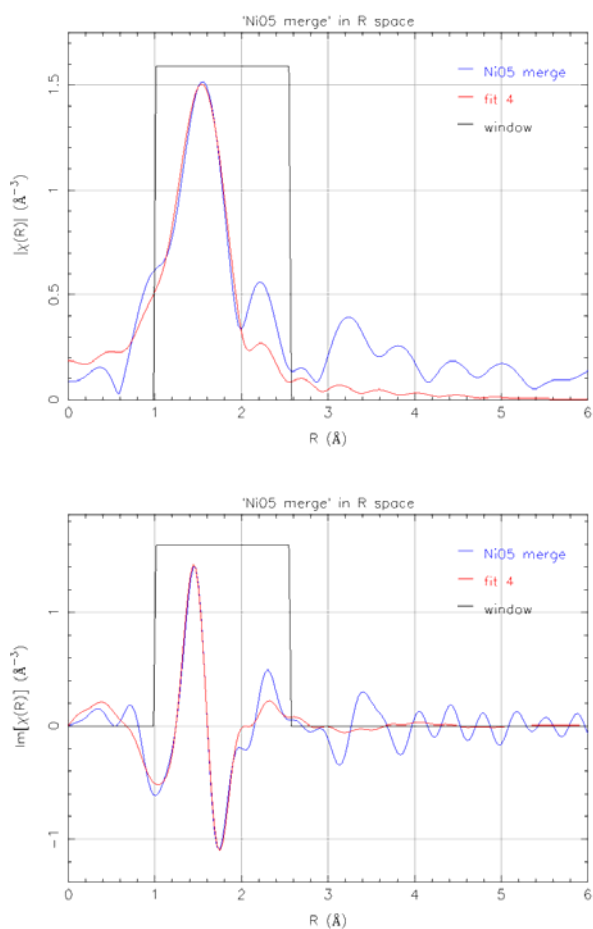
Path	N	$R_{\text{eff}}$ ( $\text{\AA}$ )	R ( $\text{\AA}$ )	$\sigma^2 \times 10^3$ ( $\text{\AA}^2$ )
Co–O	$4.7 \pm 0.4$	1.9995	$1.959 \pm 0.005$	$4.6 \pm 0.7$
Co–C	$9 \pm 7$	3.0130	$2.98 \pm 0.05$	$17 \pm 15$
Co–Co	$4 \pm 3$	3.0276	$3.20 \pm 0.02$	$12 \pm 5$





**Figure S24.** Data and fit of the EXAFS spectrum of Ni(2-ethylhexanoate)<sub>2</sub> plotted as (a)  $\chi(k)$ ; (b) the magnitude of the FT; and (c) the imaginary portion of the FT. The  $k$ -range used for FT was 2–13.5  $\text{\AA}^{-1}$ .  $k$ -weighting and  $R$ -range used for the fit were  $k^2$  and 1.0–2.0  $\text{\AA}$ , respectively.  $\Delta E_0 = -2.6 \pm 0.5$  eV. The only path used to fit the spectrum is Ni–O,  $R_{\text{eff}} = 2.0494$   $\text{\AA}$ ; results from the fit are tabulated in the main text.

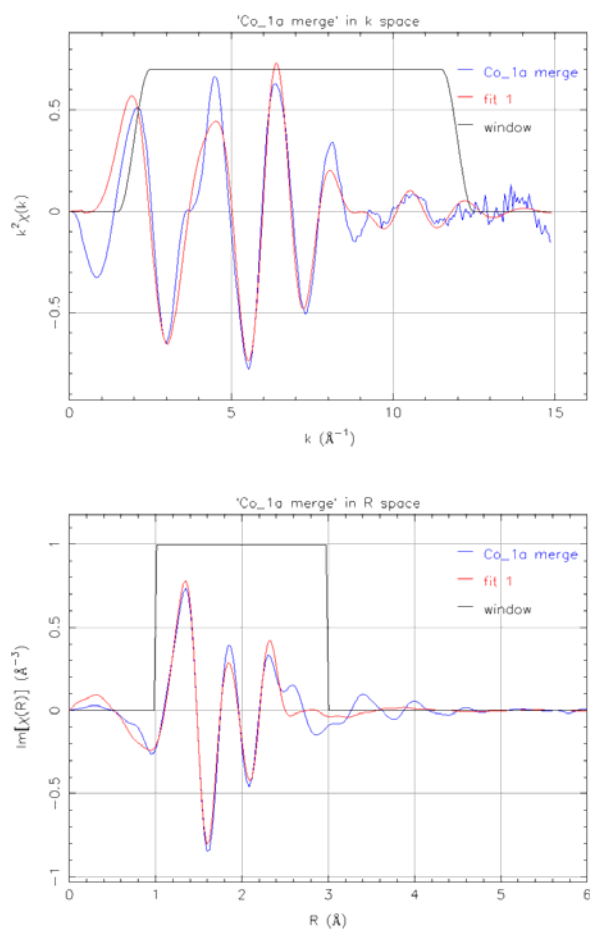




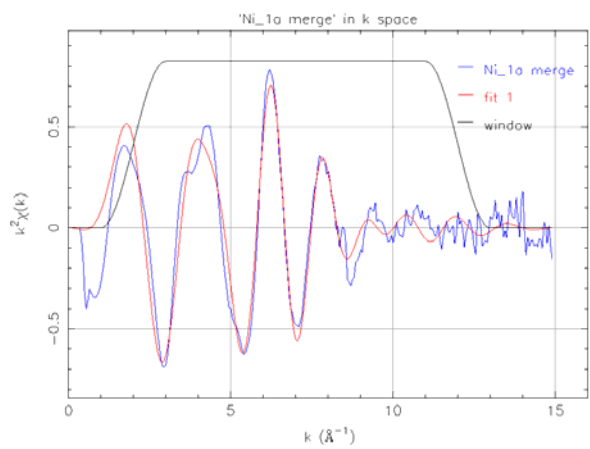
**Figure S25.** Data and fit of the EXAFS spectrum Ni(2-ethylhexanoate)<sub>2</sub> plus AlEt<sub>3</sub>, with an Al/Ni ratio of 0.5, plotted as (a)  $\chi(k)$ ; (b) the magnitude of the FT; and (c) the imaginary portion of the FT. The  $k$ -range used for FT was 2–9  $\text{\AA}^{-1}$ .

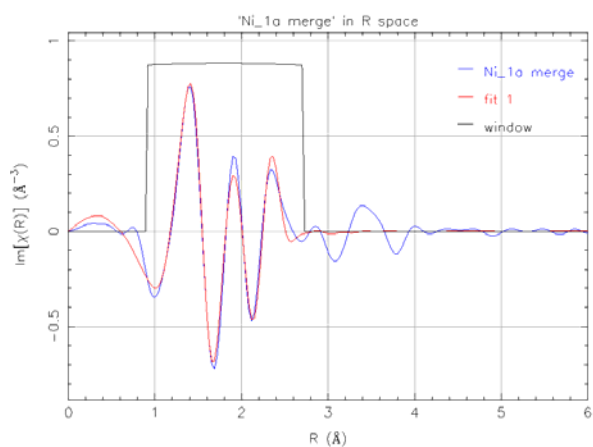
**Table S4.** Fit results for Ni(2-ethylhexanoate)<sub>2</sub> plus AlEt<sub>3</sub>, with an Al/Ni ratio of 0.5.  $\Delta E_0 = -1 \pm 2$  eV.  $k$ -weighting and  $R$ -range used for the fit were  $k^2$  and 1.0–2.55  $\text{\AA}$ , respectively.

Path	N	$R_{\text{eff}}$ ( $\text{\AA}$ )	$R$ ( $\text{\AA}$ )	$\sigma^2 \times 10^3$ ( $\text{\AA}^2$ )
Ni–O	$5 \pm 1$	2.0494	$2.06 \pm 0.02$	$9 \pm 4$

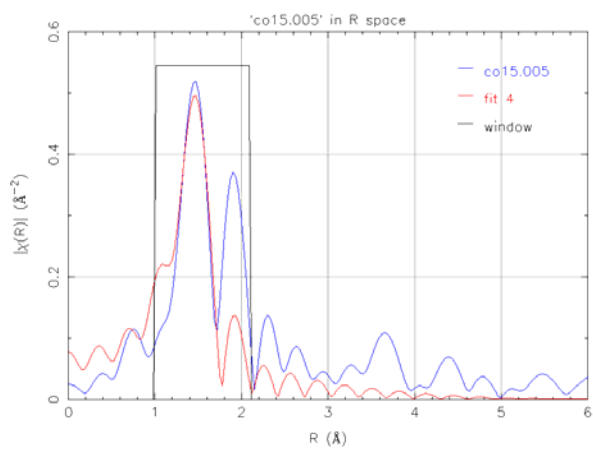
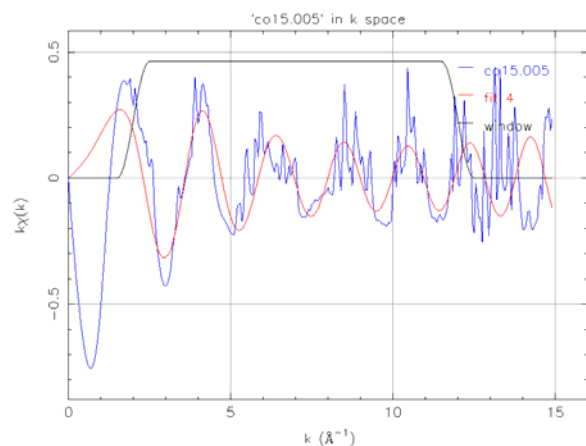


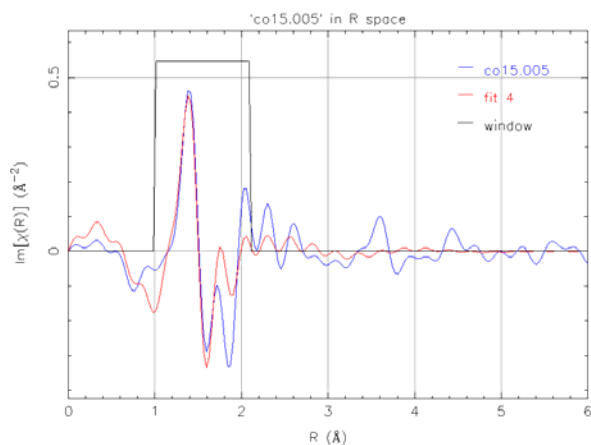
**Figure S26.** Data and fit of the EXAFS spectrum of  $\text{Co}(\text{neodecanoate})_2$  plus  $\text{AlEt}_3$ , with an Al/Co ratio of 1.0, plotted as (a)  $\chi(k)$ ; and (b) as the imaginary portion of the FT. The magnitude of the FT is shown in the main text. The k-range used for FT was 2–12  $\text{\AA}^{-1}$ . K-weighting and R-range used for the fit were  $k^2$  and 1.0–3.0  $\text{\AA}$ , respectively.  $\Delta E_0 = 1 \pm 2$  eV. Results from the fit are tabulated in the main text.





**Figure S27.** Data and fit of the EXAFS spectrum  $\text{Ni}(\text{2-ethylhexanoate})_2$  plus  $\text{AlEt}_3$ , with an Al/Ni ratio of 1.0, plotted as (a)  $\chi(k)$ ; and (b) as the imaginary portion of the FT. The magnitude of the FT is shown in the main text. The  $k$ -range used for FT was  $2\text{--}12 \text{ \AA}^{-1}$ .  $k$ -weighting and  $R$ -range used for the fit were  $k^2$  and  $1.0\text{--}2.6 \text{ \AA}$ , respectively.  $\Delta E_0 = -3 \pm 2 \text{ eV}$ . Results from the fit are tabulated in the main text.

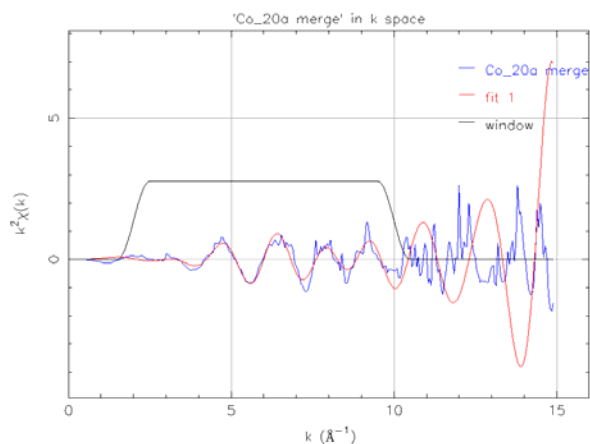


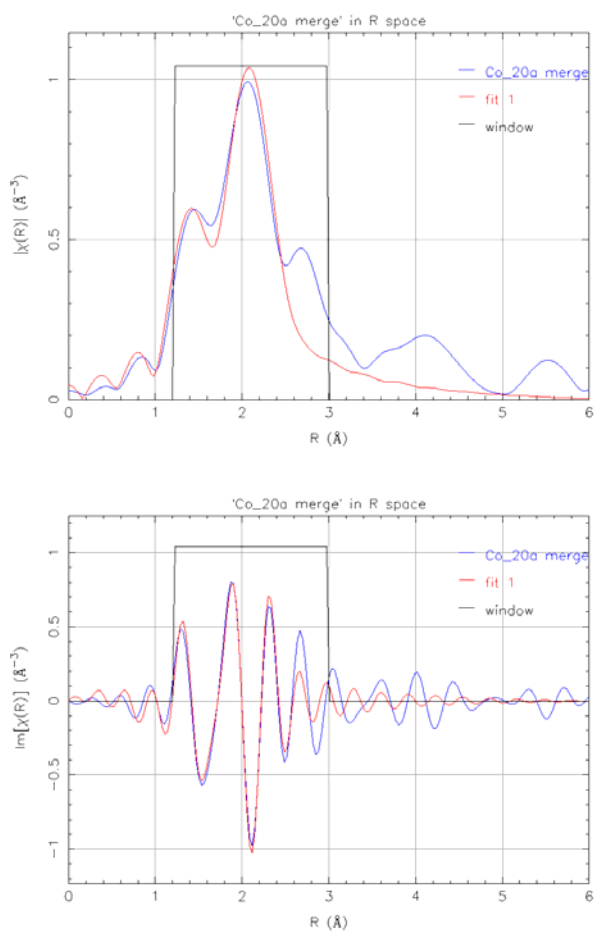


**Figure S28.** Data and fit of the EXAFS spectrum of Co(neodecanoate)<sub>2</sub> plus AlEt<sub>3</sub>, with an Al/Co ratio of 1.5, plotted as (a)  $\chi(k)$ ; (b) the magnitude of the FT; and (c) the imaginary portion of the FT. The k-range used for FT was 2–12  $\text{\AA}^{-1}$ .

**Table S5.** Fit results for Co(neodecanoate)<sub>2</sub> plus AlEt<sub>3</sub>, with an Al/Co ratio of 1.5.  $\Delta E_0 = -4 \pm 6$  eV. K-weighting and R-range used for the fit were  $k^1$  and 1.0–2.1  $\text{\AA}$ , respectively.

Path	N	$R_{\text{eff}}$ ( $\text{\AA}$ )	R ( $\text{\AA}$ )	$\sigma^2 \times 10^3$ ( $\text{\AA}^2$ )
Co–O	$3 \pm 2$	1.9014	$1.92 \pm 0.03$	$5 \pm 5$

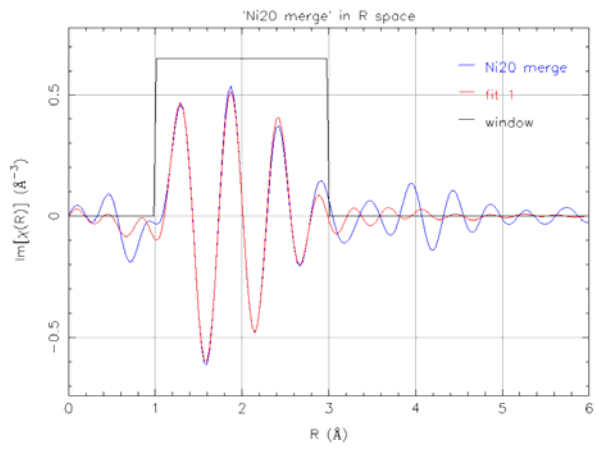
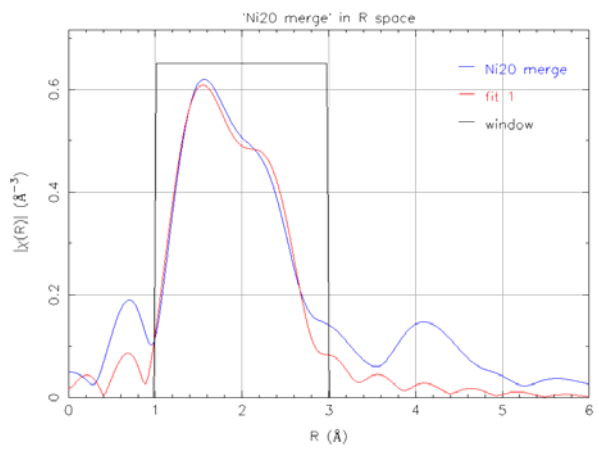
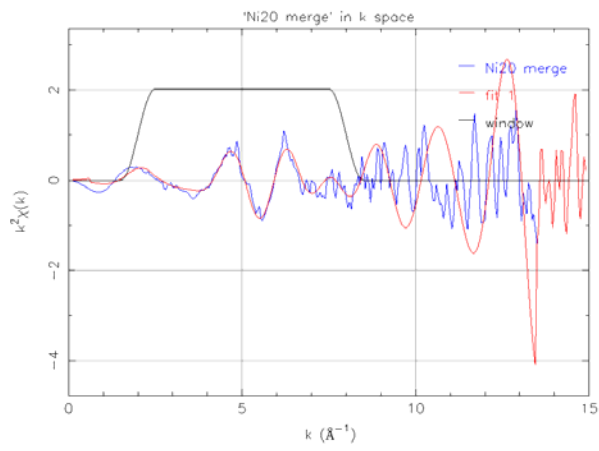


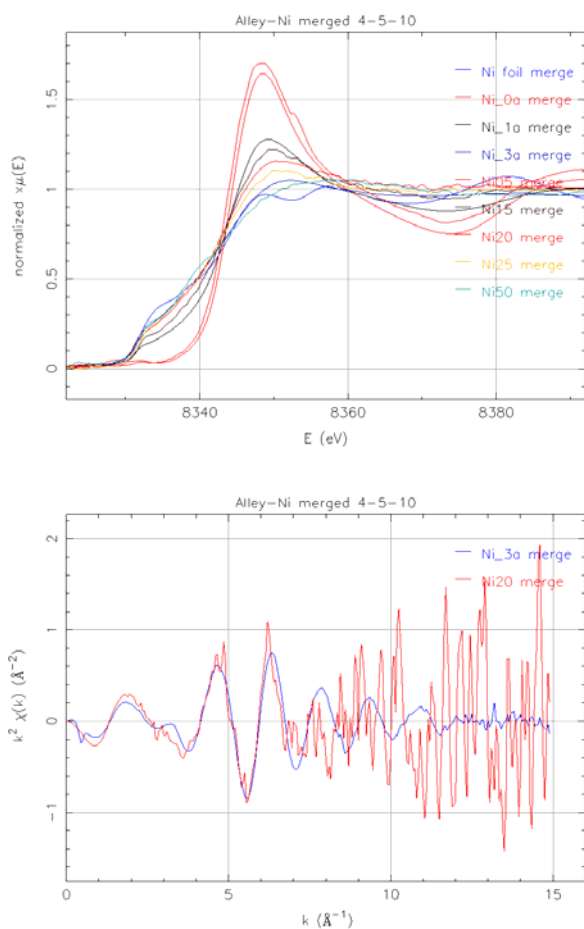


**Figure S29.** Data and fit of the EXAFS spectrum of Co(neodecanoate)<sub>2</sub> plus AlEt<sub>3</sub>, with an Al/Co ratio of 2.0, plotted as (a)  $\chi(k)$ ; (b) the magnitude of the FT; and (c) the imaginary portion of the FT. The  $k$ -range used for FT was 2–10  $\text{\AA}^{-1}$ .

**Table S6.** Fit results for Co(neodecanoate)<sub>2</sub> plus AlEt<sub>3</sub>, with an Al/Co ratio of 2.0.  $\Delta E_0 = -8 \pm 9$  eV.  $K$ -weighting and  $R$ -range used for the fit were  $k^2$  and 1.2–3.0  $\text{\AA}$ , respectively.

Path	N	$R_{\text{eff}}$ ( $\text{\AA}$ )	R ( $\text{\AA}$ )	$\sigma^2 \times 10^3$ ( $\text{\AA}^2$ )
Co–O	$0.3 \pm 0.7$	1.9014	$1.84 \pm 0.05$	$-12 \pm 16$
Co–Co	$2 \pm 1$	2.4982	$2.45 \pm 0.05$	$3 \pm 6$

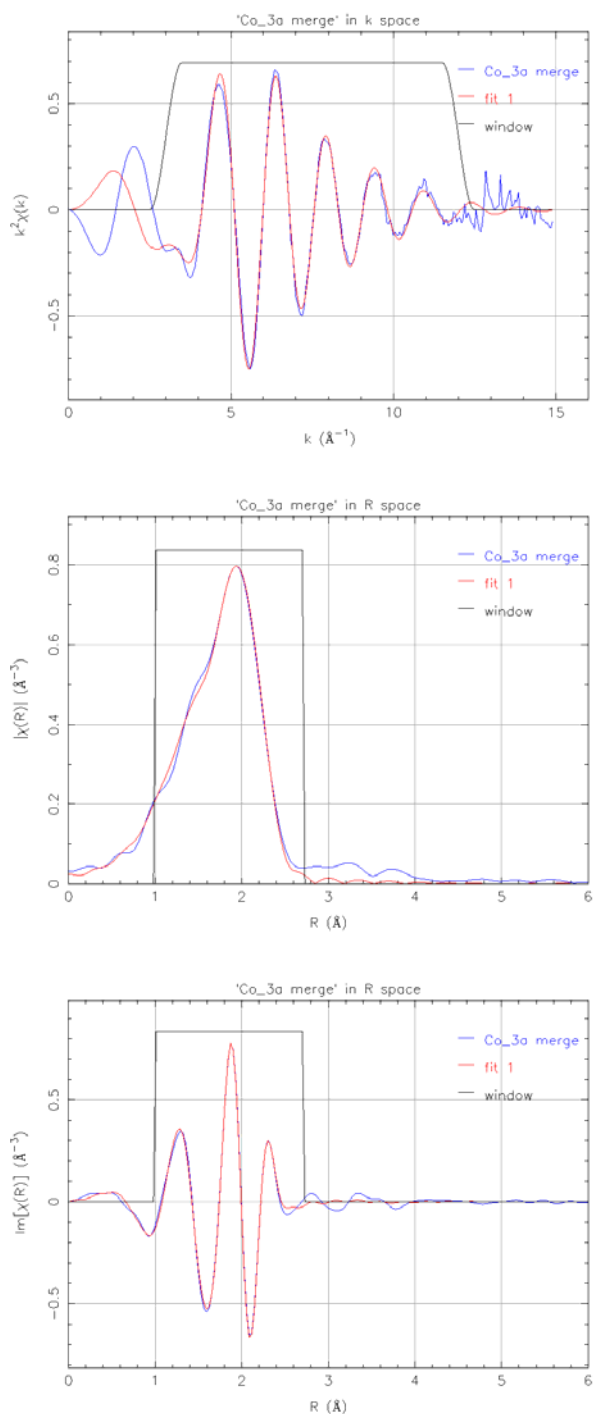




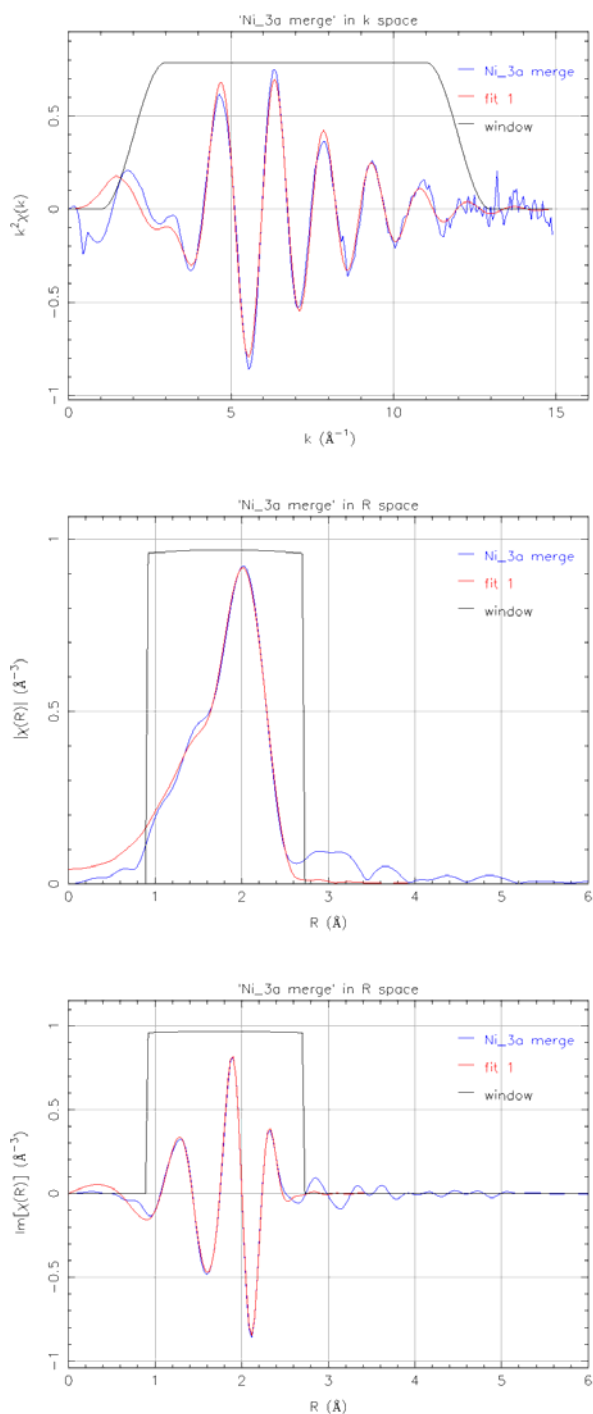
**Figure S30.** Data and fit of the EXAFS spectrum of Ni(2-ethylhexanoate)<sub>2</sub> plus AlEt<sub>3</sub>, with an Al/Ni ratio of 2.0, plotted as (a)  $\chi(k)$ ; (b) the magnitude of the FT; and (c) the imaginary portion of the FT. The k-range used for FT was 2–8 Å<sup>-1</sup>. (d) The XANES spectra of Ni foil, Ni(2-ethylhexanoate)<sub>2</sub>, and Ni(2-ethylhexanoate)<sub>2</sub> plus AlEt<sub>3</sub> catalyst samples with Al/Ni ratios of 0.5, 1.0, 1.5, 2.0, 2.5, 3.0 and 5.0. Aside from the Al/Ni = 0.5 sample, which is very similar to Ni(2-ethylhexanoate)<sub>2</sub>, the catalyst samples show a smooth progression of changes toward Ni foil with increasing Al/Ni ratio. (e) A  $\chi(k)$  plot of the Al/Ni = 2.0 and 3.0 samples shows their close similarity up to  $\sim 7$  Å<sup>-1</sup>, where the data for the Al/Ni = 2.0 sample becomes excessively noisy.

**Table S7.** Fit results for Ni(2-ethylhexanoate)<sub>2</sub> plus AlEt<sub>3</sub>, with an Al/Ni ratio of 2.0.  $\Delta E_0 = -2 \pm 6$  eV. K-weighting and R-range used for the fit were  $k^2$  and 1.0–3.0 Å, respectively

Path	N	R <sub>eff</sub> (Å)	R (Å)	$\sigma^2 \times 10^3$ (Å <sup>2</sup> )
Ni–O	0.5 ± 0.3	2.0494	1.89 ± 0.05	-12 ± 9
Ni–Ni	3 ± 2	2.4890	2.57 ± 0.05	10 ± 11



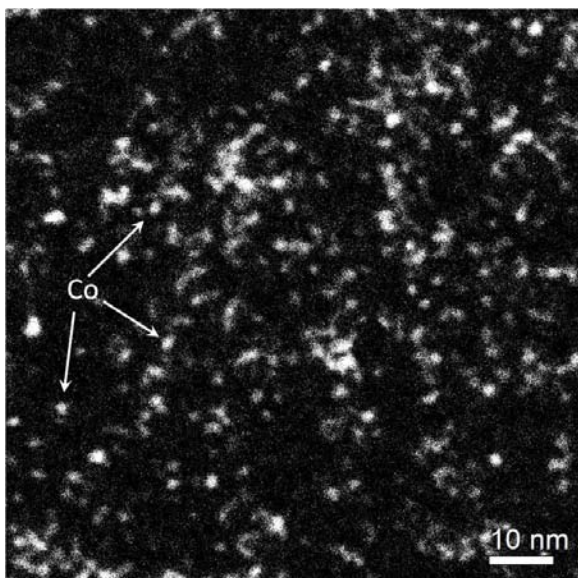
**Figure S31.** Data and fit of the EXAFS spectrum of  $\text{Co}(\text{neodecanoate})_2$  plus  $\text{AlEt}_3$ , with an Al/Co ratio of 3.0, plotted as (a)  $\chi(k)$ ; (b) the magnitude of the FT; and (c) the imaginary portion of the FT. The  $k$ -range used for FT was  $3\text{--}12 \text{\AA}^{-1}$ .  $k$ -weighting and  $R$ -range used for the fit were  $k^2$  and  $1.0\text{--}2.7 \text{\AA}$ , respectively.  $\Delta E_0 = -13 \pm 1 \text{ eV}$ . Results from the fit are tabulated in the main text.

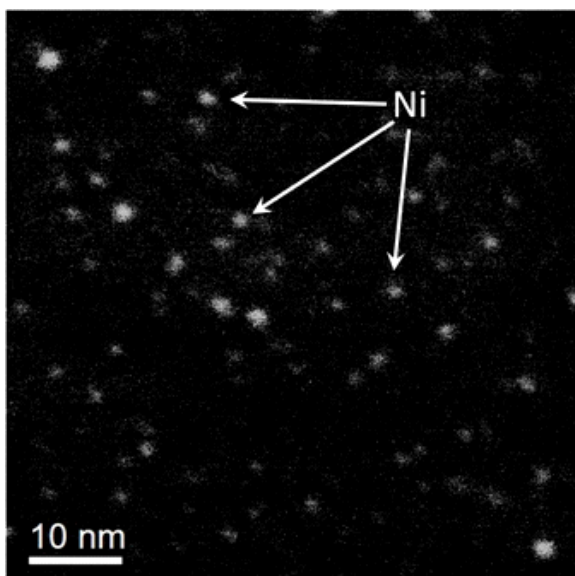


**Figure S32.** Data and fit of the EXAFS spectrum of Ni(2-ethylhexanoate)<sub>2</sub> plus AlEt<sub>3</sub>, with an Al/Ni ratio of 3.0, plotted as (a)  $\chi(k)$ ; (b) the magnitude of the FT; and (c) the imaginary portion of the FT. The k-range used for FT was 2–12  $\text{\AA}^{-1}$ . K-weighting and R-range used for the fit were  $k^2$  and 1.0–2.6  $\text{\AA}$ , respectively.  $\Delta E_0 = -10.8 \pm 0.9$  eV. Results from the fit are tabulated in the main text.

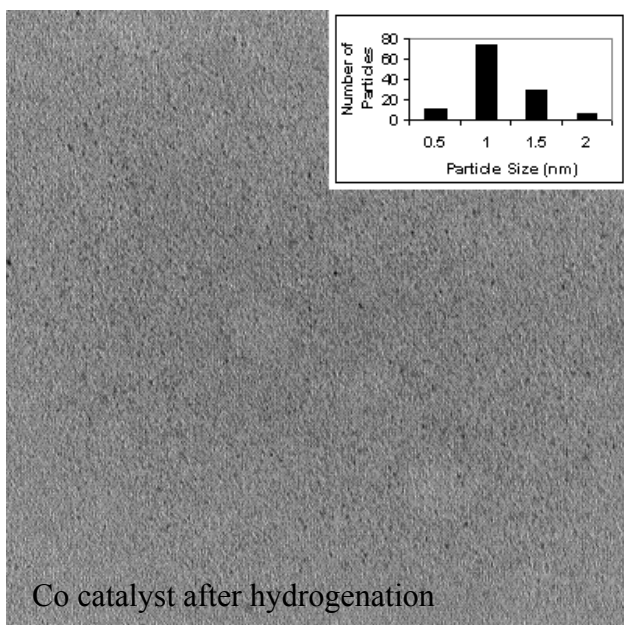
### Nuclearity of $M_n$ Species *after* Hydrogenation: Z-Contrast STEM Bright Field

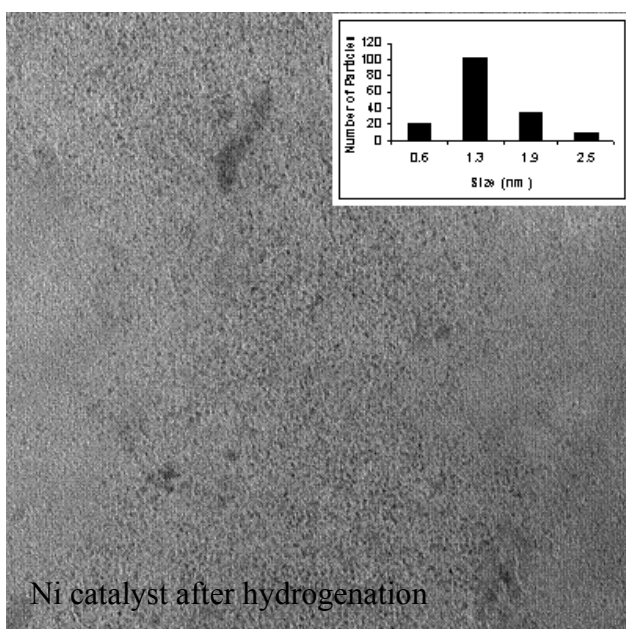
**TEM.** Additional Z-contrast STEM images of the  $\text{Co}(\text{neodecanoate})_2$  or  $\text{Ni}(\text{2-ethylhexanoate})_2$ , plus  $\text{AlEt}_3$  catalyst samples, with an Al/Co ratio of 3 or an Al/Ni ratio of 2, *after* their use for cyclohexene hydrogenation are shown in Figure S33. Additionally, bright field TEM was used to image catalyst samples *after* hydrogenation, Figure S34. Measurement of particles from bright field TEM images gives mean Co and Ni clusters  $1.1 \pm 0.3$ , and  $1.4 \pm 0.5$  nm in diameter, respectively. The results from bright field TEM imaging for the *after* hydrogenation samples are in close agreement with those obtained using Z-contrast STEM.





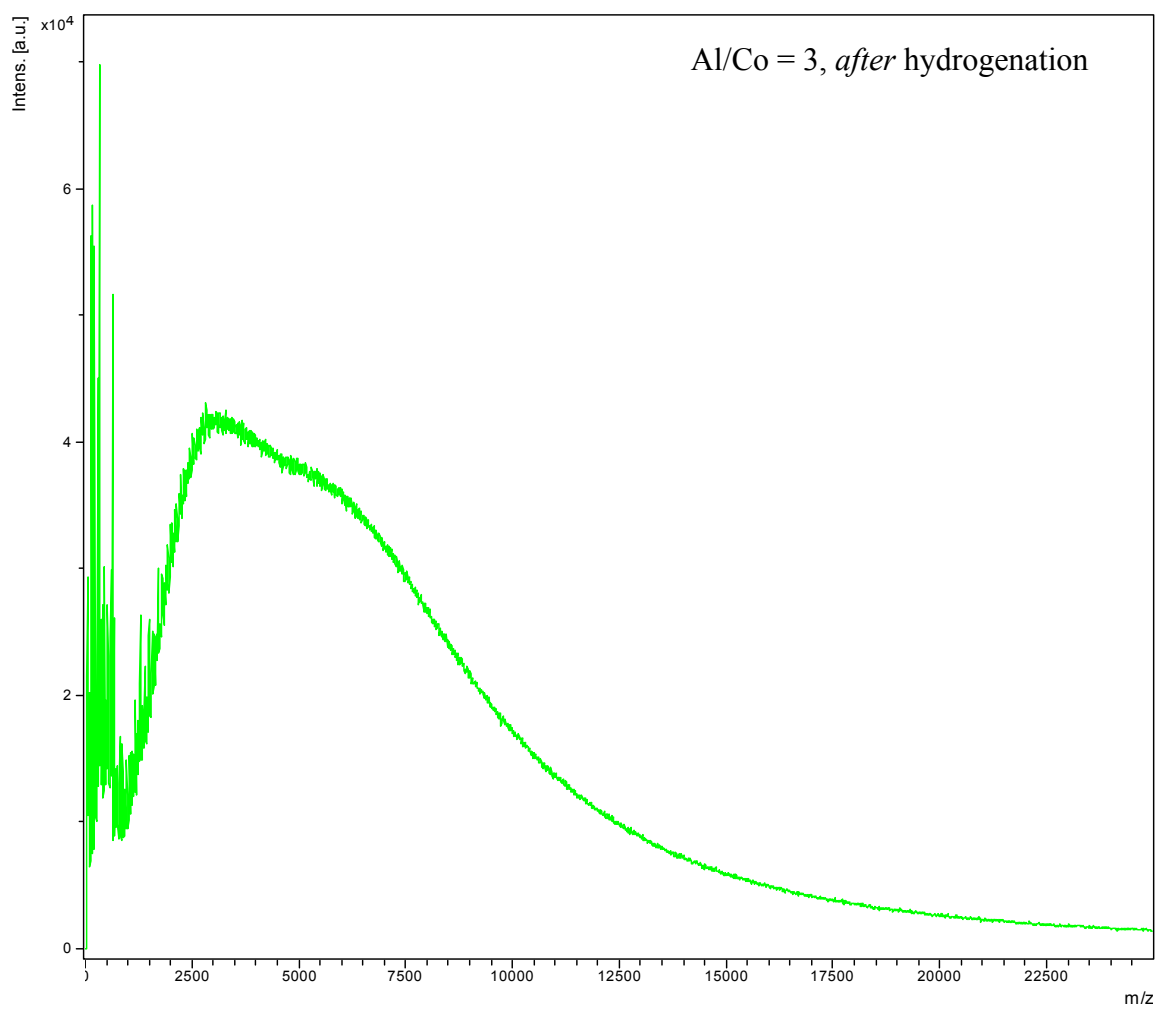
**Figure S33.** Additional example Z-contrast STEM images of catalyst samples made from  $\text{Co}(\text{neodecanoate})_2$  and  $\text{AlEt}_3$  (top), or  $\text{Ni}(\text{2-ethylhexanoate})_2$ , and  $\text{AlEt}_3$  (bottom) *after* their use for catalytic cyclohexene hydrogenation. The histograms shown in the main text include cluster diameter measurements from several images at the same levels of magnification and contrast.



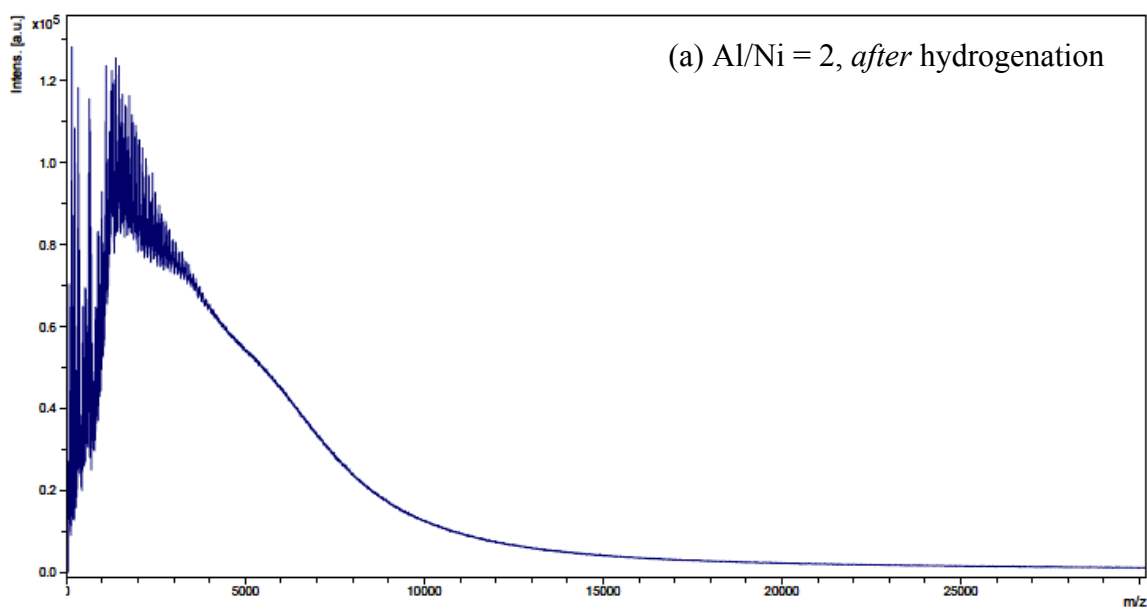


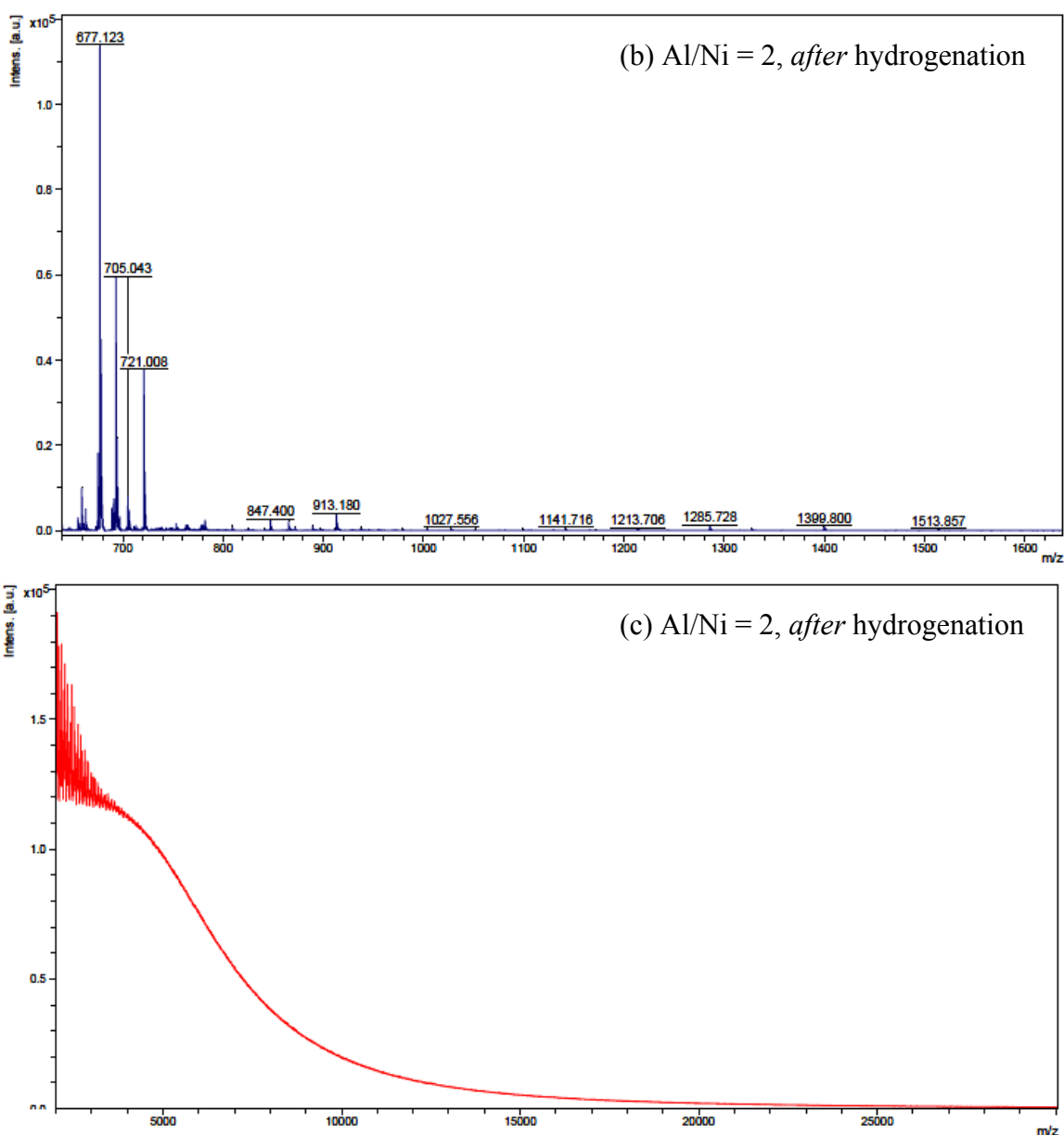
**Figure S34.** TEM and corresponding particle size histogram of the  $\text{Co}(\text{neodecanoate})_2$  plus  $\text{AlEt}_3$  catalyst, with an Al/Co ratio of 3.0, *after* the catalyst was used for cyclohexene hydrogenation (top). The mean diameter calculated by manually counting 119 Co clusters is  $1.1 \pm 0.3$  nm. TEM and corresponding particle size histogram of the  $\text{Ni}(\text{2-ethylhexanoate})_2$  plus  $\text{AlEt}_3$ , with an Al/Ni ratio of 2, catalyst *after* its use in cyclohexene hydrogenation (bottom). The mean diameter of the observed Ni clusters is  $1.4 \pm 0.5$  nm.

**Nuclearity of  $M_n$  Species *after* Hydrogenation: MALDI MS.** The MALDI MS results using catalyst samples made from  $\text{Co}(\text{neodecanoate})_2$  plus  $\text{AlEt}_3$ , with an Al/Co ratio of 3, and from  $\text{Ni}(\text{2-ethylhexanoate})_2$  plus  $\text{AlEt}_3$ , with an Al/Ni ratio of 2, both *after* hydrogenation are shown in Figures S35 and S36, respectively. An example hi-resolution spectrum of the low  $m/z$  region for the Ni catalyst is shown in Figure S36b. Repeat experiments show that the MALDI MS peaks are reproducibly obtained, even when taken from separately prepared catalyst batches. An example repeat MALDI MS of the Ni catalyst is shown in Figure S36c.



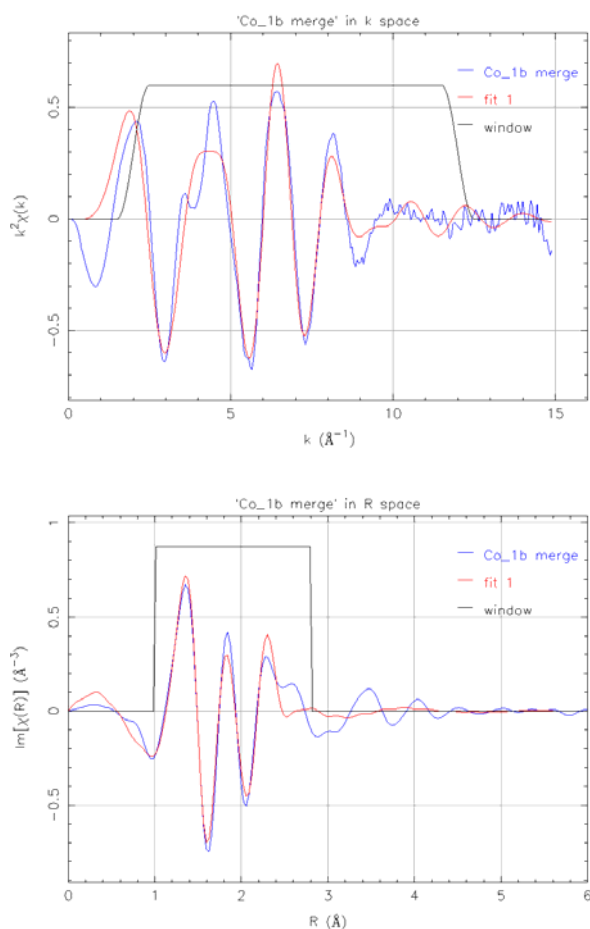
**Figure S35.** MALDI MS of the  $\text{Co}(\text{neodecanoate})_2$  plus  $\text{AlEt}_3$  catalyst, with an Al/Co ratio of 3, *after* its use for cyclohexene hydrogenation.



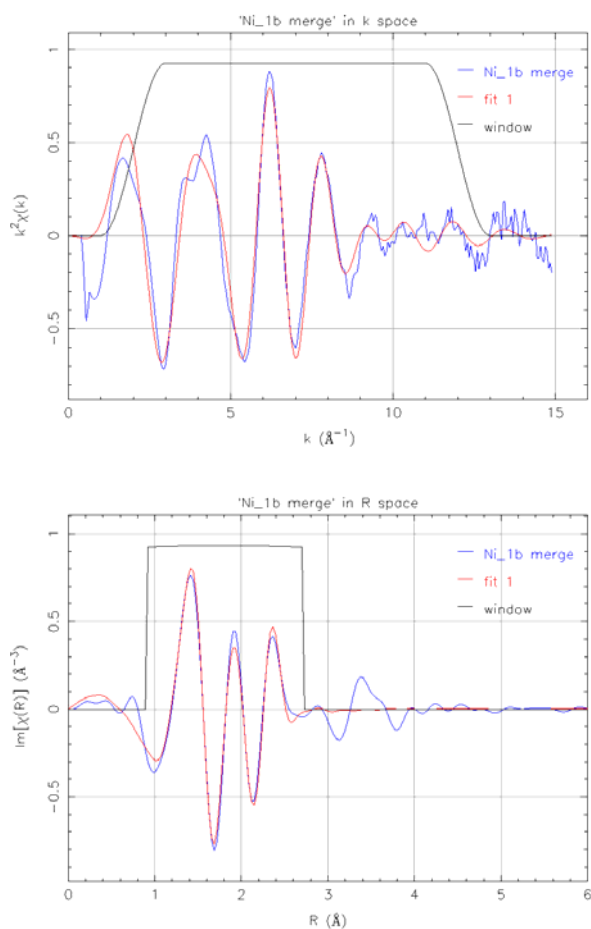


**Figure S36.** (a) MALDI MS of the Ni(2-ethylhexanoate)<sub>2</sub> plus AlEt<sub>3</sub> catalyst, with an Al/Ni ratio of 2, *after* its use in cyclohexene hydrogenation. (b) High resolution MALDI MS of the Ni(2-ethylhexanoate)<sub>2</sub> plus AlEt<sub>3</sub> catalyst sample, with Al/Ni ratio of 2.0, *after* it is used in cyclohexene hydrogenation. Same as with the catalyst samples analyzed before hydrogenation, these observed peaks represent species that do not contain Ni, evidenced by the absence of characteristic Ni isotope peak distributions. Therefore, they can be assigned to either detached stabilizer species, trihydroxyacetophenone (THAP, used as the matrix), or both. (c) An example of a repeat MALDI MS of the Ni(2-ethylhexanoate)<sub>2</sub> plus AlEt<sub>3</sub> catalyst, with an Al/Ni ratio of 2, *after* it is used in cyclohexene hydrogenation. Despite being shown here on a different scale, the peak is consistent with others of the same sample, demonstrating that the MALDI MS observations are reproducible for these catalyst samples when performed under exactly the same conditions.

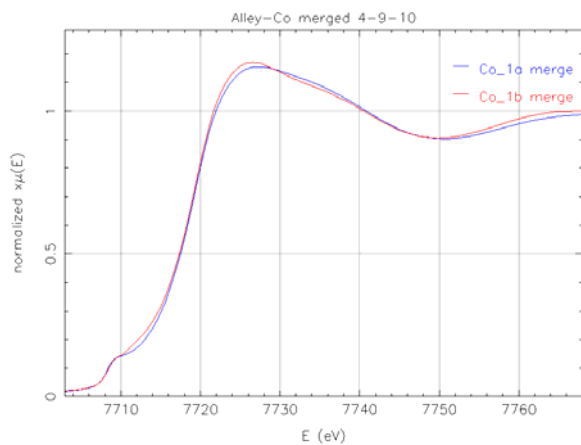
**Nuclearity of  $M_n$  Species *after* Hydrogenation: EXAFS.** Samples of  $\text{Co}(\text{neodecanoate})_2$  or  $\text{Ni}(\text{2-ethylhexanoate})_2$ , plus  $\text{AlEt}_3$  catalyst *solutions*,  $\text{Al}/\text{M} = 1.0$ , *after* hydrogenation were analyzed by EXAFS spectroscopy. The EXAFS spectra, with fits, plotted as  $\chi(k)$  and as the imaginary portion of the FT are shown here in Figures S37 and S38. The XANES spectra of the Co and Ni catalysts *after* hydrogenation are shown alongside their prehydrogenation counterparts, Figure S39; each shows that the hydrogenation process has a negligible effect on the transition-metal catalyst material.



**Figure S37.** Data and fit of the EXAFS spectrum  $\text{Co}(\text{neodecanoate})_2$  plus  $\text{AlEt}_3$ , with an  $\text{Al}/\text{Co}$  ratio of 1.0, and after hydrogenation, plotted as (a)  $\chi(k)$ ; and (b) as the imaginary portion of the FT. The magnitude of the FT and fitting results are shown in the main text. The  $k$ -range used for FT was  $2\text{--}12 \text{\AA}^{-1}$ .  $k$ -weighting and  $R$ -range used for the fit were  $k^2$  and  $1.0\text{--}2.8 \text{\AA}$ , respectively.  $\Delta E_0 = -0.3 \pm 3 \text{ eV}$ .



**Figure S38.** Data and fit of the EXAFS spectrum  $\text{Ni}(\text{2-ethylhexanoate})_2$  plus  $\text{AlEt}_3$ , with an Al/Ni ratio of 1.0, and after hydrogenation, plotted as (a)  $\chi(k)$ ; and (b) as the imaginary portion of the FT. The magnitude of the FT and fitting results are shown in the main text. The k-range used for FT was 2–12  $\text{\AA}^{-1}$ . K-weighting and R-range used for the fit were  $k^2$  and 1.0–2.6  $\text{\AA}$ , respectively.  $\Delta E_0 = -2 \pm 1$  eV.



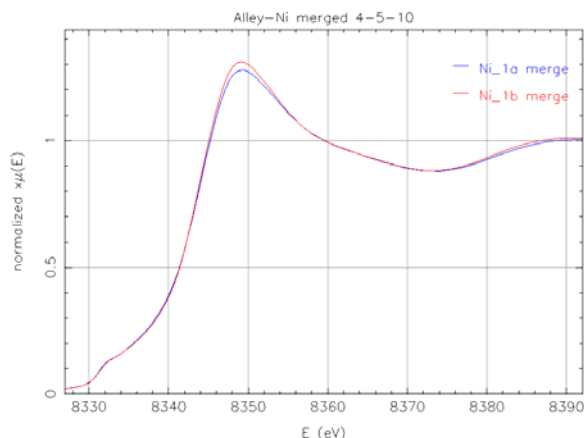


**Figure S39.** Posthydrogenation XANES spectra of the Co (top) and Ni (bottom) catalysts are shown alongside the corresponding prehydrogenation XANES spectra. The similarity in each case supports the other evidence showing that use of the catalyst solutions for cyclohexene hydrogenation has a negligible effect on the transition metal catalyst material.

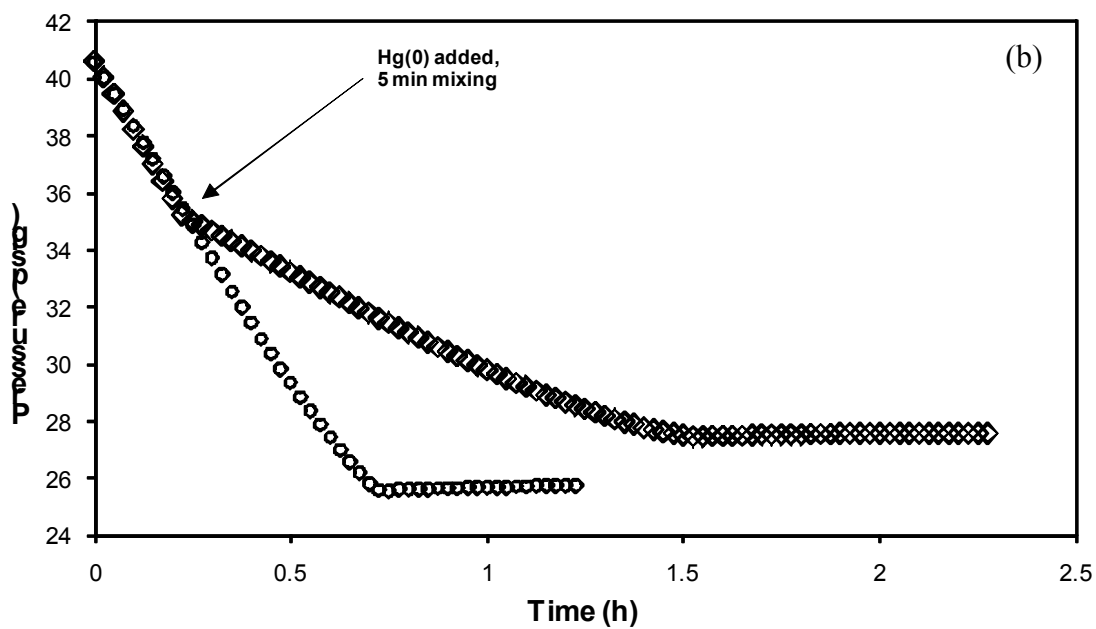
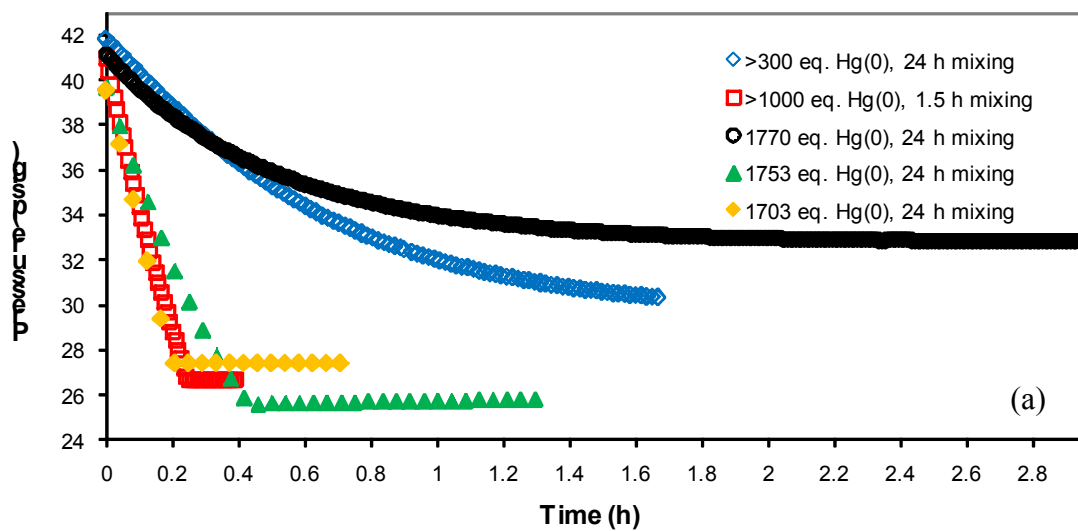
### Hg(0) Poisoning Experiments

Control experiments showing the effects of aging the Co and Ni catalysts for 24 h before use, Fig S3, also show that the observed initial catalyst poisoning by Hg(0) is not due to the mixing time involved in carrying out the Hg(0) poisoning experiment. This is also true for poisoning of the Ni catalyst, which required only 1.5 h of mixing time with Hg(0), as opposed to the 24 h shown in Fig S3.

For the Co catalyst, additional control experiments show that the poisoning of catalysis, depending on the amount of Hg(0) used and the time allowed for mixing, Figure S40a, is ultimately irreproducible. These results make the Hg(0) poisoning experiments with the Co catalyst system unreliable.

For the Ni catalyst, a control experiment shows that  $\geq 1.5$  hours of mixing (with 1000 rpm stirring in the sealed FP bottle) was necessary and sufficient to thoroughly contact the  $\geq 300$  Hg(0) with all of the Ni(2-ethylhexanoate)<sub>2</sub> plus AlEt<sub>3</sub> catalyst, with an Al/Ni ratio of 2.0, in solution, Figure S40b. In addition, a control experiment also shows that the procedure used to halt catalysis after about half the cyclohexene had been consumed and add Hg(0) at that stage

does not account for the observed poisoning Figure S40c. In all cases the catalyst solutions retain substantial catalytic activity when subjected to the handling procedures required for Hg(0) addition, which demonstrates that it is the addition of Hg(0), and not just the experimental procedures employed, that poison the catalyst.



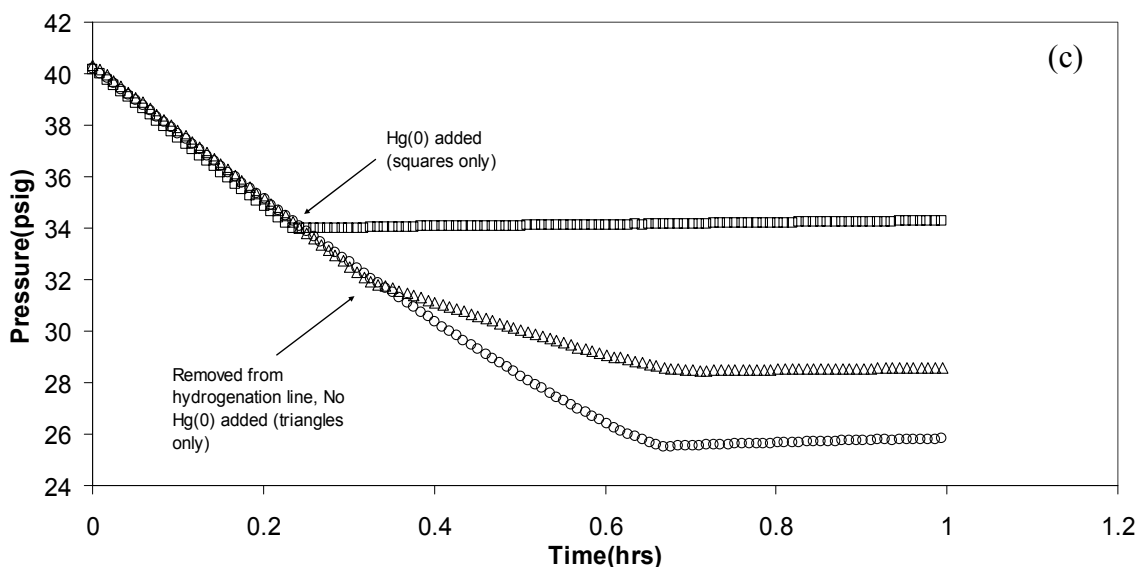


**Figure S40.** The results of Hg(0) poisoning control experiments are shown here using the Co(neodecanoate)<sub>2</sub> or Ni(2-ethylhexanoate)<sub>2</sub>, plus AlEt<sub>3</sub> catalysts, with an Al/Co ratio of 3.0 and an Al/Ni ratio of 2.0. (a) Control experiments using the Co catalyst show that the amount of poisoning depending on both on the quantity of Hg(0) used (in equivalents per Co) and on the mixing time with the catalyst solution, is ultimately irreproducible. (b) An example control hydrogenation is shown where  $\geq 300$  equivalents of Hg(0) per Ni were added after about half the cyclohexene had been consumed (diamonds) next to a standard conditions hydrogenation run for comparison (circles). The Hg(0) was stirred vigorously ( $1000 \pm 200$  rpm) with the catalyst solution for 5 min before putting the catalyst solution back under an atmosphere of pressurized H<sub>2</sub>. The H<sub>2</sub> uptake rate has been slowed, but not completely poisoned, implying that 5 min is not sufficient time to allow the Hg(0) to contact/react with the Ni catalyst in solution. (c) A control experiment is shown whereby a Ni catalyst solution is handled *as if* Hg(0) was being added after about half the cyclohexene had been consumed (i.e., the solution was removed from the pressurized H<sub>2</sub> line, transported into the drybox, opened, resealed, and stirred at  $1000 \pm 200$  rpm for 1.5 h before reconnecting with the pressurized H<sub>2</sub> line and resuming data acquisition). This run (triangles) is shown next to a standard hydrogenation run (circles) and a catalyst solution handled identically, but with  $\geq 300$  equivalents of Hg(0) per Ni *actually* added (squares). The H<sub>2</sub> uptake of the control run (triangles) is slowed somewhat by the procedure, but does not display the immediate and total poisoning exhibited by the run where Hg(0) was actually added (squares). This result demonstrates that the Hg(0), and not the procedure itself, accounts for total poisoning of catalysis.

## Reference 18d

The full reference for ref 18d in the main text is: Angermund, K.; Bühl, M.; Endruschat, U.; Mauschick, F. T.; Mörtel, R.; Mynott, R.; Tesche, B.; Waldöfner, N.; Bönemann, H.; Köhl, G.; Modrow, H.; Hormes, J.; Dinjus, E.; Gassner, F.; Haubold, H.-G.; Vad, T.; Kaupp, M. *J.*

*Phys. Chem. B* **2003**, *107*, 7507–7515.

## References

---

- <sup>1</sup> Aiken, J. D., III; Finke, R. G. *J. Am. Chem. Soc.* **1998**, *120*, 9545–9554.
- <sup>2</sup> Alley, W. M.; Hamdemir, I. K.; Johnson, K. A.; Finke, R. G. *J. Mol. Catal. A: Chem.* **2010**, *315*, 1–27.
- <sup>3</sup> Alley, W. M.; Girard, C. W.; Özkar, S.; Finke, R. G. *Inorg. Chem.* **2009**, *48*, 1114–1121.
- <sup>4</sup> Alley, W. M.; Hamdemir, I. K.; Wang, Q.; Frenkel, A.; Li, L.; Yang, J. C.; Menard, L. D.; Nuzzo, R. G.; Özkar, S.; Johnson, K.; Finke, R. G. *Inorg. Chem.* **2010**, in press.
- <sup>5</sup> Buzzeo, M. C.; Iqbal, A. H.; Long, C. M.; Millar, D.; Patel, S.; Pellow, M.; Saddoughi, S. A.; Smenton, A. L.; Turner, J. F.; Wadhawan, J. D.; Compton, R. G.; Golen, J. A.; Rheingold, A. L.; Doerrer, L. H. *Inorg. Chem.* **2004**, *43*, 7709–7725.
- <sup>6</sup> Downie, T. C.; Harrison, W.; Raper, E. S.; Hepworth, M. A. *Acta Cryst.* **1971**, *B27*, 706.

## CHAPTER VI

### SUMMARY

This dissertation has focused on a fundamental study of industrially relevant Ziegler–type hydrogenation catalysts. A critical review of the related literature discussed what was already known—and unknown—about Ziegler–type hydrogenation catalysts concerning the variables their synthesis, and whether the catalytically active species were believed to be truly homogenous versus heterogeneous in nature. Since one of the important insights from the literature review is that answering the five-decades-old homogenous or heterogeneous catalysis question for these industrial catalysts could be aided through the use of a well characterized, third-row transition metal precatalyst. Hence, the synthesis and unequivocal characterization of such a precatalyst was described in Chapter III. Then, in Chapter IV, that Ir precatalyst was shown, upon addition of  $\text{AlEt}_3$ , to initially make active Ziegler–type hydrogenation catalyst solutions containing a range of  $\text{Ir}_n$  species, from which crystalline  $\text{Ir}(0)_{-40-150}$  “Ziegler nanoclusters” develop as the most active catalysts under working conditions, and according to kinetic studies. Last, the homogeneous versus heterogeneous nature of industrial Co- or Ni-based

Ziegler-type hydrogenation catalysts was investigated, using an approach similar to that used with the Ir system, and with the results from the model Ir system available for comparison. The results indicated that Co and Ni industrial catalysts are probably heterogeneous ( $M_{\geq 4}$ ) based on the combination of data from multiple physical methods plus Hg(0) poisoning studies.

An additional manuscript draft has been prepared by William M. Alley describing an interesting inverse [Ir]-TOF relationship obtained from kinetics studies of the Ir model system formed by [1,5-COD)Ir( $\mu$ -O<sub>2</sub>C<sub>8</sub>H<sub>15</sub>)]<sub>2</sub> plus AlEt<sub>3</sub>. It has not been included in this dissertation, but is a promising avenue for future study in the area of Ziegler-type hydrogenation catalysts. In addition, work related to the results described herein is currently in various stages of completion as part of Isil K. Hamdemir's PhD dissertation. There are also several other potential avenues for additional research stemming directly from the results described herein. They include: (i) investigating the details of Ziegler nanocluster/ catalyst formation using Ir, Pt, or both systems; (ii) study of the "aging" process, especially in the Co and Ni catalyst systems—does aging give larger clusters? If so, then one has achieved an important result indicating that the smaller,  $M_{\sim 4}$  say, (sub)nanometer clusters or hydrides,  $M_4H_4$  for example, are the better catalysts. Also, (iii) similar studies of the model Rh precatalyst could be of interest, as well as (iv) operando spectroscopy studies (i.e., under operating conditions) of the Ir, Rh, Co, and Ni catalysts, (v) obtaining the full rate law for these systems, and (vi) studies to understand better the origins of the enhanced, apparently AlR<sub>3</sub>-based, novel stabilization and high stability of these catalysts—including why Ir–Al, but no Co– or Ni–Al, peaks are seen in the respective catalysts by EXAFS.

## APPENDIX A

### GENERAL STATEMENT ON “JOURNALS-FORMAT” THESES

(Written by Professor Richard G. Finke)

The Graduate School at Colorado State University allows, and the Finke Group in particular encourages, so-called journals-format theses. Journals-format theses, such as the present one, consist of a student written and ideally lightly edited literature background section, chapters corresponding (in the limiting, ideal case) to final-form papers either accepted or at least submitted for publication, a summary or conclusions chapter, and short bridge or transition sections between the chapters as needed to make the thesis cohesive and understandable to the reader. The “bridge” sections and summary are crucial so that the thesis fulfills the requirement that the thesis be an entity (an official requirement of most Graduate Schools). All chapters (manuscripts) in a journals-format thesis must of course be written initially by the student, with subsequent (ideally light) editing by the Professor, the student’s committee, and even the student’s colleagues where appropriate and productive.

The advantages for doing a journals-format thesis are several-fold and compelling. Specifically, some of the major advantages are: the level of science (i.e., of refereed, accepted publications) is at the highest level; the student and Professor must

interact closely and vigorously (i.e., to bring both the science and the writing to their highest level), hence the student is getting the best education possible and is being at least exposed to (if not held to) the highest standards; the needed clean-up or control experiments that invariably come up have all been identified and completed before the student leaves; there are no further time demands once the student has left the University (since all publications are at least submitted; it is terribly inefficient to try to complete either writing or often specialized experiments once the student has left); and the American tax payers, who ultimately pay the bill for the research, are getting their money's worth since all the research is published and thus widely disseminated in the highest form, as refereed science. Professorial experience teaches that a student who has achieved a journals-format thesis has indeed received a better education and has learned critical thinking and clear writing skills that will serve them well for a lifetime.

Experience also teaches, however, that much more than light editing is often needed in at least some student theses; it follows, then, that considerable professorial writing and editing might be needed for at least the initial chapters of most journals-format theses. Indeed, a journals-format thesis is not recommended (and may not even be possible) for less strong students. Hence, the issue arises of exactly how much of the science and the writing, in the final (or submittable) chapters, is due to the student vs. the Professor and whether or not this level of contribution constitutes that acceptable of a new Ph.D. and independent investigator.

To deal with this issue, several recommendations are made; the recommendations below have been discussed with the committee signing William M Alley's dissertation. (Mr. Alley's dissertation is the seventeenth such thesis from the Finke group following

Dr. C. Garr's, Dr. Y. Lin's, Dr. M. Pohl's, Dr. J. Sirovatka's, Dr. J. Aiken's, Dr. R. Suto's, Dr. J. Widegren's, Dr. K. Doll's, Dr. C.-X. Yin's, Dr. L. Ott's, Dr. A. Morris', and Dr. E. Finney's dissertations, and Ms. K. Weddle's, Mr. W. White's, Mr. C. Hagen's, and Mr. C. Graham's Masters theses.)

## Recommendations

The recommendations are:

(i) That the present pages be enclosed in the thesis until such a time as it is no longer needed (i.e., when the policies and procedures for journals-format theses become routine);

(ii) That for each chapter it is detailed, and to the satisfaction of the committee and the advisor, who made what contributions, both of intellectual substance and writing. [Substantial contributions of other students or Professors should of course be acknowledged. In the case of disagreements, the various drafts (i.e., as their electronic files) can be examined by the committee (in light of a knowledge of who wrote which draft) to easily determine who contributed what. In possible borderline or controversial cases it may even be advisable to keep all (electronic) drafts of the papers as a record];

(iii) That it be specifically stated whether or not all the experimental work is the Ph.D. candidate's [as is usually the case, although the increasing (desirable) collaboration among scientists worldwide makes this a non-trivial point].

(iv) Furthermore, it is recommended that allowances be made for the expectation that a greater degree of involvement of the professorial advisor is likely in a journals-format thesis than in a traditional thesis. [That this is reasonable follows from the fact

that some Professors write 100% of all their papers; this, unfortunately, robs the student of the valuable experience of participating in the science and the end product as practiced at the highest levels. (It also creates an unmanageable writing burden for Professors involved in all but the narrowest of research areas or for Professors involved in more than one competitive research area)];

(v) Notwithstanding (iv), there needs to be ideally no more than ca. 40% Professorial writing contribution in a given *early* chapter in the thesis, and there should be a clear evolution in the thesis of a decreasing professorial involvement to, say, a 10-20% direct contribution in the last chapter or two.

(vi) As a further aid towards separating out the candidate's and the professorial (and other) contributions, it is recommended that the Introductory (usually literature background) chapter(s) and at least the final chapter be lightly edited only, so that authentic examples of the student's contributions are documented in an unambiguous form.

(vii) In order to avoid the loss of useful, but unpublished/unpublishable, experimental work by the student writing a journals-format thesis, the Finke Group requires the following: (1) carefully kept laboratory notebooks; (2) mandatory research reports detailing the results of any unpublished work; and (3) the extensive use of Supporting Information and textual footnotes, where appropriate, in all published work.

## APPENDIX B

### RESEARCH PROPOSAL

#### **Synthesis and Use of Chiral Metallocyclic Supramolecular Systems as Enantioselective Molecular Sensors in Differential Sensing Arrays**

##### **Abstract/ Specific Aims**

Molecular recognition using chemical sensors is a rapidly growing field with the potential for application in a variety of areas such as the analysis of important bioanalytes for medical purposes, cellular imaging, environmental analysis of toxic heavy metals or pesticides, chemical and biological warfare agent detection, and quality control in manufacturing. Several of these important functions of chemical sensing technology involve chiral analytes, and could therefore benefit significantly from improvements in the abilities of enantioselective sensors. Chiral metallocyclic supramolecular systems (MSSs), which are macrocycles, often metallocyclophanes, and typically form via self-assembly from transition metal coordination compounds and linking ligands, are an interesting class of compounds with considerable potential for use as enantioselective

sensors. However, the relatively small amount of research conducted so far into use of chiral MSSs as enantioselective sensors has yet to produce many examples of real utility. An untried approach to enantioselective molecular recognition using chiral MSSs as sensors might be needed. Testing the enantioselective sensing ability of chiral MSSs in differential sensing arrays has never been attempted, and may be the fresh approach needed to advance this field.

Recently, great strides in molecular recognition have been made using differential sensing arrays (DSAs). These arrays of cross-reactive sensors give a composite response, or “fingerprint,” for an analyte. This method possesses several advantages, among them are that the number of analytes that can be identified is greater than the number of individual sensors needed in the array, complex mixtures can be analyzed, and the difficulties involved in the targeted synthesis of highly selective sensors can be avoided. Interestingly this is the chemosensory approach taken by the mammalian senses of smell and taste. However, very few studies so far have applied this approach to enantioselective sensing applications. Enantioselective DSAs (E-DSAs) could be improved by the availability of a wider variety of chemical sensors. Using metallocyclic supramolecular systems in enantioselective differential sensing arrays is one novel approach to expanding the range of useful array-based sensors. The hypothesis to be tested herein is that chiral metallocyclic supramolecular systems will be useful sensors in enantioselective differential sensing arrays.

The initial test of this hypothesis will be to synthesize two chiral MSSs that have a demonstrated ability to discriminate between enantiomers of analytes, and use them in an E-DSA. That E-DSA will also include other non-MSS sensors previously used in E-

DSAs that were able to differentiate between enantiomers in samples of chiral amino acids. The results will be analyzed using principle component analysis (PCA), which should show whether or not the incorporation of the MSS sensors into the array has added to the discriminatory ability of the array. The full test of the hypothesis will involve the eventual synthesis and analysis of other chiral MSSs.

### **Background and Significance**

*Supramolecular Chemical Sensors and Applications.* Research in the field of molecular recognition using chemical sensors has experienced significant growth, particularly over the last several decades.<sup>1,2,3</sup> Precise definition of the term “chemical sensor” is somewhat open to debate, but is used herein to describe a compound that acts as a “receptor” for an analyte and gives a measureable signal (e.g., colorimetric, fluorescent, etc.) in response.<sup>1,2,3</sup> Many of the different chemical sensors developed have been supramolecular systems.<sup>2</sup> It is generally accepted that supramolecular chemistry is focused on the creation and study of multi-molecular assemblies using intermolecular forces (i.e., ion-dipole, van der Waals, solvophobicity, etc.).<sup>4</sup> However, in part because most supramolecular chemistry is aimed at synthetic receptors,<sup>5</sup> a more inclusive, sensor-based definition of the term “supramolecular” seems justified.<sup>2,6,7</sup>

Synthetic compounds for use as sensing materials have since been sought for analytical purposes in a broad variety of fields. The appetite for synthetic chemical sensing materials has therefore grown considerably, and is “driven by the ever-expanding monitoring needs” of their widening applicability.<sup>3</sup> Chemists have sought to satiate that appetite by developing chemical sensors based on a variety of approaches.<sup>2,3,8</sup> Organic

species are frequently used,<sup>9,10,11,12,13,14,15,7,16</sup> as are sensors explicitly based on biological systems.<sup>17,18,19</sup> Sensing strategies using metalloporphyrins,<sup>20</sup> or enzymes<sup>21,22</sup> are just two examples. Molecularly imprinted polymers,<sup>23</sup> and composites of conductive polymers, often incorporating a variety of metallic or metal-containing components,<sup>24</sup> are two examples of polymer-based sensor materials. Recent examples from the literature of inorganic sensor materials include photoluminescent CdSe semiconductor nanocrystals,<sup>25</sup> certain Zn,<sup>26</sup> or Cu complexes<sup>27,28</sup> and the organometallic compound [Cp\*RhCl<sub>2</sub>]<sub>2</sub>.<sup>29</sup>

Compounds with potential for increased use as chemical sensors, and the particular focus of this proposal, are the transition metal-based metallocyclic supramolecular systems (MSSs).<sup>1,,30,31</sup> The term MSS is used herein to describe a macrocycle, often a metallocyclophane, typically formed via self-assembly from transition metal coordination compounds and linking ligands, and that has potential toward chemical sensing capabilities. Early examples of MSSs are the luminescent “molecular squares” with Re corners, Figure 1.<sup>32</sup> A wide variety of MSSs exists, and several have shown promise as receptors for a similarly wide variety of potential analytes.<sup>1</sup> More specifically, chiral MSSs for use as enantioselective sensors are at the heart of the current proposal.<sup>33</sup>

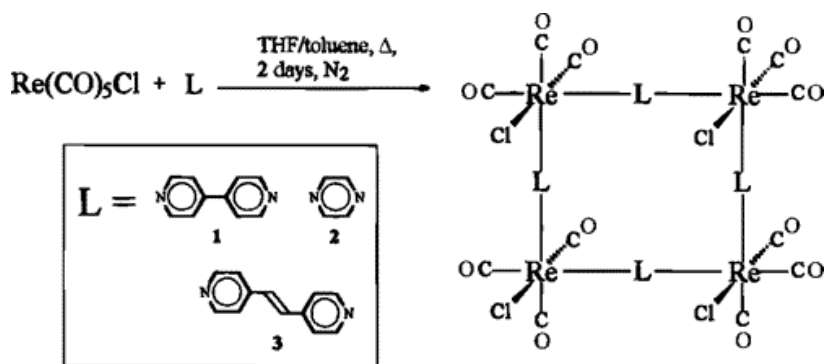


**Figure 1.** Luminescent “molecular squares” with rhenium corners. Reproduced with permission from Slone et al. *Inorg. Chem.* **1996**, *35*, 4096-4097. Copyright 1996 American Chemical Society.

*Enantioselective Sensors.* The “ever-expanding”<sup>3</sup> analysis applications for chemical sensors include molecular recognition problems in the fields of environmental contaminants, food processing,<sup>34,35</sup> and medicine. Indeed, “the future of using synthetic receptors as sensors is in the interrogation of complex mixtures of bioanalytes (blood, urine, saliva), cellular imaging, environmental analytes (streams, industrial wastes), and quality control (manufacturing, process).”<sup>2</sup> The sheer variety of analytes of interest in these fields is huge.<sup>9,36,37,38,39</sup> Chemical sensors are particularly desired for the wide variety of analytes of biological interest.<sup>40</sup> Interesting bioanalytes include metal ions,<sup>40</sup> glucose,<sup>22</sup> drugs,<sup>7</sup> amino acids,<sup>13,26-29,41</sup> nucleic acids, complex carbohydrates, and proteins.<sup>19</sup> Chirality is a feature of critical importance in many analytes of biological interest including drugs and biomolecules themselves.

For biological systems and their interactions, the importance of chirality cannot be overstated. A classic example of what is at stake is the case of (*N*-phthalidomido)-glutarimide (thalidomide). The (*R*) enantiomer is at least of negligible toxicity, but the drug was marketed as the racemic mixture and prescribed to pregnant women despite the fact that the (*S*) enantiomer is a potent teratogen.<sup>42</sup> Based on the knowledge that different stereoisomers of pharmaceutical compounds “may have different pharmacokinetic properties,” and result in “quantitatively or qualitatively different pharmacologic or toxicologic effects,” the United States Food and Drug Administration made mandatory via a 1992 policy statement the study of individual stereoisomers.<sup>43</sup> The impetus for developing methods for the production and detection of optically pure compounds should

therefore be obvious. Yet despite the involvement of the lucrative pharmaceutical industry, asymmetric syntheses are still often “laborious and limited,”<sup>7</sup> and the most successful separation approaches (HPLC, GC, and capillary electrophoresis) are “usually time consuming and rather expensive,”<sup>7</sup> or at least “do not lend themselves to rapid analysis”<sup>13</sup> as desired in commonly high-scale or high-throughput industrial processes. The development of enantioselective chemical sensors, then, is highly desired, and one of their most immediate practical applications may be in the high-throughput analysis of the products of potential pharmaceutical-producing reactions and syntheses, catalytic and otherwise.

Surprisingly, relatively few studies in molecular recognition and sensing have focused specifically on chiral differentiation. Studies of enantioselective molecular recognition include the pioneering work, of Kubo and coworkers who used calixarene-based sensors for the visual enantiomeric distinction between chiral amines and amino acids.<sup>44</sup> Recent advancements in enantioselective molecular recognition include, among others,<sup>10,11,13,14</sup> chiral dendroclefts for the enantio- and diastereoselective sensing of monosaccharides,<sup>15</sup> a chiral Cu<sup>II</sup> complex for sensing and enantiomeric excess (ee) determination of amino acids,<sup>27</sup> and cyclodextrin derivatives for the enantioselective sensing of a variety of potential analytes.<sup>7</sup> Other systems currently being explored for enantioselective molecular recognition are chiral MSSs.<sup>1,33</sup>

Multiple studies report the synthesis of chiral MSSs that are of interest as potential enantioselective chemical sensors.<sup>45,46</sup> The general strategies<sup>1,33</sup> used for the design and synthesis of chiral MSSs involve the use of auxiliary (i.e., non-bridging) chiral ligands,<sup>47,48</sup> metal complexes that are inherently chiral due to their coordination

arrangements,<sup>49,50</sup> chiral bridging ligands,<sup>51,52</sup> or some combination thereof. Some of the reasons to specifically pursue chiral MSSs as sensors for the enantioselective recognition of chiral substrates are the remarkably large variety of metallocycles available via self assembly into predictable systematic structures,<sup>30</sup> their ability to be readily modified or functionalized,<sup>1</sup> their ability to form meso- and nano-porous thin films,<sup>53,54</sup> and their capacity for ancillary properties such as luminescence.<sup>1,33,55</sup> The “introduction of chromogenic or luminescent properties is especially interesting” in MSSs,<sup>1</sup> in part because some have claimed that, at least in luminescent sensors, the signal transduction aspect of the sensing process is of primary importance.<sup>9</sup> Thus, “while organic reagents are widely employed in existing optical sensors, such reagents often suffer from their intrinsic limitations such as rapid photobleaching and short shelf life.”<sup>25</sup> This is in contrast to MSSs, which tend to give robust, air-stable structures.<sup>30</sup>

Despite the numerous studies investigating the synthesis and photophysical properties of chiral MSSs,<sup>1,33</sup> very little work has been reported on their enantioselective molecular recognition properties. An early study in this area by Stang and coworkers sought to increase understanding of the function of chiral elements in supramolecular structures by investigating their host-guest chemistry.<sup>56</sup> This study provides an important foundation, but did not address the ability of the MSSs therein in terms of enantioselective analyte sensing; the guest species used were non-chiral tetramethylpyrazine and phenazine.<sup>56</sup> Lee and Lin used axially chiral binaphthyl bridging ligands in Re metallocycles to make sensors for chiral amino alcohols.<sup>51</sup> Their 2002 study provides the first observation of enantioselective luminescence sensing by a chiral metallocycle.<sup>51</sup> In a 2006 paper, Heo and Mirkin report the enantioselective luminescent

sensing of chiral mandelic acid using a Cu<sup>I</sup> metallocyclophane.<sup>57</sup> Because of the potential advantages of using chiral MSSs in enantioselective molecular recognition, and the numerous studies of their syntheses and photophysical properties, yet near complete lack of studies demonstrating their use, this area is poised for discovery.

It may be that simply increased study of the potential of chiral MSSs for use as enantioselective chemical sensors would lead to advances in the field of molecular recognition by expanding the range of potential analytes. However, there are other desired improvements for the aforementioned applications of interest as well. These include the ability to use chemical sensors for the analysis of mixtures containing an analyte and multiple other species, simultaneous sensing of multiple analytes from complex mixtures, and reduced experimental uncertainties in ee determination. It is arguable that the mentioned improvements could not conceivably be achieved to the desired degree given an approach based exclusively on the rational design of selective receptors;<sup>58</sup> an innovation in the way chemical sensors for molecular recognition are designed and used is needed. That innovation is provided by *differential sensing arrays*.<sup>2,8</sup>

*Enantioselective Differential Sensing Arrays.* Recent efforts in synthetic chemical sensor design have hit upon a strategy found in Nature in the chemosensory abilities of smell and taste in organisms: the use of imperfectly selective receptors in arrays.<sup>58</sup> In our sense of smell, for example, the human brain interprets the aggregate response of about 1000 different types of receptors as a particular scent.<sup>59</sup> If each type of receptor was perfectly selective according to a “lock and key” model,<sup>60</sup> human olfaction would be

limited to the ability to detect only about 1000 possible chemical species, and mixtures thereof. Instead, imperfectly selective receptors can distinguish among types of molecules or functional groups (e.g., aldehydes<sup>61</sup>), and are cross-reactive within types. The composite receptor response to a particular mixture of analytes then, gives a “fingerprint” that is interpreted and recorded by the brain as a particular odor. This approach to chemosensory design taken by Nature allows an organism with a finite number of individual receptors to differentiate the from among the vast range of imaginable compounds and mixtures thereof it would encounter in its environment. Because of the importance of chirality in biological systems, it is not surprising that the ability to enantiodiscriminate is built into our own chemosensory arrays. For example, a considerable part of the smell and taste of caraway seeds or spearmint is due to d- or l-carvone, respectively.<sup>42</sup> Working from Nature’s examples when designing synthetic chemosensory systems is an approach that has the potential to further both synthetic chemosensor design, and our understanding of the complicated biological systems themselves.<sup>62</sup>

#### Lock and Key Sensor



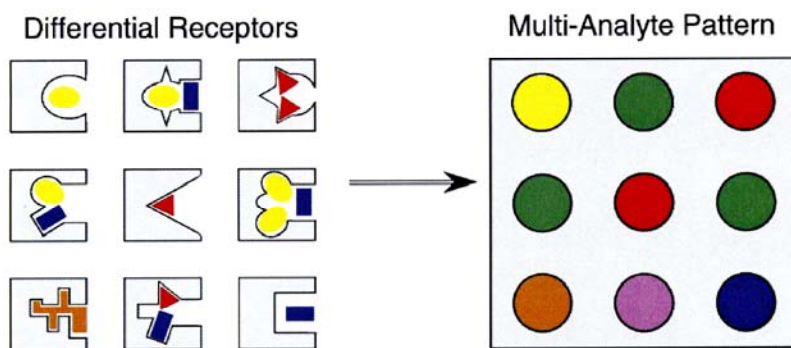


**Figure 2.** Schematic representation of molecular recognition by an analyte-specific sensor (top) and a differential sensing array (bottom), adapted with permission from reference 58, Lavigne, J. J.; Anslyn, E. V. *Angew. Chem., Int. Ed.* **2001**, *40*, 3118-3130. Copyright 2001 Wiley-VCH Verlag GmbH & Co. KGaA. The recognition event is shown on the left and the signaling event is shown on the right. Sensors in differential arrays are necessarily “cross-reactive” giving a “fingerprint” response allowing the analysis of even complicated mixtures of analytes using a limited number of sensor types.

Synthetic molecular recognition systems designed in this manner have been aptly termed “differential sensing arrays” (DSAs), Figure 2.<sup>2,8</sup> Efforts in molecular recognition have advanced significantly from applying the DSA approach.<sup>58</sup> Recent examples include the detection of metal ions,<sup>9</sup> steroids,<sup>18</sup> and a variety of metal-ligating compounds,<sup>20</sup> using arrays of hydroxyquinoline-,<sup>9</sup> oligonucleotide-,<sup>18</sup> or metalloporphyrin-based sensors,<sup>20</sup> respectively. However, there have been very few reports in the literature of enantioselective differential sensing arrays (E-DSAs). Lewis and coworkers reported the array-based differential detection of chiral gases. Their approach utilized an “electronic nose” comprised of chiral polymer composite sensors. The focus of this proposal, however, is on solution-phase analyses. In a 2001 paper, Shair and coworkers described a breakthrough; kinetic resolution of the response of arrays of sensors, made from □- and □-proline covalently coupled to fluorophores, was used to calculate ee in samples of chiral amino acids.<sup>41</sup> Preparation of the arrays, however, was somewhat laborious; each sample of an *N*-Boc-protected amino acid

analyte had to be covalently attached to the amine-derivatized surface of a glass slide, deprotected, and covalently connected to the proline-fluorophore sensor. More recently, Anslyn and coworkers improved on the use of E-DSAs by showing how arrays of Cu<sup>II</sup> complex-based sensors can be used to achieve simultaneous chemo- and enantioselective sensing of multi-analyte mixtures of chiral amino acids.<sup>63</sup>

Despite the recent advances in E-DSAs, the wide range of receptor-analyte interaction modes (e.g., solvophobic, ion pairing, hydrogen bonding, etc.), analyte sizes, and other factors giving rise to the wide variety of analyte classes of potential interest, requires a significant inventory of receptor types; the existing receptors used in E-DSAs are insufficient. As others have stated, “the molecular frameworks suitable for introducing the incremental variations of structure needed to achieve differential cross-reactivity are currently limited.”<sup>18</sup> The importance of enantioselective chemical sensors, coupled with the nascent state of the science of E-DSAs means that a great opportunity currently exists to find improvements in this field. Current research with chiral MSSs is still largely focused on the rational design of molecules with *potential* use as chemical sensors for enantioselective molecular recognition. In order to tap this unrealized potential, a novel approach is proposed herein: using chiral MSSs in E-DSAs. The hypothesis that will be tested is that MSSs will show utility in this regard. The idea is that a wider variety of available chemical sensor types that have proven to be useful in E-DSA will lead to an expansion in the range of analytes to which E-DSAs can be applied, and thereby improve the outlook for chemical sensing technology using E-DSAs. Such eventual improvements hold the potential, for example, to revolutionize the methodology used in high throughput screening of potential chiral catalysts of key importance in,

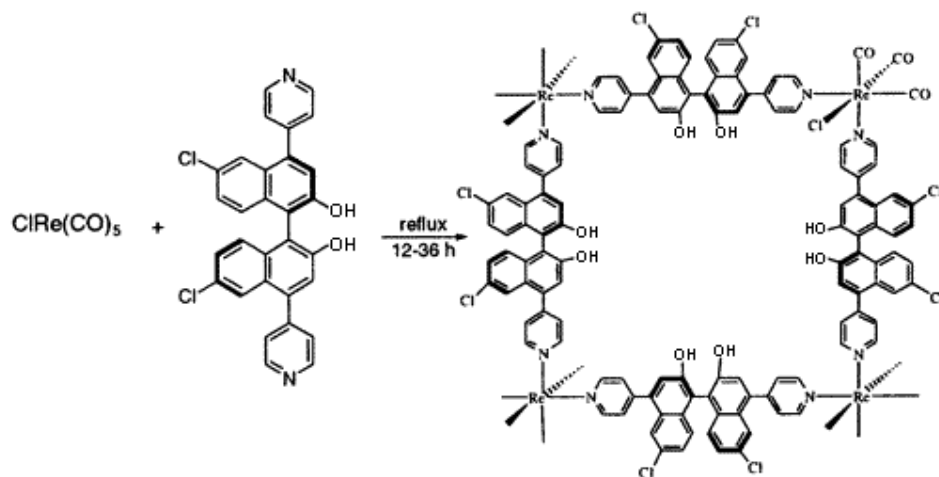
among other areas, the development of chiral pharmaceutical compounds, as well as to advance our understanding of, and ability to mimic, mammalian chemosensory systems.

## Research Design and Methods

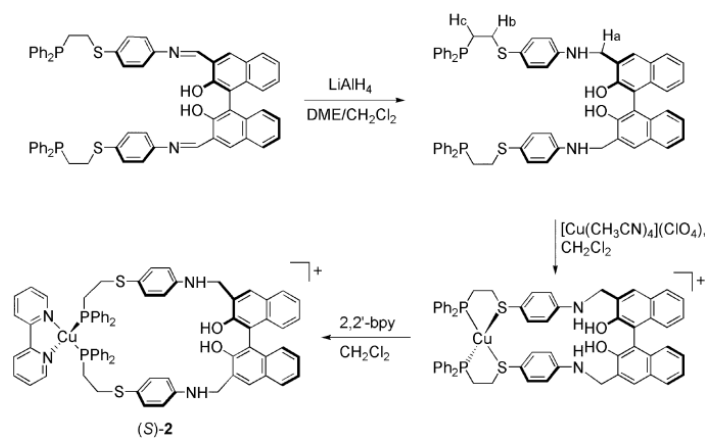
The research proposed herein will be conducted in three stages. The first two are (i) synthesis and characterization of the necessary sensor compounds including the known chiral MSSs with enantioselective molecular recognition capabilities, and (ii) use of these chiral MSSs together in an E-DSA *along with* other chemical sensors from the literature that have been used in E-DSAs. The specifics of the third stage depend on the findings obtained from stage two. In general, it will involve the synthesis of known chiral MSSs suggested to have promise as enantioselective sensors, and by making incremental variations, novel chiral MSSs. These will then be tested for applicability in E-DSAs in an approach parallel to stage two.

*Stage 1: Synthesis and Characterization of Sensor Compounds Including Known Chiral MSSs with Enantioselective Molecular Recognition Capabilities.* The proposed research will begin with a reproduction of the published synthesis of both enantiomers of  $[\text{Cl}(\text{CO})_3\text{Re}(\text{L})]_4$ , (hereafter (*R*)- or (*S*)-**1**), where L is enantiopure atropisomeric 6,6'-dichloro-2,2'-dihydroxy-4,4'-bis(4-pyridyl)-1,1'-binaphthalene.<sup>51</sup> First, the linking ligand, L, was synthesized starting with enantiopure 1,1'-bi-2-naphthol (binol). Refluxing L with  $\text{ClRe}(\text{CO})_5$  in a 1:1 molar ratio in benzene gave either (*S*)- or (*R*)-**1**, Scheme 1. To ensure that the correct compound is obtained, and is of acceptable purity, characterization of **1** will be accomplished by C, H, and N analyses, FAB MS, <sup>1</sup>H and

$^{13}\text{C}$  NMR, IR, UV-vis, and CD as reported in the literature.<sup>51</sup> It will also be necessary to reproduce the syntheses of both enantiomers of the  $\text{Cu}^{\text{I}}$  metallocyclophane (hereafter (*R*)- or (*S*)-**2**) reported by Heo and Mirkin, Scheme 2.<sup>57</sup> The starting compound in Scheme 2 was formed by coupling enantiopure binol-3,3'-dicarbaldehyde to 4-(2-diphenylphosphanylethylthio)-phenylamine via imine condensation. As with **1**, characterization of **2** will be accomplished by all methods reported in the literature, which in this case are C, H, and N analyses, ESI MS,  $^1\text{H}$ ,  $^{13}\text{C}$ , and  $^{31}\text{P}$  NMR, and CD.<sup>57</sup>



**Scheme 1.** The synthesis of **1** (right) from  $\text{ClRe}(\text{CO})_5$  and linking ligand, **L**, in a 1:1 molar ratio by refluxing in benzene. **L** was synthesized starting from enantiopure 1,1'-bi-2-naphthol by a procedure described in detail.<sup>51</sup> Reproduced with permission from Lee, S. J.; Lin, W. *J. Am. Chem. Soc.* **2002**, *124*, 4554–4555. Copyright 2002 American Chemical Society.



**Scheme 2.** The synthesis of (*S*)-**2** (bottom left). The synthesis of (*R*)-**2** was accomplished in the same fashion using enantiopure (*R*)-binaphthol-3,3'-dicarbaldehyde to start.<sup>57</sup> Reproduced with permission from Heo, J.; Mirkin, C. A. *Angew. Chem., Int. Ed.* **2006**, *45*, 941–944. Copyright 2006 Wiley-VCH Verlag GmbH & Co. KGaA.

After successful syntheses have been assured, but before the next stage of the research will be undertaken, control experiments will be performed; both enantiomers of both compounds **1** and **2** will be tested using fluorescence spectroscopy for their abilities to enantioselectively coordinate chiral 2-amino-1-propanol (alaninol) and chiral mandelic acid, respectively. In the literature, the luminescent signal at 412 nm of (*S*)-**1** was quenched more rapidly by (*R*)-alaninol than the (*S*) form, and vice versa for (*R*)-**1**, which resulted in measurable enantioselective sensing.<sup>51</sup> The net fluorescence intensity increase upon binding of (*S*)-mandelic acid by (*S*)-**2** was more than twice the increase upon its binding with (*R*)-mandelic acid, and vice versa with (*R*)-**2**, also a clearly discernable enantioselective sensing event.<sup>57</sup>

*Stage 2: Using Chiral MSSs Together in an E-DSA with Other Chemical Sensors Previously Used in E-DSAs.* Multiple E-DSAs incorporating **1** and **2** alongside the Cu<sup>II</sup>-based sensors used previously in enantioselective arrays will be created. Use of the

MSSs in the same sensing arrays as the other sensors should permit direct evaluation of the usefulness of MSSs in E-DSAs. The methods used will be analogous to how those arrays were prepared in the literature without incorporating **1** and **2**,<sup>63</sup> to form a sensor array, solutions of each of the Cu<sup>II</sup>-based and MSS sensors will be deposited into separate wells of polystyrene 96-well flat bottom plates.

After collection of blank array spectra, the composite response of an array to the addition of various analyte mixtures will be measured by multi-well plate spectroscopy. The analytes to be tested may include each enantiomer of the following chiral and achiral molecules and amino acids: alaninol, mandelic acid, norpinephrine, metoprolol, sphingosine, Leu, Val, Trp, Phe, Tle, Gly, Ala, Pro, Ser, Cys, or any others of similar size and/or functionality of interest. Enantioselective sensing of many of these analytes has been previously studied using one or more of these sensors. Use of the array of sensors, however, means that this will be the first time many of these sensors will be tested for their ability to recognize many of these analytes. The effects of both the sensor and analyte concentrations, and thus the sensor/analyte ratios should, therefore, be tested as well. An obvious weakness of this research, and at least at present, the DSA approach to enantioselective chemical sensing in general, is the large amount of data that must be collected and handled. Despite this difficulty, and depending on the results of the described set of experiments, it may be important to also test MSSs in differential arrays alongside the sensors reported by Shair and coworkers (described above).<sup>41</sup>

The pattern recognition aspect of data analysis will be accomplished through the use of principal component analysis (PCA), the most common of the pattern recognition protocols typically used in similar analyses.<sup>2</sup> PCA is a statistical treatment used to

visualize the clustering of data<sup>29</sup> without regard for which analyte-sensor combination the data points have originated from, but instead defines data clusters based simply on similarity (i.e., an “unsupervised” statistical method).<sup>9</sup> It works using mathematics analogous to those used to solve for molecular orbitals (i.e., an Eigenvector problem).<sup>2</sup> Essentially the data patterns obtained from the sensor arrays are reduced to single data points along an axis of maximum variance (the first principle component (PC) axis). Subsequent orthogonal PC axes are ordered according to decreasing variance.<sup>8,25</sup> A PCA test of the discriminatory power of the sensor is to see if the PC-analyzed data points for a given analyte cluster together.<sup>9</sup> A comparison of PCA plots from arrays without MSS sensors to arrays with MSS sensors, but from otherwise identical experiments and conditions should show how MSSs contribute to the discriminatory ability of the array. To carry out PCA, the program XLSTAT-Pro (Addinsoft) has been used previously,<sup>63</sup> and should be sufficient for the proposed work herein. However, other pattern recognition protocols such as hierarchical cluster theory, artificial neural networks, or linear discriminant analysis have the potential to work as well.<sup>2,36</sup>

Stage 3: *Synthesis of Chiral MSSs and Their Use in E-DSAs*. Depending on the results of the previous stages of the proposed research, there should be a clear indication at this point whether **1** and **2** are, or are not useful as chemical sensors in E-DSAs. A test of the hypothesis that chiral MSSs **1** and **2** can be used in E-DSAs is a test of the implicit hypothesis that **1** and **2** will act as *cross-reactive* sensors. The original reports of the synthesis and enantioselective sensing properties of **1** and **2** do not describe the degree of cross-reactivity of sensors **1** and **2** using a broad variety of similar analytes.<sup>51,57</sup>

Regardless of whether or not **1** and **2** exhibit sufficient cross-reactivity and make a beneficial contribution to the discriminatory power of the sensing array, that finding alone says little about the entire class of chiral MSS sensors. To fully test the hypothesis of this proposal (that chiral MSSs, as a class of chemical sensor, will be useful in E-DSAs) other MSSs sensors will need to be explored as well.

Research in the field of chiral MSSs has produced many examples which show promise for utility as enantioselective sensors, but that ability has yet to be demonstrated in numerous cases.<sup>52</sup> Screening these compounds for their usefulness as enantioselective sensors will be an important, but time consuming and laborious endeavor best approached using E-DSAs. Syntheses of novel chiral MSSs should be conducted as well. Initial efforts in this regard will be to make incremental variations to existing chiral MSSs that have shown ability or promise for enantioselective sensing. In doing so, it is possible that important and useful sensor materials are found. Additionally, the efforts are likely add to the general understanding of how to best make chemical sensors for use in enantioselective differential arrays.

To conclude, molecular recognition using chemical sensors is a rapidly growing field. Important potential applications of chemical sensing technology require improvements to the abilities of enantioselective sensors. Great strides in molecular recognition have been made using differential sensing arrays, yet very few studies have applied this approach to enantioselective sensing applications. Enantioselective differential sensing arrays could be improved by the availability of a wider variety of chemical sensors. Using metallocyclic supramolecular systems in enantioselective

differential sensing arrays is one novel approach to expanding the range of useful array-based sensors. The hypothesis that chiral metallocyclic supramolecular systems will be useful sensors in enantioselective differential sensing arrays will be tested according the efforts delineated in this proposal.

### Literature Cited

- 
- <sup>1</sup> Kumar, A.; Sun, S.-S.; Lees, A. J. Directed assembly metallocyclic supramolecular systems for molecular recognition and chemical sensing. *Coordination Chemistry Reviews* **2008**, *252*, 922-939.
- <sup>2</sup> Anslyn, E. V. Supramolecular Analytical Chemistry. *J. Org. Chem.* **2007**, *72*, 687-699.
- <sup>3</sup> Potyrailo, R. A.; Mirsky, V. M. Combinatorial and High-Throughput Development of Sensing Materials: The First 10 Years. *Chem. Rev.* **2008**, *108*, 770-813.
- <sup>4</sup> Lehn, J.-M. *Supramolecular Chemistry*; VCH: New York, 1995.
- <sup>5</sup> Schrader, T.; Hamilton, A. *Functional Synthetic Receptors*; John Wiley & Sons: New York, 2005.
- <sup>6</sup> Gokel, G. W.; Leevy, W. M.; Weber, M. E.; Crown Ethers: Sensors for Ions and Molecular Scaffolds for Materials and Biological Models. *Chem. Rev.* **2004**, *104*, 2723-2750.
- <sup>7</sup> Shahgaldian, P.; Pieles, U. Cyclodextrin Derivatives as Chiral Supramolecular Receptors for Enantioselective Sensing. *Sensors* **2006**, *6*, 593-615
- <sup>8</sup> Wright, A. T.; Anslyn E. V. Differential receptor arrays and assays for solution-based molecular recognition. *Chem. Soc. Rev.* **2006**, *35*, 14-28.

- 
- <sup>9</sup> Palacios, M. A.; Wang, Z.; Montes, V. A.; Zyryanov, G. V.; Anzenbacher, P., Jr. Rational Design of a Minimal Size Sensor Array for Metal Ion Detection. *J. Am. Chem. Soc.* **2008**, *130*, 10307-10314.
- <sup>10</sup> Zhu, L.; Anslyn, E. V. Facile Quantification of Enantiomeric Excess and Concentration with Indicator-Displacement Assays: An Example in the Analyses of  $\alpha$ -Hydroxyacids. *J. Am. Chem. Soc.* **2004**, *126*, 3676-3677.
- <sup>11</sup> Zhu, L.; Zhong, Z.; Anslyn, E. V. Guidelines in Implementing Enantioselective Indicator-Displacement Assays for  $\alpha$ -Hydroxycarboxylates and Diols. *J. Am. Chem. Soc.* **2005**, *127*, 4260-4269.
- <sup>12</sup> Mohr, G. J. Chromo- and Fluororeactands: Indicators for Detection of Neutral Analytes by Using Reversible Covalent-Bond Chemistry. *Chem. Eur. J.* **2004**, *10*, 1082-1090.
- <sup>13</sup> Moghimi, A.; Maddah, B.; Yari, A.; Shamsipur, M.; Boostani, M.; Rastegar, M. F.; Ghaderi, A. R. Molecular recognition of amino acids with some fluorescent ditopic pyrylium- and pyridinium-based crown ether receptors. *J. Mol. Struct.* **2005**, *752*, 68-77.
- <sup>14</sup> Kim, J.; Kim, S.-G.; Seong, H. R.; Ahn, K. H. Breaking the  $C_3$ -Symmetry of Chiral Tripodal Oxazolines: Enantio-Discrimination of Chiral Organoammonium Ions. *J. Org. Chem.* **2005**, *70*, 7227-7231.
- <sup>15</sup> Smith, D. K.; Zingg, A.; Diederich, F. Dendroclefts: Optically Active Dendritic Receptors for the Selective Recognition and Chiroptical Sensing of Monosaccharide Guests. *Helv. Chim. Acta* **1999**, *82*, 1225-1241.
- <sup>16</sup> Ogoshi, T.; Harada, A. Chemical Sensors Based on Cyclodextrin Derivatives. *Sensors* **2008**, *8*, 4961-4982.
- <sup>17</sup> McCleskey, S. C.; Griffin, M. J.; Schneider, S. E.; McDevitt, J. T.; Anslyn, E. V. Differential Receptors Create Patterns Diagnostic for ATP and GTP. *J. Am. Chem. Soc.* **2003**, *125*, 1114-1115.

- 
- <sup>18</sup> Stojanović, M. N.; Green, E. G.; Semova, S.; Nikić, D. B.; Landry, D. W. Cross-Reactive Arrays Based on Three-Way Junctions. *J. Am. Chem. Soc.* **2003**, *125*, 6085-6089.
- <sup>19</sup> Baldini, L.; Wilson, A. J.; Hong, J.; Hamilton, A. D. Pattern-Based Detection of Different Proteins Using an Array of Fluorescent Protein Receptors. *J. Am. Chem. Soc.* **2004**, *126*, 5656-5657.
- <sup>20</sup> Rakow, N. A.; Suslick, K. S. A colorimetric sensor array for odour visualization. *Nature* **2000**, *406*, 710-713.
- <sup>21</sup> Marty, J. L.; Garcia, D.; Rouillion, R. Biosensors: potential in pesticide detection. *Trends Anal. Chem.* **1995**, *14*, 329-333.
- <sup>22</sup> Wilson, G. S.; Hu, Y. Enzyme-Based Biosensors for in Vivo Measurements. *Chem. Rev.* **2000**, *100*, 2693-2704.
- <sup>23</sup> Haupt, K.; Mosbach, K. Molecularly Imprinted Polymers and Their Use in Biomimetic Sensors. *Chem. Rev.* **2000**, *100*, 2495-2504.
- <sup>24</sup> Hatchett, D. W.; Josowicz, M. Composites of Intrinsically Conducting Polymers as Sensing Nanomaterials. *Chem. Rev.* **2008**, *108*, 746-769.
- <sup>25</sup> Potyrailo, R. A.; Leach, A. M. Selective gas nanosensors with multisize CdSe nanocrystal/polymer composite films and dynamic pattern recognition. *Appl. Phys. Lett.* **2006**, *88*, 134110.
- <sup>26</sup> Aït-Haddou, H.; Wiskur, S. L.; Lynch, V. M.; Anslyn, E. V. Achieving Large Color Changes in Response to the Presence of Amino Acids: A Molecular Sensing Ensemble with Selectivity for Aspartate. *J. Am. Chem. Soc.* **2001**, *123*, 11296-11297.
- <sup>27</sup> Folmer-Andersen, J. F.; Lynch, V. M.; Anslyn, E. V. Colorimetric Enantiodiscrimination of  $\alpha$ -Amino Acids in Protic Media. *J. Am. Chem. Soc.* **2005**, *127*, 7986-7987.

- 
- <sup>28</sup> Folmer-Andersen, J. F.; Kitamura, M.; Anslyn, E. V. Pattern-Based Discrimination of Enantiomeric and Structurally Similar Amino Acids: An Optical Mimic of the Mammalian Taste Response. *J. Am. Chem. Soc.* **2006**, *128*, 5652-5653.
- <sup>29</sup> Buryak, A.; Severin, K. A Chemosensor Array for the Colorimetric Identification of 20 Natural Amino Acids. *J. Am. Chem. Soc.* **2005**, *127*, 3700-3701.
- <sup>30</sup> Stang, P. J.; Olenyuk, B. Self-Assembly, Symmetry, and Molecular Architecture: Coordination as the Motif in the Rational Design of Supramolecular Metallacyclic Polygons and Polyhedra. *Acc. Chem. Res.* **1997**, *30*, 502-518.
- <sup>31</sup> Sun, S.-S.; Lees, A. J. Transition metal based supramolecular systems: synthesis photophysics, photochemistry and their potential applications as luminescent anion chemosensors. *Coordination Chemistry Reviews* **2002**, *230*, 171-192.
- <sup>32</sup> Slone, R. V.; Hupp, J. T.; Stern, C. L.; Albrecht-Schmitt, T. E. Self-Assembly of Luminescent Molecular Squares Featuring Octahedral Rhenium Corners. *Inorg. Chem.* **1996**, *35*, 4096-4097.
- <sup>33</sup> Lee, S. J.; Lin, W. Chiral Metallocycles: Rational Synthesis and Novel Applications. *Acc. Chem. Res.* **2008**, *41*, 521-537.
- <sup>34</sup> Stella, R.; Barisci, J. N.; Serra, G.; Wallace, G. G.; Rossi, D. D. Characterization of olive oil by an electronic nose based on conducting polymer sensors. *Sensors and Actuators B* **2000**, *63*, 1-9.
- <sup>35</sup> Piątek, A. M.; Bomble, Y. J.; Wiskur, S. L.; Anslyn, E. V. Threshold Detection Using Indicator-Displacement Assays: An Application in the Analysis of Malate in Pinot Noir Grapes. *J. Am. Chem. Soc.* **2004**, *126*, 6072-6077.
- <sup>36</sup> Wang, Z.; Palacios, M. A.; Anzenbacher, P., Jr. Fluorescence Sensor Array for Metal Ion Detection Based on Various Coordination Chemistries: General Performance and Potential Application. *Anal. Chem.* **2008**, *80*, 7451-7459.

- 
- <sup>37</sup> Zampolli, S.; Betti, P.; Elmi, I.; Dalcanale, E. A supramolecular approach to sub-ppb aromatic VOC detection in air. *Chem. Commun.* **2007**, 2790-2792.
- <sup>38</sup> Jenkins, A. L.; Yin, R.; Jensen, J. L. Molecularly imprinted polymer sensors for pesticide and insecticide detection in water. *Analyst (Cambridge, U.K.)* **2001**, *126*, 798-802.
- <sup>39</sup> Jenkins, A. L.; Uy, O. M.; Murray G. M. Polymer-Based Lanthanide Luminescent Sensor for Detection of the Hydrolysis Product of the Nerve Agent Soman in Water. *Anal. Chem.* **1999**, *71*, 373-378.
- <sup>40</sup> Czarnik, A. W. Desperately seeking sensors. *Chem. Biol.* **1995**, *2*, 423-428.
- <sup>41</sup> Korbel, G. A.; Lalic, G.; Shair, M. D. Reaction Microarrays: A Method for Rapidly Determining the Enantiomeric Excess of Thousands of Samples. *J. Am. Chem. Soc.* **2001**, *123*, 361-362.
- <sup>42</sup> Hoffmann, R. *The Same and Not the Same*, George B Pegram lecture series; Columbia University Press: New York, 1995; pp 42, 43, 129-138.
- <sup>43</sup> <http://www.fda.gov/cder/guidance/stereo.htm>
- <sup>44</sup> Kubo, Y.; Maeda, S.; Tokita, S.; Kubo, M. Colorimetric chiral recognition by a molecular sensor. *Nature* **1996**, *382*, 522-524.
- <sup>45</sup> Jiang, H.; Lin, W. Self-Assembly of Chiral Molecular Polygons. *J. Am. Chem. Soc.* **2003**, *125*, 8084–8085.
- <sup>46</sup> Jiang, H.; Lin, W. Chiral Molecular Polygons Based on the Pt-Alkynyl Linkage: Self-Assembly, Characterization, and Functionalization. *J. Organomet. Chem.* **2005**, *690*, 5159–5169.
- <sup>47</sup> Oenyuk, B.; Whiteford, J. A.; Stang, P. J. Design and Study of Synthetic Chiral Nanoscopic Assemblies. Preparation and Characterization of Optically Active Hybrid,

---

Iodonium-Transition-Metal and All-Transition-Metal Macrocyclic Molecular Squares. *J. Am. Chem. Soc.* **1996**, *118*, 8221–8230.

<sup>48</sup> Fan, J.; Whitehold, J. A.; Olenyuk, B.; Levin, M. D.; Stang, P. J.; Fleischer, E. B. Self-Assembly of Porphyrin Arrays via Coordination to Transition Metal Bisphosphine Complexes and the Unique Spectral Properties of the Product Metallacyclic Ensembles. *J. Am. Chem. Soc.* **1999**, *121*, 2741–2752.

<sup>49</sup> Zhang, Y.; Wang, S.; Enright, G. D.; Breeze, S. R. Tetraacetylene Dianion (Tae) As a Bridging Ligand for Molecular Square Complexes:  $\text{Co}^{\text{II}}_4(\text{Tae})_4(\text{Dpa})_4$ , Dpa = Di-2-pyridylamine, a Chiral Molecular Square in the Solid State. *J. Am. Chem. Soc.* **1998**, *120*, 9398–9399.

<sup>50</sup> Ali, M. M.; MacDonnell, F. M. Topospecific Self-Assembly of Mixed-Metal Molecular Hexagons with Diameters of 5.5 nm Using Chiral Control. *J. Am. Chem. Soc.* **2000**, *122*, 11527–11528.

<sup>51</sup> Lee, S. J.; Lin, W. A Chiral Molecular Square with Metallo-Corners for Enantioselective Sensing. *J. Am. Chem. Soc.* **2002**, *124*, 4554–4555.

<sup>52</sup> Lee, S. J.; Kim, J. S.; Lin, W. Chiral Molecular Squares Based on Angular Bipyridines: Self-Assembly, Characterization, and Photophysical Properties. *Inorg. Chem.* **2004**, *43*, 6579–6588.

<sup>53</sup> Bélanger, S.; Hupp, J. T.; Stern, C. L.; Slone, R. V.; Watson, D. F.; Carrell, T. G. Thin-Film Molecular Materials Based on Tetrametallic “Squares”: Nanoscale Porosity and Size-Selective Guest Transport Characteristics. *J. Am. Chem. Soc.* **1999**, *121*, 557–563.

<sup>54</sup> Keefe, M. H.; Slone, R. V.; Hupp, J. T.; Czaplewski, K. F.; Snurr, R. Q.; Stern, C. L. Mesoporous Thin Films of “Molecular Squares” as Sensors for Volatile Organic Compounds. *Langmuir* **2000**, *16*, 3964–3970.

- 
- <sup>55</sup> Lee, S. J.; Luman, C. R.; Castellano, F. N.; Lin, W. Directed Assembly of Chiral Organometallic Squares that Exhibit Dual Luminescence. *Chem. Commun.* **2003**, *17*, 2124–2125.
- <sup>56</sup> Müller, C.; Whiteford, J. A.; Stang, P. J. Self-Assembly, Chiroptical Properties, and Host-Guest Chemistry of Chiral Pt–Pt and Pt–Pd Tetranuclear Macrocycles. Circular Dichroism Studies on Neutral Guest Inclusion Phenomena. *J. Am. Chem. Soc.* **1998**, *120*, 9827–9837.
- <sup>57</sup> Heo, J.; Mirkin, C. A. Pseudo-Allosteric Recognition of Mandelic Acid with an Enantioselective Coordination Complex. *Angew. Chem., Int. Ed.* **2006**, *45*, 941–944.
- <sup>58</sup> Lavigne, J. J.; Anslyn, E. V. Sensing A Paradigm Shift in the Field of Molecular Recognition: From Selective to Differential Receptors. *Angew. Chem., Int. Ed.* **2001**, *40*, 3118–3130.
- <sup>59</sup> Zozulya, S.; Echeverri, F.; Nguyen, T. The human olfactory receptor repertoire. *Genome Biol.* **2001**, *2*, research0018.
- <sup>60</sup> *The Lock-and-Key Principle : The State of the Art – 100 Years On*, Behr, J.-P., Ed.; Perspectives in supramolecular chemistry; Wiley & Sons: New York, 1994; Vol. 1.
- <sup>61</sup> Firestein, S. Olfactory Receptor Neuron Signaling in *Chemistry of Taste: Mechanisms, Behaviors, and Mimics* Given, P.; Paredes, D., Eds.; ACS symposium series (Vol. 825) 2003, Ch 9.
- <sup>62</sup> Persaud, K.; Dodd, G. Analysis of discrimination mechanisms in the mammalian olfactory system using a model nose. *Nature* **1982**, *299*, 352–355.
- <sup>63</sup> Folmer-Andersen, J. F.; Kitamura, M.; Anslyn, E. V. Pattern-Based Discrimination of Enantiomeric and Structurally Similar Amino Acids: An Optical Mimic of the Mammalian Taste Response. *J. Am. Chem. Soc.* **2006**, *128*, 5652–5653.